

Dissertation zur Erlangung des Doktorgrades
der Fakultät für Chemie und Pharmazie
der Ludwig-Maximilians-Universität München

**One-Bond-Nucleophilicity and One-Bond-Electrophilicity Parameters:
An Efficient Ordering System for 1,3-Dipolar Cycloadditions**

Le Li

aus

Weinan, Shaanxi, China

2022

Erklärung

Diese Dissertation wurde im Sinne von § 7 der Promotionsordnung vom 07. November 2017 von Herrn PD Dr. Armin R Ofial betreut.

Eidesstattliche Versicherung

Diese Dissertation wurde eigenständig und ohne unerlaubte Hilfe erarbeitet.

München, den 22.11.2022

.....

Le Li

Dissertation eingereicht am: ...24.11.2022...

1. Gutachter: PD Dr. Armin Ofial
2. Gutachter: Prof. Dr. Oliver Trapp

Mündliche Prüfung am: ...19.01.2023...

Acknowledgement

I'm thankful to PD Dr. Armin R. Ofial for showing me the labs the first day when I came to Munich, for his helpful suggestions and enlightening discussions regarding my research projects, his support when it comes to trying out new ideas, his detailed corrections of all my reports, papers, posters and presentations, and his offering of opportunities to German courses, scientific trainings, conferences, trade fairs and fundings.

I deeply appreciate Prof. Dr. Herbert Mayr for giving me the opportunity to join the research group, his trust in me to manage the fascinating PhD project, his dedicated investment of time and energy in my project after his retirement, his informative discussions, his kindness of always offering me help when I came to him, and his delightful encouragement, without which it would be impossible for me to achieve what I have done.

Additionally, I would like to thank Prof. Dr. Oliver Trapp for reviewing my thesis and Prof. Dr. Anne Schuetz, Prof. Dr. Hendrik Zipse and Prof. Dr. Thomas M. Klapoetke for their participation in my defense.

I would also like to thank all my lab mates for the friendly lab atmosphere. Thank Dr. Artem Leonov for his help when I first came to the lab, Dr. Li Zhen for letting me 'inherit' his stuff in the lab, Dr. Daria Timofeeva for useful discussions, Dr. An Feng for picking me up from the airport the first day when I came to Munich, Dr. Patrick Jüstel for teaching me German words, Nathalie Hampel for preparing the benzhydrylium ions, Christoph Groß for his constant help, Dr. Magenta Hensinger for her discussions, Dr. Andreas Eitzinger and Dr. Robert Mayer for kindly showing me how to do DFT calculations.

Many thanks to Dr. Anja Haniel, Sabina Ferrara, Elisabeth Wutz and Top Sefa for their help with my work contracts, especially during Covid time.

Thank the Department of Chemistry, LMU München for the financial support of my PhD study, Ciska Voelmle and Andrea Blei for granting me the +Erasmus funding, which supported me during my summer school in Italy.

Thank Dr. David S. Stephenson for his low-temperature NMR kinetic measurements, Claudia Ober and Mariia Palchyk for their NMR measurements, Carrie Louis for being a good friend.

Special thanks to Ni Yinan and Hsu Jer-Ray for working with me to accomplish their Bachelor thesis.

Last but not least, I'm thankful to my parents and my partner Yu Weibo for their constant support and love.

Publications

- (1) “An Overlooked Pathway in 1,3-Dipolar Cycloadditions of Diazoalkanes with Enamines.”
Li, L.; Mayer, P.; Stephenson, D. S.; Ofial, A. R.; Mayer, R. J.; Mayr, H. *Angew. Chem. Int. Ed.* **2022**, *61*, e202117047; *Angew. Chem.* **2022**, *134*, e202117047.

- (2) “Quantification of the Electrophilicities of Diazoalkanes: Kinetics and Mechanism of Azo Couplings with Enamines and Sulfonium Ylides.”
Li, L.; Mayer, R. J.; Stephenson, D. S.; Mayer, P.; Ofial, A. R.; Mayr, H. *Chem. Eur. J.* **2022**, *28*, e202201376.

- (3) “Cyclobutane Formation by the Reaction of Ethenesulfonyl Fluoride with Dimethyl Diazomalonate.”
Li, L.; Mayer, P.; Ofial, A. R.; Mayr, H. *E. J. Org. Chem.* **2022**, e202200865.

Contributions to Conferences

Parts of this work were presented at the following scientific conferences:

2019-09 17th European Symposium on Organic Reactivity (XVII ESOR)

Dubrovnik (Croatia)

Poster presentation: “Ambiphilic Reactivity of Dimethyl Diazomalonate.”

2022-06 46th “A. Corbella” International Summer School on Organic Synthesis (XLVI ISOS) Gargnano (Italy)

Poster and oral presentation: “Quantification of the One-Bond Nucleophilicities and the One-Bond Electrophilicities of Diazoalkanes: A Novel Approach to 1,3-Dipolar Cycloadditions.”

2022-07 17th Belgian Organic Synthesis Symposium (XVII BOSS) Namur (Belgium)

Poster presentation: “Quantification of the One-Bond Nucleophilicities and the One-Bond Electrophilicities of Diazoalkanes: A Novel Approach to 1,3-Dipolar Cycloadditions.”

Table of Contents

Chapter 1. Summary	1
1.1 An Overlooked Pathway in 1,3-Dipolar Cycloadditions of Diazoalkanes	1
1.2 Quantification of the Electrophilicities of Diazoalkanes	3
1.3 Cyclobutane Formation by the Reaction of Ethenesulfonyl Fluoride with Dimethyl Diazomalonate	5
1.4 One-Bond-Nucleophilicity and -Electrophilicity Parameters: An Efficient Ordering System for 1,3-Dipolar Cycloadditions	6
Chapter 2. Introduction and Objectives	10
2.1 Mayr-Patz Equation	10
2.2 Nucleophilic Reactions of Diazoalkanes	11
2.2.1 Nucleophilic Reactions of Diazoalkanes with Carbonyl Compounds	11
2.2.2 Nucleophilic Reactions of Diazoalkanes with Benzhydrylium Ions	11
2.3 Electrophilic Reactions of Diazoalkanes	12
2.3.1 Electrophilic Reactions of Diazoalkanes with Organometallic Compounds	12
2.3.2 Electrophilic Reactions of Diazoalkanes with Carbanions	12
2.3.3 Electrophilic Reactions of Diazoalkanes with Sulfonium Ylides and Enamines	13
2.4 1,3-Dipolar Cycloadditions of Diazoalkanes	13
2.4.1 Concepts of 1,3-DCAs	13
2.4.2 Mechanism of 1,3-DCAs	14
2.4.3 Models for Interpretation of Structure-Reactivity Relationship in 1,3-DCAs	14
2.5 Objectives	19
2.6 References	21
Chapter 3. An Overlooked Pathway in 1,3-Dipolar Cycloadditions of Diazoalkanes with Enamines	24
3.1 Copies of Manuscript	25
3.2 Supporting Information	32
3.2.1 Product Studies	32
3.2.2 Kinetics	38
3.2.3 Single Crystal X-ray Crystallography	42
3.2.4 References	46
Chapter 4. Quantification of the Electrophilicities of Diazoalkanes: Kinetics and Mechanism of Azo Couplings with Enamines and Sulfonium Ylides	47
4.1 Copies of Manuscript	48
4.2 Supporting Information	61
4.2.1 Product Studies	61
4.2.2 Kinetics	81
4.2.3 Single Crystal X-ray Crystallography	98
4.2.4 References	103
Chapter 5. Cyclobutane Formation by the Reaction of Ethenesulfonyl Fluoride with Dimethyl Diazomalonate	104

5.1 Copies of Manuscript	105
5.2 Supporting Information	111
5.2.1 Additional Figure	111
5.2.2 Copies of ¹ H, ¹³ C and ¹⁹ F NMR Spectra	112
5.2.3 Single Crystal X-ray Crystallography	121
Chapter 6. One-Bond-Nucleophilicity and -Electrophilicity Parameters: An Efficient Ordering System for 1,3-Dipolar Cycloadditions	123
6.1 One-Bond-Nucleophilicity and -Electrophilicity Parameters: An Efficient Ordering System for 1,3-DCAs ..	124
6.2 Supporting Information	144
6.2.1 General.....	144
6.2.2 Product Studies	146
6.2.3 Kinetics	166
6.2.4 Single Crystal X-ray Crystallography	207
6.2.5 References.....	210

Chapter 1. Summary

1.1 An Overlooked Pathway in 1,3-Dipolar Cycloadditions of Diazoalkanes with Enamines

Reactions of methyl diazoacetate with enamines derived from five- and six-membered cyclic ketones were studied and the reaction mechanism was clarified.

Kinetics of the reactions of methyl diazoacetate with enamines were measured by time-resolved ^1H NMR spectroscopy in CDCl_3 at low temperatures (range ≥ 20 K) by following the decrease of the integral for the vinylic hydrogens of enamines (Figure 1A) relative to an internal standard (1,1,2,2-tetrachloroethane). Equimolar amounts of diazoacetate and enamines were used and the second-order rate constants k_2 were derived from the slopes of the plots of $1/[\text{enamine}]_t$ versus time t according to $1/[\text{enamine}]_t = k_2 t + 1/[\text{enamine}]_0$ (Figure 1B). Eyring plots of $\ln(k_2/T)$ versus $1/T$ gave the activation parameters ΔH^\ddagger and ΔS^\ddagger , from which the second-order rate constants k_2 at 20 °C were calculated (Figure 1C).

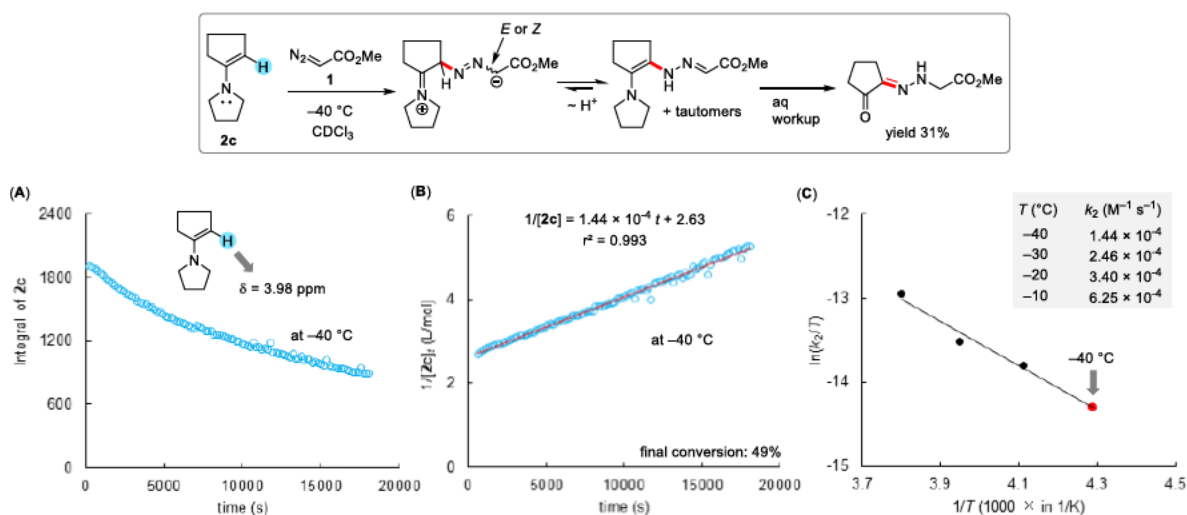
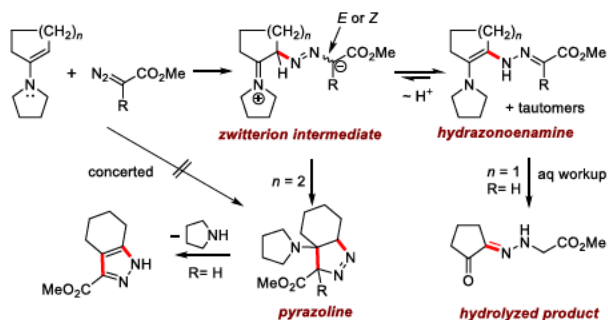


Figure 1. (A) Reaction of methyl diazoacetate (0.399 M) with enamine **2c** (0.371 M) monitored by the decrease of the integral for the vinylic H of **2c** vs. 1,1,2,2-tetrachloroethane (0.276 M) as internal standard in CDCl_3 at -40 °C. (B) Plot of $1/[\mathbf{2c}]_t$ vs. time t for the determination of the second-order rate constant k_2 of the reaction of methyl diazoacetate with **2c** at -40 °C. (C) Eyring plot for the reactions of methyl diazoacetate with **2c** at -40 to -10 °C.

^1H NMR spectroscopic monitoring of the reaction of methyl diazoacetate with pyrrolidinocyclopentene **2c** confirmed the preliminary formation of the hydrazoneenamine and tautomers (Figure 1, top). They were generated presumably via the zwitterionic intermediate formed by azo coupling of enamine **2c** to diazoacetate. Aqueous workup of the hydrazoneenamine and tautomers gave the final product.

Although 1,3-dipolar cycloadducts were obtained as the final products from the reactions of α -diazo esters with pyrrolidinocyclohexene, ^1H NMR monitoring of these reactions in CDCl_3 at low temperatures proved that the heterocycles were formed at later stage of the reactions.

The rate-determining step for both the azo coupling and the 1,3-dipolar cycloadditions (Huisgen reactions) of enamines with α -diazo esters can thus be confirmed as the formation of the zwitterionic intermediates. Proton shifts of the zwitterions afford the hydrazone enamines and tautomers, which may hydrolyze during aqueous workup or regenerate the zwitterions to give pyrazolines via cyclization (Scheme 1).



Scheme 1. Mechanism for the reactions of diazo esters with cyclopentanone- and cyclohexanone-derived enamines.

1.2 Quantification of the Electrophilicities of Diazoalkanes

Reactions of methyl diazoacetate, dimethyl diazomalonate, *p*-nitrophenyl diazomethane and diphenyldiazomethane with sulfonium ylides and enamines were investigated. And the one-bond electrophilicities of the diazoalkanes were determined.

Kinetics of the reactions of dimethyl diazomalonate with sulfonium ylide **2a** were investigated photometrically by monitoring the decay of the absorbance of **2a** at 372 nm in DMSO at 20 °C under pseudo-first-order conditions (Figure 2A).

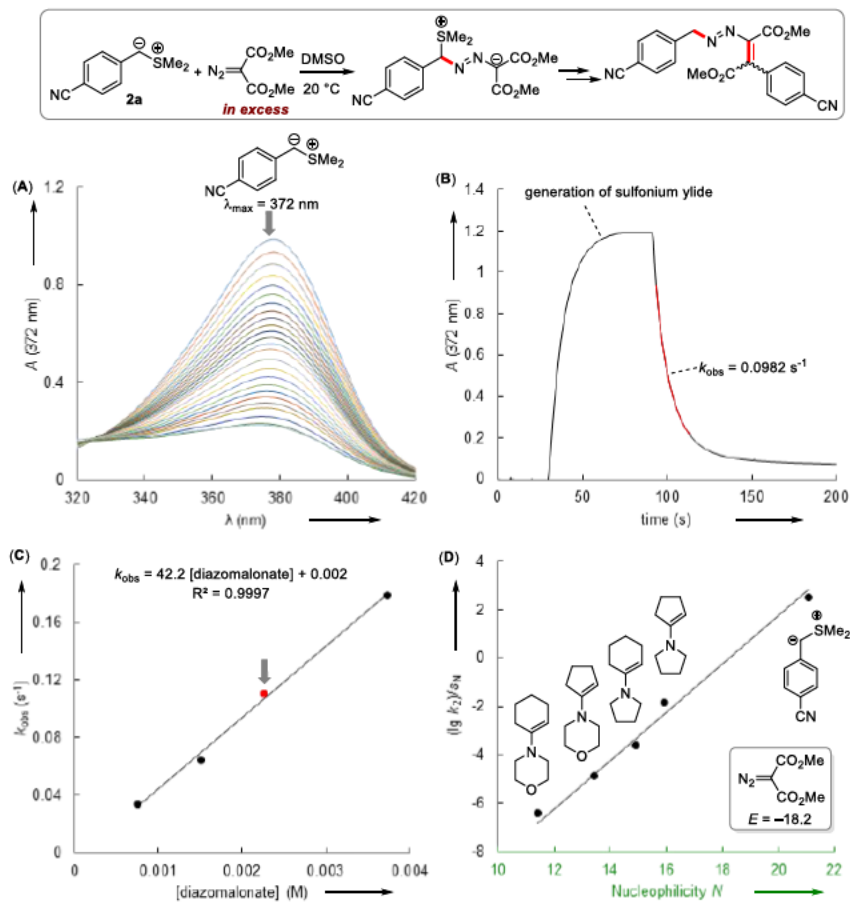


Figure 2. (A) UV-Vis spectroscopic monitoring of the reaction of dimethyl diazomalonate (2.26×10^{-3} M) with sulfonium ylide **2a** (8.32×10^{-5} M) at 372 nm in DMSO at 20 °C. (B) Mono-exponential decay of the absorbance A at 372 nm vs. time for the reaction of diazomalonate with sulfonium ylide in DMSO at 20 °C. (C) Linear correlation of the observed first-order rate constants k_{obs} with [diazomalonate] for determining the second-order rate constant $k_2 = 42.2 \text{ M}^{-1} \text{ s}^{-1}$ at 20 °C. (D) Plots of $(\lg k_2)/s_N$ vs. N for the reactions of diazomalonate with sulfonium ylide (in DMSO) and enamines (in CDCl $_3$) at 20 °C.

By following the mono-exponential decay of the absorbance of sulfonium ylide **2a** the observed first-order rate constants k_{obs} of its reactions with diazomalonate were derived (Figure 2B). The slope of the linear plot of k_{obs} versus the concentrations of diazomalonate gave the second-order

rate constant k_2 of the reaction of diazomalonate with sulfonium ylide **2a** at 20 °C (Figure 2C). The k_2 values of the reactions of diazoalkanes with enamines in CDCl_3 or CD_2Cl_2 at 20 °C were obtained using similar approach as described in the first part of this *Summary* chapter.

The equation $\lg k_{20\text{C}} = s_N(N + E)$ [eq. (1)] was applied to determine the electrophilicity parameters E of the diazoalkanes. The linear correlation of $(\lg k)/s_N$ with the N parameters of sulfonium ylide and enamines indicated the common nature of the rate-determining steps in the reactions of diazomalonate with sulfonium ylide **2a** and enamines (Figure 2D). The one-bond electrophilicity parameters E of the diazoalkanes were derived from least-squares analysis according to eq. (1).

α -Ester substitutions have only limited influence on the one-bond electrophilicities of diazoalkanes, as indicated by the similar E parameters of diazoacetate ($E = -18.5$) and diazomalonate ($E = -18.2$). This can be explained by the limited interactions between the π orbitals of the α -ester substituents and the $\pi^*_{\text{N=N}}$ orbitals of the diazo compounds.

The thus obtained E parameters of diazoalkanes can be used to rationalize reported azo couplings of diazoalkanes with other nucleophiles. As indicated by their N parameters (about 14 to 16), carbanions derived from active methylene compounds react with diazo esters ($E \approx -18$) smoothly as reported (Figure 3).

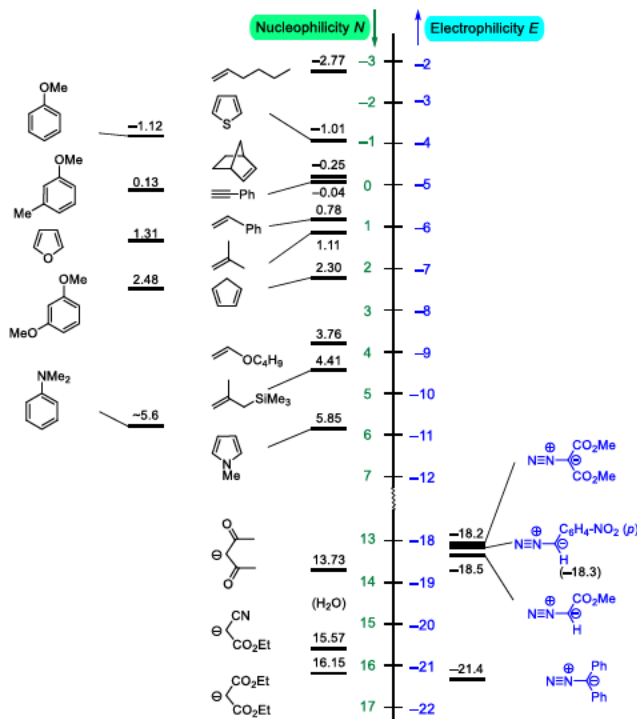


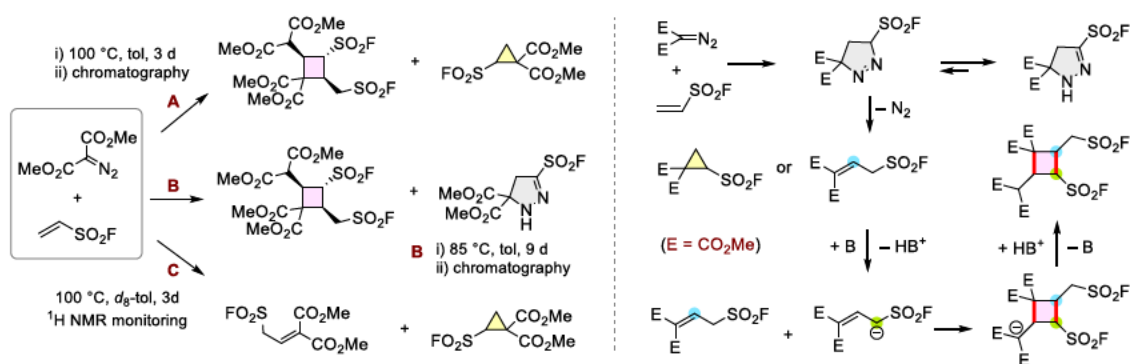
Figure 3. Potential nucleophilic reaction partners for diazoalkanes.

In contrast, ordinary alkenes such as styrene, cannot be expected to react with diazoalkanes via azo couplings at room temperature due to their weak nucleophilicities. The fact that these reactions have been observed suggests that the reaction mechanism has switched from polar to concerted processes.

1.3 Cyclobutane Formation by the Reaction of Ethenesulfonyl Fluoride with Dimethyl Diazomalonate

Reaction of dimethyl diazomalonate with ethenesulfonyl fluoride was studied and the mechanism for the formation of the cyclobutane product was investigated.

A highly functionalized cyclobutane and a cyclopropane were isolated from the reaction of ethenesulfonyl fluoride (ESF) with diazomalonate in toluene after 3 days at 100 °C (Scheme 2 left, A). While column chromatographic workup of the reaction of ESF with diazomalonate in toluene after 9 days at 85 °C led to the isolation of the cyclobutane and a Δ^2 -pyrazoline (Scheme 2 left, B). ^1H NMR spectroscopic monitoring of the reaction of ESF with diazomalonate in d_8 -toluene after 3 days at 100 °C detected the formation of an alkylidene malonate and the cyclopropane (Scheme 2 left, C), from which the cyclobutane and the cyclopropane were isolated by column chromatographic workup on silica gel.



Scheme 2. Left: Reactions of ESF with dimethyl diazomalonate under different conditions. Right: Proposed reaction mechanism for the formation of the cyclobutane.

^1H NMR monitoring of the solution of the isolated Δ^2 -pyrazoline in d_8 -toluene at 95 °C confirmed that both the alkylidene malonate and the cyclopropane were generated from thermolysis of the pyrazoline. Integration of the respective ^1H NMR signals suggested that the ratio of the alkylidene malonate and the cyclopropane remained constant after 72 h at 95 °C, which indicated that no interconversion occurred between the olefin and the cyclopropane.

After adding triethylamine to the mixture, the alkylidene malonate disappeared and transformation of it to the cyclobutane was detected by ^{19}F NMR spectroscopy (see Chapter 5). The cyclopropane remained inert under these conditions.

The mechanism for the formation of the cyclobutane can thus be proposed as in Scheme 2, right. 1,3-Dipolar cycloaddition of ESF with diazomalonate gives the Δ^1 -pyrazoline, which is in fast equilibrium with its thermodynamically more favorable Δ^2 -pyrazoline tautomer. Under heating, the Δ^1 -pyrazoline extrudes molecular nitrogen and generates the alkylidene malonate and the cyclopropane. The strong electron-withdrawing SO_2F substituent facilitates deprotonation of the CH_2 group in the alkylidene malonate under base catalysis. The thus formed carbanion undergoes a Michael addition to another alkylidene malonate furnishing the cyclobutylmalonyl anion after an intramolecular Michael addition. Protonation of the anion then yields the final cyclobutane.

1.4 One-Bond-Nucleophilicity and -Electrophilicity Parameters: An Efficient Ordering System for 1,3-Dipolar Cycloadditions

One-bond nucleophilicities of methyl diazoacetate and dimethyl diazomalonate were determined. Reactions of methyl diazoacetate, dimethyl diazomalonate, *p*-nitrophenyl diazomethane and diphenyldiazomethane with nucleophilic and electrophilic dipolarophiles were studied.

The equation $\lg k_{20\text{C}} = s_{\text{N}}(N + E)$ [eq. (1)] was applied to investigate the one-bond electrophilicities (as in the second part of this *Summary* chapter) and the one-bond nucleophilicities of ambiphilic diazoalkanes. The one-bond nucleophilicities of α -diazo esters were determined by measuring the kinetics of their reactions with benzhydrylium ions Ar_2CH^+ in CH_2Cl_2 at 20 °C. By plotting the $\lg k_2$ of these reactions versus the known E parameters of Ar_2CH^+ , the nucleophilicity parameters N and s_{N} of the diazo compounds were derived according to eq. (1) (Figure 4).

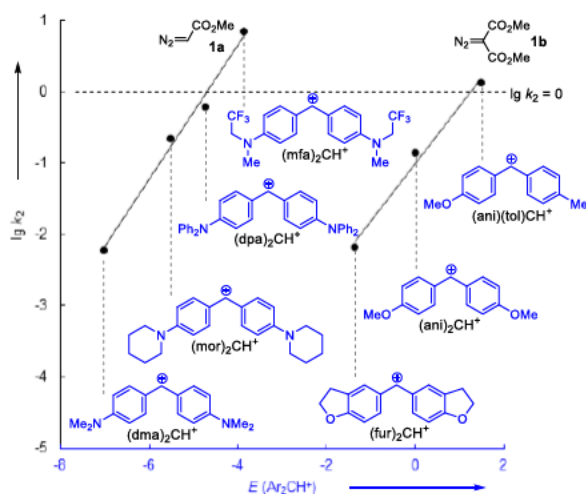


Figure 4. Plots of $\lg k_2$ of the reactions of α -diazo esters with benzhydrylium ions Ar_2CH^+ (in CH_2Cl_2 at 20 °C) versus their electrophilicity parameters E .

Kinetics of the 1,3-dipolar cycloadditions (1,3-DCAs) of diazoalkanes with nucleophilic and electrophilic dipolarophiles (structures as exemplified in Figs 5A & 5B) were investigated by time-resolved ^1H NMR spectroscopy and conventional UV-Vis spectroscopy. The second-order rate constants k_2 of these reactions at 20 °C were obtained either from the activation parameters derived from Eyring plots of the k_2 values measured at various temperatures or from the plots of observed first-order rate constants k_{obs} vs. the concentrations of the excessive diazoalkanes at 20 °C (see Chapter 6). Previously reported kinetic data of the 1,3-DCAs of diazoalkanes with additional dipolarophiles were collected and transformed to k_2 values at 20 °C by assuming appropriate entropies of activation (Chapter 6).

Product analyses for the 1,3-DCAs of diazoalkanes with donor- and acceptor-substituted ethylenes were performed. In most cases Δ^2 -pyrazolines, cyclopropanes and/or ethylene derivatives were isolated as the final products. ^1H NMR spectroscopic monitoring of some of the 1,3-DCAs confirmed the initial formation of the Δ^1 -pyrazolines, which underwent proton shifts or extrusion of molecular nitrogen to yield the isolated products.

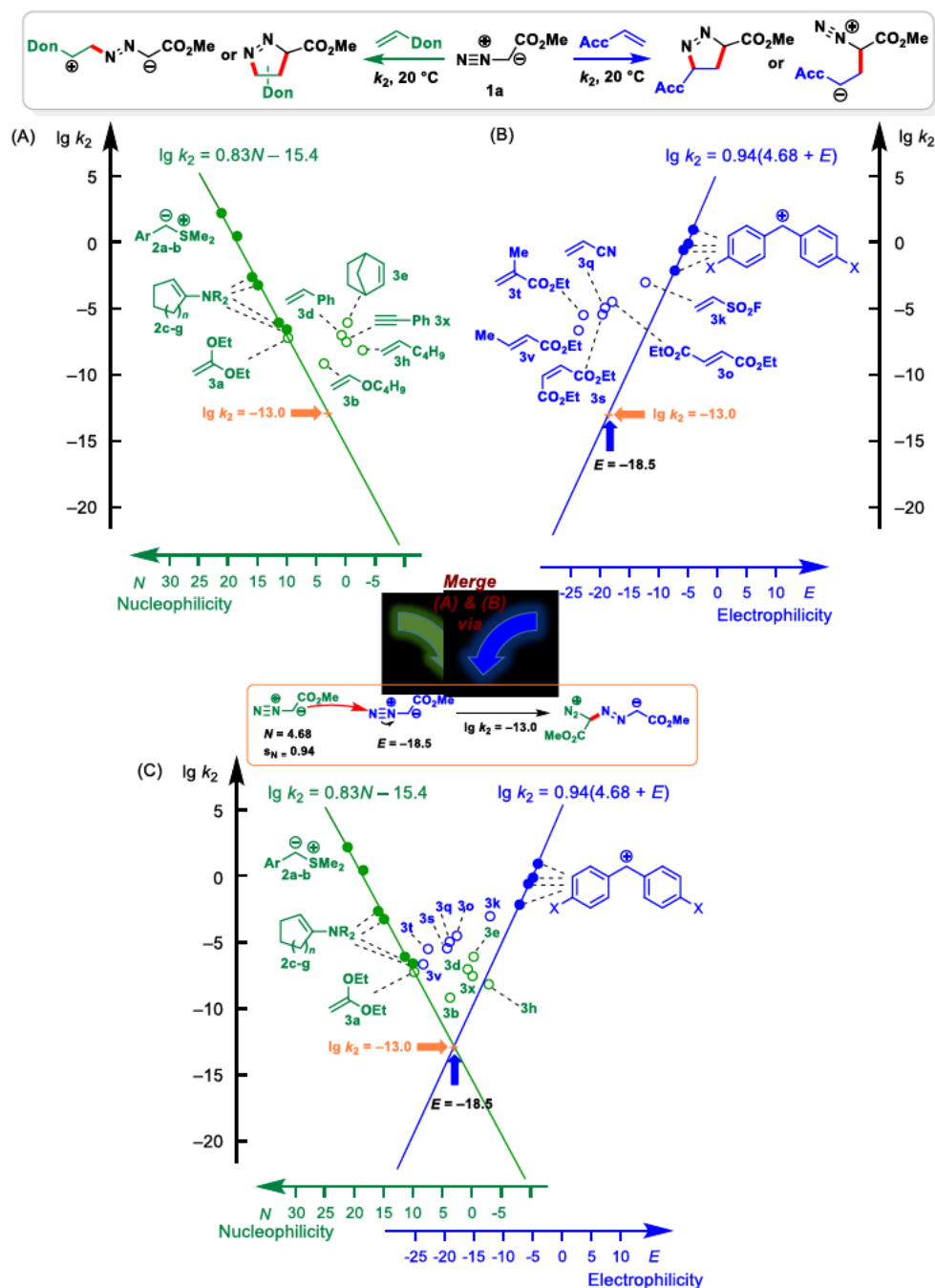


Figure 5. Correlation of $\lg k_2(20\text{ }^\circ\text{C})$ for the reactions of diazoacetate **1a** with (A) nucleophilic reaction partners vs. their N parameters and (B) electrophilic reaction partners vs. their E parameters. (C) Merger of Figures (A) and (B) at $\lg k = -13.0$ – Filled dots: One-bond electrophiles (blue) and one-bond nucleophiles (green) used for the construction of the correlation lines.

Figure 5B plots the $\lg k_2$ for the reactions of diazoacetate **1a** with benzydrylium ions Ar_2CH^+ and acceptor-substituted ethylenes **3** against their one-bond electrophilicity parameters E . The blue correlation line is derived from the reactions of diazoacetate with Ar_2CH^+ and is the same as the linear plot in Figure 4 for determination of the one-bond nucleophilicity parameters N and s_N of diazoacetate.

The acceptor-substituted ethylenes **3** should also lie on the blue correlation line if they would react as one-bond electrophiles with **1a** with rate-determining formation of zwitterions. Figure 5B shows, however, that the measured rate constants for the cycloadditions of all acceptor-substituted ethylenes lie above the linear correlation for one-bond electrophiles, indicating that the transition states (TS) of these reactions are more stable than those leading to zwitterions. The separation of the rate constants from the blue line increases with decreasing electrophilicities E of the dipolarophiles **3** due to increasing synchronicity of the formation of the two δ -bonds. Additionally, the one-bond electrophilicity parameters E of the electrophilic ethylenes **3** reflect their relative reactivities towards diazoacetate, i.e., the lower the E parameters of the dipolarophiles **3**, the slower their cycloadditions with diazoacetate.

This observation can be illustrated in more detail as in Figure 6. The blue line in the left part of Figure 6 shows Gibbs activation energies derived from rate constants $k_2(20\text{ }^\circ\text{C})$ calculated by eq. (1) for the hypothetical formation of zwitterions by attack of the nucleophilic carbon of **1a** at the β -position of the acceptor-substituted ethylenes **3** (structures in Figure 6, right). The orange correlation line plots experimental Gibbs activation energies $\Delta G^\ddagger(\text{exp})$ for the concerted cycloadditions of diazoacetate with dipolarophiles **3** against their one-bond electrophilicities E . The linear plot of $\Delta G^\ddagger(\text{exp})$ vs. E indicates that relative Gibbs activation energies for the concerted cycloadditions are identical with those for the hypothetical stepwise processes.

The two correlation lines intersect at $E = -6$, which implies that the reactions of diazoacetate with one-bond electrophiles of $E > -6$ will give zwitterions as intermediates. As the electrophilicity parameters E decline from the right to the left of the abscissa, the two linear correlations separate from each other and the zwitterionic character of the TS diminishes. Accordingly, the extent of concertedness in the reaction TS increases and the synchronicity of the formation of the two bonds improves as the one-bond electrophilicities E become smaller.

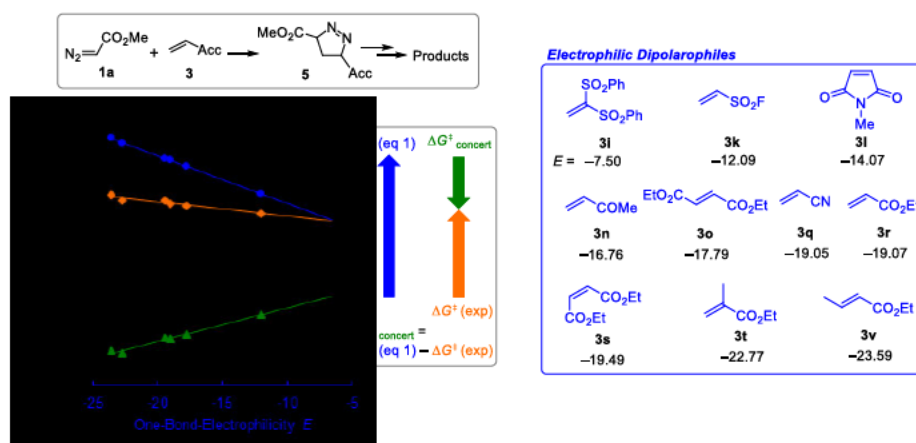


Figure 6. Left: Correlation of Gibbs energies ΔG for the 1,3-DCAs of diazoacetate **1a** with Michael acceptors **3k**, **3o**, **3q**, **3s-t** and **3v** at $20\text{ }^\circ\text{C}$ vs. their electrophilicities E . $-\Delta G^\ddagger(\text{eq 1})$: Gibbs activation energy calculated from eq. (1); $\Delta G^\ddagger(\text{exp})$: Gibbs activation energy measured experimentally; $\Delta G_{\text{concert}}$: energy of concert, i.e., stabilization of the concerted TS relative to the transition state yielding a zwitterion. Right: Structures of the electrophilic dipolarophiles **3** used in this section.

The difference of the blue and the orange lines, thus, is a measure of the energy of concert, as shown by the green line in Figure 6. The Gibbs activation energy of the concerted cycloaddition can formally be regarded as the gap between the activation energy for formation of zwitterion and the energy of concert (the box in the middle of Figure 6).

Figure 5A plots the rate constants of the reactions of diazoacetate **1a** with sulfonium ylides **2a-b**, enamines **2c-g** and weak donor-substituted ethylenes **3** against the corresponding one-bond nucleophilicity parameters N . The green linear correlation of $\lg k_2$ for the reactions of diazoacetate with sulfonium ylides and enamines versus their N parameters is established based on the fact that these reactions proceed via azo couplings and the s_N parameters [according to eq. (1)] of these nucleophiles are similar. In contrast to other dipolarophiles, which are far above the green correlation line, ketene acetal **3a** and enol ether **3b** are on or very close to the green linear correlation, which indicates that their reactions with diazoacetate proceed via stepwise mechanism. On the other hand, the large positive deviation of $\lg k_2$ for the reactions of diazoacetate with nucleophilic dipolarophiles except from **3a** and **3b** indicates concerted processes. This explains the experimentally observed regioselectivity that cannot be rationalized by polarization of ordinary alkenes in their 1,3-DCA with diazoalkanes.

If diazoacetate would react as a one-bond nucleophile with another diazoacetate, $\lg k_2 = -13.0$ would be derived from the one-bond nucleophilicity parameters N , s_N and the one-bond electrophilicity parameter E of diazoacetate as pointed out by the horizontal arrows in Figures 5A & 5B. By linking the two correlation lines at $\lg k_2 = -13.0$, Figure 5C can be derived. Although this approach cannot predict the absolute rate constants for the concerted cycloadditions of diazoalkanes, Figure 7 shows, however, that the experimental $\lg k_2$ values correlate much better with the one-bond electrophilicity parameters E than with the LUMO energies of the acceptor-substituted ethylenes **3** for their 1,3-DCA with diazoacetate **1a** (black lines) and 4-nitrophenyl diazomethane **1c** (red lines).

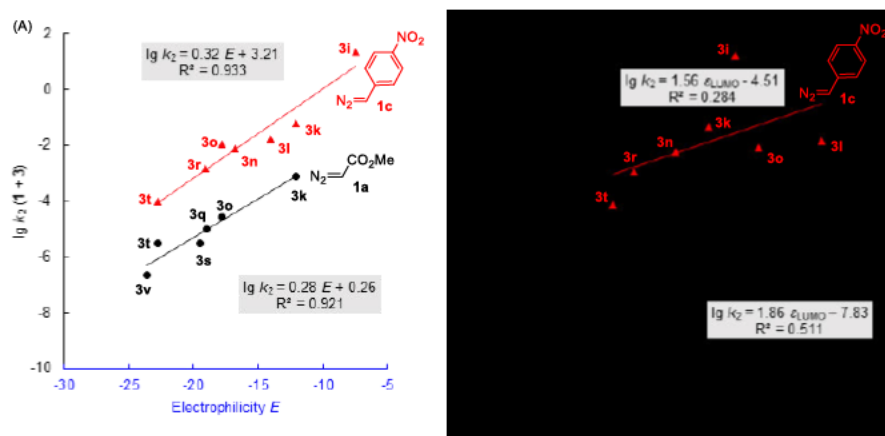


Figure 7. Correlation of $\lg k_2$ for the reactions of the diazo compounds **1a** (in black) and **1c** (in red) with electrophilic dipolarophiles **3** with (A) the electrophilicities E and (B) gas-phase LUMO energies ϵ_{LUMO} (eV) of **3** (from ref.³³ in section 6.1). Structures of dipolarophiles **3** are given in Figure 6, right.

Chapter 2. Introduction and Objectives

2.1 Mayr-Patz Equation

Combination of a nucleophile with an electrophile is one of the most fundamental reaction types in organic chemistry.¹ The two terms “cationoid” and “anionoid” were first used by Lapworth in 1925² to describe the reagents in polar bond-forming processes. Ingold updated the concepts and introduced the terms of “electrophiles” and “nucleophiles”,³ which are nowadays generally used.

In 1953, Swain and Scott⁴ published a two-parameter equation where k^0 is the rate constant of the S_N2 reaction of alkyl halide with water, k the rate constant of the reaction with other nucleophiles than water, s the electrophile-dependent constant (= 1 for methyl bromide in water at 25 °C), and n the nucleophile-characteristic parameter (= 0 for water). By this approach, the relative reactivities of common nucleophiles in aqueous solution were characterized.

$$\lg (k/k^0) = sn$$

For a wider range of applicable reactions, correction factors such as polarizability, basicity and solvation were later incorporated by Edwards and Parker.⁵ Bunnett further detailed 17 aspects influential to nucleophilicities.⁶

In 1972, Ritchie simplified the model by selecting the reaction partners as covalent bond-forming anions and cations including triarylmethyl cations and aryldiazonium ions, which excluded the influence of leaving groups on the TS of S_N2 reactions.^{7a} In the correlation, $\lg k_0$ is electrophile-specific, while N_+ is characteristic of a nucleophile in a certain solvent. Further applicability of the approach was also found in the reactions of amines with triarylmethyl cations^{7b} as well as of simple anions with substrates containing leaving groups.^{7c,d}

$$\lg k = \lg k_0 + N_+$$

Limited applicability owing to the constraints of the ‘constant selectivity relationship’ used by Ritchie was eased when Mayr and Patz extended the correlation by adding an additional parameter s representing the sensitivity of nucleophiles to changes in electrophiles.⁸ Here $\lg k_0$, a measure of electrophilicity, represents the rate constants for the reactions of electrophiles with 2-methyl-1-pentene, while nucleophilicity is described by c (= 0 for 2-methyl-1-pentene) and s (= 1 for 2-methyl-1-pentene).

$$\lg k = s \lg k_0 + c$$

To avoid large uncertainties caused by the parameter s to the rate constants in cases of large absolute values of $\lg k_0$ for very strong or very weak electrophiles, the equation was slightly rearranged as follows.

$$\lg k_{20} c = s(E + N) \quad \text{eq. (1)}$$

In eq. (1), k is the second-order rate constant of a polar reaction at 20 °C, E the electrophilicity, N the solvent-dependent nucleophilicity, and s the nucleophile-specific sensitivity parameter.

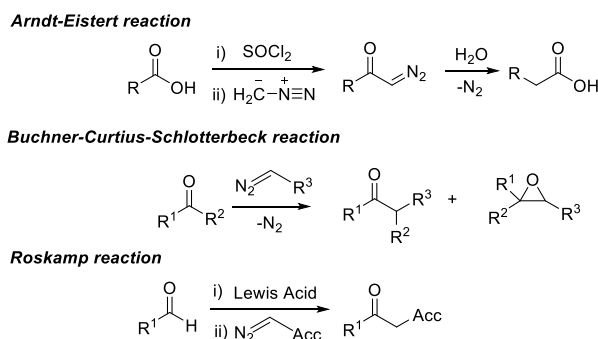
This linear free energy relationship has so far proven applicable in the quantification of the

reactivities of 1251 nucleophiles and 349 electrophiles, covering a scale of more than 30 orders of magnitude.⁹ Generally, eq. (1) applies to polar reactions in which only one new bond is formed in the rate-determining step. For the concerted 1,3-DCAs of phenyldiazomethanes with electron-deficient dipolarophiles, the experimentally derived rate constants are faster than predicted from eq. (1), which indicates that these 1,3-DCAs are concerted processes.¹⁰

2.2 Nucleophilic Reactions of Diazoalkanes

2.2.1 Nucleophilic Reactions of Diazoalkanes with Carbonyl Compounds

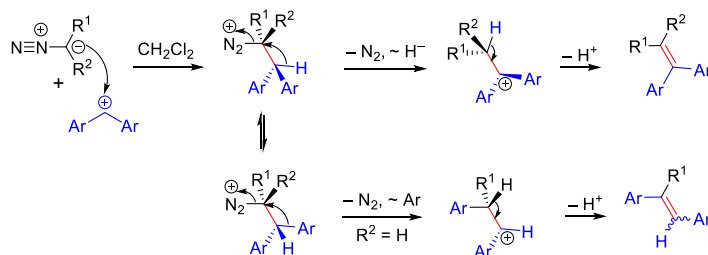
Established reaction procedures such as Arndt-Eistert reaction, Buchner-Curtius-Schlotterbeck reaction and Roskamp reaction (Scheme 1) involve the nucleophilic reactions of the α -carbon atoms of diazoalkanes with carbonyl chlorides, ketones or aldehydes, respectively.



Scheme 1. Reactions of diazoalkanes with carbonyl compounds.

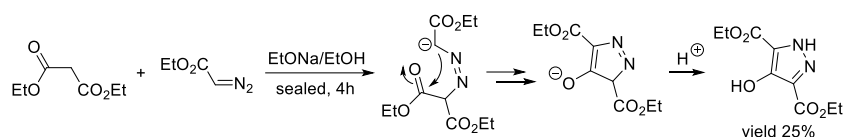
2.2.2 Nucleophilic Reactions of Diazoalkanes with Benzhydrylium Ions

Product studies and kinetics of the nucleophilic reactions of diazoalkanes with benzhydrylium ions Ar_2CH^+ in anhydrous CH_2Cl_2 were reported in 2003,^{11a} 2018¹⁰ and 2022.^{11b} As shown in Scheme 2, the reactions of acyclic diazoalkanes with benzhydrylium ions generally afford substituted ethylenes as the final products. The mechanism for their formation is rationalized as follows. The nucleophilic attack of the diazoalkanes at the carbocations yields the diazonium ions, which undergo elimination of molecular nitrogen followed by or concomitant with 1,2-hydride transfer¹² or aryl shift and abstraction of proton to give the isolated olefins.



Scheme 2. Proposed mechanism for the reactions of diazoalkanes with benzhydrylium ions.^{10,11a}

carbanions generated from active methylene compounds under base catalysis to afford terminal nitrogen functionalized hydrazones.¹⁴ Substituted pyrazoles can be obtained when diazoacetates react with carbanions generated from malonates. The mechanism of their formation can be formulated as in Scheme 4. Azo couplings of diazoacetates with deprotonated malonates give anions, which undergo intramolecular addition-elimination processes followed by proton abstraction and afford cyclic enolate ions. Protonation of the enolate ions yields the isolated pyrazoles.^{14b}



Scheme 4. Reaction of ethyl diazoacetate with diethyl malonate under catalysis of EtONa.^{14b}

2.3.3 Electrophilic Reactions of Diazoalkanes with Sulfonium Ylides and Enamines

Highly functionalized hydrazones can also be isolated from the electrophilic reactions of diazoalkanes with sulfonium ylides.¹⁵

Reactions of diazo esters with cyclopentanone-derived enamines have been reported by Huisgen and colleagues to give hydrazonoenamines or hydrolyzed derivatives via the initial electrophilic attack of the terminal nitrogens of diazoalkanes to the enamines.^{16a,b} In contrast, reactions of diazo esters with cyclohexanone-derived enamines were claimed to yield pyrazolines or pyrazoles via concerted 1,3-DCAs.^{16a,c}

2.4 1,3-Dipolar Cycloadditions of Diazoalkanes

1,3-Dipolar cycloadditions (Huisgen reactions) of diazoalkanes are one of the most fundamental approaches to afford N-heterocycles¹⁷ such as pyrazoles and indazoles,¹⁸ which have been utilized in a variety of fields.¹⁹⁻²¹ 1,3-Dipolar cycloadditions (1,3-DCAs) of diazoalkanes have also been utilized for the preparation of functionalized cyclopropanes.²²

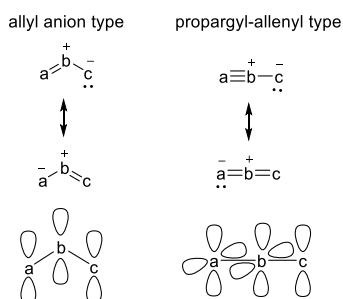
The concept and mechanism of 1,3-DCAs as well as the models applied for interpreting the reactivities of dipolarophiles in their 1,3-DCAs with diazoalkanes will be shortly presented in the following sections 2.4.1 to 2.4.4.

2.4.1 Concepts of 1,3-DCAs

Curtius in 1883 discovered diazoacetic ester.²³ Five years later Buchner published the first cycloaddition of diazoacetates with dimethyl and diethyl fumarates.²⁴ Smith in 1938 reviewed by then the available reactions (quoted as ‘1,3-additions’) of 1,3-dipoles including diazomethane with carboxylic acids, aldehydes, ketones, halides and carbon-carbon multiple bond systems.²⁵

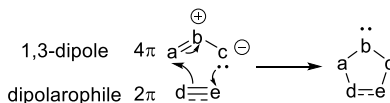
Huisgen recognized the generality among the reactions of multiple-bond systems with compounds bearing similar structures to diazoalkanes and extended in 1961 the scope of 1,3-dipoles up to 18 types,²⁶ some of which were unknown at that time but successfully synthesized and investigated afterwards.²⁷

Generally, 1,3-dipoles can be categorized into two types, namely, the allyl anion and the propargyl/allenyl anion type (Scheme 5). Apart from the three parallel p_z orbitals perpendicular to the 1,3-dipole plane in the allyl anion type 1,3-dipoles, the propargyl/allenyl anion type dipoles have extra π orbitals oriented orthogonal to the 1,3-dipole plane. One example of the propargyl/allenyl anion type 1,3-dipole is diazoalkane.



Scheme 5. Allyl anion type and propargyl-allenyl type 1,3-dipoles.

In 1963, Huisgen systematically elaborated the concept of 1,3-DCAs.^{28a} Similar to Diels-Alder reaction, 1,3-DCA refers to the pericyclic reaction of a 4π system with an unsaturated system providing 2π electrons, namely a dipolarophile, to yield (3+2)-cycloadducts (Scheme 6).



Scheme 6. 1,3-DCA postulated by Huisgen.

2.4.2 Mechanism of 1,3-DCAs

Huisgen recognized in 1961 and detailed in 1963 the concerted mechanism of 1,3-DCAs based on the common features of higher dipolarophilic reactivities of strained-ring systems, stereospecificity, low solvent dependence as well as great influence of steric hindrance on reaction rates and highly negative entropies of activation.^{26,28b}

Firestone proposed later an alternative two-step mechanism involving diradical intermediates in 1,3-DCAs,²⁹ which, on a certain extent, led to Huisgen's later discovery of the few examples of 1,3-DCAs with zwitterionic intermediates.³⁰

2.4.3 Models for Interpretation of Structure-Reactivity Relationship in 1,3-DCAs

Due to limited space, only frontier molecular orbital (FMO) theory, complete neglect of differential overlap (CNDO/2) method and the distortion/interaction (or activation-strain) model will be discussed here.

2.4.3.1 FMO Approach

Conservation of orbital symmetry developed by Woodward and Hoffmann provides a useful tool for the understanding of the concertedness of 1,3-DCAs.³¹ What also needs to be mentioned is Fukui's frontier molecular orbital (FMO) theory,³² which focuses on the interactions of the frontier orbitals, namely the HOMOs and LUMOs of the reactants.

Based on the FMO model, Sustmann presented in 1971^{33a} and 1974^{33b} three types of 1,3-DCAs (Figure 2) according to the HOMO-LUMO energy differences of 1,3-dipoles and dipolarophiles. Specifically, 1,3-DCA of type I is characteristic of smaller HOMO(1,3-dipole)-LUMO(dipolarophile) energy separation, type III lower HOMO(dipolarophile)-LUMO(1,3-dipole) energy interval, while type II similar energy difference of HOMO(1,3-dipole)-LUMO(dipolarophile) and HOMO(dipolarophile)-LUMO(1,3-dipole). The interaction of HOMO and LUMO with smaller energy gap leads to stronger overlap and therefore better stabilized TS.

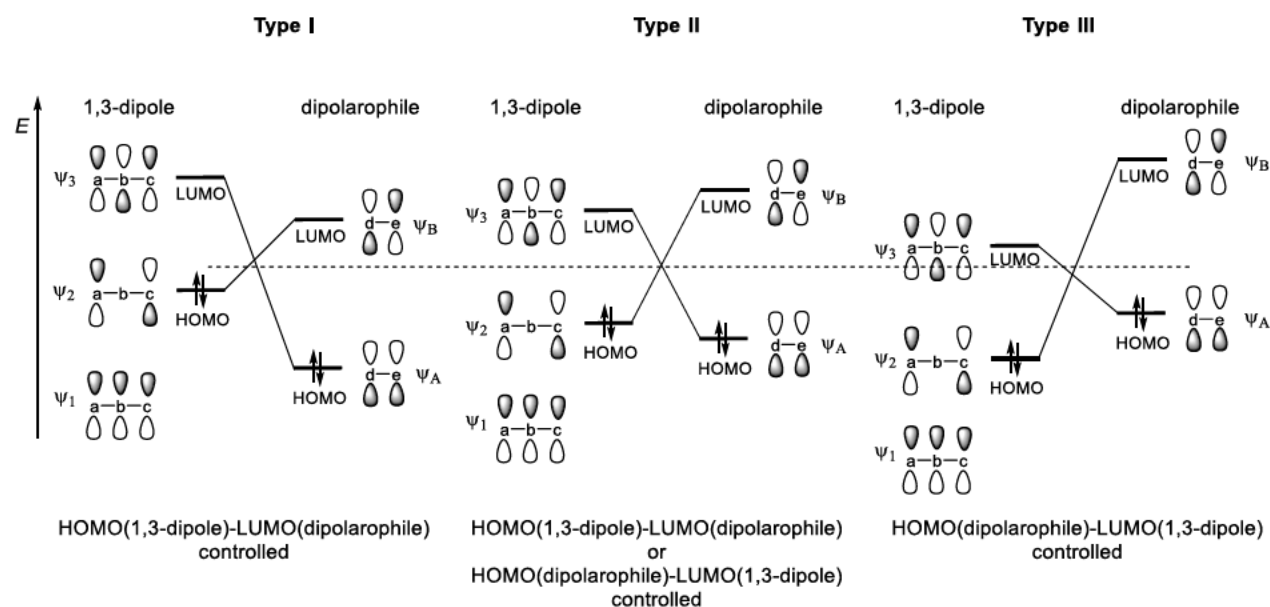


Figure 2. Sustmann's classification of three types of 1,3-DCAs.

In 1,3-DCA of type I, where the reaction is HOMO(1,3-dipole)-LUMO(dipolarophile) controlled, introduction of electron-withdrawing groups to dipolarophiles would accelerate the reaction by lowering the LUMO(dipolarophile), thus leading to a more narrow HOMO(1,3-dipole)-LUMO(dipolarophile) distance. Accordingly, electron-releasing substituents on 1,3-dipoles would also increase the reaction rate by raising the HOMO(1,3-dipole).

In contrast, the reactivities of dipolarophiles in 1,3-DCA of type III would be enhanced by adding

electron-donating groups to the dipolarophiles by increasing the HOMO(dipolarophile).

In 1,3-DCA of type II, introduction of both electron-attracting and electron-releasing groups to the dipolarophiles would facilitate the cycloaddition. While ethylene would be the most unreactive dipolarophile.

According to perturbation theory, the interaction energy of the HOMO(1,3-dipole)-LUMO(dipolarophile) and the HOMO(dipolarophile)-LUMO(1,3-dipole) as the two addends approach each other can be formulated as in eq (2).³⁴ In this equation, E_I and E_{II} are the energy differences of HOMO(1,3-dipole)-LUMO(dipolarophile) and HOMO(dipolarophile)-LUMO(1,3-dipole), respectively. Quantities c and c' are the atomic orbital coefficients of HOMO and LUMO, respectively, at the centers where the new bonds are formed. Variable β_{ad} is the resonance integral of the newly formed δ bond a–d, which is a measure for the strength of the interaction.

$$\Delta E = \frac{(c_a c'_d \beta_{ad} + c_c c'_e \beta_{ce})^2}{E_I} + \frac{(c'_a c_d \beta_{ad} + c'_c c_e \beta_{ce})^2}{E_{II}} \quad \text{eq. (2)}$$

$$E_I = E_{\psi_2} - E_{\psi_B} = \text{HOMO}(1,3\text{-dipole}) - \text{LUMO}(\text{dipolarophile})$$

$$E_{II} = E_{\psi_A} - E_{\psi_3} = \text{HOMO}(\text{dipolarophile}) - \text{LUMO}(1,3\text{-dipole})$$

In 1977,³⁵ Huisgen, Geittner and Sustmann reported a linear function between the $\lg k_2$ of the 1,3-DCAs of diazomethane with alkenes and the converted HOMO(diazomethane)-LUMO(alkenes) distance represented by the quantity D (Figure 3). Under the assumption that only the interaction of HOMO(diazomethane)-LUMO(alkenes) matters and that for all olefins the atomic orbital coefficients as well as the resonance integrals are constant in the numerator of eq. (2), they derived eq. (3).

$$\Delta E = \frac{k\beta^2}{E_{\text{HOMO(diazomethane)}} - E_{\text{LUMO(alkenes)}}} \quad \text{eq. (3)}$$

Ionization potential (IP) of diazomethane was taken as the negative value of HOMO(diazomethane) energy according to Koopmans' theorem.³⁶ And the LUMO(alkenes) energies were replaced by electron affinities (EAs) of the double-bond systems, which were approximated by the differences between the IPs of the dipolarophiles and their energies of $\pi \rightarrow \pi^*$ transition $E_{\pi \rightarrow \pi^*}$ ($= E_{\text{LUMO(alkenes)}} - E_{\text{HOMO(alkenes)}}$) as shown in eq. (4).

$$D = E_{\text{HOMO(diazomethane)}} - E_{\text{LUMO(alkenes)}} = -\text{IP}_{\text{diazomethane}} + (\text{IP} - E_{\pi \rightarrow \pi^*})_{\text{alkenes}} \quad \text{eq. (4)}$$

The correlation between the $\lg k_2$ of the 1,3-DCAs of diazomethane with alkenes and the approximated HOMO(diazomethane)-LUMO(alkenes) energy intervals roughly illustrates the effect of substituents of alkenes on the rates of their 1,3-DCAs with diazomethane. That is, the smaller the HOMO(diazomethane)-LUMO(alkenes) energy gap, the faster the 1,3-DCAs. The reasons for the large deviations of ethylene, butyl vinyl ether and cyclohexene, however, were not clarified.

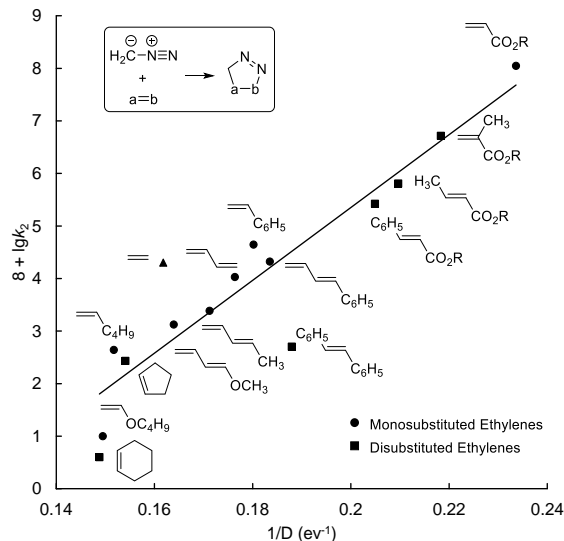


Figure 3. Correlation between the $\lg k_2$ of the 1,3-DCAs of diazomethane with alkenes and the approximated HOMO(diazomethane)-LUMO(alkenes) energy differences (represented by the quantity D).

In 1979, Huisgen and coworkers reported the kinetic studies of the 1,3-DCAs of diazoacetate, diazomalonate and diazo(phenylsulfonyl) acetic ester with multiple-bond systems.³⁷ Based on Sustmann's approach, they plotted the $\lg k_2$ of the 1,3-DCAs against the IPs of the dipolarophiles, which led to parabolic functions (as exemplified for diazoacetate in Figure 4).

Introduction of α -ester group to diazomethane lowers its LUMO energy to a bigger extent than to the HOMO energy, which renders the 1,3-DCAs of diazoacetate features of type II 1,3-DCAs. Namely, both the HOMO(diazoacetate)-LUMO(dipolarophiles) and the HOMO(dipolarophiles)-LUMO(diazoacetate) interactions control the reactivity. That is, introduction of both electron-donating and electron-withdrawing groups to the unsaturated systems results in higher reaction rates of their 1,3-DCAs with diazoacetate, whereas ethylene should have the lowest reactivity.

One might have already noticed that instead of plotting $\lg k_2$ versus the approximated HOMO-LUMO energy gaps as in the 1977 publication (Figure 3),³⁵ IPs were directly taken here as the measure for HOMO-LUMO energy separation due to the difficulty of obtaining reliable electron affinities of the dipolarophiles.

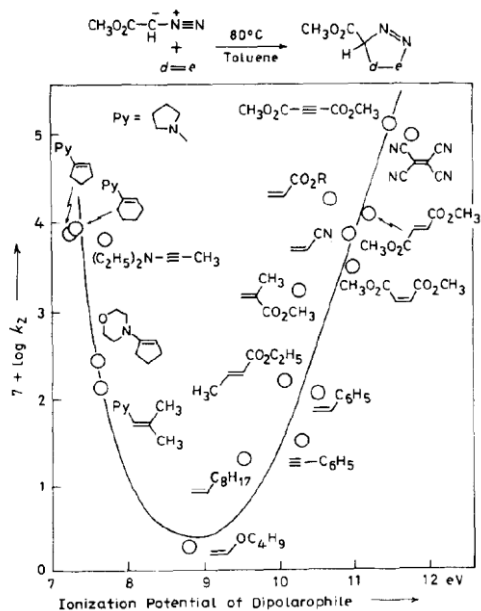


Figure 4. Relationship between the rate constants of the reactions of methyl diazoacetate with different dipolarophiles and the ionization potentials of the dipolarophiles (Reprinted from ref.³⁷ with permission from Elsevier).

2.4.3.2 Quantum Chemical Approach

Complete Neglect of Differential Overlap (CNDO/2) Method

Based on the simplified second-order perturbation theory^{34a,38} (electrostatic interactions, closed-shell repulsions and steric hindrance were neglected), Houk interpreted in 1973 the regioselectivity in the 1,3-DCAs of diazoalkanes with common dipolarophiles by comparing the calculated terminal coefficients of the HOMOs and the LUMOs of the two addends by CNDO/2³⁹ method. It was reported that orbitals with larger coefficients overlap better, thus leading to certain regioselectivity. For example, the formation of 3-substituted Δ^1 -pyrazolines from the 1,3-DCAs of diazomethane with electron-deficient dipolarophiles was ascribed to the bigger HOMO coefficient on the α -carbon of diazomethane and the greater LUMO coefficients on the unsubstituted carbons of the dipolarophiles. The preference for interactions between orbitals with bigger coefficients was also proposed to explain the non-synchronicity in the concerted 1,3-DCAs.

Bastide investigated the regioselectivity in the 1,3-DCAs of diazoalkanes with alkenes and alkynes using the similar approach.⁴⁰

Distortion/Interaction (or activation-strain) model

The distortion/interaction (or activation strain) model⁴¹ provides new interpretation of reactivity trends in 1,3-DCAs.

Houk and Bickelhaupt applied the distortion/interaction or activation strain model which splits the activation energy (ΔE^\ddagger) of a bimolecular reaction into the destabilizing strain or distortion energy (ΔE_{dist} , energy required to distort the reactants to their TS geometries) and the stabilizing energy of interaction between the distorted fragments (ΔE_{int}).^{42,43} ΔE_{dist} is related to two factors, namely, the rigidity of the reactants and the reaction mechanism which decides to what extent the starting materials are distorted to afford the TS geometries. ΔE_{int} reflects the bonding capability of the distorted reactants.

FMO approach assumes that the HOMO-LUMO interactions between 1,3-dipoles and dipolarophiles control reactivities. In contrast, it was discovered that ΔE_{dist} of 1,3-dipoles were generally responsible for exerting reactivity differences in 1,3-DCAs. Only in cases where distortion or strain energies were constant within a series of reactants, the interaction energies would become significant in affecting reactivities.⁴²

2.5 Objectives

The reactions of α -diazo esters with cyclopentanone-derived enamines were reported to proceed via azo couplings.^{16b} In contrast, the reactions with cyclohexanone-derived enamines were claimed to occur via concerted 1,3-DCAs because cycloadducts were isolated from these reactions.^{16c} Further experiments should be carried out to examine if preliminary formation of acyclic intermediates takes place in cases where pyrazolines or pyrazoles were obtained as final products from the reactions of diazo esters with enamines.

Previous kinetic measurements of the reactions of diazo esters with enamines were performed at relatively high temperatures, e.g. at 80.3 or 110 °C. Yet immediate changes of color in some of these reactions were generally observed even at -20 °C,^{16a} which indicates that these reactions should proceed relatively fast at room temperature. Therefore, kinetics of these reactions should be measured at lower temperatures for more reliable data.

The one-bond nucleophilicities of diazoalkanes have been determined by studying the kinetics of their reactions with benzhydrylium ions Ar_2CH^+ at 20 °C based on the Mayr-Patz equation.^{10,11} The one-bond electrophilicities of diazoalkanes should also be quantifiable by measuring the kinetics of their reactions with appropriate reaction partners. The thus derived electrophilicity parameters of diazoalkanes should provide a rationalization for the reported azo couplings of diazoalkanes with nucleophiles.

Due to the perpendicular orientation of the two sets of MOs in diazoalkanes, it is generally believed that the $\pi^*_{\text{N=N}}$ MOs do not participate in the 1,3-DCAs of diazoalkanes with dipolarophiles.^{33b,44} However, detailed examinations of whether the $\pi^*_{\text{N=N}}$ MOs of diazoalkanes participate in their reactions with nucleophilic alkenes should be performed.

FMO theory provides a useful tool in qualitatively analyzing the reactivity sequence of dipolarophiles in 1,3-DCAs. However, applications of FMO approach in the quantitative analysis of the structure-reactivity relationship in 1,3-DCAs are restricted. That orbital energies control reactivity does not necessarily apply to every system. For example, ethylene and acetylene have

similar reactivity in 1,3-DCAs despite their different ground state HOMO-LUMO energy gaps.⁴²

Although the HOMO energies of organic molecules can be replaced by the negative values of ionization potentials according to Koopmans' theorem,³⁶ the approximation of LUMO energies to electron affinities is somewhat controversial.⁴⁵

Additionally, the drastic simplification of HOMO(diazoalkane)-LUMO(dipolarophile) energy gaps as IP values of the dipolarophiles (Figure 4 in Chapter 1) by Huisgen³⁷ assumes constant HOMO-LUMO distances for all the dipolarophiles. That is, substituents move the HOMO(dipolarophiles) and LUMO(dipolarophiles) energies to the same extent,^{33b} which is not necessarily true since electron-donating groups usually raise the HOMO energies higher than the LUMO energies, whereas electron-attracting groups lower the LUMO energies more than the HOMO energies.⁴⁶

The linear free energy relationship $\lg k_{20} = s_N(N + E)$ has been utilized to interpret the relationship between the one-bond electrophilicities E of acceptor-substituted ethylenes and the rates of their 1,3-DCAs with aryldiazomethanes.¹⁰ For the reactions of aryldiazomethanes with electron-deficient dipolarophiles, deviations from the linear correlation of $\lg k_2$ versus E were observed. The degree of deviation was interpreted as extent of concertedness in the TS and was quantified as energy of concert. If the one-bond electrophilicities E of diazoalkanes could be determined, then the degree of concertedness in the TS of the 1,3-DCAs of diazoalkanes with weak donor-substituted ethylenes of known nucleophilicities N could also be quantified. For a given diazo compound, when one combines the correlation of $\lg k_2$ versus the one-bond E parameters of electron-deficient ethylenes with that of $\lg k_2$ versus the one-bond N parameters of electron-rich alkenes, an intuitive presentation of the reactivity sequence for various dipolarophiles would be achieved. By varying the substitutions of the diazoalkanes, it would allow clear comparisons of the 1,3-dipole-specific reactivities towards the same series of dipolarophiles.

2.6 References

- (1) a) Mayr, H.; Ofial, A. R. *Pure Appl. Chem.* **2005**, *77*, 1807–1821. b) Ma, J.-A.; Cahard, D. *Angew. Chem. Int. Ed.* **2004**, *43*, 4566–4583. c) Emer, E.; Sinisi, R.; Capdevila, M. G.; Petruzzello, D.; Vincentiis, F. D.; Cozzi, G. *Eur. J. Org. Chem.* **2011**, *2011*, 647–666. d) Chattaraj, P. K.; Roy, D. *R. Chem. Rev.* **2007**, *107*, PR46–PR74.
- (2) Lapworth, A. *Nature* **1925**, *115*, 625.
- (3) a) Ingold, C. K. *Recl. Trav. Chim. Pays-Bas* **1929**, *42*, 797–812. b) Ingold, C. K. *J. Chem. Soc.* **1933**, 1120–1127. c) Ingold, C. K. *Chem. Rev.* **1934**, *15*, 225–274.
- (4) Swain, C. G.; Scott, C. B. *J. Am. Chem. Soc.* **1953**, *75*, 141–147.
- (5) a) Edwards, J. O. *J. Am. Chem. Soc.* **1954**, *76*, 1540–1547. b) Edwards, J. O. *J. Am. Chem. Soc.* **1956**, *78*, 1819–1820. c) Parker, A. J. *Chem. Rev.* **1969**, *69*, 1–32.
- (6) Bunnett, J. F. *Annu. Rev. Phys. Chem.* **1963**, *14*, 271–290.
- (7) a) Ritchie, C. D. *Acc. Chem. Res.* **1972**, *5*, 348–354. b) Ritchie, C. D.; Virtanen, P. O. I. *J. Am. Chem. Soc.* **1973**, *95*, 1882–1889. c) Ritchie, C. D.; Sawada, M. *J. Am. Chem. Soc.* **1977**, *99*, 3754–3761. d) Ritchie, C. D. *J. Am. Chem. Soc.* **1975**, *97*, 1170–1179.
- (8) a) Mayr, H.; Schneider, R.; Grabis, U. *J. Am. Chem. Soc.* **1990**, *112*, 4460–4467. b) Mayr, H.; Patz, M. *Angew. Chem.* **1994**, *106*, 990–1010; *Angew. Chem. Int. Ed.* **1994**, *33*, 938–957.
- (9) For a database of nucleophilicity parameters N/S_N , and electrophilicity parameters E , check the link: <https://www.cup.lmu.de/oc/mayr/reaktionsdatenbank2/>.
- (10) Jangra, H.; Chen, Q.; Fuks, E.; Zenz, I.; Mayer, P.; Ofial, R. A.; Zipse, H.; Mayr, H. *J. Am. Chem. Soc.* **2018**, *140*, 16758–16772.
- (11) a) Bug, T.; Hartnagel, M.; Schlierf, C.; Mayr, H. *Chem. Eur. J.* **2003**, *9*, 4068–4076. b) Hartnagel, M.; Ofial, R. A.; Mayr, H. *Synthesis* **2022** (doi: 10.1055/s-0041-1737327).
- (12) a) Streitwieser, A. Jr. *J. Org. Chem.* **1957**, *22*, 861–869. b) Friedman, L. *Carbonium Ions* Vol. II; Olah, G. A., Schleyer, P. v. R., Eds.; Wiley-Interscience: New York, **1970**; Chapter 16, pp 655–713. c) Zollinger, H. *Diazo Chemistry II*; VCH: Weinheim, **1995**; Chapter 7, pp 241–304. d) Katz, C. E.; Ribelin, T.; Withrow, D.; Basseri, Y.; Manukyan, A. K.; Bermudez, A.; Nuera, C. G.; Day, V. W.; Powell, D. R.; Poutsma, J. L.; Aubé, J. *J. Org. Chem.* **2008**, *73*, 3318–3327. (e) Gutierrez, O.; Aubé, J.; Tantillo, D. J. *J. Org. Chem.* **2012**, *77*, 640–647.
- (13) a) Müller, E.; Rundel, W. *Chem. Ber.* **1956**, *89*, 1065–1071. b) Müller, E.; Rundel, W. *Chem. Ber.* **1957**, *90*, 1299–1302. c) Coleman, G. H.; Gilman, H.; Adams, C. E.; Pratt, P. E. *J. Org. Chem.* **1938**, *3*, 99–107. d) Takamura, N.; Yamada, S.-I. *Chem. Pharm. Bull.* **1976**, *24*, 800–803. e) Yasui, E.; Wada, M.; Takamura, N. *Tetrahedron Lett.* **2006**, *47*, 743–746. f) Yasui, E.; Wada, M.; Takamura, N. *Tetrahedron* **2009**, *65*, 461–468.
- (14) a) Wolff, L. *Liebigs Ann. Chem.* **1902**, *325*, 129–195. b) Bertho, A.; Nüssel, H. *Liebigs Ann. Chem.* **1927**, *457*, 278–307. c) Farnum, D. G.; Yates, P. *Proc. Chem. Soc.* **1960**, 224. d) Regitz, M.; Liedhegener, A.; Stadler, D. *Liebigs Ann. Chem.* **1968**, *713*, 101–112. e) Arkhipov, A. V.; Arkhipov, V. V.; Cossy, J.; Kovtunencko, V. O.; Myhkailiuk, P. K. *Org. Lett.* **2016**, *18*, 3406–3409.

- (15) Wu, D.; Wang, Y.; Zhou, J. W.; Sun, Q. L.; Zhao, Y. J.; Xu, X. C. *Org. Lett.* **2019**, *21*, 8722–8725.
- (16) a) H.-U. Reissig, Dissertation, Ludwig-Maximilians-Universität München, **1978**. b) R. Huisgen, W. Bihlmaier, H.-U. Reissig, *Angew. Chem. Int. Ed.* **1979**, *18*, 331–332; *Angew. Chem.* **1979**, *91*, 347–348. c) R. Huisgen, H.-U. Reissig, *Angew. Chem. Int. Ed.* **1979**, *18*, 330–331; *Angew. Chem.* **1979**, *91*, 346–347.
- (17) a) Padwa, A.; Pearson, W. H. Eds. *Synthetic Applications of 1,3-Dipolar Cycloaddition Chemistry toward Heterocycles and Natural Products*. John Wiley and Sons; New York, **2002**. b) Kissane, M.; Maguire, A. R. *Chem. Soc. Rev.* **2010**, *39*, 845–883. c) Fustero, S.; Sánchez-Roselló, M.; Barrio, P.; Simón-Fuentes, A. *Chem. Rev.* **2011**, *111*, 6984–7034. d) Dadiboyena, S. *Eur. J. Med. Chem.* **2013**, *63*, 347–377. e) Singh, M. S.; Chowdhury, S.; Koley, S. *Tetrahedron* **2016**, *72*, 1603–1644. f) Breugst, M.; Reissig, H.-U. *Angew. Chem. Int. Ed.* **2020**, *59*, 12293–12307.
- (18) Jin, T.; Yamamoto, Y. *Angew. Chem. Int. Ed.* **2007**, *46*, 3323–3325.
- (19) Taylor, R. D.; MacCoss, M.; Lawson, A. D. G. *J. Med. Chem.* **2014**, *57*, 5845–5859.
- (20) *The Pesticide Manual*. MacBean, C. Ed. British Crop Production Council, **2012**.
- (21) Dias, H. V. R.; Lovely, C. J. *Chem. Rev.* **2008**, *108*, 3223–3238.
- (22) Lebel, H.; Marcoux, J-F.; Molinaro, C.; Charette, A. B. *Chem. Rev.* **2003**, *103*, 977–1050.
- (23) Curtius, T. *Ber. Dtsch. Chem. Ges.* **1883**, *16*, 2230.
- (24) Buchner, E. *Ber. Dtsch. Chem. Ges.* **1888**, *21*, 2637–2647.
- (25) Smith, L. I. *Chem. Rev.* **1938**, *23*, 193–285.
- (26) Huisgen, R. *Proc. Chem. Soc. London* **1961**, 357–369.
- (27) a) Huisgen, R.; Grashey, R.; Steingruber E. *Tetrahedron Lett.* **1963**, *4*, 1441–1445. b) Huisgen, R.; Eckell, A. *Tetrahedron Lett.* **1960**, *1*, 5–8. c) Huisgen, R.; Stangl, H.; Sturm, H. J.; Wagenhofer, H. *Angew. Chem. Int. Ed.* **1962**, *1*, 50; *Angew. Chem.* **1962**, *74*, 31. d) Huisgen, R.; Seidel, M.; Wallbillich, G.; Knupfer, H. *Tetrahedron* **1962**, *17*, 3–29.
- (28) a) Huisgen, R. *Angew. Chem. Int. Ed.* **1963**, *2*, 565–598. b) Huisgen, R. *Angew. Chem. Int. Ed.* **1963**, *2*, 633–696.
- (29) a) Firestone, R. A. *J. Org. Chem.* **1968**, *33*, 2285–2290. b) Firestone, R. A. *J. Org. Chem.* **1972**, *37*, 2181–2191. c) Firestone, R. A. *J. Org. Chem.* **1976**, *41*, 2212–2214. d) Firestone, R. A. *Tetrahedron* **1977**, *33*, 3009–3039. e) Firestone, R. A. *Int. J. Chem. Kinet.* **2013**, *45*, 415–428.
- (30) a) Huisgen, R.; Mlostoń, G.; Langhals, E. *J. Am. Chem. Soc.* **1986**, *108*, 6401–6402. b) Huisgen, R.; Mlostoń, G.; Langhals, E. *J. Org. Chem.* **1986**, *51*, 4085–4087. c) Huisgen, R.; Langhals, E.; Mlostoń, G.; Oshima, T. *Heterocycles* **1989**, *29*, 2069–2074. d) Huisgen, R.; Mlostoń, G.; Langhals, E.; Oshima, T. *Helv. Chim. Acta* **2002**, *85*, 2668–2685.
- (31) a) Woodward, R. B.; Hoffmann, R. *J. Am. Chem. Soc.* **1965**, *87*, 395–397. b) Woodward, R. B.; Hoffmann, R. *Angew. Chem. Int. Ed.* **1969**, *8*, 781–932.
- (32) Fukui, K. *Fortschr. Chem. Forsch.* **1970**, *15*, 1.

- (33) a) Sustmann, R. *Tetrahedron Lett.* **1971**, *12*, 2717–2720; b) Sustmann, R. *Pure Appl. Chem.* **1974**, *40*, 569–593.
- (34) a) Herndon, W. C. *Chem. Rev.* **1972**, *72*, 157–179. b) Hudson, R. F. *Angew. Chem. Int. Ed.* **1973**, *12*, 36–56. c) Huisgen, R. *J. Org. Chem.* **1976**, *41*, 403–419.
- (35) Geittner, J.; Huisgen, R.; Sustmann, R. *Tetrahedron Lett.* **1977**, *18*, 881–884.
- (36) Koopmans, T. *Physica.* **1934**, *1*, 104–113.
- (37) Bihlmaier, W.; Huisgen, R.; Reissig, H.-U.; Voss, S. *Tetrahedron Lett.* **1979**, *20*, 2621–2624.
- (38) Salem, L. *J. Am. Chem. Soc.* **1968**, *90*, 543–552, 553–566.
- (39) a) Houk, K. N. *J. Am. Chem. Soc.* **1972**, *94*, 8953–8955; b) Houk, K. N.; Sims, J.; Duke Jr, R. E.; Strozier, R. W.; George, J. K. *J. Am. Chem. Soc.* **1973**, *95*, 7287–7301. c) Houk, K. N.; Sims, J.; Watts, C. R.; Luskus, L. *J. Am. Chem. Soc.* **1973**, *95*, 7301–7315.
- (40) a) Bastide, J.; Ghandour, N. El.; Henri-Rousseau, O. *Tetrahedron Lett.* **1972**, 4225–4228. b) Bastide, J.; Ghandour, N. El.; Henri-Rousseau, O. *Bull. Soc. Chim. Fr.* **1973**, 2290–2293. c) Bastide, J.; Henri-Rousseau, O.; Aspart-Pascot, L. *Tetrahedron* **1974**, *30*, 3355–3363.
- (41) Nagase, S.; Morokuma, K. *J. Am. Chem. Soc.* **1978**, *100*, 1666–1672.
- (42) a) Ess, D. H.; Houk, K. N. *J. Am. Chem. Soc.* **2007**, *129*, 10646–10647. b) Ess, D. H.; Houk, K. N. *J. Am. Chem. Soc.* **2008**, *130*, 10187–10198. c) Chen, P.-P.; Ma, P.; He, X.; Svatunek, D.; Liu, F.; Houk, K. N. *J. Org. Chem.* **2021**, *86*, 5792–5804.
- (43) a) Zeist, W.-J.; Bickelhaupt, F. M. *Org. Biomol. Chem.* **2010**, *8*, 3118–3127. b) Bickelhaupt, F. M.; Houk, K. N. *Angew. Chem. Int. Ed.* **2017**, *56*, 10070–10086; *Angew. Chem.* **2017**, *129*, 10204–10221.
- (44) a) Eckell, A.; Huisgen, R.; Sustmann, R.; Wallbillich, G.; Grashey, D.; Spindler, E. *Chem. Ber.* **1967**, *100*, 2192. b) Gothelf, K. V.; Jørgensen, K. A. *Chem. Rev.* **1998**, *98*, 863–909.
- (45) a) Frank, J. *Introduction to Computational Chemistry*. Wiley. **1990**. b) Kronik, L.; Stein, T.; Rafaely-Abramson, S.; Baer, R. *J. Chem. Theory Comput.* **2012**, *8*, 1515–1531. c) Cohen, A. J.; Mori-Sanchez, P.; Yang, W. *Chem. Rev.* **2012**, *112*, 289–320. d) Payán-Gómez, S. A.; Flores-Holguín, N.; Pérez-Hernández, A.; Piñón-Miramontes, M.; Glossman-Mitnik, D. *J. Mol. Model* **2011**, *17*, 979–985. e) Tsuneda, T.; Hirao, K. *WIREs. Comput. Mol. Sci.* **2014**, *4*, 375–390. f) Frau, J.; Muñoz, F.; Glossman-Mitnik, D. *Quim. Nova.* **2017**, *40*, 402–406.
- (46) a) Kaur, I.; Jia, W.; Kopreski, R. P.; Selvarasah, S.; Dokmeci, M. R.; Pramanik, C.; McGruer, N. E.; Miller, G. P. *J. Am. Chem. Soc.* **2008**, *130*, 16274–16286. b) Eakins, G. L.; Alford, J. S.; Tiegs, B. J.; Breyfogle, B. E.; Stearman, C. J. *J. Phys. Org. Chem.* **2011**, *24*, 1119–1128.

Chapter 3. An Overlooked Pathway in 1,3-Dipolar Cycloadditions of Diazoalkanes with Enamines

Li, L.; Mayer, P.; Stephenson, D. S.; Ofial, A. R.; Mayer, R. J.; Mayr, H. *Angew. Chem. Int. Ed.* **2022**, *61*, e202117047; *Angew. Chem.* **2022**, *134*, e202117047.

Author Contributions

Li, L. performed all the experiments. Mayer, P. characterized the single crystal X-ray structures. Stephenson, D. S. measured the low temperature NMR kinetics. Mayer, R. J. conducted the DFT calculations. The manuscript was drafted by Li, L. and jointly revised by Li, L., Mayer, R. J., Ofial, A. R. and Mayr, H.

Copyright

Reproduced with permission from: Li, L.; Mayer, P.; Stephenson, D. S.; Ofial, A. R.; Mayer, R. J.; Mayr, H. *Angew. Chem. Int. Ed.* **2022**, *61*, e202117047; *Angew. Chem.* **2022**, *134*, e202117047. Copyright 2022 John Wiley & Sons, Inc.

Parts of the supporting data are presented in section 3.2. The complete supporting information is available under the following link:

<https://onlinelibrary.wiley.com/doi/full/10.1002/anie.202117047>

3.1 Copies of Manuscript



An Overlooked Pathway in 1,3-Dipolar Cycloadditions of Diazoalkanes with Enamines

Le Li, Peter Mayer, David S. Stephenson, Armin R. Ofial, Robert J. Mayer,* and Herbert Mayr*

Dedicated to Professor Wolfgang Beck on the occasion of his 90th birthday

Abstract: Methyl diazoacetate reacts with 1-(*N*-pyrrolidino)cycloalkenes to give products of 1,3-dipolar cycloadditions and azo couplings. The kinetics and mechanisms of these reactions were investigated by NMR spectroscopy and DFT calculations. Orthogonal π -systems in the 1,3-dipoles of the propargyl-allenyl type allow for two separate reaction pathways for the (3+2)-cycloadditions. The commonly considered concerted pathway is rationalized by the interaction of the enamine HOMO with LUMO+1, the lowest unoccupied orbital of the heteropropargyl anion fragment of methyl diazoacetate. We show that HOMO/LUMO($\pi^*_{N=N}$) interactions between enamines and methyl diazoacetate open a previously unrecognized reaction path for stepwise cycloadditions through zwitterionic intermediates with barriers approximately 40 kJ mol⁻¹ lower in energy in CHCl₃ (DFT calculations) than for the concerted path.

Huisgen (3+2)-cycloadditions can be considered to be the most general synthesis for five-membered heterocycles.^[1] They usually proceed via concerted mechanisms, which are rationalized by interactions of the frontier orbitals of the heteroallyl or heteropropargyl anion fragments of the 1,3-dipoles with the frontier orbitals of the dipolarophiles.^[2] Whereas interactions of ψ_2 (1,3-dipole) with LUMO(dipolarophile) are considered to control the reactions of electron-rich 1,3-dipoles with electron-poor dipolarophiles, the interactions of HOMO(dipolarophile) with ψ_3 (1,3-dipole) have been assumed to be dominating in

reactions of electron-rich dipolarophiles with electron-deficient 1,3-dipoles (Figure 1).

In diazoalkanes, however, ψ_3 does not correspond to LUMO, but to LUMO+1, since the perpendicular $\pi^*_{N=N}$ is lower in energy (Figure 1). Hamlin and co-workers have already reported this ordering of orbitals in diazomethane and stated that in the reaction of diazomethane with ethylene “the orientation of the LUMO of diazomethane, being perpendicular to the HOMO(ethylene), prevents it from overlapping in a favorable manner and thus the HOMO(ethylene)-LUMO+1(diazomethane) interaction dominates”.^[2b] Chen, Hu, and Houk also reported that the lowest unoccupied orbital of the heteropropargyl fragment (ψ_3) does not correspond to the LUMO of diazomethane. They did not comment, however, why the interaction with the LUMO of diazomethane was neglected in their analysis.^[2i] We now report that the 1,3-dipolar cycloadditions of methyl diazoacetate (**1**) with electron-rich dipolarophiles may proceed via different pathways arising from interactions of the enamines’ HOMO with either LUMO or LUMO+1 of the diazoalkane.

Reissig obtained 15% of pyrazole **3a** when methyl diazoacetate (**1**) and pyrrolidino-cyclopentene (**2a**) were heated under reflux in chloroform and subsequently treated with HCl in methanol (Scheme 1).^[3a] The formation of a mixture of (*E/Z*)-isomers of **4a** was reported, when the same experiment was carried out at 0 °C and worked up by chromatography.^[3a] Since cyclization was not observed when the hydrazonoenamine obtained from **1** and 1-(*N*-morpholino)cyclopentene (that is, the non-hydrolyzed precursor of **4a**) was treated with acid, the direct formation of **3a** through concerted cycloaddition was postulated.^[3a] X-ray

*] L. Li, Dr. P. Mayer, Dr. D. S. Stephenson, Dr. A. R. Ofial, Prof. Dr. H. Mayr
Department Chemie, Ludwig-Maximilians-Universität München
Butenandtstraße 5–13, 81377 München (Germany)
E-mail: herbert.mayr@cup.uni-muenchen.de
Dr. R. J. Mayer
Institut de Science et d’Ingénierie Supramoléculaires (ISIS)
Université de Strasbourg & CNRS,
8 Allée Gaspard Monge, 67000 Strasbourg (France)
E-mail: rjmayer@unistra.fr

© 2022 The Authors. Angewandte Chemie International Edition published by Wiley-VCH GmbH. This is an open access article under the terms of the Creative Commons Attribution Non-Commercial License, which permits use, distribution and reproduction in any medium, provided the original work is properly cited and is not used for commercial purposes.

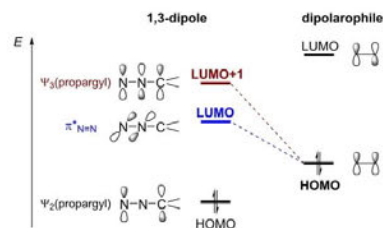
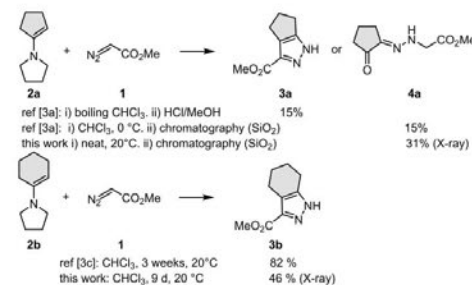


Figure 1. Qualitative description of orbital interactions of electron-rich dipolarophiles with acceptor-substituted diazoalkanes.



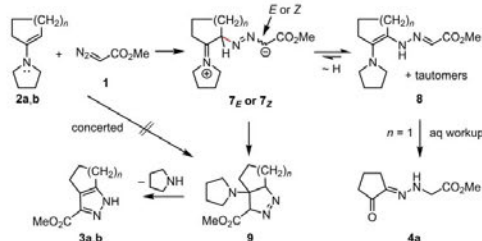
Scheme 1. Products of the reactions of methyl diazoacetate (**1**) with enamines **2a** and **2b**.

analysis and NMR spectra of **4a**, which we obtained by combining **1** and **2a** without solvent at room temperature, showed the presence of a single isomer of **4a** (Supporting Information).

The formation of 82 % of pyrazole **3b** by the reaction of **1** with **2b** at room temperature was reported by Huisgen and Reissig.^[3c] While our experiments confirmed the formation of **3b**, NMR monitoring of this reaction showed signals of unidentified intermediates before the appearance of the signals of **3b** (Supporting Information, Figure S2). In order to elucidate the nature of the unidentified intermediates we investigated the analogous reaction of diazomalonate **1'** with **2b** by NMR spectroscopy (Scheme 2).



Scheme 2. NMR monitoring of the reaction of **1'** with enamine **2b** (^1H NMR spectra are shown in Supporting Information, Figure S3).



Scheme 3. Proposed mechanism for the reactions of **1** with enamines **2a,b**.

When Huisgen and Reissig kept a solution of **2b** and **1'** in diethyl ether for four days at room temperature, they obtained the bicyclic pyrazoline **6** in 73 % yield.^[3a,c] Accordingly, in this work, **6** was isolated in 65 % yield (Et_2O , one week at room temperature) and characterized by X-ray analysis (Scheme 2). Monitoring this reaction by ^1H NMR spectroscopy in CDCl_3 showed that initially the reactants were quantitatively converted into a mixture of hydrazone-enamines **5** and **5'**, which subsequently underwent cyclization with formation of **6** (Supporting Information, Figure S3). We, therefore, suggest that all reactions in Schemes 1 and 2 proceed by the mechanism illustrated in Scheme 3 and disagree with earlier conclusions that pyrazolines **6** and **9** are formed via concerted 1,3-dipolar cycloadditions.^[3]

Electrophilic attack of the diazo ester **1** at the enamines **2** yields zwitterions **7**, which may undergo proton shifts to yield **8** or several other tautomers whose hydrolyses give hydrazonecyclopentanone **4a**. Pyrazoline **9**, the supposed precursor of **3**, is formed in a subsequent process by cyclization of zwitterions **7**, which may be regenerated through proton shifts from **8** or its tautomers. The reason why this cyclization is more favorable in the reaction with **2b** than with **2a** is discussed in the computational section below.

The kinetics of the reactions of methyl diazoacetate (**1**) with the enamines **2a** and **2b** were investigated by time-resolved ^1H NMR spectroscopy, following the decrease of the vinylic hydrogens of the enamines **2** relative to an internal standard (1,1,2,2-tetrachloroethane) in CDCl_3 at low temperatures. Equimolar amounts of **1** and **2** were used, and the second-order rate constants k_2 were obtained as the slopes of plots of $1/[2]_t$ versus time t according to $1/[2]_t = k_2 t + 1/[2]_0$ (Figure 2a).^[4]

Plots of $\ln(k_2/T)$ versus $1/T$ provided the Eyring activation parameters ΔH^\ddagger and ΔS^\ddagger in CDCl_3 (Figure 2b), from which the second-order rate constants k_2 at $+80.3^\circ\text{C}$ were extrapolated that gave values 3 and 12 times higher than reported^[3a,d] for this temperature in toluene (Table 1). Table 1 shows that both reactions **1** + **2a,b** are characterized by highly negative activation entropies, again demonstrating that highly negative activation entropies cannot be used as a criterion for the occurrence of multicenter processes.^[5]

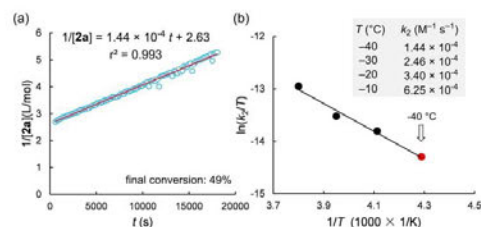


Figure 2. a) Kinetics of the reaction of **1** (0.399 M) with **2a** (0.371 M) monitored by the decrease of the NMR signals of the vinylic H of **2a** vs. 1,1,2,2-tetrachloroethane (0.276 M) as internal standard in CDCl_3 at -40°C . b) Eyring plot for the reactions of **1** with **2a** at -40 to -10°C .

Table 1: Second-order rate constants k_2 in CDCl_3 for the reactions of **1** with **2a, b** at various temperatures, and k_2 at +25 and +80.3 °C calculated from the Eyring activation parameters ΔH^\ddagger and ΔS^\ddagger .

Enamine	T [°C]	k_2 [$\text{M}^{-1}\text{s}^{-1}$]	ΔH^\ddagger [kJ mol^{-1}]	ΔS^\ddagger [J $\text{mol}^{-1}\text{K}^{-1}$]
2a	-40	1.44×10^{-4}	22.0 ± 2.1	-222 ± 9
	-30	2.46×10^{-4}		
	-20	3.40×10^{-4}		
	-10	6.25×10^{-4}		
	+25	$2.17 \times 10^{-3[a]}$		
	+80.3	$1.03 \times 10^{-2[b]}$		
2b	+80.3	$8.28 \times 10^{-4[b]}$	23.5 ± 1.8	-228 ± 7
	-30	5.46×10^{-5}		
	-20	8.48×10^{-5}		
	-10	1.43×10^{-4}		
	+25	$5.59 \times 10^{-4[a]}$		
	+80.3	$2.91 \times 10^{-3[a]}$		
	+80.3	$8.90 \times 10^{-4[b]}$		

[a] Extrapolated from rate constants at lower temperatures in this table by using the Eyring equation. [b] k_2 in toluene, as reported in refs. [3a, d].

After an extensive conformational search^[6] the geometries of all structures were optimized at the B3LYP-D3BJ/def2-SVP^[7] level of theory considering solvation with the SMD model^[8] for chloroform within the Gaussian set of codes.^[9] For improved accuracy, the thermal corrections at this level were combined with single-point energies using the (SMD= CHCl_3)/MN15/def2-TZVPD method.^[10] Lastly, the Gibbs energies of all conformers were Boltzmann weighted.

Let us first consider the reaction of methyl diazoacetate (**1**) with pyrrolidinocyclopentene (**2a**). Diazoacetate **1** exists as two almost isoenergetic conformers which interconvert via a rotational barrier of 52.2 kJ mol^{-1} (at 25 °C) as determined by NMR spectroscopy and confirmed by DFT calculations (Figure 3a).^[11]

Figure 3b replaces the qualitative orbital representations of LUMO and LUMO+1 for 1,3-dipoles in Figure 1 by the calculated images of these two orbitals for **1**.^[12] As expected, $\pi^*_{\text{N=N}}$ (LUMO) is significantly lower in energy than LUMO

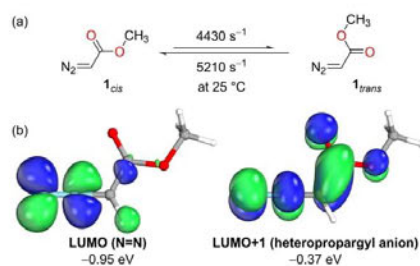


Figure 3. a) Conformational equilibrium of methyl diazoacetate (**1**) experimentally determined by dynamic ^1H NMR spectroscopy in CDCl_3 .^[11] b) Lowest unoccupied molecular orbitals of **1** and their energies at the (SMD= CHCl_3)/MN15/def2-TZVPD/(SMD= CHCl_3)/B3LYP-D3BJ/def2-SVP level of theory.

+1, independent of the computational method and basis set (see Supporting Information for a systematic investigation).

Interaction of the enamine HOMO with LUMO+1 of **1_{trans}** directly leads to the (3+2)-cycloadduct as illustrated in Figure 4a. For the location of the transition state of this trajectory, the C–N and C–C bonds of the cycloadduct were simultaneously elongated. The structure lying at the saddle point of the resulting three-dimensional energy surface was further optimized to give a transition state, where the formation of the new C–N bond (1.85 Å) is much further advanced than that of the new C–C bond (2.77 Å).

The intrinsic reaction coordinate (IRC) shows that after passing the transition state, the C–N bond continues to shorten much faster than the C–C bond. Though the resulting structures closely resemble a zwitterion, a local minimum for an intermediate is not involved, and the C–C bond is formed without additional barrier.

A slightly more favorable concerted pathway arises from interaction of HOMO(**2a**) with LUMO+1 of **1_{cis}**. The corresponding transition state shows a higher degree of asynchronicity (Figures S8 and S9; C–N bond: 1.73 Å, C–C bond: 3.14 Å) and the reaction might be considered as a two-step no-intermediate process. Detailed discussions of the concerted mechanisms are shifted into the Supporting Information, because none of them is followed in reality.

The actually occurring reaction pathway (Figure 4b)^[15] arises from the interaction of the HOMO(enamine) with $\pi^*_{\text{N=N}}$, that is, the LUMO of **1**, as substantiated by analysis of the overlap integrals of the involved orbitals.^[13,14] This pathway leads to the formation of zwitterion **7_Z** faster than to its isomer **7_E** despite the higher thermodynamic stability of the latter (for geometries and charges of zwitterions **7**, see Figure S11). Transition state TS_{Z} , which is 51 and 42 kJ mol^{-1} lower in Gibbs energy than the transition states TS_{conc} of the two concerted cycloadditions, was located by stepwise elongation of the C–N bond in the zwitterion **7_Z** and optimization of the structure at the energetic maximum of the resulting pathway on the potential energy surface. As cyclization of **7_Z** occurs with a smaller barrier ($\Delta E_{\text{rel}}=7.7$, $\Delta G^\ddagger=26 \text{ kJ mol}^{-1}$) than the retroaddition regenerating the reactants, the formation of **7_Z** via TS_{Z} corresponds to the rate-determining step of the stepwise cycloaddition (Figure 5a).^[16] Thus, the stepwise cycloaddition in Figure 4b is highly preferred over the concerted pathway in Figure 4a.

However, the isolation of hydrazonocyclopentanone **4a**, a hydrolysis product of **8** in the reaction of **1** with **2a**, implies that proton shifts in the zwitterion **7_Z** or **7_E** must be even faster than cyclization. Since calculations revealed a high barrier for the intramolecular 1,2-proton shift from **7** to **8**,^[17] intermolecular processes must account for these tautomerizations, as previously reported for the 1,2-proton shifts generating Breslow intermediates from the zwitterions initially formed from aldehydes and NHCs.^[18] Because of the manifold of potential intermolecular proton shifts, we have not tried to calculate barriers for these proton shifts, at least one of which must be even smaller than the low barriers calculated for the cyclizations of **7_Z**.

Comparison of the two Gibbs energy profiles in Figure 5 shows close similarity for the reactions of **1** with the

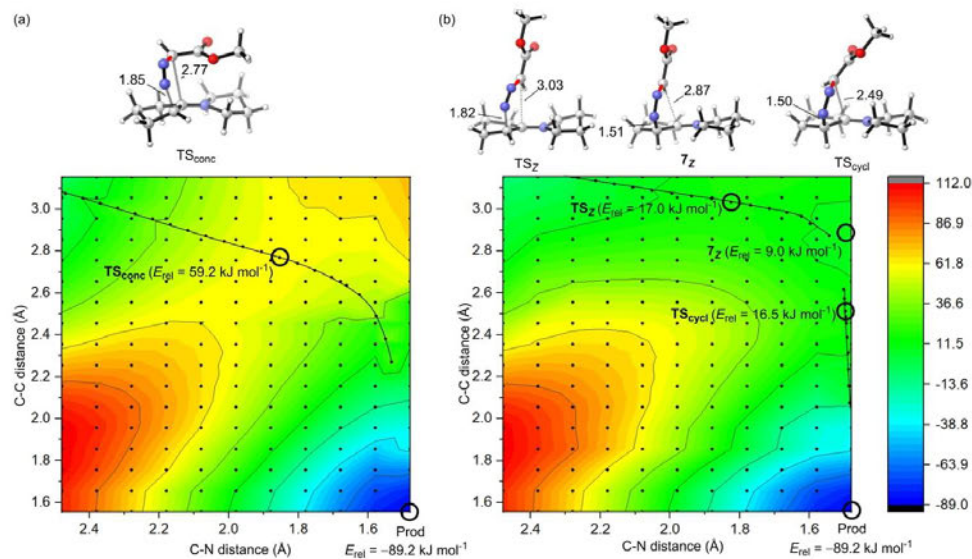


Figure 4. 3D potential energy surfaces at the (SMD = CHCl₃)/B3LYP-D3BJ/def2-SVP level for the reaction of methyl diazoacetate (**1**_{trans}) with pyrrolidinocyclopentene (**2a**) for (a) the concerted pathway (for the related surface with **1**_{cis}, see Figure S9b) and (b) the stepwise pathway. All energies E_{rel} (in kJ mol⁻¹) are given relative to the reactants and are scaled identically for both pathways. Isolines are drawn at an energy difference of 25 kJ mol⁻¹. Black lines connect the reaction pathway derived from IRC calculations starting from the respective transition states. Note: Since zwitterion **7_z** is located on a flat region of the potential energy surface, relaxation of **TS_z** by means of an IRC calculation did not end up exactly at **7_z**, but stopped in close vicinity to **7_z** due to the low gradient in the surroundings.

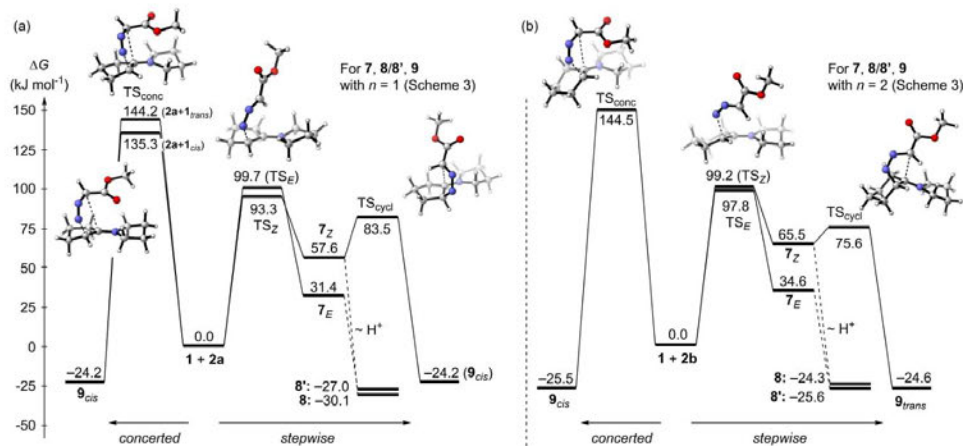


Figure 5. Comparison of the Gibbs activation energies ΔG (kJ mol⁻¹) of the concerted and stepwise cycloadditions of **1** with **2a** (a) and **2b** (b) as computed at the (SMD = CHCl₃)/MN15/def2-TZVPD/(SMD = CHCl₃)/B3LYP-D3BJ/def2-SVP level of theory. In **9**, *cis* and *trans* refer to the relative orientation of the pyrrolidine and ester moieties. Less favorable **TS_{zycl}** are shown in Figures S7 and S10.

enamines **2a** and **2b**. In both cycloadditions, the stepwise process with rate-determining formation of the zwitterion **7** is highly favored over the concerted processes. The agreement of the experimentally determined activation Gibbs

energies $\Delta G^{\ddagger}_{\text{exp}}$ (298 K) of 88 (**1+2a**) and 92 kJ mol⁻¹ (**1+2b**) with the calculated barriers for the formation of the zwitterions **7** (93 and 98 kJ mol⁻¹, respectively) leads to the conclusion that zwitterions **7** are common intermediates for cycloadditions (\rightarrow **9**) and azo couplings (\rightarrow **8**).

A distortion/interaction analysis^[19] for the reaction **1+2a** shows that the higher activation barrier for the concerted pathway is predominantly caused by the higher distortion energy of methyl diazoacetate **1** (Figures S12 and S13). The differences of the interaction energies are much smaller but are also in favor of the stepwise pathway. Further energy decomposition analysis of the interaction energies with the SAPT method^[20] shows that in addition to its higher steric constraints, it is predominantly Pauli repulsion that disfavors the concerted pathways (Figures S14 and S15).^[21]

Figure 5 rationalizes why the azo-coupling products initially formed from aminocyclohexene **2b** cyclize under the reaction conditions, while those obtained from aminocyclopentene **2a** do not. Since the proton shifts in the zwitterions **7** (\rightarrow **8** or **8'**) were experimentally found to be faster than their cyclizations, one can conclude that the equilibration of **8** and **8'** with **7_F** and **7_Z** is faster than the cyclizations. Thus the Curtin–Hammett principle applies, and one can calculate barriers of 113.6 (Figure 5a) and 101.2 kJ mol⁻¹ (Figure 5b) for the formation of **9** from the more stable of the azo coupling products **8** or **8'** (difference between **8** or **8'** and TS_{cycl}). The differences of the Gibbs energies in Figures 5a and b are thus in line with the observation of different types of products in reactions of diazoalkanes with five- and six-membered enamines, but cannot be considered as definite proof because of the error limits of the computed energies. Since the pyrazolines **9** undergo further stabilization by elimination of the amines and proton shifts, the relative Gibbs energies of **8/8'** and **9** do not account for the different behavior of 5- and 6-membered enamines. Formation of **9** via electrocyclicization of an N-alkenyl azomethine imine, a tautomer of **8**, was calculated to have a much higher barrier than the pathway via cyclization of **7** (Supporting Information, p S37).

What is the link between the two trajectories depicted in Figures 4a and b? Rotation around the red C–N bond in TS_Z of the stepwise process (while the C–N bond length is constrained to 1.83 Å and the C–C bond length to 3.03 Å) transforms TS_Z (Figure 4b) into a structure similar to the structure of TS_{conc}, the transition state of the concerted cycloaddition in Figure 4a. In the initial phase of this rotation, which corresponds to a change of the N=N–C–C dihedral angle from 180° (in TS_Z) to roughly 260° or 100°, the potential energy increases by 55–58 kJ mol⁻¹ due to loss of the partial double-bond character of the red bond. Further rotation leads to a decrease of energy by approximately 11 kJ mol⁻¹ due to interaction of the termini of the incipient zwitterion. This barrier accounts for the existence of separate concerted and stepwise trajectories, as quantitatively described in Figure S16.^[22]

The question whether 1,3-dipolar cycloadditions proceed by concerted (Huisgen)^[23b,24a] or stepwise mechanisms (Firestone)^[23a] has been a long-lasting controversy. While Huisgen rejected Firestone's diradical hypothesis in

general,^[23b] in 1986 Huisgen, Mloston, and Langhals reported the first nonstereospecific 1,3-dipolar cycloadditions in reactions of thiocarbonyl ylides with electron-acceptor substituted ethylenes, which they interpreted by stepwise processes via intermediate zwitterions.^[25] Nevertheless, the concerted mechanism of most 1,3-dipolar cycloadditions is now well established, and their rates are commonly rationalized by the interactions of the frontier orbitals of the allyl/propargyl fragment of the 1,3-dipoles with the frontier orbitals of the dipolarophiles.^[2]

Reaction rates of acceptor-substituted diazoalkanes, such as **1** and **1'**, have been the preferred examples to illustrate this FMO model,^[24] probably because these 1,3-dipoles display the most spectacular variations of reactivity – fast reactions with electron-deficient dipolarophiles (acrylic esters) as well as with electron-rich dipolarophiles (enamines), and slow reactions with alkyl- and alkoxy-substituted ethylenes (Figure 3 in ref. [3d]). Our work has shown, however, that these examples are not suitable for demonstrating the dependence of cycloaddition rates on the interactions of the frontier orbitals of the dipolarophiles with the frontier orbitals of the 3-center/4-electron π -systems in 1,3-dipoles, because (1) the measured rate constants with enamines refer to azo-couplings, not to cycloadditions, and (2) the reactions with enamines are not controlled by HOMO(dipolarophile)- Ψ_3 (1,3-dipole) interactions, but by interactions of HOMO(enamine) with $\pi^*_{N=N}$, the LUMO of methyl diazoacetate, an orbital whose role has so far been neglected.

We now found that the availability of two perpendicular low-lying unoccupied molecular orbitals in acceptor-substituted diazoalkanes (e.g. **1** and **1'**) opens the possibility for nucleophilic attack at two different orbitals. Interaction of the enamines' HOMO with LUMO+1(diazoacetate) is calculated to result in concerted (3+2)-cycloadditions through transition states which are considerably higher in energy than the experimentally observed stepwise processes with formation of the zwitterions **7**, which proceed by attack of the enamines at LUMO($\pi^*_{N=N}$) of the diazoalkanes. This situation thus differs from most other concomitant concerted and stepwise cycloadditions, where both pathways are controlled by the interactions of the same orbitals and only differ by unlike orientations of the reactants (cyclic vs stretched).

We are presently investigating the switch from stepwise cycloadditions (attack at LUMO of diazoalkane) to concerted cycloadditions (attack at LUMO+1 of diazoalkane), which is expected to take place when enamines are replaced by less nucleophilic dipolarophiles. Furthermore, we are exploring the role of the two perpendicular π -orbitals in (3+2)-cycloadditions of other 1,3-dipoles of the propargyl/allenyl type (e.g., azides).

Acknowledgements

L.L., A.R.O. and H.M. are grateful to the Department Chemie (LMU München) and the Deutsche Forschungsgemeinschaft (DFG, SFB 749, project B1) for financial

support. R.J.M. thanks the Deutsche Forschungsgemeinschaft (DFG, German Research Foundation) for a fellowship (MA 9687/1-1). We thank the Faculty of Chemistry and Pharmacy (LMU München) for providing the computational resources and Professors H.-U. Reißig, C. Y. Legault and the anonymous reviewers for helpful comments. Open Access funding enabled and organized by Projekt DEAL.

Conflict of Interest

The authors declare no conflict of interest.

Data Availability Statement

The data that support the findings of this study are available in the Supporting Information of this article.

Keywords: Diazoalkane · Enamine · Kinetics · Orbital Interactions · Quantum Chemical Calculations

- [1] a) R. Huisgen, *Angew. Chem. Int. Ed. Engl.* **1963**, *2*, 565–598; *Angew. Chem.* **1963**, *75*, 604–637; b) *1,3-Dipolar Cycloaddition Chemistry, Vols. 1 & 2* (Ed.: A. Padwa), Wiley, New York, **1984**; c) *The Chemistry of Heterocyclic Compounds, Volume 59: Synthetic Applications of 1,3-Dipolar Cycloaddition Chemistry Toward Heterocycles and Natural Products* (Eds.: A. Padwa, W. H. Pearson), Wiley, New York, **2002**; d) H. Suga, K. Itoh, *Methods and Applications of Cycloaddition Reactions in Organic Syntheses* (Ed.: N. Nishiwaki), Wiley, Hoboken, **2014**, chap. 7, pp. 175–204; e) M. Breugst, H.-U. Reißig, *Angew. Chem. Int. Ed.* **2020**, *59*, 12293–12307; *Angew. Chem.* **2020**, *132*, 12389–12404.
- [2] a) R. Sustmann, *Tetrahedron Lett.* **1971**, *12*, 2717–2720; b) R. Sustmann, H. Trill, *Angew. Chem. Int. Ed. Engl.* **1972**, *11*, 838–840; *Angew. Chem.* **1972**, *84*, 887–888; c) K. N. Houk, *J. Am. Chem. Soc.* **1972**, *94*, 8953–8955; d) K. N. Houk, J. Sims, C. R. Watts, L. J. Luskus, *J. Am. Chem. Soc.* **1973**, *95*, 7301–7315; e) R. Sustmann, W. Sicking, *Chem. Ber.* **1987**, *120*, 1653–1658; f) B. Engels, M. Christl, *Angew. Chem. Int. Ed.* **2009**, *48*, 7968–7970; *Angew. Chem.* **2009**, *121*, 8110–8112; g) M. Breugst, R. Huisgen, H.-U. Reißig, *Eur. J. Org. Chem.* **2018**, 2477–2485; h) T. A. Hamlin, D. Svatunek, S. Yu, L. Ridder, I. Infante, L. Visscher, F. M. Bickelhaupt, *Eur. J. Org. Chem.* **2019**, 378–386; i) S. Chen, T. Hu, K. N. Houk, *J. Org. Chem.* **2021**, *86*, 6840–6846.
- [3] a) H.-U. Reißig, Dissertation, Ludwig-Maximilians-Universität München, **1978**; b) R. Huisgen, W. Bihlmaier, H.-U. Reißig, *Angew. Chem. Int. Ed. Engl.* **1979**, *18*, 331–332; *Angew. Chem.* **1979**, *91*, 347–348; c) R. Huisgen, H.-U. Reißig, *Angew. Chem. Int. Ed. Engl.* **1979**, *18*, 330–331; *Angew. Chem.* **1979**, *91*, 346–347; d) W. Bihlmaier, R. Huisgen, H.-U. Reißig, S. Voss, *Tetrahedron Lett.* **1979**, *20*, 2621–2624; e) R. Huisgen, H.-U. Reißig, H. Huber, S. Voss, *Tetrahedron Lett.* **1979**, *20*, 2987–2990. f) Formation of **9** via diradical intermediates has been excluded by Huisgen and Reißig in ref. [3c] because in this case they would have expected opposite regioselectivity in reactions with enamines, where pyrazolines of type **9** can be observed (e.g., **6**).
- [4] P. Atkins, J. de Paula, J. Keeler, *Atkins' Physical Chemistry*, 11th ed., Oxford Univ. Press, Oxford (UK), **2018**, p. 733.
- [5] Activation entropies of similar magnitude have previously been reported by Huisgen and Steiner for stepwise (2+2)-cycloadditions of tetracyanoethylene with enol ethers: G. Steiner, R. Huisgen, *Tetrahedron Lett.* **1973**, *14*, 3769–3772.
- [6] Conformational sampling was performed with the OPLS3 force field as implemented in MacroModel: a) E. Harder, W. Damm, J. Maple, C. Wu, M. Reboul, J. Y. Xiang, L. Wang, D. Lupyan, M. K. Dahlgren, J. L. Knight, J. W. Kaus, D. S. Cerutti, G. Krilov, W. L. Jorgensen, R. Abel, R. A. Friesner, *J. Chem. Theory Comput.* **2016**, *12*, 281–296; b) Schrödinger Release 2019-4: MacroModel, Schrödinger, LLC, New York, NY, **2019**.
- [7] a) A. D. Becke, *J. Chem. Phys.* **1993**, *98*, 5648–5652; b) S. Grimme, S. Ehrlich, L. Goerigk, *J. Comput. Chem.* **2011**, *32*, 1456–1465; c) F. Weigend, R. Ahlrichs, *Phys. Chem. Chem. Phys.* **2005**, *7*, 3297–3305.
- [8] A. V. Marenich, C. J. Cramer, D. G. Truhlar, *J. Phys. Chem. B* **2009**, *113*, 6378–6396.
- [9] Gaussian16, Revision A.03, Gaussian, Inc., Wallingford CT, **2016**. For the full reference including all authors, see the Supporting Information.
- [10] H. S. Yu, X. He, S. L. Li, D. G. Truhlar, *Chem. Sci.* **2016**, *7*, 5032–5051; H. S. Yu, X. He, S. L. Li, D. G. Truhlar, *Chem. Sci.* **2016**, *7*, 6278–6279.
- [11] a) F. Kaplan, G. K. Meloy, *J. Am. Chem. Soc.* **1966**, *88*, 950–956; b) for dynamic NMR spectroscopy in this work, see Figure S4; c) for a computational analysis, see Figure S6.
- [12] Molecular orbitals in Figure 3 were visualized within the IboView software using the frontier molecular orbitals calculated with Gaussian: G. Knizia, J. E. M. N. Klein, *Angew. Chem. Int. Ed.* **2015**, *54*, 5518–5522; *Angew. Chem.* **2015**, *127*, 5609–5613. See Supporting Information for details.
- [13] Analysis of the orbital overlap of the HOMO of **2a** with the unoccupied orbitals of **1** at different C–N distances along the reaction pathway was performed with the Multiwfn package (Supporting Information): T. Lu, F. Chen, *J. Comput. Chem.* **2012**, *33*, 580–592.
- [14] Since the reactions of **1_{eq}** and **1_{non}** with enamines **2** yield the zwitterions **7** with almost identical rates, much more slowly than **1_{eq}** and **1_{non}** interconvert (cf. Figure 3a), only the Boltzmann-weighted average of all conformers of these reactions is discussed in the following.
- [15] a) Unlike in the well-known More O'Ferrall–Jencks diagrams (see refs [15b,c]) the two reaction pathways in Figure 4 cannot be depicted on the same potential energy surface. Since different orientations of the reactants are involved, the two pathways differ fundamentally and not only by the different lengths of the new C–C and C–N bonds; b) R. A. More O'Ferrall, *J. Chem. Soc. B* **1970**, 274–277; c) W. P. Jencks, *Chem. Rev.* **1972**, *72*, 705–718.
- [16] Cyclizations of **7_z** via a *trans* orientation are not depicted in Figure 5 because they are very unfavorable with barriers higher than those of the reverse reactions (Tables S3 and S4).
- [17] Hydrazonoenamines of type **8**, formally arising from 1,2-proton shifts in **7**, have been identified by X-ray analysis as the kinetically controlled products in reactions with other diazo compounds (manuscript in preparation).
- [18] a) M. Pareek, Y. Reddi, R. B. Sunoj, *Chem. Sci.* **2021**, *12*, 7973–7992; b) Y. He, Y. Xue, *J. Phys. Chem. A* **2011**, *115*, 1408–1417. The general problems to analyze proton-shuttle processes computationally have been described: c) R. E. Plata, D. A. Singleton, *J. Am. Chem. Soc.* **2015**, *137*, 3811–3826.
- [19] a) F. M. Bickelhaupt, K. N. Houk, *Angew. Chem. Int. Ed.* **2017**, *56*, 10070–10086; *Angew. Chem.* **2017**, *129*, 10204–10221; b) P. Vermeeren, S. C. C. van der Lubbe, C. F. Guerra, F. M. Bickelhaupt, T. A. Hamlin, *Nat. Protoc.* **2020**, *15*, 649–667.
- [20] a) B. Jeziorski, R. Moszynski, K. Szalewicz, *Chem. Rev.* **1994**, *94*, 1887–1930; b) T. M. Parker, L. A. Burns, R. M. Parrish,

- A. G. Ryno, C. D. Sherrill, *J. Chem. Phys.* **2014**, *140*, 094106; c) Computations were performed with the *Psi4* package. For the full reference, see the Supporting Information.
- [21] T. A. Hamlin, F. M. Bickelhaupt, I. Fernández, *Acc. Chem. Res.* **2021**, *54*, 1972–1981.
- [22] When trying to optimize the transition states of various conformations of the concerted pathway, we observed rotation around the C–N bond during optimization and convergence into the stepwise pathway. This suggests that switchover from a concerted to a stepwise pathway proceeds barrierless for some conformations.
- [23] a) R. A. Firestone, *J. Org. Chem.* **1968**, *33*, 2285–2290; b) R. Huisgen, *J. Org. Chem.* **1968**, *33*, 2291–2297.
- [24] a) “1,3-Dipolar Cycloadditions—Introduction, Survey, Mechanism”: R. Huisgen, *1,3-Dipolar Cycloaddition Chemistry*, Vols. 1 & 2 (Ed.: A. Padwa), Wiley, New York, **1984**, pp. 1–176; b) I. Fleming, *Molecular Orbitals and Organic Chemical Reactions*, Wiley, Chichester, **2010**, pp. 327–328; c) R. Brückner, *Reaktionsmechanismen*, 3. Aufl., Spektrum, Springer-Verlag, Berlin, **2007**, p. 670.
- [25] a) R. Huisgen, G. Mloston, E. Langhals, *J. Org. Chem.* **1986**, *51*, 4085–4087; b) R. Huisgen, G. Mloston, E. Langhals, *J. Am. Chem. Soc.* **1986**, *108*, 6401–6402.

Manuscript received: December 14, 2021

Accepted manuscript online: January 13, 2022

Version of record online: February 3, 2022

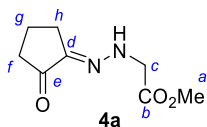
3.2 Supporting Information

3.2.1 Product Studies

General procedure A (GP A). Diazo compounds **1** and **1'** were mixed with **2a,b** in solvents (chloroform, dry diethyl ether) in an oven-dried GC vial (or a round-bottom flask) under argon atmosphere at room temperature. The GC vial (or round-bottom flask) was then sealed and the reaction mixture was kept till the reactions completed (TLC monitoring). Solvents were then evaporated and the resulting crude products were recrystallized or worked up by column chromatography on silica gel to give the purified products.

Reaction of methyl diazoacetate (**1**) with 1-pyrrolidinocyclopentene (**2a**)

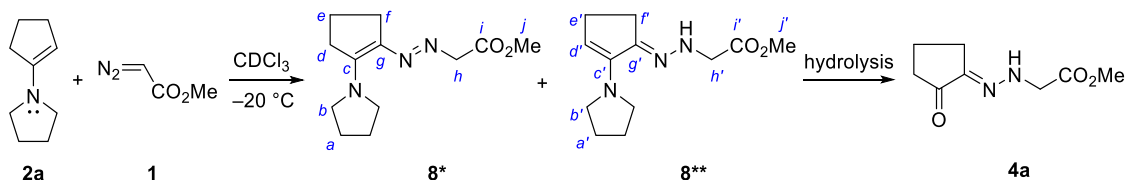
Methyl (*E*)-((2-oxocyclopentylidene)amino)glycinate (4a**)** was obtained from **1** (206 mg, 2.06 mmol) and **2a** (281 mg, 2.05 mmol) according to *GP A* as gray solid (GC vial, neat, room temperature, 1 h, eluent for column chromatography: n-pentane/diethyl ether = 1:1), which was further purified by recrystallization (CH₂Cl₂/hexane): colorless crystals (118 mg, 31%); mp 106.7 °C.



¹H NMR (400 MHz, CDCl₃): δ = 2.10 (quint, *J* = 7.7 Hz, 2 H, H^g), 2.43 (t, *J* = 7.9 Hz, 2 H, H^h), 2.54 (t, *J* = 7.4 Hz, 2 H, H^f), 3.74 (s, 3 H, H^a), 4.28 (d, *J* = 5.1 Hz, 2 H, H^c), 5.99 (br s, 1 H, NH). **¹³C NMR** (101 MHz, CDCl₃): δ = 17.5 (CH₂, C^g), 24.5 (CH₂, C^h), 37.7 (CH₂, C^f), 51.8 (CH₃, C^a), 52.4 (CH₂, C^a), 143.3 (C, C^d), 171.2 (C, C^b), 203.3 (C, C^e). **HRMS** (ESI⁺) [M+Na]⁺: calcd for [C₈H₁₂N₂NaO₃]⁺: 207.0740, found 207.0738. **IR** (neat, ATR): 3237, 2988, 2947, 1746, 1698, 1547, 1458, 1450, 1433, 1393, 1367, 1275, 1190, 1168, 1133, 1118, 1044, 1000, 945, 914, 826, 702 cm⁻¹. **Single crystal X-ray crystallography (4a)**: C₈H₁₂N₂O₃ (xv798).

Reissig reported that the reaction of **1** with **2a** in chloroform at 0 °C yielded **4a** (15%), which was isolated after purification on silica as a mixture of *E/Z*-isomers.^{1a} When the mixture of **1** and enamine **2a** was heated to reflux in chloroform and subsequently treated with HCl in methanol, the pyrazole **3a** (15%) furnished.^{1a}

NMR monitoring of the reaction of **1** with **2a** at -20 °C in CDCl₃ showed the formation of hydrazoneenamines **8*** and **8**** as intermediates (Figure S1), which were further characterized by NMR spectra at +25 °C.



NMR data assigned to **8***: ^1H NMR (400 MHz, CDCl_3 , +25 °C): δ = 1.75–1.82 (m, 1.8 H, H^a , superimposed with $\text{H}^{a'}$ in **8****), 1.86–1.90 (m, 3.4 H, H^e , superimposed with unassigned peaks), 2.64 (dt, J = 12.7, 7.7 Hz, 2.3 H, H^d and H^f), 3.04 (s, 1.4 H, H^b), 3.69 (s, 1.5 H, H^j , superimposed with $\text{H}^{j'}$ in **8****), 4.51 (s, 1 H, H^h). ^{13}C NMR (101 MHz, CDCl_3): δ = 19.5 (CH_2 , C^e), 25.1 (CH_2 , C^a), 28.7 (CH_2 , C^d), 34.8 (CH_2 , C^f), 46.1 (CH_2 , C^b), 51.9 (CH_3 , C^j , superimposed with $\text{C}^{j'}$ in **8****), 67.1 (CH_2 , C^h), 129.6 (C, C^g), 155.0 (C, C^c), 171.5 (C, C^i).

NMR data assigned to **8****: ^1H NMR (400 MHz, CDCl_3 , +25 °C): δ = 1.75–1.82 (m, 4 H, $\text{H}^{a'}$, superimposed with H^a in **8***), 2.38–2.50 (m, 4 H, $\text{H}^{e'}$ and $\text{H}^{f'}$), 3.18–3.21 (m, 4 H, $\text{H}^{b'}$), 3.69 (s, 3 H, $\text{H}^{j'}$, superimposed with H^j in **8***), 3.94 (d, J = 5.6 Hz, 2 H, $\text{H}^{h'}$), 4.87 (t, J = 5.8 Hz, 1 H, NH), 5.02 (t, J = 2.3 Hz, 1 H, $\text{H}^{d'}$). ^{13}C NMR (101 MHz, CDCl_3): δ = 24.6 (CH_2 , $\text{C}^{a'}$), 25.2 (CH_2 , $\text{C}^{f'}$), 26.2 (CH_2 , $\text{C}^{e'}$), 49.7 (CH_2 , $\text{C}^{b'}$), 51.9 (CH_3 , $\text{C}^{j'}$, superimposed with C^j in **8***), 52.6 (CH_2 , $\text{C}^{h'}$), 111.1 (CH, $\text{C}^{d'}$), 147.3 (C, $\text{C}^{c'}$), 156.8 (C, $\text{C}^{g'}$), 172.7 (C, $\text{C}^{i'}$).

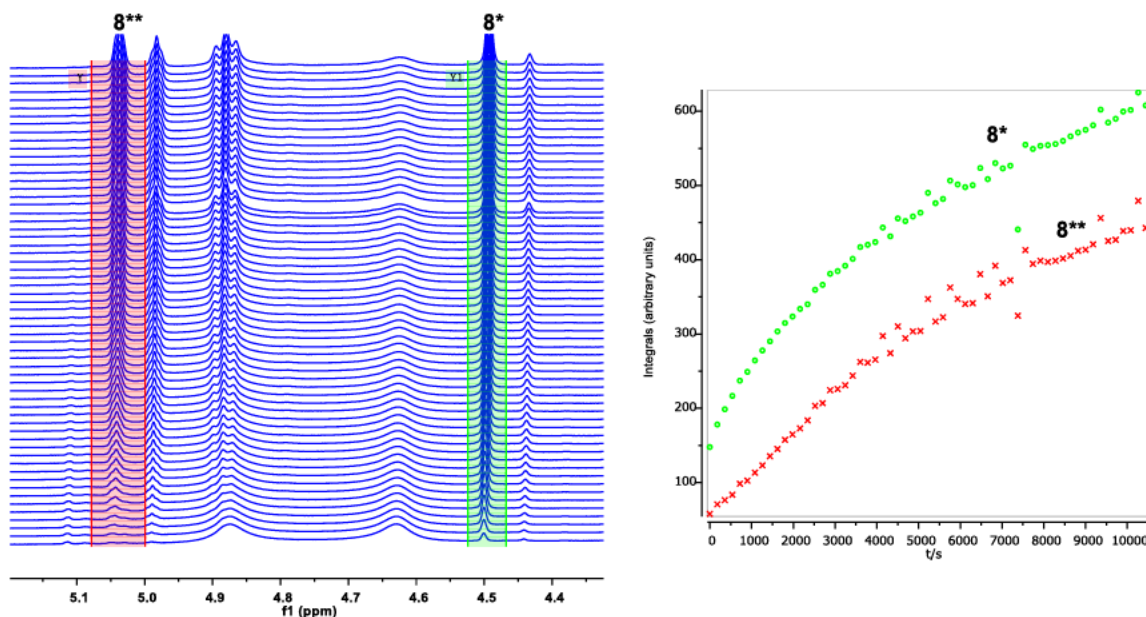
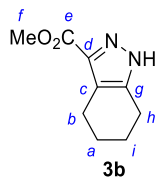


Figure S1. Kinetic monitoring of the reaction of **1** with **2a** in CDCl_3 at -20 °C: increase of the resonances assigned to **8*** (4.50 ppm, resonance and time-dependent integral marked in green color) and **8**** (5.04 ppm, resonance and time-dependent integral marked in red color).

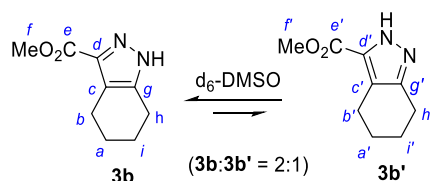
Reaction of methyl diazoacetate (**1**) with 1-pyrrolidinocyclohexene (**2b**)

Methyl 4,5,6,7-tetrahydro-1*H*-indazole-3-carboxylate (**3b**)^{1a,c,2} was obtained from **1** (203 mg, 2.03 mmol) and **2b** (304 mg, 2.01 mmol) in chloroform (1 mL) according to *GPA* (GC vial, room temperature, 9 days, eluent for column chromatography: n-pentane/diethyl ether = 1:1 ~ diethyl ether, recrystallization from CH_2Cl_2 /hexane): white powder (165 mg, 46%); mp 128.9 °C (lit.^{1a}, mp 127-128 °C)



¹H NMR (400 MHz, CDCl₃): δ = 1.76–1.81 (m, 4 H, H^{a,i}), 2.69 (t, *J* = 5.8 Hz, 2 H, H^b), 2.74 (t, *J* = 5.8 Hz, 2 H, H^b), 3.89 (s, 3 H, H^f), 11.4 (br s, 1 H, NH). **¹³C NMR** (101 MHz, CDCl₃): δ = 21.5 and 22.6 (2 × CH₂, C^b and C^h), 22.0 and 22.9 (2 × CH₂, C^a and Cⁱ), 51.7 (CH₃, C^f), 119.7 (C, C^c), 137.5 (C, C^d), 162.9 (C, C^e).² The signal intensity of C^g was too low to be assigned. The position of the proton bound to the nitrogen in **3b** was identified by single crystal X-ray analysis (see below). **HRMS** (ESI⁺) [M+Na]⁺: calcd for [C₉H₁₂N₂NaO₂]⁺: 203.0791, found 203.0791. **IR** (neat, ATR): 3182, 3125, 3079, 2941, 2860, 1730, 1453, 1411, 1353, 1262, 1234, 1193, 1142, 1049, 970, 932, 852, 812, 786 cm⁻¹.

NMR spectra of **3b** in *d*₆-DMSO solution suggest a mixture of tautomers, presumably **3b** and **3b'** in a ratio of 2:1. The chemical shifts for C^{a'} and C^{i'} in **3b'** could not be determined. The partially determined NMR data of **3b** and **3b'** in *d*₆-DMSO are listed below:



¹H NMR (400 MHz, *d*₆-DMSO): δ = 1.68 (br s, 6 H, H^{a,i,a',i'}), 2.58 (br s, 6 H, H^{b,h,b',h'}), 3.75 (s, 3 H, H^f), 3.80 (s, 1.4 H, H^f), 13.0 (s, 1 H, NH^{3b}), 13.4 (s, 0.5 H, NH^{3b'}). **¹³C NMR** (101 MHz, CDCl₃): δ = 20.5 and 21.2 (2 × CH₂, C^b and C^h), 21.9 and 22.6 (2 × CH₂, C^a and Cⁱ), 22.7, 22.9 (2 × CH₂, C^{b'} and C^{h'}), 51.0 (CH₃, C^f), 51.6 (CH₃, C^f), 117.7 (C, C^c), 119.7 (C, C^{c'}), 128.6 (C, C^d), 139.2 (C, C^d), 139.8 (C, C^g), 149.1 (C, C^{g'}), 160.0 (C, C^e), 163.3 (C, C^{e'}).

To get crystals of **3b** for X-ray analysis, the reaction of **1** (20.0 mg) with **2b** (30.5 mg) was carried out in pentane:diethyl ether = 1:1 (0.2 mL) at -26 °C for a month. **Single crystal X-ray crystallography** of the precipitated crystals showed the formation of **3b** (C₉H₁₂N₂O₂), which co-crystallized with pyrrolidinium chloride in a 1:1 ratio: (C₉H₁₂N₂O₂)·(C₄H₁₀N)·(Cl) (yv060).

Figure S2 shows the NMR spectroscopic monitoring of the reaction of **1** with **2b** in CDCl₃ at -30 °C. As the resonance of the olefinic proton of enamine **2b** decreases (δ = 4.22 ppm), the resonances of the intermediate(s) at δ = 6.42, 3.78, and 3.75 ppm increase initially, but then the resonances of the transient species vanish. Resonances of the intermediate(s) at 2.67 and 2.59 ppm appear at later stage of the reaction and keep steadily increasing at -30 °C. Though the structures of the intermediates could not be clarified, Figure S2 provides evidence for a stepwise reaction of **1** with **2b**.

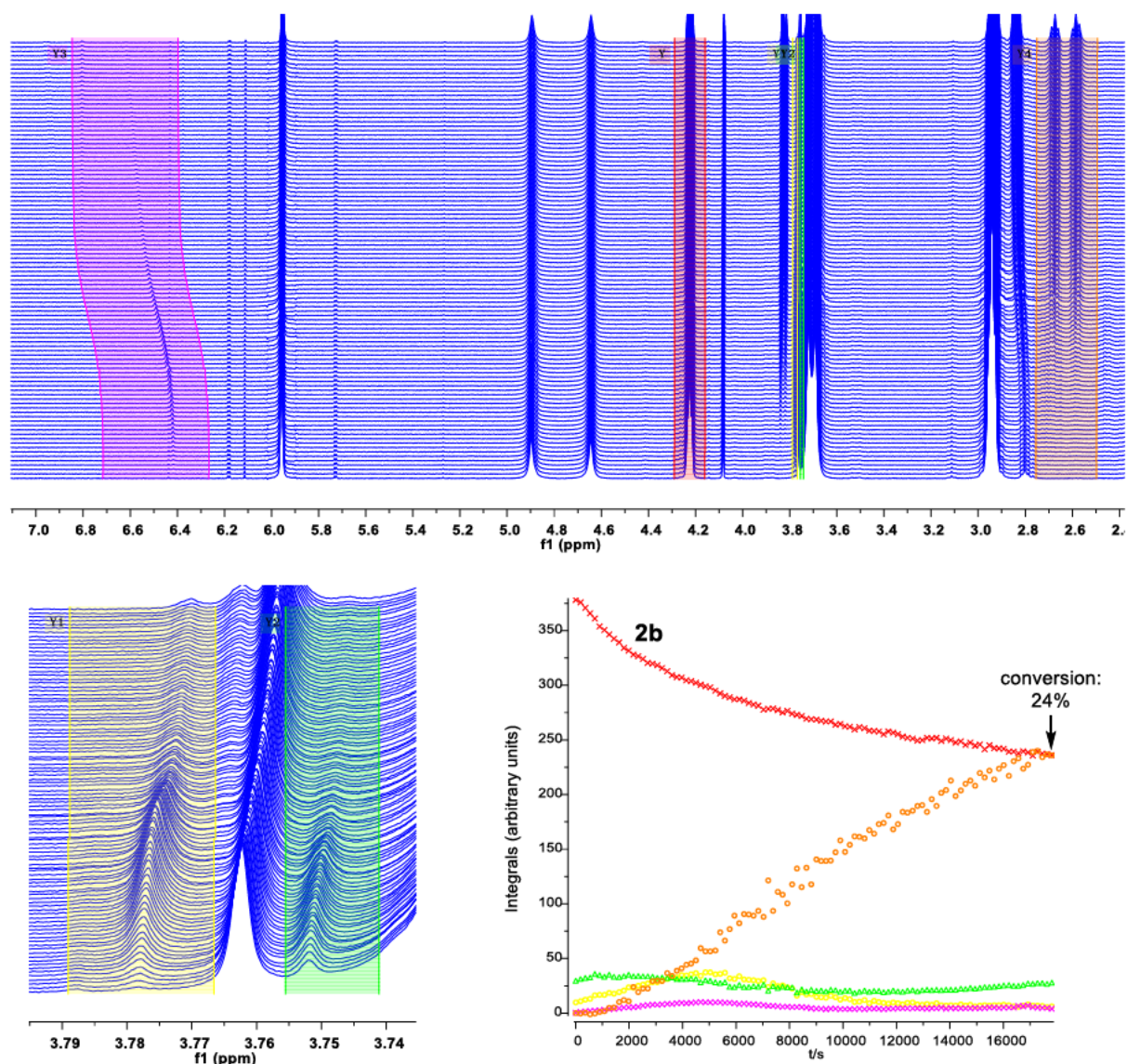
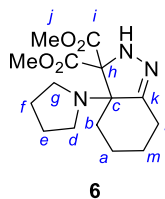


Figure S2. ^1H NMR spectroscopic monitoring of the initial phase of the reaction of **1** with **2b** in CDCl_3 at $-30\text{ }^\circ\text{C}$: decay of **2b** (4.22 ppm, resonance and time-dependent integral marked in red color) and emergence of unknown intermediates (6.42 ppm, resonance and time-dependent integral marked in magenta color, 3.78 ppm, resonance and time-dependent integral marked in yellow color, 3.75 ppm, resonance and time-dependent integral marked in lime color, 2.67 and 2.59 ppm, resonance and time-dependent integral marked in orange color).

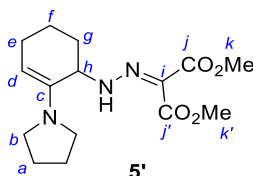
Reaction of dimethyl diazomalonate (**1'**) with 1-pyrrolidinocyclohexene (**2b**)

Dimethyl 3a-(pyrrolidin-1-yl)-2,3a,4,5,6,7-hexahydro-3H-indazole-3,3-dicarboxylate (6**)^{1a,c,3,4}** was obtained from **1'** (548 mg, 3.47 mmol) and **2b** (509 mg, 3.37 mmol) in diethyl ether (2 mL) according to *GP A* (round-bottom flask, room temperature, 1 week, recrystallization: hexane/EtOAc): colorless crystals (677 mg, 65%); mp $92.7\text{ }^\circ\text{C}$. Spectroscopic data agree with those reported in refs.^{1a,c,3,4}



¹H NMR (400 MHz, CDCl₃): δ = 1.21–1.38 (m, 2 H, H^{b,m}), 1.57 (tt, *J* = 11.9, 3.0 Hz, 2 H, H^a), 1.69 (t, *J* = 6.1 Hz, 4 H, H^{e,f}), 1.85 (ddd, *J* = 10.4, 4.9, 2.4 Hz, 1 H, H^b), 2.15 (td, *J* = 13.6, 5.4 Hz, 1 H, H^l), 2.47–2.54 (m, 2 H, H^{l,m}), 2.76–3.10 (br s, 4 H, H^{d,g}), 3.73 and 3.74 (2 s, 2 × 3 H, H^j), 6.16 (br s, 1 H, NH). **¹³C NMR** (101 MHz, CDCl₃): δ = 22.3 (CH₂, C^a), 25.5 (CH₂, C^{e,f}), 26.3 (CH₂, C^{b,l}), 35.1 (CH₂, C^m), 45.7 (CH₂, C^{d,g}), 52.9 and 53.2 (2 × CH₃, C^j), 78.2 (C, C^c), 78.3 (C, C^h), 156.0 (C, C^k), 168.2 and 169.6 (2 × C, Cⁱ). **HRMS** (ESI⁺) [M+Na]⁺: calculated for [C₁₅H₂₃N₃NaO₄]⁺: 332.1581 found 332.1579. **IR** (neat, ATR): 3353, 3315, 2939, 2863, 1736, 1720, 1456, 1436, 1429, 1413, 1260, 1227, 1122, 1089, 1038, 985, 933, 913, 788, 782, 704 cm⁻¹. **UV-vis** (CH₂Cl₂): λ_{max} = 230 nm (log ε = 0.83). **Single crystal X-ray crystallography** (**6**): C₁₅H₂₃N₃O₄ (wv097).

NMR monitoring of the reaction of **1'** with **2b** in CDCl₃ from -20 to +40 °C (Figure S3) showed the initial formation of open chain products **5'** and **5**, which then slowly transformed to the isolated cyclic product **6** at +40 °C.



NMR data of intermediate **5'**: **¹H NMR** (400 MHz, CDCl₃, -20 °C): δ = 1.31–1.42 and 1.52–1.54 (2 m, 2 H, H^f), 1.74–1.75 (m, 5 H, H^a and H^e), 1.99–2.01 (m, 1 H, H^e), 2.06–2.11 (m, 2 H, H^g), 2.87–2.90 (m, 4 H, H^b), 3.75 and 3.77 (2 s, 2 × 3 H, H^k and H^{k'}), 4.32 (s, 1 H, H^h), 4.43 (dd, *J* = 5.0, 2.8 Hz, 1 H, H^d), 11.6 (br, 1 H, NH). **¹³C NMR** (101 MHz, CDCl₃): δ = 17.5 (CH₂, C^f), 24.0 (CH₂, C^g), 24.4 (CH₂, C^a), 30.3 (CH₂, C^e), 47.5 (CH₂, C^b), 51.8 and 52.2 (2 × CH₃, C^k and C^{k'}), 58.0 (CH, C^h), 99.1 (CH, C^d), 116.0 (C, Cⁱ), 138.9 (C, C^c), 164.1 and 164.3 (2 × C, C^j and C^{j'}); some of the reported multiplet ranges for **5'** might be inaccurate due to significant superimposition with resonances of residual **1'** and **2b**.

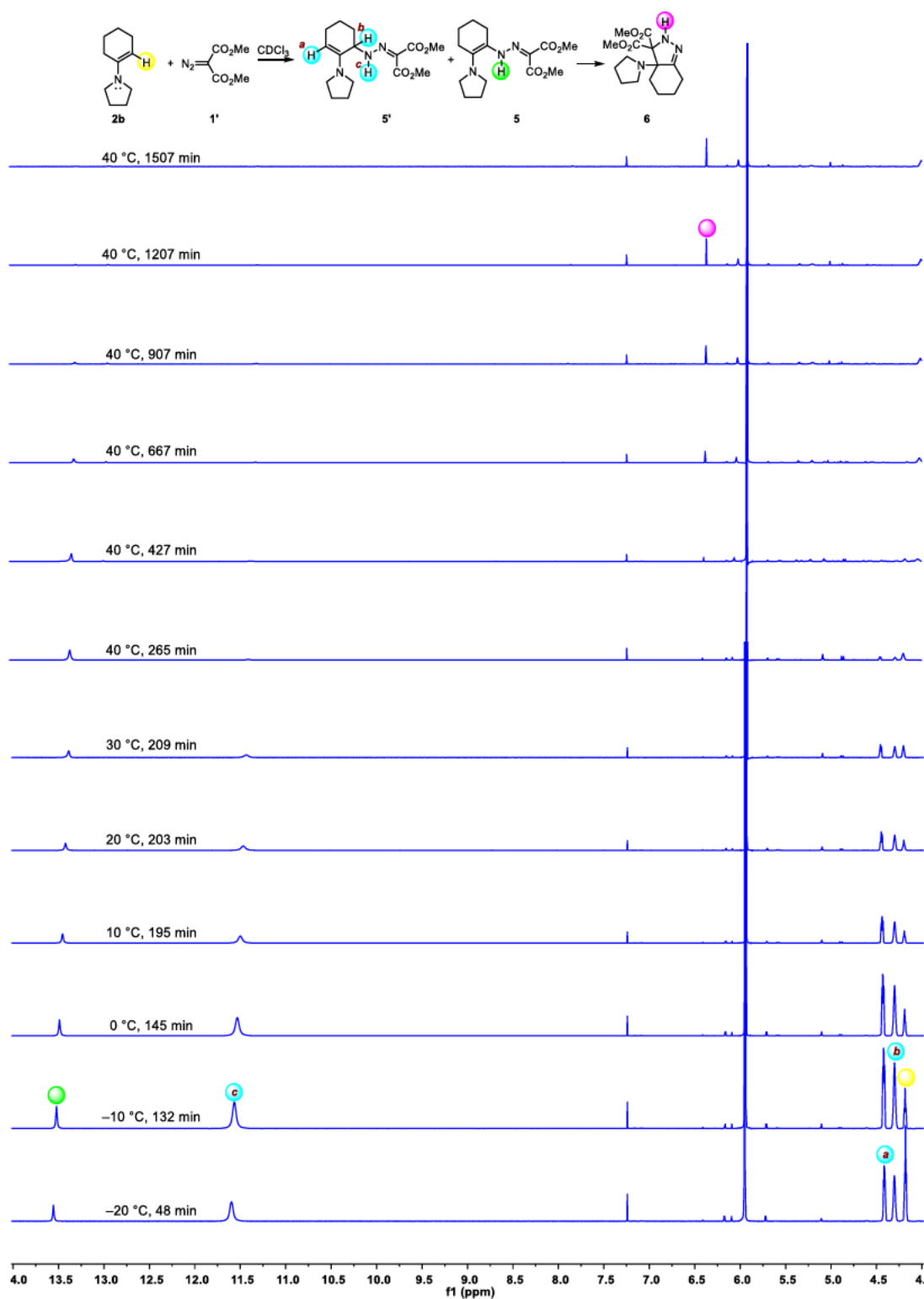


Figure S3. The reaction of 1' ($c_0 = 0.480$ M) with 2b ($c_0 = 0.465$ M) in CDCl₃ at -20 to 40 °C with 1,1,2,2-tetrachloroethane ($c = 0.340$ M) as internal standard monitored by ¹H NMR spectroscopy (400 MHz).

3.2.2 Kinetics

In the NMR kinetic measurement of the reactions of **1** with **2a** and **2b**, two sets of resonances for both the Me and the CH hydrogens in **1** were detected (Figure S4, at -40 and -30 °C), which are caused by conformers of **1**, due to hindered rotation around the C–C bond.

To measure the rotation barrier of the C–C bond in **1** (Figure S4a), the ^1H NMR spectra (400 MHz) of **1** ($c = 0.424$ M solution) were measured in CD_2Cl_2 at various temperatures ($-50 \sim -4$ °C, Figure S4b). Line shape analysis of the α -hydrogen resonances of **1** was performed by fitting the experimental measurements by the program DNMR5 software (Figure S4c)^{5a-b} to determine the exchange rate constants k_{ex} (s^{-1}) in the temperature range between -50 and -4 °C (Figure S4d). Then, an Eyring plot (Figure S4e) was used to determine the rotation barrier ΔG^\ddagger of 52.2 kJ mol^{-1} ($= 12.5$ kcal mol^{-1}), consistent with reported value.^{5c}

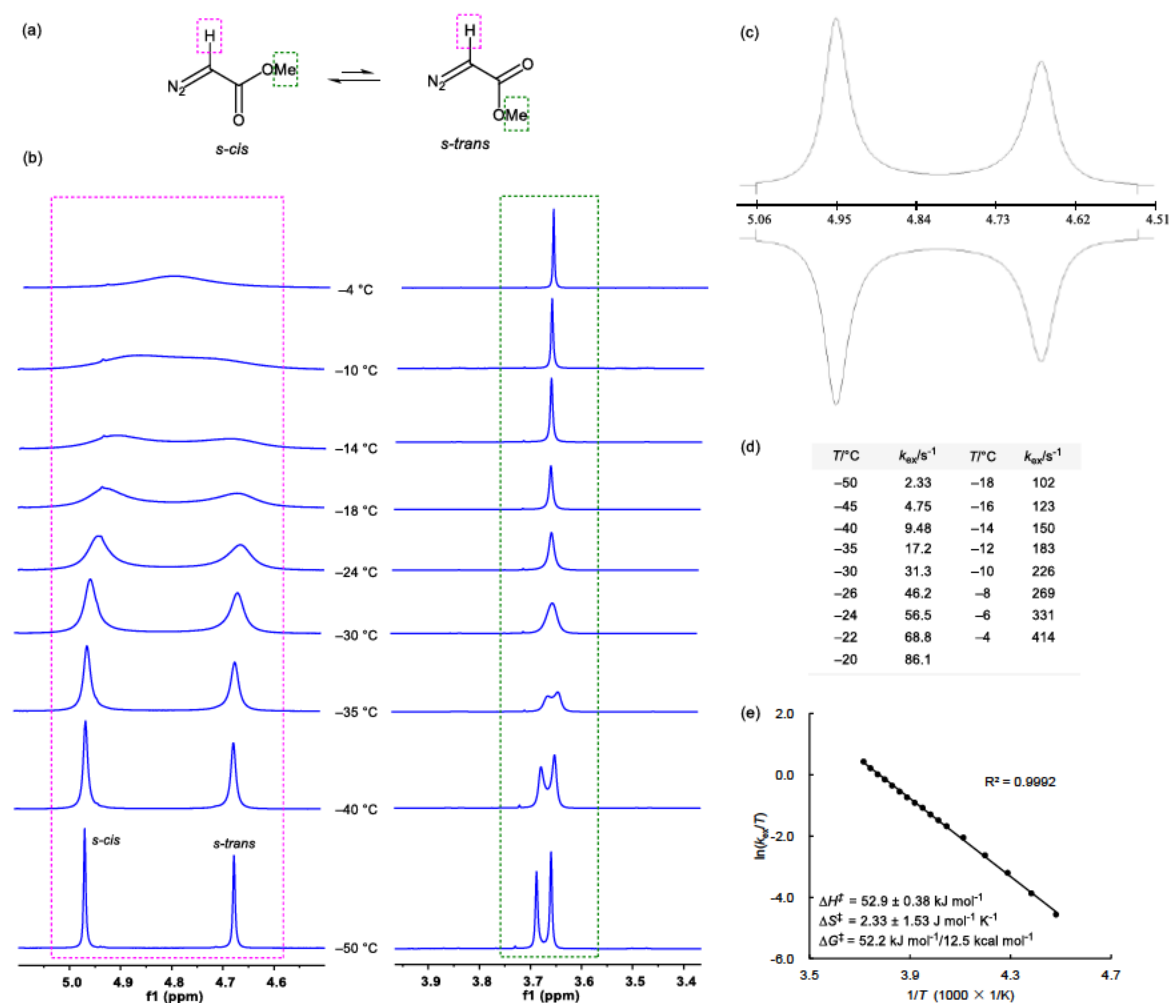


Figure S4. (a) *S-cis* and *s-trans* rotamers of **1**. (b) Stack of the ^1H NMR spectral sections (400 MHz) with resonance for the α -CH hydrogen and the methyl group hydrogens, respectively, of **1** ($c = 0.424$ M) in CD_2Cl_2 at $-50 \sim -4$ °C. (c) Experimental (above) and DNMR5 fitted resonances of the α -CH hydrogen in **1** at -26 °C. (d) Temperature-dependent DNMR exchange rate constants k_{ex} (s^{-1}) of **1** in CD_2Cl_2 . (e) Eyring plot for the exchange rate constants k_{ex} (s^{-1}), at $-50 \sim -4$ °C.

In Figure S5, the two resonances of the CH group in **1** (at 4.90 and 4.64 ppm, *cis/trans* = 1/0.9) decay equally fast during the kinetic measurement of the reaction of **1** with **2b** at $-30\text{ }^{\circ}\text{C}$ (see Table S1). At each of the relevant temperatures, the rotation in **1** occurs faster (on the second to millisecond time scale) than the reaction with the enamines **2a** or **2b** (hours time scale).

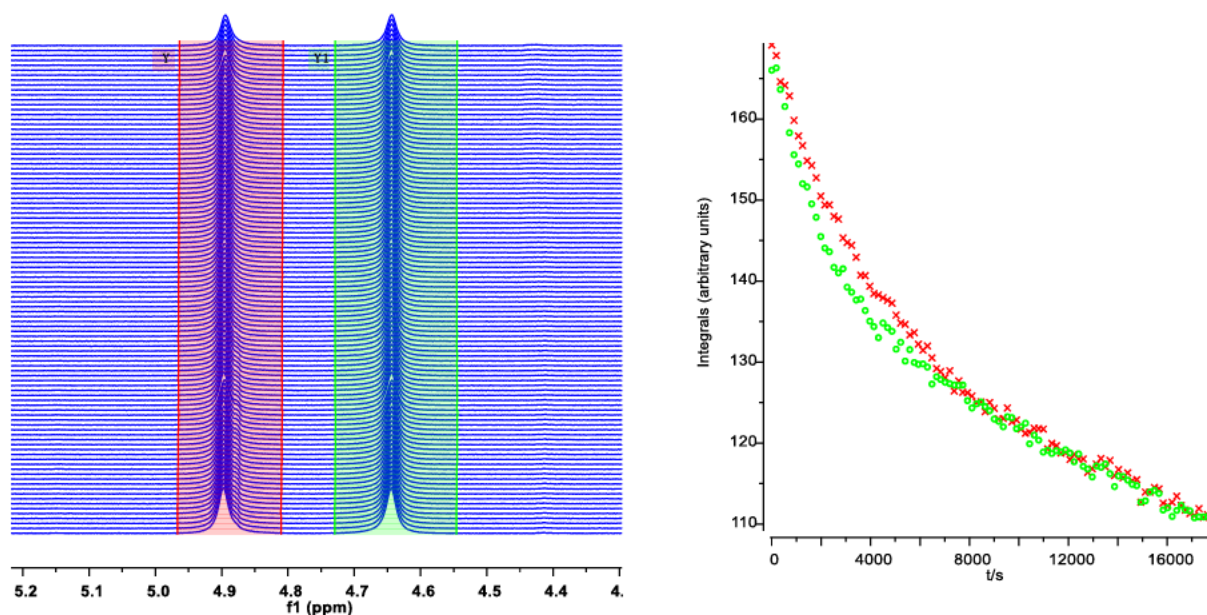


Figure S5. ¹H NMR spectroscopic monitoring of the initial phase of the reaction of **1** with **2b** in CDCl₃ at $-30\text{ }^{\circ}\text{C}$: the decrease of both resonances assigned to the CH groups of the **1** conformers is equally fast.

Table S1. k_2^{exptl} of the reactions of **1** with **2a** in CDCl_3 at -40 (A), -30 (B), -20 (C), -10 °C (D) (^1H NMR kinetics, 1,1,2,2-tetrachloroethane as the internal standard IS). Activation parameters from Eyring plot (E) were used to calculate $\Delta G^\ddagger(25^\circ\text{C})$ and k_2 at $+25$ and $+80.3$ °C. Initial reactant concentrations were determined by using the integration ranges of the IS from -40 °C to -10 °C at 6.05–5.85, 6.05–5.85, 6.00–5.89, 6.05–5.85 ppm, respectively, of the vinylic hydrogen of **2a** at 4.02–3.955, 4.02–3.955, 4.02–3.94, 4.04–3.95 ppm, respectively, of the CH_3 hydrogen of **1** at -40 , -20 and -10 °C at 3.76–3.64, 3.745–3.67, 3.74–3.68 ppm, respectively. The integration range of the $\alpha\text{-CH}$ hydrogen of **1** at -30 °C is 4.98–4.54 ppm. Relaxation delay and acquisition time are always 0.10 and 3.65 s, respectively.

T (°C)	$[\mathbf{1}]_0$ (M)	$[\mathbf{2a}]_0$ (M)	$[\text{IS}]_0$ (M)	k_2^{exptl} ($\text{M}^{-1} \text{s}^{-1}$)	k_2 ($\text{M}^{-1} \text{s}^{-1}$)	ΔG^\ddagger (kJ mol^{-1})
-40	3.99×10^{-1}	3.71×10^{-1}	2.76×10^{-1}	1.44×10^{-4}		
-30	3.74×10^{-1}	4.16×10^{-1}	2.63×10^{-1}	2.46×10^{-4}		
-20	3.85×10^{-1}	3.82×10^{-1}	1.88×10^{-1}	3.40×10^{-4}		
-10	3.73×10^{-1}	3.64×10^{-1}	2.70×10^{-1}	6.25×10^{-4}		
+25					$(2.17 \pm 0.38) \times 10^{-3}$	88.2
+80.3					$(1.03 \pm 0.32) \times 10^{-2}$	

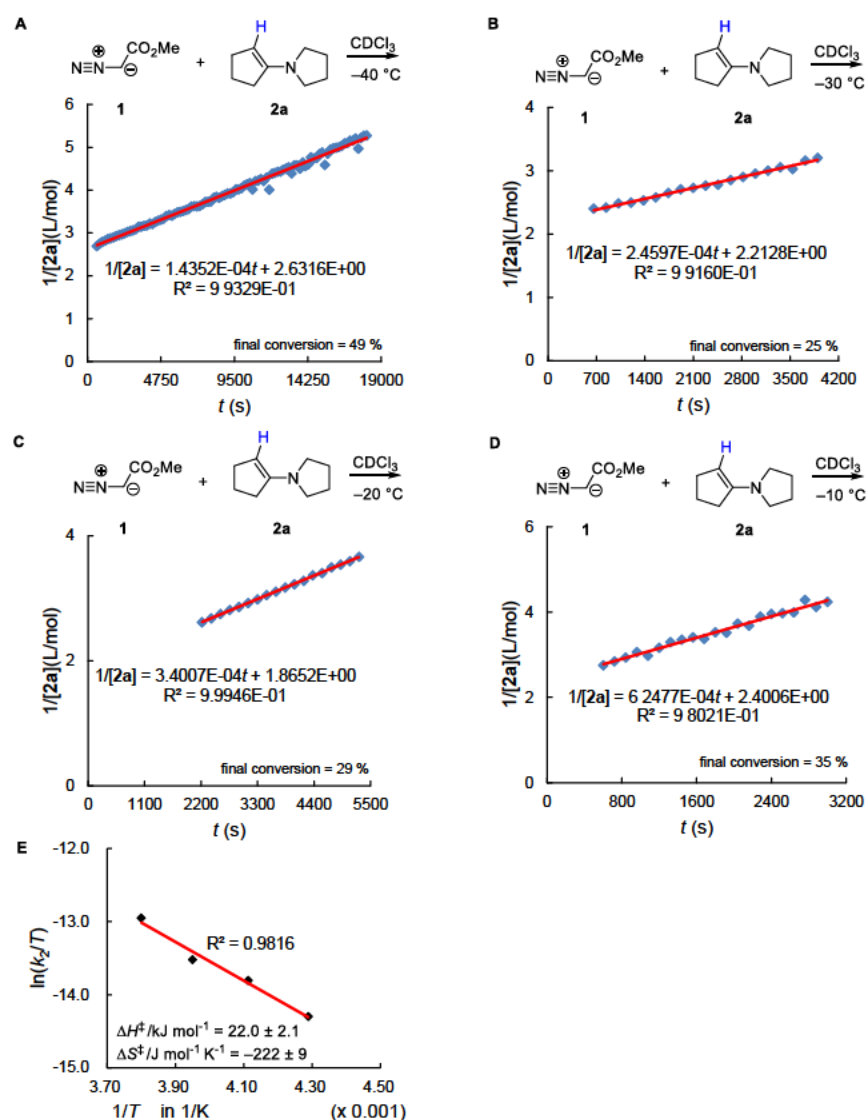
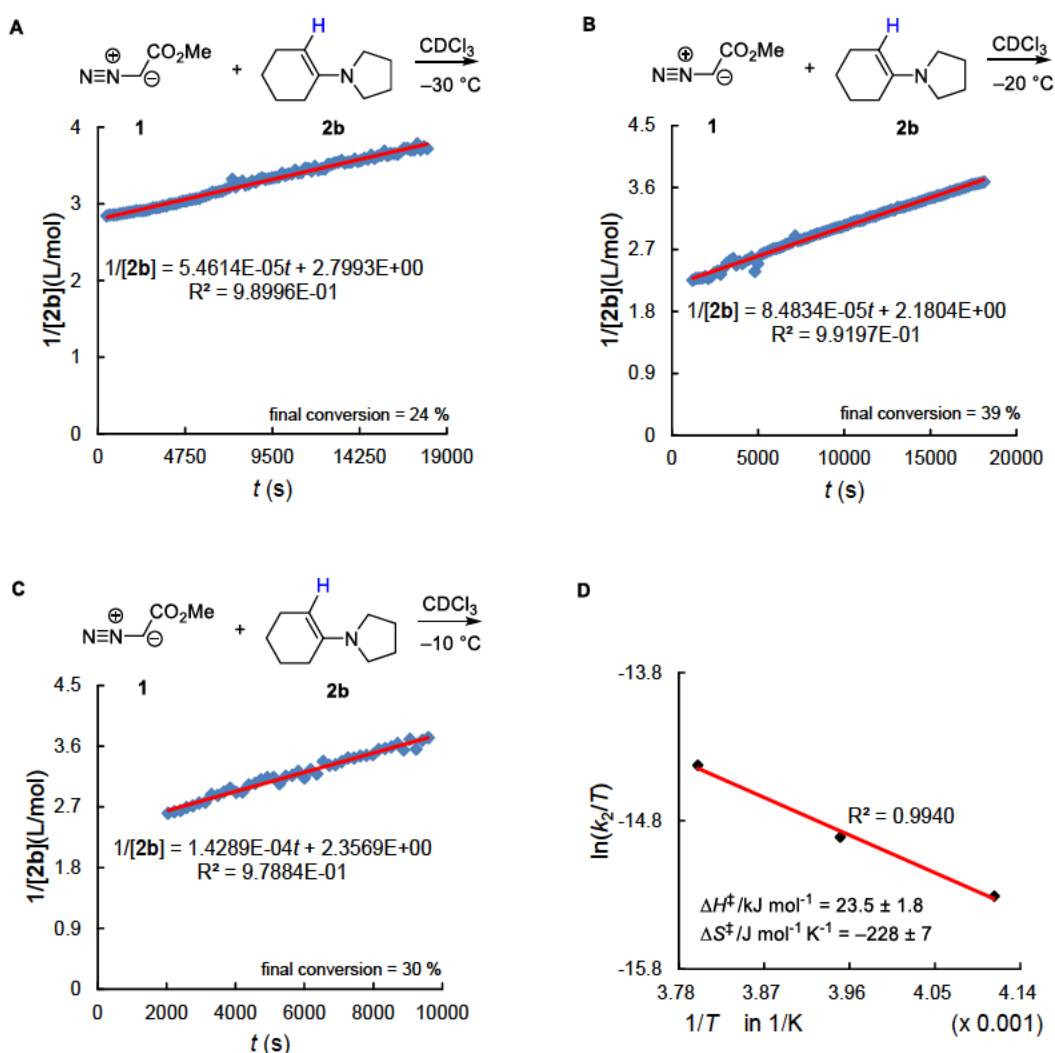
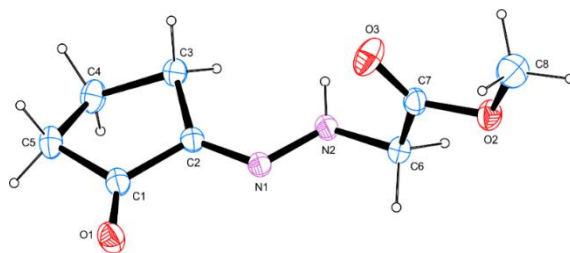


Table S2. Kinetics of the reactions of **1** with **2b** in CDCl₃ at -30 (A), -20 (B), -10 °C (C) (¹H NMR kinetics, 1,1,2,2-tetrachloroethane as the internal standard IS). Activation parameters from Eyring plot (D) were used to calculate $\Delta G^\ddagger(25^\circ\text{C})$ and k_2 at +25 and +80.3 °C. Initial reactant concentrations were determined by using the integration ranges of the IS from -30 °C to -10 °C at always 6.08–5.80 ppm, of the vinylic hydrogen of **2b** at always 4.29–4.16 ppm, of the CH₃ hydrogen of **1** at 3.75–3.63, 3.745–3.63, 3.75–3.66 ppm. Relaxation delay and acquisition time are always 0.10 and 3.65 s, respectively.

T (°C)	$[\mathbf{1}]_0$ (M)	$[\mathbf{2b}]_0$ (M)	$[\text{IS}]_0$ (M)	k_2^{exptl} (M ⁻¹ s ⁻¹)	k_2 (M ⁻¹ s ⁻¹)	ΔG^\ddagger (kJ mol ⁻¹)
-30	3.64×10^{-1}	3.52×10^{-1}	2.49×10^{-1}	5.46×10^{-5}		
-20	4.65×10^{-1}	4.44×10^{-1}	2.76×10^{-1}	8.48×10^{-5}		
-10	4.11×10^{-1}	3.84×10^{-1}	3.16×10^{-1}	1.43×10^{-4}		
+25					$(5.59 \pm 0.74) \times 10^{-4}$	91.6
+80.3					$(2.91 \pm 0.73) \times 10^{-3}$	



3.2.3 Single Crystal X-ray Crystallography

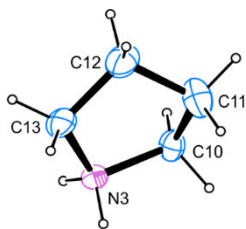
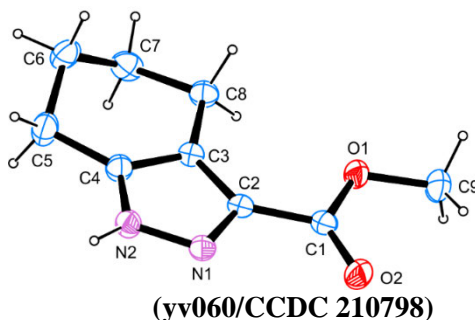
Methyl (*E*)-((2-oxocyclopentylidene)amino)glycinate (**4a**)

(xv798/CCDC 2102952)

Crystallographic data.

net formula	C ₈ H ₁₂ N ₂ O ₃
<i>M_r</i> /g mol ⁻¹	184.20
crystal size/mm	0.100 × 0.030 × 0.030
<i>T</i> /K	102.(2)
radiation	MoK α
diffractometer	'Bruker D8 Venture TXS'
crystal system	monoclinic
space group	'P 1 21/c 1'
<i>a</i> /Å	8.6488(7)
<i>b</i> /Å	13.5518(10)
<i>c</i> /Å	7.5975(6)
α /°	90
β /°	90.245(3)
γ /°	90
<i>V</i> /Å ³	890.47(12)
<i>Z</i>	4
calc. density/g cm ⁻³	1.374
μ /mm ⁻¹	0.106
absorption correction	Multi-Scan
transmission factor range	0.93–1.00
refls. measured	10047
<i>R</i> _{int}	0.0356
mean $\sigma(I)/I$	0.0264
θ range	2.681–26.370
observed refls.	1727
<i>x</i> , <i>y</i> (weighting scheme)	0.0253, 0.3880
hydrogen refinement	H(C) constr, H(N) reffall
refls in refinement	1821
parameters	124
restraints	0
<i>R</i> (<i>F</i> _{obs})	0.0347
<i>R</i> _w (<i>F</i> ²)	0.0795
<i>S</i>	1.102
shift/error _{max}	0.001
max electron density/e Å ⁻³	0.163
min electron density/e Å ⁻³	-0.172

Pseudomerohedral twin, BASF refined to 0.26.

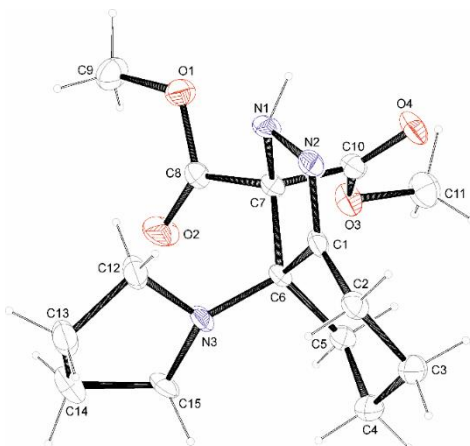
Methyl 4,5,6,7-tetrahydro-1*H*-indazole-3-carboxylate (3b)
 Cl1
**Crystallographic data.**

net formula	C ₁₃ H ₂₂ ClN ₃ O ₂
<i>M_r</i> /g mol ⁻¹	287.78
crystal size/mm	0.080 × 0.040 × 0.030
<i>T</i> /K	102.(2)
radiation	MoKα
diffractometer	'Bruker D8 Venture TXS'
crystal system	triclinic
space group	'P -1'
<i>a</i> /Å	8.2892(6)
<i>b</i> /Å	9.0891(7)
<i>c</i> /Å	10.0072(7)
α/°	99.156(3)
β/°	90.021(2)
γ/°	93.010(3)
<i>V</i> /Å ³	743.29(9)
<i>Z</i>	2
calc. density/g cm ⁻³	1.286
μ/mm ⁻¹	0.260
absorption correction	Multi-Scan
transmission factor range	0.94–0.99
refls. measured	12989
<i>R</i> _{int}	0.0426
mean σ(<i>I</i>)/ <i>I</i>	0.0392
θ range	3.197–27.482
observed refls.	2948
<i>x</i> , <i>y</i> (weighting scheme)	0.0340, 0.4466
hydrogen refinement	H(C) constr, H(N) reffall

refls in refinement	3373
parameters	194
restraints	0
$R(F_{\text{obs}})$	0.0403
$R_w(F^2)$	0.0998
S	1.064
shift/error _{max}	0.001
max electron density/e \AA^{-3}	0.536
min electron density/e \AA^{-3}	-0.274

Disorder described by a split model, sof ratio refined to 0.81/0.19, disordered atoms of minor part refined isotropically.

Dimethyl 3a-(pyrrolidin-1-yl)-2,3a,4,5,6,7-hexahydro-3H-indazole-3,3-dicarboxylate (6)



(wv097/CCDC 2102956)

Crystallographic data.

net formula	$\text{C}_{15}\text{H}_{23}\text{N}_3\text{O}_4$
$M_r/\text{g mol}^{-1}$	309.36
crystal size/mm	$0.090 \times 0.060 \times 0.040$
T/K	100.(2)
radiation	MoK α
diffractometer	'Bruker D8 Venture TXS'
crystal system	triclinic
space group	'P -1'
$a/\text{\AA}$	8.3250(3)
$b/\text{\AA}$	12.1239(5)
$c/\text{\AA}$	15.1683(7)
$\alpha/^\circ$	88.910(2)
$\beta/^\circ$	85.091(2)
$\gamma/^\circ$	85.7000(10)
$V/\text{\AA}^3$	1520.93(11)
Z	4
calc. density/ g cm^{-3}	1.351
μ/mm^{-1}	0.099
absorption correction	Multi-Scan
transmission factor range	0.92–1.00

refls. measured	15740
R_{int}	0.0395
mean $\sigma(I)/I$	0.0495
θ range	3.161–26.370
observed reffs.	5058
x, y (weighting scheme)	0.0789, 0.7652
hydrogen refinement	H(C) constr, H(N) refall
refls in refinement	6189
parameters	419
restraints	0
$R(F_{\text{obs}})$	0.0513
$R_w(F^2)$	0.1449
S	1.020
shift/error _{max}	0.001
max electron density/e \AA^{-3}	0.445
min electron density/e \AA^{-3}	-0.297

Disorder in one of the two molecules of the asymmetric unit described by a split model, anisotropic refinement, sof ratio 0.7/0.3.

One of the two molecules (the one without disorder) is depicted above.

3.2.4 References

- (1) a) Reissig, H.-U. Dissertation, Ludwig-Maximilians-Universität München, **1978**. b) Huisgen, R.; Bihlmaier, W.; Reissig, H.-U. *Angew. Chem. Int. Ed.* **1979**, *18*, 331–332. c) Huisgen, R.; Reissig, H.-U. *Angew. Chem. Int. Ed.* **1979**, *18*, 330–331. d) Bihlmaier, W.; Huisgen, R.; Reissig, H.-U.; Voss, S. *Tetrahedron Lett.* **1979**, *20*, 2621–2624.
- (2) Wang, L.; Huang, J. Y.; Gong, X. J.; Wang, J. *Chem. Eur. J.* **2013**, *19*, 7555–7560.
- (3) Galloway, N.; Dent, B. R.; Halton, B. *Aust. J. Chem.* **1983**, *36*, 593–599.
- (4) Dietrich-Buchecker, C.; Franck-Neumann, M. *Tetrahedron* **1977**, *33*, 745–749.
- (5) a) Stephenson, D. S.; Binsch, G. *J. Magn. Res.* **1978**, *32*, 145–152. b) Stephenson, D. S. Programm DNMR5, Ludwig-Maximilians-Universität München, **1994**. c) Kaplan, F.; Meloy, G. K. *J. Am. Chem. Soc.* **1966**, *88*, 950–956.

Chapter 4. Quantification of the Electrophilicities of Diazoalkanes: Kinetics and Mechanism of Azo Couplings with Enamines and Sulfonium Ylides

Li, L.; Mayer, R. J.; Stephenson, D. S.; Mayer, P.; Ofial, A. R.; Mayr, H. *Chem. Eur. J.* **2022**, 28, e202201376.

Author Contributions

Li, L. performed all the experiments. Mayer, P. characterized the single crystal X-ray structures. Stephenson, D. S. measured the low temperature NMR kinetics. Mayer, R. J. conducted the DFT calculations. The manuscript was drafted by Li, L. and jointly revised by Li, L., Mayer, R. J., Ofial, A. R. and Mayr, H.

Copyright

Reproduced with permission from: Li, L.; Mayer, R. J.; Stephenson, D. S.; Mayer, P.; Ofial, A. R.; Mayr, H. *Chem. Eur. J.* **2022**, 28, e202201376. Copyright 2022 John Wiley & Sons, Inc.

Parts of the supporting data are presented in section 4.2. The complete supporting information is available under the following link:

<https://chemistry-europe.onlinelibrary.wiley.com/doi/full/10.1002/chem.202201376>

4.1 Copies of Manuscript

Quantification of the Electrophilicities of Diazoalkanes: Kinetics and Mechanism of Azo Couplings with Enamines and Sulfonium Ylides

Le Li,^[a] Robert J. Mayer,^[b] David S. Stephenson,^[a] Peter Mayer,^[a] Armin R. Ofial,^{*[a]} and Herbert Mayr^{*[a]}

Dedicated to Professor Paul Knochel in recognition of his outstanding contributions to modern metalorganic chemistry.

Abstract: Kinetics and mechanism of the reactions of methyl diazoacetate, dimethyl diazomalonate, 4-nitrophenyldiazomethane, and diphenyldiazomethane with sulfonium ylides and enamines were investigated by UV-Vis and NMR spectroscopy. Ordinary alkenes undergo 1,3-dipolar cycloadditions with these diazo compounds. In contrast, sulfonium ylides and enamines attack at the terminal nitrogen of the diazo alkanes to give zwitterions, which undergo various subsequent reactions. As only one new bond is formed in the rate-determining step of these reactions, the correlation

$\lg k_2(20^\circ\text{C}) = s_N(N + E)$ could be used to determine the one-bond electrophilicities E of the diazo compounds from the measured second-order rate constants and the known reactivity indices N and s_N of the sulfonium ylides and enamines. The resulting electrophilicity parameters ($-21 < E < -18$), which are 11–14 orders of magnitude smaller than that of the benzenediazonium ion, are used to define the scope of one-bond nucleophiles which may react with these diazoalkanes.

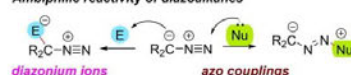
Introduction

Diazoalkanes are versatile reagents for organic synthesis. They are widely used 1,3-dipoles that react with dipolarophiles to give five-membered heterocycles (Huisgen reactions).^[1] As ambiphilic reagents they have the ability to react with electrophiles as well as with nucleophiles (Scheme 1). While electrophiles attack at the carbon atom to yield diazonium ions, nucleophiles attack at the terminal nitrogen to yield azo compounds.^[2] Mechanistically, the attack of a nucleophile at the terminal nitrogen of the diazoalkane parallels the well-known azo couplings of diazonium ions.^[3]

Azo coupling of diazonium ions with nucleophiles



Ambiphilic reactivity of diazoalkanes



Scheme 1. Reactions of diazoalkanes with electrophiles and nucleophiles and mechanistically analogous azo couplings with diazonium ions.

Kinetic investigations of the reactions of diazoalkanes with a series of benzydrylium ions (Aryl_2CH^+) of known electrophilicity E have previously been performed to characterize the nucleophilicities of diazoalkanes, which are described by the parameters N and s_N in Equation (1).^[4]

$$\lg k_{20^\circ\text{C}} = s_N(N + E) \quad (1)$$

In this way, diazoalkanes have been integrated in the currently most comprehensive nucleophilicity scales^[5] showing that diazomethane has a nucleophilic reactivity comparable to enamines, whereas stabilized diazoalkanes, such as diazoacetates and diphenyldiazomethane, have nucleophilic reactivities similar to silylated enol ethers and allylsilanes (Figure 1). The least nucleophilic diazoalkanes characterized so far were diazomalonates with N parameters slightly lower than those of 1,1-dialkylethylenes and styrene. Based on these comparisons it

[a] L. Li, Dr. D. S. Stephenson, Dr. P. Mayer, Dr. A. R. Ofial, Prof. Dr. H. Mayr
Department Chemie
Ludwig-Maximilians-Universität München
Butenandstr. 5–13, 81377 München (Germany)
E-mail: ofial@lmu.de
herbert.mayr@cup.uni-muenchen.de
Homepage: www.cup.uni-muenchen.de/oc/ofial/
www.cup.uni-muenchen.de/oc/mayr/

[b] Dr. R. J. Mayer
Institut des Science et d'Ingénierie Supramoléculaires (ISIS)
Université de Strasbourg & CNRS
8 Allée Gaspard Monge, 67000 Strasbourg (France)

Supporting information for this article is available on the WWW under <https://doi.org/10.1002/chem.202201376>

© 2022 The Authors. Chemistry – A European Journal published by Wiley-VCH GmbH. This is an open access article under the terms of the Creative Commons Attribution Non-Commercial License, which permits use, distribution and reproduction in any medium, provided the original work is properly cited and is not used for commercial purposes.

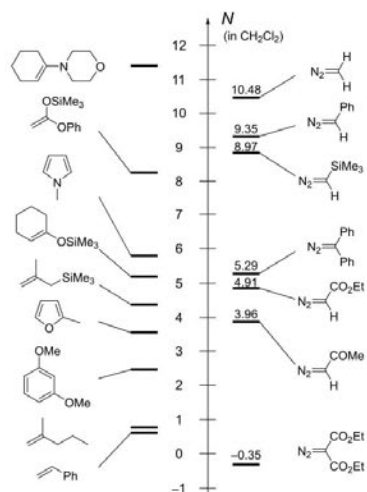


Figure 1. Comparison of the nucleophilicity parameters N of diazoalkanes (N in CH_2Cl_2 from Ref. [4a]) with those of other $\pi_{\text{C}=\text{C}}$ -nucleophiles (N in CH_2Cl_2 from Ref. [5f]).

was possible to derive a general ordering principle for the reactions of diazoalkanes with electrophiles.^[4a]

We have now complemented this work by an analogous quantification of the electrophilicities E of the α -diazoesters **1a** and **1b**, p -nitrophenyldiazomethane (**1c**), and diphenyldiazomethane (**1d**) (Figure 2) by studying the rates of their reactions with the sulfonium ylides **2a–b** and the enamines **3a–e** as reference nucleophiles. The nucleophile-specific reactivity descriptors N and s_N of **2** and **3**, needed for these derivations by Equation (1), have previously been derived from the rates of

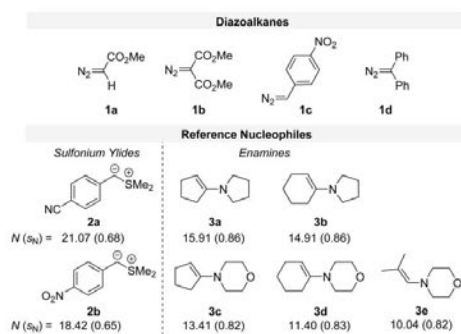


Figure 2. Diazoalkanes **1** and nucleophiles (N and s_N parameters of **2** in DMSO ^[6a] and of **3** in dichloromethane^[6b,6c]) used in this work for determining the electrophilicities E of **1a–d**.

Chem. Eur. J. 2022, 28, e202201376 (2 of 13)

their reactions with benzhydrylium ions and structurally related quinone methides (Figure 2).

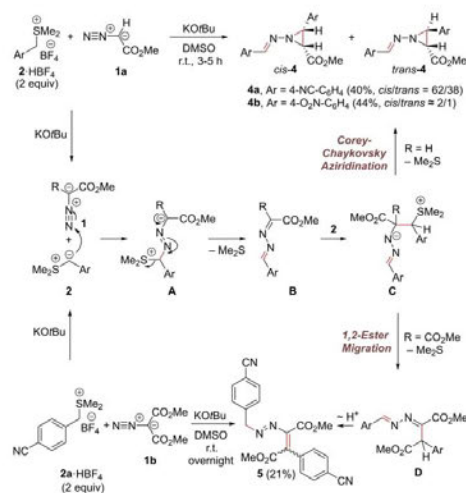
Prerequisite for the applicability of Equation (1) is a reaction mechanism, in which one, and only one, new σ -bond is generated in the rate-determining step.^[5] Though earlier work had claimed concerted 1,3-dipolar cycloadditions of diazoacetate **1a** and diazomalonate **1b** with pyrrolidincyclohexene **3b**,^[7a,c] we have recently demonstrated that these reactions proceed via rate-determining formation of azo coupling products, which undergo subsequent cyclizations.^[6] Thus, the measured rate constants for these reactions reflect the one-bond electrophilicities of the diazoalkanes, as needed for our analysis.

Herein, we report on the reactions of the diazoalkanes **1** with sulfonium ylides **2** and enamines **3**. The second-order rate constants of these reactions are used for determining the one-bond electrophilicities E of diazoalkanes **1a–d**. By demonstrating that the E values thus obtained allow one to rationalize previously reported azo couplings of diazoalkanes, it is shown that these parameters reflect the electrophilic potential of diazoalkanes and enable synthetic chemists to predict the scope of nucleophiles accessible for azo couplings with **1**.

Results and Discussion

Product analysis of the reactions of **1a–b** with the sulfonium ylides **2a–b**

Methyl diazoacetate **1a** reacts with two equivalents of the sulfonium ylides **2a** and **2b** in DMSO to give mixtures of *cis/trans* aziridines **4** with a total yield of about 40% (Scheme 2). Their formation can be explained by attack of **2** at the N



Scheme 2. Reactions of diazoalkanes **1** with sulfonium ylides **2**.

© 2022 The Authors. Chemistry - A European Journal published by Wiley-VCH GmbH

terminus of **1a** (\rightarrow A) followed by elimination of Me_2S to give a 2,3-diazabuta-1,3-diene (**B**), which reacts with a second equivalent of **2** to yield **C**. An intramolecular nucleophilic substitution eventually furnishes the aziridines **4** (Scheme 2). An analogous Corey-Chaykovsky reaction of electrophilic 2,3-diazabutadienes affording aziridines has previously been reported.^[9]

The formation of the azo compound **5** from **1b** with **2a** (Scheme 2) can analogously be explained by attack of a second equivalent of **2a** at the intermediate **B**. The resulting zwitterion **C** ($\text{R}=\text{CO}_2\text{Me}$) does not cyclize as in the case of $\text{R}=\text{H}$, but undergoes 1,2-ester migration concomitantly with or after Me_2S elimination to form **D** which gives **5** by a proton shift (Scheme 2). Related reactions of diazoalkanes with sulfonium ylides giving 2:1-products have recently been reported.^[10]

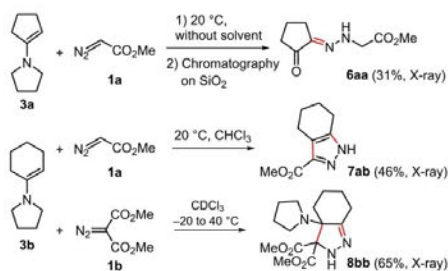
Products of the reactions of diazoalkanes with 1-(dialkylamino)cycloalkenes **3(a–d)**

In recent work, we have confirmed the formation of **6aa**, **7ab** and **8bb** by the reactions of diazoacetate **1a** and diazomalonnate **1b** with pyrrolidinocyclopentene **3a** and pyrrolidinocyclohexene **3b** (Scheme 3).^[7,8]

In contrast to earlier statements^[7c] we found, however, that the heterocycles **7ab** and **8bb** are not formed via concerted 1,3-dipolar cycloadditions, but via azo couplings to give hydrazoneenamines **9** and other tautomers of the initially formed zwitterions E_F and E_Z , which undergo subsequent cyclizations (Scheme 4). We now report that Scheme 4, which has been shown to rationalize the mechanisms of the formation of **6aa**, **7ab**, and **8bb** can also be used to explain the products and mechanisms of other combinations of the diazoalkanes **1a–d** with enamines **3a–e**.

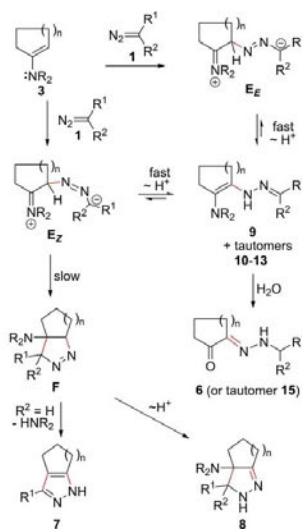
Reactions of diazoalkanes **1** with the 1-(dialkylamino)cyclopentenes **3a** and **3c**

In line with an earlier report by Huisgen, Bihlmaier, and Reissig,^[7b] combination of diazomalonnate **1b** with pyrrolidinocyclopentene **3a** in Et_2O at 0°C resulted in the precipitation of



Scheme 3. Products of the reactions of diazoacetate **1a** and diazomalonnate **1b** with the enamines **3a** and **3b**.

Chem. Eur. J. 2022, 28, e202201376 (3 of 13)



Scheme 4. Mechanism for the reactions of diazoalkanes **1** with enamines **3**. Note: In designating specific reaction products, the first letter refers to the diazoalkane precursor, and the second letter specifies the enamine precursor; thus product **9ba** refers to structure **9** formed from diazoalkane **1b** and enamine **3a**.

brick-red needles (yield: 90%). The identity of the precipitated material was attributed by Huisgen et al. to the zwitterionic structure **Eba**.^[7b] However, when we analyzed the precipitate by NMR and UV-Vis spectroscopy as well as by single crystal X-ray crystallography, we identified the red needles as the hydrazoneenamine **9ba** (Figure 3; UV-vis spectrum in Supporting Information: Figure S2a, black curve). From the electron densities calculated using X-ray diffraction data, a hydrogen bond from N2 to O4 (Figure 3a) was derived.

When isolated **9ba** was dissolved in CDCl_3 at -50°C , only the signals of **9ba** were seen in the ^1H and ^{13}C NMR spectra (pp. S58–S59, Supporting Information). When this sample was warmed up to 20°C , tautomerization led to a 2:3:5 mixture of **9ba**, **11ba**, and **12ba**, the ratio of which was derived from the ^1H NMR signals at $\delta = 2.77$ (t, **9ba**), 5.25 (s, **11ba**), and 4.86 ppm (d, **12ba**). A signal of low intensity at $\delta = 4.26$ ppm, which appeared during warming up at 0°C and disappeared at 20°C , was probably due to traces of **10ba** (Figure S3). As depicted in Figure S2a, the UV-vis spectrum of the red needles (**9ba**) measured at -50°C in CHCl_3 showed an absorption maximum at $\lambda = 491$ nm which is close to that reported in Ref. [7b] ($\lambda = 477$ nm). The shape of the experimental spectrum is in agreement with the calculated spectrum for **9ba** (Supporting Information: Figure S2a, red curve). The originally suggested zwitterionic structure **Eba**^[7b] for the red needles must, therefore, be revised. The decrease of the absorbance at 491 nm (**9ba**) during warming up (Figure S2b) is in line with the NMR-spectroscopically observed tautomerization of **9ba** (Figure S3).

© 2022 The Authors. Chemistry - A European Journal published by Wiley-VCH GmbH

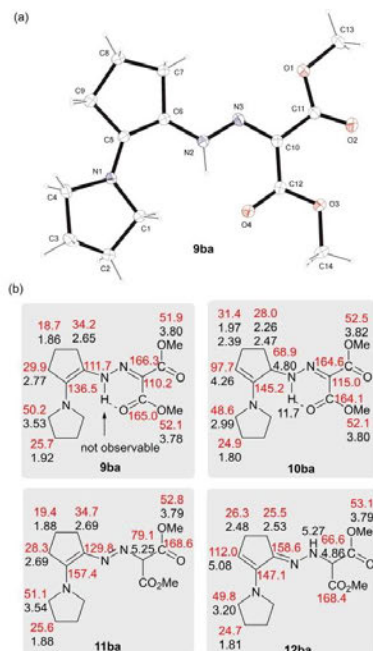
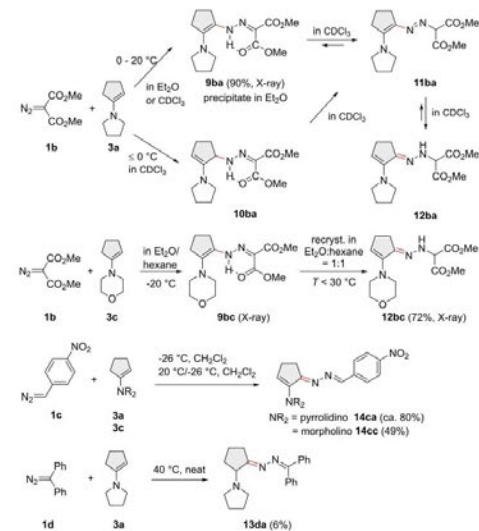


Figure 3. (a) Crystal structure of hydrazoneenamine **9ba**. (b) ¹H and ¹³C NMR chemical shifts of the azo coupling products **9ba**, **10ba**, **11ba**, and **12ba**.

When the reaction of **1b** with **3a** in CDCl₃ at −50 °C was followed by ¹H NMR spectroscopy, the simultaneous formation of **9ba**, **10ba** and **11ba** was observed (Figure S4). Whereas **9ba** and **10ba** are directly generated from zwitterion **Eba**, it is not clear whether **11ba** is directly formed from **Eba** or through tautomerization of **10ba**. NMR monitoring of the reaction at −30 °C showed that the concentration of **10ba** (Figure S4), originally formed from **Eba**, decreases at longer reaction times due to tautomerization, predominantly into **11ba**. At 20 °C, hydrazoneenamine **12ba** is the most stable tautomer. Of all the tautomers formed in the reaction of **1b** with **3a**, **12ba** is formed most slowly, which can be explained by the fact that in **12ba**, like in the tautomer **11ba**, a new C–H bond is generated, which has a higher intrinsic barrier than proton transfer to nitrogen.

The reaction of diazomalonnate **1b** with morpholinocyclopentene **3c** in Et₂O/hexane at −20 °C proceeded analogously (Scheme 5), and an orange needle formed in the reaction mixture was characterized as **9bc** by X-ray crystallography. Attempts to recrystallize **9bc** from Et₂O/hexane led to tautomerization and formation of **12bc** (72%), which was unequivocally identified by X-ray crystallography. In contrast to the equilibrium mixture of **12ba/11ba/9ba**, **12bc** appears to be the most stable tautomer, as it is the only species observed by NMR



Scheme 5. Reactions of diazoalkanes **1b–d** with the cyclopentanone-derived enamines **3a** and **3c**.

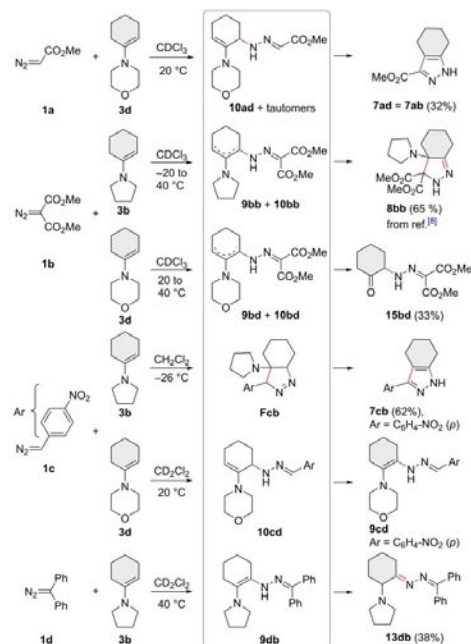
spectroscopy (pp. S79–S80, Supporting Information). Hydrazoneenamine **12bc** has previously been obtained from **1b** and **3c** in 66% yield in Et₂O at −30 °C,^[7b] and the reported ¹³C NMR spectra are in accord with our spectra. The close analogy of the ¹³C NMR spectra of **12bc** and **12ba** (pp. S70–S74, Supporting Information) is another confirmation of the structure of **12ba**. When the reaction of **1b** with **3c** in CDCl₃ was followed by ¹H NMR spectroscopy at 20 to 40 °C, **12bc** was generally observed as the predominant species.

Combination of *p*-nitrophenyldiazomethane (**1c**) with the aminocyclopentenes **3a** and **3c** furnished compounds **14ca** and **14cc**, respectively. It is not clear, why neither **9ca**, **9cc**, nor any of their tautomers were detectable, and only the oxidized products **14ca** and **14cc** were observed.

Heating of diphenyldiazomethane (**1d**) with pyrrolidinocyclopentene **3a** without solvent for two days at 40 °C yielded **13da** in very poor yield (6%).

Reactions of diazoalkanes **1** with the 1-(dialkylamino)-cyclohexenes **3b** and **3d**

While cyclization products have not commonly been observed in the reactions of **1** with the cyclopentenyl amines **3a** and **3c** (Schemes 1 and 5),^[11] pyrazole **7ad** (= **7ab**, Scheme 6) was the only product obtained in moderate yield from the reaction of methyl diazoacetate (**1a**) with pyrrolidinocyclohexene **3b** (Scheme 3) and morpholinocyclohexene **3d** (Scheme 6), in agreement with a previous report of Reissig and Huisgen who obtained 82% of **7ab** by the reaction of **1a** with **3b** in



Scheme 6. Reactions of diazoalkanes **1** with the cyclohexanone-derived enamines **3b** and **3d** (framed: intermediates detected by NMR spectroscopic monitoring).

chloroform at ambient temperature.^[7c] ¹H NMR monitoring of this reaction in CDCl₃ showed the initial formation of the azo coupling product **10ad** (pp. S95-S98, Supporting Information), followed by the appearance of other tautomers and eventual cyclization with formation of **7ad** by elimination of morpholine and proton migration.

The initial formation of **10bd** followed by occurrence of **9bd** (pp. S101-S106, Supporting Information) was observed by ¹H NMR spectroscopy in the reaction of **1b** with morpholinocyclohexene **3d** at 20 to 40 °C, in analogy to the reaction of **1b** with **3b**, which initially gave a mixture of **9bb** and **10bb**. While the hydrazoneenamines **9bb** and **10bb** underwent ring closure and eventually gave **8bb**,^[9] the hydrazoneenamines **9bd** and **10bd** did not cyclize, and the cyclohexanone derivative **15bd** was isolated in 33% yield after chromatography on silica gel.^[12]

The ¹H NMR spectroscopic monitoring of the reaction of **1c** with **3b** at -10 °C allowed to identify the 1-pyrazoline **Fcb** (pp. S85-S88, Supporting Information) as an intermediate, before it underwent elimination of pyrrolidine and proton shift to give 62% of **7cb**.

The reaction of *p*-nitrophenyldiazomethane (**1c**) with morpholinocyclohexene **3d** yields enamine **10cd** initially (pp. S109-S110, Supporting Information), which also does not cyclize, but tautomerizes with formation of **9cd**. A plausible

reason why only azo coupling products generated from cyclohexanone-derived enamines can undergo subsequent cyclization is given below.

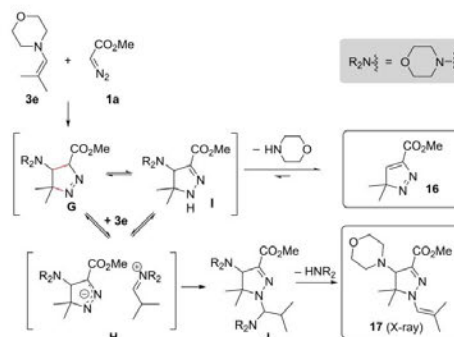
While mainly decomposition of pyrrolidinocyclopentene **3a** took place when treated with diphenyldiazomethane (**1d**, Scheme 5), we observed the formation of compound **9db** (pp. S91-S94, Supporting Information) in the reaction of **1d** with **3b**, as previously reported by Bettinetti and co-workers.^[13] In repeating this reaction several times, we could not reproduce this result and instead isolated **13db**, a tautomer of **9db**.

Reactions of diazoalkane **1a** with 1-morpholinoisobutene (**3e**)

The reaction of 1-morpholinoisobutene (**3e**) with **1a** in the dark (3 days at +50 °C)^[14] furnished a mixture of the 1:1-product **16** and 2:1-product **17**, which was separated by column chromatography. In analogy to the reactions described in Scheme 4 we assume that the Δ¹-pyrazoline **G** is formed via stepwise Huisgen cycloaddition, followed by morpholine elimination, either directly or via tautomer **I**, to yield the isolated pyrazole **16**, which has previously been obtained by the reaction of **1a** with 1-pyrrolidinoisobutene.^[7c] The 2:1 product **17**, whose structure was characterized by NMR spectroscopy and X-ray crystallography (Scheme 7), may be formed through proton transfer from **G** or **I** to enamine **3e** to give **H**, which may collapse with formation of **J**, the precursor of **17**. An alternative mechanism for the formation of **17** is suggested in Scheme S2. Both mechanisms are in line with the observed formation of **17** from isolated **16** and **3e** (Figure S6).

Kinetics of the reactions of **1a**–**d** with **2** and **3**

The reactions of diazoalkanes **1** with sulfonium ylides **2** were studied photometrically by monitoring the decay of the UV-Vis absorbances of the sulfonium ylides in DMSO at 20 °C (Fig-



Scheme 7. Products and suggested mechanism for the reaction of **1a** with **3e**.

ure 4a). Due to the slow decomposition of the sulfonium ylides **2** (product formed by decomposition: p. S5, Supporting Information), they were generated in the flask used for the kinetic experiments by treating the solution of **2**(H)BF₄ in DMSO with KOtBu (1.03–1.15 equiv) immediately before adding the diazoalkanes **1** (Figure 4b). In order to achieve pseudo-first-order kinetics, more than 9 equivalents of the diazoalkanes were used. The mono-exponential decays of the absorbances of the sulfonium ylides indicate that the reactions proceed with first-order in sulfonium ylides. The first-order in diazoalkanes **1** is indicated by the linear correlations of the pseudo-first-order rate constants k_{obs} with **[1]** (Figure 4c).

As previously reported,¹⁸ the kinetics of the reactions of the diazoalkanes **1** with enamines **3** were investigated by time-resolved ¹H NMR spectroscopy, following the decrease of the vinylic hydrogens of the enamines **3** relative to an internal standard (mesitylene, dibromomethane, or 1,1,2,2-tetrachloroethane) in CDCl₃, CD₂Cl₂ or d₈-toluene/mesitylene (1:1) at various temperatures. Usually equimolar amounts of **1** and **3** were used, and the second-order rate constants k_2 were obtained as the slopes of plots of $1/[3]_t$ versus time t according to $1/[3]_t = k_2 t + 1/[3]_0$; in some cases 2 equivalents of **1** were used and evaluated as described on p. S4 (Supporting Information).¹⁵ Plots of $\ln(k_2/T)$ versus $(1/T)$ provided the Eyring activation parameters ΔH^\ddagger and ΔS^\ddagger , from which the second-order rate constants k_2 at 20 °C were calculated (Table 1).

Kinetics of some of these reactions, which were measured by us between –50 to +50 °C in CDCl₃ had previously been studied by Reissig and Huisgen at +80.3 °C in toluene or at +110 °C in mesitylene.¹⁷ In order to compare these data with our results, we used the Eyring activation parameters in Table 1 to calculate rate constants at the higher temperatures of the previous studies (Table S20). Due to the highly negative activation entropies and the small activation enthalpies, the rates of these reactions are not strongly affected by variation of temperature. Extrapolation of our previously reported rate constants for the reactions of methyl diazoacetate **1a** with **3a** and **3b** in CDCl₃ at –40 to –10 °C¹⁸ by the Eyring equation gave values on average one order of magnitude greater than

those reported at 80.3 °C in toluene.^{17d} Analogous extrapolation of the rate constants in Table 1 (CDCl₃ and CD₂Cl₂, –50 to +50 °C) by the Eyring equation led to values, generally one order of magnitude higher, in the case of **1b**+**3a** 500 times higher than previously measured at +110 °C in mesitylene solution (Supporting Information).^{17a,d} Solvent effects can only partially account for this discrepancy because our NMR studies showed that the reactions of **1b** with **3b** and **3c** are 3 and 6 times faster in CDCl₃ than in d₈-toluene/mesitylene = 1:1 (v/v) (Table S20).

Quantum chemical calculations

Quantum chemical calculations have been performed in order to examine our conclusion that zwitterions **E** are common intermediates of all reactions of the diazoalkanes **1a–d** with the enamines **3**, as depicted in Scheme 4. For that purpose, a conformational sampling was performed for all structures using the OPLS3 force field as implemented in MacroModel.¹¹⁶ Subsequently, the geometries were optimized at the B3LYP–D3BJ/def2-SVP¹¹⁷ level of theory considering solvation with the SMD model¹¹⁸ for chloroform within the Gaussian set of codes.¹¹⁹ For improved accuracy, the thermal corrections at this level were combined with single-point energies using the (SMD = CHCl₃)/MN15/def2-TZVPD method.¹²⁰ Eventually, the Gibbs energies of all conformers were Boltzmann weighted.

As previously reported for diazoacetate **1a**,¹⁸ the lowest unoccupied orbital of the heteropropargyl system (ψ_3) does not correspond to LUMO of **1a**, but to LUMO + 1. Figure 5 shows that the situation is similar in **1b–d**. In all cases, the previously neglected $\pi^*_{N=N}$ is significantly lower in energy than ψ_3 and generally corresponds to the LUMO. Only in 4-nitrophenyldiazoacetate (**1c**), there is an even lower lying unoccupied molecular orbital which is largely localized at the nitro group. Since it is not relevant for the reactivity of **1c**, it is not depicted in Figure 5, but shown in Figure S10 (Supporting Information).

As reported for **1a**,¹⁸ two separate trajectories have also been identified for the reactions of **1b–d** with enamines **3a** and

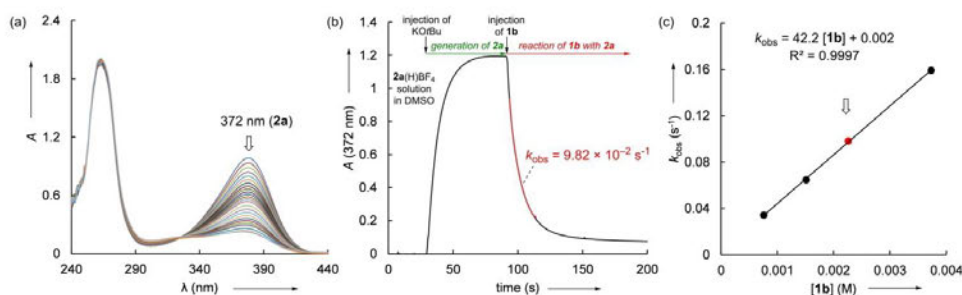


Figure 4. (a) UV-Vis spectroscopic monitoring of the reaction of **1b** (2.26×10^{-3} M) with **2a** (8.32×10^{-5} M) generated from a KOtBu solution (1.14 equiv) and a **2a**(H)BF₄ solution in DMSO at 20 °C. (b) Mono-exponential decay of the absorbance A at 372 nm vs. time for the reaction of **1b** with **2a** in DMSO at 20 °C. (c) Linear correlation of k_{obs} with **[1b]** for determining the second-order rate constant $k_2 = 42.2 \text{ M}^{-1} \text{ s}^{-1}$ at 20 °C.

Table 1. Second-order rate constants k_2 and Eyring activation parameters ΔH^\ddagger and ΔS^\ddagger for the reactions of 1 a-d with 2 and 3.

Diazoalkanes	Nucleophiles (solvents)	T [°C]	k_2 [M ⁻¹ s ⁻¹]	ΔH^\ddagger [kJ mol ⁻¹]	ΔS^\ddagger [J mol ⁻¹ K ⁻¹]
Reactions with 1 a					
1 a	2 a (DMSO)	+20	1.18×10^2		
1 a	2 b (DMSO)	+20	2.17		
1 a	3 a (CDCl ₃)	+20	$(1.83 \pm 0.30) \times 10^{-5}$ [a,b]	22.0 ± 2.1	-222 ± 9
1 a	3 b (CDCl ₃)	+20	$(4.68 \pm 0.56) \times 10^{-6}$ [a,b]	23.5 ± 1.8	-228 ± 7
1 a	3 d (CDCl ₃)	+50	4.82×10^{-6}		
		+40	2.75×10^{-6}		
		+30	1.38×10^{-6}		
		+20	$(7.03 \pm 0.38) \times 10^{-7}$ [a]	48.4 ± 2.1	-198 ± 7
1 a	3 e (CDCl ₃)	+50	1.97×10^{-6}		
		+40	1.01×10^{-6}		
		+30	4.77×10^{-7}		
		+20	$(2.20 \pm 0.05) \times 10^{-7}$ [a]	55.2 ± 0.9	-184 ± 3
Reactions with 1 b					
1 b	2 a (DMSO)	+20	4.22×10^1		
1 b	3 a (CDCl ₃)	-50	6.96×10^{-4}		
		-40	1.40×10^{-3}		
		-30	2.38×10^{-3}		
		+20	$(2.59 \pm 0.42) \times 10^{-2}$ [a]	25.8 ± 1.5	-187 ± 7
1 b	3 b (CDCl ₃)	-50	8.98×10^{-5}		
		-40	1.40×10^{-4}		
		-30	1.84×10^{-4}		
		+20	$(7.59 \pm 1.50) \times 10^{-4}$ [a]	14.3 ± 1.8	-256 ± 8
1 b	3 c (CDCl ₃)	+40	1.92×10^{-4}		
		+30	1.47×10^{-4}		
		+20	9.71×10^{-5}		
		+20	$(9.91 \pm 0.37) \times 10^{-5}$ [a]	23.6 ± 2.8	-241 ± 9
1 b	3 d (CDCl ₃)	+40	7.25×10^{-6}		
		+30	6.19×10^{-6}		
		+20	4.74×10^{-6}		
		+20	$(4.81 \pm 0.13) \times 10^{-6}$ [a]	13.7 ± 2.1	-300 ± 7
Reactions with 1 c					
1 c	3 a (CD ₂ Cl ₂)	-40	1.03×10^{-3}		
		-30	1.47×10^{-3}		
		-20	2.18×10^{-3}		
		+20	$(7.20 \pm 0.59) \times 10^{-3}$ [a]	16.4 ± 1.0	-230 ± 4
1 c	3 b (CD ₂ Cl ₂)	-30	2.87×10^{-4}		
		-20	4.61×10^{-4}		
		-10	6.63×10^{-4}		
		+20	$(1.93 \pm 0.15) \times 10^{-3}$ [a]	20.2 ± 1.2	-228 ± 5
1 c	3 c (CD ₂ Cl ₂)	+20	7.59×10^{-5}		
1 c	3 d (CD ₂ Cl ₂)	+20	1.80×10^{-6}		
Reactions with 1 d					
1 d	3 b (CD ₂ Cl ₂)	+20	2.89×10^{-6}		

[a] Extrapolated from rate constants at other temperatures by using the Eyring equation; [b] Data from Ref. [8].

3b. In all cases, the stepwise process, which involves rate-determining formation of the intermediate zwitterions E₁ or E₂ by attack of the enamine at π_{N=N} proceeds via considerably

lower barriers than the concerted pathway (Table 2). For details of the non-occurring concerted pathway, which involves the

Table 2. Comparison of experimental and calculated activation Gibbs energies at 25 °C (in kJ mol⁻¹, at the (SMD = CHCl₃)/MN15/def2-TZVPD//((SMD = CHCl₃)/B3LYP-D3BJ/def2-SVP level of theory). - See text for the meaning of the color markings.

Entry	$\Delta G^\ddagger_{\text{exp}}$	$\Delta G^\ddagger_{\text{E}}$	$\Delta G^\ddagger_{\text{Z}}$	$\Delta G^\ddagger(\text{E}_1)$	$\Delta G^\ddagger(\text{E}_2)$	$\Delta G^\ddagger(\text{F})$	$\Delta G^\ddagger(\text{9})$	$\Delta G^\ddagger(\text{10})$	$\Delta G^\ddagger(\text{11})$	$\Delta G^\ddagger(\text{12})$	$\Delta G^\ddagger_{\text{concl}}$	$\Delta G^\ddagger_{\text{conc}}$	
1 ^[a]	1 a + 3 a	88.2	99.7	93.3	31.4	57.6	-24.2	-30.1	-27.0	-34.3	-45.0	83.5	135.3
2	1 b + 3 a	81.6	93.0	109.6	42.6	79.1	1.5	-30.6	-17.4	-19.5	-31.8	— ^[b]	116.8
3	1 c + 3 a	84.9 ^[c]	104.6	90.6	21.9	49.0	-26.9	-32.9	-33.7	-39.3	-43.5	72.9	— ^[b]
4	1 d + 3 a ^[d]	—	108.6	124.3	42.0	102.1	2.0	-35.9	-35.5	-36.5	-43.5	— ^[b]	151.0
5 ^[e]	1 a + 3 b	91.6	97.8	99.2	34.6	65.5	-24.6	-24.3	-25.6	-21.8	-28.9	75.6	144.5
6	1 b + 3 b	90.5	91.6	116.6	48.2	83.2	2.4	-20.5	-19.7	-8.8	-15.2	— ^[b]	119.9
7	1 c + 3 b	88.1 ^[c]	107.4	95.5	28.0	55.3	-32.9	-37.5	-34.1	-28.5	-28.9	67.6	145.4
8	1 d + 3 b	104.0 ^[c,e]	105.6	126.5	51.2	110.7	3.3	-40.9	-35.3	-23.4	-27.0	— ^[b]	173.8

[a] From Ref. [8]. [b] TS could not be localized. [c] In CD₂Cl₂. [d] $\Delta G^\ddagger(\text{13 da}) = -37.3$ kJ mol⁻¹. [e] Calculated from $k_2(20^\circ\text{C})$ with an estimated $\Delta S^\ddagger = -230$ J mol⁻¹ K⁻¹.

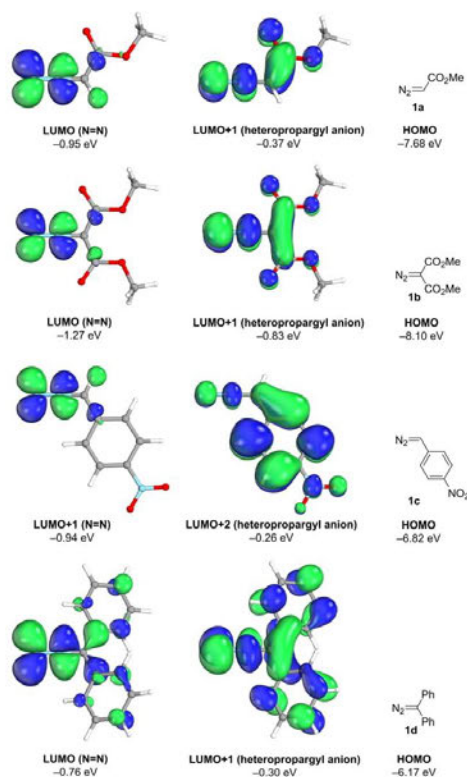


Figure 5. Lowest unoccupied molecular orbitals of 1a–d and their energies at the (SMD = CHCl₃)/MN15/def2-TZVPD// (SMD = CHCl₃)/B3LYP-D3BJ/def2-SVP level of theory. Orbital energies of 1a were reported in Ref. [8].

lowest unoccupied orbital of the propargyl system (ψ_3) see ref.^[8] and Supporting Information (Figures S11 and S12).

All zwitterions E_z are more stable than E_z (structures in Scheme 4), in line with the well-known higher stability of (*E*)-azo compounds relative to their (*Z*)-isomers.^[3] The energy difference [$\Delta G^0(E_z) - \Delta G^0(E_z)$] increases with increasing steric effects and is largest for $R^1 = R^2 = \text{Ph}$ ($\approx 60 \text{ kJ mol}^{-1}$, Table 2, entries 4 and 8) and smallest for $R^2 = \text{H}$, $R^1 = \text{aryl}$ ($\approx 27 \text{ kJ mol}^{-1}$, entries 3 and 7). However, the less-stable *cis*-isomers (E_z) are generally formed faster if one of the substituents (R^1 or R^2 , Scheme 4) equals hydrogen (exception 1a + 3b). Coulomb interactions between the two termini, which give rise to the second bond in the corresponding 1,3-dipolar cycloadditions, may account for the faster formation of E_z in these cases. If none of the substituents R^1 and R^2 is hydrogen, this stabilization of the transition state is overruled by steric effects, which account for the higher stability of the *trans* zwitterions E_z compared to E_z (Table 2).

The barriers for cyclization of the zwitterions E_z are calculated to be very low (reactions of 1a and 1c) or cannot be calculated at all, because attempts to localize transition states for the cyclizations of E_z (reactions of 1b and 1d) led to collapse of the selected structures into the cycloadducts **F** (Figures 6 and S12). However, since in all reactions of the diazoalkanes 1 with the enamines 3, tautomers of the zwitterions E_z and E_z (i. e., 9–13) were observed as intermediates or final products, proton shifts must generally be faster than cyclization. As discussed for the reactions of 1a with 3a and 3b, the proton shifts in the zwitterions E_z/E_z proceed by intermolecular processes, which we could not describe computationally.^[8]

Anyway, since the proton shifts are faster than the cyclizations, Figures 6, S11, and S12 imply that the formation of the zwitterions E_z or E_z corresponds to the rate-determining step of all reactions. This conclusion is supported by the excellent agreement between the experimentally determined activation Gibbs energies $\Delta G^{\ddagger}_{\text{exp}}$ and the calculated barriers for the rate-determining step (smaller value of ΔG^{\ddagger}_E and ΔG^{\ddagger}_z in Table 2). The green marked values in Table 2 show that the calculated barriers are generally 1–7 kJ mol^{-1} (11 kJ mol^{-1} for 1b + 3a) higher than the experimental values, whereas the calculated barriers $\Delta G^{\ddagger}_{\text{conc}}$ for the concerted processes (last column in Table 2) are 29 to 70 kJ mol^{-1} larger than the experimental numbers.

Figure 6 depicts the calculated Gibbs energy profiles for the reactions of 1b with 3a and 3b (entries 2 and 6 of Table 2). Analogous illustrations for the reactions of enamines with 1a (entries 1 and 5) are shown in Ref. [8], those for the reactions of enamines with 1c and 1d (entries 3, 4, 7, 8) in the Supporting Information (Figures S11 and S12).

In our recent analysis of the reaction of 1a with the enamines 3a and 3b, we have discussed that cyclization of the initially formed azo coupling products proceeds via the (*Z*)-zwitterion E_z . The course of the reactions of 1b–1d with 3a and 3b can now be rationalized analogously. Since the interconversions of the tautomers 9, 10, 11, and 12 are faster than the cyclizations, the Curtin-Hammett principle applies, and the rate of cyclization depends on the difference of the Gibbs energies of the most stable of these tautomers (marked by yellow background in Table 2) and the Gibbs energy of the cyclization step ($\Delta G^{\ddagger}_{\text{cycl}}$ in Table 2). If a barrier between E_z and the cycloadduct **F** could not be localized (as in the reactions with 1b, Figure 6), $\Delta G^{\ddagger}_{\text{cycl}}$ can be replaced by $\Delta G^0(E_z)$. The barrier for cyclization can, therefore, be derived from the difference of the grey highlighted energies [$\Delta G^{\ddagger}_{\text{cycl}}$ or $\Delta G^0(E_z)$] in Table 2 and the yellow marked values (most stable tautomers). One can see that for all reactions with pyrrolidinocyclopentene 3a (entries 1–4 in Table 2), as well as for the reaction of diphenyldiazomethane 1d with 3b (entry 8), these differences are greater than 110 kJ mol^{-1} , in accord with the observation that cyclized products are not commonly observed for these reactions. On the other hand, the corresponding energy differences are smaller than 105 kJ mol^{-1} in entries 5–7, in accord with the observation that in these reactions with pyrrolidinocyclohexene 3b, formation of the pyrazolines has been observed. Because of

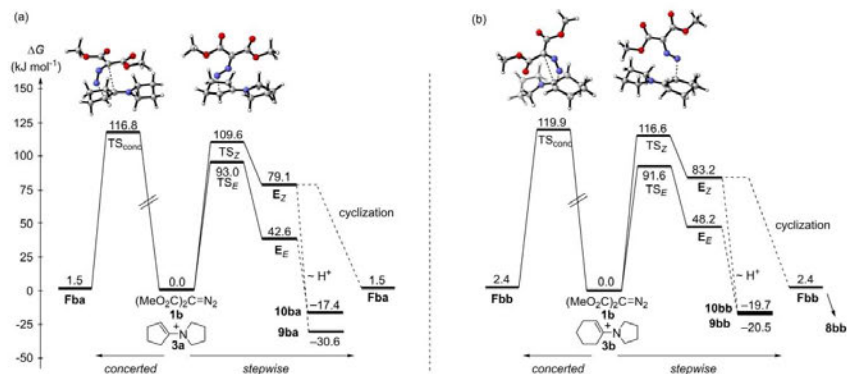


Figure 6. Gibbs energy profiles for the concerted and stepwise cycloadditions of **1b** with (a) **3a** and (b) **3b** as computed at the (SMD = CHCl_3)/MN15/def2-TZVPD/(SMD = CHCl_3)/B3LYP-D3BJ/def2-SVP level of theory. Analogous illustrations for the reactions of enamines with **1a** are shown in Ref. [8] and for **1c** and **1d** in Figures S11 and S12 (Supporting Information).

the error limits of these calculations, illustrated by the observation of **11ba** in equilibrium with **9ba** and **12ba** (Scheme 5) despite its calculated 12 kJ/mol higher Gibbs energy (Table 2), this analysis should be considered as a plausible rationalization for the different behavior of **3a** and **3b**, but not as an unequivocal proof.

Table 2 (entries 1 & 2 and 5 & 6) shows that the calculated activation Gibbs energies for the reactions of both enamines **3a** and **3b** to give the (*E*)-zwitterions **E_E** (ΔG^{\ddagger}_E) are only 6 kJ mol^{-1} lower for diazomalonnate **1b** than for diazoacetate **1a**. Intuitively, one might explain this small difference by the fact that the additional ester group in **1b** has little effect on $\pi^*_{\text{N}=\text{N}}$ (LUMO), because this orbital is not in conjugation with the π -system of the ester group. On the other hand, conjugation of the π -system of the ester group with ψ_3 of the heteropropargyl anion system (LUMO + 1) might account for the fact that the transition states for the concerted cycloadditions ($\Delta G^{\ddagger}_{\text{conc}}$) are lowered by 19 to 25 kJ mol^{-1} by the additional ester group in **1b** (Table 2, entries 1 & 2 and 5 & 6).

This rationalization is not explicitly supported by the calculated orbital energies. Figure 5 shows that ψ_3 of the heteropropargyl anion system (LUMO + 1), which is in conjugation with the π -system of the ester group is only slightly more lowered in energy by the additional ester group in **1b** (-0.46 eV) than $\pi^*_{\text{N}=\text{N}}$ (-0.32 eV). While we find a good agreement between calculated and experimental activation energies, the calculated orbital energies of the reactants correlate only poorly with the observed reactivity ordering of the diazo compounds.

Determination of the Electrophilicity Parameters *E* of the Diazoalkanes **1**

Experimental studies and quantum chemical calculations thus agree that azo couplings as well as 1,3-dipolar cycloadditions of **1a–1d** with the enamines **3** proceed by rate-determining electrophilic attack of the diazoalkanes at the enamines yielding zwitterions **E** as short-lived intermediates (Scheme 4). These reactions thus fulfill the criteria for the applicability of Equation (1), in particular formation of one and only one new bond in the rate-determining step. Since solvent effects on rate constants are included in the nucleophile-specific parameters *N* and s_N in Equation (1), it is possible to use rate constants in different solvents for determining the solvent-independent electrophilicity parameters *E*.

Accordingly, Figure 7 shows linear correlations of $(\lg k_2)/s_N$ versus the 1-bond nucleophilicity parameters *N* of sulfonium ylides **2** and enamines **3** (Figure 2). The common nature of the rate-determining step in the reactions of diazoalkanes **1** with sulfonium ylides **2** and enamines **3** is thus confirmed. Least-squares analysis according to Equation (1), enforcing a slope of 1.00, yields the electrophilicity parameters *E* of **1a–c**, which are given in Figure 7. Slopes between 0.93 and 1.04 are obtained when the correlations in Figure 7 are performed without restrictions of the slopes. Assuming that Equation (1) also holds for the reactions of diphenyldiazomethane **1d** with enamines, $E(\mathbf{1d}) = -21.4$ is derived from the second-order rate constant k_2 for the reaction of **1d** with **3b**.

As shown in Figure 8, the electrophilicities of diazoalkanes **1a–d** ($E = -21.4$ to -18.2) are much smaller than those of aryldiazonium ions ($E = -10.4$ to -2.5 in acetonitrile),^[21] which can be rationalized by the electron-donating effect of the formal negative charge on the carbon adjacent to the N_2 group expressed by the ylide structures of **1a–d** (Scheme 1). The similar electrophilicities of **1a–c** as well as the three orders of

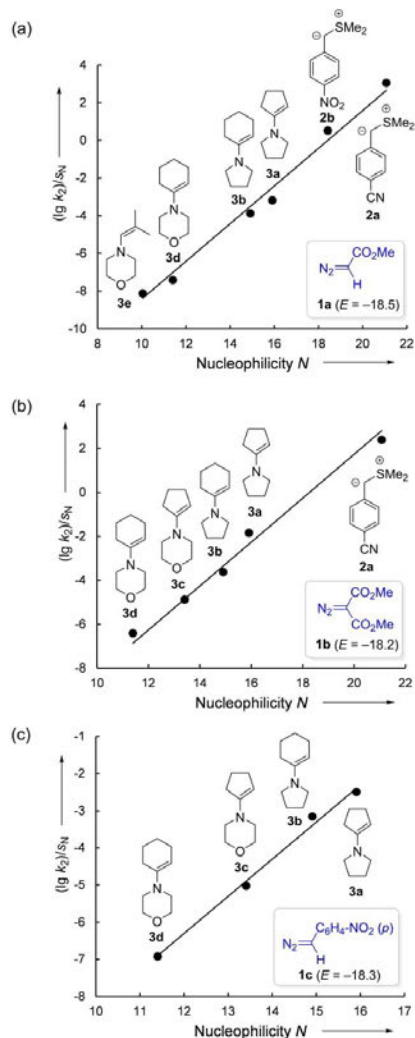


Figure 7. Plots of $(\lg k_2)/s_N$ vs. N for the reactions of (a) **1a** with **2a–b** (in DMSO) and **3a–e** (in CDCl_3), (b) **1b** with **2a** (in DMSO) and **3a–d** (in CDCl_3), and (c) **1c** with **3a–d** (in CD_3Cl_3); electrophilicity parameters E of **1a–1c** were calculated by the method of least-squares through iterative minimization of $\Delta^2 = \sum (\lg k_2 - s_N(E + N))^2$, which implies enforcing a unity slope in the $(\lg k_2)/s_N$ vs N plots.

magnitude lower electrophilicity of diphenyldiazomethane (**1d**) are in good agreement with the quantum chemically calculated Gibbs activation energies for their reactions with enamines, while a consistent rationalization by FMO analysis failed (see above).

Chem. Eur. J. 2022, 28, e202201376 (16 of 13)

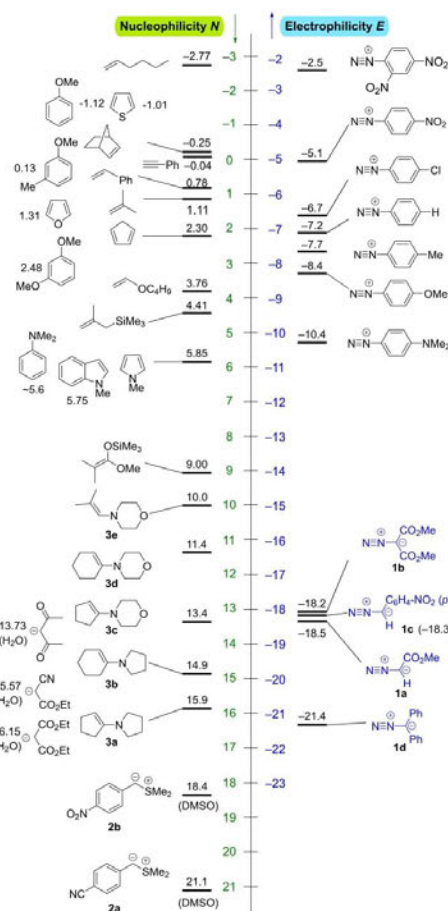


Figure 8. Potential nucleophilic reaction partners for diazoalkanes **1a–d** and diazonium ions. Note: E parameters for diazonium ions Ar-N_2^+ are from Ref. [21] and have not been parametrized through reactions with the usually used reference nucleophiles. Reactivity descriptors N for nucleophiles refer to CH_2Cl_2 (if not mentioned otherwise) and were taken from Ref. [5f].

In previous work we have reported that the reactivity parameters E and N can be used for a first guess whether certain reactions of electrophiles with nucleophiles can be expected to take place at room temperature. When electrophiles and nucleophiles are arranged as in Figure 8, where $E + N = -5$ for reactants on the same level, Equation (1) predicts $\lg k_2(20^\circ\text{C}) = -5s_N$ for reactions of electrophiles with nearby nucleophiles. Since s_N is close to 1 for most $\pi_{\text{C-C}}$ nucleophiles,^[5] one can expect that the diazonium ions and diazo compounds in Figure 8 will undergo azo couplings with substrates on the same horizontal level with second-order rate constants of

© 2022 The Authors. Chemistry - A European Journal published by Wiley-VCH GmbH

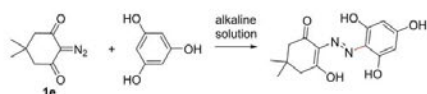
approximately $10^{-5} \text{ M}^{-1} \text{ s}^{-1}$ at 20°C , corresponding to half-reaction times of about 1 day for 1 M solutions. As a consequence, azo couplings at ambient temperature can be expected with all nucleophiles, which are positioned below the corresponding electrophiles in Figure 8, but not with those nucleophiles located at significantly higher positions.

The suitability of this rule of thumb as an ordering principle for the reactions of diazonium ions with aromatic and aliphatic π -systems has already been demonstrated in refs.^[21,22] Let us now consider literature reports on reactions of diazoalkanes with C-centered nucleophiles.

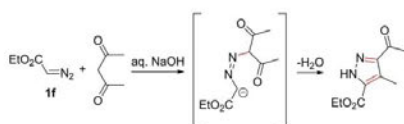
In Figure 8, arenes are positioned at significantly higher positions than the diazo compounds **1a–d**. Accordingly, azo couplings of the diazoalkanes **1a–d** with arenes have to our knowledge not been reported. While diazodimedone (**1e**) was found to react readily with phloroglucine under alkaline conditions (Scheme 8), an analogous reaction of diazoacetate was also mentioned in ref.^[23] without giving details. Ciganek's report^[24] that dicyanodiazomethane undergoes azo coupling with *N,N*-dimethylaniline indicates an electrophilicity level of this diazoalkane that is higher than that of **1a–d**.

In line with the relative position of **1a** and enamine **3e** in Figure 8, their combination required heating at 50°C for 3 days (Scheme 7). Since enamines are among the strongest neutral C-nucleophiles, the electrophilic character of diazoalkanes has predominantly been observed in reactions with the more nucleophilic carbanions.^[25]

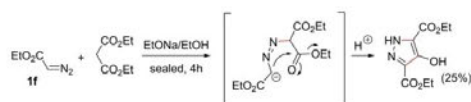
Klages reported the formation of a pyrazoline, when ethyl diazoacetate (**1f**) was combined with 1,3-diketones and aqueous NaOH, as depicted for the reaction with pentane-2,4-dione in Scheme 9.^[26] Its formation can be rationalized by initial electrophilic attack of the diazoester **1f** at the anion of the diketone (in H_2O : $N=13.73$), followed by cyclization and



Scheme 8. Reaction of diazodimedone (**1e**) with phloroglucine.^[23]



Scheme 9. Reaction of ethyl diazoacetate (**1f**) with pentane-2,4-dione.^[26]



Scheme 10. Reaction of ethyl diazoacetate (**1f**) with diethyl malonate.^[27a]

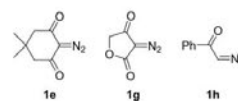
dehydration. Since the enolates derived from pentan-2,4-dione and diethyl malonate have nucleophilicities in water comparable to enamines, we consider the formation of the pyrazoles via concerted 1,3-dipolar cycloaddition across the C=C bond of the enolates unlikely.

An analogous reaction of ethyl diazoacetate (**1f**) with diethyl malonate catalyzed by sodium ethoxide has been reported by Bertho and Nüssel in 1927 (Scheme 10).^[27a] In line with the relative position of **1a** and the anion of diethyl malonate (in H_2O : $N=16.15$) in Figure 8, this reaction can again be rationalized by initial azo coupling of the diazo ester with the malonate anion, followed by cyclization.

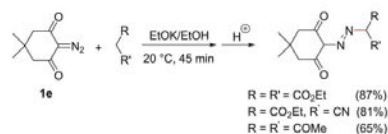
Assuming that structurally related diazoketones and diazoesters will also have similar electrophilicities as the diazoalkanes **1a–c**, one can analogously interpret the reactions of the diazo compounds **1e**,^[27b] **1g**,^[27c] and **1h**^[27d] (Scheme 11) with CH acidic compounds by initial electrophilic attack of the diazo compounds at the corresponding carbanions, followed by proton shifts or cyclization. The most comprehensive studies in this field have been performed by Regitz and coworkers, as depicted in Scheme 12.^[27b]

Azo couplings of CH acidic compounds have also been observed with the parent diazomethane under neutral conditions,^[28] which has been suggested to proceed via protonation of diazomethane and attack of the resulting methyldiazonium ion at the simultaneously formed carbanion.^[28b–d] Analogous reactions of diazonium ions are known as Japp-Klingemann reactions.^[29]

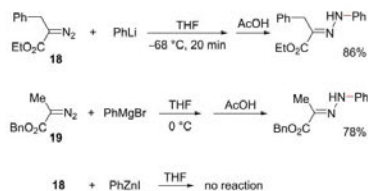
Alkylolithium and aryllithium, as well as the corresponding magnesium reagents are among the strongest C-centered nucleophiles. Though their nucleophilicities have so far not been quantified, they can be expected to be located at the very bottom of Figure 8, in line with the long-known reactions of organometallics with diazoalkanes.^[2] Scheme 13 illustrates that the diazo esters **18** and **19** derived from α -amino acid esters react with PhLi at -68°C , with PhMgBr at 0°C , but not with PhZnI, even when raising the temperature.^[30]



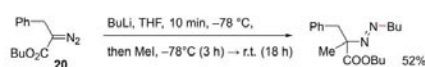
Scheme 11. Diazoketones and esters which have been reported to react with carbanions derived from CH-acidic compounds.



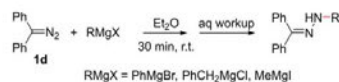
Scheme 12. Reactions of diazodimedone (**1e**) with C–H acids under catalysis of potassium ethoxide.^[27b]



Scheme 13. Reactions of the α -diazo esters **18** and **19** with organometallic reagents.^[10]



Scheme 14. Synthesis of an α -azo ester by sequential reaction of butyl lithium and methyl iodide with α -diazoester **20**.^[11]



Scheme 15. Reactions of Grignard reagents with diphenyldiazomethane (**1d**).^[12]

Electrophilic amination of butyl lithium combined with subsequent trapping of the resulting azo-substituted carbanion by methyl iodide was used by Takamura and Yamada to introduce two different alkyl groups at both reactive sites of the diazoalkane functionality in the diazoester **20** (Scheme 14).^[11]

The three orders of magnitude less electrophilic diphenyldiazomethane (**1d**) reacted with Grignard reagents, such as phenylmagnesium bromide, benzyl magnesium chloride or methylmagnesium iodide within 30 min at room temperature to yield *N*-substituted hydrazones (Scheme 15).^[12]

As mentioned at the beginning of this paragraph, **1a–d** have not been reported to react with the arenes depicted in Figure 8. As expected, no reaction was observed when 1,3-dimethoxybenzene ($N=2.48$) was heated with **1b** for 2 days in CDCl_3 at 55 °C. The fact that ordinary alkenes, which have similar nucleophilic reactivity as 1,3-dimethoxybenzene, react with diazoalkanes indicates a change of mechanism (see below).

Conclusions

Nucleophilic attack of sulfonium ylides **2** and enamines **3** at the terminal nitrogen of the diazoalkanes **1a–d** yields transient zwitterions, which undergo various subsequent reactions. NMR spectroscopic monitoring of the reactions with enamines showed that the pyrazoles **7** and pyrazolines **8** are formed by stepwise processes via intermediate hydrazone enamines (Scheme 4) and not via concerted 1,3-dipolar cycloadditions, as previously postulated.^[7c]

For all reactions of the diazoalkanes with enamines investigated in this work, the experimentally determined activation Gibbs energies agreed well with the quantum-chemically calculated values for the formation of the zwitterions, which arise from the interaction of the HOMO(enamine) with $\pi^*_{\text{N=N}}$ (diazoalkane), i.e., LUMO(diazoalkane). The alternative concerted 1,3-dipolar cycloadditions, arising from the interaction of the HOMO(enamine) with ψ_3 of the heteropropargyl fragments of the diazoalkanes were calculated to have 29–70 kJ mol^{-1} higher Gibbs activation energies (Table 2) and did not occur.

Since only one new bond is formed in the first, rate-determining step of all reactions described in this article, Equation (1) applies and was used to calculate the electrophilicity parameters E of the diazoalkanes **1a–d** from the measured second-order rate constants k_2 in Table 1 and the known nucleophile-specific parameters N and s_N of sulfonium ylides and enamines in Chart 1. Earlier studies^[4a] have shown that the nucleophilicity of diethyl diazomalonate is five orders of magnitude lower than that of ethyl diazoacetate. Experimental investigations and quantum chemical calculations now concordantly show that the electrophilicities of **1a**, **1b**, and **1c** are almost the same, while diphenyldiazomethane (**1d**) has a three orders of magnitude lower electrophilicity. This observation can be rationalized by the fact that the π -acceptor orbitals of the substituents are in direct conjugation with the nucleophilic reaction center of diazoalkanes but perpendicular to $\pi^*_{\text{N=N}}$ which accounts for the electrophilic reactivity of diazoalkanes.

In accord with the E parameters of the diazoalkanes **1a–d**, which are 8 to 19 orders of magnitude smaller than those of diazonium ions, azo couplings of diazoalkanes with arenes do usually not occur and have only been observed in rare cases. The well-known azo couplings of diazoalkanes with 1,3-diketones, 1,3-dicarboxylates, and related CH-acidic compounds under basic conditions can be rationalized by the high nucleophilicities of the corresponding enolates.

Figure 8 suggests that azo couplings of **1a–d** with ordinary alkenes, styrene, or phenylacetylene cannot be expected to take place at room temperature. Equation (1) predicts reaction times of billions of years for these reactions. The fact that these reactions have actually been observed,^[1] indicates a different mechanism. In a subsequent paper we will discuss the change from stepwise processes to concerted 1,3-dipolar cycloadditions when the enamines described in this article are replaced by less nucleophilic $\pi_{\text{C=C}}$ systems.

Experimental Section

For experimental details please see Supporting Information.

CCDC 2102953 (**9ba**, vv842), 2102954 (**9bc**, vv088), 2102955 (**12bc**, vv086), and 2102958 (**17**, yv006) contain the supplementary crystallographic data for this paper. These data are provided free of charge by The Cambridge Crystallographic Data Centre.

Acknowledgements

We thank Prof. H.-U. Reißig for helpful discussions and valuable suggestions and the Faculty of Chemistry and Pharmacy (LMU München) for providing the computational resources. LL, A.R.O. and H.M. are grateful to the Department Chemie (LMU München), the Fonds der Chemischen Industrie (FCI), and the Deutsche Forschungsgemeinschaft (DFG, SFB 749, project B1) for financial support. R.J.M. thanks the Deutsche Forschungsgemeinschaft (DFG, German Research Foundation) for a fellowship (MA 9687/1-1). Open Access funding enabled and organized by Projekt DEAL.

Conflict of Interest

The authors declare no conflict of interest.

Data Availability Statement

The data that support the findings of this study are available from the corresponding author upon reasonable request.

Keywords: diazoalkane · enamine · electrophilicity · kinetics · quantum chemical calculations

- [1] a) R. Huisgen, *Angew. Chem. Int. Ed. Engl.* **1963**, *2*, 565–598; *Angew. Chem.* **1963**, *75*, 604–637; b) *1,3-Dipolar Cycloaddition Chemistry*, Vol. 1 and 2 (Ed.: A. Padwa), Wiley, New York, **1984**; c) *Synthetic Applications of 1,3-Dipolar Cycloaddition Chemistry Toward Heterocycles and Natural Products* (Eds.: A. Padwa, W. H. Pearson), Wiley, New York, **2002**; d) H. Suga, K. Itoh, *Methods and Applications of Cycloaddition Reactions in Organic Syntheses* (Ed.: N. Nishiwaki), Wiley, Hoboken, **2014**, p 175; e) M. Breugst, H.-U. Reißig, *Angew. Chem. Int. Ed.* **2020**, *59*, 12293–12307; *Angew. Chem.* **2020**, *132*, 12389–12404; f) R. Jasinski, E. Dresler, *Organics* **2020**, *1*, 49–69.
- [2] a) R. Huisgen, *Angew. Chem.* **1955**, *67*, 439–463; b) S. Patai, *The Chemistry of Diazonium and Diazo Groups*, Wiley, Chichester, **1978**; c) M. Regitz, *Diazoalkane*, Thieme, Stuttgart, **1977**; d) B. Eistert, M. Regitz, G. Heck, H. Schwab, *Houben-Weyl, Methoden der Organischen Chemie*, 4th ed., Vol. 10/4, Georg Thieme Verlag Stuttgart, **1968**, pp. 589–710.
- [3] H. Zollinger, *Diazo Chemistry I: Aromatic and Heteroaromatic Compounds*, VCH, Weinheim, **1994**.
- [4] a) T. Bug, M. Hartnagel, C. Schlierf, H. Mayr, *Chem. Eur. J.* **2003**, *9*, 4068–4076; b) M. Hartnagel, A. R. Ofial, H. Mayr, *Synthesis* **2022**, *54*, doi: 10.1055/s-0041-1737327.
- [5] a) H. Mayr, M. Patz, *Angew. Chem.* **1994**, *106*, 990–1010; *Angew. Chem. Int. Ed. Engl.* **1994**, *33*, 938–957; b) H. Mayr, T. Bug, M. F. Gotta, N. Hering, B. Irrgang, B. Janker, B. Kempf, R. Loos, A. R. Ofial, G. Remennikov, H. Schimmel, *J. Am. Chem. Soc.* **2001**, *123*, 9500–9512; c) H. Mayr, B. Kempf, A. R. Ofial, *Acc. Chem. Res.* **2003**, *36*, 66–77; d) H. Mayr, A. R. Ofial, *Pure Appl. Chem.* **2005**, *77*, 1807–1821; e) H. Mayr, *Tetrahedron* **2015**, *71*, 5095–5111; f) For a database of nucleophilicity parameters (N/s_p) and electrophilicity parameters (E), check the link: <https://www.cup.lmu.de/oc/mayr/reaktionsdatenbank2/>.
- [6] a) R. Appel, N. Hartmann, H. Mayr, *J. Am. Chem. Soc.* **2010**, *132*, 17894–17900; b) B. Kempf, N. Hampel, A. R. Ofial, H. Mayr, *Chem. Eur. J.* **2003**, *9*, 2209–2218.
- [7] a) H.-U. Reißig, Dissertation, Ludwig-Maximilians-Universität München, **1978**; b) R. Huisgen, W. Bihlmaier, H.-U. Reißig, *Angew. Chem. Int. Ed. Engl.* **1979**, *18*, 331–332; *Angew. Chem.* **1979**, *91*, 347–348; c) R. Huisgen, H.-U. Reißig, *Angew. Chem. Int. Ed. Engl.* **1979**, *18*, 330–331; *Angew. Chem.* **1979**, *91*, 346–347; d) W. Bihlmaier, R. Huisgen, H.-U. Reißig, S. Voss, *Tetrahedron Lett.* **1979**, *20*, 2621–2624.
- [8] L. Li, P. Mayer, D. S. Stephenson, A. R. Ofial, R. J. Mayer, H. Mayr, *Angew. Chem. Int. Ed.* **2022**, *61*, e202117047; *Angew. Chem.* **2022**, *134*, e202117047.
- [9] H. Metzger, K. Seelert, *Z. Naturforsch. B* **1963**, *18*, 336.
- [10] D. Wu, Y. Wang, J. Zhou, Q. Sun, Y. Zhao, X. Xu, *Org. Lett.* **2019**, *21*, 8722–8725.
- [11] For the formation of small quantities of cyclized products, see Ref. [7b].
- [12] A structurally analogous azo coupling product was isolated when enamine **3b** was combined with ethyl 2-diazo-3,3,3-trifluoropropanoate (80 °C, 5 days, work-up by column chromatography on silica gel and subsequent purification by HPLC): D. Gladow, S. Doniz-Kettenmann, H.-U. Reißig, *Helv. Chim. Acta* **2014**, *97*, 808–821.
- [13] G. F. Bettinetti, A. Cogoli, A. O. Sale, *Ric. Sci.* **1968**, *38*, 806–809.
- [14] Previous work reported photo decomposition of 3H-pyrazoles to give cyclopropanes, which underwent subsequent [2 + 2] cycloadditions with enamines a) M. Franck-Neumann, M. Miesch, H. Kempf, *Tetrahedron* **1988**, *44*, 2933–2942; b) M. Franck-Neumann, M. Miesch, H. Kempf, *Synthesis* **1989**, *11*, 820–824.
- [15] P. W. Atkins, J. Paula in *Physical Chemistry*, Eighth Edition, W. H. Freeman and Co., New York, **2006**, p 802.
- [16] a) E. Harder, W. Damm, J. Maple, C. Wu, M. Reboul, J. Y. Xiang, L. Wang, D. Lupyan, M. K. Dahlgren, J. L. Knight, J. W. Kaus, D. S. Cerutti, G. Krilov, W. L. Jorgensen, R. Abel, R. A. Friesner, *J. Chem. Theory Comput.* **2016**, *12*, 281–296; b) *Schrödinger Release 2019–4: MacroModel*, Schrödinger, LLC, New York, NY, **2019**.
- [17] a) A. D. Becke, *J. Chem. Phys.* **1993**, *98*, 5648–5652; b) S. Grimme, S. Ehrlich, L. Goerigk, *J. Comput. Chem.* **2011**, *32*, 1456–1465; c) F. Weigend, R. Ahlrichs, *Phys. Chem. Chem. Phys.* **2005**, *7*, 3297–3305.
- [18] A. V. Marenich, C. J. Cramer, D. G. Truhlar, *J. Phys. Chem. B* **2009**, *113*, 6378–6396.
- [19] *Gaussian 16, Revision A.03*, Gaussian, Inc., Wallingford CT, **2016**. For the full reference including all authors, see the Supporting Information.
- [20] H. S. Yu, X. He, S. L. Li, D. G. Truhlar, *Chem. Sci.* **2016**, *7*, 5032–5051; 6278–6279.
- [21] H. Mayr, M. Hartnagel, K. Grimm, *Liebigs Ann.* **1997**, 55–69.
- [22] W. Gabsi, T. Boubaker, R. Goumont, *Int. J. Chem. Kinet.* **2016**, *48*, 266–273.
- [23] T. Severin, *Angew. Chem.* **1958**, *70*, 745.
- [24] E. Ciganek, *J. Org. Chem.* **1965**, *30*, 4198–4204.
- [25] Since Equation (1) cannot be applied to the formation of heteroatom-heteroatom bonds, reactions of diazo compounds with phosphines, amines, hydride donors, thiolates or hydroxide ions (see Ref. [2]) are not considered here.
- [26] a) A. Klages, *J. Prakt. Chem.* **1902**, *65*, 387–393; b) A. Klages, A. Rönneburg, *Ber. Dtsch. Chem. Ges.* **1903**, *36*, 1128–1132; c) W. Hampel, *J. Prakt. Chem.* **1969**, *311*, 1058–1064.
- [27] a) A. Bertho, H. Nüssel, *Liebigs Ann. Chem.* **1927**, *457*, 278–307; b) M. Regitz, A. Liedhegener, D. Stadler, *Liebigs Ann. Chem.* **1968**, *713*, 101–112; c) L. Wolff, *Liebigs Ann. Chem.* **1902**, *325*, 129–195; d) D. G. Farnum, P. Yates, *Proc. Chem. Soc.* **1960**, 224.
- [28] a) R. Schmiechen, *Tetrahedron Lett.* **1969**, *10*, 4995–4996; b) S. Nesnow, R. Shapiro, *J. Org. Chem.* **1969**, *34*, 2011–2013; c) W. Uhde, K. Hartke, *Chem. Ber.* **1970**, *103*, 2675–2686; d) J. S. Pyrek, O. Achmatowicz, *Tetrahedron Lett.* **1970**, *11*, 2651–2652.
- [29] a) F. R. Japp, F. Klingemann, *Ber. Dtsch. Chem. Ges.* **1887**, *20*, 2942–2944; b) F. R. Japp, F. Klingemann, *Ber. Dtsch. Chem. Ges.* **1887**, *20*, 3398–3401; c) R. R. Phillips, *The Japp-Klingemann Reaction*. In: *Organic Reactions*, Wiley, **2004**, doi: 10.1002/0471264180.or010.02.
- [30] a) E. Yasui, M. Wada, N. Takamura, *Tetrahedron Lett.* **2006**, *47*, 743–746; b) E. Yasui, M. Wada, N. Takamura, *Tetrahedron* **2009**, *65*, 461–468.
- [31] N. Takamura, S.-I. Yamada, *Chem. Pharm. Bull.* **1976**, *24*, 800–803.
- [32] G. H. Coleman, H. Gilman, C. E. Adams, P. E. Pratt, *J. Org. Chem.* **1938**, *3*, 99–107.

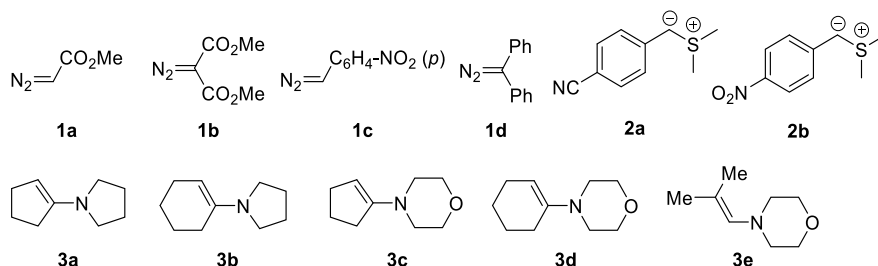
Manuscript received: May 4, 2022
Accepted manuscript online: June 27, 2022
Version of record online: August 4, 2022

4.2 Supporting Information

4.2.1 Product Studies

General procedure A (GP A). Sulfonium ylides **2a** and **2b** were generated by adding KO^tBu in dry DMSO to the vigorously stirred solution of the corresponding sulfonium tetrafluoroborates in DMSO under argon atmosphere. Solutions of diazo compounds **1a** or **1b** in DMSO were then immediately added in one portion. After stirring for a certain time, distilled water (300 mL) was added to the mixture (about 50 mL brine was also added for better separation) and CH₂Cl₂ (3 × 200 mL) was used for extraction. The combined organic layer was washed with distilled water (3 × 200 mL), brine, and dried over anhydrous MgSO₄. Volatiles were removed under reduced pressure and the crude products were purified by column chromatography on silica gel (n-pentane/dichloromethane/ethyl acetate = 4:2:1 ~ 4:1:2).

General procedure B (GP B). Diazo compounds **1a-d** were mixed with enamines **3a-e** in solvents (chloroform, CDCl₃, dry diethyl ether, diethyl ether:hexane = 1:1, CH₂Cl₂ or CD₂Cl₂) in an oven-dried GC vial (round-bottom flask or a NMR tube) under argon atmosphere at room temperature (cooling or heating also used when necessary). The GC vial (round-bottom flask or NMR tube) was then sealed and the reaction mixture was kept for a certain time (till reactions completed or reached a certain conversion). Solvents were then evaporated and the resulting crude products were filtered, recrystallized (hexane/EtOAc, diethyl ether:hexane = 1:1 or CH₂Cl₂/hexane), or worked up by column chromatography on silica gel (n-pentane/EtOAc = 5:1, n-pentane/diethyl ether = 5:1 ~ diethyl ether, or dichloromethane/methanol = 10:1) to give the purified products.



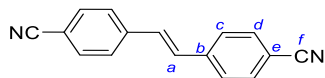
Scheme S1. Electrophiles and nucleophiles used in this work.

Reaction of methyl diazoacetate (**1a**) with sulfonium ylide **2a**

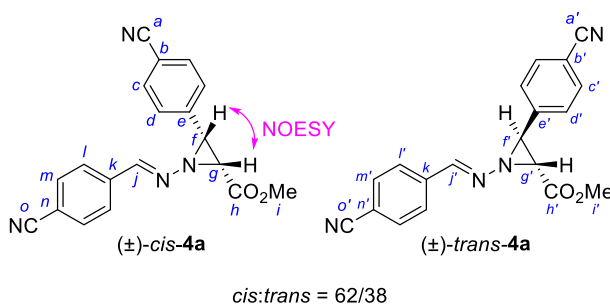
Methyl (**2R***, **3R***)-1-((4-cyanobenzylidene)amino)-3-(4-cyanophenyl)aziridine-2-carboxylate (\pm)-*cis*-**4a** and methyl (**2R***, **3S***)-1-((4-cyanobenzylidene)amino)-3-(4-cyanophenyl)aziridine-2-carboxylate (\pm)-*trans*-**4a** were obtained as a mixture from (4-cyanobenzyl)dimethylsulfonium tetrafluoroborate (399 mg, 1.51 mmol) in DMSO (5 mL), KO^tBu (176 mg, 1.57 mmol) in DMSO (2 mL) and **1a** (80.2 mg, 0.80 mmol) in DMSO (1 mL) according to *GP A* (reaction time: 3 h, column chromatography: n-pentane/CH₂Cl₂/EtOAc = 4:1:1): viscous yellow oil (98.7 mg, yield 40%); *cis/trans*-**4a** = 62:38 (¹H NMR spectroscopy).

Additionally, (*E*)-4,4'-dicyanostilbene¹ (30.2 mg, yield 17%) was isolated: light-yellow crystals.

The photolytic decomposition of stabilized sulfonium ylides via carbene intermediates to form *trans*-alkenes has been reported by Trost.²



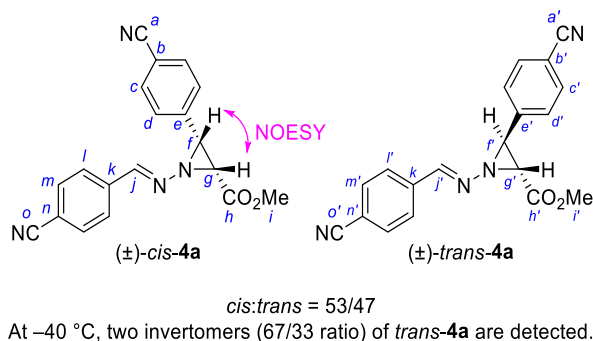
¹H NMR (400 MHz, CDCl₃): δ = 7.20 (s, 2 H, H^a), 7.61 (d, *J* = 8.5 Hz, 4 H, H^c), 7.68 (d, *J* = 8.5 Hz, 4 H, H^d).¹ **¹³C NMR** (101 MHz, CDCl₃): δ = 111.8 (C, C^e), 118.9 (C, C^f), 127.4 (CH, C^c), 130.4 (CH, C^a), 132.8 (CH, C^d), 140.8 (C, C^b). **HRMS** (EI⁺): *m/z* calcd for C₁₆H₁₀N₂⁺ (M⁺): 230.0838, found 230.0842.



NMR signals assigned to *cis*-**4a** (from NMR spectra acquired at r.t.):

¹H NMR (400 MHz, CDCl₃): δ = 3.42 (d, *J* = 8.2 Hz, 1 H, H^g), 3.59 (s, 3 H, Hⁱ), 3.71 (d, *J* = 8.2 Hz, 1 H, H^f), 7.58–7.60 (m, 2 H, H^d), 7.62–7.67 (m, 2 H, H^c, superimposed with resonances of *trans*-**4a**), 7.68–7.70 (m, 2 H, H^m, superimposed with resonances of *trans*-**4a**), 7.76–7.78 (m, 2 H, H^l), 8.64 (s, 1 H, H^j). The configuration of *cis*-**4a** was derived by a NOESY experiment. **¹³C NMR** (101 MHz, CDCl₃) δ = 49.2 (CH, C^g), 49.6 (CH, C^f), 52.5 (CH₃, Cⁱ), 112.0 (C, C^b), 114.5 (C, Cⁿ), 118.4 (C, C^o), 118.7 (C, C^a), 128.4 (CH, C^l), 128.7 (CH, C^d), 132.1 (CH, C^c), 132.7 (CH, C^m), 137.2 (C, C^k), 138.9 (C, C^e), 159.6 (CH, C^j), 166.6 (C, C^h). **HRMS** (ESI⁺): *m/z* calcd for C₁₉H₁₅N₄O₂⁺ (M+H⁺): 331.1190, found 331.1189.

At ambient temperature, ¹H and ¹³C NMR signals of *trans*-**4a** are broadened, presumably because of the dynamics of the pyramidal inversion at the aziridine nitrogen.³ To achieve better analyzable NMR spectra, an independently prepared sample (conditions as described above) was analyzed by 1D and 2D NMR spectra at –40 °C, and a *cis/trans* ratio of 53:47 was determined for **4a**.



For *cis*-**4a** one set of resonances was observed at –40 °C. The signals of *trans*-**4a** split into two

separate sets for the two invertomers (in a 67:33 ratio, ^1H NMR spectroscopy). The NMR data at hand did not allow us *endo*-/*exo*-assignments for the individual sets of signals of *trans*-**4a**.

NMR signals assigned to (\pm)-*trans*-**4a** (major invertomer):

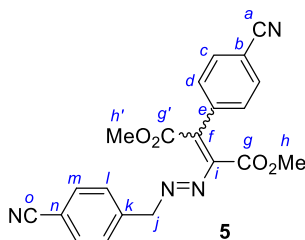
^1H NMR (400 MHz, CDCl_3 , -40°C): $\delta = 3.34$ (d, $J = 3.5$ Hz, 0.6 H, $\text{H}^{\text{g}'}$), 3.79 (s, 1.7 H, $\text{H}^{\text{i}'}$), 3.82–3.84 (m, 1.4 H, $\text{H}^{\text{f}'}$, superimposed with $\text{H}^{\text{i}'}$ resonances of the minor invertomer), 7.44 (d, $J = 8.0$ Hz, 1.2 H, $\text{H}^{\text{d}'}$), 7.58–7.73 (m, 10.7 H, $\text{H}^{\text{c}'}$, $\text{H}^{\text{l}'}$, and $\text{H}^{\text{m}'}$, superimposed with $\text{H}^{\text{c}'}$ and $\text{H}^{\text{m}'}$ resonances of the minor isomer and H^{c} , H^{d} , and H^{m} of *cis*-**4a**), 8.26 (s, 0.9 H, $\text{H}^{\text{j}'}$, superimposed with the $\text{H}^{\text{j}'}$ resonance of the minor invertomer). ^{13}C NMR (101 MHz, CDCl_3 , -40°C): $\delta = 48.6$ (CH, $\text{C}^{\text{g}'}$), 48.89 (CH, $\text{C}^{\text{f}'}$), 53.2 (CH_3 , $\text{C}^{\text{i}'}$), 111.44 (C, $\text{C}^{\text{b}'}$), 113.3 (C, $\text{C}^{\text{n}'}$), 118.7 (C, $\text{C}^{\text{a}'}$ or $\text{C}^{\text{o}'}$), 118.8 (C, $\text{C}^{\text{a}'}$ or $\text{C}^{\text{o}'}$), 127.1 (CH, $\text{C}^{\text{d}'}$), 127.8 (CH, $\text{C}^{\text{l}'}$), 132.47 (CH, $\text{C}^{\text{e}'}$), 132.54 (CH, $\text{C}^{\text{m}'}$, superimposed with the $\text{C}^{\text{m}'}$ resonance of the minor invertomer), 137.2 (C, $\text{C}^{\text{k}'}$), 141.2 (C, $\text{C}^{\text{e}'}$), 155.6 (CH, $\text{C}^{\text{j}'}$), 165.67 (C, $\text{C}^{\text{h}'}$).

NMR signals assigned to (\pm)-*trans*-**4a** (minor invertomer):

^1H NMR (400 MHz, CDCl_3 , -40°C): $\delta = 3.62$ (d, $J = 4.5$ Hz, 0.3 H, $\text{H}^{\text{g}'}$), 3.82–3.84 (m, 1.4 H, $\text{H}^{\text{i}'}$, superimposed with $\text{H}^{\text{f}'}$ resonances of the major invertomer), 3.97 (d, $J = 4.6$ Hz, 0.3 H, $\text{H}^{\text{f}'}$), 7.39 (d, $J = 8.1$ Hz, 0.6 H, $\text{H}^{\text{d}'}$), 7.55 (d, $J = 8.1$ Hz, 0.6 H, $\text{H}^{\text{l}'}$), 7.58–7.73 (m, 10.7 H, $\text{H}^{\text{c}'}$ and $\text{H}^{\text{m}'}$, superimposed with $\text{H}^{\text{c}'}$, $\text{H}^{\text{l}'}$, and $\text{H}^{\text{m}'}$ resonances of the major isomer and H^{c} , H^{d} , and H^{m} of *cis*-**4a**), 8.27 (s, 0.9 H, $\text{H}^{\text{j}'}$, superimposed with the $\text{H}^{\text{j}'}$ resonance of the major invertomer). ^{13}C NMR (101 MHz, CDCl_3 , -40°C): $\delta = 47.4$ (CH, $\text{C}^{\text{g}'}$), 51.1 (CH, $\text{C}^{\text{f}'}$), 53.3 (CH_3 , $\text{C}^{\text{i}'}$), 111.8 (C, $\text{C}^{\text{b}'}$), 113.8 (C, $\text{C}^{\text{n}'}$), 118.50 (C, $\text{C}^{\text{a}'}$ or $\text{C}^{\text{o}'}$), 118.55 (C, $\text{C}^{\text{a}'}$ or $\text{C}^{\text{o}'}$), 127.9 (CH, $\text{C}^{\text{l}'}$), 130.6 (CH, $\text{C}^{\text{d}'}$), 131.9 (CH, $\text{C}^{\text{e}'}$), 132.54 (CH, $\text{C}^{\text{m}'}$, superimposed with the $\text{C}^{\text{m}'}$ resonance of the major invertomer), 135.7 (C, $\text{C}^{\text{e}'}$), 136.6 (C, $\text{C}^{\text{k}'}$), 159.9 (CH, $\text{C}^{\text{j}'}$), 169.2 (C, $\text{C}^{\text{h}'}$).

Reaction of dimethyl diazomalonate (**1b**) with sulfonium ylide **2a**

Dimethyl 2-((E)-(4-cyanobenzyl)diazenyl)-3-(4-cyanophenyl)but-2-enedioate (5) was obtained from (4-cyanobenzyl)dimethylsulfonium tetrafluoroborate (395 mg, 1.49 mmol) in DMSO (8 mL), KO^tBu (174 mg, 1.55 mmol) in DMSO (10 mL) and **1b** (229 mg, 1.45 mmol) in DMSO (1.5 mL) according to *GP A* (reaction time: overnight, column chromatography: n-pentane/ CH_2Cl_2 / $\text{EtOAc} = 4:1:2$): yellow foam (61.0 mg, yield 21%).



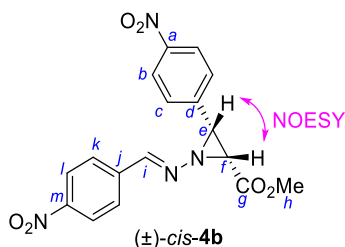
^1H NMR (400 MHz, CDCl_3): $\delta = 3.57$ and 3.94 (2 s, 2×3 H, H^{h} and $\text{H}^{\text{h}'}$), 4.02 (s, 2 H, H^{j}), 7.21–7.23 (m, 4 H, H^{d} and H^{l}), 7.48–7.50 (m, 4 H, H^{c} and H^{m}). ^{13}C NMR (151 MHz, CDCl_3): $\delta = 53.0$ (CH_3 , C^{h} or $\text{C}^{\text{h}'}$), 53.3 (CH_2 , C^{j}), 53.8 (CH_3 , C^{h} or $\text{C}^{\text{h}'}$), 112.1 (C, C^{b} and C^{n}), 118.4 (C, C^{a} and C^{o}),

128.4 (CH, C^{d,l}), 132.2 (CH, C^c and C^m), 138.2 (C, C^e and C^k), 153.8 (C, C^f and Cⁱ), 160.4 (C, C^g or C^{g'}), 162.3 (C, C^g or C^{g'}). **HRMS** (ESI⁺): *m/z* calcd for C₂₁H₁₇N₄O₄⁺ (M+H⁺): 389.1244, found 389.1247. **IR** (neat, ATR): 2954, 2227, 1738, 1609, 1506, 1435, 1331, 1256, 1193, 1167, 1085, 1046, 1019, 831, 804, 762, 726 cm⁻¹.

Reaction of methyl diazoacetate (**1a**) with sulfonium ylide **2b**

Methyl (2R*, 3R*)-1-((4-nitrobenzylidene)amino)-3-(4-nitrophenyl)aziridine-2-carboxylate (\pm)-*cis*-**4b** and **Methyl (2R*, 3S*)-1-((4-nitrobenzylidene)amino)-3-(4-nitrophenyl)aziridine-2-carboxylate** (\pm)-*trans*-**4b** were obtained as a mixture (*cis:trans* = 2:1, NMR integration) from (4-nitrobenzyl)dimethylsulfonium tetrafluoroborate (506 mg, 1.78 mmol) in DMSO (5 mL), KO^tBu (211 mg, 1.88 mmol) in DMSO (2 mL) and **1a** (95.0 mg, 0.95 mmol) in DMSO (1 mL) according to *GP A* (reaction time 5 h, column chromatography: n-pentane/dichloromethane/ethyl acetate = 4:1:2): yellow foam (144 mg, yield 44%).

The reaction was repeated, and pure *cis*-**4b** was isolated by column chromatography with a long column and an eluent of low polarity (n-pentane/CH₂Cl₂/EtOAc = 4:2:1). The configuration of *cis*-**4b** was derived by a NOESY experiment.



¹H NMR (600 MHz, CDCl₃): δ = 3.47 (d, *J* = 8.3 Hz, 1 H, H^f), 3.60 (s, 3 H, H^h), 3.79 (d, *J* = 8.2 Hz, 1 H, H^e), 7.66–7.68 (m, 2 H, H^c), 7.84–7.86 (m, 2 H, H^k), 8.21–8.23 (m, 2 H, H^b), 8.26–8.29 (m, 2 H, H^l), 8.72 (s, 1 H, Hⁱ). **¹³C NMR** (151 MHz, CDCl₃): δ = 49.4 (CH, C^f), 49.5 (CH, C^e), 52.6 (CH₃, C^h), 123.6 (CH, C^b), 124.2 (CH, C^l), 128.7 (CH, C^k), 128.9 (CH, C^c), 138.9 (C, C^j), 140.9 (C, C^d), 147.8 (C, C^a), 149.5 (C, C^m), 159.4 (CH, Cⁱ), 166.5 (C, C^g). **HRMS** (ESI⁺): *m/z* calcd for C₁₇H₁₅N₄O₆⁺ (M+H⁺): 371.0986, found 371.0988. **IR** (neat, ATR): 3077, 2924, 2851, 1742, 1597, 1513, 1438, 1338, 1202, 1174, 1107, 1051, 1013, 853, 833, 749, 739, 690 cm⁻¹.

At ambient temperature, ¹H and ¹³C NMR signals of *trans*-**4b** are broadened, presumably because of the dynamics of the pyramidal inversion at the aziridine nitrogen.³ To straighten the interpretation of the NMR data for *trans*-**4b**, the reaction of **1a** with **2b** was repeated and worked up by column chromatography (conditions as described above) to give a purified mixture of *cis*- and *trans*-**4b**. To achieve an enriched content of *trans*-**4b**, only those fractions of the column chromatographic separation were combined, which were rich of *trans*-**4b**. In the finally used NMR sample, the *cis/trans* ratio of **4b** was 42:58. After removal of the eluent solvents by evaporation (rotary evaporator) and dissolution of the residual in CDCl₃, the 1D and 2D NMR spectra of this sample were measured at variable temperatures in the range from +50 to –40°C (Figure S1).

Heating to +50 °C did not lead to full coalescence of the broadened signals of *trans*-**4b**. However, at –40 °C the signals of *trans*-**4b** split into two separate sets for the two invertomers (in a 70:30 ratio, ¹H NMR spectroscopy). The NMR data at hand did not allow us *endo*-/*exo*-assignments for the individual sets of signals of *trans*-**4b**.

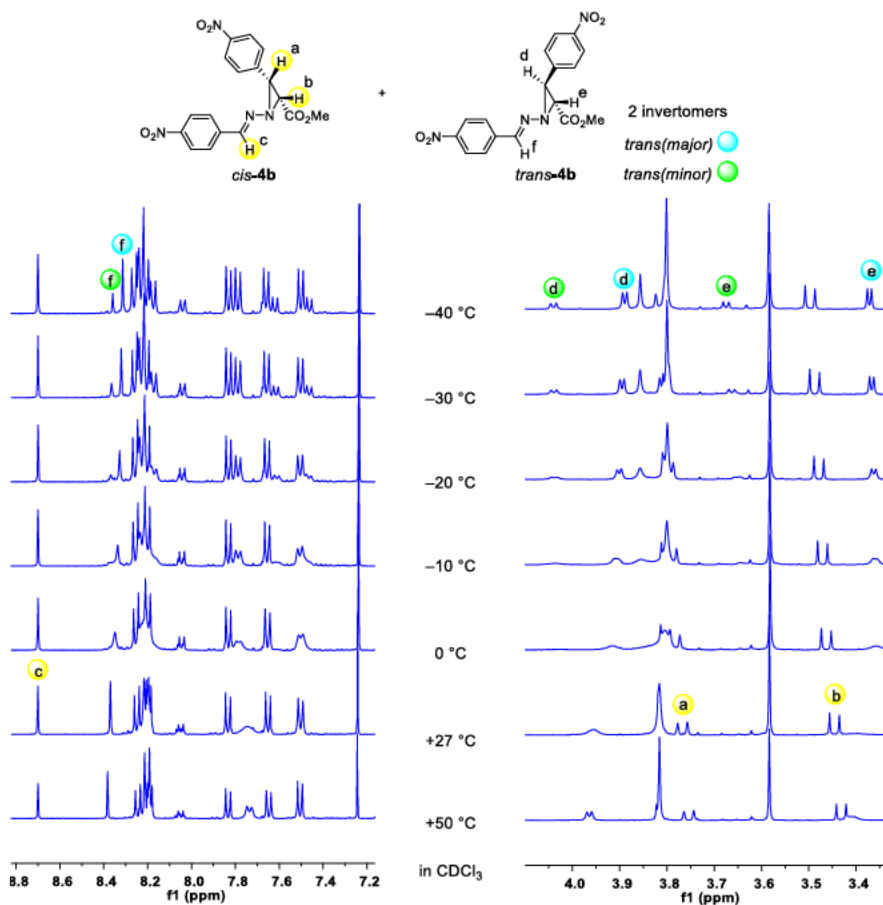
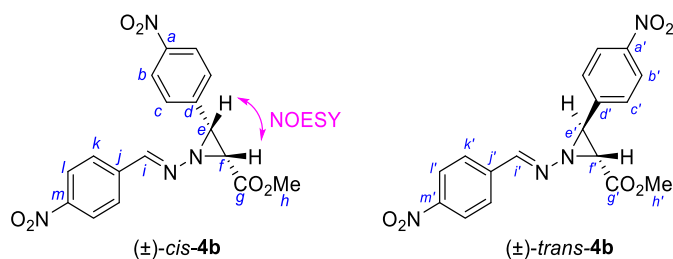


Figure S1. Temperature-dependent ¹H NMR spectra of a 42:58 *cis/trans*-mixture of **4b** in CDCl₃.

For *cis*-**4b**, only one set of resonances was observed in the temperature range from +50 to –40 °C. This indicates a high energetic barrier for the pyramidal inversion at the aziridine nitrogen of *cis*-**4b**, which may prefer to exist in the more stable *endo*-form.



cis:trans = 42/58

At $-40\text{ }^{\circ}\text{C}$, two invertomers (70/30 ratio) of *trans*-**4b** are detected.

NMR signals assigned to (\pm) -*trans*-**4b** (major invertomer):

^1H NMR (400 MHz, CDCl_3 , $-40\text{ }^{\circ}\text{C}$): $\delta = 3.40$ (d, $J = 3.5$ Hz, 1 H, H^f), 3.83 (s, 3 H, H^h , superimposed with resonances for H^e of *cis*-**4b**), 3.91 (d, $J = 3.5$ Hz, 1 H, H^e), 7.51–7.54 (m, 2 H, H^c), 7.80–7.83 (m, 2 H, H^k), 8.19–8.30 (m, 10 H, H^b and H^l superimposed with resonances of the minor invertomer and those for H^b and H^l of *cis*-**4b**), 8.34 (s, 1 H, H^i). **^{13}C NMR** (101 MHz, CDCl_3 , $-40\text{ }^{\circ}\text{C}$): $\delta = 48.8$ (CH, C^e), 48.9 (CH, C^f), 53.35 (CH_3 , C^h), 124.17 (CH, $\text{C}^{b'}$ or $\text{C}^{l'}$), 124.21 (CH, $\text{C}^{b'}$ or $\text{C}^{l'}$), 127.4 (CH, C^c), 128.3 (CH, $\text{C}^{k'}$), 139.0 (C, $\text{C}^{j'}$), 143.3 (C, $\text{C}^{d'}$), 147.2 (C, $\text{C}^{a'}$), 148.5 (C, $\text{C}^{m'}$), 155.4 (CH, $\text{C}^{i'}$), 165.7 (C, C^g).

NMR signals assigned to (\pm) -*trans*-**4b** (minor invertomer):

^1H NMR (400 MHz, CDCl_3 , $-40\text{ }^{\circ}\text{C}$): $\delta = 3.70$ (d, $J = 4.7$ Hz, 0.5 H, H^f), 3.88 (s, 1.2 H, H^h), 4.06 (d, $J = 4.7$ Hz, 0.4 H, H^e), 7.48–7.50 (m, 0.8 H, H^c), 7.63–7.66 (m, 0.8 H, H^k), 8.19–8.30 (m, 10 H, H^b and H^l superimposed with resonances of the major invertomer and those for H^b and H^l of *cis*-**4b**), 8.38 (s, 0.4 H, H^i). **^{13}C NMR** (101 MHz, CDCl_3 , $-40\text{ }^{\circ}\text{C}$): $\delta = 47.8$ (CH, C^f), 50.9 (CH, C^e), 53.44 (CH_3 , C^h), 123.4 (CH, $\text{C}^{b'}$ or $\text{C}^{l'}$), 124.17 (CH, $\text{C}^{b'}$ or $\text{C}^{l'}$), 128.4 (CH, $\text{C}^{k'}$), 131.0 (CH, C^c), 137.8 (C, $\text{C}^{d'}$), 138.4 (C, $\text{C}^{j'}$), 147.3 (C, $\text{C}^{a'}$), 148.7 (C, $\text{C}^{m'}$), 159.8 (CH, $\text{C}^{i'}$), 169.2 (C, C^g).

Reaction of 1-pyrrolidinocyclopentene (3a**) with methyl diazoacetate (**1a**):** see ref.⁴

Reaction of 1-pyrrolidinocyclopentene (3a**) with dimethyl diazomalonate (**1b**)**

Dimethyl 2-(2-(2-(pyrrolidin-1-yl)cyclopent-1-en-1-yl)hydrazono)malonate (9ba**)** was obtained from **1b** (196 mg, 1.24 mmol) and **3a** (176 mg, 1.28 mmol) in diethyl ether (2 mL) according to *GP B* (round bottom flask, $0\text{ }^{\circ}\text{C}$ addition, then room temperature 40 min, filtration): brick-red needles (329 mg, yield 90%); m.p. $91.2\text{ }^{\circ}\text{C}$. NMR and UV-vis spectra (Figure S2) of **9ba** were measured with the temperature strictly controlled at $-50\text{ }^{\circ}\text{C}$.

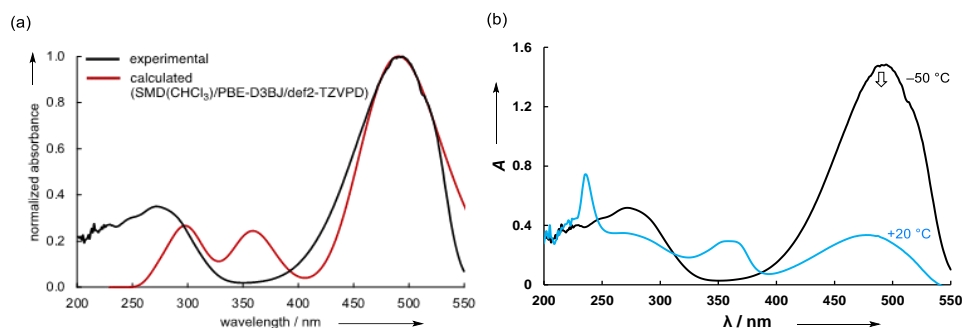
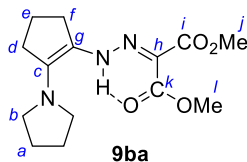


Figure S2. (a) Black curve: UV-vis absorbance of **9ba** (9.67×10^{-5} M) in CHCl_3 at -50 °C (under a dry N_2 atmosphere, pre-cooled CHCl_3 and **9ba** were mixed in a volumetric flask at -50 °C and a known volume of this chilled **9ba** solution was immediately injected into CHCl_3 in the flask for the photometric measurement at -50 °C); red curve: calculated UV-vis spectrum of **9ba**.⁵ The absorbance of **9ba** is normalized to 1 A.U. at the $\lambda_{\text{max}} = 491$ nm. The λ_{max} of the calculated spectrum was matched with the experimental spectrum ($\lambda + 29$ nm) and a line-broadening function applied (0.3 eV). (b) UV-Vis spectroscopic monitoring of **9ba** (9.67×10^{-5} M) in CHCl_3 at -50 and $+20$ °C.



^1H NMR (400 MHz, CDCl_3 , -50 °C): $\delta = 1.82\text{--}1.89$ (m, 2 H, H^e), $1.91\text{--}1.94$ (m, 4 H, H^a), 2.65 (t, $J = 7.4$ Hz, 2 H, H^f), 2.77 (t, $J = 7.3$ Hz, 2 H, H^d), $3.51\text{--}3.55$ (m, 4 H, H^b), 3.78 (s, 3 H, H^l), 3.80 (s, 3 H, H^j). **^{13}C NMR** (151 MHz, CDCl_3 , -50 °C): $\delta = 18.7$ (CH_2 , C^e), 25.7 (CH_2 , C^a), 29.9 (CH_2 , C^d), 34.2 (CH_2 , C^f), 50.2 (CH_2 , C^b), 51.9 (CH_3 , C^j or C^l), 52.1 (CH_3 , C^j or C^l), 110.2 (C, C^h), 111.7 (C, C^g), 136.5 (C, C^c), 165.0 (C, C^k), 166.3 (C, C^i). **HRMS** (ESI⁺): m/z calcd for $\text{C}_{14}\text{H}_{22}\text{N}_3\text{O}_4^+$ ($\text{M}+\text{H}^+$): 296.1605, found 296.1603. **IR** (neat, ATR): 2942, 2848, 1683, 1652, 1645, 1588, 1506, 1441, 1418, 1343, 1283, 1224, 1177, 1084, 1021, 982, 948, 932, 842, 785, 744 cm^{-1} . **UV-vis** (CHCl_3 , -50 °C): $\lambda_{\text{max}} = 491$ nm ($\lg \epsilon = 4.49$) (Figure S2). **Single crystal X-ray crystallography** (**9ba**): $\text{C}_{14}\text{H}_{21}\text{N}_3\text{O}_4$ (vv842).

When a solution of **9ba** in CDCl_3 was prepared at -50 °C and then warmed up to $+20$ °C, tautomerization of **9ba** led to a mixture of **9ba**, **11ba**, and **12ba**. A tiny resonance at δ 4.26 ppm, which appeared during warming up at 0 °C and disappeared at $+20$ °C, was probably due to traces of **10ba** (Figure S3).

As depicted in Figure S2b, the absorbance of **9ba** at 491 nm in CHCl_3 at -50 °C decreased during warming up to $+20$ °C due to tautomerization, which is consistent with the results of the NMR spectroscopic monitoring of a solution of **9ba** in CDCl_3 in the temperature range from -50 to $+20$ °C (Figure S3).

Chapter 4. Quantification of the Electrophilicities of Diazoalkanes

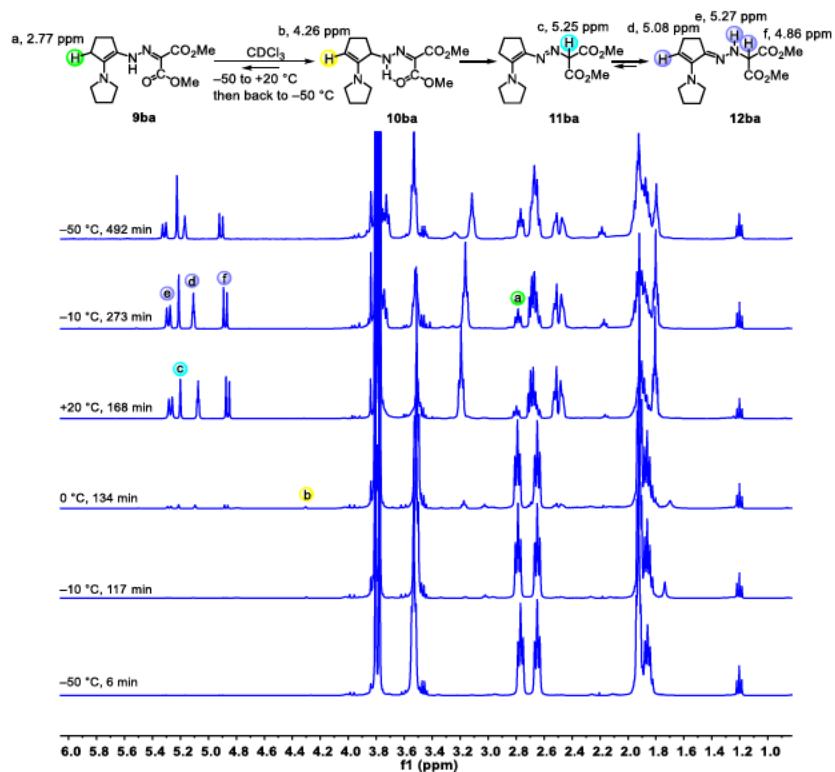


Figure S3. ^1H NMR (400 MHz) spectroscopic monitoring of the tautomerization of **9ba** (2.98×10^{-5} mol) in CDCl_3 (0.55 mL) at -10 to $20\text{ }^\circ\text{C}$ and then to $-50\text{ }^\circ\text{C}$.

^1H NMR spectroscopic monitoring of the reactions of **1b** with **3a** in CDCl_3 at $-50\text{ }^\circ\text{C}$ and $-40\text{ }^\circ\text{C}$ suggests the simultaneous formation of **9ba** and **10ba**, accompanied by a subsequent formation of **11ba**. Species **12ba** appears with the lowest growth rate and was observed only in the kinetics at $-30\text{ }^\circ\text{C}$ (Figure S4).

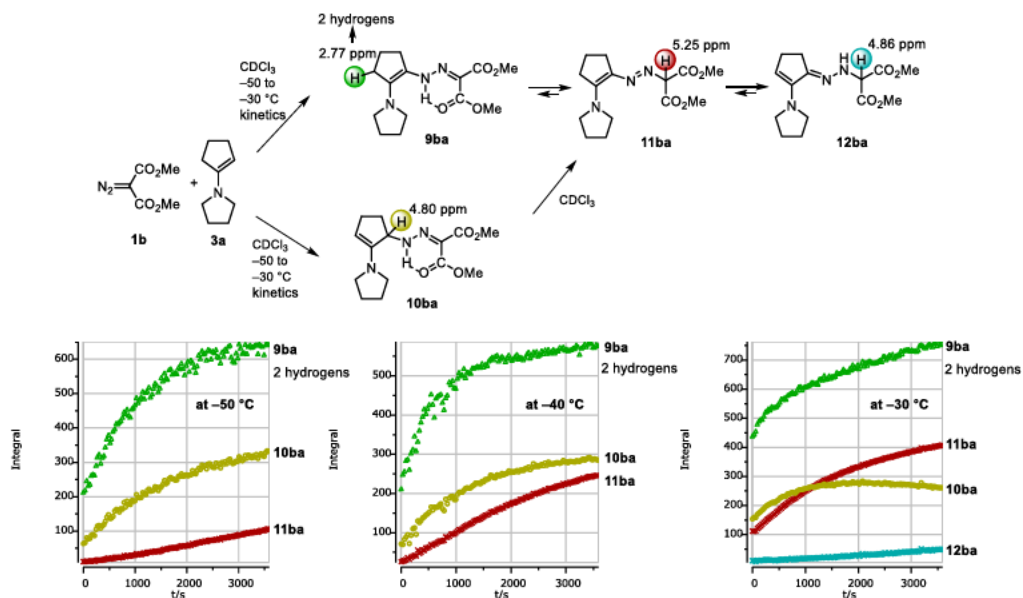
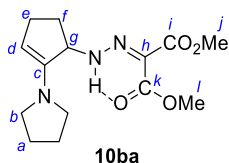


Figure S4. Changes in the integrals of **9ba** (green curves, 2 hydrogens), **10ba** (yellow curves), **11ba** (brick-red curves), and **12ba** (blue curve, only at $-30\text{ }^{\circ}\text{C}$) during ^1H NMR spectroscopic monitoring of the reactions of **1b** with **3a** at -50 , -40 and $-30\text{ }^{\circ}\text{C}$ in CDCl_3 .

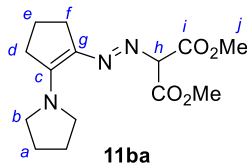
Enamines **10ba**, **11ba**, and **12ba** are tautomers of the crystallized **9ba**. To elucidate the structures of **10ba**, **11ba**, and **12ba** and assign the NMR chemical shifts, different approaches were used:

The structural characterization of **10ba** was based on the NMR spectroscopic investigation of the reaction mixture of **1b** + **3a** in CDCl_3 at $-50\text{ }^{\circ}\text{C}$. One-dimensional (^1H and $^{13}\text{C}\{^1\text{H}\}$) and two-dimensional (^1H , ^1H -COSY, ^1H , ^{13}C -HSQC, and HMBC) NMR experiments were used to assign the individual chemical shifts of nuclei in **10ba**. Thus, **10ba** was characterized in a mixture, which also contained the unreacted educts (**1b**, **3a**), other products (**9ba** and **11ba**), the integration standard (IS = mesitylene), and traces of decomposition products (cP = cyclopentanone).



Characteristic NMR signals assigned to **10ba**: ^1H NMR (400 MHz, CDCl_3 , $-50\text{ }^{\circ}\text{C}$): $\delta = 1.79$ – 1.80 (4 H, H^a , superimposed with hydrogens of **3a**), 1.94 – 1.98 (1 H, H^e , superimposed with hydrogens of **3a**, **9ba** and **11ba**), 2.25 – 2.29 (m, 1 H, H^f , superimposed with hydrogens of **3a**), 2.37 – 2.41 (1 H, H^e , superimposed with hydrogens of **3a**), 2.46 – 2.50 (m, 1 H, H^f , superimposed with hydrogens of **3a**), 2.98 – 3.01 (m, 4 H, H^b , superimposed with NCH_2 of **3a**), 3.80 and 3.82 (2 s, H^j and H^i , superimposed with OCH_3 of **1b** and **9ba**), 4.26 (s, 1 H, H^d), 4.80 (br d, $J = 7.8$ Hz, 1 H, H^g), 11.7 (br s, 1 H, NH). ^{13}C NMR (101 MHz, CDCl_3 , $-50\text{ }^{\circ}\text{C}$): $\delta = 24.9$ (CH_2 , C^a), 28.0 (CH_2 , C^f), 31.4 (CH_2 , C^e), 48.6 (CH_2 , C^b), 52.1 (CH_3 , C^j or C^i), 52.5 (CH_3 , C^j or C^i), 68.9 (CH , C^g), 97.7 (CH , C^d), 115.0 (C, C^h), 145.2 (C, C^c), 164.1 (C, C^i or C^k), 164.6 (C, C^i or C^k).

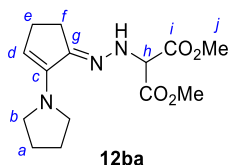
The structural characterization of **11ba** was based on the NMR spectroscopic investigation of the reaction mixture of **1b** + **3a** in CDCl_3 at $-30\text{ }^{\circ}\text{C}$. One-dimensional (^1H and $^{13}\text{C}\{^1\text{H}\}$) and two-dimensional (^1H , ^1H -COSY, ^1H , ^{13}C -HSQC, and HMBC) NMR experiments were used to assign the individual chemical shifts of nuclei in **11ba**. Thus, **11ba** was characterized in a mixture, which also contained unreacted educts (**1b**, **3a**), other products (**9ba**, **10ba** and **12ba**), the integration standard (mesitylene), and traces of decomposition products (cP = cyclopentanone).



Characteristic NMR signals assigned to **11ba**: ^1H NMR (400 MHz, CDCl_3 , $-30\text{ }^{\circ}\text{C}$): $\delta = 1.87$ – 2.01 (m, 6 H, H^a and H^e , superimposed with hydrogens of **9ba** and **10ba**), 2.66 – 2.73 (m, 4 H, H^d

and H^f, superimposed with H^f of **9ba**), 3.53–3.56 (m, 4 H, H^b, superimposed with NCH₂ of **9ba**), 3.79 (s, 6 H, Hⁱ, superimposed with OCH₃ of **9ba**), 5.25 (s, 1 H, H^h). ¹³C NMR (101 MHz, CDCl₃, –30 °C): δ = 19.4 (CH₂, C^e), 25.8 (CH₂, C^a), 28.3 (CH₂, C^d), 34.7 (CH₂, C^f), 51.1 (CH₂, C^b), 52.8 (CH₃, C^j), 79.1 (CH, C^h), 129.8 (C, C^g), 157.4 (C, C^c), 168.6 (C, Cⁱ).

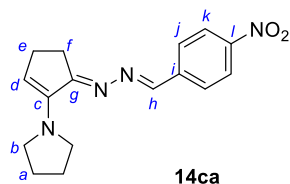
The structural characterization of **12ba** was based on the NMR spectroscopic investigation of a sample, which was prepared by dissolving crystalline **9ab** in CDCl₃ at ambient temperature. One-dimensional (¹H and ¹³C{¹H}) and two-dimensional (¹H,¹H-COSY, ¹H,¹³C-HSQC, and HMBC) NMR experiments were used to assign the individual chemical shifts of nuclei in **12ba**. In this way, **12ba** was characterized in a mixture, which also contained the initially dissolved tautomer **9ba**, another product (**11ba**) as well as traces of decomposition products (cP = cyclopentanone, DMM = dimethyl malonate) and diethyl ether (residual from the crystallization of **9ab**).



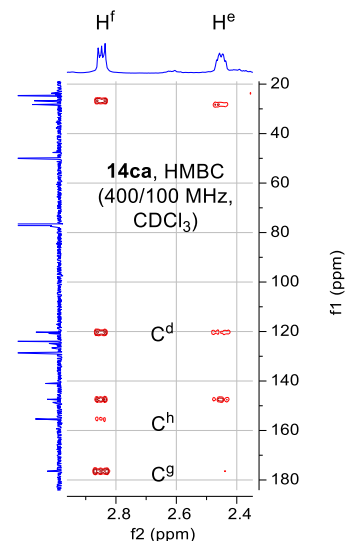
Characteristic NMR signals assigned to **12ba**: ¹H NMR (600 MHz, CDCl₃, +30 °C): δ = 1.80–1.82 (m, 4 H, H^a), 2.47–2.49 (m, 2 H, H^e), 2.52–2.54 (m, 2 H, H^f), 3.19–3.21 (m, 4 H, H^b), 3.79 (s, 6 H, Hⁱ), 4.86 (d, *J* = 9.6 Hz, 1 H, H^h), 5.08 (t, *J* = 2.9 Hz, 1 H, H^d), 5.27 (d, *J* = 9.5 Hz, 1 H, NH). ¹³C NMR (151 MHz, CDCl₃, +30 °C): δ = 24.7 (CH₂, C^a), 25.5 (CH₂, C^f), 26.3 (CH₂, C^e), 49.8 (CH₂, C^b), 53.1 (CH₃, C^j), 66.6 (CH, C^h), 112.0 (CH, C^d), 147.1 (C, C^c), 158.6 (C, C^g), 168.4 (C, Cⁱ).

Reaction of 1-pyrrolidinocyclopentene (**3a**) with *p*-nitrophenyldiazomethane (**1c**)

1-((E)-5-(E)-4-Nitrobenzylidene)hydrazineylidene)cyclopent-1-en-1-ylpyrrolidine (14ca) was obtained from **1c** (193 mg, 1.18 mmol) in dry CH₂Cl₂ (4.5 mL) and **3a** (206 mg, 1.50 mmol) in dry CH₂Cl₂ (0.5 mL) according to *GP B* (–26 °C, 12 days, low temperature recrystallization from CH₂Cl₂/hexane): red solid (318 mg). The NMR spectra show that the precipitated crystals were contaminated with the diazo compound **1c** and further unknown impurities. Attempts to purify **14ca** failed, however, because **14ca** decomposed during column chromatography on silica gel.

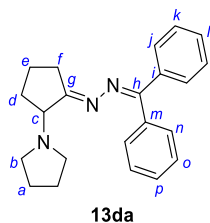


^1H NMR (400 MHz, CDCl_3): δ = 1.88–1.92 (m, 4 H, H^a , superimposed with unassigned peaks), 2.50–2.53 (m, 2 H, H^e), 2.90–2.93 (m, 2 H, H^f), 3.33–3.37 (m, 4 H, H^b), 5.53 (t, J = 3.2 Hz, 1 H, H^d), 7.92–7.96 (m, 2 H, H^i), 8.25–8.28 (m, 2 H, H^k), 8.46 (s, 1 H, H^h); the chemical shifts for H^e/C^e and H^f/C^f were assigned on the basis of the HMBC spectrum. **^{13}C NMR** (101 MHz, CDCl_3): δ = 24.8 (CH_2 , C^a), 26.9 (CH_2 , C^e), 28.4 (CH_2 , C^f), 50.1 (CH_2 , C^b), 120.4 (CH , C^d), 124.1 (CH , C^k), 128.7 (CH , C^j), 141.1 (C, C^i), 147.5 (C, C^c), 148.8 (C, C^l), 155.5 (CH, C^h), 176.6 (C, C^g). **HRMS** (ESI^+): m/z calcd for $\text{C}_{16}\text{H}_{19}\text{N}_4\text{O}_2^+$ ($\text{M}+\text{H}^+$): 299.1503, found 299.1505. **IR** (neat, ATR): 3067, 2842, 1622, 1589, 1552, 1511, 1419, 1396, 1335, 1300, 1161, 1138, 1105, 1029, 974, 958, 944, 851, 794, 739, 690 cm^{-1} .



Reaction of 1-pyrrolidinocyclopentene (**3a**) with diphenyldiazomethane (**1d**)

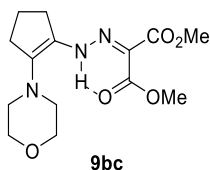
(*E*)-1-(2-((Diphenylmethylene)hydrazineylidene)cyclopentyl)pyrrolidine (**13da**) was obtained from **1d** (488 mg, 2.51 mmol) and **3a** (470 mg, 3.42 mmol) without solvent according to *GP B* (round-bottom flask, $40\text{ }^\circ\text{C}$, 2 days, column chromatography: dichloromethane/methanol = 10:1): yellow oil (52 mg, yield 6.3%).



^1H NMR (400 MHz, CDCl_3): δ = 1.63–1.69 (m, 5 H, $4 \times \text{H}^a$ and $1 \times \text{H}^e$), 1.87–2.05 (m, 2 H, H^d and H^e), 2.16–2.24 (m, 1 H, H^d), 2.38 (dt, J = 17.8, 8.4 Hz, 1 H, H^f), 2.67–2.89 (m, 5 H, $4 \times \text{H}^b$ and $1 \times \text{H}^f$), 3.61 (t, J = 7.8 Hz, 1 H, H^c), 7.20–7.22 (m, 2 H, Ph), 7.32–7.44 (m, 6 H, Ph), 7.62–7.64 (m, 2 H, Ph). **^{13}C NMR** (101 MHz, CDCl_3): δ = 21.1 (CH_2 , C^e), 23.3 (CH_2 , C^a), 29.4 (CH_2 , C^d), 29.8 (CH_2 , C^f), 51.2 (CH_2 , C^b), 65.3 (CH, C^c), 128.3 (CH, Ph), 128.47 (CH, Ph), 128.50 (CH, Ph), 128.6 (CH, Ph), 130.3 (CH, Ph), 136.1 (C, Ph), 137.4 (C, Ph), 161.1 (C, C^h), 168.1 (C, C^g). **HRMS** (ESI^+): m/z calcd for $\text{C}_{22}\text{H}_{26}\text{N}_3^+$ ($\text{M}+\text{H}^+$): 332.2121, found 332.2123. **IR** (neat, ATR): 3416, 3055, 2962, 2875, 2349, 1741, 1699, 1643, 1557, 1490, 1444, 1415, 1320, 1300, 1074, 1030, 970, 909, 777, 731, 694 cm^{-1} .

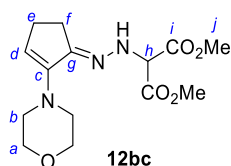
Reaction of 1-morpholinocyclopentene (3c) with dimethyl diazomalonate (1b)

Dimethyl 2-(2-(2-morpholinocyclopent-1-en-1-yl)hydrazinenyl)malonate (9bc) was isolated from the reaction of **1b** (50.0 mg, 0.32 mmol) and **3c** (49.4 mg, 0.32 mmol) in diethyl ether:hexane = 1:1 (1 mL) according to *GP B* (sealed round-bottom flask, $-20\text{ }^{\circ}\text{C}$, 3 weeks): orange needles. Crystals of **9bc** were isolated from the $-20\text{ }^{\circ}\text{C}$ reaction mixture and directly analyzed by low-temperature single crystal X-ray diffraction. At room temperature and open air, **9bc** decomposes rapidly.

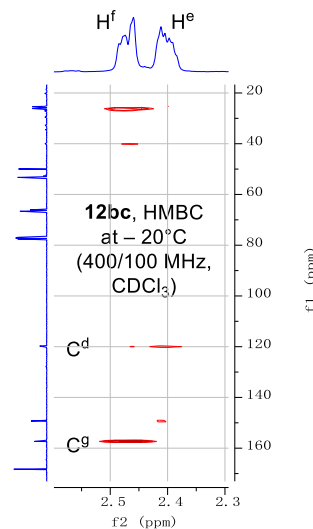


Single crystal X-ray crystallography (9bc): $\text{C}_{14}\text{H}_{21}\text{N}_3\text{O}_5$ (wv088).

Dimethyl (E)-2-(2-(2-morpholinocyclopent-2-en-1-ylidene)hydrazinyl)malonate (12bc) was obtained from **1b** (27.7 mg, 0.18 mmol) and **3c** (26.9 mg, 0.18 mmol) in diethyl ether:hexane = 1:1 (0.5 mL) according to *GP B* (sealed vial, $-20\text{ }^{\circ}\text{C}$, 3 weeks, recrystallized with the cap still sealed, heating to max. $30\text{ }^{\circ}\text{C}$): orange-yellow crystals (40.8 mg, yield 72%); m.p. $89.9\text{ }^{\circ}\text{C}$. Spectroscopic data agree with those reported in refs.^{6a,b} **12bc** is stable both in solid state and in solution (CDCl_3) for a couple of months.



$^1\text{H NMR}$ (400 MHz, CDCl_3): $\delta = 2.45\text{--}2.48$ (m, 2 H, H^e), $2.52\text{--}2.55$ (m, 2 H, H^f), $3.05\text{--}3.07$ (m, 4 H, H^b), $3.76\text{--}3.78$ (m, 4 H, H^a), 3.79 (s, 6 H, H^j , partially superimposed with H^a), 4.86 (d, $J = 9.3\text{ Hz}$, 1 H, H^h , simplifies to a singlet when D_2O is added), 5.29 (d, $J = 9.3\text{ Hz}$, 1 H, NH, vanishes with added D_2O), 5.47 (t, $J = 2.9\text{ Hz}$, 1 H, H^d). **$^{13}\text{C NMR}$** (101 MHz, CDCl_3): $\delta = 25.5$ (CH_2 , C^f), 26.2 (CH_2 , C^e), 50.1 (CH_2 , C^b), 53.1 (CH_3 , C^j), 66.4 (CH , C^h), 66.8 (CH_2 , C^a), 118.9 (CH , C^d), 149.5 (C , C^c), 157.2 (C , C^g), 168.4 (C , C^i). **HRMS** (ESI⁺): m/z calcd for $\text{C}_{14}\text{H}_{22}\text{N}_3\text{O}_5^+$ ($\text{M}+\text{H}^+$): 312.1554, found 312.1551. **IR** (neat, ATR): 3268, 2985, 2958, 2885, 2854, 2822, 1754, 1750, 1732, 1622, 1601, 1455, 1429, 1383, 1326, 1303, 1242, 1230, 1212, 1190, 1161, 1132, 1115, 1069, 1019, 968, 947, 922, 889, 762, 692, 667 cm^{-1} . **UV-vis** (CH_2Cl_2) $\lambda_{\text{max}} = 269\text{ nm}$ ($\log_{10} \epsilon = 4.03$) (Figure S5). **Single crystal X-ray crystallography (12bc):** $\text{C}_{14}\text{H}_{21}\text{N}_3\text{O}_5$ (wv086).



In contrast to **9ba** (Figure S2b), the UV-Vis absorbance of **12bc** in CH_2Cl_2 at $20\text{ }^{\circ}\text{C}$ (Figure S5) remained constant over a time range of 60 min. This suggests that **12bc** is the most stable tautomer.

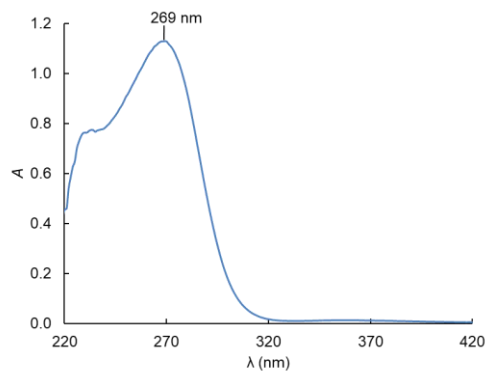
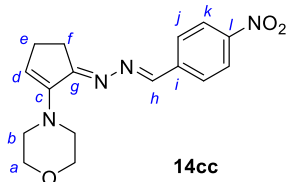


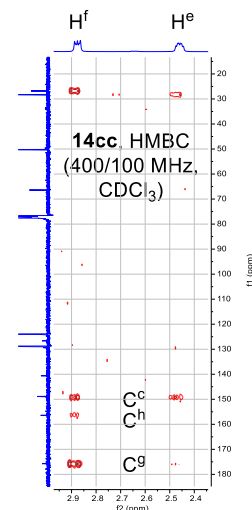
Figure S5. UV-Vis spectrum of **12bc** (0.209 mM) in CH_2Cl_2 at 20 °C.

Reaction of 1-morpholinocyclopentene (**3c**) with *p*-nitrophenyldiazomethane (**1c**)

4-((5*E*)-5-((4-Nitrobenzylidene)hydrazineylidene)cyclopent-1-en-1-yl)morpholine (14cc**)** was obtained from **1c** (189 mg, 1.16 mmol) in dry CH_2Cl_2 (4.5 mL) and **3c** (207 mg, 1.35 mmol) in dry CH_2Cl_2 (0.5 mL) according to *GP B* (room temperature for 1 hour, then -26 °C for 39 days, low temperature recrystallization: CH_2Cl_2 /hexane): red solid (178 mg, yield 49%); m.p. 170.8 °C (dec.).



^1H NMR (400 MHz, CDCl_3): δ = 2.51–2.54 (m, 2 H, H^e), 2.93–2.95 (m, 2 H, H^f), 3.20–3.22 (m, 4 H, H^b), 3.85–3.88 (m, 4 H, H^a), 5.95 (br s, 1 H, H^d), 7.92–7.96 (m, 2 H, H^j), 8.25–8.29 (m, 2 H, H^k), 8.48 (s, 1 H, H^h). **^{13}C NMR** (101 MHz, CDCl_3): δ = 26.9 (CH_2 , C^e), 28.4 (CH_2 , C^f), 50.4 (CH_2 , C^b), 66.5 (CH_2 , C^a), 124.1 (CH, C^k), 128.9 (CH, C^j), 140.7 (C, C^i), 149.0 (C, C^l), 149.2 (C, C^c , detected only in the HMBC spectrum), 156.5 (CH, C^h), 175.8 (C, C^g); the chemical shifts for H^e/C^e and H^f/C^f were assigned on the basis of the HMBC spectrum, C^d could not be detected. **HRMS** (ESI⁺): m/z calcd for $\text{C}_{16}\text{H}_{19}\text{N}_4\text{O}_3^+$ ($\text{M}+\text{H}^+$): 315.1452, found 315.1451. **IR** (neat, ATR): 3074, 2963, 2836, 2067, 1625, 1590, 1556, 1514, 1448, 1413, 1384, 1341, 1304, 1265, 1170, 1146, 1114, 1071, 1026, 989, 954, 898, 881, 850, 839, 795, 772, 751, 688 cm^{-1} .

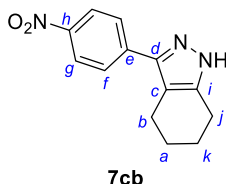


Reaction of 1-pyrrolidinocyclohexene (3b**) with methyl diazoacetate (**1a**):** See ref.⁴

Reaction of 1-pyrrolidinocyclohexene (3b) with methyl diazoacetate (1b): See ref.⁴

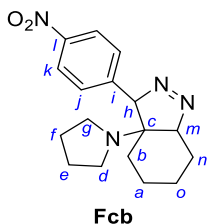
Reaction of 1-pyrrolidinocyclohexene (3b) with *p*-nitrophenyldiazomethane (1c)

3-(4-Nitrophenyl)-4,5,6,7-tetrahydro-1*H*-indazole (7cb) was obtained from **1c** (188 mg, 1.15 mmol) in dry CH₂Cl₂ (4.5 mL) and **3b** (182 mg, 1.20 mmol) in dry CH₂Cl₂ (0.5 mL) according to *GP B* (−26 °C, 33 days, low temperature recrystallization: CH₂Cl₂/hexane): light-yellow solid (172 mg, yield 62%); m.p. 180.2 °C (reported m.p.: 177–178 °C^{7a}, 183–185 °C^{7b})



¹H NMR (400 MHz, CDCl₃): δ = 1.81–1.90 (m, 4 H, H^a and H^k), 2.70 (t, *J* = 5.8 Hz, 2 H, H^j), 2.76 (t, *J* = 5.7 Hz, 2 H, H^b), 5.60 (br s, 2 H, NH, overlapped with resonance of trace water), 7.86–7.90 (m, 2 H, H^f), 8.23–8.27 (m, 2 H, H^g). **¹³C NMR** (101 MHz, CDCl₃): δ = 21.8 (CH₂, C^j), 22.21 (CH₂, C^b), 22.23 (CH₂, C^k), 23.3 (CH₂, C^a), 114.7 (C, C^c), 124.2 (CH, C^g), 127.2 (CH, C^f), 139.4 (C, C^e), 143.0 (C, Cⁱ), 144.5 (C, C^d), 147.0 (C, C^h). **HRMS** (EI): *m/z* calcd for C₁₃H₁₃N₃O₂⁺ (M⁺): 243.1002, found 243.1002. **IR** (neat, ATR): 3560, 3193, 3129, 3068, 2922, 2852, 1598, 1510, 1504, 1445, 1335, 1321, 1274, 1105, 993, 934, 852, 825, 759, 740, 708 cm^{−1}.

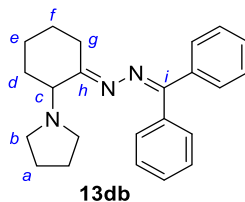
During NMR monitoring of the reaction of **1c** with **3b**, initial formation of **Fcb** was observed. NMR data assigned to **Fcb** (in a mixture with **1c** and **3b**) are listed below:



¹H NMR (400 MHz, CD₂Cl₂, −10 °C): δ = 0.92–1.01 (m, 1 H, H^b), 1.04–1.10 (m, 1 H, H^a), 1.19–1.37 (m, 3 H, H^a, H^b, and H^o), 1.57–1.64 (m, 1 H, H^o, superimposed with hydrogens of **3b**), 1.72–1.81 (m, 4 H, H^e and H^f, superimposed with hydrogens of **3b**), 1.85–1.94 (m, 1 H, Hⁿ), 2.37–2.45 (m, 1 H, Hⁿ), 2.61–2.72 (m, 4 H, H^d and H^g), 4.08–4.11 (m, 1 H, H^m), 5.24–5.25 (m, 1 H, H^h), 7.48–7.52 (m, 2 H, H^j), 8.18–8.21 (m, 2 H, H^k). **¹³C NMR** (101 MHz, CD₂Cl₂, −10 °C): δ = 19.9 (CH₂, C^a), 22.1 (CH₂, C^o), 24.3 (CH₂, C^{e,f}), 24.5 (CH₂, Cⁿ), 28.2 (CH₂, C^b), 46.4 (CH₂, C^{d,g}), 69.3 (C, C^c), 85.7 (CH, C^h), 86.0 (CH, C^m), 123.4 (CH, C^k), 129.4 (CH, C^j), 145.2 (C, Cⁱ), 147.2 (C, C^l).

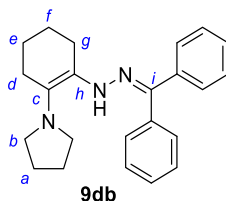
Reaction of 1-pyrrolidinocyclohexene (3b) with diphenyldiazomethane (1d)

1-(2-((Diphenylmethylene)hydrazineylidene)cyclohexyl)pyrrolidine (13db) was obtained from **1d** (150 mg, 0.77 mmol) and **3b** (155 mg, 1.02 mmol) in CD₂Cl₂ (0.5 mL) according to *GP B* (NMR tube, 40 °C, 6 days, column chromatography: dichloromethane/methanol = 10:1): yellow oil (104 mg, yield: 38%, calculated by considering a 26 mol-% content of MeOH in the sample).



¹H NMR (400 MHz, CDCl₃): δ = 1.43–1.74 (m, 7 H, H^e, H^f, and H^a), 1.87 (br s, 3 H, H^e and H^g), 2.36–2.57 (m, 6 H, H^d and H^b), 3.03 (br s, 1 H, H^c), 7.14–7.16 (m, 2 H, Ph), 7.29–7.39 (m, 6 H, Ph), 7.60–7.63 (m, 2 H, Ph); additional resonance: 3.38 (s, integral: 0.94 for 3 H corresponding to a 26 mol-% contamination with MeOH, eluent of the column chromatography). **¹³C NMR** (101 MHz, CDCl₃): δ = 21.4 (CH₂, C^e), 23.6 (CH₂, C^a), 26.3 (CH₂, C^f), 26.9 (CH₂, C^d), 32.1 (CH₂, C^g), 51.0 (CH₂, C^b), 66.3 (CH, C^c), 128.17 (CH, Ph), 128.18 (CH, Ph), 128.21 (CH, Ph), 128.4 (CH, Ph), 128.5 (CH, Ph), 129.9 (CH, Ph), 135.9 (C, Ph), 137.5 (C, Ph), 159.8 (C, Cⁱ), 163.0 (C, C^h); additional resonance: 50.4 (MeOH). **HRMS** (ESI⁺): *m/z* calcd for C₂₃H₂₈N₃⁺ (M+H⁺): 346.2278, found 346.2283. **IR** (neat, ATR): 3059, 2935, 2858, 2797, 2423, 2201, 1622, 1561, 1490, 1443, 1349, 1320, 1299, 1074, 1029, 1018, 1000, 970, 907, 775, 726, 692 cm⁻¹.

During in situ NMR monitoring of the **1d** + **3b** reaction, **9db** was the observed product.^{7c} NMR data assigned to **9db** (in a mixture with **1d** and **3b**) are listed below. Upon work up by column chromatography on silica gel **9db** tautomerized to give **13db**.

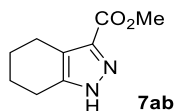


¹H NMR (400 MHz, CD₂Cl₂): δ = 1.55–1.58 (m, 4 H, H^a), 1.69–1.72 (m, 2 H, H^f), 1.76–1.79 (m, 2 H, H^e), 2.06–2.10 (m, 2 H, H^d), 2.52–2.55 (m, 4 H, H^b), 2.64–2.68 (m, 2 H, H^g), 7.28–7.34 (m, 4 H, Ph), 7.47–7.53 (m, 2 H, Ph), 7.54–7.62 (m, 4 H, Ph), 8.62 (s, 1 H, NH). **¹³C NMR** (101 MHz, CD₂Cl₂): δ = 20.1 (CH₂, C^d), 23.0 (CH₂, C^e), 23.7 (CH₂, C^f), 24.3 (CH₂, C^a and C^g), 49.1 (CH₂, C^b), 117.2 (C, C^h), 126.0 (CH, Ph), 127.0 (CH, Ph), 128.4 (CH, Ph), 128.8 (CH, Ph), 129.6 (CH, Ph), 129.8 (CH, Ph), 133.2 (C, C^c), 134.6 (C, Ph), 139.6 (C, Ph), 140.4 (C, Cⁱ).

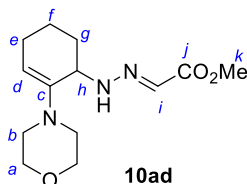
Reaction of 1-morpholinocyclohexene (**3d**) with methyl diazoacetate (**1a**)

Methyl 4,5,6,7-tetrahydro-1H-indazole-3-carboxylate (7ad = 7ab) was obtained from **1a** (209 mg, 2.09 mmol) and **3d** (340 mg, 2.03 mmol) in CDCl₃ (250 μL) according to *GP B* (NMR tube, 30 °C, 3 weeks, column chromatography: n-pentane/diethyl ether = 1:1 ~ diethyl ether): white

powder (118 mg, yield 32%). The spectroscopic data of **7ab** has been reported in ref.⁴ for the reaction of **1a** with **3b**.



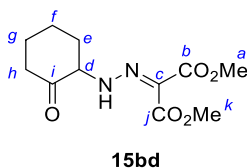
During NMR monitoring of the reaction of **1a** with **3d**, initial formation of **10ad** was observed, and the NMR data assigned to **10ad** are listed below:



¹H NMR (400 MHz, CDCl₃): δ = 1.42–1.49 (m, 2 H, H^f, superimposed with hydrogens of **3d**), 1.74–1.82 (m, 2 H, H^g, superimposed with hydrogens of **3d**), 1.99–2.00 (m, 2 H, H^e, superimposed with hydrogens of **3d**), 2.80–2.83 (m, 4 H, H^b), 3.61–3.64 (m, 4 H, H^a, superimposed with OCH₂ of **3d**), 4.11 (q, J = 5.0 Hz, 1 H, H^h), 4.82 (t, J = 4.1 Hz, 1 H, H^d), 6.77 (s, 1 H, Hⁱ), 6.92 (d, J = 5.4 Hz, 1 H, NH). **¹³C NMR** (101 MHz, CDCl₃): δ = 18.3 (CH₂, C^f), 24.3 (CH₂, C^e), 26.9 (CH₂, C^g), 46.1 (CH₂, C^b), 51.7 (CH₂, C^h, superimposed), 67.6 (CH₂, C^a), 106.3 (CH, C^d), 120.8 (CH, Cⁱ), 143.2 (C, C^c), 165.1 (C, C^j); an unequivocal assignment of H^k/C^k could not be made.

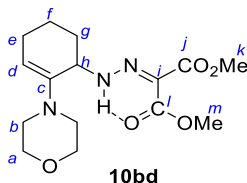
Reaction of 1-morpholinocyclohexene (**3d**) with dimethyl diazomalonate (**1b**)

Dimethyl 2-(2-(2-oxocyclohexyl)hydrazineylidene)malonate (15bd**)** was obtained from **1b** (194 mg, 1.23 mmol) and **3d** (202 mg, 1.21 mmol) in CDCl₃ (200 μ L) according to *GP B* (sealed NMR tube, 40 °C, 2 days, conversion 62%, 1,1,2,2-tetrachloroethane as internal standard, column chromatography: n-pentane/EtOAc = 5:1): light-orange oil (103 mg, yield 33%).



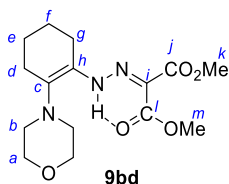
¹H NMR (400 MHz, CDCl₃): δ = 1.61–1.81 (m, 3 H, H^e, H^f, and H^g), 1.96–2.01 (m, 1 H, H^f), 2.10–2.18 (m, 1 H, H^g), 2.39 (td, J = 13.6, 6.4 Hz, 1 H, H^h), 2.53–2.66 (m, 2 H, H^e and H^h), 3.80 (m, 3 H, H^a or H^k), 3.84 (m, 3 H, H^a or H^k), 4.35 (dt, J = 12.1, 6.0 Hz, 1 H, H^d), 11.69 (d, J = 5.0 Hz, 1 H, NH). **¹³C NMR** (101 MHz, CDCl₃): δ = 24.0 (CH₂, C^f), 27.5 (CH₂, C^g), 35.2 (CH₂, C^e), 41.2 (CH₂, C^h), 52.0 and 52.3 (2 \times CH₃, C^a and C^k), 68.2 (CH, C^d), 118.6 (C, C^c), 163.8 and 164.0 (2 \times C, C^b and C^j), 206.2 (C, Cⁱ). **HRMS** (ESI⁺): m/z calcd for C₁₁H₁₆N₂NaO₅⁺ (M+Na⁺): 279.0951, found 279.0956. **IR** (neat, ATR): 3228, 2952, 2866, 1714, 1673, 1515, 1435, 1332, 1280, 1200, 1153, 1122, 1084, 841, 802 cm⁻¹.

Dimethyl 2-(2-(2-morpholinocyclohex-2-en-1-yl)hydrazineylidene)malonate (10bd) was observed and characterized by 2D NMR spectroscopy as the initial product from **1b** (79.7 mg, 0.50 mmol) and **3d** (83.5 mg, 0.50 mmol) in CDCl₃ (400 μL) at room temperature 1 day after the reactants were mixed. Listed NMR chemical shifts were obtained from the crude reaction mixture without workup.



¹H NMR (400 MHz, CDCl₃): δ = 1.39–1.49 (m, 2 H, H^f, superimposed with hydrogens of **3d**), 1.79–1.88 (m, 2 H, H^g), 1.97–2.11 (m, 2 H, H^e), 2.52 (dt, *J* = 11.8, 4.7 Hz, 2 H, H^b), 2.76 (dt, *J* = 11.8, 4.8 Hz, 2 H, H^b), 3.55 (t, *J* = 4.7 Hz, 4 H, H^a), 3.66 (s, 3 H, H^m), 3.70 (s, 3 H, H^k), 4.23 (q, *J* = 5.5 Hz, 1 H, H^h), 4.81 (t, *J* = 4.0 Hz, 1 H, H^d), 11.48 (d, *J* = 5.4 Hz, 1 H, NH). **¹³C NMR** (101 MHz, CDCl₃): δ = 18.4 (CH₂, C^f), 24.2 (CH₂, C^e), 29.9 (CH₂, C^g), 48.8 (CH₂, C^b), 51.4 (CH₃, C^m), 51.7 (CH₃, C^k), 55.9 (CH, C^h), 66.6 (CH₂, C^a), 106.6 (CH, C^d), 116.3 (C, Cⁱ), 142.9 (C, C^c), 163.8 (C, C^l), 163.9 (C, C^j).

In the same NMR sample, **dimethyl 2-(2-(2-morpholinocyclohex-1-en-1-yl)hydrazineylidene)malonate (9bd)** was detected 4 days after the reactants were mixed. Due to the slow formation of **9bd** under the above-mentioned conditions, the experiment was repeated at higher concentrations of **1b** (284 mg, 1.80 mmol) and **3d** (205 mg, 1.23 mmol) in CDCl₃ (220 μL) at 50 °C. NMR spectra for **9bd** were recorded 2 days after the reactants were mixed. Listed NMR chemical shifts were obtained from the crude reaction mixture without workup.

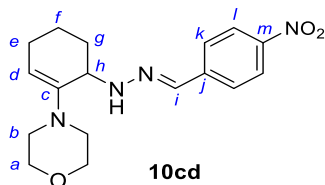


¹H NMR (400 MHz, CDCl₃): δ = 1.31–1.36 (m, 4 H, H^e and H^f), 1.81–1.86 (m, 2 H, H^g), 2.06 (dt, *J* = 6.3, 3.0 Hz, 2 H, H^d), 2.29–2.33 (m, 4 H, H^b), 3.46 (s, 7 H, H^a and H^m, superimposed with hydrogens of **1b** and **10bd**), 3.49 (s, 3 H, H^k), 13.24 (s, 1 H, NH). **¹³C NMR** (101 MHz, CDCl₃): δ = 20.1 (CH₂, C^g), 20.8 (CH₂, C^e), 21.5 (CH₂, C^d), 21.8 (CH₂, C^f), 49.4 (CH₂, C^b), 50.7 (CH₃, C^m), 51.4 (CH₃, C^k), 66.4 (CH₂, C^a), 115.0 (C, Cⁱ), 130.9 (C, C^h), 131.2 (C, C^c), 163.0 (C, C^l), 163.3 (C, C^j).

Reaction of 1-morpholinocyclohexene (**3d**) with *p*-nitrophenyldiazomethane (**1c**)

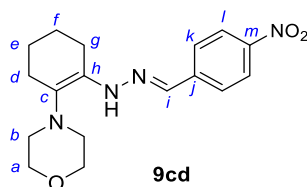
4-(6-(2-(4-Nitrobenzylidene)hydrazineyl)cyclohex-1-en-1-yl)morpholine (10cd) and **4-(2-(2-(4-nitrobenzylidene)hydrazineyl)cyclohex-1-en-1-yl)morpholine (9cd)** were observed by NMR spectroscopic methods during the reaction **1c** (50.8 mg, 0.31 mmol) with **3d** (52.4 mg, 0.31

mmol) in CD_2Cl_2 (450 μL). The structures of **10cd** and **9cd** were assigned based on their NMR resonances. However, **10cd** and **9cd** both decomposed upon workup with column chromatography. At the beginning of the sluggish reaction of **1c** with **3d** at room temperature, only the resonances of product **10cd** (in a mixture with the educts **1c** and **3d**) were detected. After 11 days at room temperature, **9cd** became detectable and slowly increased in amount.



^1H NMR (400 MHz, CD_2Cl_2): $\delta = 1.57\text{--}1.60$ (m, 2 H, H^f , superimposed with resonances of **3d**), $1.79\text{--}1.87$ (m, 1 H, H^g), $1.98\text{--}2.01$ (m, 1 H, H^g , superimposed with resonances of **3d**), $2.08\text{--}2.20$ (m, 2 H, H^e), $2.60\text{--}2.66$ (m, 2 H, H^b), $2.87\text{--}2.93$ (m, 2 H, H^b), $3.64\text{--}3.65$ (m, 4 H, H^a , superimposed with resonances of **3d**), 4.17 (q, $J = 4.8$ Hz, 1 H, H^h), 4.91 (t, $J = 4.1$ Hz, 1 H, H^d), 6.38 (d, $J = 4.8$ Hz, 1 H, NH), 7.62 (s, 1 H, H^i), $7.62\text{--}7.65$ (m, 2 H, H^k), $8.12\text{--}8.15$ (m, 2 H, H^l , superimposed with resonances of **1c**). **^{13}C NMR** (101 MHz, CD_2Cl_2): $\delta = 18.6$ (CH_2 , C^f), 25.0 (CH_2 , C^e), 29.6 (CH_2 , C^g), 49.5 (CH_2 , C^b), 52.7 (CH, C^h), 67.3 (CH_2 , C^a , superimposed with resonances of **3d**), 106.5 (CH, C^d), 124.3 (CH, C^l), 125.7 (CH, C^k), 132.0 (CH, C^i), 143.4 (C, C^j), 144.9 (C, C^c), 146.7 (C, C^m).

Analyzing the same sample after 25 days at room temperature made it possible to characterize **9cd** (in a mixture with **1c**, **3d**, and **10cd**) by NMR spectroscopy:

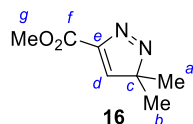


^1H NMR (400 MHz, CD_2Cl_2): $\delta = 1.64\text{--}1.69$ (m, 4 H, H^e and H^f), $2.10\text{--}2.13$ (m, 2 H, H^d), $2.46\text{--}2.49$ (m, 2 H, H^g), $2.60\text{--}2.62$ (m, 4 H, H^b), $3.73\text{--}3.76$ (m, 4 H, H^a), 7.53 (s, 1 H, H^i), $7.58\text{--}7.62$ (m, 2 H, H^k), $8.10\text{--}8.12$ (m, 2 H, H^l), 9.16 (br s, 1 H, NH). **^{13}C NMR** (101 MHz, CD_2Cl_2): $\delta = 20.0$ (CH_2 , C^d), 22.5 (CH_2 , C^f), 23.3 (CH_2 , C^e), 24.1 (CH_2 , C^g), 50.3 (CH_2 , C^b), 67.7 (CH_2 , C^a), 122.1 (C, C^h), 124.3 (CH, C^l), 125.4 (CH, C^k), 130.4 (CH, C^i), 132.5 (C, C^c), 143.6 (C, C^j), 146.2 (C, C^m).

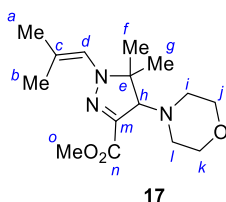
Reaction of 1-morpholinoisobutene (**3e**) with methyl diazoacetate (**1a**)

Methyl 3,3-dimethyl-3H-pyrazole-5-carboxylate (**16**) and **methyl 5,5-dimethyl-1-(2-methylprop-1-en-1-yl)-4-morpholino-4,5-dihydro-1H-pyrazole-3-carboxylate** (**17**) were obtained from **1a** (254 mg, 2.54 mmol) and **3e** (359 mg, 2.54 mmol) in CDCl_3 (200 μL) according to *GP B* (NMR tube, 50°C , 3 days, conversion 60%, 1,1,2,2-tetrachloroethane as internal standard, column chromatography: n-pentane/diethyl ether = 1:1): white powder (**16**, 98.1 mg,

yield 25%), m.p. 95.4 °C (reported m.p.: 95 °C^{8c}), and yellow crystals (**17**, 40.0 mg, 11%), m.p. 103.7 °C.



¹H NMR (400 MHz, CDCl₃): δ = 1.49 (d, *J* = 1.1 Hz, 6 H, H^a and H^b), 3.97 (d, *J* = 1.2 Hz, 3 H, H^g), 7.68 (s, 1 H, H^d). **¹³C NMR** (101 MHz, CDCl₃): δ = 19.9 (CH₃, C^a and C^b), 52.7 (CH₃, C^g), 95.2 (C, C^c), 146.9 (C, C^e), 154.5 (CH, C^d), 161.6 (C, C^f). **HRMS** (ESI⁺): *m/z* calcd for C₇H₁₀N₂NaO₂⁺ (M+Na⁺): 177.0634, found 177.0634. Spectroscopic data consistent with those reported in ref.^{6a,8}



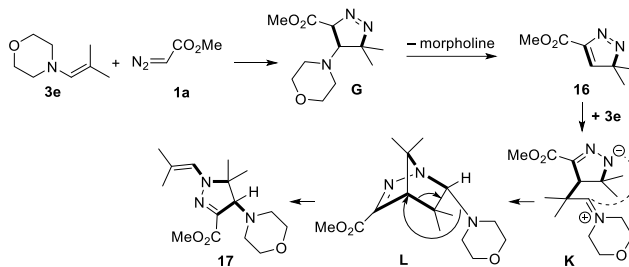
¹H NMR (400 MHz, CDCl₃): δ = 1.07 (s, 3 H, H^f or H^g), 1.30 (s, 3 H, H^f or H^g), 1.74 (d, *J* = 1.4 Hz, 3 H, H^a or H^b), 1.79 (d, *J* = 1.4 Hz, 3 H, H^a or H^b), 2.55–2.85 (m, 4 H, Hⁱ and H^l), 3.48 (s, 1 H, H^h), 3.59–3.67 (m, 4 H, H^j and H^k), 3.84 (s, 3 H, H^o), 5.84 (hept, *J* = 1.5 Hz, 1 H, H^d). **¹³C NMR** (101 MHz, CDCl₃): δ = 18.7 (CH₃, C^a or C^b), 19.3 (CH₃, C^f or C^g), 23.4 (CH₃, C^a or C^b), 24.5 (CH₃, C^f or C^g), 50.9 (CH₂, Cⁱ and C^l, detected only in the HMBC spectrum), 52.0 (CH₃, C^o), 67.7 (CH₂, C^j and C^k), 69.4 (C, C^e), 74.4 (CH, C^h), 119.5 (CH, C^d), 128.6 (C, C^c), 135.6 (C, C^m), 164.8 (C, Cⁿ). At room temperature, the resonances of Cⁱ and C^l were only detected in the HMBC spectrum of **17**.

To support the structural assignment, the NMR spectra of **17** were also recorded at –50 °C in CDCl₃. **¹H NMR** (400 MHz, CDCl₃, –50 °C): δ = 1.05 (s, 3 H, H^f or H^g), 1.27 (s, 3 H, H^f or H^g), 1.71 (s, 3 H, H^a or H^b), 1.75 (s, 3 H, H^a or H^b), 2.29 (d, *J* = 11.6 Hz, 1 H, Hⁱ or H^l), 2.50 (t, *J* = 12.1 Hz, 1 H, Hⁱ or H^l), 2.66 (d, *J* = 11.9 Hz, 1 H, Hⁱ or H^l), 3.15 (t, *J* = 11.9 Hz, 1 H, Hⁱ or H^l), 3.47 (s, 1 H, H^h), 3.50–3.59 (m, 2 H, H^j and H^k), 3.67–3.69 (m, 1 H, H^j or H^k), 3.77–3.78 (m, 1 H, H^j or H^k), 3.82 (s, 3 H, H^o), 5.83–5.84 (m, 1 H, H^d). **¹³C NMR** (101 MHz, CDCl₃, –50 °C): δ = 18.7 (CH₃, C^a or C^b), 19.1 (CH₃, C^f or C^g), 23.3 (CH₃, C^a or C^b), 24.0 (CH₃, C^f or C^g), 46.8 (CH₂, Cⁱ or C^l), 52.3 (CH₃, C^o), 53.8 (CH₂, Cⁱ or C^l), 66.8 (CH₂, C^j or C^k), 68.2 (CH₂, C^j or C^k), 69.3 (C, C^e), 73.4 (CH, C^h), 119.2 (CH, C^d), 129.2 (C, C^c), 135.1 (C, C^m), 164.8 (C, Cⁿ). **HRMS** (ESI⁺): *m/z* calcd for C₁₅H₂₅N₃NaO₃⁺ (M+Na⁺): 318.1788, found 318.1787. **IR** (neat, ATR): 2945, 2846, 1676, 1501, 1440, 1395, 1287, 1257, 1215, 1207, 1181, 1115, 1083, 1044, 1018, 998, 970, 868, 854, 830, 784, 766, 688 cm⁻¹.

A mechanism for the formation of **17** is shown in Scheme 7 (Chapter 4.1). Alternatively, the 2:1 product **17** may be formed by stepwise or concerted Diels-Alder reaction of **16** with **3e** to give the diazabicyclo[2.2.1]heptane (**L**) followed by ring opening and migration of the morpholino group (Scheme S2). Both mechanisms are in line with the observed formation of **17** from isolated **16** and

3e (Figure S6).

When pure **16** was mixed with **3e** in CDCl_3 and heated at $+60^\circ\text{C}$, first traces of **17** were observed (^1H NMR spectroscopy) within a reaction time of less than one day (Figure S6). The concentration of **17** further increased at elongated reaction times (CDCl_3 , 60°C).



Scheme S2. Alternative mechanism for the formation of **17** from **16** and **3e**.

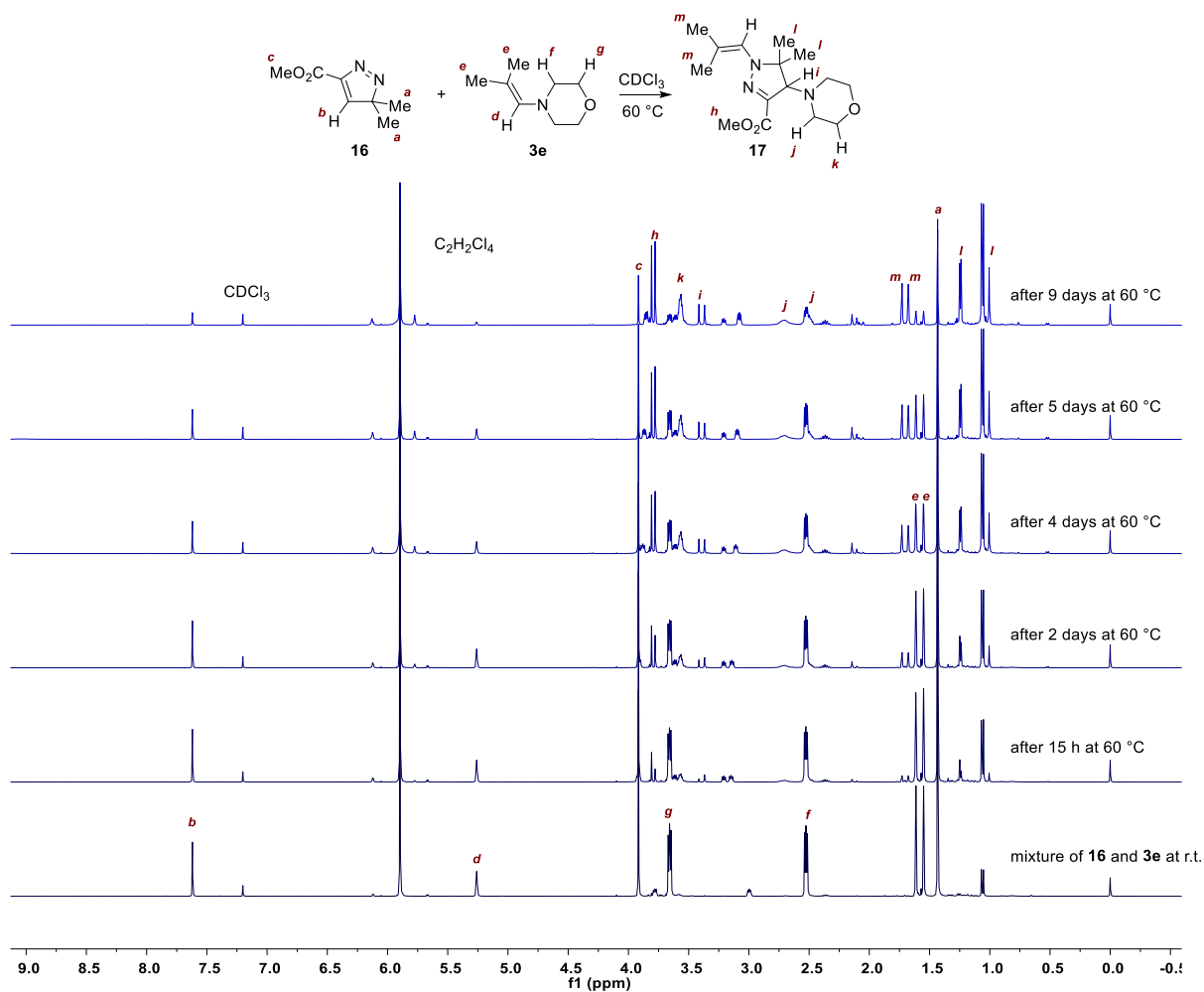
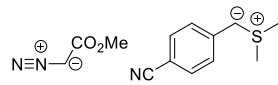
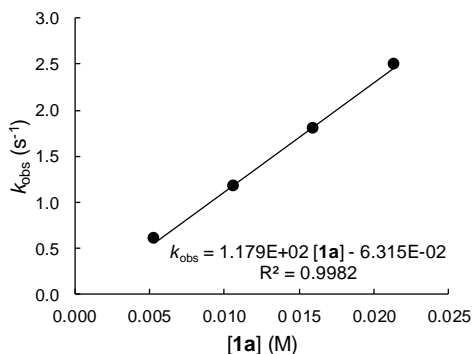
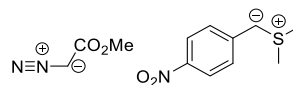


Figure S6. Formation of **17** from **16** ($c_0 = 37.7$ mM) and **3e** ($c_0 = 46.6$ mM) in CDCl_3 at $+60^\circ\text{C}$ with 1,1,2,2-tetrachloroethane ($c = 184$ mM) as internal standard monitored by ^1H NMR spectroscopy (400 MHz).

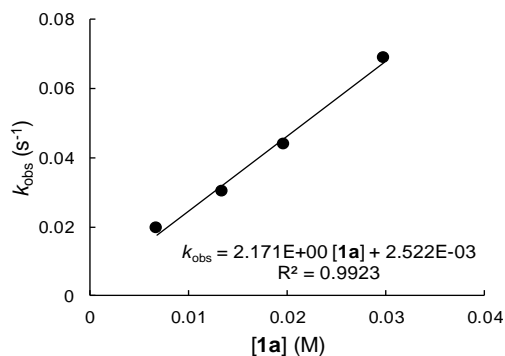
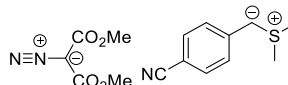
4.2.2 Kinetics

Reactions of diazo compounds **1a** and **1b** with S-ylides **2a** or **2b** in DMSO**Table S1.** Kinetics of the reaction of **1a** with **2a** in DMSO at 20 °C (stopped-flow method, detection at 372 nm).


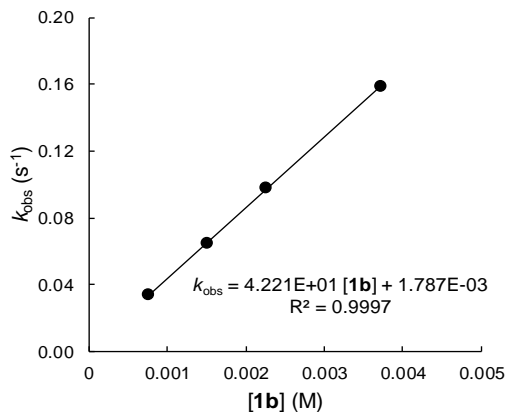
[1a] (M)	[2a (H)BF ₄] (M)	[KO ^t Bu] (M)	<i>k</i> _{obs} (s ⁻¹)
5.35 × 10 ⁻³	8.11 × 10 ⁻⁵	9.36 × 10 ⁻⁵	5.97 × 10 ⁻¹
1.07 × 10 ⁻²	8.11 × 10 ⁻⁵	9.36 × 10 ⁻⁵	1.17
1.60 × 10 ⁻²	8.11 × 10 ⁻⁵	9.36 × 10 ⁻⁵	1.79
2.14 × 10 ⁻²	8.11 × 10 ⁻⁵	9.36 × 10 ⁻⁵	2.49
<i>k</i>₂ = 1.18 × 10² M⁻¹ s⁻¹			

**Table S2.** Kinetics of the reaction of **1a** with **2b** in DMSO at 20 °C (conventional method, evaluated at 518 nm).


[1a] (M)	[2b (H)BF ₄] (M)	[KO ^t Bu] (M)	<i>k</i> _{obs} (s ⁻¹)
6.87 × 10 ⁻³	7.67 × 10 ⁻⁵	7.94 × 10 ⁻⁵	1.93 × 10 ⁻²
1.35 × 10 ⁻²	7.52 × 10 ⁻⁵	7.78 × 10 ⁻⁵	3.02 × 10 ⁻²
1.98 × 10 ⁻²	7.37 × 10 ⁻⁵	7.63 × 10 ⁻⁵	4.39 × 10 ⁻²
2.99 × 10 ⁻²	7.67 × 10 ⁻⁵	7.94 × 10 ⁻⁵	6.88 × 10 ⁻²
<i>k</i>₂ = 2.17 M⁻¹ s⁻¹			

**Table S3.** Kinetics of the reaction of **1b** with **2a** in DMSO at 20 °C (conventional method, evaluated at 372 nm).


[1b] (M)	[2a (H)BF ₄] (M)	[KO ^t Bu] (M)	<i>k</i> _{obs} (s ⁻¹)
7.59 × 10 ⁻⁴	8.38 × 10 ⁻⁵	9.54 × 10 ⁻⁵	3.41 × 10 ⁻²
1.51 × 10 ⁻³	8.35 × 10 ⁻⁵	9.50 × 10 ⁻⁵	6.45 × 10 ⁻²
2.26 × 10 ⁻³	8.32 × 10 ⁻⁵	9.46 × 10 ⁻⁵	9.82 × 10 ⁻²
3.73 × 10 ⁻³	8.25 × 10 ⁻⁵	9.38 × 10 ⁻⁵	1.59 × 10 ⁻¹
<i>k</i>₂ = 4.22 × 10¹ M⁻¹ s⁻¹			



Kinetic investigations of the reactions of **1a-c** with enamines **3** in CDCl_3 or CD_2Cl_2

Table S4. Second-order rate constants k_2^{exptl} of the reactions of **1a** with **3d** in CDCl_3 at +50 (A), +40 (B), +30 °C (C) (^1H NMR kinetics, 1,1,2,2-tetrachloroethane as the internal standard IS). Activation parameters from Eyring plot (D) were used to calculate ΔG^\ddagger (25°C) and k_2 at +20 and +25 °C. Initial reactant concentrations were determined by using the integration ranges of the IS from +50 to +30 °C at 6.22–5.90, 6.06–5.68, 6.00–5.80 ppm, respectively, with the related reference of IS at 5.93, 5.92 ppm for measurement at 40 and 30 °C, of the vinylic hydrogen of **3d** at 4.66–4.44, 4.50–4.25, 4.47–4.25 ppm, respectively, with the related reference of the vinylic hydrogen of **3d** at 4.56, 4.39, 4.38 ppm, respectively, of the CH hydrogen of **1a** at 4.98–4.62, 4.84–4.46, 4.81–4.46 with the related reference of the CH hydrogen of **1a** at 4.81, 4.66, 4.66 ppm, respectively. Relaxation delay and acquisition time are always 1.00 and 4.09 s, respectively.

T (°C)	$[\mathbf{1a}]_0$ (M)	$[\mathbf{3d}]_0$ (M)	$[\text{IS}]_0$ (M)	k_2^{exptl} ($\text{M}^{-1} \text{s}^{-1}$)	k_2 ($\text{M}^{-1} \text{s}^{-1}$)	ΔG^\ddagger (kJ mol^{-1})
+50	1.92	2.15	0.597	4.82×10^{-6}		
+40	1.99	2.36	0.705	2.75×10^{-6}		
+30	2.13	2.32	0.639	1.38×10^{-6}		
+20					$(7.03 \pm 0.38) \times 10^{-7}$	106
+25					$(9.98 \pm 0.40) \times 10^{-7}$	107

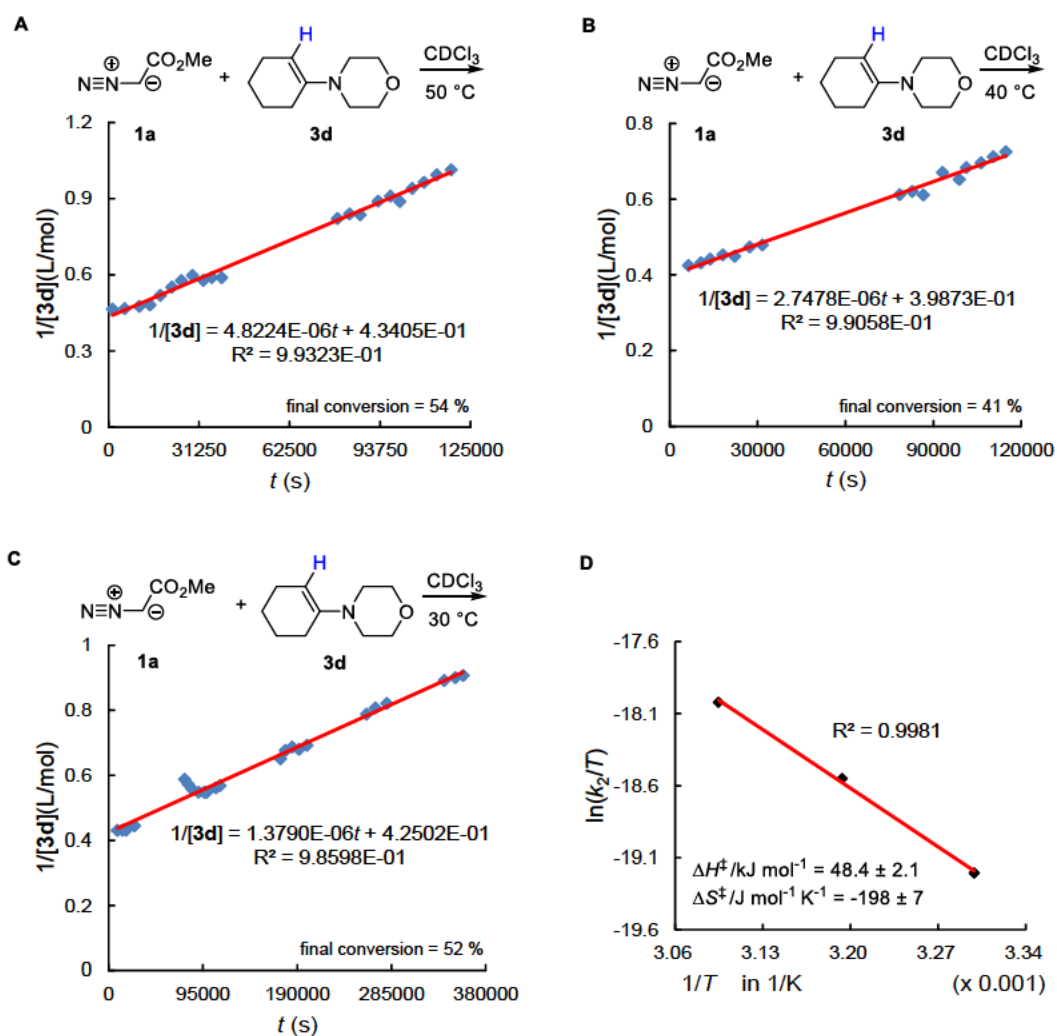


Table S5. Second-order rate constants k_2^{exptl} of the reactions of **1a** with **3e** in CDCl_3 at 50 (A), 40 (B), 30 °C (C) (^1H NMR kinetics, 1,1,2,2-tetrachloroethane as the internal standard IS). Activation parameters from Eyring plot (D) were used to calculate ΔG^\ddagger and k_2 at +25 and +20 °C. Initial reactant concentrations were determined by using the integration ranges of the IS from +50 to +30 °C at always 5.98–5.85 ppm with the reference of IS at 5.93 ppm, of the vinylic hydrogen of **3e** at always 5.18–4.84 ppm, of the CH hydrogen of **1a** at always 4.78–4.44 ppm. Relaxation delay and acquisition time are always 1.00 and 4.09 s, respectively.

T (°C)	$[\mathbf{1a}]_0$ (M)	$[\mathbf{3e}]_0$ (M)	$[\text{IS}]_0$ (M)	k_2^{exptl} ($\text{M}^{-1} \text{s}^{-1}$)	k_2 ($\text{M}^{-1} \text{s}^{-1}$)	ΔG^\ddagger (kJ mol^{-1})
+50	2.26	2.73	0.681	1.97×10^{-6}		
+40	2.31	2.25	0.699	1.01×10^{-6}		
+30	2.32	2.50	0.727	4.77×10^{-7}		
+20					$(2.20 \pm 0.05) \times 10^{-7}$	109
+25					$(3.27 \pm 0.06) \times 10^{-7}$	110

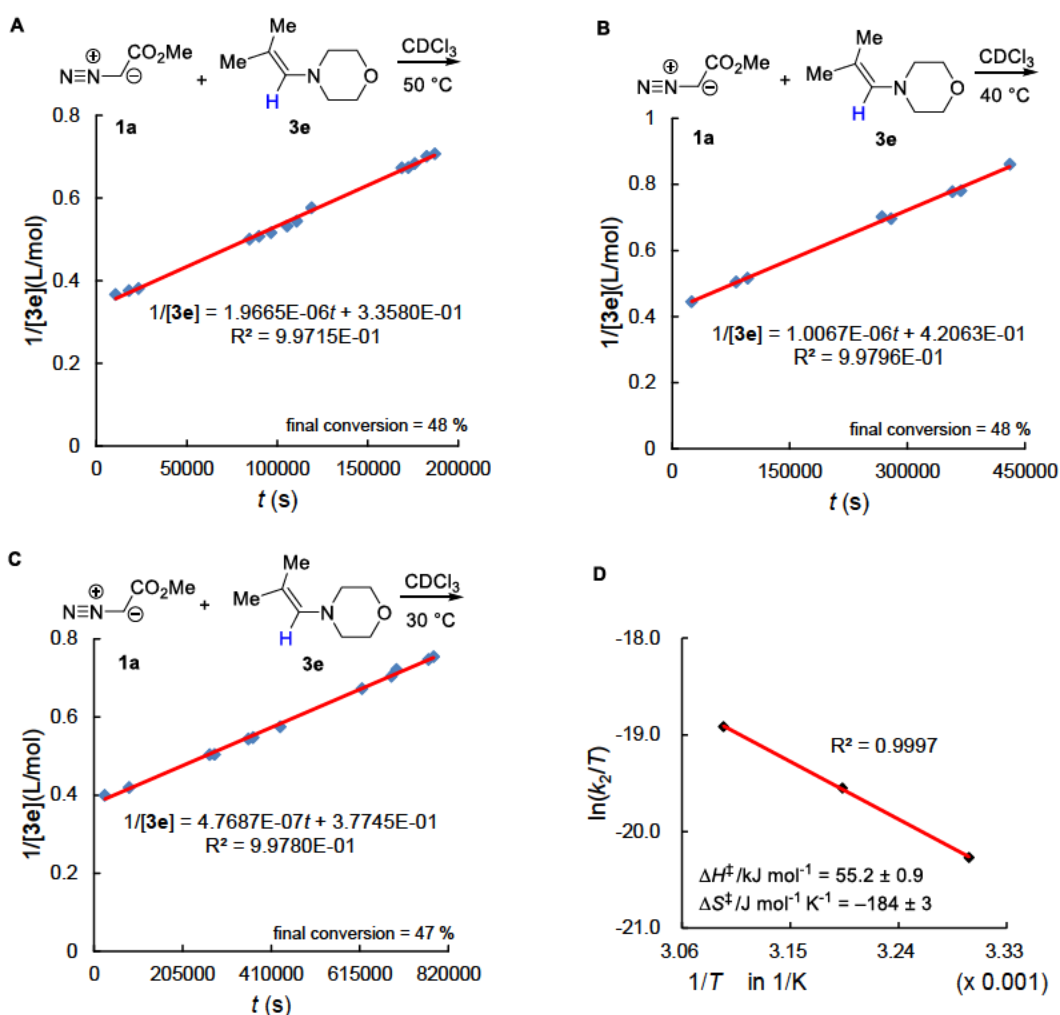


Table S6. Second-order rate constants k_2^{exptl} of the reaction of **1b** with **3a** in CDCl_3 at -50 (A), -40 (B), -30 °C (C) (^1H NMR kinetics, mesitylene CH_3 hydrogens as the internal standard IS). Activation parameters from Eyring plot (D) were used to calculate ΔG^\ddagger and k_2 at $+110$, $+25$ and $+20$ °C. Initial reactant concentrations were determined by using the integration ranges of the IS from -50 to -30 °C at 2.305–2.22, 2.31–2.23, 2.30–2.23 ppm, respectively, of the vinylic hydrogen of **3a** at 4.07–3.97, 4.07–3.975, 4.07–3.975 ppm, respectively, of the CH_3 hydrogens of **1b** at 3.90–3.825, 3.86–3.82 ppm at -50 and -40 °C, respectively. Relaxation delay and acquisition time are always 0.10 and 3.60 s, respectively.

T (°C)	$[\mathbf{1b}]_0$ (M)	$[\mathbf{3a}]_0$ (M)	$[\text{IS}]_0$ (M)	k_2^{exptl} ($\text{M}^{-1} \text{s}^{-1}$)	k_2 ($\text{M}^{-1} \text{s}^{-1}$)	ΔG^\ddagger (kJ mol^{-1})
-50	2.17×10^{-1}	2.61×10^{-1}	2.48×10^{-1}	6.96×10^{-4}		
-40	2.08×10^{-1}	2.33×10^{-1}	2.84×10^{-1}	1.40×10^{-3}		
-30	2.95×10^{-1} [a]	2.15×10^{-1}	2.82×10^{-1}	2.38×10^{-3}		
+20					$(2.59 \pm 0.42) \times 10^{-2}$	80.7
+25					$(3.15 \pm 0.55) \times 10^{-2}$	81.6
+110					4.08×10^{-1}	

[a] Calculated from weighed mass of **1b** due to overlap of the CH_3 resonance of **1b** with product signals.

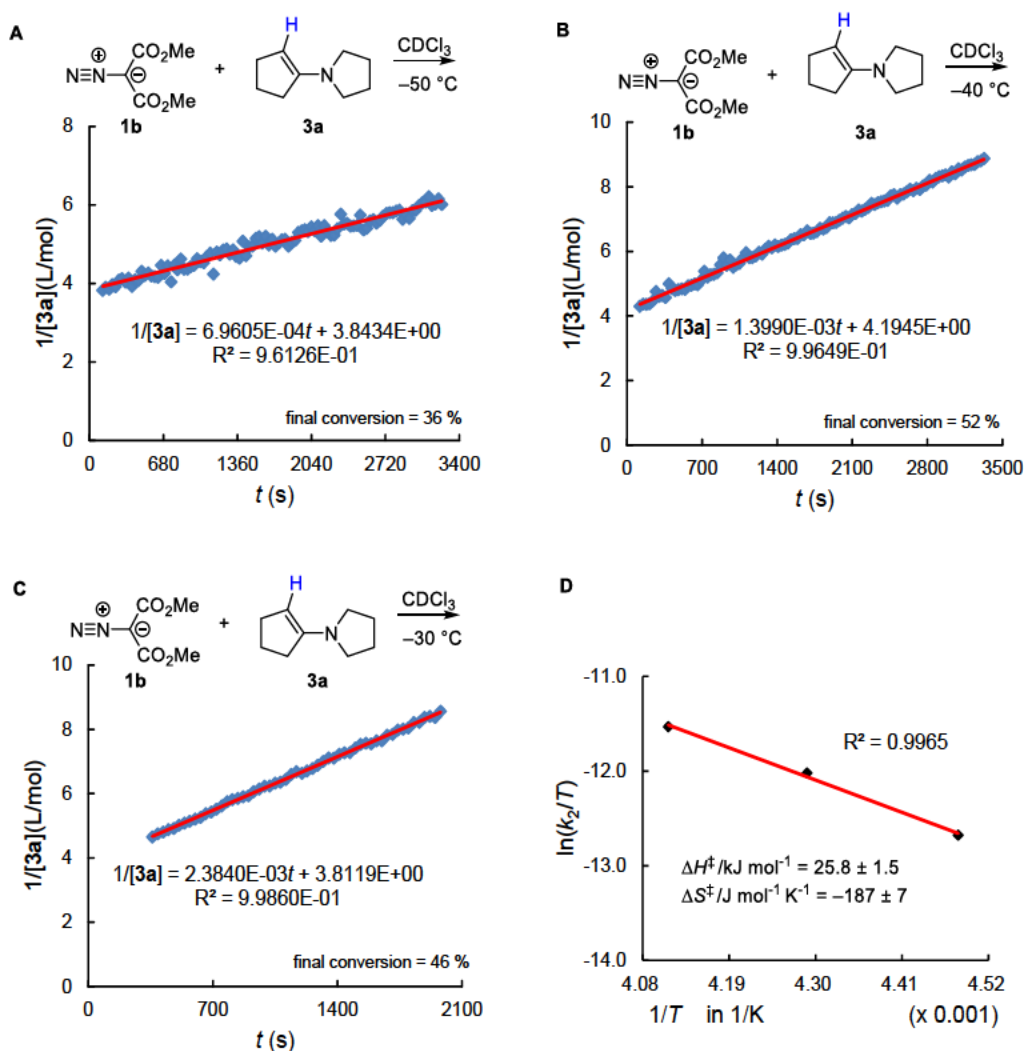


Table S7. Second-order rate constants k_2^{exptl} of the reactions of **1b** with **3b** in CDCl_3 at -50 (A), -40 (B), -30 °C (C) (^1H NMR kinetics, mesitylene CH_3 hydrogens as the internal standard IS). Activation parameters from Eyring plot (D) were used to calculate ΔG^\ddagger and k_2 at $+110$, $+25$ and $+20$ °C. Initial reactant concentrations were determined by using the integration ranges of the IS from -50 to -30 °C at 2.31–2.22, 2.31–2.22, 2.30–2.21 ppm, respectively, of the vinylic hydrogen of **3b** at 4.32–4.18, 4.32–4.20, 4.32–4.21 ppm, respectively, of the CH_3 hydrogens of **1b** at 3.89–3.795, 3.86–3.82, 3.85–3.81 ppm, respectively. Relaxation delay and acquisition time are always 0.10 and 3.65 s, respectively.

T (°C)	$[\mathbf{1b}]_0$ (M)	$[\mathbf{3b}]_0$ (M)	$[\text{IS}]_0$ (M)	k_2^{exptl} ($\text{M}^{-1} \text{s}^{-1}$)	k_2 ($\text{M}^{-1} \text{s}^{-1}$)	ΔG^\ddagger (kJ mol^{-1})
-50	4.10×10^{-1}	2.03×10^{-1}	2.79×10^{-1}	8.98×10^{-5}		
-40	4.18×10^{-1}	2.24×10^{-1}	3.35×10^{-1}	1.40×10^{-4}		
-30	3.78×10^{-1}	2.37×10^{-1}	2.63×10^{-1}	1.84×10^{-4}		
+20					$(7.59 \pm 1.50) \times 10^{-4}$	89.3
+25					$(8.52 \pm 1.79) \times 10^{-4}$	90.5
+110					3.93×10^{-3}	

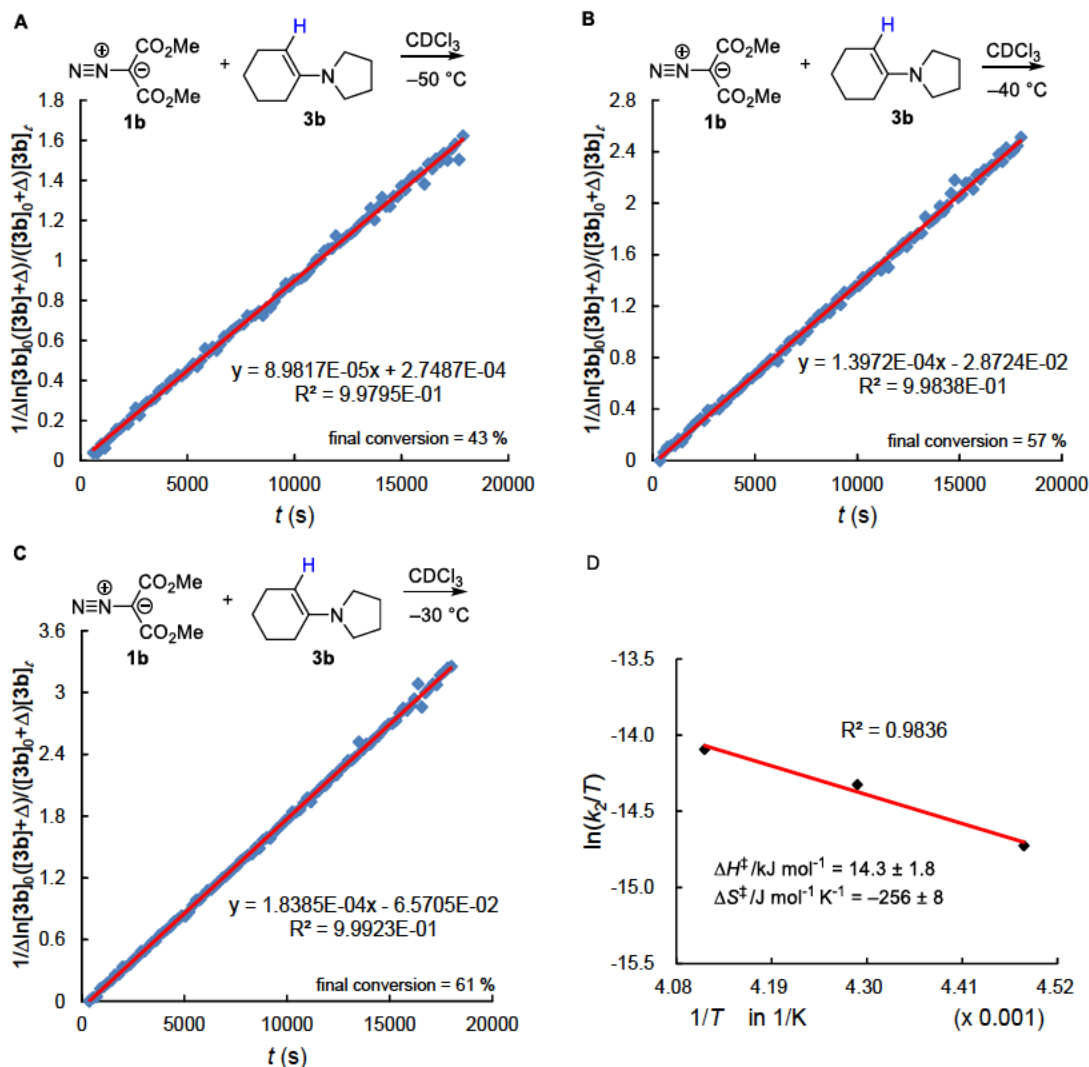


Table S8. Second-order rate constants k_2^{exptl} of the reactions of **1b** with **3b** in d_8 -toluene:mesitylene = 1:1 at -30 (A), -20 (B), -10 °C (C) (^1H NMR kinetics, 1,1,2,2-tetrachloroethane as the internal standard IS). Activation parameters from Eyring plot (D) were used to calculate ΔG^\ddagger and k_2 at $+110$, $+25$ and $+20$ °C. Initial reactant concentrations were determined by using the integration ranges of the IS from -30 to -10 °C at 5.21–5.09, 5.26–5.17, 5.18–5.09 ppm, respectively, of the vinylic hydrogen of **3b** at 4.26–4.17, 4.39–4.30, 4.26–4.18 ppm, respectively, of the CH_3 hydrogens of **1b** at 3.34–3.24, 3.48–3.37 ppm at -30 and -20 °C, respectively. Relaxation delay and acquisition time are always 0.10 and 3.65 s, respectively.

T (°C)	$[\mathbf{1b}]_0$ (M)	$[\mathbf{3b}]_0$ (M)	$[\text{IS}]_0$ (M)	k_2^{exptl} ($\text{M}^{-1} \text{s}^{-1}$)	k_2 ($\text{M}^{-1} \text{s}^{-1}$)	ΔG^\ddagger (kJ mol^{-1})
-30	5.10×10^{-1}	5.49×10^{-1}	3.61×10^{-1}	1.19×10^{-4}		
-20	4.67×10^{-1}	4.96×10^{-1}	2.96×10^{-1}	1.55×10^{-4}		
-10	5.35×10^{-1} [a]	5.49×10^{-1}	3.17×10^{-1}	1.96×10^{-4}		
+20					$(3.69 \pm 0.04) \times 10^{-4}$	91.0
+25					$(4.05 \pm 0.05) \times 10^{-4}$	92.4
+110					1.42×10^{-3}	

[a] Calculated from weighed mass of **1b** due to overlap of the CH_3 resonance of **1b** with product signals.

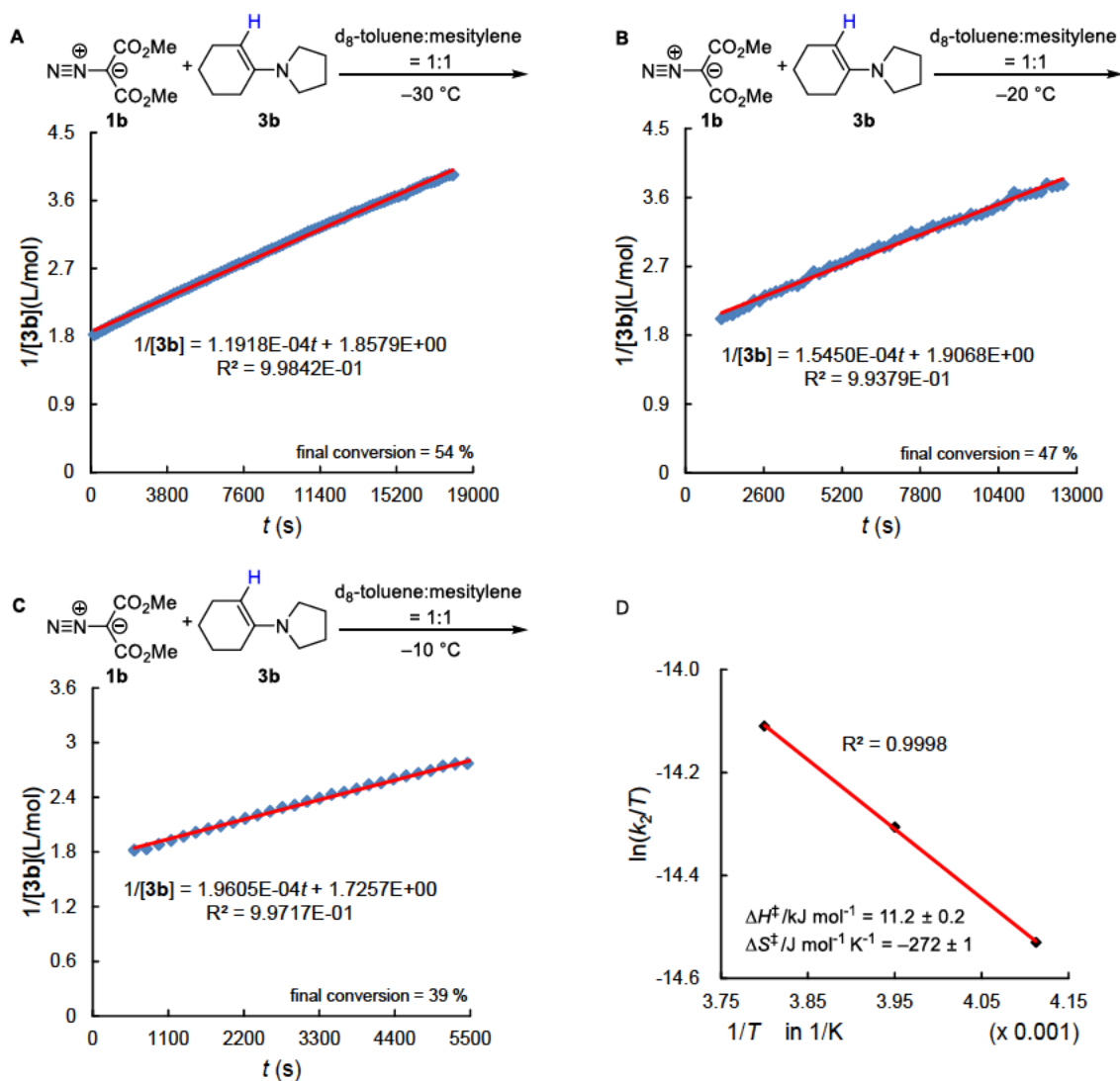


Table S9. Second-order rate constants k_2^{exptl} of the reactions of **1b** with **3c** in CDCl_3 at +40 (A), +30 (B), +20 °C (C) (^1H NMR kinetics, mesitylene CH_3 hydrogens as the internal standard IS). Activation parameters from Eyring plot (D) were used to calculate ΔG^\ddagger and k_2 at +110, +25 and +20 °C. Initial reactant concentrations were determined by using the integration ranges of the IS from +40 to +20 °C at 2.265–2.195, 2.26–2.18, 2.29–2.22 ppm, respectively, of the vinylic hydrogen of **3c** at 4.48–4.35, 4.48–4.35, 4.51–4.40 ppm, respectively, of the CH_3 hydrogens of **1b** at 3.83–3.78, 3.82–3.77, 3.87–3.80 ppm, respectively. Relaxation delay and acquisition time are 0.10 and 3.65 s, respectively, for measurements at 40 and 30 °C, and 1.00 and 5.12 s for the measurement at 20 °C.

T (°C)	$[\mathbf{1b}]_0$ (M)	$[\mathbf{3c}]_0$ (M)	$[\text{IS}]_0$ (M)	k_2^{exptl} ($\text{M}^{-1} \text{s}^{-1}$)	k_2 ($\text{M}^{-1} \text{s}^{-1}$)	ΔG^\ddagger (kJ mol^{-1})
+40	4.82×10^{-1}	2.49×10^{-1}	2.80×10^{-1}	1.92×10^{-4}		
+30	4.42×10^{-1}	2.29×10^{-1}	2.51×10^{-1}	1.47×10^{-4}		
+20	4.58×10^{-1}	2.57×10^{-1}	1.97×10^{-1}	9.71×10^{-5}		
+20					$(9.91 \pm 0.37) \times 10^{-5}$	94.2
+25					$(1.19 \pm 0.06) \times 10^{-4}$	95.4
+110					1.25×10^{-3}	

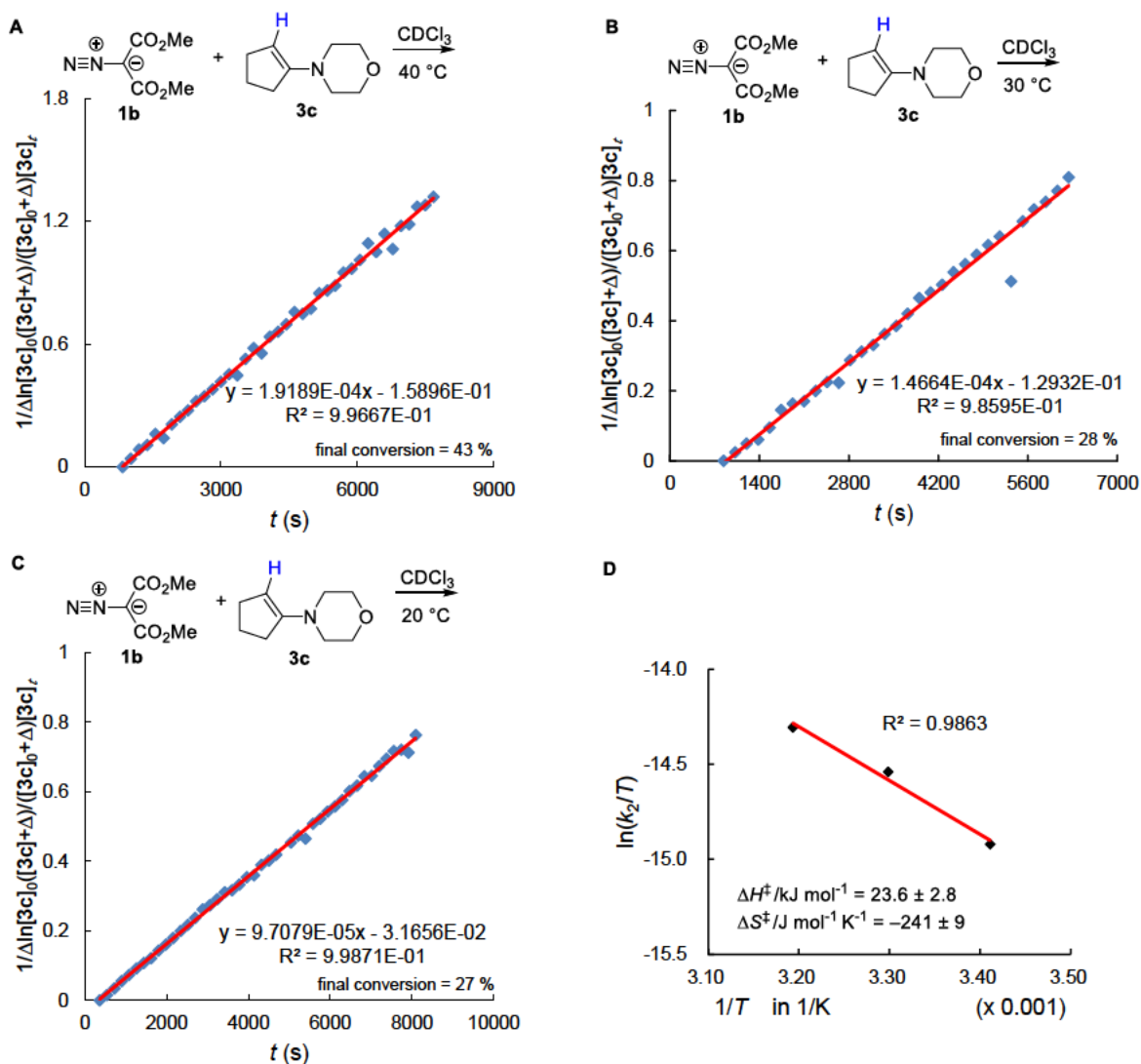


Table S10. Second-order rate constants k_2^{exptl} of the reactions of **1b** with **3c** in d_8 -toluene:mesitylene = 1:1 at +50 (A), +40 (B), +20 °C (C) (^1H NMR kinetics, aromatic hydrogens of mesitylene as the internal standard IS). Activation parameters from Eyring plot (D) were used to calculate ΔG^\ddagger and k_2 at +110, +25 and +20 °C. Initial reactant concentrations were determined by using the integration ranges of the IS from +50 to +20 °C at 6.71–6.51, 6.72–6.46, 6.75–6.46 ppm, respectively, of the vinylic hydrogen of **3c** at 4.36–4.16, 4.35–4.19, 4.36–4.23 ppm, respectively, of the CH_3 hydrogens of **1b** at 3.418–3.376, 3.414–3.366, 3.445–3.37 ppm, respectively. Relaxation delay and acquisition time are 0.10 and 3.65 s, respectively for measurement at 50 and 40 °C, 1.00 and 4.09 s for measurement at 20 °C.

T (°C)	$[\mathbf{1b}]_0$ (M)	$[\mathbf{3c}]_0$ (M)	$[\text{IS}]_0$ (M)	k_2^{exptl} ($\text{M}^{-1} \text{s}^{-1}$)	k_2 ($\text{M}^{-1} \text{s}^{-1}$)	ΔG^\ddagger (kJ mol^{-1})
+50	4.57×10^{-1}	4.82×10^{-1}	2.84	4.81×10^{-5}		
+40	4.56×10^{-1}	5.48×10^{-1}	2.84	3.61×10^{-5}		
+20	5.33×10^{-1}	5.87×10^{-1}	2.84	1.81×10^{-5}		
+20					$(1.82 \pm 0.02) \times 10^{-5}$	98.4
+25					$(2.17 \pm 0.03) \times 10^{-5}$	99.6
+110					2.23×10^{-4}	

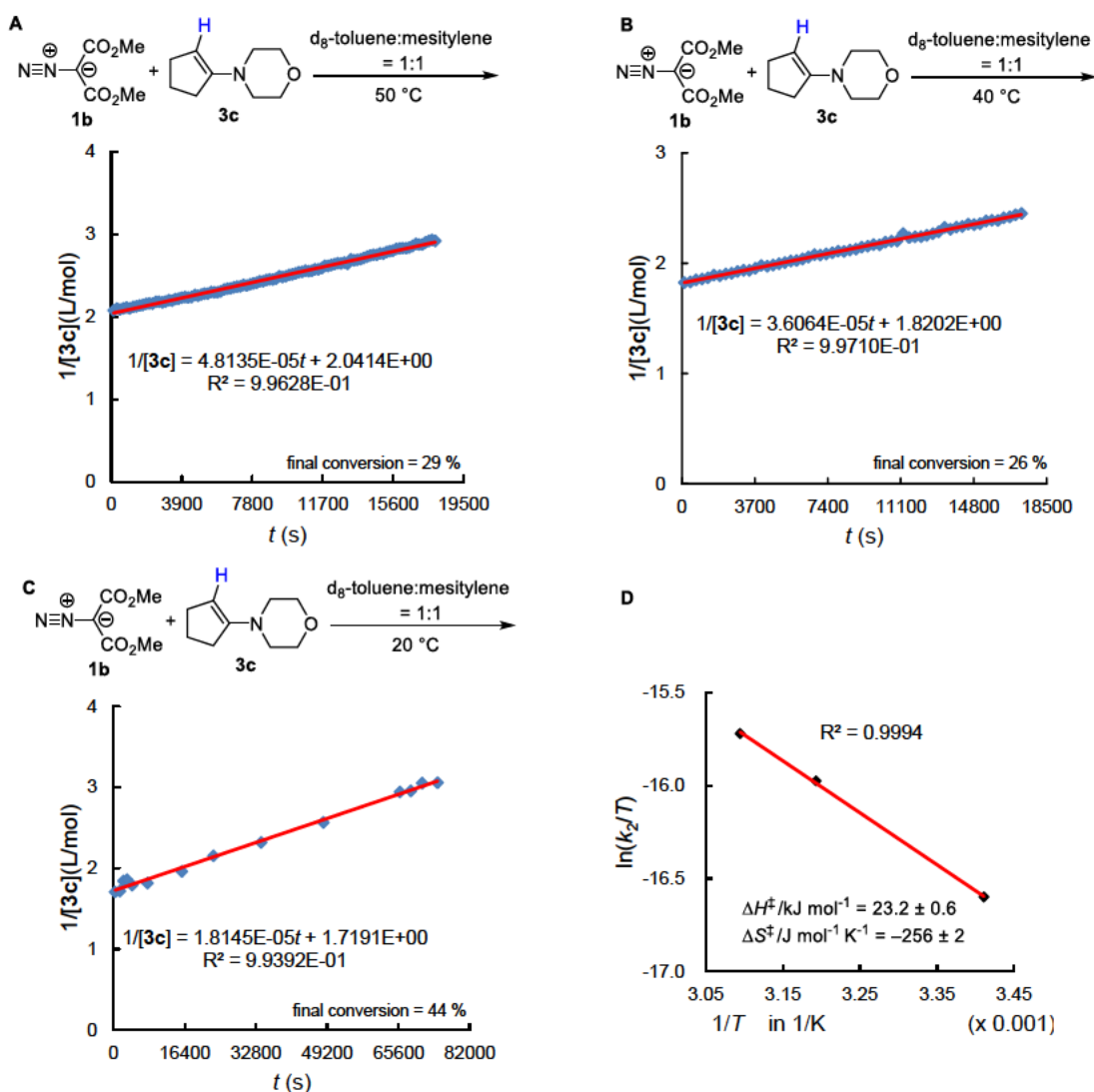


Table S11a. Second-order rate constants k_2^{exptl} of the reactions of **1b** with **3d** in CDCl_3 at +40 (A), +30 (B), +20 °C (C) (^1H NMR kinetics, 1,1,2,2-tetrachloroethane as the internal standard IS). Activation parameters from Eyring plot (D) were used to calculate ΔG^\ddagger and k_2 at +25 and +20 °C. Initial reactant concentrations were determined by using the integration ranges of the IS from +40 to +20 °C at always 6.04–5.95 ppm with the reference of IS at 6.00 ppm for the measurement at 40 and 30 °C, of the vinylic hydrogen of **3d** at always 4.66–4.44 ppm with the reference of the vinylic hydrogen of **3d** at 4.57 ppm, of the CH_3 hydrogens of **1b** at 3.76–3.68, 3.78–3.71, 3.75–3.69 ppm, respectively, with the reference of **1b** at 3.72, 3.75, 3.72 ppm, respectively. Relaxation delay and acquisition time are always 1.00 and 4.09 s, respectively.

T (°C)	$[\mathbf{1b}]_0$ (M)	$[\mathbf{3d}]_0$ (M)	$[\text{IS}]_0$ (M)	k_2^{exptl} ($\text{M}^{-1} \text{s}^{-1}$)	k_2 ($\text{M}^{-1} \text{s}^{-1}$)	ΔG^\ddagger (kJ mol^{-1})
+40	1.17	1.23	1.07	7.25×10^{-6}		
+30	1.10	1.13	1.18	6.19×10^{-6}		
+20	1.10	1.10	1.13	4.74×10^{-6}		
+20					$(4.81 \pm 0.13) \times 10^{-6}$	102
+25					$(5.38 \pm 0.21) \times 10^{-6}$	103

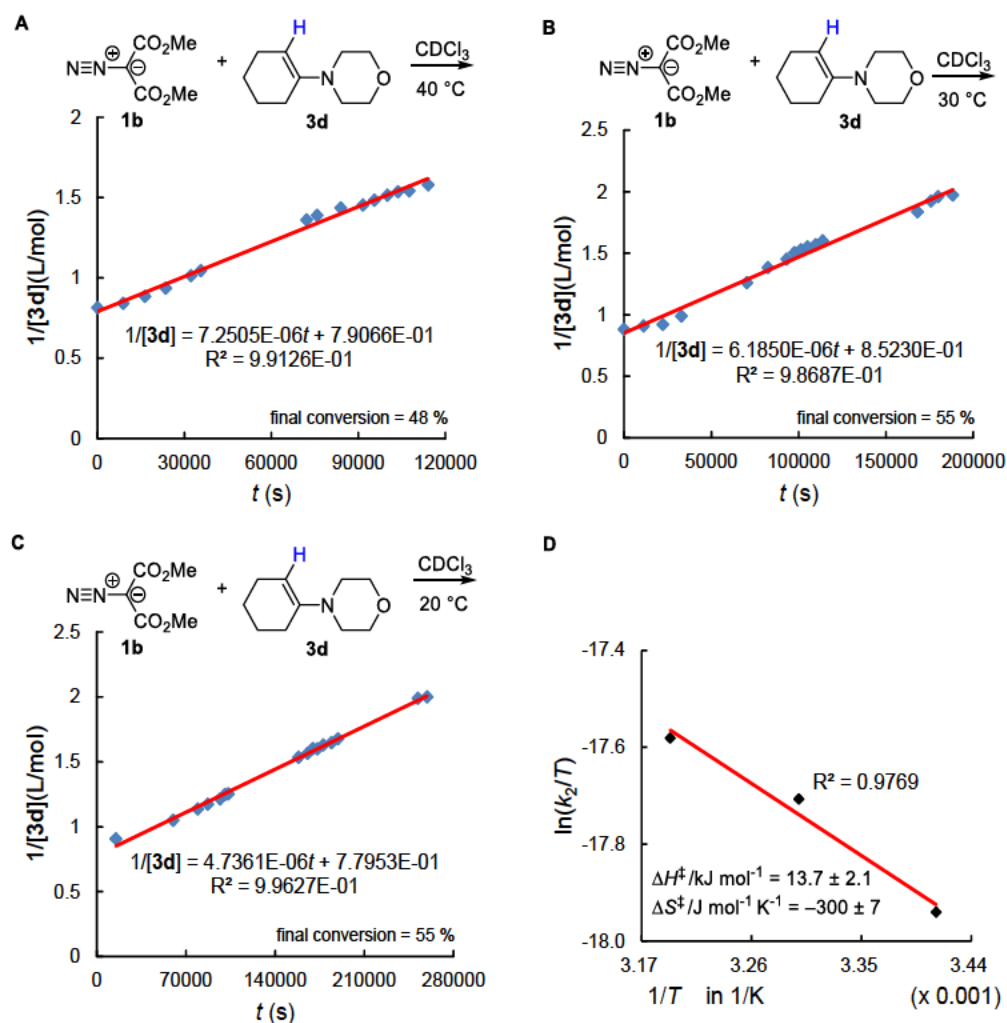
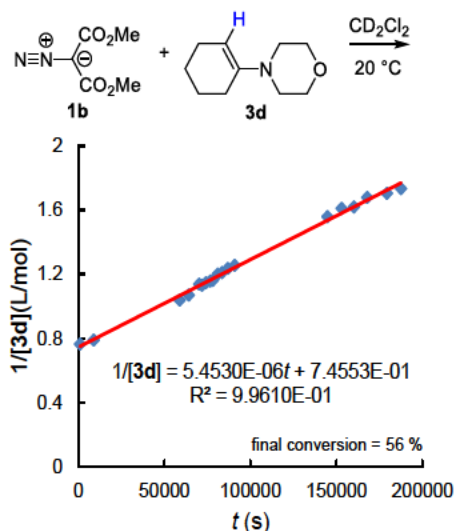


Table S11b. Second-order rate constant k_2^{exptl} of the reactions of **1b** with **3d** in CD_2Cl_2 at $+20\text{ }^\circ\text{C}$ (^1H NMR kinetics, 1,1,2,2-tetrachloroethane as the internal standard IS). Initial reactant concentrations were determined by using the integration ranges of the IS at always 6.24–5.98 ppm, of the vinylic hydrogen of **3d** at 4.70–4.48 ppm, of the CH_3 hydrogens of **1b** at 3.80–3.73 ppm, respectively. Relaxation delay and acquisition time are 1.00 and 4.09 s, respectively.

T ($^\circ\text{C}$)	$[\mathbf{1b}]_0$ (M)	$[\mathbf{3d}]_0$ (M)	$[\text{IS}]_0$ (M)	k_2^{exptl} ($\text{M}^{-1} \text{s}^{-1}$)	ΔG^\ddagger (kJ mol^{-1})
+20	1.21	1.31	9.67×10^{-1}	5.45×10^{-6}	101



Changing the solvent only slightly enhanced the second-order rate constant k_2 for the reaction of **1b** with **3d** at $20\text{ }^\circ\text{C}$ from 4.81×10^{-6} in CDCl_3 (Table S11a) to $5.45 \times 10^{-6} \text{ M}^{-1} \text{ s}^{-1}$ in CD_2Cl_2 (Table S11b). We conclude, therefore, that the effect of switching the solvent from CDCl_3 to CD_2Cl_2 on the reaction rate is negligible. Thus, it is justified to apply the kinetic data measured in CDCl_3 to derive the E parameters of the diazoalkanes from their reactions with enamines whose N/S_N parameters have been determined by eq. (1) from reactions in CH_2Cl_2 solutions.

Table S12. Second-order rate constants k_2^{exptl} of the reactions of **1c** with **3a** in CD_2Cl_2 at -40 (A), -30 (B), -20 °C (C) (^1H NMR kinetics, 1,1,2,2-tetrachloroethane as the internal standard IS). Activation parameters from Eyring plot (D) were used to calculate ΔG^\ddagger and k_2 at $+25$ and $+20$ °C. Initial reactant concentrations were determined by using the integration ranges of the IS from -40 to -20 °C at 6.16–5.97, 6.09–6.02, 6.09–6.02 ppm, respectively, of the vinylic hydrogen of **3a** at 4.00–3.84, 4.03–3.82, 4.03–3.86 ppm, respectively, of the α -CH hydrogen of **1c** at 5.28–5.21, 5.27–5.21, 5.25–5.21 ppm, respectively. Relaxation delay and acquisition time are always 0.10 and 3.65 s, respectively.

T (°C)	$[\mathbf{1c}]_0$ (M)	$[\mathbf{3a}]_0$ (M)	$[\text{IS}]_0$ (M)	k_2^{exptl} ($\text{M}^{-1} \text{s}^{-1}$)	k_2 ($\text{M}^{-1} \text{s}^{-1}$)	ΔG^\ddagger (kJ mol^{-1})
-40	2.11×10^{-1}	1.83×10^{-1}	2.65×10^{-1}	1.03×10^{-3}		
-30	1.69×10^{-1}	1.99×10^{-1}	2.67×10^{-1}	1.47×10^{-3}		
-20	1.34×10^{-1}	1.60×10^{-1}	2.37×10^{-1}	2.18×10^{-3}		
$+20$					$(7.20 \pm 0.59) \times 10^{-3}$	83.8
$+25$					$(8.20 \pm 0.72) \times 10^{-3}$	84.9

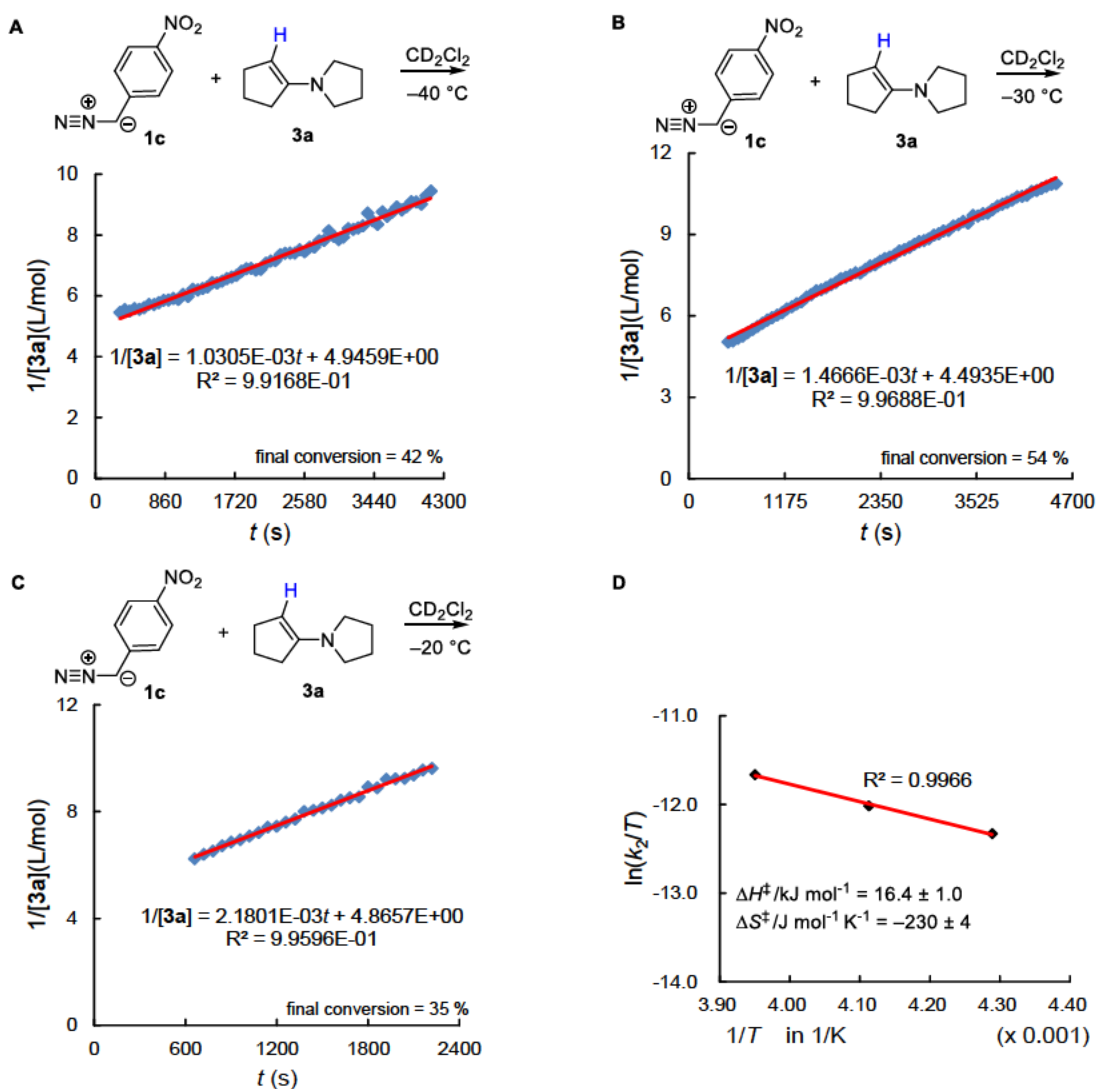


Table S13. Second-order rate constants k_2^{exptl} of the reactions of **1c** with **3b** in CD_2Cl_2 at -30 (A), -20 (B) and -10 °C (C) (^1H NMR kinetics, 1,1,2,2-tetrachloroethane as the internal standard IS). Activation parameters from Eyring plot (D) were used to calculate ΔG^\ddagger and k_2 at $+25$ and $+20$ °C. Initial reactant concentrations were determined by using the integration ranges of the IS from -30 to -10 °C at 6.14–5.97, 6.16–5.97, 6.18–5.94 ppm, respectively, of the vinylic hydrogen of **3b** at 4.23–4.11, 4.21–4.12, 4.23–4.13 ppm, respectively, of the aromatic hydrogens of **1c** at 7.08–6.86, 7.09–6.89, 8.15–8.05 ppm, respectively. Relaxation delay and acquisition time are always 0.10 and 3.65 s, respectively.

T (°C)	$[\mathbf{1c}]_0$ (M)	$[\mathbf{3b}]_0$ (M)	$[\text{IS}]_0$ (M)	k_2^{exptl} ($\text{M}^{-1} \text{s}^{-1}$)	k_2 ($\text{M}^{-1} \text{s}^{-1}$)	ΔG^\ddagger (kJ mol^{-1})
-30	3.45×10^{-1}	2.93×10^{-1}	1.74×10^{-1}	2.87×10^{-4}		
-20	3.34×10^{-1}	3.06×10^{-1}	1.86×10^{-1}	4.61×10^{-4}		
-10	2.98×10^{-1}	3.40×10^{-1}	2.18×10^{-1}	6.63×10^{-4}		
$+20$					$(1.93 \pm 0.15) \times 10^{-3}$	87.0
$+25$					$(2.25 \pm 0.20) \times 10^{-3}$	88.1

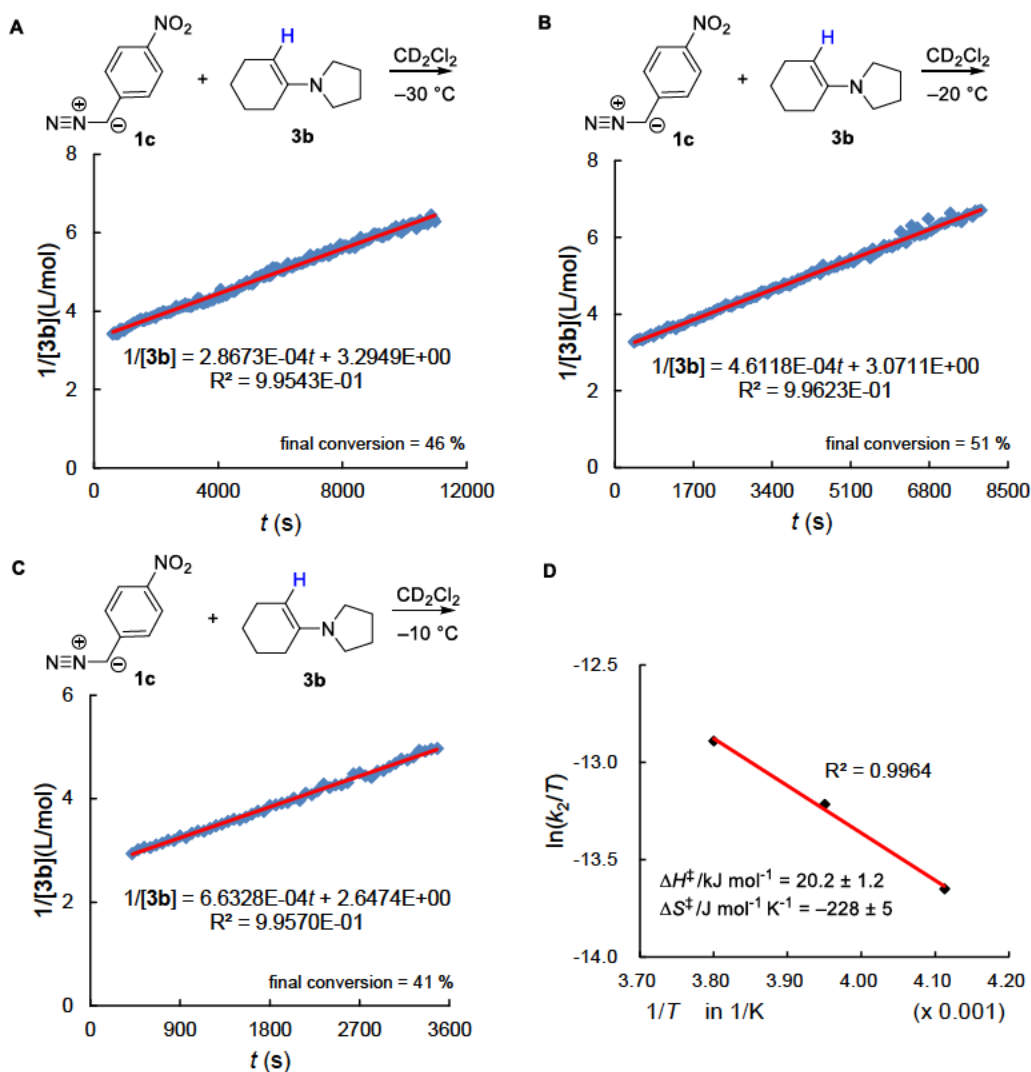


Table S14. Second-order rate constant k_2^{exptl} of the reaction of **1c** with **3c** in CD_2Cl_2 at +20 °C (^1H NMR kinetics, 1,1,2,2-tetrachloroethane as the internal standard IS). Initial reactant concentrations were determined by using the integration ranges of the IS at 6.17–5.97 ppm, of the vinylic hydrogen of **3c** at 4.44–4.36 ppm, of the α -CH hydrogen of **1c** at 5.28–5.16 ppm. Relaxation delay and acquisition time are 0.10 and 3.65 s, respectively.

T (°C)	$[\mathbf{1c}]_0$ (M)	$[\mathbf{3c}]_0$ (M)	$[\text{IS}]_0$ (M)	k_2^{exptl} ($\text{M}^{-1} \text{s}^{-1}$)	ΔG^\ddagger (kJ mol^{-1})
+20	5.29×10^{-1}	5.75×10^{-1}	2.83×10^{-1}	7.59×10^{-5}	94.9

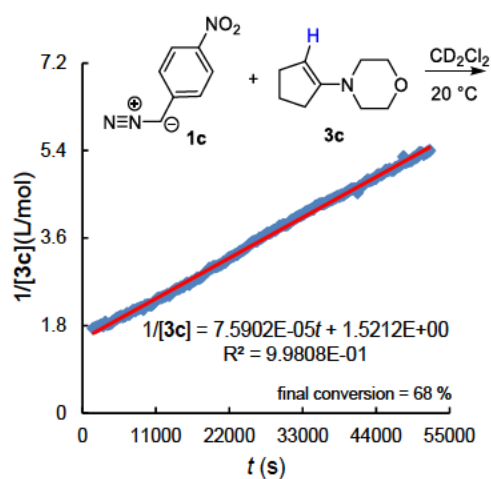


Table S15. Second-order rate constant k_2^{exptl} of the reaction of **1c** with **3d** in CD_2Cl_2 at +20 °C (^1H NMR kinetics, 1,1,2,2-tetrachloroethane as the internal standard IS). Initial reactant concentrations were determined by using the integration ranges of the IS at 6.12–5.76 ppm, of the vinylic hydrogen of **3d** at 4.66–4.36 ppm, of the aromatic hydrogens of **1c** at 7.07–6.77 ppm. Relaxation delay and acquisition time are 1.00 and 4.09 s, respectively.

T (°C)	$[\mathbf{1c}]_0$ (M)	$[\mathbf{3d}]_0$ (M)	$[\text{IS}]_0$ (M)	k_2^{exptl} ($\text{M}^{-1} \text{s}^{-1}$)	ΔG^\ddagger (kJ mol^{-1})
+20	6.64×10^{-1}	7.93×10^{-1}	3.76×10^{-1}	1.80×10^{-6}	104

Chapter 4. Quantification of the Electrophilicities of Diazoalkanes

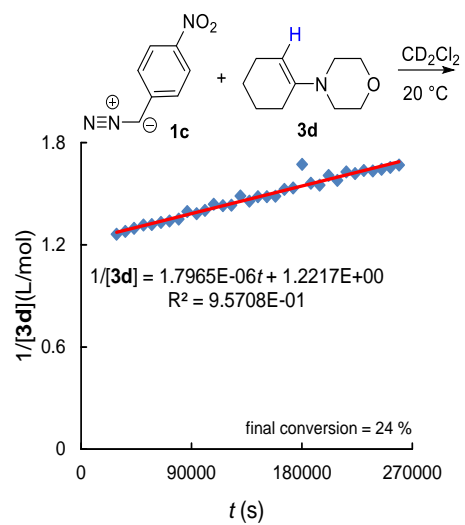
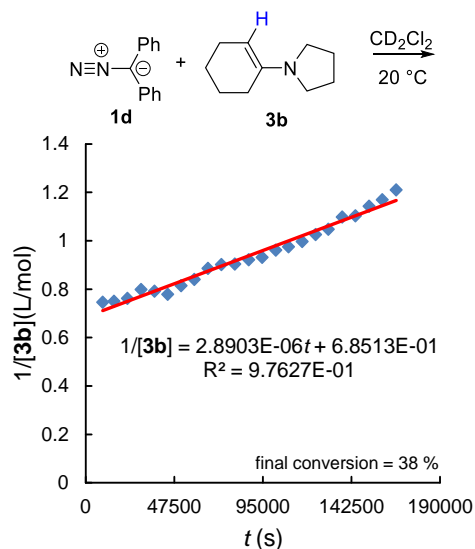


Table S16. Second-order rate constant k_2^{exptl} of the reaction of **1d** with **3b** in CD_2Cl_2 at +20 °C (^1H NMR kinetics, dibromomethane as the internal standard IS). Initial reactant concentrations were determined by using the integration ranges of the IS at 5.20–4.80 ppm with the reference of IS at 5.00 ppm, of the vinylic hydrogen of **3b** at 4.42–4.28 ppm, of the aromatic hydrogen of **1d** at 7.52–7.45 ppm. Relaxation delay and acquisition time are 1.00 and 4.09 s, respectively.

T (°C)	$[\mathbf{1d}]_0$ (M)	$[\mathbf{3b}]_0$ (M)	$[\text{IS}]_0$ (M)	k_2^{exptl} ($\text{M}^{-1} \text{s}^{-1}$)	ΔG^\ddagger (kJ mol^{-1})
+20	1.08	1.34	1.01	2.89×10^{-6}	103



Determination of the electrophilicity parameters E for **1a-c**

Table S17. Determination of the electrophilicity parameter E for **1a**.

Nucleophiles	$\text{N}=\text{N}-\text{C}(\text{CO}_2\text{Me})_2$ 1a		k_2^{exptl} ($\text{M}^{-1} \text{s}^{-1}$)	$\lg k_2$	E ^[a]	$\lg k_2^{\text{calc}}$ ^[b]	Δ ^[c]	Δ^2	sum ^[d]
	N	s_N							
2a	21.07	0.68	1.18×10^2	2.07		1.72	-0.35	0.13	
2b	18.42	0.65	2.17	0.34		-0.08	-0.42	0.17	
3a	15.91	0.86	1.83×10^{-3}	-2.74		-2.26	0.47	0.22	
3b	14.91	0.86	4.68×10^{-4}	-3.33		-3.12	0.21	0.04	
3d	11.40	0.83	7.03×10^{-7}	-6.15		-5.93	0.22	0.05	
3e	10.04	0.82	2.20×10^{-7}	-6.66	-18.5	-6.97	-0.31	0.10	0.71
$E = -18.5$									

^[a] Optimal E parameter resulting from the least-squares analysis according to the Mayr-Patz equation. ^[b] Calculated by applying N , s_N , and E in the equation. ^[c] $\Delta = \lg k_2^{\text{exptl}} - \lg k_2^{\text{calc}}$. ^[d] sum = $\Sigma \Delta^2$, to be minimized by variation of E in the least-squares analysis.

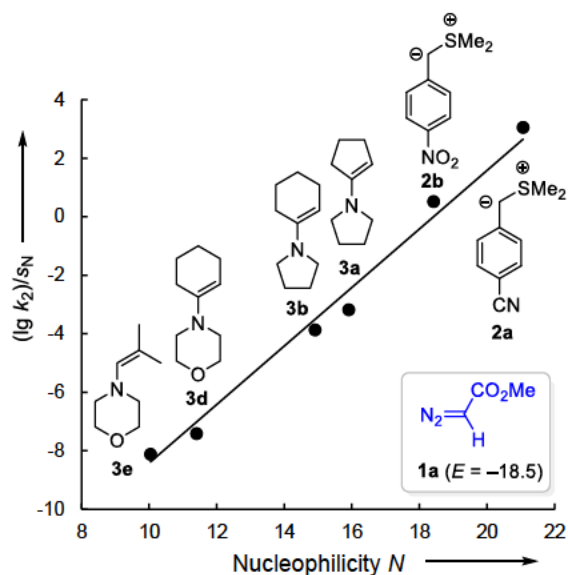


Figure S7. Linear correlation of $(\lg k_2)/s_N$ with the nucleophilicity parameters N for reactions of the diazo compound **1a** with the nucleophiles **2** and **3**. The depicted linear correlation has a fixed slope of unity as required by the Mayr-Patz equation. The linear regression for the data in this figure gives a slope of 1.04.

Table S18. Determination of the electrophilicity parameter E for **1b**.

1b

Nucleophiles	N	s_N	$k_2^{\text{exptl}}/\text{M}^{-1} \text{s}^{-1}$	$\lg k_2$	$E^{[a]}$	$\lg k_2^{\text{calc}}^{[b]}$	$\Delta^{[c]}$	Δ^2	sum ^[d]
2a	21.07	0.68	4.22×10^1	1.63		1.96	0.34	0.12	
3a	15.91	0.86	2.59×10^{-2}	-1.59		-1.95	-0.37	0.13	
3b	14.91	0.86	7.59×10^{-4}	-3.12		-2.81	0.31	0.09	
3c	13.41	0.82	9.91×10^{-5}	-4.00		-3.91	0.09	0.01	
3d	11.4	0.83	4.81×10^{-6}	-5.32	-18.2	-5.63	-0.31	0.10	0.45

$E = -18.2$

^[a] Optimal E parameter resulting from the least-squares analysis according to the Mayr-Patz equation. ^[b] Calculated by applying N , s_N , and E in the equation. ^[c] $\Delta = \lg k_2^{\text{exptl}} - \lg k_2^{\text{calc}}$. ^[d] sum = $\Sigma \Delta^2$, to be minimized by variation of E in the least-squares analysis.

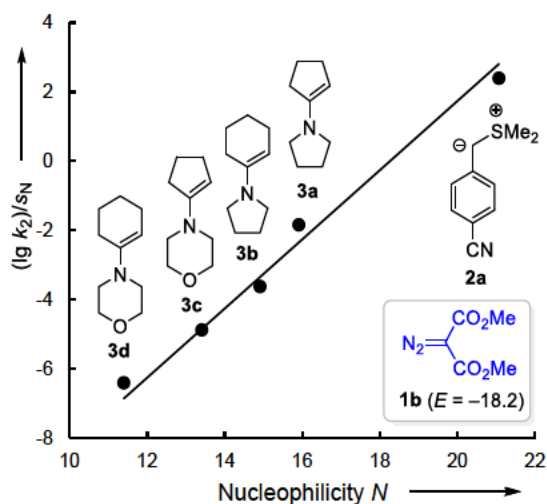
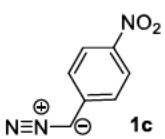


Figure S8. Linear correlation of $(\lg k_2)/s_N$ with the nucleophilicity parameters N for reactions of the diazo compound **1b** with the nucleophiles **2a** and **3a-d**. The depicted linear correlation has a fixed slope of unity as required by the Mayr-Patz equation. The linear regression for the data in this figure gives a slope of 0.93.

Table S19. Determination of the electrophilicity parameter E for **1c**.


Nucleophiles	N	s_N	k_2^{exptl} ($\text{M}^{-1} \text{s}^{-1}$)	$\lg k_2$	E ^[a]	$\lg k_2^{\text{calc}}$ ^[b]	Δ ^[c]	Δ^2	sum ^[d]
3a	15.91	0.86	7.20×10^{-3}	-2.14		-2.06	0.09	0.01	
3b	14.91	0.86	1.93×10^{-3}	-2.71		-2.92	-0.20	0.04	
3c	13.41	0.82	7.59×10^{-5}	-4.12		-4.01	0.11	0.01	
3d	11.40	0.83	1.80×10^{-6}	-5.74	-18.3	-5.73	0.02	0.00	0.06

$E = -18.3$

^[a] Optimal E parameter resulting from the least-squares analysis according to the Mayr-Patz equation. ^[b] Calculated by applying N , s_N , and E in the equation. ^[c] $\Delta = \lg k_2^{\text{exptl}} - \lg k_2^{\text{calc}}$. ^[d] sum = $\Sigma \Delta^2$, to be minimized by variation of E in the least-squares analysis.

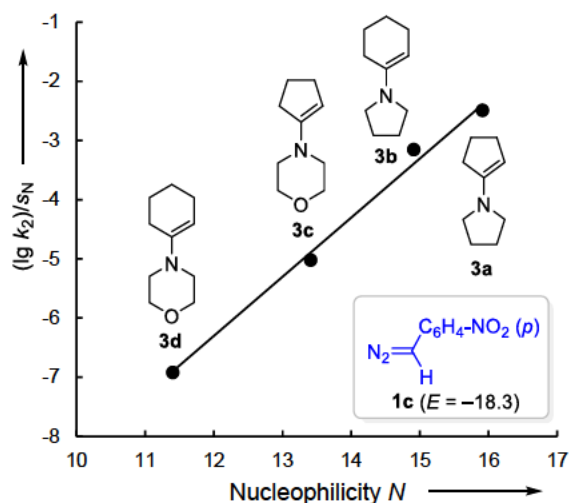
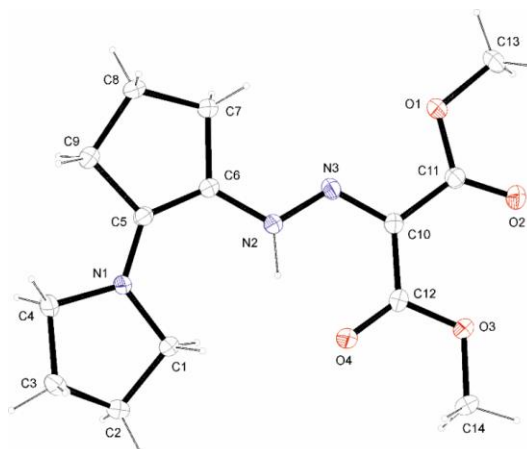


Figure S9. Linear correlation of $(\lg k_2)/s_N$ with the nucleophilicity parameters N for reactions of the diazo compound **1c** with the nucleophiles **3a-d**. The depicted linear correlation has a fixed slope of unity as required by the Mayr-Patz equation. The linear regression for the data in this figure gives a slope of 1.01.

4.2.3 Single Crystal X-ray Crystallography

Dimethyl 2-(2-(2-(pyrrolidin-1-yl)cyclopent-1-en-1-yl)hydrazono)malonate (9ba)



(vv842/CCDC 2102953)

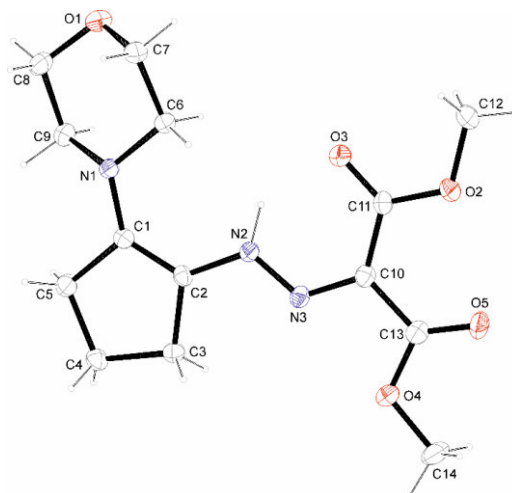
Crystallographic data.

net formula	$C_{14}H_{21}N_3O_4$
$M_r/g\ mol^{-1}$	295.34
crystal size/mm	$0.070 \times 0.050 \times 0.030$
T/K	103.(2)
radiation	MoK α
diffractometer	'Bruker D8 Venture TXS'
crystal system	triclinic
space group	'P -1'
$a/\text{\AA}$	8.0460(5)
$b/\text{\AA}$	9.3723(6)
$c/\text{\AA}$	10.5732(6)
$\alpha/^\circ$	110.359(2)
$\beta/^\circ$	91.662(2)
$\gamma/^\circ$	106.409(2)
$V/\text{\AA}^3$	709.85(8)
Z	2
calc. density/ $g\ cm^{-3}$	1.382
μ/mm^{-1}	0.102
absorption correction	Multi-Scan
transmission factor range	0.93–1.00
refls. measured	7335
R_{int}	0.0292
mean $\sigma(I)/I$	0.0350
θ range	3.139–26.362
observed refls.	2447
x, y (weighting scheme)	0.0429, 0.2212
hydrogen refinement	H(C) constr, H(N) refall
refls in refinement	2873
parameters	201
restraints	0
$R(F_{obs})$	0.0371
$R_w(F^2)$	0.0971

S	1.059
shift/error _{max}	0.001
max electron density/e Å ⁻³	0.279
min electron density/e Å ⁻³	-0.198

Disorder of C8 described in a split model, sof ratio 0.8/0.2. Minor part refined isotropically. Indication of an intramolecular hydrogen bond: [N-H 0.97(2) Å, O...H 1.76(2) Å, angle NHO 137.1(15)°, the hydrogen atom bound to N has been refined freely].

Dimethyl 2-(2-(2-morpholinocyclopent-1-en-1-yl)hydrazono)malonate (9bc)



(wv088/CCDC 2102954)

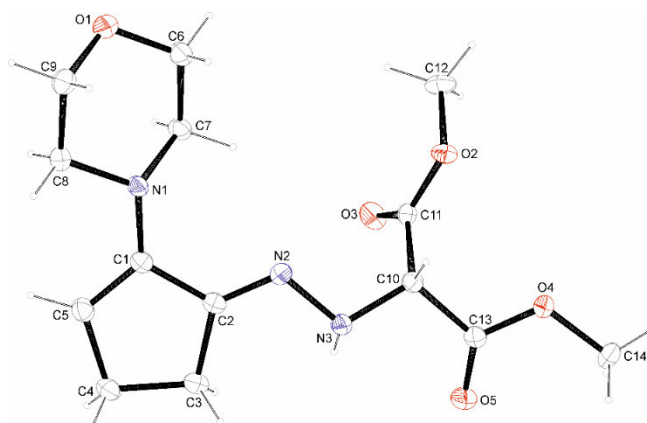
Crystallographic data.

net formula	C ₁₄ H ₂₁ N ₃ O ₅
M_r /g mol ⁻¹	311.34
crystal size/mm	0.100 × 0.090 × 0.050
T /K	100.(2)
radiation	MoK α
diffractometer	'Bruker D8 Venture TXS'
crystal system	triclinic
space group	'P -1'
a /Å	8.1532(4)
b /Å	9.5318(5)
c /Å	10.5959(5)
α /°	113.562(2)
β /°	99.210(2)
γ /°	97.431(2)
V /Å ³	727.87(6)
Z	2
calc. density/g cm ⁻³	1.421
μ /mm ⁻¹	0.109
absorption correction	Multi-Scan
transmission factor range	0.88–0.99
refls. measured	6657
R_{int}	0.0264
mean $\sigma(I)/I$	0.0429

θ range	3.550–26.366
observed refls.	2239
x, y (weighting scheme)	0.0342, 0.5168
hydrogen refinement	H(C) constr, H(N) refall
refls in refinement	2903
parameters	205
restraints	0
$R(F_{\text{obs}})$	0.0435
$R_w(F^2)$	0.1083
S	1.061
shift/error _{max}	0.001
max electron density/e \AA^{-3}	0.252
min electron density/e \AA^{-3}	-0.258

Indication of an intramolecular hydrogen bond: [N-H 0.94(2) \AA , O...H 1.82(2) \AA , angle NHO 135.9(19) $^\circ$].

Dimethyl (*E*)-2-(2-(2-morpholinocycloprop-2-en-1-ylidene)hydrazinyl)malonate (12bc)



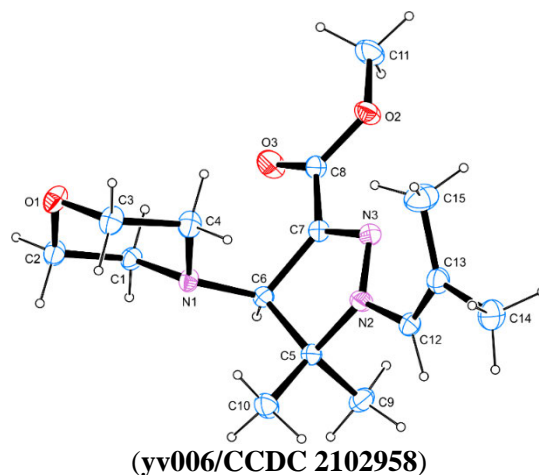
(**wv086/CCDC 2102955**)

Crystallographic data.

net formula	$\text{C}_{14}\text{H}_{21}\text{N}_3\text{O}_5$
$M_r/\text{g mol}^{-1}$	311.34
crystal size/mm	0.100 \times 0.080 \times 0.050
T/K	100.(2)
radiation	MoK α
diffractometer	'Bruker D8 Venture TXS'
crystal system	monoclinic
space group	'P 1 21/n 1'
$a/\text{\AA}$	7.9977(4)
$b/\text{\AA}$	14.2996(7)
$c/\text{\AA}$	13.7547(7)
$\alpha/^\circ$	90
$\beta/^\circ$	103.142(2)
$\gamma/^\circ$	90
$V/\text{\AA}^3$	1531.84(13)
Z	4
calc. density/ g cm^{-3}	1.350
μ/mm^{-1}	0.103
absorption correction	Multi-Scan

transmission factor range	0.94–0.99
refls. measured	16896
R_{int}	0.0331
mean $\sigma(I)/I$	0.0238
θ range	3.230–26.366
observed refls.	2657
x, y (weighting scheme)	0.0314, 0.9159
hydrogen refinement	H(C) constr, H(N) reffall
refls in refinement	3111
parameters	205
restraints	0
$R(F_{\text{obs}})$	0.0382
$R_w(F^2)$	0.0894
S	1.058
shift/error $_{\text{max}}$	0.001
max electron density/e \AA^{-3}	0.275
min electron density/e \AA^{-3}	-0.233

Methyl 5,5-dimethyl-1-(2-methylprop-1-en-1-yl)-4-morpholino-4,5-dihydro-1H-pyrazole-3-carboxylate (17)



Crystallographic data.

net formula	$\text{C}_{15}\text{H}_{25}\text{N}_3\text{O}_3$
$M_r/\text{g mol}^{-1}$	295.38
crystal size/mm	$0.100 \times 0.080 \times 0.040$
T/K	102.(2)
radiation	$\text{MoK}\alpha$
diffractometer	'Bruker D8 Venture TXS'
crystal system	monoclinic
space group	'P 1 21/c 1'
$a/\text{\AA}$	15.7536(6)
$b/\text{\AA}$	6.5292(2)
$c/\text{\AA}$	15.7587(6)
$\alpha/^\circ$	90
$\beta/^\circ$	100.6290(10)
$\gamma/^\circ$	90

Chapter 4. Quantification of the Electrophilicities of Diazoalkanes

$V/\text{\AA}^3$	1593.10(10)
Z	4
calc. density/g cm^{-3}	1.232
μ/mm^{-1}	0.086
absorption correction	Multi-Scan
transmission factor range	0.95–1.00
refls. measured	27593
R_{int}	0.0321
mean $\sigma(I)/I$	0.0210
θ range	3.360–28.282
observed refls.	3469
x, y (weighting scheme)	0.0414, 0.6439
hydrogen refinement	constr
refls in refinement	3955
parameters	195
restraints	0
$R(F_{\text{obs}})$	0.0369
$R_w(F^2)$	0.0957
S	1.042
shift/error _{max}	0.001
max electron density/e \AA^{-3}	0.371
min electron density/e \AA^{-3}	-0.215

4.2.4 References

- (1) a) Huang, T.; Chen, T.; Han, L.-B. *J. Org. Chem.* **2018**, *83*, 2959–2965. b) Esfandiartard, K.; Mai, J.; Ott, S. *J. Am. Chem. Soc.* **2017**, *139*, 2940–2943.
- (2) Trost, B. M. *J. Am. Chem. Soc.* **1966**, *88*, 1587–1588.
- (3) a) Rauk, A.; Allen, L. C.; Mislow, K. *Angew. Chem. Int. Ed. Engl.* **1970**, *9*, 400–414. b) Kessler, H. *Naturwissenschaften* **1971**, *58*, 46–51. c) de Loera, D.; Liu, F.; Houk, K. N.; Garcia-Garibay, M. A. *J. Org. Chem.* **2013**, *78*, 11623–11626.
- (4) Li, L.; Mayer, P.; Stephenson, D. S.; Ofial, A. R.; Mayer, R. J.; Mayr, H. *Angew. Chem. Int. Ed.* **2022**, *61*, e202117047; *Angew. Chem.* **2022**, *134*, e202117047.
- (5) Bruhn, T.; Schaumlöffel, A.; Hemberger, Y.; Bringmann, G. *Chirality* **2013**, *25*, 243–249.
- (6) a) Reissig, H.-U. Dissertation, Ludwig-Maximilians-Universität München, **1978**. b) Huisgen, R.; Bihlmaier, W.; Reissig, H.-U. *Angew. Chem. Int. Ed. Engl.* **1979**, *18*, 331–332; *Angew. Chem.* **1979**, *91*, 347–348. c) Bihlmaier, W.; Huisgen, R.; Reissig, H.-U.; Voss, S. *Tetrahedron Lett.* **1979**, *20*, 2621–2624.
- (7) a) Mikhailovskii, A. G.; Aliev, Z. G.; Bazina, N. G.; Pantyukhin, A. A.; Vakhrin, M. I. *Chem. Heterocycl. Comp.* **2010**, *46*, 730–735. b) Sharp, J. T.; Findlay, R. H.; Thorogood, P. B. *J. Chem. Soc. Perkin Trans. 1*, **1975**, 102–113. c) Bettinetti, G. F.; Cogoli, A.; Sale, A. O. *Ric. Sci.* **1968**, *38*, 806–809.
- (8) a) Huisgen, R.; Reissig, H.-U. *Angew. Chem. Int. Ed. Engl.* **1979**, *18*, 330–331; *Angew. Chem.* **1979**, *91*, 346–347. b) Galloway, N.; Dent, B. R.; Halton, B. *Aust. J. Chem.* **1983**, *36*, 593–599. c) Dietrich-Buchecker, C.; Franck-Neumann, M. *Tetrahedron* **1977**, *33*, 745–749.

Chapter 5. Cyclobutane Formation by the Reaction of Ethenesulfonyl Fluoride with Dimethyl Diazomalonate

Li, L.; Mayer, P.; Ofial, A. R.; Mayr, H. *E. J. Org. Chem.* **2022**, e202200865.

Author contributions

Li, L. performed all the experiments. Mayer, P. characterized the single crystal X-ray structure. The manuscript was written by Ofial, A. R.

Copyright

It is an open access article.

Link to article: <https://chemistry-europe.onlinelibrary.wiley.com/doi/10.1002/ejoc.202200865>

5.1 Copies of Manuscript

Cyclobutane Formation by the Reaction of Ethenesulfonyl Fluoride with Dimethyl Diazomalonate

Le Li,^[a] Peter Mayer,^[a] Armin R. Ofial,^{*(a)} and Herbert Mayr^{*(a)}

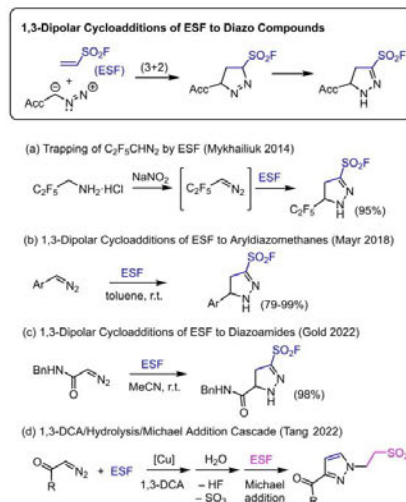
Attempts to synthesize fluorosulfonyl-substituted pyrazolines by Huisgen reactions (1,3-dipolar cycloadditions) of dimethyl diazomalonate with ethenesulfonyl fluoride led to the formation of dimethyl (2*R**,3*S**,4*R**)-2-(1,3-dimethoxy-1,3-dioxopropan-2-yl)-3-(fluorosulfonyl)-4-(fluorosulfonyl)methylcyclobutane-1,1-dicarboxylate, a highly substituted cyclobutane derivative, which was characterized by NMR spectroscopy and single crystal X-ray crystallography. The mechanism of its

formation was elucidated by carrying out the reaction at different temperatures and workup conditions. It is shown that an initial 1,3-dipolar cycloaddition yields a pyrazoline which extrudes nitrogen with formation of 1-fluorosulfonyl-2,2-bis(methoxycarbonyl)cyclopropane and dimethyl 2-(2-(fluorosulfonyl)ethylidene)malonate, the latter of which dimerized during chromatography on silica gel with formation of the isolated cyclobutane.

Introduction

Organic sulfonyl fluorides have already been known since the 1920s.^[1–3] Though the synthetic potential of alkenesulfonyl fluorides to react as Michael acceptors as well as the general ability of organic sulfonyl fluorides to undergo reactions at the SO₂F group had already been recognized in the late 1970s,^[2–4] this class of organic compounds had attracted little attention until Sharpless and associates introduced sulfonyl fluoride exchange (SuFEx) reactions^[5,6] as a new generation of click chemistry in 2014.^[7] Since then numerous applications in organic synthesis,^[8] materials chemistry,^[3] polymer chemistry,^[9] drug discovery,^[10,11] medicinal chemistry,^[12] and chemical biology^[13] have been reported.^[14] Furthermore, the electrophilic reactivity of alkenesulfonyl fluorides has been characterized and embedded in the currently most comprehensive reactivity scales for polar reactions.^[15]

Alkenesulfonyl fluorides may also act as dipolarophiles in Huisgen reactions (1,3-dipolar cycloadditions) to provide a straightforward access to fluorosulfonyl substituted heterocycles.^[16] In reactions with organic azides R-N₃, ethenesulfonyl fluoride (ESF)^[6] acted as formal acetylene equivalent, however, because the initially formed cycloadducts rapidly eliminated SO₂ and HF to yield 1-alkyl or 1-aryl-1,2,3-triazoles.^[17] On the other hand, the reactions of ESF with diazoalkanes were reported to generate SO₂F-functionalized heterocycles (Scheme 1). Mykhailiuk, for example, used ESF as a highly



Scheme 1. Reported 1,3-dipolar cycloadditions (1,3-DCA) of ESF with diazo compounds.

efficient trapping reagent for the in situ generated 1,3-dipole pentafluorodiazopropane (C₂F₅CHN₂) to yield 3-SO₂F-5-pentafluoroethyl-Δ²-pyrazoline regioselectively (Scheme 1a).^[18,19] Analogously, reactions of ESF with aryldiazomethanes gave 5-arylpiprazolines that carried an SO₂F group at position 3 (Scheme 1b).^[20] Very recently, ESF was reported by Gold and coworkers to undergo an uncatalyzed 1,3-dipolar cycloaddition with *N*-benzyl-2-diazoacetamide to deliver a 3,5-disubstituted pyrazoline (Scheme 1c).^[21] Copper(II) fluoride catalysis was used by Tang and coworkers to synthesize the (3+2)-cycloadducts of ESF with α-keto-stabilized diazoalkanes, hydrolysis of which led to HF/SO₃ elimination with formation of pyrazoles that under-

[a] L. Li, Dr. P. Mayer, Dr. A. R. Ofial, Prof. Dr. H. Mayr
Department Chemie
Ludwig-Maximilians-Universität München
Butenandtstr. 5–13, 81377 München, Germany
E-mail: ofial@lmu.de
herbert.mayr@cup.uni-muenchen.de

Supporting information for this article is available on the WWW under <https://doi.org/10.1002/ejoc.202200865>

© 2022 The Authors. European Journal of Organic Chemistry published by Wiley-VCH GmbH. This is an open access article under the terms of the Creative Commons Attribution License, which permits use, distribution and reproduction in any medium, provided the original work is properly cited.

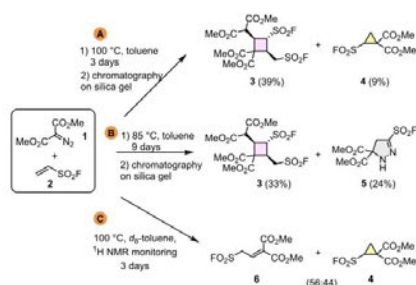
went a Michael addition to a second equivalent of ESF (Scheme 1d).^[22]

During our ongoing studies to quantify the reactivities of diazo compounds,^[20,23] we envisioned the cycloaddition of ESF with dimethyl diazomalonate to furnish fluorosulfonyl substituted pyrazolines without the need for metal catalysis, in analogy to the reports summarized in Scheme 1.

Herein, we report that the initially formed cycloadduct from diazomalonate and ESF underwent a cascade of subsequent reactions, which ultimately generated highly functionalized cyclobutanes. Online-NMR spectroscopic monitoring of the reaction was used to identify further intermediates in the course of the reaction, which enabled us to elucidate the individual transformations on the way to the isolated cyclobutane.

Results and Discussion

When we tried to synthesize fluorosulfonyl substituted pyrazolines by the reaction of ESF (2) with dimethyl diazomalonate (1), we isolated cyclobutane 3 as the major product along with a



Scheme 2. Reactions of ethenesulfonyl fluoride (2) with dimethyl diazomalonate (1) under different conditions.

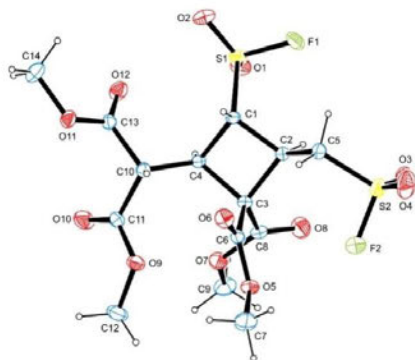


Figure 1. X-ray crystal structure of cyclobutane 3 (CCDC 2183363). Within the cyclobutane ring the atomic distances are for C1–C2 155.1(2), C2–C3 157.2(2), C3–C4 157.6(2), and C4–C1 155.2(2) pm.

small amount of cyclopropane 4 (Scheme 2A). Cyclobutane 3 showed four singlets for methoxy groups in the proton NMR spectrum as well as two signals in the ¹⁹F NMR spectrum, indicating that 3 is a 2:2 product of 1 and 2.

Since 3 crystallized nicely after column chromatographic purification, its molecular structure could be investigated by single-crystal X-ray crystallography (Figure 1). The solid state structure shows that the cyclobutane moiety adopts a butterfly conformation with a ring puckering angle of 20.5°. Slightly elongated C–C single bonds (as compared with 153.6 pm in cyclohexane)^[24] are due to the ring strain in the four-membered carbocycle. Only one diastereomer with the SO₂F group trans to the vicinal CH₂SO₂F and CH(CO₂Me)₂ was obtained.

Cyclobutanes with similar substitution patterns have been formed by gallium chloride-mediated (2+2) dimerization of donor-acceptor cyclopropanes.^[25]

Since cyclopropanes, such as 4, are known to be formed by thermolysis of Δ^1 -pyrazolines,^[26] the cycloadducts from the reactions of diazoalkanes with dipolarophiles, we repeated the reaction of 1 with 2 at lower temperature, hoping to isolate the precursors of 3 and 4. However, as depicted in Scheme 2B, cyclobutane 3 was the main product again when the reaction was run at 85 °C, now accompanied by the Δ^2 -pyrazoline 5.

Because of the slow reaction of 1 with 2, we did not further lower the temperature, but monitored the 100 °C reaction in a sealed tube by ¹H NMR spectroscopy. As depicted in Scheme 2C and documented by the original spectra (Supporting Information), cyclobutane 3 and Δ^2 -pyrazoline 5 were not detectable. Instead, the formation of a 44:56 mixture of cyclopropane 4 and alkyldiene malonate 6 was observed.

While a solution of 5 (0.128 M) in *d*₈-toluene remained unchanged over a period of more than 4 months when stored at ambient temperature, the assumption that both, 4 and 6, are generated by thermolysis of pyrazoline 5 was confirmed by ¹H NMR monitoring of the thermal decomposition of isolated 5 in *d*₈-toluene at 95 °C. Figure 2 shows that the cyclopropane 4 and the acyclic product 6 are formed in parallel reactions. As soon as the resonances of 4 and 6 have both reached signal-to-noise levels that enable a reliable integration of the ¹H NMR signals (after 72 h), the 55/45 ratio of 4 and 6 remains constant, suggesting that 4 and 6 do not interconvert. The fact that the sum of the concentrations of 4 and 6 is smaller by about 10% than the initial concentration of the starting material 5 may indicate that thermolysis of 5 yields small amounts of further, so far not identified products.

Further experiments were undertaken to gain insight in the mechanisms that ultimately generate cyclobutane 3 from the 4/6-mixture initially obtained by heating 1 and 2 in an inert solvent (Scheme 2C). In particular, we sought to clarify whether the cyclopropane 4 or the alkyldiene malonate 6 or both are the precursors of 3. A solution of equimolar amounts (2.54 mmol) of methyl diazomalonate (1) and ESF (2) in *d*₈-toluene was kept at 100 °C for 52 h to generate a 42:58-mixture of 4 and 6 (Figure 3). Stirring of this solution with a small amount of added silica gel at ambient temperature for 30 min did not noticeably change the composition of the mixture ([4]:[6] = 45:55, Figure 3B). A quick workup of this sample by

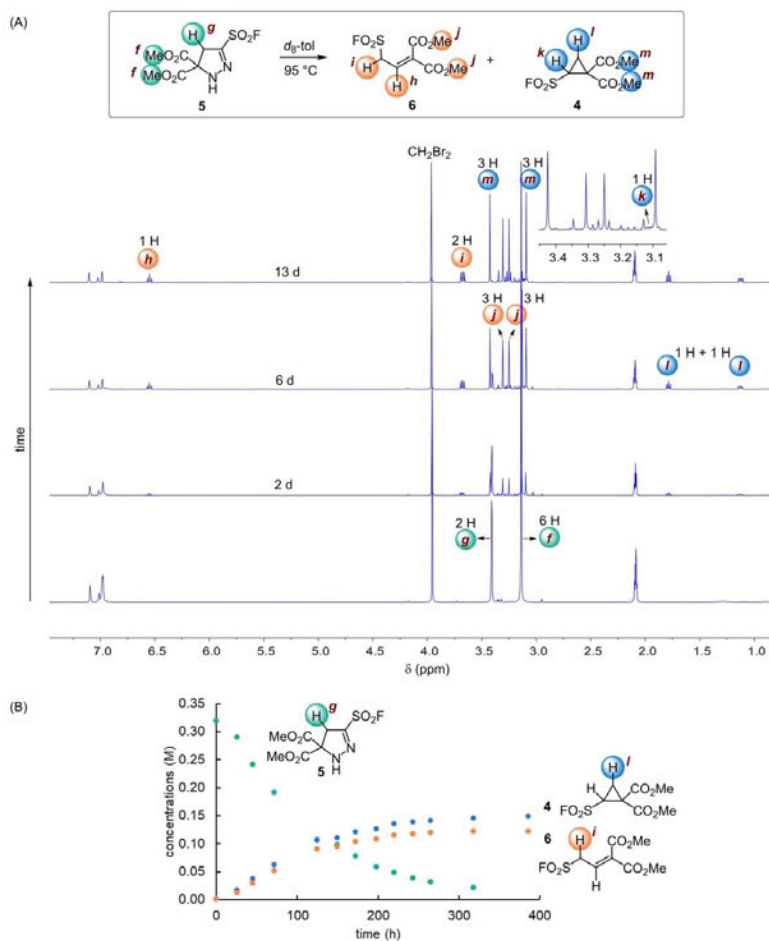


Figure 2. (A) ^1H NMR (400 MHz) monitoring of the transformation of **5** ($c_0 = 0.318\text{ M}$) in d_8 -toluene at $95\text{ }^\circ\text{C}$ with CH_2Br_2 (0.277 M) as the internal integration standard. (B) Concentration profiles for the starting material **5**, the alkylidene malonate **6**, and the cyclopropane **4** in d_8 -toluene at $95\text{ }^\circ\text{C}$ determined by monitoring the thermal decomposition of **5** by ^1H NMR spectroscopy [evaluated protons are marked by colored dots, the resonance at $\delta_{\text{H}} = 1.66\text{--}1.86\text{ ppm}$ (H) was used to determine the content of **4**, integrals for **4**, **5**, and **6** were normalized to 1 H and concentrations were calculated relative to CH_2Br_2 as the internal integration standard].

filtration through a plug of silica gel (pentane/ethyl acetate and dichloromethane as eluents) followed by removal of the solvents (vacuum) furnished a residue, which was dissolved in CDCl_3 and analyzed by ^1H NMR spectroscopy to contain **4** and **6** in a 45:55 ratio (Figure 3C). At this point, the NMR spectrum did not yet indicate formation of the cyclobutane **3**. Then, drops of triethylamine (NEt_3) were added to the **4/6**-mixture. NMR monitoring showed that the characteristic resonances for the alkylidene malonate **6** disappeared within minutes (Figure 3D). Yet, due to overlapping resonances, it was not possible to derive the selective conversion of **6** into the cyclobutane **3** from

the ^1H NMR spectrum. Therefore, the formation of **3** was substantiated by identifying both ^{19}F resonances of **3** in the ^{19}F NMR spectrum (377 MHz) of this sample (Supporting Information, Figure S1).

In contrast to the acyclic product **6**, cyclopropane **4** was not altered by the addition of NEt_3 to the reaction mixture (Figure 3D and Figure S1). It can, therefore, be concluded that basic sites on silica used for the chromatographic purification of the product mixtures (cf. Scheme 2A or Scheme 2B) led to the formation of cyclobutane **3**. Accordingly, acidic additives, such

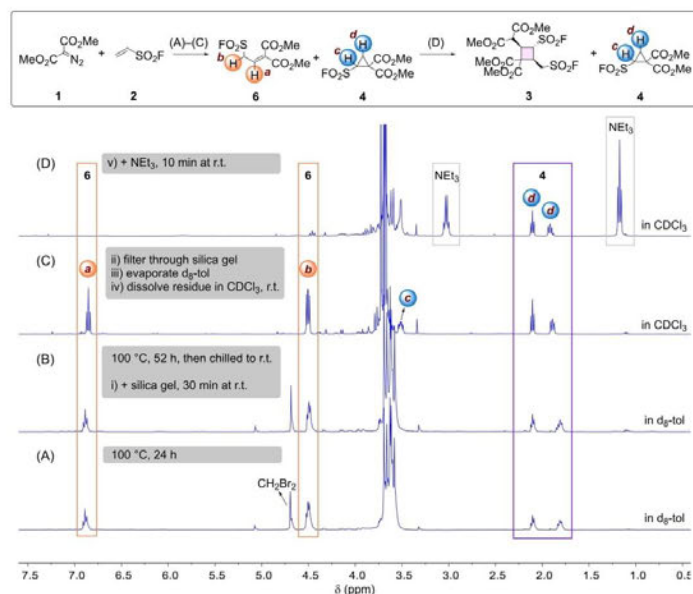


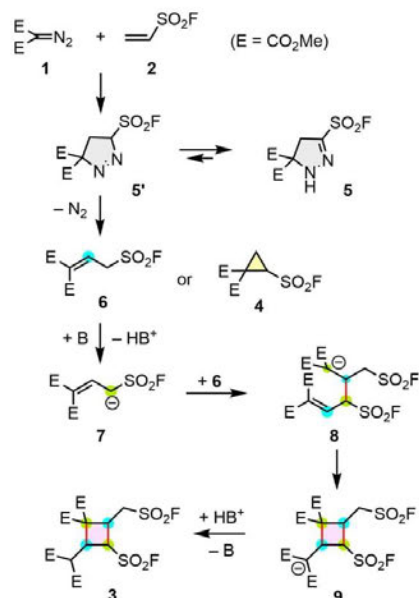
Figure 3. (A) Generation of a mixture of **4** and **6** through the reaction of **1** with **2** (100 °C, in *d*₆-toluene, CH₂Br₂ as the internal integration standard) with subsequent addition of (B) silica gel, (C) filtration through silica gel and solvent exchange to *d*-chloroform as well as (D) addition of triethylamine.

as acetic acid or boron trifluoride etherate, failed to induce cyclobutane formation from **4/6** mixtures in CDCl₃ within 24 h.

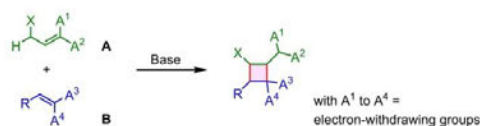
We, therefore, suggest the reaction mechanism described in Scheme 3. 1,3-Dipolar cycloaddition of dimethyl diazomalonate (**1**) and ESF (**2**) generates the Δ¹-pyrazoline **5'**, which is in rapid equilibrium with its thermodynamically more stable tautomer **5** that is observed by NMR spectroscopy. At higher temperatures, **5'** extrudes molecular nitrogen with formation of cyclopropane **4** and the alkylidene malonate **6**. While **4** is persistent under the reaction and workup conditions, the strong electron-withdrawing nature of the SO₂F group (Hammett substituent parameter σ_p⁻ = 1.54 for SO₂F, as compared to σ_p⁻ = 1.27 for NO₂)^[27] facilitates deprotonation of the CH₂ group of **6**. The resulting allyl anion **7** is sufficiently nucleophilic to undergo a Michael addition with another equivalent of the alkylidene malonate **6** to furnish the diester stabilized anion **8**, which is intramolecularly trapped in a second Michael addition leading to the formation of the cyclobutylmalonyl anion **9**. Protonation of **9** yields the isolated and characterized cyclobutane **3**.

Conclusion

The highly functionalized cyclobutane **3**, isolated as the major product by the reaction of dimethyl diazomalonate (**1**) with ethenesulfonyl fluoride (**2**) is formed by a series of well-established reactions. Initial Huisgen (3+2)-cycloaddition of **1** with **2** yields the Δ¹-pyrazoline **5'**, which tautomerizes into the



Scheme 3. Proposed reaction mechanism for the formation of cyclobutane **3**.



Scheme 4. Suggestion of a versatile cyclobutane synthesis.

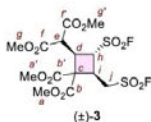
thermodynamically more stable Δ^2 -pyrazoline 5 in a reversible reaction. Thermolysis of 5' leads to extrusion of nitrogen and concomitant formation of the cyclopropane 4 and the Michael acceptor 6, which dimerizes under basic conditions to give cyclobutane 3, while cyclopropane 4 remained unaffected.

Scheme 4 shows a generalization of the observed dimerization of 6 which might give access to cyclobutanes of large structural variety.^[28] By combining CH-acids of type A with Michael acceptors B, which are more electrophilic than A, mixed variants of the dimerization of 6 might become viable.^[28b,29] Electrophilicity parameters of numerous types of Michael acceptors are available and can be used for designing suitable reactions.^[30] An extension to acetylenic variants of A and B appears feasible.

Experimental Section

Cyclobutane 3 and cyclopropane 4. Dimethyl diazomalonate (1) (400 mg, 2.53 mmol) was mixed with ethenesulfonyl fluoride (ESF, 2) (279 mg, 2.53 mmol) in toluene (0.2 mL) in an oven-dried NMR tube with screw cap under argon atmosphere at room temperature. The NMR tube was then sealed and the reaction mixture was heated at 100 °C for 3 days (TLC showed quantitative consumption of the starting material). At the end of the reaction time, the reaction mixture was transferred to a 25 mL round-bottom flask and the NMR tube was washed with CH_2Cl_2 (3 × 2 mL). Solvents were evaporated and the resulting crude products were then worked up by column chromatography (diameter of the column: 20 mm) on silica gel (50 mL, 0.035–0.070 mm, 60 Å) with n-pentane/EtOAc (4:1 ~ 2:1) as the eluent to give dimethyl (2*R**,3*S**,4*R**)-2-(1,3-dimethoxy-1,3-dioxopropan-2-yl)-3-(fluorosulfonyl)-4-(fluorosulfonyl)methylcyclobutane-1,1-dicarboxylate (3) as a white solid (241 mg, yield 39%; mp 144.9 °C) and dimethyl 2-(fluorosulfonyl)cyclopropane-1,1-dicarboxylate (4) as a light-yellow oil (54.3 mg, yield 9%).

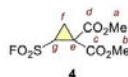
Spectroscopic characterization of cyclobutane 3:



¹H NMR (400 MHz, CDCl_3): δ = 3.73–3.86 (m, 3 H, H^d, Hⁱ, and H^j, superimposed with resonances of OCH_3 groups), 3.75, 3.78, 3.82 and 3.85 (4 s, 4 × 3 H, 4 OCH_3 , superimposed with resonances of H^d, Hⁱ, and H^j), 4.05 (app t, J = 9.1 Hz, 1 H, H^k), 4.13–4.20 (m, 1 H, H^l), 4.33 (t, J = 9.5 Hz, 1 H, H^m). ¹³C NMR (101 MHz, CDCl_3): δ = 37.3 (CH, C), 41.9 (CH, C^a), 49.2 (CH₂, d, ² J_{CF} = 19.9 Hz, C^b), 51.2 (CH, C^d), 53.39 and 53.44 (2 CH₂, C^a and C^c), 53.82 and 53.87 (2 × CH₂, C^a and C^b), 55.5 (C_q, C), 57.5 (CH, d, ² J_{CF} = 19.0 Hz, C^b), 166.1 (C_q, C^o or C^p),

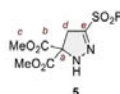
166.6 (C_q, C^b or C^b), 167.5 (C_q, C^f or C^f), 167.8 (C_q, C^f or C^f). ¹⁹F NMR (377 MHz, CDCl_3): δ = 50.83–50.84 (m, 1 F), 58.80–58.81 (m, 1 F). HRMS (ESI⁺): m/z calcd for $\text{C}_{16}\text{H}_{18}\text{F}_2\text{O}_{12}\text{NaS}_2$ ⁺ (M + Na⁺): 503.0100; found 503.0100. IR (neat, ATR): 2991, 2963, 1751, 1738, 1719, 1439, 1416, 1409, 1351, 1311, 1288, 1268, 1251, 1211, 1196, 1186, 1160, 1020, 964, 889, 817, 798, 779, 770, 762, 747, 722 cm^{-1} .

Spectroscopic characterization of cyclopropane 4:



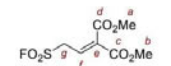
NMR spectra in CDCl_3 : ¹H NMR (400 MHz, CDCl_3): δ = 1.99 (ddd, ³ J_{HH} = 9.0, ² J_{HH} = 6.2, ⁴ J_{HF} = 1.6 Hz, 1 H, H^a), 2.26 (dd, ³ J_{HH} = 6.8, ² J_{HH} = 6.2 Hz, 1 H, H^b), 3.56 (ddd, ³ J_{HH} = 9.0, ³ J_{HH} = 6.7, ³ J_{HF} = 4.3 Hz, 1 H, H^c), 3.83 (s, 3 H, H^d or H^e), 3.84 (s, 3 H, H^d or H^e). ¹³C NMR (101 MHz, CDCl_3): δ = 18.6 (CH₂, C^f), 36.3 (C_q, C^g), 39.3 (CH, d, ² J_{CF} = 32.3 Hz, C^h), 54.0 (CH₂, C^a or C^b), 54.2 (CH₂, C^a or C^b), 163.7 (C_q, C^c or C^c), 166.9 (C_q, C^c or C^c). ¹⁹F NMR (376 MHz, CDCl_3): δ = 61.83 (dd, ³ J_{FH} = 4.4, ⁴ J_{FH} = 1.6 Hz). NMR spectra in d_6 -toluene: ¹H NMR (400 MHz, d_6 -toluene): δ = 1.10 (ddd, ³ J_{HH} = 9.0, ² J_{HH} = 6.2, ⁴ J_{HF} = 1.5 Hz, 1 H, H^a), 1.76–1.79 (m, 1 H, H^b), 3.06–3.11 (m, 1 H, H^c, superimposed with H^d or H^e resonance), 3.07 (s, 3 H, H^d or H^e, superimposed with H^d), 3.42 (s, 3 H, H^d or H^e). ¹³C NMR (101 MHz, d_6 -toluene): δ = 17.9 (CH₂, C^f), 36.3 (C_q, C^g), 39.2 (CH, d, ² J_{CF} = 32.6 Hz, C^h), 53.1 (CH₂, C^a or C^b), 53.2 (CH₂, C^a or C^b), 163.3 (C_q, C^c or C^c), 166.6 (C_q, C^c or C^c). NMR spectra in CD_2Cl_2 : ¹H NMR (400 MHz, CD_2Cl_2): δ = 2.01 (ddd, ³ J_{HH} = 9.0, ² J_{HH} = 6.3, ⁴ J_{HF} = 1.6 Hz, 1 H, H^a), 2.24 (app t, J = 6.5 Hz, 1 H, H^b), 3.61 (ddd, ³ J_{HH} = 9.0, ³ J_{HH} = 6.8, ³ J_{HF} = 4.3 Hz, 1 H, H^c), 3.80 (s, 3 H, H^d or H^e), 3.81 (s, 3 H, H^d or H^e). ¹³C NMR (101 MHz, CD_2Cl_2): δ = 18.8 (CH₂, C^f), 36.6 (C_q, C^g), 39.4 (CH, d, ² J_{CF} = 32.0 Hz, C^h), 54.1 (CH₂, C^a or C^b), 54.4 (CH₂, C^a or C^b, superimposed with resonances of the solvent CD_2Cl_2), 164.0 (C_q, C^c or C^c), 167.0 (C_q, C^c or C^c). HRMS (EI): m/z calcd for $\text{C}_7\text{H}_9\text{FO}_5\text{S}^+$ (M⁺): 240.0098; found 240.0102. IR (neat, ATR): 3113, 3047, 2960, 2921, 2853, 1736, 1437, 1408, 1352, 1318, 1261, 1218, 1200, 1179, 1128, 1008, 915, 879, 793, 767, 718 cm^{-1} .

Dimethyl 5-(fluorosulfonyl)-2,4-dihydro-3H-pyrazole-3,3-dicarboxylate (5). When the product mixture obtained from the reaction of 1 (442 mg, 2.80 mmol) with 2 (296 mg, 2.69 mmol) in d_6 -toluene: mesitylene = 1:1 (200 μL) at 85 °C for 9 days was worked up by column chromatography on silica gel (n-pentane/EtOAc = 5:1 ~ 1:1), we isolated cyclobutane 3 (213 mg, yield 33%) and the pyrazole 5 as a colorless oil (170 mg, yield 24%).



¹H NMR (400 MHz, CDCl_3): δ = 3.77 (d, ⁴ J_{HF} = 1.6 Hz, 2 H, H^a), 3.87 (s, 6 H, H^b), 7.51 (br s, 1 H, NH). ¹³C NMR (101 MHz, CDCl_3): δ = 38.4 (CH₂, C^d), 54.5 (CH₂, C^e), 76.3 (C_q, C^f), 141.0 (C_q, d, ² J_{CF} = 37.8 Hz, C^g), 167.0 (C_q, C^h). ¹⁹F NMR (377 MHz, CDCl_3): δ = 59.84–59.86 (m). HRMS (EI): m/z calcd for $\text{C}_7\text{H}_9\text{FN}_2\text{O}_6\text{S}^+$ (M⁺): 268.0160; found 268.0166. IR (neat, ATR): 3347, 2962, 2851, 1740, 1557, 1415, 1282, 1254, 1223, 1164, 1134, 1078, 1046, 956, 879, 769 cm^{-1} .

Dimethyl 2-(2-(fluorosulfonyl)ethylidene)malonate (6) was characterized by analyzing the NMR spectra of the mixture of 4 and 6 obtained at the end of the reaction of 1 (404 mg, 2.56 mmol) with 2 (287 mg, 2.61 mmol) in d_6 -toluene (0.2 mL) at 100 °C for 3 days.



6 (in a 56/44 mixture with 4)

^1H NMR (400 MHz, d_8 -toluene): δ = 3.53 (s, 3 H, H^a or H^b), 3.60 (s, 3 H, H^a or H^b), 4.39 (dd, $^3J_{\text{HH}} = 7.7$, $^3J_{\text{HF}} = 5.6$ Hz, 2 H, H^c), 6.79 (t, $^3J_{\text{HH}} = 7.7$ Hz, 1 H, H^d). ^{13}C NMR (101 MHz, d_8 -toluene): δ = 50.2 (CH_2 , d, $^2J_{\text{CF}} = 19.4$ Hz, C^a), 52.9 (CH_3 , C^a or C^b), 53.0 (CH_3 , C^a or C^b), 132.5 (CH , C^c), 135.0 (C_{qu} , C^c or C^d), 163.6 (C_{qu} , C^c or C^d), 164.1 (C_{qu} , C^c or C^d). ^{19}F NMR (376 MHz, d_8 -toluene): δ 54.89 (t, $^3J_{\text{FH}} = 5.6$ Hz).

Deposition Number CCDC 2183363

Deposition Number 2183363 (for 3) contains the supplementary crystallographic data for this paper. These data are provided free of charge by the joint Cambridge Crystallographic Data Centre and Fachinformationszentrum Karlsruhe Access Structures service www.ccdc.cam.ac.uk/structures.

Acknowledgements

We thank the Department Chemie (LMU München) for financial support. Open Access funding enabled and organized by Projekt DEAL.

Conflict of Interest

The authors declare no conflict of interest.

Data Availability Statement

The data that support the findings of this study are available from the corresponding author upon reasonable request.

Keywords: Azo compounds · (3+2)-Cycloadditions · Cyclobutanes · Reaction monitoring · Sulfonyl fluorides

- [1] a) W. Steinkopf, *J. Prakt. Chem.* **1927**, *117*, 1–82; b) W. Steinkopf, P. Jaeger, *J. Prakt. Chem.* **1930**, *128*, 63–88; c) W. Steinkopf, R. Hübner, *J. Prakt. Chem.* **1934**, *141*, 193–200.
- [2] P. K. Chinthakindi, P. I. Arvidsson, *Eur. J. Org. Chem.* **2018**, 3648–3666.
- [3] A. S. Barrow, C. J. Smedley, Q. Zheng, S. Li, J. Dong, J. E. Moses, *Chem. Soc. Rev.* **2019**, *48*, 4731–4758.
- [4] J. J. Krutak, R. D. Burpitt, W. H. Moore, J. A. Hyatt, *J. Org. Chem.* **1979**, *44*, 3847–3858.
- [5] J. Dong, L. Krasnova, M. G. Finn, K. B. Sharpless, *Angew. Chem. Int. Ed.* **2014**, *53*, 9430–9448; *Angew. Chem.* **2014**, *126*, 9584–9603.
- [6] M.-C. Giel, C. J. Smedley, J. E. Moses, in *Science of Synthesis: Click Chemistry*, Vol. 1 (Ed: F. P. J. T. Rutjes), Thieme, Stuttgart, **2021**, Ch. 5, pp. 435–484.
- [7] Y.-P. Meng, S.-M. Wang, W.-Y. Fang, Z.-Z. Xie, J. Leng, H. Alsulami, H.-L. Qin, *Synthesis* **2020**, *52*, 673–687.
- [8] T. S.-B. Lou, M. C. Willis, *Nat. Chem. Rev.* **2022**, *6*, 146–162.

- [9] T. A. Fattah, A. Saeed, F. Albericio, *J. Fluorine Chem.* **2018**, *213*, 87–112.
- [10] Z. Liu, J. Li, S. Li, G. Li, K. B. Sharpless, P. Wu, *J. Am. Chem. Soc.* **2018**, *140*, 2919–2925.
- [11] J. J. Rojas, R. A. Croft, A. J. Sterling, E. L. Briggs, D. Antermite, D. C. Schmitt, L. Blagojevic, P. Haycock, A. J. P. White, F. Duarte, C. Choi, J. J. Mousseau, J. A. Bull, *Nat. Chem.* **2022**, *14*, 160–169.
- [12] O. O. Grygorenko, D. M. Volochnyuk, B. V. Vashchenko, *Eur. J. Org. Chem.* **2021**, 6478–6510.
- [13] Q. Zheng, J. L. Woehl, S. Kitamura, D. Santos-Martins, C. J. Smedley, G. Li, S. Forli, J. E. Moses, D. W. Nolan, K. B. Sharpless, *Proc. Natl. Acad. Sci. USA* **2019**, *116*, 18808–18814.
- [14] N. D. Ball in *Emerging Fluorinated Motifs: Synthesis, Properties, and Applications*, Vol. 2 (Eds: J.-A. Ma, D. Cahard), Wiley-VCH, Weinheim, **2020**, Ch. 21, pp. 621–674.
- [15] Q. Chen, P. Mayer, H. Mayr, *Angew. Chem. Int. Ed.* **2016**, *55*, 12664–12667; *Angew. Chem.* **2016**, *128*, 12854–12858.
- [16] a) J. Chanet-Ray, R. Vessière, A. Zéroual, *Heterocycles* **1987**, *26*, 101–108; b) V. L. Mykhailiuk, V. S. Yarmolchuk, R. O. Doroschuk, A. A. Tolmachev, O. O. Grygorenko, *Eur. J. Org. Chem.* **2018**, 2870–2876.
- [17] M.-C. Giel, C. J. Smedley, E. R. R. Mackie, T. Guo, J. Dong, T. P. Soares da Costa, J. E. Moses, *Angew. Chem. Int. Ed.* **2020**, *59*, 1181–1186; *Angew. Chem.* **2020**, *132*, 1197–1202.
- [18] P. K. Mykhailiuk, *Chem. Eur. J.* **2014**, *20*, 4942–4947.
- [19] P. K. Mykhailiuk, *Chem. Rev.* **2021**, *121*, 1670–1715.
- [20] H. Jangra, Q. Chen, E. Fuks, I. Zenz, P. Mayer, A. R. Ofial, H. Zipse, H. Mayr, *J. Am. Chem. Soc.* **2018**, *140*, 16758–16772.
- [21] P. Yamanushkin, K. Kaya, M. A. M. Feliciano, B. Gold, *J. Org. Chem.* **2022**, *87*, 3868–3873.
- [22] W.-F. Yang, T. Shu, H.-R. Chen, H.-L. Qin, H. Tang, *Org. Biomol. Chem.* **2022**, *20*, 3506–3510.
- [23] a) T. Bug, M. Hartnagel, C. Schlierf, H. Mayr, *Chem. Eur. J.* **2003**, *9*, 4068–4076; b) J. Zhang, Q. Chen, R. J. Mayer, J.-D. Yang, A. R. Ofial, J.-P. Cheng, H. Mayr, *Angew. Chem. Int. Ed.* **2020**, *59*, 12527–12533; *Angew. Chem.* **2020**, *132*, 12628–12634; c) M. Hartnagel, A. R. Ofial, H. Mayr, *Synthesis* **2022**, *54*, doi: 10.1055/s-0041-1737327; d) L. Li, P. Mayer, D. S. Stephenson, A. R. Ofial, R. J. Mayer, H. Mayr, *Angew. Chem. Int. Ed.* **2022**, *61*, e202117047; e) L. Li, R. J. Mayer, D. S. Stephenson, P. Mayer, A. R. Ofial, H. Mayr, *Chem. Eur. J.* **2022**, doi: 10.1002/chem.202201376.
- [24] K. B. Wiberg in *The Chemistry of Cyclobutanes* (Eds.: Z. Rappoport, J. F. Liebman), Wiley, **2005**, Ch. 1, pp. 1–15.
- [25] R. A. Novikov, A. V. Tarasova, V. A. Korolev, V. P. Timofeev, Y. V. Tomilov, *Angew. Chem. Int. Ed.* **2014**, *53*, 3187–3191; *Angew. Chem.* **2014**, *126*, 3251–3255.
- [26] a) W. M. Jones, *J. Am. Chem. Soc.* **1958**, *80*, 6687; b) W. M. Jones, *J. Am. Chem. Soc.* **1959**, *81*, 5153–5156; c) W. M. Jones, *J. Am. Chem. Soc.* **1960**, *82*, 3136–3137.
- [27] C. Hansch, A. Leo, D. Hoekman, *Exploring QSAR – Hydrophobic, Electronic, and Steric Constants*, ACS Professional Reference Book, American Chemical Society, Washington D. C. (U. S. A.), **1995**.
- [28] For reviews on the synthesis of functionalized cyclobutanes, see: a) F. Secci, A. Frongia, P. Piras, *Molecules* **2013**, *18*, 15541–15572; b) K.-G. Wen, Y.-Y. Peng, X.-P. Zeng, *Org. Chem. Front.* **2020**, *7*, 2576–2597.
- [29] For a selection of organocatalytic reactions that furnish cyclobutanes, see: a) E. Albrecht, G. Dickmeiss, F. Cruz Acosta, C. Rodríguez-Escrich, R. L. Davis, K. A. Jørgensen, *J. Am. Chem. Soc.* **2012**, *134*, 2543–2546; b) K. Patora-Komisarska, M. Benohoud, H. Ishikawa, D. Seebach, Y. Hayashi, *Helv. Chim. Acta* **2011**, *94*, 719–745; c) G. Talavera, E. Reyes, J. L. Vicario, L. Carrillo, *Angew. Chem. Int. Ed.* **2012**, *51*, 4104–4107; *Angew. Chem.* **2012**, *124*, 4180–4183; d) P. S. Akula, B.-C. Hong, G.-H. Lee, *Org. Lett.* **2018**, *20*, 7835–7839.
- [30] For a freely accessible database of electrophilicity parameters E , see: www.cup.lmu.de/oc/mayr/DBintro.html (accessed on August 8th, 2022).

Manuscript received: July 18, 2022
Revised manuscript received: August 8, 2022
Accepted manuscript online: August 9, 2022

5.2 Supporting Information

5.2.1 Additional Figure

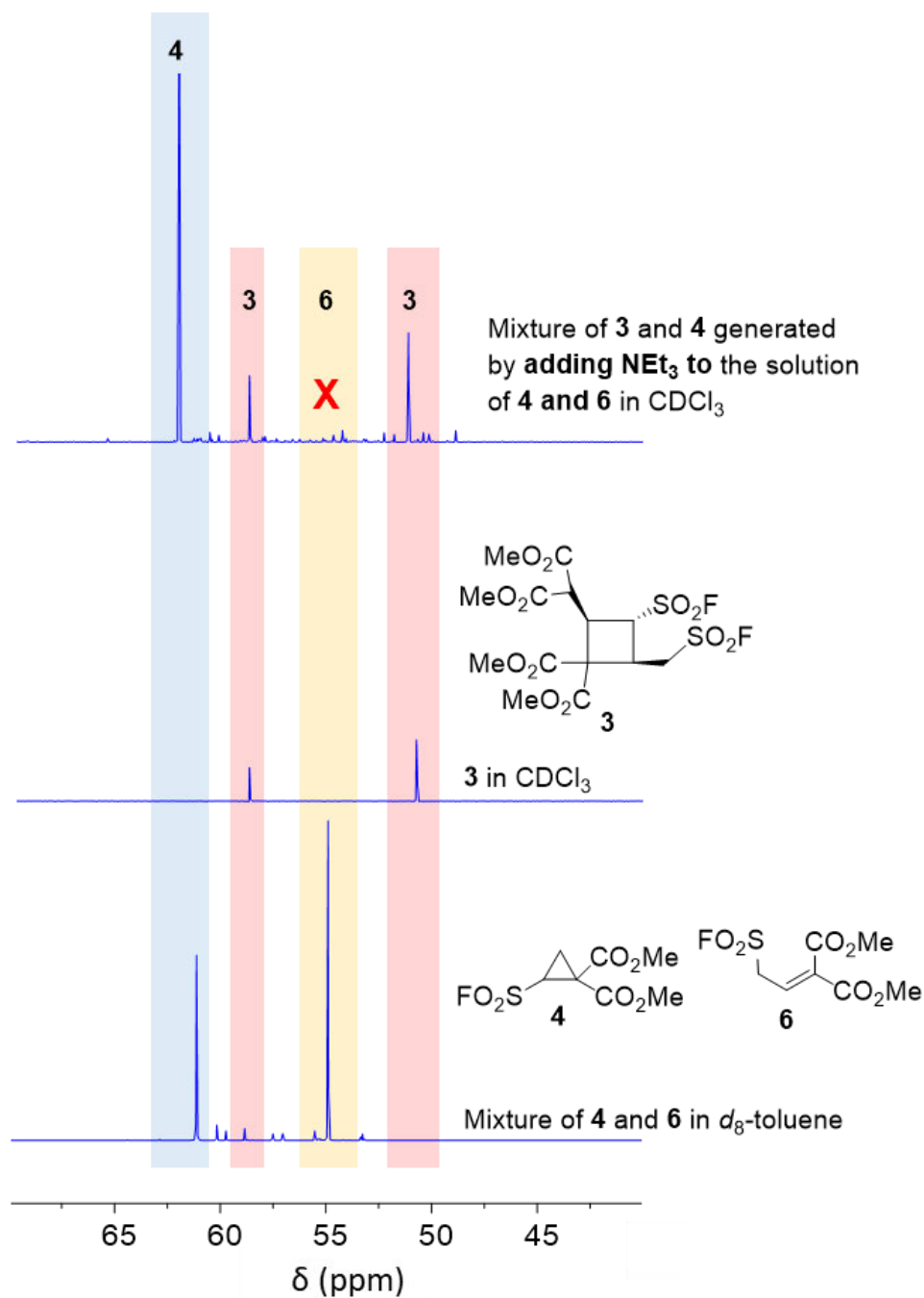
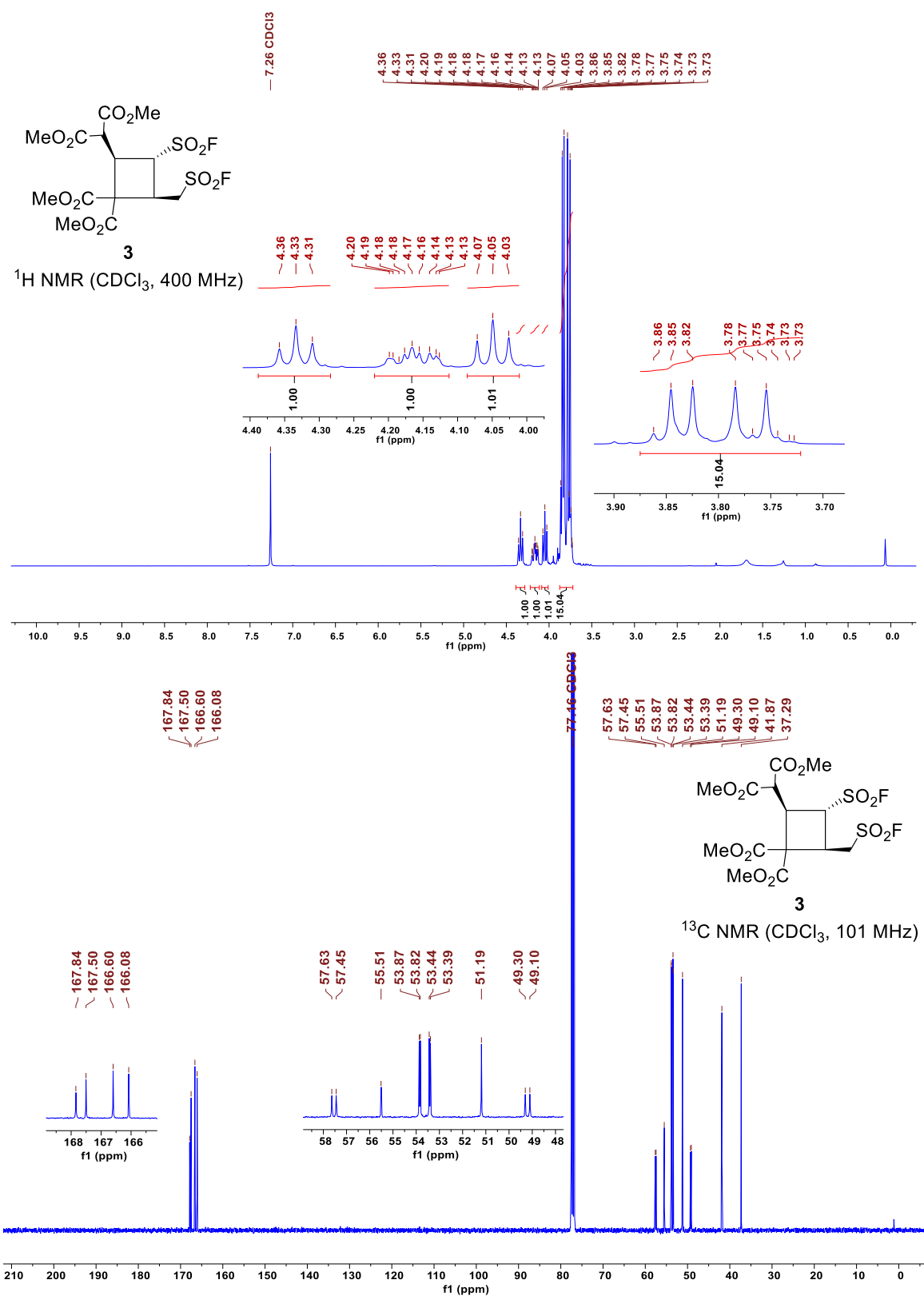
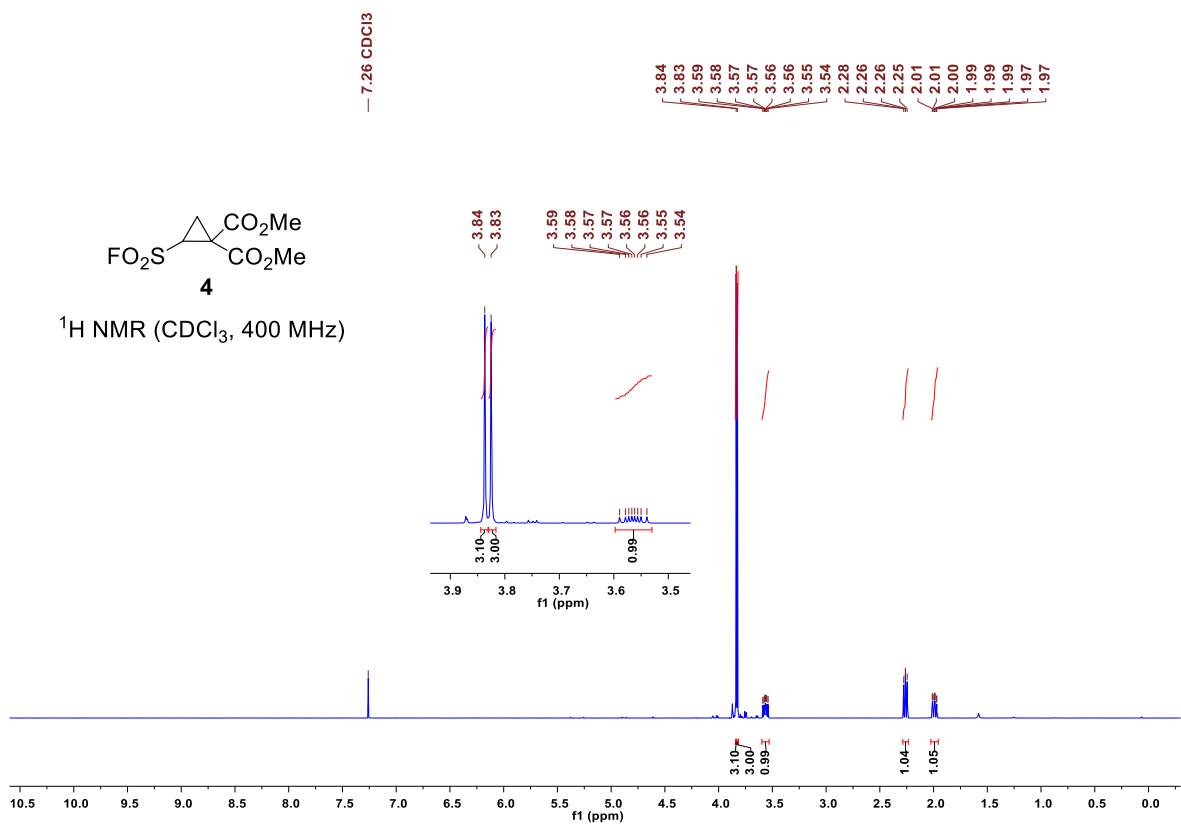
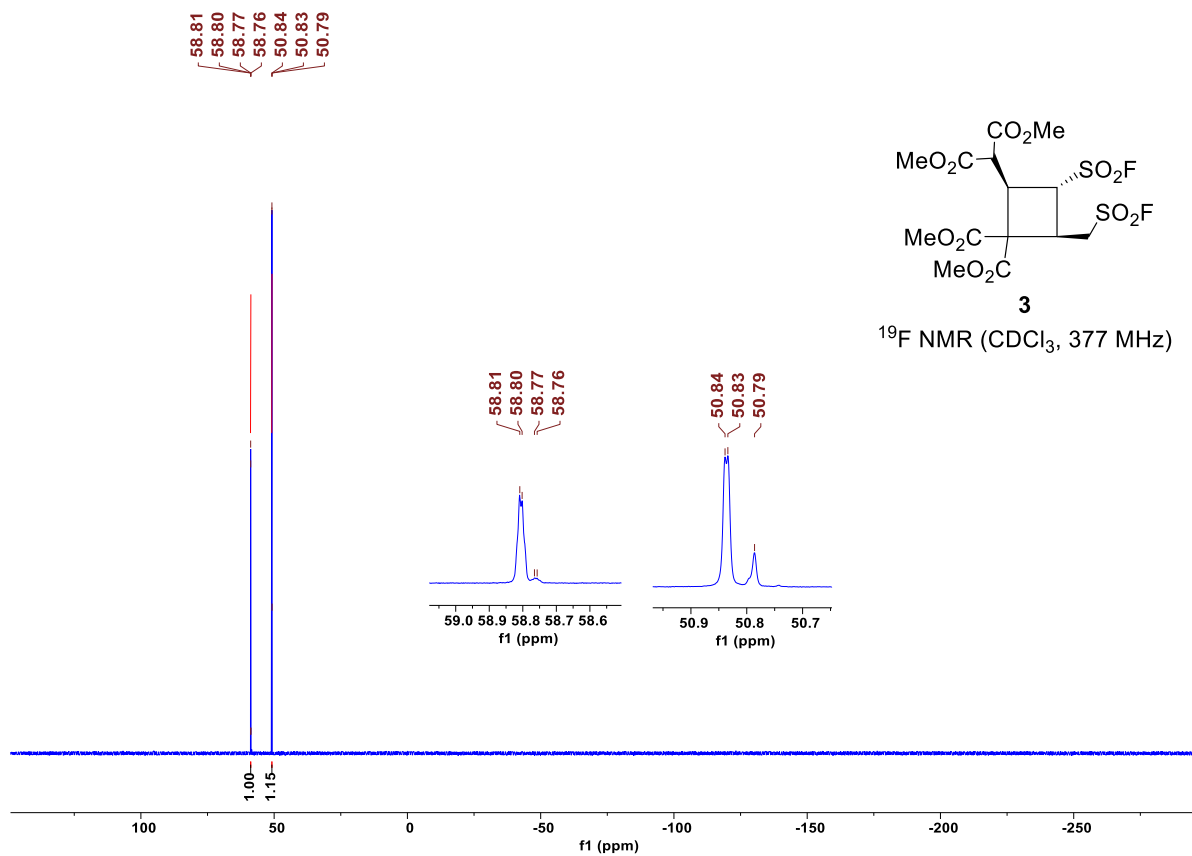
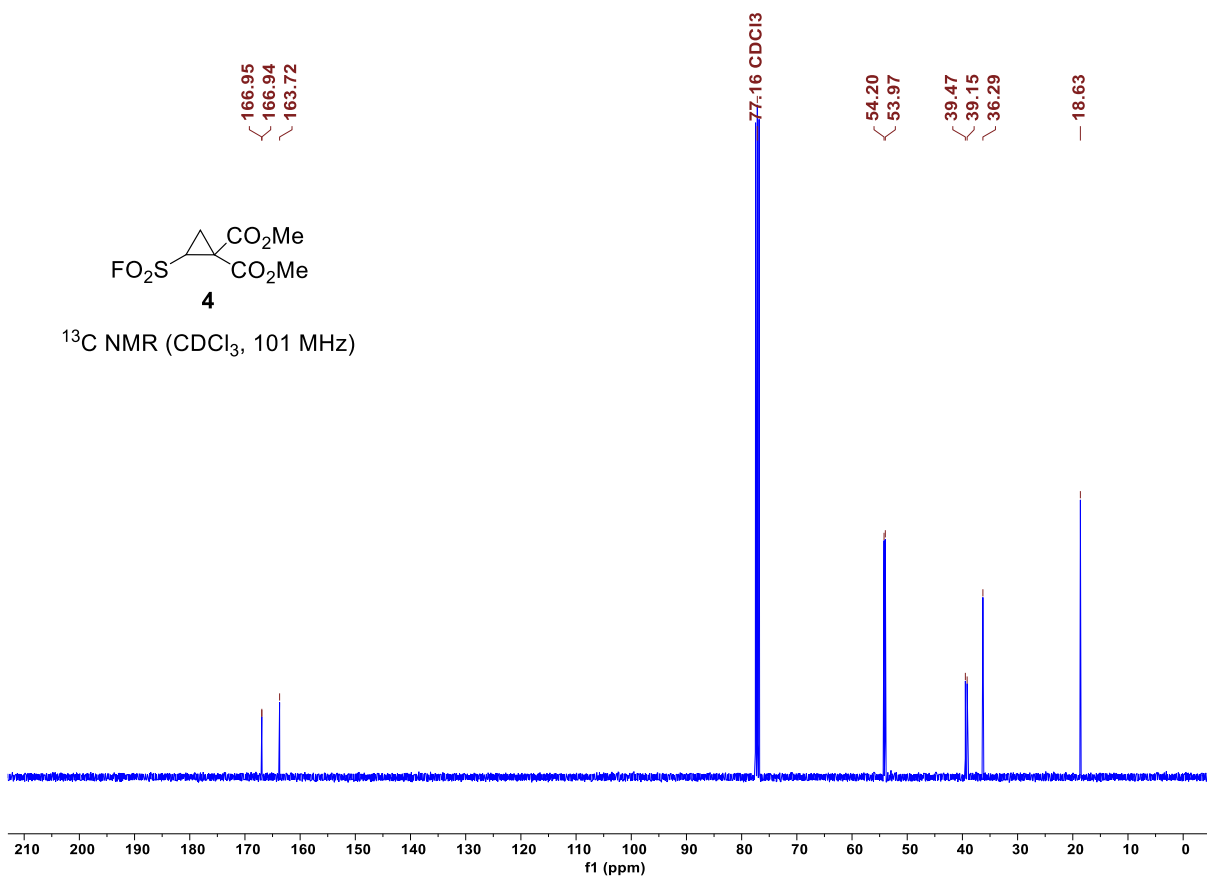


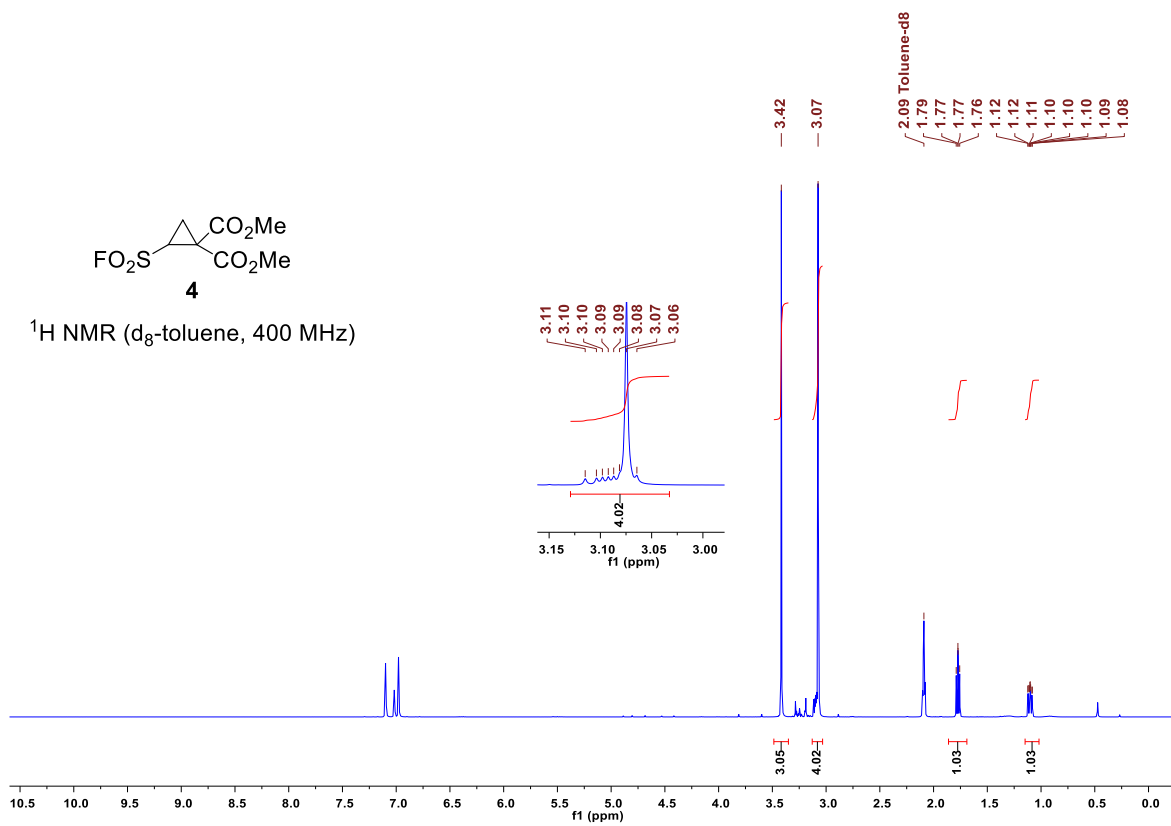
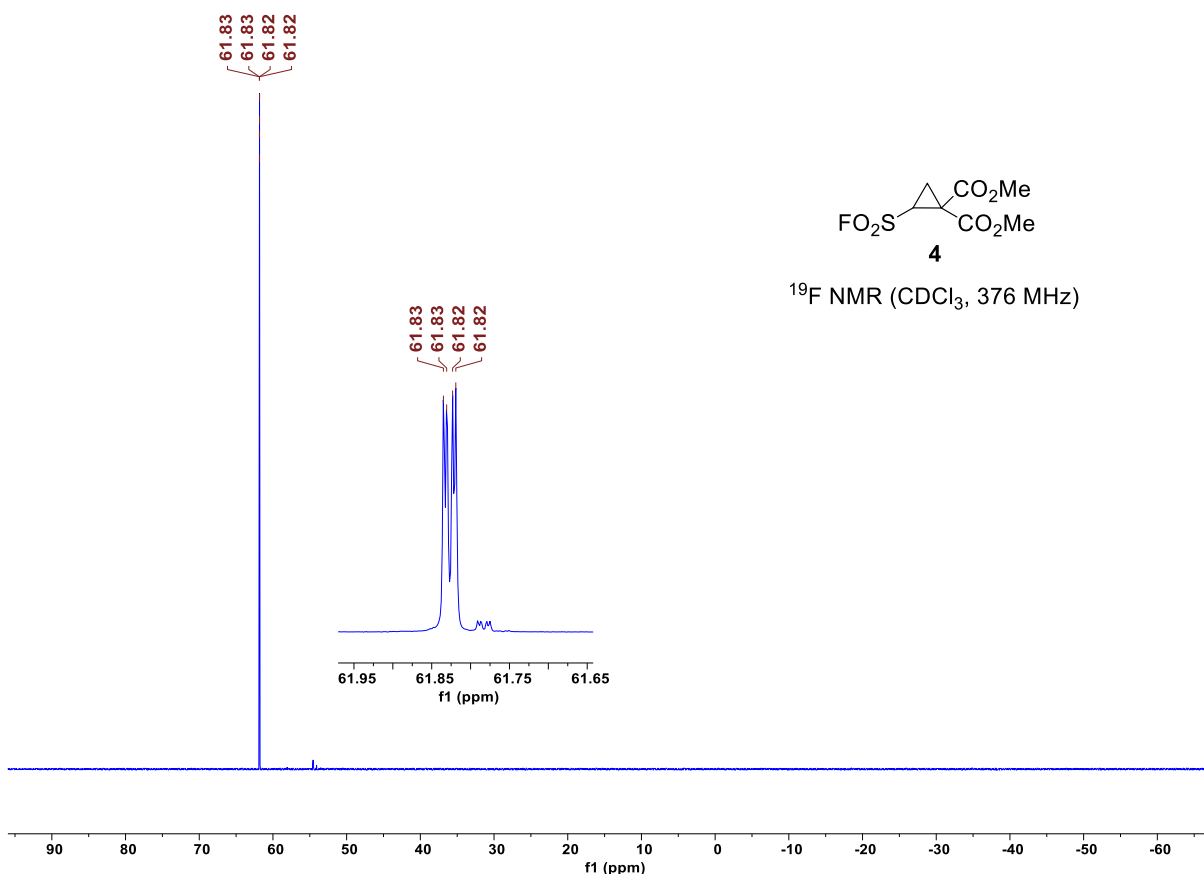
Figure S1. ^{19}F NMR spectra (377 MHz) show the conversion of the acyclic compound **6** to the cyclobutane **3** upon the addition of triethylamine to a mixture of the cyclopropane **4** and the alkydione malonate **6**.

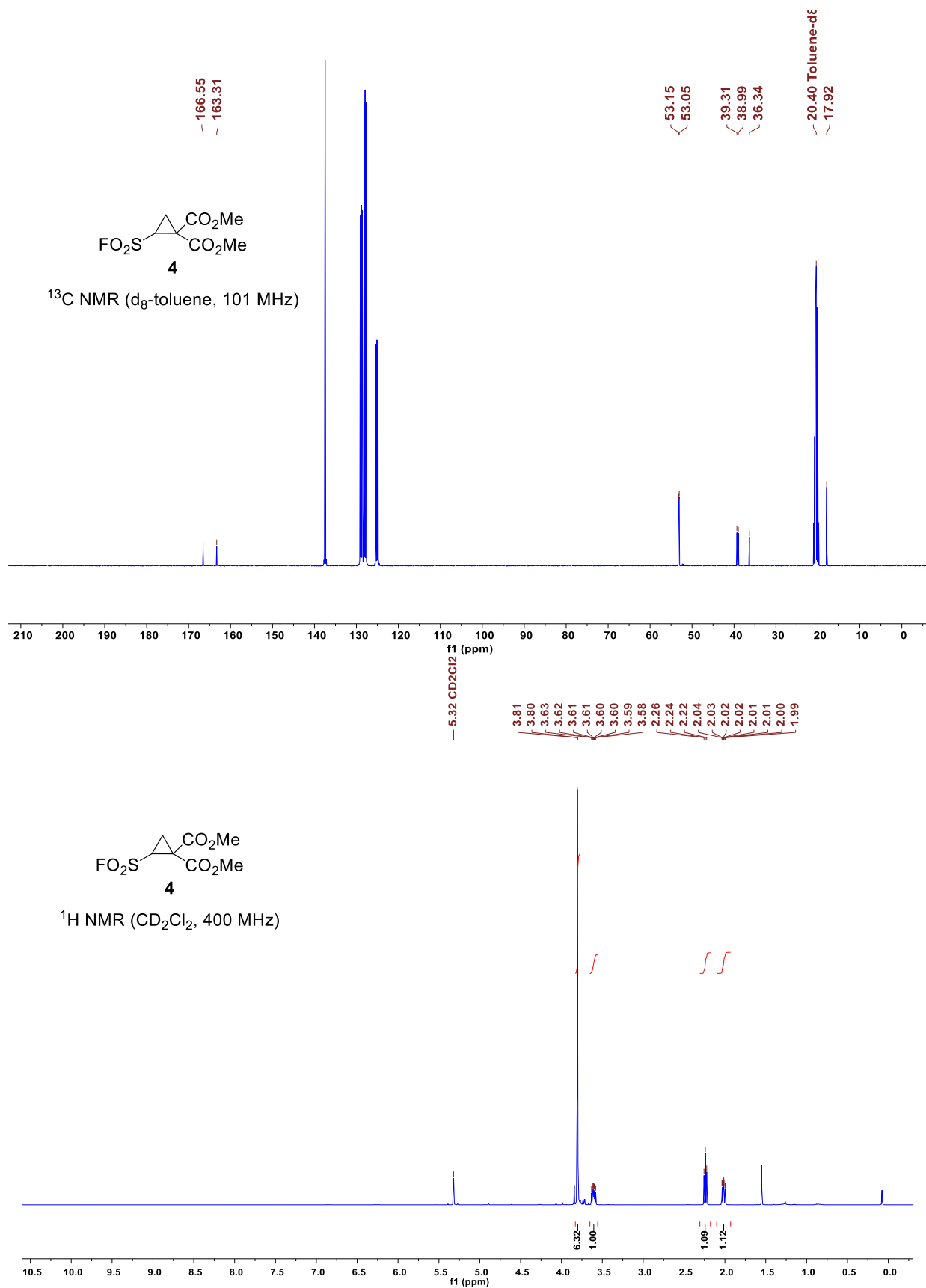
5.2.2 Copies of ^1H , ^{13}C and ^{19}F NMR Spectra

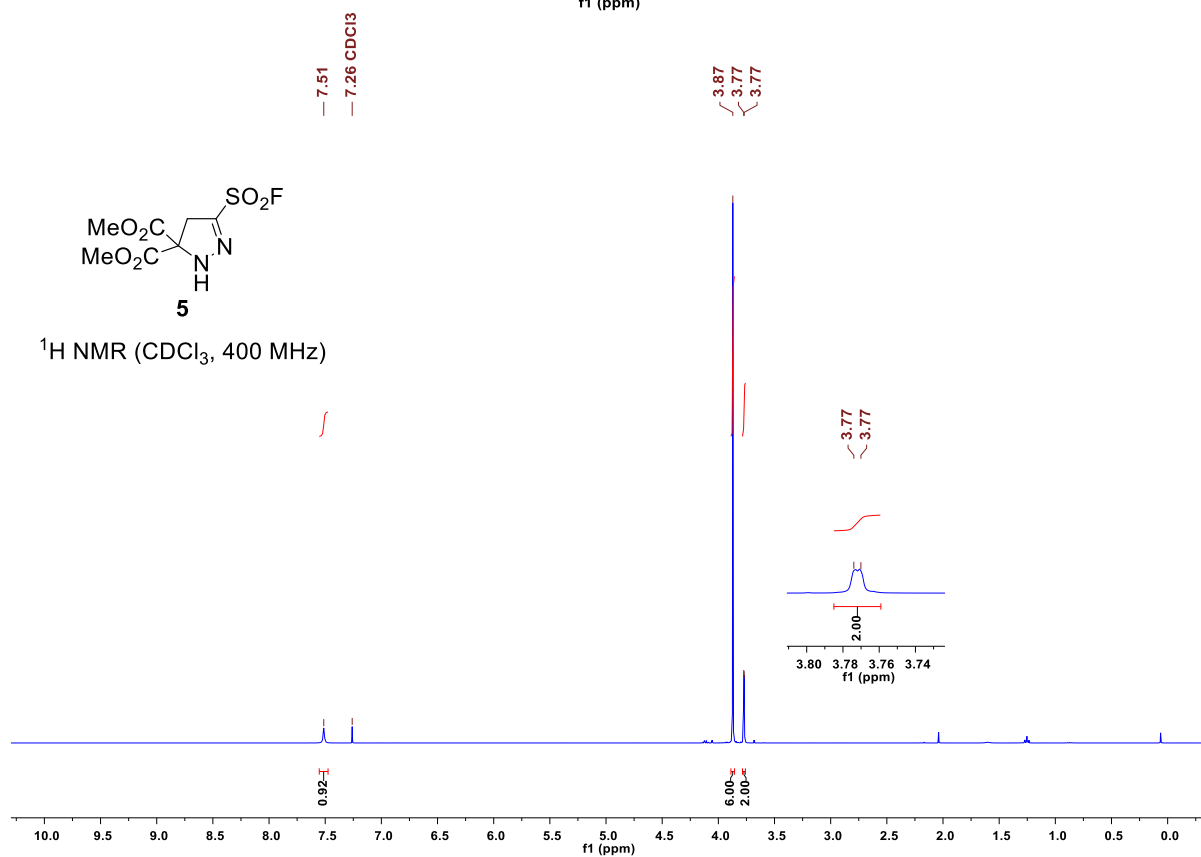
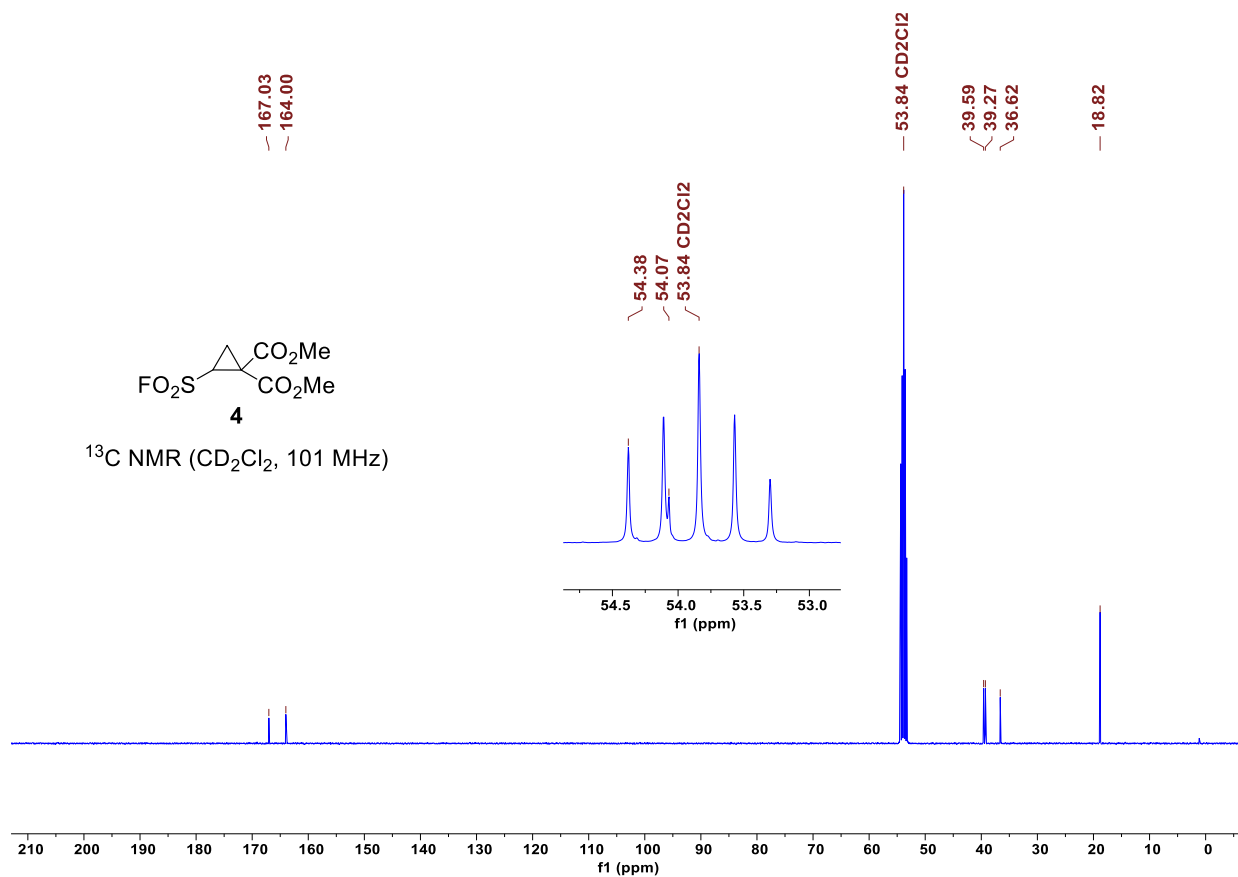
Chapter 5. Cyclobutane Formation by the Reaction of Ethenesulfonyl Fluoride with Dimethyl Diazomalonate

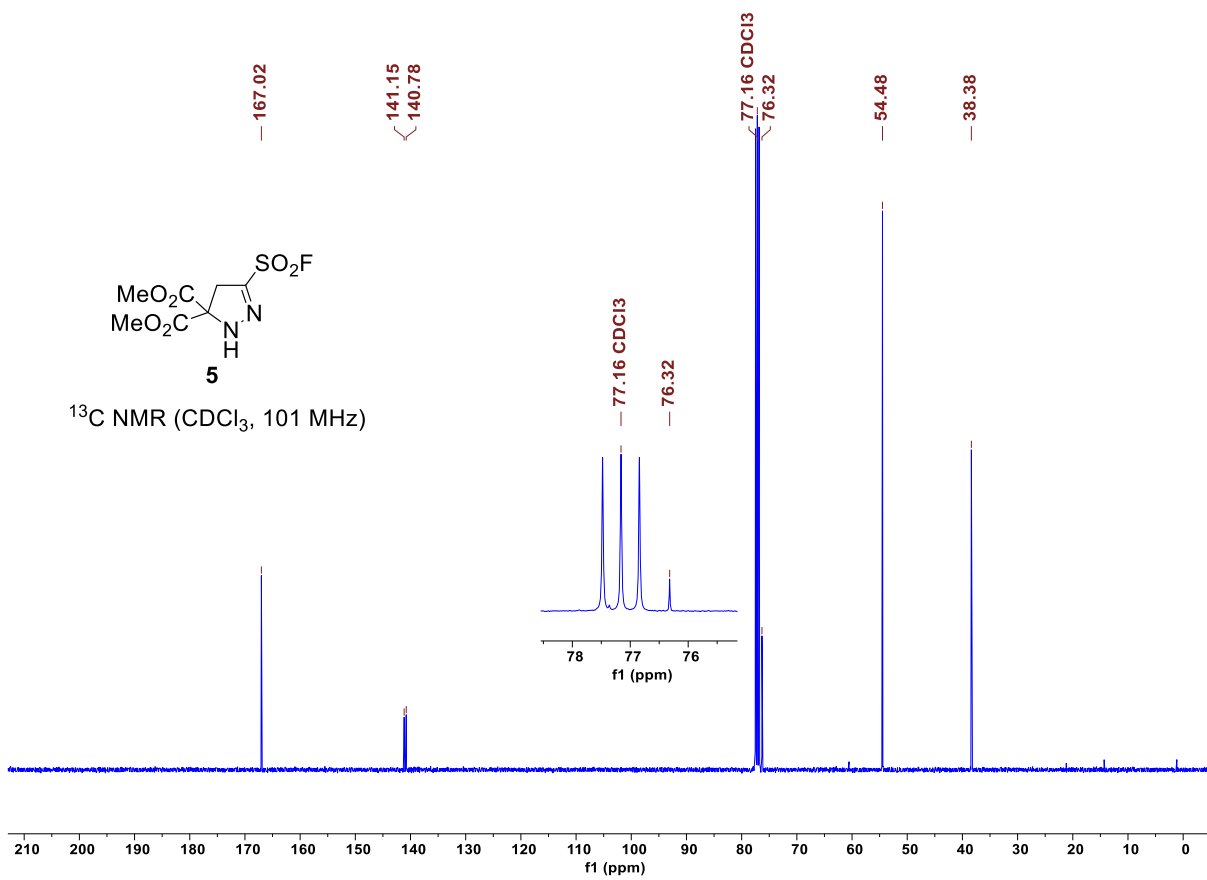




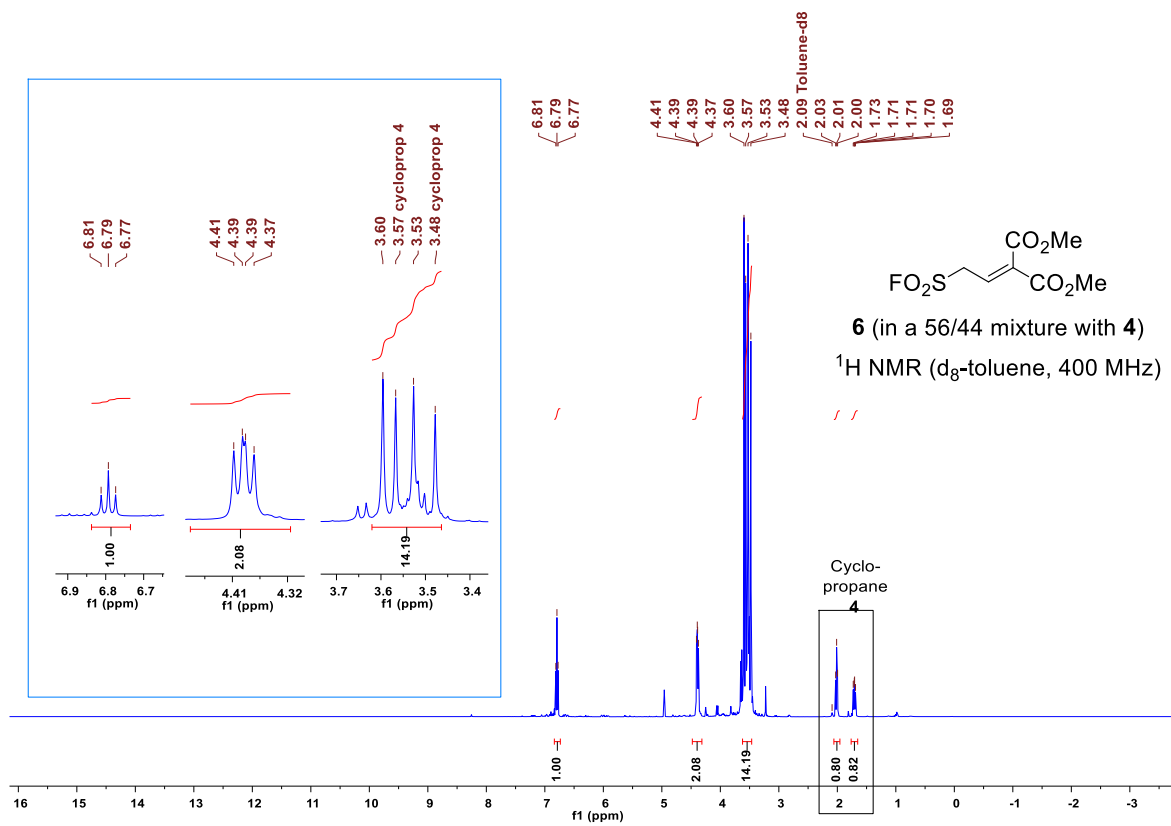
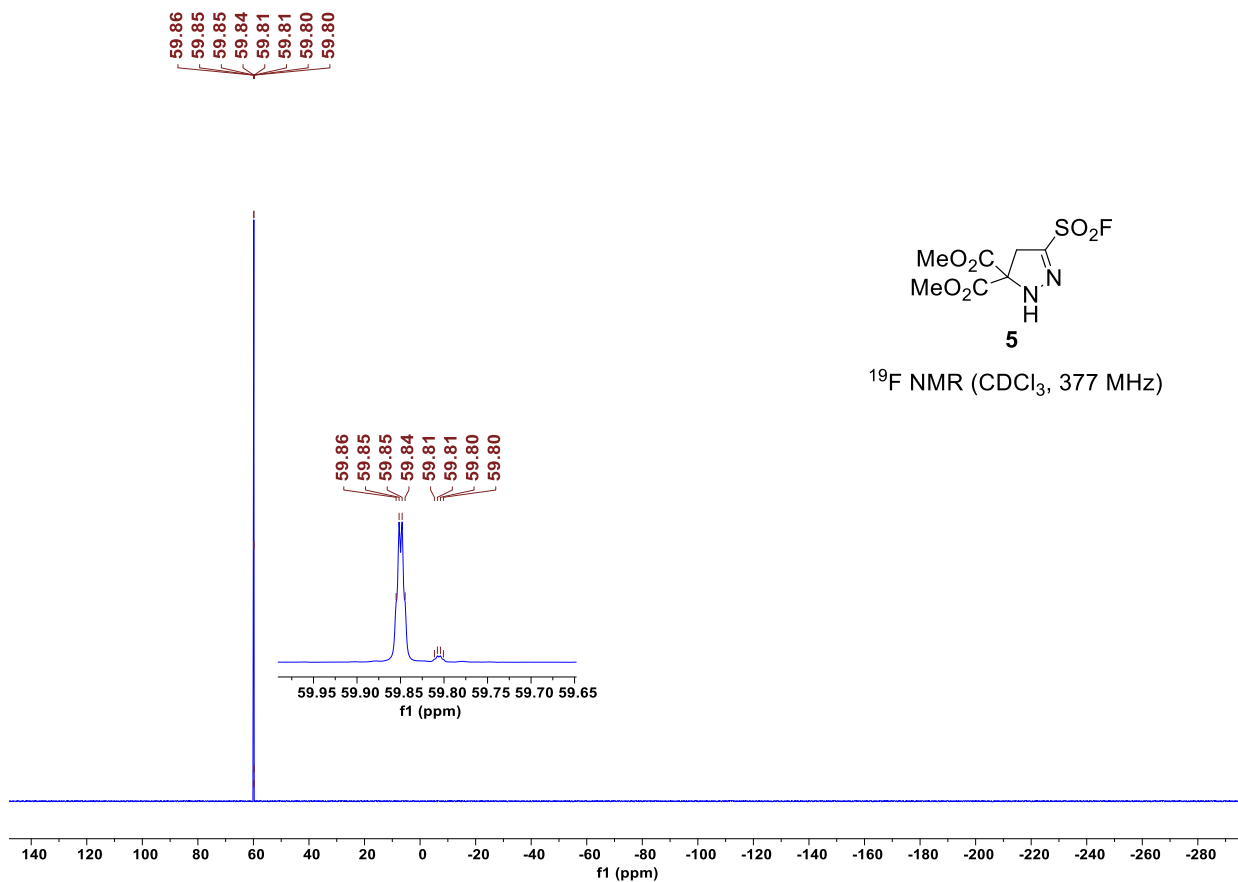


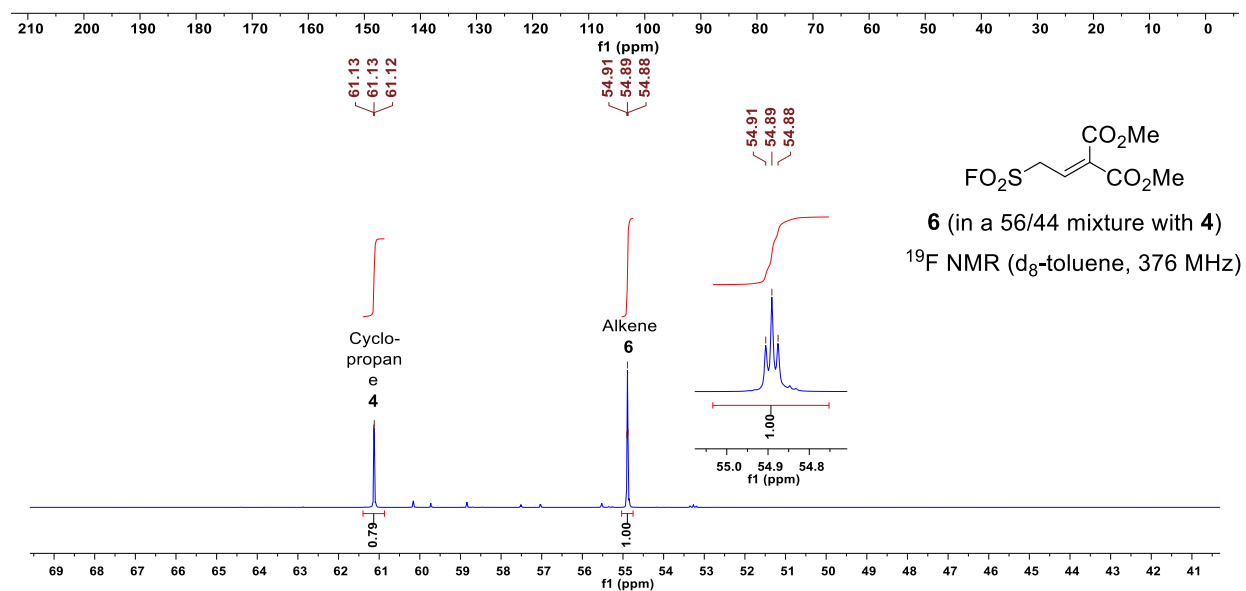
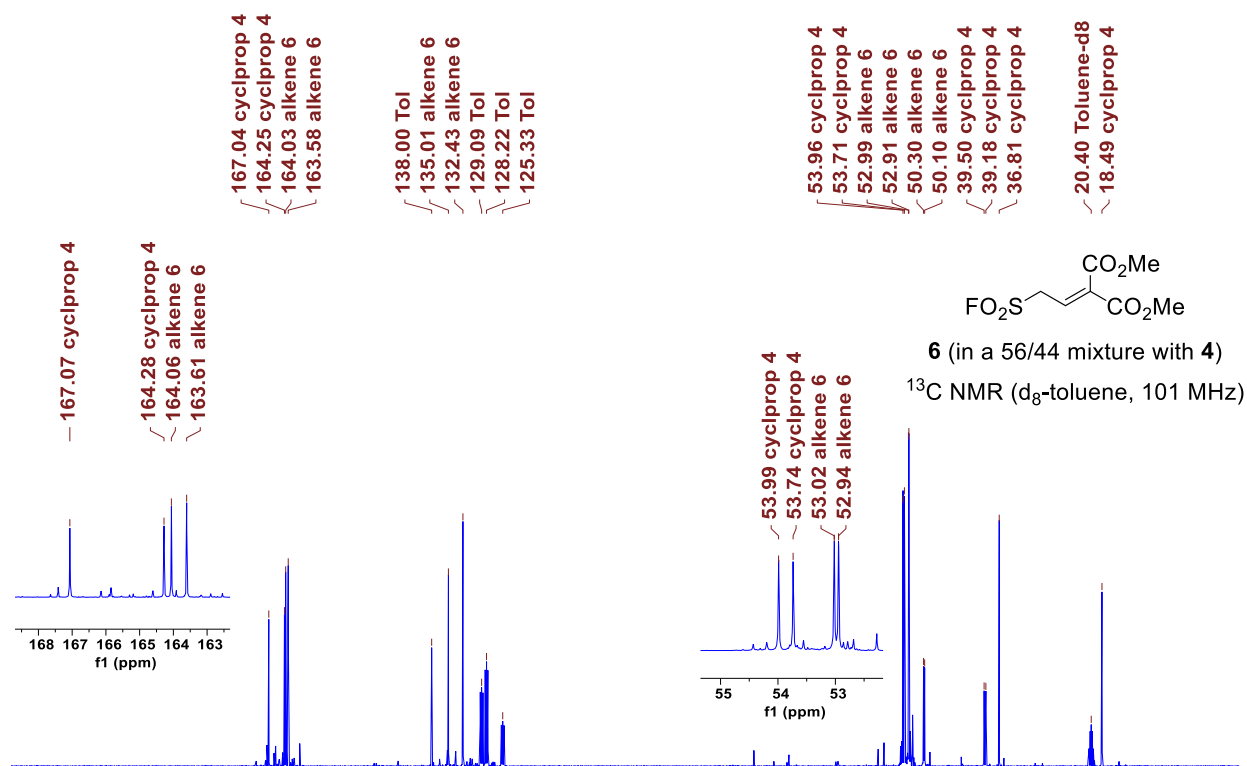






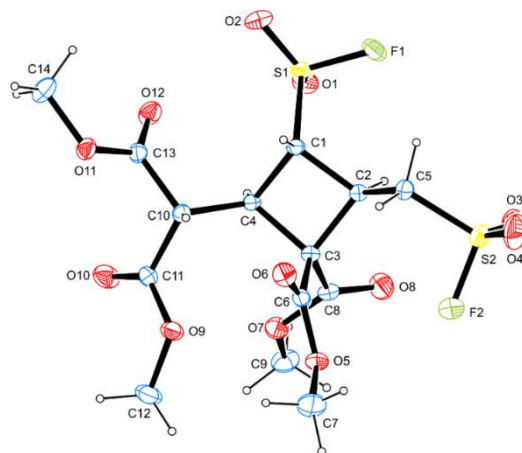
Chapter 5. Cyclobutane Formation by the Reaction of Ethenesulfonyl Fluoride with Dimethyl Diazomalonate





5.2.3 Single Crystal X-ray Crystallography

Dimethyl 2-(1,3-dimethoxy-1,3-dioxopropan-2-yl)-3-(fluorosulfonyl)-4-((fluorosulfonyl)methyl)cyclobutane-1,1-dicarboxylate (3)



(xv236/CCDC 2183363)

Crystallographic data.

net formula	$C_{14}H_{18}F_2O_{12}S_2$
$M_r/g\ mol^{-1}$	480.40
crystal size/mm	$0.090 \times 0.050 \times 0.040$
T/K	107.(2)
radiation	MoK α
diffractometer	'Bruker D8 Venture TXS'
crystal system	monoclinic
space group	'P 1 21/n 1'
$a/\text{\AA}$	13.4798(5)
$b/\text{\AA}$	8.5798(3)
$c/\text{\AA}$	16.9534(6)
$\alpha/^\circ$	90
$\beta/^\circ$	90.9820(10)
$\gamma/^\circ$	90
$V/\text{\AA}^3$	1960.44(12)
Z	4
calc. density/ $g\ cm^{-3}$	1.628
μ/mm^{-1}	0.353
absorption correction	Multi-Scan
transmission factor range	0.96–0.99
refls. measured	35309
R_{int}	0.0406
mean $\sigma(I)/I$	0.0269
θ range	3.070–28.698
observed refls.	4420
x, y (weighting scheme)	0.0352, 2.2146
hydrogen refinement	constr
refls in refinement	5072
parameters	275
restraints	0
$R(F_{obs})$	0.0374

$R_w(F^2)$	0.0967
S	1.047
shift/error _{max}	0.001
max electron density/e \AA^{-3}	1.101
min electron density/e \AA^{-3}	-0.776

Chapter 6. One-Bond-Nucleophilicity and -Electrophilicity Parameters: An Efficient Ordering System for 1,3-Dipolar Cycloadditions

Li, L.; Mayer, R. J.; Ofial, A. R.; Mayr, H. *J. Am. Chem. Soc.* **2023**, *under revision*.

Author Contributions

Li, L. performed all the experiments. Mayer, R. J. conducted the DFT calculations. The manuscript was drafted by Li, L. and jointly revised by Li, L., Mayer, R. J., Ofial, A. R. and Mayr, H.

6.1 One-Bond-Nucleophilicity and -Electrophilicity Parameters: An Efficient Ordering System for 1,3-DCAs

Le Li,⁺ Robert J. Mayer,[§] Armin R. Ofial,^{*,+} Herbert Mayr^{*,+}

⁺ Department Chemie, Ludwig-Maximilians-Universität München, Butenandtstr. 5-13, 81377 München (Germany)

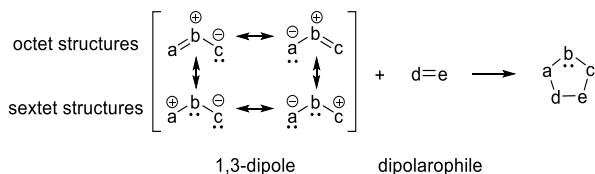
[§] Université de Strasbourg, CNRS, ISIS, 8 Allée Gaspard Monge, 67000 Strasbourg (France)

ABSTRACT: Diazoalkanes are ambiphilic 1,3-dipoles that undergo fast Huisgen cycloadditions with both electron-rich and electron-poor dipolarophiles but react slowly with alkenes of low polarity. Frontier molecular orbital (FMO) theory considering the 3-center-4-electron π -system of the propargyl fragment of diazoalkanes is commonly applied to rationalize these reactivity trends. However, we recently found that a change in mechanism from cycloadditions to azo couplings takes place due to the existence of a previously overlooked lower lying unoccupied molecular orbital. We now propose an alternative approach to analyze 1,3-dipolar cycloaddition reactions, which relies on the linear free energy relationship $\lg k_2(20\text{ }^\circ\text{C}) = s_N(N + E)$ (eq. 1) with two solvent-dependent parameters (N , s_N) to characterize nucleophiles and one parameter (E) for electrophiles. Rate constants for the cycloadditions of diazoalkanes with dipolarophiles were measured and compared with those calculated for the formation of zwitterions by equation (1). The difference between experimental and predicted Gibbs energies of activation is interpreted as the energy of concert, i.e., the stabilization of the transition states by the concerted formation of two new bonds. By linking the plot of $\lg k_2$ vs. N for nucleophilic dipolarophiles with that of $\lg k_2$ vs. E for electrophilic dipolarophiles, one obtains V-shaped plots which provide absolute rate constants for the stepwise reactions on the borderlines. These plots furthermore predict relative reactivities of dipolarophiles in concerted, highly asynchronous cycloadditions more precisely than the classical correlations of rate constants with FMO energies or ionization potentials. DFT calculations using the SMD solvent model confirm these interpretations.

Introduction

1,3-Dipolar cycloadditions (Huisgen reactions) represent the most general approach for the synthesis of five-membered heterocycles.^{1,2} According to Huisgen, “the 1,3-dipole is defined as a species that is represented by zwitterionic octet structures (top in Scheme 1) and undergoes 1,3-cycloadditions to a multiple-bond system, the dipolarophile. The formal charges are lost in the [3 + 2 \rightarrow 5] cycloaddition”.^{1c} Huisgen emphasized that the term 1,3-dipole does not imply a high dipole moment and that the resonance structures should not be associated with reactivity. A feature shared by all 1,3-dipoles is an allyl anion (or propargyl anion)-type π -system, that is, four electrons in three parallel atomic p-orbitals.

Scheme 1. General Scheme for 1,3-Dipolar Cycloadditions.^a



^a The 1,3-dipoles depicted here share an allyl type π -system; 1,3-dipoles of the propargyl-allyl type have an additional π -bond perpendicular to the allyl anion π -system and are usually linear.

Since Sustmann’s seminal discovery that a simple Hückel-MO-perturbational model can qualitatively explain substituent effects on the rates of 1,3-dipolar cycloadditions,³ frontier molecular orbital (FMO) theory has become the most popular method to describe and predict the course of these reactions,⁴ though alternative theoretical treatments have also been

reported.⁵ As illustrated in Figure 1, Sustmann identified three types of 1,3-dipolar cycloadditions which result from the energy differences between HOMOs and LUMOs of the reactants.

Cycloadditions of 1,3-dipoles of type I, which are controlled by the interaction of ψ_2 with ψ_B , are accelerated by electron-donating substituents in the 1,3-dipole and electron-accepting substituents in the dipolarophile, while the opposite substituent effects hold for cycloadditions of 1,3-dipoles of type III. If the energy differences $\psi_2 - \psi_B$ and $\psi_3 - \psi_A$ are similar (cycloadditions of type II) additional electron-donating and electron-accepting substituents in either of the reaction partners lead to an increase of the reaction rates.

Sustmann’s “Paradigmatic Parabola”,⁴ⁱ first reported for 1,3-dipolar cycloadditions of phenyl azide in 1972^{3b} and later applied to other cycloadditions, e.g., of diazoalkanes (Figure 2), have several limitations, however. Thus, Breugst, Huisgen, and Reissig investigated the reactions of diazoalkanes with methyl 3-(diethylamino)propionate and concluded, “It is evident that the oversimplifying FMO model does not work in this borderline case”.⁶ Liu, Houk, and coworkers recently stated that “The reactivity differences between dipoles are often controlled by the distortion energies of the 1,3-dipoles ..., rather than by FMO interactions or reaction thermodynamics”.⁴ⁱ

Though 1,3-dipolar cycloadditions of diazoalkanes have been the most prominent examples for demonstrating the use of FMO theory, it is exactly this class of reactions which should not be explained by Figure 1, because ψ_3 is not the LUMO of diazoalkanes. The previously neglected $\pi^*_{N=N}$, perpendicular to ψ_3 , is lower in energy and thus corresponds to the real LUMO of diazoalkanes. As a consequence, the HOMOs of enamines

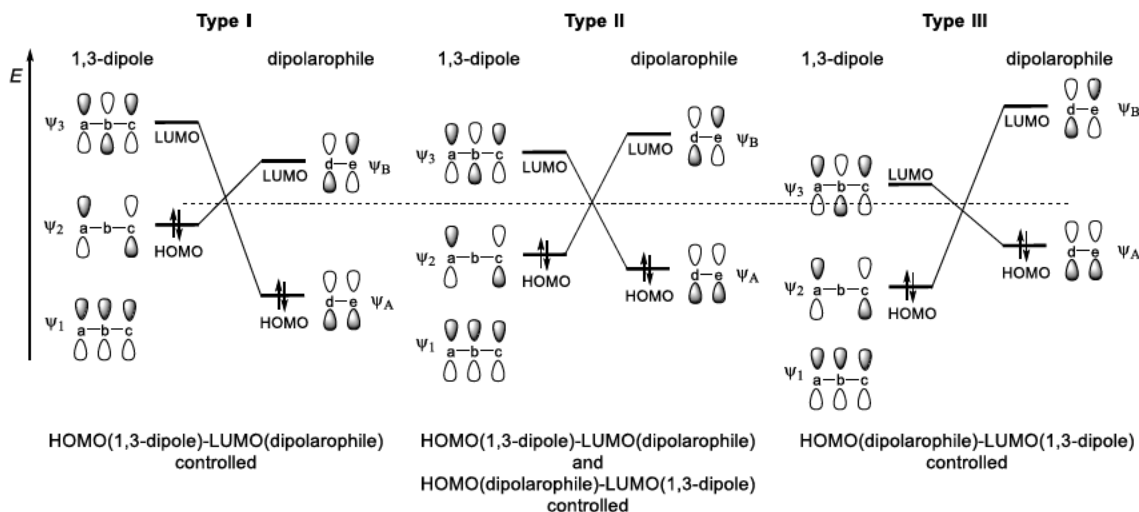


Figure 1. Sustmann's classification of three types of 1,3-dipolar cycloadditions.

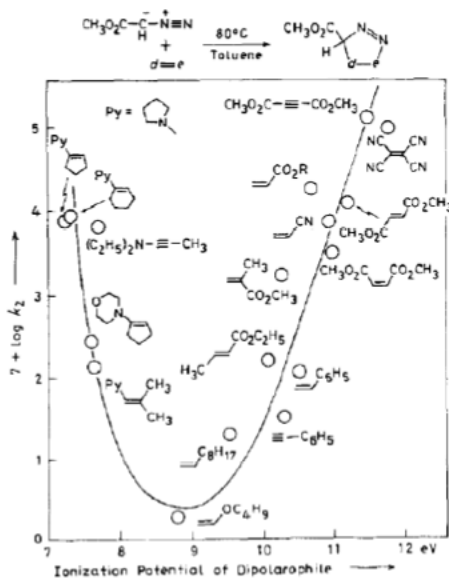


Figure 2. Relationship between the rate constants of the reactions of methyl diazoacetate with different dipolarophiles and the ionization potentials of the dipolarophiles (Reprinted from *Tetrahedron Lett.* 1979, 20, W. Bihlmaier, R. Huisgen, H. U. Reissig, S. Voss, Reactivity Sequences of Dipolarophiles towards Diazoacetyl Compounds - MO Perturbation Treatment, 2621–2624 (ref. 11), Copyright 1979, with permission from Elsevier).

interact with $\pi^*_{\text{N}=\text{N}}$ and not with ψ_3 , which accounts for the fact that diazoalkanes undergo azo couplings with enamines and not concerted cycloadditions as stated previously.^{7a}

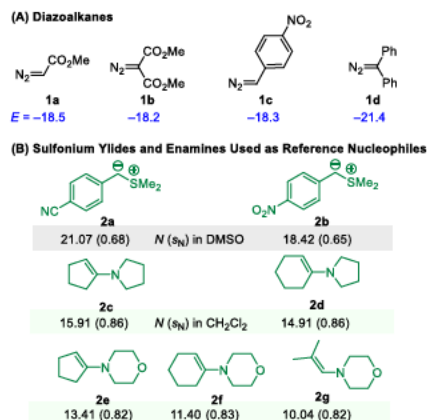
Correlations of rate constants against ionization potentials, as shown in Figure 2, which are claimed to be the result of FMO interactions, suffer from a further problem. According to FMO theory, the relative reactivities of

electron-rich dipolarophiles are controlled by their HOMO energies, and the relative reactivities of electron-deficient dipolarophiles are controlled by their LUMO energies. While HOMO energies are considered to equal the negative values of the experimentally accessible ionization potentials⁸ (Koopmans' theorem⁹), energies of the LUMOs cannot directly be measured. For that reason, it was assumed that substituents shift HOMOs and LUMOs in the same way, and ionization potentials are not only used as a measure for HOMO but also for LUMO energies. The inherent assumption of a constant HOMO-LUMO gap implies that chemical hardness η ¹⁰ is similar for all dipolarophiles. This assumption contrasts common experience and neglects the fact that conjugation generally raises HOMO and lowers LUMO.^{4f-h}

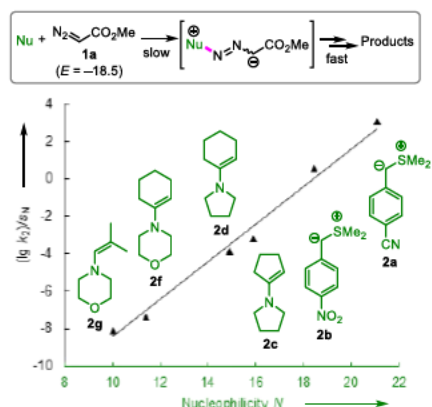
These discrepancies prompted us to search for an alternative organizing principle for these cycloadditions, which is based on the one-bond nucleophilicity parameters N and s_N and one-bond electrophilicity parameters E defined by equation (1). This correlation has been demonstrated to reproduce and predict rate constants for reactions of nucleophiles with electrophiles when one and only one new bond is formed in the rate-determining step and no σ -bond is broken.¹² More than 1250 solvent-dependent nucleophile-specific parameters, N and s_N , and 350 electrophilicity parameters, E , have so far been determined;^{12e} theoretical and statistical analyses of these parameters have also been reported.^{10b,13}

$$\lg k_{20^\circ\text{C}} = s_N(N + E) \quad (1)$$

Diazoalkanes are ambiphilic reagents, i.e., they may react with electrophiles as well as with nucleophiles. Several years ago, we had already determined the one-bond nucleophilicity parameters of a series of diazoalkanes,¹⁴ and very recently, we have derived the one-bond electrophilicity parameters E of diazo compounds **1a–1d** (Chart 1) from the rates of their reactions with sulfonium ylides **2a,b** and enamines **2c–2g** as illustrated in Figure 3.^{7b}

Chart 1. (A) Diazoalkanes with Their E Parameters (from ref. 7b) and (B) Sulfonium Ylides and Enamines with Their N (s_N) Parameters (from ref. 12e) Used in This Work

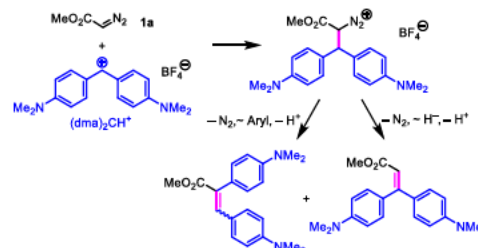
In the rate-determining step of the reactions of diazoalkanes **1** with **2a–2g** only one new bond is formed. Therefore, equation (1) is applicable, and the intercept of the correlations of $(\lg k_2)/s_N$ vs. N , illustrated for the reactions of methyl diazoacetate (**1a**) with **2a–2g** in Figure 3, yielded the electrophilicity parameters E listed in Chart 1.

**Figure 3.** Determination of the electrophilicity parameter E for **1a** (with data from ref 7b).

Results and Discussion

Determination of the One-Bond Nucleophilicity Parameters N and s_N for **1a and **1b**.** While N and s_N for **1c** and **1d** have been determined previously,¹⁴ the nucleophilicities of the diazoesters **1a** and **1b** in dichloromethane have now analogously been derived from the rates of their reactions with benzhydrylium ions. The general course of these reactions has been reported in ref. 14. We have now obtained analogous products by the reactions of methyl diazoacetate (**1a**) with bis(4-(dimethylamino)phenyl)methyl tetrafluoroborate

$(\text{dma})_2\text{CH}^+\text{BF}_4^-$. As illustrated in Scheme 2, the initial formation of a diazonium ion is followed by nitrogen loss, accompanied by hydride or aryl migration, and deprotonation.

Scheme 2. Products and Mechanism of the Reaction of Benzhydrylium Tetrafluoroborate $(\text{dma})_2\text{CH}^+\text{BF}_4^-$ with Methyl Diazoacetate (**1a**).

The rates of these reactions have been measured photometrically in dichloromethane by following the decays of the absorbances of the blue or red solutions of benzhydrylium ions (Ar_2CH^+) using the equipment described previously.¹⁴ All reactions were studied under pseudo-first order conditions using more than 10 equivalents of the diazoalkanes **1a** or **1b**. As described in the Supporting Information (Tables S1–S4 and S6–S8), the observed first-order rate constants k_{obs} (s^{-1}), derived from the exponential absorption decays, were plotted against the concentrations of the diazoalkanes **1** to give the second-order rate constants k_2 ($\text{M}^{-1} \text{s}^{-1}$) listed in the left part of Table 1. The right part of Table 1 lists previously reported rate constants for **1c** and **1d**, which will be used for constructing some diagrams below.

Figure 4 shows linear plots of the second-order rate constants k_2 vs. the electrophilicities E of the benzhydrylium ions (Ar_2CH^+) indicating the applicability of equation (1). Their slopes, which correspond to s_N , and their intercepts on the abscissa, which correspond to $-N$, are given in the bottom line of Table 1.

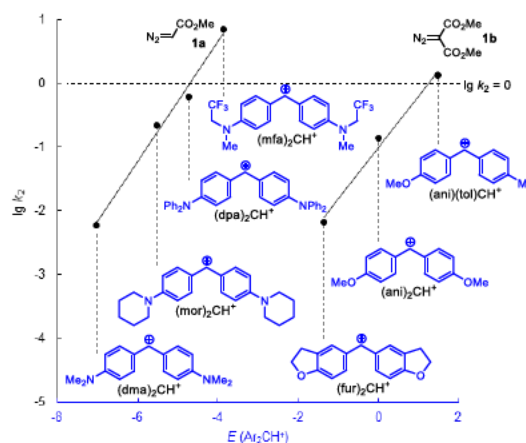
**Figure 4.** Plots of $\lg k_2$ for the reactions of **1a** and **1b** with benzhydrylium ions Ar_2CH^+ (in CH_2Cl_2 at 20 °C) versus the electrophilicity parameters E of Ar_2CH^+ (ref. 12a,e).

Table 1. Second-Order Rate Constants k_2 for the Reactions of the Diazoalkanes **1a–1d** with the Benzhydrylium Salts Ar_2CH^+ (counterions: BF_4^- or TfO^-) in CH_2Cl_2 and Resulting Nucleophilicity Parameters N (and s_N).

Ar_2CH^+ ^a	E	$k_2(20\text{ }^\circ\text{C}) / \text{M}^{-1} \text{s}^{-1}$			
		$(\text{MeO}_2\text{C})\text{CH}=\text{N}_2$ (1a)	$(\text{MeO}_2\text{C})_2\text{C}=\text{N}_2$ (1b)	$(\text{O}_2\text{NC}_6\text{H}_4)\text{CH}=\text{N}_2$ (1c) ^b	$\text{Ph}_2\text{C}=\text{N}_2$ (1d) ^c
$(\text{ani})(\text{tol})\text{CH}^+$	1.48		1.33		
$(\text{ani})_2\text{CH}^+$	0		1.41×10^{-1}		
$(\text{fur})_2\text{CH}^+$	-1.36		6.67×10^{-3}		
$(\text{mfa})_2\text{CH}^+$	-3.85	6.94			2.30×10^1
$(\text{dpa})_2\text{CH}^+$	-4.72	6.22×10^{-1}		1.26×10^2	2.93
$(\text{mor})_2\text{CH}^+$	-5.53	2.19×10^{-1}		2.16×10^1	
$(\text{mpa})_2\text{CH}^+$	-5.89			9.49	2.88×10^{-1}
$(\text{dma})_2\text{CH}^+$	-7.02	5.92×10^{-3}		1.51	2.71×10^{-2}
N (s_N)		4.68 (0.94)	-1.24 (0.81)	7.17 (0.83)	5.29 (0.92)

^a See Figure 4 for meaning of the abbreviations, $(\text{mpa})_2\text{CH}^+$ = bis[(4-(methylphenylamino)phenyl)methyl]methylum. ^b Data from ref. 14b.

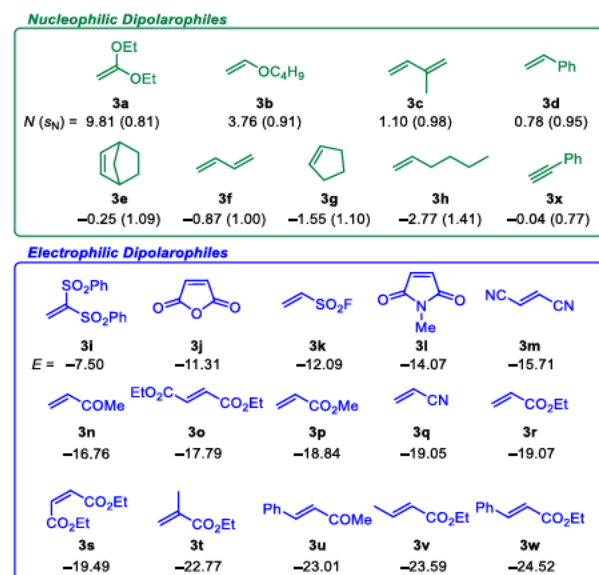
^c Data from ref. 14a.

As expected, the rate constants for the reactions of the methyl esters **1a** and **1b** with the benzhydrylium ions (Table 1) differ by less than a factor of 4 (1.2 to 3.9) from those of the ethyl esters previously reported.^{14a} We thus independently confirmed the previously reported five orders of magnitude lower nucleophilicities of diazomalonates compared to diazoacetates,^{14a} despite the almost identical electrophilicities E of **1a** and **1b** (Chart 1).

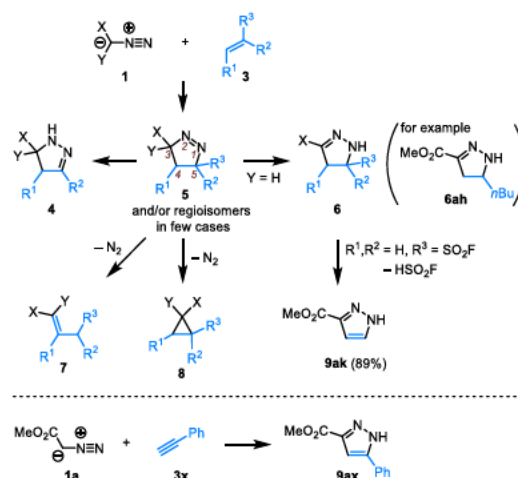
Products from Diazoalkanes and Dipolarophiles.

Reactions of diazoalkanes with dipolarophiles are among the best investigated 1,3-dipolar cycloadditions.^{1,15} In line with earlier investigations, all products obtained by the reactions of **1a–1d** with the dipolarophiles **3** (Chart 2) can be rationalized by initial Huisgen reaction to give the Δ^1 -pyrazolines **5**, which generally tautomerize with formation of the Δ^2 -pyrazolines **4** or **6** if there is an acidic proton at C-3 or C-5 position (Scheme 3).

Chart 2. Nucleophilic and Electrophilic Dipolarophiles Studied in This Work (Reactivity Parameters E or N and s_N from ref. 12e).



Scheme 3. Reactions of Diazoalkanes **1** with Dipolarophiles **3**^a



^a Products from individual reactions are identified by numbers followed by two letters; that is, **6ah** means structure **6** formed from diazoalkane **1a** and dipolarophile **3h**.

As described in the Supporting Information, several intermediate Δ^1 -pyrazolines **5**, which had been postulated, but were not observed in previous investigations, have now been characterized by NMR-monitoring of the corresponding reactions. The isolation of methyl 5-butyl-4,5-dihydro-1H-pyrazole-3-carboxylate (**6ah**) from the reaction of methyl diazoacetate (**1a**) with hex-1-ene (**3h**) confirmed the counter-intuitive earlier reports that terminal alkenes react with the same regioselectivity with diazoalkanes as acceptor-substituted ethylenes to give cycloadducts **5**, where the diazoalkane substituents X and Y and the substituents R^2 and R^3 of the dipolarophile end up in 3- and 5-position, respectively. In the case of unsymmetrical 1,2-disubstituted ethylenes, the stronger electron acceptor adopts the 5-position of pyrazoline **5**.

In several cases we also observed the formation of cyclopropanes **8** or their acyclic isomers **7** by nitrogen loss from the initially formed Δ^1 -pyrazolines **5**, sometimes after

reversible formation of the tautomers **4** and **6**. The mechanisms of these dediazotations have previously been reported.¹⁶ The reaction of methyl diazoacetate (**1a**) with ethenesulfonyl fluoride (**3k**) gave pyrazole **9ak** as the only product which can be rationalized by initial formation of **6ak** (or **4ak**) followed by elimination of HSO₂F.¹⁷ A different behavior was observed for the reaction of **3k** with dimethyl diazomalonate (**1b**). Now, the initially formed pyrazoline **4bk** did not eliminate HSO₂F, but lost nitrogen with formation of **8bk** and **7bk**, the latter of which dimerized to give a cyclobutane as described previously.¹⁸

Phenylacetylene (**3x**) reacted with **1a** to give methyl 5-phenyl-1*H*-pyrazole-3-carboxylate (**9ax**) in analogy to earlier reports on reactions of diazoalkanes with alkynes.^{6,19}

We have now collected kinetic data for the reactions of **1a**–**1d** with dipolarophiles **3** of known one-bond nucleophilicity or electrophilicity parameters^{12e} in the literature and complemented them by the investigation of further combinations of **1a**–**1d** with dipolarophiles **3** (Chart 2) for examining the relationship between the rates of 1,3-dipolar cycloadditions and the one-bond nucleophilicity and electrophilicity parameters of dipolarophiles. In order to link the new data with the rate constants reported in the literature, we have selected solvents identical or similar to those previously used for the reactions of a particular diazoalkane.

Kinetic Investigations. The kinetics of the reactions of diazoalkanes **1a** and **1b** with dipolarophiles **3** and those of the reactions of **1c** with **3d** were investigated by time-resolved ¹H NMR spectroscopy, following the decrease of the resonances of the red-marked hydrogens (Figure 5 and Supporting Information) of **1** or **3** relative to an internal standard (1,1,2,2-tetrachloroethane, mesitylene, or dibromomethane) in CDCl₃, CD₂Cl₂, *d*₈-toluene or *d*₈-toluene/mesitylene (1:1) at various temperatures. Usually equimolar amounts of **1** and **3** were used, and the second-order rate constants *k*₂ were obtained as the slopes of plots of 1/[**1**]_{*t*} or 1/[**3**]_{*t*} vs. time *t* according to 1/[**1**]_{*t*} = *kt* + 1/[**1**]₀ or 1/[**3**]_{*t*} = *kt* + 1/[**3**]₀ (Figure 5A). The kinetics of the reaction of **1b** with **3r** was performed with 3 equivalents of **1b** and evaluated as described in the Supporting Information (p S3).²⁰ Plots of ln(*k*₂/*T*) vs. (1/*T*) (Figure 5B) provided the Eyring activation parameters Δ*H*[‡] and Δ*S*[‡], from which the second-order rate constants *k*₂(20 °C) were extrapolated (Table 2).

The highly negative activation entropies of these reactions imply that the *T*Δ*S*[‡] term makes a large contribution to Δ*G*[‡], and the resulting small value of Δ*H*[‡] accounts for the small temperature-dependence of the cycloadditions.

Rate constants for several reactions of **1a** and **1b** listed in Table 2 had previously been determined with different methods at different temperatures. In order to examine the consistency of the data reported in the literature and those in Table 2, we used the Eyring activation parameters in Table 2 to calculate rate constants *k*₂ for *T* = 80.3 or 110 °C, the temperatures used in the earlier studies.^{11,21a} Table

S30 (Supporting Information) shows that the deviations are generally less than a factor of 2.5. This observation encouraged us to apply the Eyring equation and an averaged value of Δ*S*[‡] for reactions of structurally related compounds to convert second-order rate constants *k*(*T*) reported in the literature to *k*₂(20 °C) listed in Table 3. In order to indicate the uncertainty introduced by this extrapolation, the corresponding rate constants in Table 3 are given without decimals and should be considered as fair estimates.

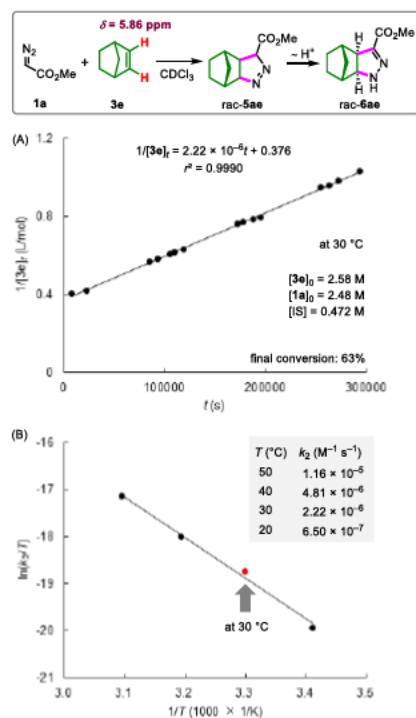


Figure 5. (A) Kinetics of the reaction of **1a** with **3e** monitored by the decrease of the vinylic hydrogens of **3e** vs. the internal standard (IS) 1,1,2,2-tetrachloroethane in CDCl₃ at 30 °C. (B) Eyring plot for the reactions of **1a** with **3e** at 20 to 50 °C.

The kinetics of the reaction of diazoalkane **1c** with styrene (**3d**) was determined by NMR spectroscopic monitoring as described above for the analogous reactions of **1a** and **1b** with dipolarophiles **3**; the second-order rate constant *k*₂(20 °C) is listed in Table 2.

Further reactions of **1c** with the Michael acceptors **3n**, **3o**, **3r** and **3t** were investigated photometrically by monitoring the decay of the UV-Vis absorbance of **1c** at 380 nm in dry dichloromethane at 20 °C (Figure 6A). In order to achieve first-order kinetics, more than 200 equivalents of the Michael acceptors were used, and the pseudo-first-order rate constants *k*_{obs} (s⁻¹) were determined by least-squares fitting of the exponential function *A*_{*t*} = *A*₀ exp(−*k*_{obs} *t*) + *C* as depicted in Figure 6B. The second-order rate constants *k*₂, which are listed in Table 3, were obtained from the linear correlations of *k*_{obs} with the concentrations of the dipolarophiles (Figure 6C).

Table 2. Second-Order Rate Constants $k_2(20\text{ }^\circ\text{C})$ and Eyring Activation Parameters (ΔH^\ddagger , ΔS^\ddagger) for the Reactions of Diazoalkanes 1a, 1b, and 1c with Dipolarophiles 3 Derived from Measurements at Variable Temperature.

Dipolarophiles (Solvents)	$k_2(20\text{ }^\circ\text{C}) / \text{M}^{-1} \text{s}^{-1}$	$T\text{-Range} / ^\circ\text{C}$	$\Delta H^\ddagger / \text{kJ mol}^{-1}$	$\Delta S^\ddagger / \text{J mol}^{-1} \text{K}^{-1}$
Reactions with 1a				
3e (CDCl ₃)	$(7.06 \pm 0.58) \times 10^{-7}$	+20 to +50	71.8 ± 4.2	-118 ± 14
3h (CDCl ₃)	$(5.96 \pm 0.56) \times 10^{-9}$	+30 to +50	71.8 ± 3.6	-157 ± 12
3k (<i>d</i> ₈ -toluene)	$(7.92 \pm 0.16) \times 10^{-4}$	+30 to +50	36.5 ± 0.8	-180 ± 2.4
3o (<i>d</i> ₈ -toluene)	$(2.78 \pm 0.18) \times 10^{-5}$	+20 to +50	55.7 ± 3.3	-142 ± 11
3s (<i>d</i> ₈ -toluene)	$(3.21 \pm 0.47) \times 10^{-6}$	+20 to +50	54.9 ± 7.6	-163 ± 25
3t (<i>d</i> ₈ -toluene)	$(2.85 \pm 0.31) \times 10^{-6}$	+30 to +60	51.3 ± 3.6	-176 ± 12
3v (<i>d</i> ₈ -toluene)	$(2.07 \pm 0.85) \times 10^{-7}$	+50 to +80	59.2 ± 7.6	-171 ± 23
3x (<i>d</i> ₈ -toluene)	$(2.48 \pm 0.57) \times 10^{-8}$	+50 to +80	69.2 ± 4.2	-154 ± 12
Reactions with 1b				
3e (CDCl ₃)	$(2.44 \pm 0.18) \times 10^{-8}$	+35 to +55	68.3 ± 2.4	-158 ± 7.4
3i (CDCl ₃)	$(1.94 \pm 0.24) \times 10^{-6}$	+20 to +50	61.1 ± 5.8	-146 ± 19
3k (T+M) ^a	$(6.21 \pm 0.91) \times 10^{-8}$	+50 to +90	68.8 ± 2.4	-148 ± 6.8
3o (T+M) ^a	$(2.25 \pm 0.34) \times 10^{-10}$	+65 to +105	$(114 \pm 2.1)^b$	$(-39.4 \pm 5.8)^b$
3r (T+M) ^a	$(1.21 \pm 0.01) \times 10^{-8}$	+20 to +50	$(88.4 \pm 0.5)^b$	$(-94.8 \pm 1.7)^b$
3s (T+M) ^a	$(2.76 \pm 0.33) \times 10^{-10}$	+75 to +105	76.0 ± 1.5	-169 ± 4.1
Reaction with 1c				
3d (CD ₂ Cl ₂)	$(1.65 \pm 0.26) \times 10^{-6}$	+6 to +30	53.8 ± 6.6	-172 ± 23

^a Solvent T+M = *d*₈-toluene/mesitylene (1/1). ^b We explain the unusual ΔS^\ddagger , which are less negative than other entries in this table, by small inaccuracies in $k_2(T)$ of these very slow reactions, which cause large errors when splitting up the Gibbs energy of activation into ΔH^\ddagger and ΔS^\ddagger .

Table 3. Second-Order Rate Constants $k_2(20\text{ }^\circ\text{C})$ for the Reactions of Diazo Compounds 1 with Dipolarophiles 3 in Different Solvents.

Dipolarophiles	<i>N</i> or <i>E</i>	$k_2(20\text{ }^\circ\text{C}) / \text{M}^{-1} \text{s}^{-1}$		
		(MeO ₂ C)CH=N ₂ (1a)	(MeO ₂ C) ₂ C=N ₂ (1b)	(O ₂ NC ₆ H ₄)CH=N ₂ (1c)
H ₂ C=C(OEt) ₂ (3a)	<i>N</i> = 9.81	$5 \times 10^{-8,a}$ (toluene)	$4 \times 10^{-10,b}$ (mesitylene)	
Butyl vinyl ether (3b)	<i>N</i> = 3.76	$6 \times 10^{-10,a}$ (toluene)	$4 \times 10^{-11,b}$ (mesitylene)	
Styrene (3d)	<i>N</i> = 0.78	$8 \times 10^{-8,a}$ (toluene)	$5 \times 10^{-10,b}$ (mesitylene)	$1.65 \times 10^{-6,c}$ (CD ₂ Cl ₂)
Phenylacetylene (3x)	<i>N</i> = -0.04	$2.48 \times 10^{-8,c}$ (toluene- <i>d</i> ₈)	$6 \times 10^{-10,b}$ (mesitylene)	
Norbornene (3e)	<i>N</i> = -0.25	$7.06 \times 10^{-7,c}$ (CDCl ₃)	$2.44 \times 10^{-8,c}$ (CDCl ₃)	
Hex-1-ene (3h)	<i>N</i> = -2.77	$5.96 \times 10^{-9,c}$ (CDCl ₃)	$4 \times 10^{-10,b}$ (mesitylene)	
H ₂ C=C(SO ₂ Ph) ₂ (3i)	<i>E</i> = -7.50		$1.94 \times 10^{-6,c}$ (CDCl ₃)	$2.16 \times 10^{1,d}$ (CH ₂ Cl ₂)
ESF (3k)	<i>E</i> = -12.09	$7.92 \times 10^{-4,c}$ (toluene- <i>d</i> ₈)	$6.21 \times 10^{-8,c}$ (T+M) ^e	$5.82 \times 10^{-2,d}$ (CH ₂ Cl ₂)
<i>N</i> -Methylmaleimide (3l)	<i>E</i> = -14.07			$1.74 \times 10^{-2,d}$ (CH ₂ Cl ₂)
Methyl vinyl ketone (3n)	<i>E</i> = -16.76			$7.35 \times 10^{-3,f}$ (CH ₂ Cl ₂)
Diethyl fumarate (3o)	<i>E</i> = -17.79	$2.78 \times 10^{-5,c}$ (toluene- <i>d</i> ₈)	$2.25 \times 10^{-10,c}$ (T+M) ^e	$1.07 \times 10^{-2,f}$ (CH ₂ Cl ₂)
Acrylonitrile (3q)	<i>E</i> = -19.05	$1 \times 10^{-5,a}$ (toluene)	$4 \times 10^{-9,b}$ (mesitylene)	
Ethyl acrylate (3r)	<i>E</i> = -19.07		$1.21 \times 10^{-8,c}$ (T+M) ^e	$1.37 \times 10^{-3,f}$ (CH ₂ Cl ₂)
Diethyl maleate (3s)	<i>E</i> = -19.49	$3.21 \times 10^{-6,c}$ (toluene- <i>d</i> ₈)	$2.76 \times 10^{-10,c}$ (T+M) ^e	
Ethyl methacrylate (3t)	<i>E</i> = -22.77	$2.85 \times 10^{-6,c}$ (toluene- <i>d</i> ₈)	$3 \times 10^{-9,b}$ (mesitylene)	$9.04 \times 10^{-5,f}$ (CH ₂ Cl ₂)
Ethyl crotonate (3v)	<i>E</i> = -23.59	$2.07 \times 10^{-7,c}$ (toluene- <i>d</i> ₈)	$2 \times 10^{-10,b}$ (mesitylene)	

^a Calculated from $k_2(80.3\text{ }^\circ\text{C})$ reported in refs. 11,21a by assuming $\Delta S^\ddagger = -150\text{ J mol}^{-1} \text{K}^{-1}$. ^b Calculated from $k_2(110\text{ }^\circ\text{C})$ reported in refs. 11, 21a by assuming $\Delta S^\ddagger = -150\text{ J mol}^{-1} \text{K}^{-1}$. ^c This work (see Table 2). ^d From ref. 14b. ^e Solvent T+M = *d*₈-toluene/mesitylene (1/1). ^f This work (Supporting Information).

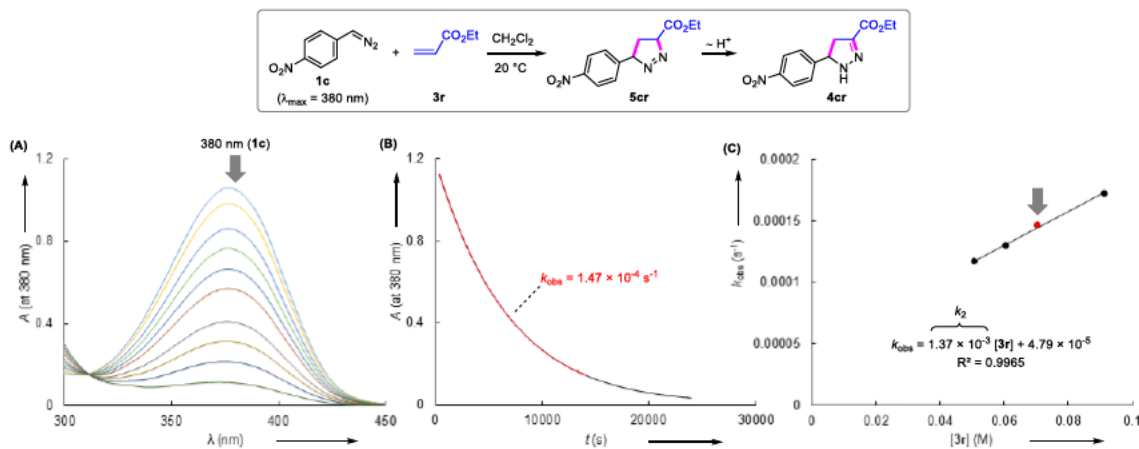


Figure 6. (A) UV-Vis spectroscopic monitoring of the reaction of **1c** (8.03×10^{-5} M) with **3r** (7.04×10^{-2} M) at 380 nm in CH_2Cl_2 at 20 °C. (B) Monoexponential decay of the absorbance A (at 380 nm) vs. time for the reaction of **1c** (8.03×10^{-5} M) with **3r** (7.04×10^{-2} M) in CH_2Cl_2 at 20 °C. (C) Correlation of k_{obs} with the concentration of **3r** used to determine the second-order rate constant $k_2(20^\circ\text{C}) = 1.37 \times 10^{-3} \text{ M}^{-1} \text{ s}^{-1}$ at 20 °C.

The second-order rate constant $k_2(20^\circ\text{C}) = 2.89 \times 10^{-6} \text{ M}^{-1} \text{ s}^{-1}$ for the reaction of diphenyldiazomethane (**1d**) with enamine **2d** (in CD_2Cl_2) has recently been determined and used to estimate the electrophilicity $E(\mathbf{1d}) = -21.4$.^{7b} Further rate constants for a series of reactions of **1d** with nucleophilic and electrophilic dipolarophiles **3** were determined by Huisgen and associates in DMF at 40 °C.²² Temperature dependent kinetics for the reactions of **1d** with norbornene (**3e**) and ethyl acrylate (**3r**) in ref. 22a gave activation entropies ΔS^\ddagger ($\text{J mol}^{-1} \text{ K}^{-1}$) = -138 ± 4 (for **3e**) and -141 ± 1 (for **3r**). The similarity of these values prompted us to use the approximated $\Delta S^\ddagger = -140 \text{ J mol}^{-1} \text{ K}^{-1}$ to convert further rate constants for the reactions of **1d** with dipolarophiles **3** measured at 40 °C to $k_2(20^\circ\text{C})$, as listed in Supporting Information (Table S43).

Correlations of the Measured Rate Constants with the One-Bond Reactivity Parameters N and E . Let us now examine the relationships between the rate constants $k_2(20^\circ\text{C})$ of the reactions of the diazoalkanes **1** with various substrates and the corresponding one-bond electrophilicity (E) and one-bond nucleophilicity parameters (N , s_N). The blue correlation line in Figure 7B corresponds to the linear plot of the rate constants ($\lg k_2$) for the reactions of diazomalonate **1b** with benzhydrylium ions (Ar_2CH^+) vs. E derived in Figure 4. The acceptor-substituted ethylenes **3** should also lie on this correlation line if they would react as one-bond electrophiles giving zwitterions with **1b**. Figure 7B shows, however, that the measured rate constants for the cycloadditions of all acceptor substituted ethylenes **3** (open blue circles) lie above the correlation line for one-bond electrophiles, indicating that the transition states of these reactions are more stable than those leading to zwitterions. We assign this deviation to the turn on of the concerted mechanism. One can see that the separation of the rate constants from the blue line increases with decreasing electrophilicities of the dipolarophiles because of decreasing zwitterionic character of the transition states

due to increasing synchronicity of the formation of the two new σ -bonds. Thus bis(phenylsulfonyl)ethylene **3i** ($E = -7.50$) reacts only 23 times faster with **1b** than expected for the formation of a zwitterion, while the less electrophilic diethyl fumarate (**3o**, $E = -17.79$) reacts 6×10^5 times faster with **1b** than predicted for the formation of a zwitterion.

Though stepwise mechanisms are excluded by the measured rate constants, the relative cycloaddition rates of the most electrophilic dipolarophiles of this series, i.e., **3i**, **3k**, and **3o**, follow the order of their one-bond electrophilicities E . For less electrophilic dipolarophiles **3** ($E < -18$), the zwitterionic character of the corresponding transition states is so low that their relative reactivities are no longer reflected by their one-bond electrophilicities E .

Figure 7A plots the rate constants of the reactions of dimethyl diazomalonate (**1b**) with sulfonium ylide **2a**, enamines **2c-f**, and dipolarophiles **3** against their one-bond nucleophilicity parameters N . The linear correlation of $\lg k_2$ for the reactions of **1b** with the sulfonium ylide **2a** and enamines **2c-2f** versus N results from the fact that only one new bond is generated in the rate-determining step^{7b} and the s_N parameters (according to eq. 1) of these nucleophiles are similar.^{23a} In addition to S -ylide **2a** and enamines, which define the green correlation line for the one-bond nucleophiles in Figure 7A, also ketene acetal **3a** is close to this correlation line, suggesting that also **3a** reacts via a stepwise mechanism,²⁴ in line with the DFT calculations discussed below.^{23b} The same is true for enol ether **3b**, whereas all other nucleophilic dipolarophiles (green open circles) are so far above the green correlation line that their cycloaddition rates are hardly affected by their nucleophilicities N . The large separation of hex-1-ene (**1h**) from the green correlation line for one-bond nucleophiles also explains why the polarization of 1-alkenes does not control the regioselectivities of their reactions with diazoalkanes (formation of 3,5- instead of 3,4-substituted Δ^1 -pyrazolines **5**).

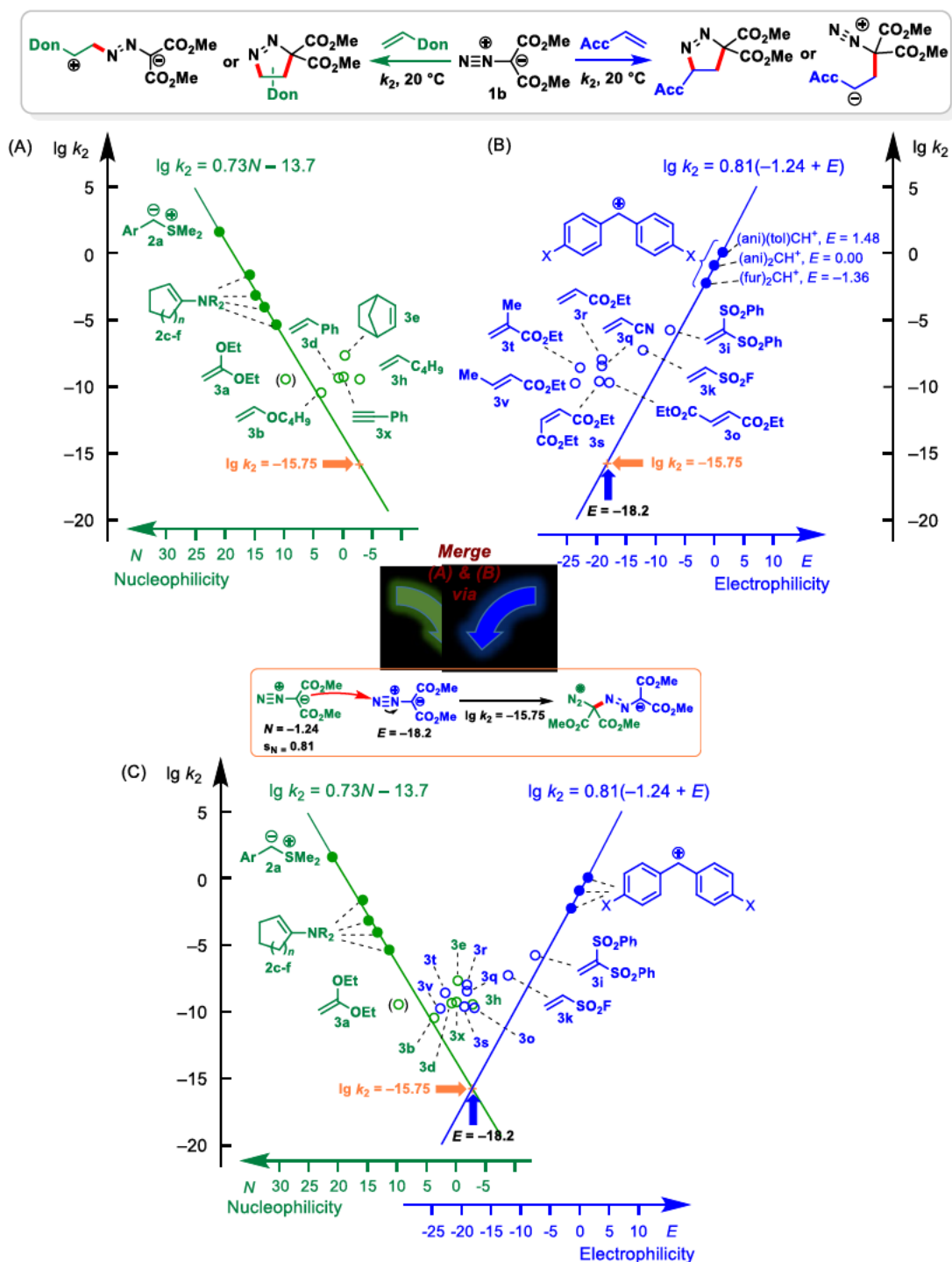


Figure 7. Correlation of $\lg k_2(20^\circ\text{C})$ for the reactions of diazomalonnate **1b** with (A) nucleophilic reaction partners versus their N parameters and (B) electrophilic reaction partners versus their E parameters. (C) Merger of Figures (A) and (B) at $\lg k = -15.75$. – Filled dots: One-bond electrophiles (blue) and one-bond nucleophiles (green) used for the construction of the correlation lines.

Since diazoalkanes are ambiphilic species, which may react as electrophiles and nucleophiles, one can consider a hypothetical dimerization of **1b**, where one molecule reacts as a one-bond nucleophile while the other one reacts as a one-bond electrophile. With the E , N , and s_N parameters for **1b** given in Chart 1 and Table 1, equation (1) gives a rate

constant of $\lg k = -15.75$ at 20°C , corresponding to a half reaction time of 180 million years for 1 M solutions, in line with the fact that this reaction has not been observed.²⁵

Substitution of this value for $\lg k_2$ into the equations above the correlation lines in Figures 7A and 7B shows that $\lg k_2 = -15.75$ is expected for the reactions of **1b** with

nucleophiles of $N = -2.81^{23c}$ as well as for its reactions with electrophiles of $E = -18.2$. The thus defined crossing point of the two correlation lines at $\lg k = -15.75$ allows one to merge Figures 7A and 7B to give Figure 7C, which resembles Sustmann's parabola (cf. Figure 2), but provides additional information as discussed below.

A similar situation is observed for the reactions of methyl diazoacetate (**1a**). Due to the almost identical electrophilicities of diazoalkanes **1b** and **1a**, the left parts of Figures 8A and 7C are nearly identical. The fact that the rate constant for the reaction of **1a** with ketene acetal **3a** is on the green correlation line in Figure 8A suggests the occurrence of a stepwise mechanism,²⁴ again in line with the DFT calculations discussed below. The cycloaddition rate constants of the less nucleophilic dipolarophiles (green open circles) are so far above the green correlation line that their one-bond nucleophilicities N do not control their cycloaddition rates. As in the reactions of diazomalonate **1b** (Figure 7) the high degree of concertedness of the reaction with hex-1-ene (**3h**) explains that the observed regioselectivity (formation of 3,5-substituted pyrazoline) is not controlled by the polarization of the dipolarophile.

Due to the significantly higher nucleophilicity of **1a** ($N = 4.68$) compared to **1b** ($N = -1.24$), the blue part on the right of Figure 8A is higher than that in Figures 7B,C (note the different benzhydrylium ions used in Figures 7 and 8). Whereas in reactions with **1b** (Figures 7B,C) only the relative reactivities of the highly electrophilic dipolarophiles **3i**, **3k** and **3o** are reflected by their one-bond electrophilicities E , now the relative reactivities of all acceptor-substituted ethylenes are roughly correlated with their E parameters. As in Figure 7B, the differences between the observed cycloaddition rates and the predicted rates for the stepwise processes (expressed by the blue correlation line) increase with decreasing electrophilicity parameters E of the electron-deficient dipolarophiles indicating increasing concertedness of the cycloadditions.

The trend observed in the change from Figure 7C to Figure 8A (**1b** to **1a**), i.e., little change in the left part of the graph due to comparable electrophilicities of these two diazoalkanes and increase of the cycloaddition rates with acceptor-substituted ethylenes on the right is continued when moving to (4-nitrophenyl)diazomethane **1c** (Figure 8B), which has a similar electrophilicity as **1a** and **1b**, but a much higher nucleophilicity [$N(\mathbf{1c}) = 7.17$].

While the rates of the reactions with enamines **2** (azo couplings) remained almost unchanged, the rates of the reactions of **1c** with electron-deficient dipolarophiles are much larger than those of the corresponding reactions of **1a** and **1b** (cf. Figure 8B with Figures 7C and 8A). Due to the unchanged electrophilicity and higher nucleophilicity of **1c**, all acceptor substituted dipolarophiles (blue circles) now react faster than morpholinocyclohexene **2f**. The relative reactivities of electron-rich and electron-poor ethylenes are thus inverted compared to those in Figure 7C. While morpholinocyclohexene **2f** reacts faster with diazomalonate **1b** than all electron-deficient dipolarophiles **3** depicted in Figure 7C, **2f** reacts more slowly with

diazoalkane **1c** than all electron-deficient dipolarophiles **3** depicted in Figure 8B. The relative reactivities of the electrophilic dipolarophiles in Figure 8B are even more

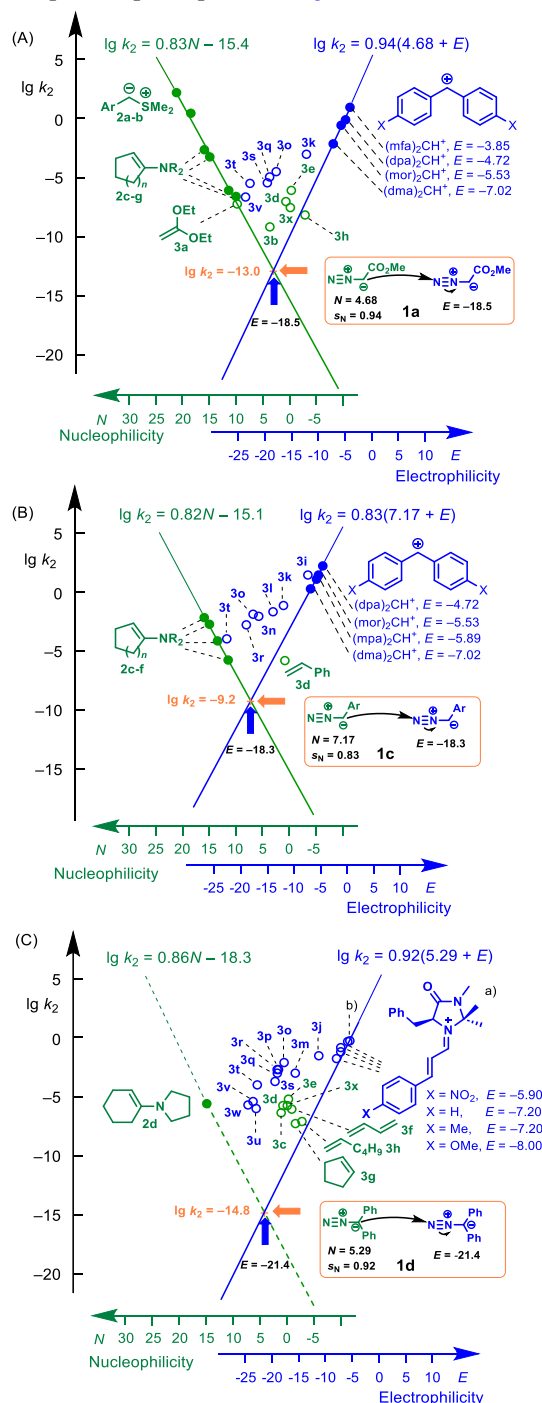


Figure 8. Correlations of $\lg k_2(20\text{ }^\circ\text{C})$ for the reactions of (A) methyl diazoacetate (**1a**), (B) 4-nitrophenyl-diazomethane (**1c**), and (C) diphenyldiazomethane (**1d**) with nucleophilic reaction partners versus their N parameters (green part, left) and electrophilic reaction partners versus their E parameters (blue part, right). – (a) Data from ref. 26. (b) Iminium ion derived from cinnamaldehyde and MacMillan type II organocatalyst ($E = -5.5$, from ref. 26).

closely correlated with their one-bond electrophilicities E than those in Figures 7B,C and 8A. The deviation of the rate constants from the blue correlation line indicates, however, that none of the cycloadditions of electron-deficient dipolarophiles in Figure 8B follows a stepwise mechanism.

Because of the lack of rate constants for the reactions of diphenyldiazomethane **1d** with a series of one-bond nucleophiles, the green line in Figure 8C does not represent a correlation line, but is based on a single rate constant for the reaction of **1d** with **2d** and the susceptibility $s_N = 0.86$ for **2d**.^{12e} The large difference between the rate constants for the reactions of **1d** with the nucleophilic dipolarophiles (green open circles) and the green line is in line with concerted mechanisms and rationalizes the lack of a correlation between the cycloaddition rate constants and the corresponding one-bond nucleophilicities N . As in the correlations in Figures 7, 8A, and 8B, the blue correlation line is based on the reactivities of the diazoalkane **1d** with benzhydrylium ions. These data points are not depicted in Figure 8C because of overlap with the reactivities of iminium ions. All neutral electrophilic dipolarophiles **3** are significantly above the blue correlation line due to the concerted mechanism of these cycloadditions. Though one can recognize a rough correlation between the cycloaddition rates of the electron-deficient dipolarophiles **3** (blue open circles) and their E -parameters, there is a significant scatter, probably due to the higher steric demand of **1d**.

Let us now look at the reactions of diazoacetate **1a** with the Michael acceptors **3** (blue entries in Figure 8A) in more detail. The blue line in Figure 9 shows Gibbs activation energies derived from rate constants $k_2(20\text{ }^\circ\text{C})$ calculated by eq. 1 for the hypothetical formation of zwitterions by attack of the nucleophilic carbon of **1a** ($N = 4.68$, $s_N = 0.94$, from Table 1) at the β -position of the acceptor-substituted ethylenes **3** (E from Chart 2). Since the electrophilicity parameters used for the calculation of these rate constants are identical to those defining the abscissa, all points are exactly on the correlation line. The remarkable fit of the experimental Gibbs energies of activation for the cycloadditions to the orange correlation line is astonishing, however, and shows that the transition states of the concerted cycloadditions reflect the relative energies of the transition states for the formation of the hypothetical zwitterions formed by a stepwise process. This observation is consistent with the results of the DFT calculations (see below) that the relative activation energies for the concerted cycloadditions of **1a** with Michael acceptors equal the relative activation energies for the corresponding stepwise cycloadditions via zwitterionic intermediates.

The point of intersection of the two lines indicates a change of mechanism, i.e. it is predicted that dipolarophiles with $E > -6$ will react with **1a** to give zwitterions which may cyclize or undergo other subsequent reactions. As one moves to the left in this diagram, the blue and the orange lines drift apart from each other, indicating that the zwitterionic character of the transition state gets smaller as

the electrophilicity of the dipolarophile decreases. The lower the electrophilicity of the dipolarophile, the greater the need for stabilizing the transition state by formation of the second bond, i.e., the higher the synchronicity of the formation of the two bonds. Accordingly, the greater concertedness of the reaction of **1a** with acrylonitrile (**3q**) compared to the analogous reaction with the more electrophilic ethylenesulfonyl fluoride (**3k**) is reflected by the corresponding transition state geometries (see DFT calculations below). While the C-C bond lengths are almost identical (2.08 and 2.07 Å), the C-N bond length is significantly shorter in the reaction with the less electrophilic **3q** (2.38 Å) than in the reaction with **3k** (2.43 Å).

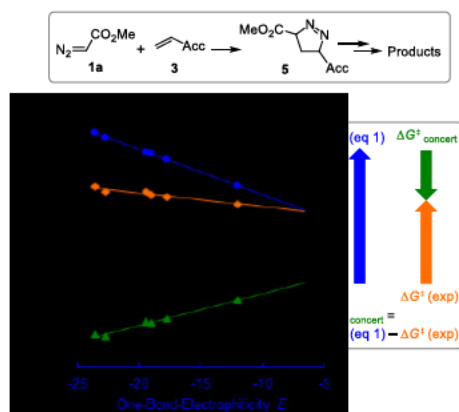


Figure 9. Correlation of Gibbs energies ΔG for the 1,3-dipolar cycloadditions of diazoacetate **1a** with Michael acceptors **3k**, **3o**, **3q**, **3s-t** and **3v** at 20 °C vs. their electrophilicities E . – $\Delta G^\ddagger(\text{eq 1})$: Gibbs activation energies calculated from rate constants predicted by eq. (1); $\Delta G^\ddagger(\text{exp})$: Gibbs activation energies measured experimentally; $\Delta G^\ddagger_{\text{concert}}$: energy of concert, i.e., stabilization of the concerted transition state relative to the transition state yielding a zwitterion.

The difference between the blue and the orange lines, thus, is a measure of the energy of concert which is shown by the green line on bottom of Figure 9. In other words: As illustrated in the right box of Figure 9, the Gibbs energy of activation of the concerted cycloaddition can formally be considered as the Gibbs energy for formation of the zwitterion minus the energy of concert.

As shown in Figure S5B (Supporting Information), a similar situation is found for the reactions of **1c** with Michael acceptors. The corresponding plot for **1b** (Figure S5A) is of poorer quality, however, because of its lower nucleophilicity which leads to a smaller zwitterionic character of the transition states of the reactions with electron-deficient dipolarophiles.

Comparison of Experimental and Quantum-Chemically Calculated Gibbs Energies of Activation. In two recent articles we have reported DFT calculations, which rationalized our experimental findings that diazoalkanes **1a–1d** generally undergo azo-couplings with enamines **2** and not concerted 1,3-dipolar cycloadditions,⁷ as previously assumed.^{11,21} We have now performed DFT

computations to obtain further information about the change of mechanism which we have derived from deviations of the measured rate constants $k_2(20\text{ }^\circ\text{C})$ from the correlation lines in Figures 7 and 8.

For that purpose, transition states for the reactions of **1a–1d** with seven representative dipolarophiles of widely differing polarity were located at the SMD(CHCl₃)/B3LYP-D3BJ/def2-SVP level of theory and combined with single point energies at the SMD(CHCl₃)/MN15/def2-TZVPD level of theory. This method is the same that we recently used for characterizing the mechanism and activation barriers of the reactions of **1** with enamines **2** allowing us to directly compare the computations for all systems.⁷ The treatment of the *cis/trans* isomers of **1a** is also described in ref.^{7a}

Scheme 4 illustrates four different types of transition state geometries for the reactions of diazoalkanes with terminal alkenes. Transition state **TS1** arises from electrophilic attack of the terminal nitrogen of **1** at the CH₂ group of the dipolarophile **3** to yield a zwitterion that is stabilized if R and/or R' are electron-donating substituents. On the other extreme, **TS4** corresponds to attack of the nucleophilic carbon center of diazoalkanes at the CH₂ group of the dipolarophile leading to a zwitterion which is stabilized if R and/or R' are electron-withdrawing substituents. **TS2** and **TS3** correspond to transition states of concerted processes, which yield regioisomeric Δ^1 -pyrazolines without involving an intermediate.

Scheme 4. Computationally Considered Transition State Geometries for the Reactions of Diazoalkanes **1** with Representative Dipolarophiles.

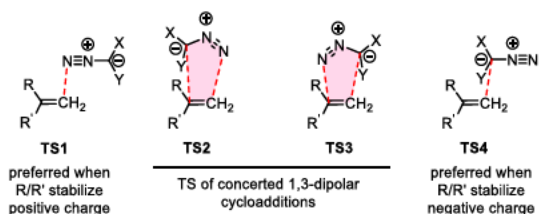


Table 4 summarizes the Gibbs energies of the four transition states **TS1** to **TS4** localized by DFT calculations. The most stable transition state calculated for each combination of **1a–1d** with a dipolarophile is highlighted in yellow and – if available – compared with the experimentally determined Gibbs energies of activation. At first glance, this comparison appears problematic because all DFT calculations have been performed with a solvation model for chloroform while the experimental data refer to kinetic measurements in a variety of solvents and were taken from different sources. This is not a serious problem, however, since Huisgen and associates have investigated the solvent dependence of the cycloadditions of diphenyldiazomethane (**1d**) with dimethyl fumarate^{22c} and of phenyldiazomethane with ethyl acrylate (**3r**) and norbornene (**3e**)²⁷ and reported that the rates of these reactions varied by less than a factor of 3 in a series of solvents with variable polarity ranging from benzene to

acetonitrile and DMF. Thus, solvent effects on the cycloaddition rates are much smaller than the expected accuracy of our computations, which allows us to neglect the nature of the solvents when comparing the Gibbs energies of activation in Table 4, which were obtained by different experimental methods.

TS1 and **TS4** refer to reactions where only one new bond is formed in the rate-determining step. For such reactions, the linear free energy relationship (eq. 1) is applicable, and the resulting values are listed as **TS1** (eq. 1) and **TS4** (eq. 1) in Table 4.

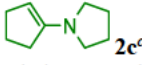
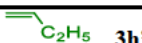
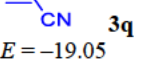
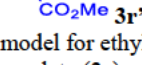
Table 4 shows that in all cases, the lowest value of **TS1–TS4** calculated by DFT, which is highlighted in yellow, is closest to the experimental Gibbs energies of activation. Though this observation confirms the consistency of experimental and computational results, the calculated DFT energies are generally higher (at most 27 kJ mol⁻¹, on average 17 kJ mol⁻¹) than the experimental values.

In the reactions of all diazoalkanes **1a–1d** with enamine **2c**, **TS1** is calculated to be significantly lower in energy than the transition state **TS2** for the analogous concerted reaction, in line with our previous report that diazoalkanes undergo azo couplings with enamines and not cycloadditions.⁷ Also in the reactions of ketene acetal **3a** with diazoalkanes **1a** or **1b** transition state **TS1** is more favorable than the alternative transition states **TS2** and **TS3** for concerted reactions. This finding is in agreement with the position of **3a** close to the correlation lines for one-bond forming processes in Figures 7 and 8.²⁴

In the reactions with the significantly less nucleophilic vinyl ether **3b'**, a model for butyl vinyl ether (**3b**), the stepwise process via **TS1** is not any longer clearly preferred, and DFT calculations for the reactions of **3b'** with **1a**, **1b**, and **1c** give similar energies for transition states **TS1**, **TS2**, and **TS3**. The calculated large values of the Gibbs energies of activation explain why attempts to isolate reaction products from alkyl vinyl ethers and **1a–1d** have failed in previous^{21a} and in our work.²⁴ The fact that the correlation equation (1) also gives a Gibbs activation energy close to those calculated for **TS1**, **TS2**, and **TS3** by DFT confirms that the reactions of diazoalkanes **1** with vinyl ether **3b'** cannot proceed with a high degree of concertedness.

For the reactions of the diazoalkanes **1a–1d** with but-1-ene (**3h'**), a model for hex-1-ene (**3h**), the concerted **TS3** is calculated to be slightly more favorable than the regioisomeric **TS2** but significantly more stable than **TS1** for the stepwise mechanism. The DFT calculations thus support our conclusions on the concerted mechanism of these reactions drawn from the position of hex-1-ene (**3h**) above the green correlation lines in Figures 7 and 8. They furthermore rationalize the observed regioselectivities of these reactions²⁸ yielding pyrazolines via **TS3** and not via **TS2** which would have been expected from the polarities of the terminal alkenes. As discussed below, relative stabilities of the products may already become noticeable in the transition states.

Table 4. Comparison of Experimental Gibbs Energies of Activation for the Reactions of Diazoalkanes 1a–1d with Seven Representative Dipolarophiles with Those Calculated for TS1–TS4 by DFT and Eq. (1) at 25 °C.^a

Dipolarophiles	(MeO ₂ C)CH=N ₂ (1a)	(MeO ₂ C) ₂ C=N ₂ (1b)	(O ₂ NC ₆ H ₄)CH=N ₂ (1c) ^b	Ph ₂ C=N ₂ (1d) ^c
	$N_{(SN)}=4.68(0.94)^b$ $E = -18.5$	$N_{(SN)} = -1.24(0.81)^b$ $E = -18.2$	$N_{(SN)}=7.17(0.83)^b$ $E = -18.3$	$N_{(SN)}=5.29(0.92)^b$ $E = -21.4$
 2c ^c $N_{(SN)} = 15.91(0.86)^b$	Exp (CDCl ₃) 88 TS1 (DFT) 93 TS1 (eq. 1) 84 TS2 (DFT) 135	Exp (CDCl ₃) 82 TS1 (DFT) 93 TS1 (eq. 1) 83 TS2 (DFT) 117	Exp(CD ₂ Cl ₂) 85 TS1 (DFT) 91 TS1 (eq. 1) 83 TS2 (DFT) – ^d	Exp n.d. TS1 (DFT) 109 TS1 (eq. 1) 100 TS2 (DFT) 151
 3a $N_{(SN)} = 9.81(0.81)^b$	Exp (tol) 113 TS1 (DFT) 123 TS1 (eq. 1) 112 TS2 (DFT) 161/175 TS3 (DFT) 171	Exp (mes) 125 TS1 (DFT) 130 TS1 (eq. 1) 110 TS2 (DFT) 144 TS3 (DFT) 182	Exp n.d. TS1 (DFT) 118 TS1 (eq. 1) 111 TS2 (DFT) 169 TS3 (DFT) 162	Exp n.d. TS1 (DFT) 147 TS1 (eq. 1) 125 TS2 (DFT) 175 TS3 (DFT) 157
 3b ^c model for butyl vinyl ether (3b) with $N_{(SN)} = 3.76(0.91)^b$	Exp (tol) (124) TS1 (DFT) 152 TS1 (eq. 1) 148 TS2 (DFT) 150 TS3 (DFT) 150	Exp (mes) (130) TS1 (DFT) – ^d TS1 (eq. 1) 146 TS2 (DFT) 154 TS3 (DFT) 162	Exp n.d. TS1 (DFT) 146 TS1 (eq. 1) 147 TS2 (DFT) 145 TS3 (DFT) 142	Exp n.d. TS1 (DFT) 171 TS1 (eq. 1) 162 TS2 (DFT) 148 TS3 (DFT) 144
 3h ^c model for 1-hexene (3h) with $N_{(SN)} = -2.77(1.41)^b$	Exp (CDCl ₃) 119 TS1 (DFT) 162 TS1 (eq. 1) 241 TS2 (DFT) 144 TS3 (DFT) 139	Exp (mes) 124 TS1 (DFT) – ^d TS1 (eq. 1) 238 TS2 (DFT) 153 TS3 (DFT) 151	Exp n.d. TS1 (DFT) 155 TS1 (eq. 1) 239 TS2 (DFT) 138 TS3 (DFT) 132	Exp (DMF) 112 TS1 (DFT) 176 TS1 (eq. 1) 264 TS2 (DFT) 143 TS3 (DFT) 135
 3k $E = -12.09$	Exp (ds-tol) 90 TS2 (DFT) 122 TS3 (DFT) 102 TS4 (DFT) – ^d TS4 (eq. 1) 111	Exp (T+M) 113 TS2 (DFT) 151 TS3 (DFT) 124 TS4 (DFT) – ^d TS4 (eq. 1) 133	Exp(CH ₂ Cl ₂) 79 TS2 (DFT) 106 TS3 (DFT) 91 TS4 (DFT) 111 TS4 (eq. 1) 95	Exp n.d. TS2 (DFT) 106 TS3 (DFT) 91 TS4 (DFT) 120 TS4 (eq. 1) 107
 3q $E = -19.05$	Exp (tol) 100 TS2 (DFT) 133 TS3 (DFT) 118 TS4 (DFT) 155 TS4 (eq. 1) 148	Exp (tol) 119 TS2 (DFT) 148 TS3 (DFT) 140 TS4 (DFT) 191 TS4 (eq. 1) 165	Exp n.d. TS2 (DFT) 119 TS3 (DFT) 109 TS4 (DFT) 141 TS4 (eq. 1) 128	Exp (DMF) 89 TS2 (DFT) 115 TS3 (DFT) 110 TS4 (DFT) 150 TS4 (eq. 1) 143
 3r ^c model for ethyl acrylate (3r) with $E = -19.07$	Exp n.d. TS2 (DFT) 130 TS3 (DFT) 113 TS4 (DFT) 153 TS4 (eq. 1) 148	Exp (T+M) 117 TS2 (DFT) 142 TS3 (DFT) 135 TS4 (DFT) 194 TS4 (eq. 1) 165	Exp(CH ₂ Cl ₂) 88 TS2 (DFT) 113 TS3 (DFT) 106 TS4 (DFT) 140 TS4 (eq. 1) 128	Exp (DMF) 87 TS2 (DFT) 111 TS3 (DFT) 109 TS4 (DFT) 149 TS4 (eq. 1) 144

^a All energies (in kJ mol⁻¹) are given relative to the reactants. The most favorable TS calculated by DFT for a certain combination of reactants is highlighted in yellow. TS1(eq. 1) and TS4(eq. 1) were calculated from the reactivity parameters E , N and s_N given for the reactants in this Table by applying eq. (1) and by subsequently converting $k_2(20^\circ\text{C})$ to $k_2(25^\circ\text{C})$ by using the Eyring equation and an assumed $\Delta S^\ddagger = -120 \text{ J mol}^{-1} \text{ K}^{-1}$. ^b In CH₂Cl₂. ^c Data from ref. 7. ^d TS could not be located.

Figures 7 and 8 have led to the conclusion that the reactions of **1** with all Michael acceptors **3i–3w** proceed through concerted pathways, because the measured rate constants are above the blue correlation lines that reflect stepwise processes via TS4. Accordingly, TS3 was calculated as the most stable transition state for the reactions of **1a–1d** with ethenesulfonyl fluoride (**3k**), acrylonitrile (**3q**), and acrylate **3r**^c. The regioselectivities of these reactions, i.e., the preference of TS3 over TS2, can be explained in the classical way by interaction of the greatest HOMO coefficients of the diazoalkanes **1** with the greatest LUMO coefficient of the Michael acceptors **3**.

Since the reactions of diazoalkanes **1a–1d** with Michael acceptors **3k**, **3q**, and **3r** proceed via concerted cycloadditions, information about the activation energies of the hypothetical stepwise processes via TS4 cannot be

derived from kinetic measurements. However, TS4 corresponds to an electrophile-nucleophile combination, where only one new bond is formed, i.e., a reaction for which equation (1) is applicable. Accordingly, Table 4 shows that the energies of TS4 obtained by equation (1) are similar to those derived by DFT calculations, and the small difference of 5 to 29 kJ mol⁻¹ between TS4(DFT) and TS4(eq. 1) is in line with the trend that the quantum chemically obtained Gibbs energies of activation are generally slightly larger than ΔG^\ddagger values derived from kinetic measurements.

Since TS4 energies corresponds to the blue correlation lines in Figures 7 and 8, the DFT calculations thus provide an independent confirmation of our conclusion that the deviations of the data points from the correlation lines in Figures 7 and 8 are a measure for the energy of concert.²⁹

FMO-Analysis. Figure 10 shows for the reactions of methyl diazoacetate (**1a**), a prototypical 1,3-dipole of the propargyl/allenyl type, how the classical FMO analysis of 1,3-dipolar cycloadditions (Figure 1) has to be modified in view of the previous discussion. Due to the presence of the low-energy $\pi^*_{N=N}$ orbital in diazoalkanes, perpendicular to the 3-center heteropropargyl anion system, not only ψ_3 has to be considered for this analysis but rather the two lowest-lying unoccupied molecular orbitals of the 1,3-dipole, that is, $\pi^*_{N=N}$ and ψ_3 .

As reported recently,⁷ the reactions of diazoalkanes **1** with enamines (**2c** in Figure 10) proceed via interaction of HOMO (enamine) with $\pi^*_{N=N}$ (**1a**) to give a zwitterion via **TS1**. Subsequent proton shifts yield azo coupling products, which in some cases undergo subsequent cyclization to give pyrazolines, formally cycloadducts of **1a** with enamines.

TS1, which leads to the formation of a zwitterion, is also the preferred pathway in the reaction of **1a** with ketene acetal **3a** and results from perpendicular orientation of the two reagents by interaction of HOMO(**3a**) with $\pi^*_{N=N}$ (\cong LUMO) of **1a**. **TS2**, arising from interaction of HOMO(**3a**) with ψ_3 , and a further transition state, arising from interaction of HOMO(**3a**) with both $\pi^*_{N=N}$ (**1a**) and ψ_3 , will

be discussed in more detail below.

For dipolarophiles **3b'** and **3h'**, models for the experimentally investigated higher homologs **3b** and **3h**, respectively, which are significantly less nucleophilic than **3a**, the stepwise pathway via **TS1** becomes less favorable relative to the concerted transition states **TS2** or **TS3**. In the reaction with vinyl ether **3b'**, interaction of HOMO(**3b'**) with LUMO(**1a**), which gives rise to **TS1**, may still compete with the interaction of HOMO(**3b'**) with LUMO+1(**1a**) which gives rise to **TS2** and **TS3**. Since experimental product studies have failed and the calculations provided three transition states which are close in energy, we cannot evaluate the preferred mechanism.

Interaction of HOMO(**3h'**) with LUMO(**1a**) leading to **TS1** is less important than the interaction of HOMO(**3h'**) with LUMO+1(**1a**) leading to **TS3**, which is slightly preferred over **TS2**, as discussed above.

In line with classical FMO analyses (Figure 1), the reactions of **1a** with **3q** and **3k** are predominantly controlled by the interaction of HOMO(**1a**) with LUMO(**3q**) and LUMO(**3k**), respectively, leading to **TS3**. However, there is also a participation of LUMO+1(**1a**) which accounts for the fact that **TS3** is favored over **TS4**.

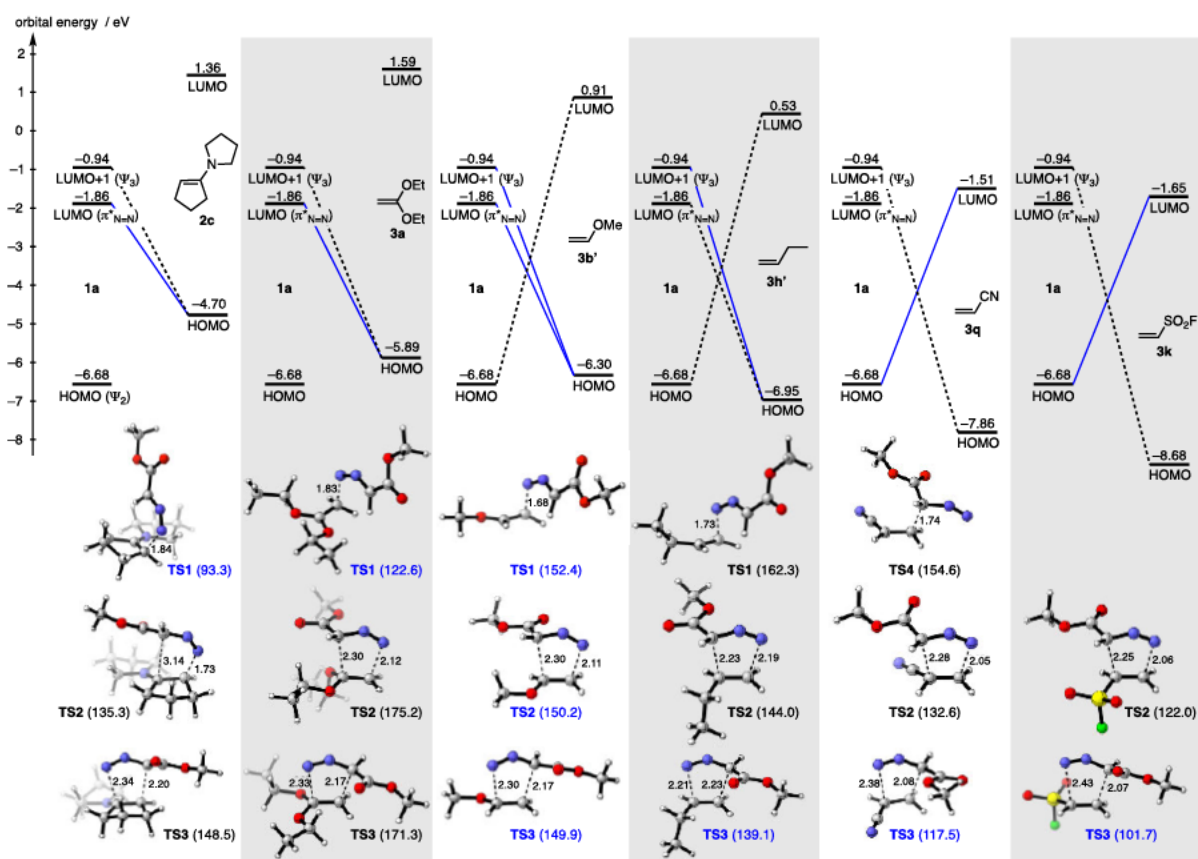


Figure 10. Orbital energies at the SMD(CHCl₃)/B3LYP-D3BJ/def2-SVP level and structures of the transition states **TS1** for azo couplings and of **TS2/3** for the concerted cycloadditions. IRC calculations for **TS1** in the reactions of **1a** with **3b'** and **3h'** indicated that these transition states do not yield zwitterions but rather aziridines.

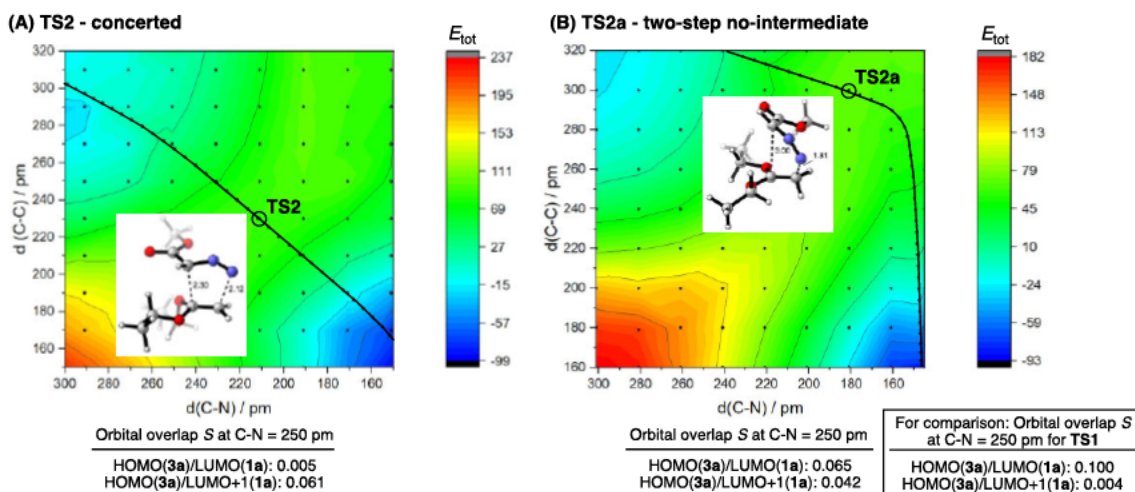


Figure 11. 3D potential energy surfaces at the (SMD=CHCl₃)/B3LYP-D3BJ/def2-SVP level for the reaction of methyl diazoacetate (**1a**^{trans}) with ketene acetal **3a** and key orbital overlaps S at a C-N distance of 2.5 Å on the intrinsic reaction coordinate for (A) the concerted transition variant via **TS2** and (B) the two-step no-intermediate pathway via **TS2a**. All energies E_{tot} (in kJ mol⁻¹) are given relative to the reactants. Black lines connect the reaction pathway derived from IRC calculations starting from the respective transition states. – See ref. 11a and Supporting Information for treatment of the *cis/trans* isomers of **1a**.

Since the reaction of diazoacetate **1a** with ketene acetal **3a** represents a borderline case where transition states for three different pathways could be localized, let us analyze this system in more detail. As illustrated in Figure 10, the most favorable transition state for this reaction (**TS1**), which leads to a zwitterion, results from interaction of HOMO(**3a**) with LUMO(**1a**), while the interaction with LUMO+1(**1a**) is insignificant (see box in Figure 11B).

When **1a** and **3a** were oriented in a way that concerted cycloadditions can result, two different types of concerted transition states were localized. In plane orientation of the heteropropargyl π -system of **1a** and the π -system of **3a** leads to **TS2** by interaction of HOMO(**3a**) with LUMO+1(**1a**) (Figure 11A). However, we located also an additional transition state **TS2a** where the reactants are twisted with respect to each other (Figure 11B). The concerted pathway *via* **TS2a**, which is approximately 14 kJ mol⁻¹ lower in energy than **TS2** (Figure 11), is highly asynchronous and can be considered as a two-stage no-intermediate mechanism (or two-step no-intermediate

mechanism) which results from interaction of HOMO(**3a**) with both LUMO(**1a**) and LUMO+1(**1a**). The potential energy surfaces in Figure 11 illustrate how interactions of the HOMO of ketene acetal **3a** with either LUMO+1 ($\cong \psi_3$) alone or with both LUMO ($\cong \pi^*_{\text{N=N}}$) plus LUMO+1 of **1a** lead to different trajectories.

Thermodynamics of the 1,3-Dipolar Cycloadditions. Recently, a comprehensive DFT study of the 1,3-dipolar cycloadditions of unsubstituted 1,3-dipoles of the allyl and the propargyl \leftrightarrow allenyl type with ethylene showed a fair correlation ($R^2 = 0.86$) between the activation energies and the corresponding exothermicities.^{5j} The slope of this correlation, which covers a range of approximately 200 kJ mol⁻¹ in activation energies and 400 kJ mol⁻¹ in reaction energies, indicated that roughly 44 % of the variation of the reaction energies are reflected by the activation energies. Let us now compare Gibbs energies of activation (Table 4) with Gibbs reaction energies for the cycloadditions described in Table 5.

Table 5. DFT-Calculated Gibbs Energies (kJ mol⁻¹) of the Reactions of **1a–1d** with Representative Dipolarophiles.^a

Dipolarophiles	(MeO ₂ C)CH=N ₂ (1a)	(MeO ₂ C) ₂ C=N ₂ (1b)	(O ₂ NC ₆ H ₄)CH=N ₂ (1c)	Ph ₂ C=N ₂ (1d)
H ₂ C=C(OEt) ₂ (3a)	$\Delta G^{02} = -34.1$ $\Delta G^{03} = -52.1$	$\Delta G^{02} = -4.1$ $\Delta G^{03} = -36.1$	$\Delta G^{02} = -40.3$ $\Delta G^{03} = -58.1$	$\Delta G^{02} = -16.3$ $\Delta G^{03} = -51.1$
H ₂ C=CH(OMe) (3b')	$\Delta G^{02} = -50.6$ $\Delta G^{03} = -61.8$	$\Delta G^{02} = -28.6$ $\Delta G^{03} = -40.8$	$\Delta G^{02} = -57.1$ $\Delta G^{03} = -63.4$	$\Delta G^{02} = -43.3$ $\Delta G^{03} = -59.2$
1-Butene (3h')	$\Delta G^{02} = -67.1$ $\Delta G^{03} = -73.9$	$\Delta G^{02} = -47.4$ $\Delta G^{03} = -55.2$	$\Delta G^{02} = -72.7$ $\Delta G^{03} = -82.7$	$\Delta G^{02} = -61.7$ $\Delta G^{03} = -72.2$
ESF (3k)	$\Delta G^{02} = -63.5$ $\Delta G^{03} = -53.7$	$\Delta G^{02} = -28.0$ $\Delta G^{03} = -28.0$	$\Delta G^{02} = -69.1$ $\Delta G^{03} = -58.7$	$\Delta G^{02} = -56.9$ $\Delta G^{03} = -53.8$
Acrylonitrile (3q)	$\Delta G^{02} = -54.7$ $\Delta G^{03} = -46.6$	$\Delta G^{02} = -29.6$ $\Delta G^{03} = -23.8$	$\Delta G^{02} = -62.6$ $\Delta G^{03} = -51.8$	$\Delta G^{02} = -57.4$ $\Delta G^{03} = -49.4$
Methyl acrylate (3r')	$\Delta G^{02} = -62.7$ $\Delta G^{03} = -56.6$	$\Delta G^{02} = -36.4$ $\Delta G^{03} = -36.7$	$\Delta G^{02} = -67.7$ $\Delta G^{03} = -61.3$	$\Delta G^{02} = -59.5$ $\Delta G^{03} = -56.1$

^a ΔG^0_2 and ΔG^0_3 refer to the reaction Gibbs energies (at 25 °C) for the formation of cycloadducts formed through **TS2** and **TS3**, respectively. When diastereomeric Δ^1 -pyrazolines are formed, ΔG^0 values correspond to the Boltzmann-weighted average of all conformers for both diastereomers.

Table 5 shows that the Δ^1 -pyrazolines from diazoalkanes **1a–1d** and but-1-ene (**3h'**) formed via **TS3** are 7–10 kJ mol⁻¹ more stable than the regioisomers formed via **TS2**. Thus, product-stabilizing factors in the transition state may account for the regioselectivities of the reactions with 1-alkenes which are opposite to those expected from the polarization of these dipolarophiles.²⁸ Figures S10 and S11 (Supporting Information) illustrate that for most cycloadditions treated in **Tables 4** and **5**, the Gibbs activation energies ΔG^\ddagger correlate poorly or not at all with the corresponding Gibbs reaction energies ΔG^0 . In fact, most kinetically controlled products formed in reactions of diazoalkanes **1a–1d** with the Michael acceptors **3k**, **3q**, **3r** via **TS3** are thermodynamically less stable than their regioisomers.

Figure 12 shows, however, that the calculated Gibbs activation energies **TS3(DFT)** for the reactions of the Michael acceptors **3k**, **3q**, and **3r'** with the diazoalkanes **1a–1d** correlate well with the corresponding reaction Gibbs energies ΔG^0_3 . We do not want to discuss the quality of these correlations, since we are almost dealing with two-point correlations due to the clustered location of diazoalkanes **1a**, **1c**, and **1d** in these plots. It is most remarkable, however, that the slopes in all three correlations of **Figure 12** are close to 1, which implies that Gibbs activation energies *and* Gibbs reaction energies for the reactions with diazomalonate **1b** are by approximately 20–30 kJ mol⁻¹ greater than those of all the other reactions. In other words, the low reaction rates of **1b** reflect fully the changes in the thermodynamic driving forces of the 1,3-dipolar cycloadditions of **1b** compared to those of the other diazoalkanes.

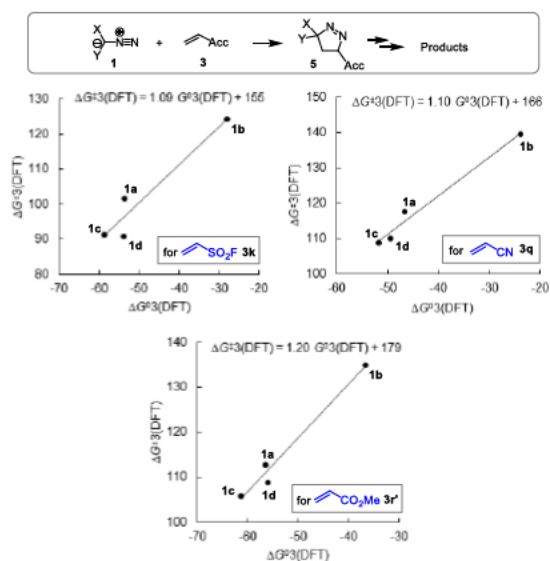


Figure 12. Correlation of Gibbs energies of activation $\Delta G^\ddagger_3(\text{DFT})$ vs. Gibbs reaction energies $\Delta G^0_3(\text{DFT})$ for the

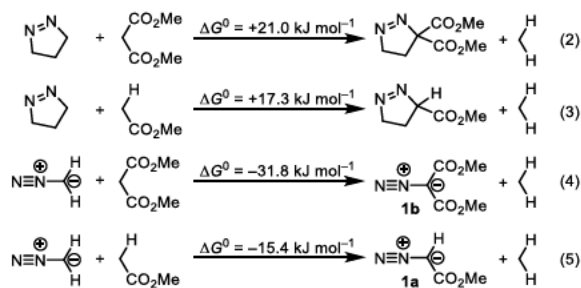
1,3-dipolar cycloadditions of the Michael acceptors **3k**, **3q**, and **3r'** with the diazoalkanes **1a–1d**. – DFT calculated energies from **Tables 4** and **5**.

What is the reason for the significantly lower exergonicities and higher activation energies for the cycloadditions of diazomalonate **1b** compared to those of the other diazoalkanes **1a**, **1c**, or **1d**? Is it due to different stabilization of the reactants or due to different stabilization of the products? In order to clarify the origin, let us compare the behavior of diazomalonate **1b** with that of diazoacetate **1a**, which can be considered as a representative for the other diazoalkanes **1c** and **1d** in **Figure 12**.

Scheme 5 shows that transfer of two ester groups from malonate to pyrazoline is endergonic (eq. 2), while the analogous transfer to diazomethane is exergonic (eq. 4). Though the absolute numbers of these two reactions are meaningless because they depend on the arbitrary choice of the ester-transfer reagent (here dimethyl malonate), the difference (52.8 kJ mol⁻¹) is independent of the nature of the ester-transfer reagent and shows the high stabilization of the diazoalkane **1b** through conjugation of the ester groups with the ylidic carbon center.

An analogous trend is found by comparison of eqs (3) and (5). While the transfer of one ester group to pyrazoline is endergonic (eq. 3), the corresponding ester transfer to diazomethane is exergonic (eq. 5). The small difference between equations (2) and (3) and the large difference between equations (4) and (5) implies that the much smaller exergonicities of the 1,3-dipolar cycloadditions of diazomalonate **1b** compared to diazoacetate **1a** are predominantly due to higher ground-state stabilization of **1b** by resonance energy (conjugation with two ester groups) and only to a minor degree due to destabilization of the cycloadducts formed from **1b**.

Scheme 5. Isodesmic Reactions for the Transfer of Ester Groups to Pyrazoline (eqs 2 and 3) and Diazomethane (eqs 4 and 5).^a



^a Energies of reactants and products (at the SMD(CHCl₃)/MN15/def2-TZVPD/def2-SVP//SMD(CHCl₃)-B3LYP-D3BJ level of theory) used for the calculation of the Gibbs energies in this Scheme are given in Table S48 (Supporting Information).

These conclusions are confirmed by the activation/strain or distortion/interaction analysis³⁰ in Figure 13, which compares the reactions of acrylonitrile **3q** with **1a** and **1b**.

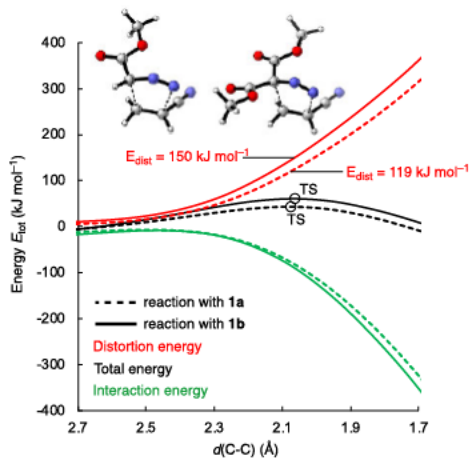


Figure 13. Distortion interaction analysis of the reaction pathway for TS3 of **3q** with **1b** and **1a** calculated at the SMD(CHCl₃)/B3LYP-D3BJ/def2-SVP level (electronic energies E_{tot} in kJ mol⁻¹). The energy values are projected on the newly forming C-C bond.

While the interaction energies of both reactions are almost identical at the transition state, the distortion energy is so much higher in the reaction with **1b** than in the reaction with **1a**, that the observed differences in activation energies for the reactions of **3q** with **1a** and **1b** are almost exclusively due to differences in the distortion energies. Since the same dipolarophile is used in both reactions, the greater loss of resonance energy in the distortion of **1b** compared to **1a** can be identified as the origin for the different reactivities of these two diazoalkanes.

Conclusions

As already mentioned in the introduction, the conventional rationalization of the reactions of diazoalkanes with dipolarophiles (Figures 1 and 2) has to be abandoned, because it was overlooked that $\pi^*_{\text{N}=\text{N}}$ and not ψ_3 corresponds to the LUMO of diazoalkanes and because ionization potentials are poor measures for relative LUMO energies. For that reason, we have developed an alternative ordering principle for cycloadditions which is based on one-bond nucleophilicity and electrophilicity parameters defined by equation (1).

In previous publications we have repeatedly emphasized that equation (1), which has become an established method to calculate rate constants for the reactions of electrophiles with nucleophiles from the electrophilicity parameters E and the solvent-dependent nucleophile-specific parameters N and s_N , cannot be applied to predict rate constants of multibond-forming reactions, e.g., concerted cycloadditions. This work demonstrates, however, that equation (1) is also a powerful tool for analyzing kinetics and mechanisms of 1,3-dipolar cycloadditions. By linking the correlation lines of $\lg k_2$ vs. E for the reactions of diazoalkanes with one-bond electrophiles and of $\lg k_2$ vs. N

for the corresponding reactions with one-bond nucleophiles (Figures 7 and 8) we arrived at graphics resembling “Sustmann’s paradigmatic parabola”. These correlations provide direct mechanistic information. Thus, rate constants on the green and blue correlation lines of Figure 14 indicate reactions with rate-determining formation of zwitterions or highly asynchronous concerted cycloadditions with transition states closely resembling zwitterions. From the deviations of cycloaddition rate constants from the correlation lines for one-bond reactivities one can derive the energies of concert, i.e., the stabilization of the transition states of the concerted cycloadditions relative to the alternative stepwise pathways via zwitterions.^{31,32}

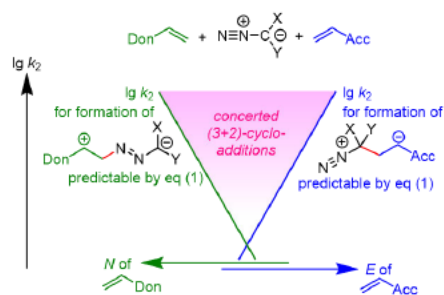


Figure 14. Schematic plots of rate constants ($\lg k_2$) of the reactions of diazoalkanes with one-bond nucleophiles (left) and one-bond electrophiles (right) vs. the corresponding reactivity indices N and E .

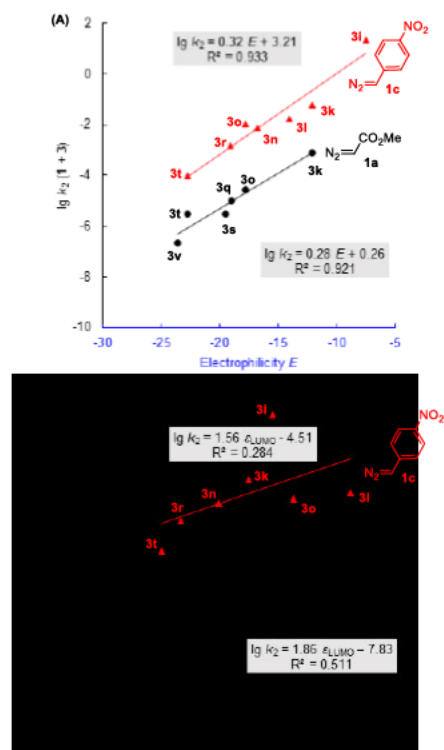


Figure 15. Correlation of $\lg k_2$ for the reactions of the diazo compounds **1a** (in black) and **1c** (in red) with electrophilic

dipolarophiles **3** with (A) the electrophilicities E and (B) gas-phase LUMO energies ϵ_{LUMO} of **3** (calculated at B3LYP/6-31G(d,p) level of theory, from ref. 33). Structures of dipolarophiles **3** are given in Chart 2.

Whereas absolute rate constants for concerted cycloadditions cannot be derived from these plots, Figure 15 shows that the rate constants of highly asynchronous concerted cycloadditions for a given diazo compound correlate much better with the one-bond electrophilicities E than with the corresponding frontier orbital energies suggesting that the one-bond reactivity indices are suitable parameters for predicting relative reactivities of dipolarophiles.²⁶

The analysis of the 1,3-dipolar cycloadditions of diazoalkanes on the basis of the one-bond electrophilicity and nucleophilicity parameters presented in this work should analogously be applicable to other 1,3-dipolar cycloadditions as well as to other types of cycloadditions, e.g., Diels-Alder reactions. We therefore expect that the widened applicability of the one-bond reactivity parameters E and N will trigger further activities to explore the prediction of these parameters by statistical and theoretical methods as recently reported.¹³

ASSOCIATED CONTENT

Supporting Information.

Procedures for the isolation of the products **4–9**, NMR spectra of characterized compounds, details of kinetic experiments, details of quantum-chemical calculations (PDF). Crystallographic data for **4as** (av173, CCDC 2233146) and **6ao** (av017, CCDC 2233145) (CIF).

This material is available free of charge via the Internet at <http://pubs.acs.org>.

AUTHOR INFORMATION

Corresponding Author

* A.R.O.: ofial@lmu.de

* H.M.: Herbert.mayr@cup.uni-muenchen.de

Author Contributions

The manuscript was written through contributions of all authors. All authors have given approval to the final version of the manuscript.

ACKNOWLEDGMENT

Dedicated to Professor Ernst-Ulrich Würthwein on the occasion of his 75th birthday. We thank Prof. H.-U. Reißig (FU Berlin) for helpful discussions and valuable suggestions. We thank Dr. Peter Mayer (Dept. Chemie, LMU München) for the single crystal X-ray structure determinations and the Faculty of Chemistry and Pharmacy (LMU München) for providing the computational resources. L.L., A.R.O. and H.M. are grateful to the Department Chemie (LMU München), the Fonds der Chemischen Industrie (FCI), and the Deutsche Forschungsgemeinschaft (DFG, SFB 749, project B1) for financial support. R.J.M. thanks the Deutsche Forschungsgemeinschaft (DFG, German Research Foundation) for a fellowship (MA 9687/1-1).

REFERENCES

- (1) (a) Huisgen, R. 1,3-Dipolar Cycloadditions. Past and Future. *Angew. Chem., Int. Ed. Engl.* **1963**, *2*, 565–598. (b) Huisgen, R. Kinetics and Mechanism of 1,3-Dipolar Cycloadditions. *Angew. Chem., Int. Ed. Engl.* **1963**, *2*, 633–645 (c) *1,3-Dipolar Cycloaddition Chemistry*, Volumes 1 and 2; Padwa, A., Ed.; Wiley: New York, 1984. (d) *Synthetic Applications of 1,3-Dipolar Cycloaddition Chemistry Toward Heterocycles and Natural Products*; Padwa, A.; Pearson, W. H., Eds.; Wiley: New York, 2002. (e) Breugst, M.; Reissig, H.-U. The Huisgen Reaction: Milestones of the 1,3-Dipolar Cycloaddition. *Angew. Chem., Int. Ed.* **2020**, *59*, 12293–12307. (f) Fustero, S.; Sánchez-Roselló, M.; Barrio, P.; Simón-Fuentes, A. From 2000 to Mid-2010: A Fruitful Decade for the Synthesis of Pyrazoles. *Chem. Rev.* **2011**, *111*, 6984–7034. (g) Dadiboyena, S. Cycloadditions and Condensations as Essential Tools in Spiropyrazoline Synthesis. *Eur. J. Med. Chem.* **2013**, *63*, 347–377. (h) Kissane, M.; Maguire, A. R. Asymmetric 1,3-Dipolar Cycloadditions of Acrylamides. *Chem. Soc. Rev.* **2010**, *39*, 845–883. (i) Singh, M. S.; Chowdhury, S.; Koley, S. Progress in 1,3-Dipolar Cycloadditions in the Recent Decade: An Update to Strategic Development towards the Arsenal of Organic Synthesis. *Tetrahedron* **2016**, *72*, 1603–1644. (j) Beutick, S. E.; Vermeeren, P.; Hamlin, T. A. The 1,3-Dipolar Cycloaddition: From Conception to Quantum Chemical Design. *Chem. Asian J.* **2022**, *17*, e202200553.
- (2) Click Chemistry: (a) Tornøe, C. W.; Christensen, C.; Meldal, M. Peptidotriazoles on Solid Phase: [1,2,3]-Triazoles by Regiospecific Copper(I)-Catalyzed 1,3-Dipolar Cycloadditions of Terminal Alkynes to Azides. *J. Org. Chem.* **2002**, *67*, 3057–3064. (b) Rostovtsev, V. V.; Green, L. G.; Fokin, V. V.; Sharpless, K. B. A Stepwise Huisgen Cycloaddition Process: Copper(I)-Catalyzed Regioselective “Ligation” of Azides and Terminal Alkynes. *Angew. Chem. Int. Ed.* **2002**, *41*, 2596–2599. (c) Evans, R. A. The Rise of Azide-Alkyne 1,3-Dipolar ‘Click’ Cycloaddition and its Application to Polymer Science and Surface Modification. *Aust. J. Chem.* **2007**, *60*, 384–395. (d) Tron, G. C.; Pirali, T.; Billington, R. A.; Canonico, P. L.; Sorba, G.; Genazzani, A. A. Click Chemistry Reactions in Medicinal Chemistry: Applications of the 1,3-dipolar Cycloaddition between Azides and Alkynes. *Med. Res. Rev.* **2008**, *28*, 278–308. (e) Tiwari, V. K.; Mishra, B. B.; Mishra, K. B.; Mishra, N.; Singh, A. S.; Chen, X. Cu-Catalyzed Click Reaction in Carbohydrate Chemistry. *Chem. Rev.* **2016**, *116*, 3086–3240. (f) Singh, M. S.; Chowdhury, S.; Koley, S. Advances of Azide-Alkyne Cycloaddition-Click Chemistry over the Recent Decade. *Tetrahedron* **2016**, *72*, 5257–5283. (g) Svatunek, D.; Houk, K. N. 1,3-Dipolar Cycloadditions in *Science of Synthesis: Click Chemistry*; Rutjes, F. P. J. T., Ed.; Thieme: Stuttgart, 2022.
- (3) (a) Sustmann, R. A Simple Model for Substituent Effects in Cycloaddition Reactions. I. 1,3-Dipolar Cycloadditions. *Tetrahedron Lett.* **1971**, *12*, 2717–2720. (b) Sustmann, R.; Trill, H. Substituent Effects in 1,3-Dipolar Cycloadditions of Phenyl Azide. *Angew. Chem., Int. Ed. Engl.* **1972**, *11*, 838–840.
- (4) (a) Houk, K. N.; Sims, J.; Duke Jr, R. E.; Strozier, R. W.; George, J. K. Frontier Molecular Orbitals of 1,3 Dipoles and Dipolarophiles. *J. Am. Chem. Soc.* **1973**, *95*, 7287–7301. (b) Houk, K. N.; Sims, J.; Watts, C. R.; Luskus, L. J. The Origin of Reactivity, Regioselectivity, and Periselectivity in 1,3-Dipolar Cycloadditions. *J. Am. Chem. Soc.* **1973**, *95*, 7301–7315. (c) Houk, K. N.; Yamaguchi, K. Theory of 1,3-Dipolar Cycloadditions. In *1,3-Dipolar Cycloaddition Chemistry*, Volume 2; Padwa, A., Ed.; Wiley: New York, 1984; pp. 407–450. (d) Sustmann, R. Orbital Energy Control of Cycloaddition Reactivity. *Pure Appl. Chem.* **1974**, *40*, 569–593. (e) Huisgen, R. The

- Concerted Nature of 1,3-Dipolar Cycloadditions and the Question of Diradical Intermediates. *J. Org. Chem.* **1976**, *41*, 403–419. (f) Fleming, I. *Molecular Orbitals and Organic Chemical Reactions: Reference Edition*, Wiley, Chichester, United Kingdom, 2010, Chap. 6.5.3, pp. 322–338. (g) Brückner, R. *Reaktionsmechanismen*, 3rd Edition, Springer, Berlin, 2004, pp. 667–671. (h) Vogel, P.; Houk, K. N. *Organic Chemistry: Theory, Reactivity and Mechanisms in Modern Synthesis*, Wiley-VCH, Weinheim, Germany, 2019, Chap. 5.3.17, pp. 420–425. (i) Chen, P.-P.; Ma, P.; He, X.; Svatunek, D.; Liu, F.; Houk, K. N. Computational Exploration of Ambiphilic Reactivity of Azides and Sustmann's Paradigmatic Parabola. *J. Org. Chem.* **2021**, *86*, 5792–5804.
- (5) (a) Grimme, S.; Mück-Lichtenfeld, C.; Würthwein, E.-U.; Ehlers, A. W.; Goumans, T. P. M.; Lammertsma, K. Consistent Theoretical Description of 1,3-Dipolar Cycloaddition Reactions. *J. Phys. Chem. A* **2006**, *110*, 2583–2586. (b) Ess, D. H.; Houk, K. N. Distortion/Interaction Energy Control of 1,3-Dipolar Cycloaddition Reactivity. *J. Am. Chem. Soc.* **2007**, *129*, 10646–10647. (c) Ess, D. H.; Houk, K. N. Theory of 1,3-Dipolar Cycloadditions: Distortion/Interaction and Frontier Molecular Orbital Models. *J. Am. Chem. Soc.* **2008**, *130*, 10187–10198. (d) Lan, Y.; Zou, L.; Cao, Y.; Houk, K. N. Computational Methods to Calculate Accurate Activation and Reaction Energies of 1,3-Dipolar Cycloadditions of 24 1,3-Dipoles. *J. Phys. Chem. A* **2011**, *115*, 13906–13920. (e) Domingo, L. R.; Emamian, S. R. Understanding the mechanisms of [3+2] cycloaddition reactions. The pseudoradical versus the zwitterionic mechanism. *Tetrahedron* **2014**, *70*, 1267–1273. (f) Miranda-Quintana, R. A.; Ayers, P. W. Charge Transfer and Chemical Potential in 1,3-Dipolar Cycloadditions. *Theor. Chem. Acc.* **2016**, *135*, 172. (g) Ríos-Gutiérrez, M.; Domingo, L. R. Unravelling the Mysteries of the [3+2] Cycloaddition Reactions. *Eur. J. Org. Chem.* **2019**, 267–282. (h) Domingo, L. R.; Ríos-Gutiérrez, M.; Acharjee, N. Unveiling the Unexpected Reactivity of Electrophilic Diazoalkanes in [3+2] Cycloaddition Reactions within Molecular Electron Density Theory. *Chemistry* **2021**, *3*, 74–91. (i) Chen, S.; Hu, T.; Houk, K. N. Energy of Concert and Origins of Regioselectivity for 1,3-Dipolar Cycloadditions of Diazomethane. *J. Org. Chem.* **2021**, *86*, 6840–6846. (j) Barrales-Martínez, C.; Martínez-Araya, J. I.; Jaque, P. 1,3-Dipolar Cycloadditions by a Unified Perspective Based on Conceptual and Thermodynamics Models of Chemical Reactivity. *J. Phys. Chem. A* **2021**, *125*, 801–815. (k) Domingo, L. R.; Ríos-Gutiérrez, M.; Barakat, M. A Molecular Electron Density Theory Study of the [3+2] Cycloaddition Reaction of an Azomethine Ylide with an Electrophilic Ethylene Linked to Triazole and Ferrocene Units. *Molecules* **2022**, *27*, 6532. (l) Adjieufack, A. I.; Liegeois, V.; Ndassa Mbouombouo, I.; Domingo, L. R.; Champagne, B. Unveiling the [3+2] cycloaddition between difluoromethyl diazomethane and 3-ylideneoxindole from the perspective of molecular electron density theory. *New J. Chem.* **2022**, *46*, 18652–18663. (m) Sengupta, A.; Li, B.; Svatunek, D.; Liu, F.; Houk, K. N. Cycloaddition Reactivities Analyzed by Energy Decomposition Analyses and the Frontier Molecular Orbital Model. *Acc. Chem. Res.* **2022**, *55*, 2467–2479. (n) The analogy of 1,3-dipolar cycloadditions to anionic 5-endo cyclizations have also been discussed: Gilmore, K.; Manoharan, M.; Wu, J. I.-C.; Schleyer, P. v. R.; Alabugin, I. Aromatic Transition States in Nonpericyclic Reactions: Anionic 5-Endo Cyclizations Are Aborted Sigmatropic Shifts. *J. Am. Chem. Soc.* **2012**, *134*, 10584–10594.
- (6) Breugst, M.; Huisgen, R.; Reissig, H.-U. Regioselective 1,3-Dipolar Cycloadditions of Diazoalkanes with Heteroatom-Substituted Alkynes: Theory and Experiment. *Eur. J. Org. Chem.* **2018**, 2477–2485.
- (7) (a) Li, L.; Mayer, P.; Stephenson, D. S.; Ofial, A. R.; Mayer, R. J.; Mayr, H. An Overlooked Pathway in 1,3-Dipolar Cycloadditions of Diazoalkanes with Enamines. *Angew. Chem., Int. Ed.* **2022**, *61*, e202117047. (b) Li, L.; Mayer, R. J.; Stephenson, D. S.; Mayer, P.; Ofial, A. R.; Mayr, H. Quantification of the Electrophilicities of Diazoalkanes: Kinetics and Mechanism of Azo Couplings with Enamines and Sulfonium Ylides. *Chem. Eur. J.* **2022**, *28*, e202201376.
- (8) According to the IUPAC recommendations, the term 'ionization potential' is outdated and should be replaced by 'ionization energy'. To avoid confusion about the wording and underlying definitions when comparing our arguments with those in quoted references, we decided to also use 'ionization potential' in this work. Perrin, C. L.; Agrat, I.; Bagno, A.; Braslavsky, S. E.; Fernandes, P. A.; Gal, J.-F.; Lloyd-Jones, G. C.; Mayr, H.; Murdoch, J. R.; Nudelman, N. S.; Radom, L.; Rappoport, Z.; Ruasse, M.-F.; Siehl, H.-U.; Takeuchi, Y.; Tidwell, T. T.; Uggerud, E.; Williams, I. H. Glossary of Terms Used in Physical Organic Chemistry (IUPAC Recommendations 2021) *Pure Appl. Chem.* **2022**, *94*, 353–534.
- (9) Koopmans, T. Über die Zuordnung von Wellenfunktionen und Eigenwerten zu den einzelnen Elektronen eines Atoms. *Physica* **1934**, *1*, 104–113.
- (10) (a) Parr, R. G.; Pearson, R. G. Absolute Hardness: Companion Parameter to Absolute Electronegativity. *J. Am. Chem. Soc.* **1983**, *105*, 7512–7516. (b) Pal, R.; Chatteraj, P. K. Electrophilicity Index Revisited. *J. Comput. Chem.* **2023**, *44*, 278–297.
- (11) Bihlmaier, W.; Huisgen, R.; Reissig, H. U.; Voss, S. Reactivity Sequences of Dipolarophiles towards Diazoalkane Compounds - MO Perturbation Treatment. *Tetrahedron Lett.* **1979**, *20*, 2621–2624.
- (12) (a) Mayr, H.; Bug, T.; Gotta, M. F.; Hering, N.; Irrgang, B.; Janker, B.; Kempf, B.; Loos, R.; Ofial, A. R.; Remennikov, G.; Schimmel, H. Reference Scales for the Characterization of Cationic Electrophiles and Neutral Nucleophiles. *J. Am. Chem. Soc.* **2001**, *123*, 9500–9512. (b) Lucius, R.; Loos, R.; Mayr, H. Kinetics of Carbocation-Carbanion Combinations: Key to a General Concept of Polar Organic Reactivity. *Angew. Chem., Int. Ed.* **2002**, *41*, 91–95. (c) Mayr, H.; Kempf, B.; Ofial, A. R. π -Nucleophilicity in Carbon-Carbon Bond-Forming Reactions. *Acc. Chem. Res.* **2003**, *36*, 66–77. (d) Mayr, H.; Ofial, A. R. A Quantitative Approach to Polar Organic Reactivity. *SAR QSAR Environm. Res.* **2015**, *26*, 619–646. (e) For a database of nucleophilicity parameters N/s_N , and electrophilicity parameters E , check the link: <https://www.cup.lmu.de/oc/mayr/reaktionsdatenbank2/>.
- (13) (a) Pérez, P.; Toro-Labbé, A.; Aizman, A.; Contreras, R. Comparison between Experimental and Theoretical Scales of Electrophilicity in Benzhydryl Cations. *J. Org. Chem.* **2002**, *67*, 4747–4752. (b) Domingo, L. R.; Pérez, P.; Contreras, R. Reactivity of the Carbon-Carbon Double Bond towards Nucleophilic Additions. A DFT Analysis. *Tetrahedron* **2004**, *60*, 6585–6591. (c) Chamorro, E.; Duque-Noreña, M.; Pérez, P. A Comparison between Theoretical and Experimental Models of Electrophilicity and Nucleophilicity. *J. Mol. Struct. THEOCHEM* **2009**, *896*, 73–79. (d) Chamorro, E.; Duque-Noreña, M.; Pérez, P. Further Relationships between Theoretical and Experimental Models of Electrophilicity and Nucleophilicity. *J. Mol. Struct. THEOCHEM* **2009**, *901*, 145–152. (e) Wang, C.; Fu, Y.; Guo, Q.-X.; Liu, L. First-Principles Prediction of Nucleophilicity Parameters for π Nucleophiles: Implications for Mechanistic Origin of Mayr's Equation. *Chem. Eur. J.* **2010**, *16*, 2586–2598. (f) Chatteraj, P. K.; Giri, S.; Duley, S. **Update 2 of: Electrophilicity Index.** *Chem. Rev.* **2011**, *111*, PR43–PR75. (g) Zhuo, L.-G.; Liao, W.; Yu, Z.-X. A Frontier Molecular Orbital

- Theory Approach to Understanding the Mayr Equation and to Quantifying Nucleophilicity and Electrophilicity by Using HOMO and LUMO Energies. *Asian J. Org. Chem.* **2012**, *1*, 336–345. (h) Kiyooka, S.-i.; Kaneno, D.; Fujiyama, R. Intrinsic Reactivity Index as a Single Scale Directed toward both Electrophilicity and Nucleophilicity Using Frontier Molecular Orbitals. *Tetrahedron* **2013**, *69*, 4247–4258. (i) Chamorro, E.; Duque-Noreña, M.; Notario, R.; Pérez, P. Intrinsic Relative Scales of Electrophilicity and Nucleophilicity. *J. Phys. Chem. A* **2013**, *117*, 2636–2643. (j) Latino, D. A. R. S.; Pereira, F. Exploration of Quantitative Structure-Reactivity Relationships for the Estimation of Mayr Nucleophilicity. *Helv. Chim. Acta* **2015**, *98*, 863–879. (k) Hoffmann, G.; Balcilar, M.; Tognetti, V.; Héroux, P.; Gaüzère, B.; Adam, S.; Joubert, L. Predicting Experimental Electrophilicities from Quantum and Topological Descriptors: A Machine Learning Approach. *J. Comput. Chem.* **2020**, *41*, 2124–2136. (l) Orlandi, M.; Escudero-Casao, M.; Licini, G. Nucleophilicity Prediction via Multivariate Linear Regression Analysis. *J. Org. Chem.* **2021**, *86*, 3555–3564. (m) Boobier, S.; Liu, Y.; Sharma, K.; Hose, D. R. J.; Blacker, A. J.; Kapur, N.; Nguyen, B. N. Predicting Solvent-Dependent Nucleophilicity Parameter with a Causal Structure Property Relationship. *J. Chem. Inf. Model.* **2021**, *61*, 4890–4899. (n) Proppe, J.; Kircher, J. Uncertainty Quantification of Reactivity Scales. *ChemPhysChem* **2022**, *23*, e202200061. (o) Tavakoli, M.; Mood, A.; Van Vranken, D.; Baldi, P. Quantum Mechanics and Machine Learning Synergies: Graph Attention Neural Networks to Predict Chemical Reactivity. *J. Chem. Inf. Model.* **2022**, *62*, 2121–2132. (p) Nie, W.; Liu, D.; Li, S.; Yu, H.; Fu, Y. Nucleophilicity Prediction Using Graph Neural Networks. *J. Chem. Inf. Model.* **2022**, *62*, 4319–4328. (q) Saini, V.; Sharma, A.; Nivatia, D. A Machine Learning Approach for Predicting the Nucleophilicity of Organic Molecules. *Phys. Chem. Chem. Phys.* **2022**, *24*, 1821–1829. (r) Cador, A.; Hoffmann, G.; Tognetti, V.; Joubert, L. A Theoretical Study on Aza-Michael Additions. *Theor. Chem. Acc.* **2022**, *141*, 70. (s) Cuesta, S. A.; Moreno, M.; López, R. A.; Mora, J. R.; Paz, J. L.; Márquez, E. A. ElectroPredictor: An Application to Predict Mayr's Electrophilicity E through Implementation of an Ensemble Model Based on Machine Learning Algorithms. *J. Chem. Inf. Model.* **2023**, *63*, 507–521.
- (14) (a) Bug, T.; Hartnagel, M.; Schlierf, C.; Mayr, H. How Nucleophilic Are Diazo Compounds? *Chem. Eur. J.* **2003**, *9*, 4068–4076. (b) Jangra, H.; Chen, Q.; Fuks, E.; Zenz, I.; Mayer, P.; Ofial, R. A.; Zipse, H.; Mayr, H. Nucleophilicity and Electrophilicity Parameters for Predicting Absolute Rate Constants of Highly Asynchronous 1,3-Dipolar Cycloadditions of Aryldiazomethanes. *J. Am. Chem. Soc.* **2018**, *140*, 16758–16772. See also (c) Li, L.; Hsu, J.-R.; Zhao, H.; Ofial, A. R. Nucleophilicities of Cyclic α -Diazo Carbonyl Compounds. *Eur. J. Org. Chem.* **2023**, EarlyView (doi: 10.1002/ejoc.202300005).
- (15) (a) Regitz, M. Diazoalkanes in ref. **1c**, Chapt. 4, pp. 393–558. (b) Patai, S. *The Chemistry of Diazonium and Diazo Groups*, Wiley, Chichester, 1978. (c) Regitz, M. *Diazoalkane*, Thieme, Stuttgart: 1977. (d) Eistert, B.; Regitz, M.; Heck, G.; Schwall, H. Houben-Weyl, *Methoden der Organischen Chemie*, 4th ed., Vol. 10/4, Thieme, Stuttgart: 1968, pp. 589–710. (e) Zollinger, H. *Diazo Chemistry I: Aromatic and Heteroaromatic Compounds*, VCH, Weinheim, 1994.
- (16) (a) Jones, W. M. The Stereochemistry of the Decomposition of 2-Pyrazolines. *J. Am. Chem. Soc.* **1958**, *80*, 6687. (b) Jones, W. M. Pyrazolines. III. The Stereochemistry of the Decomposition of 2-Pyrazolines. *J. Am. Chem. Soc.* **1959**, *81*, 5153–5156. (c) Jones, W. M. Pyrazolines. IV. On the Mechanism of Decomposition and Conformational Analyses of 2-Pyrazolines. *J. Am. Chem. Soc.* **1960**, *82*, 3136–3137.
- (17) An analogous elimination of HSO₂F (that is, SO₂ and HF) from 1,3-dipolar cycloadducts from ESF (**3k**) and organic azides has recently been reported: Giel, M.-C.; Smedley, C. J.; Mackie, E. R. R.; Guo, T.; Dong, J.; Soares da Costa, T. P.; Moses, J. E. Metal-Free Synthesis of Functional 1-Substituted-1,2,3-Triazoles from Ethenesulfonyl Fluoride and Organic Azides. *Angew. Chem., Int. Ed.* **2020**, *59*, 1181–1186.
- (18) Li, L.; Mayer, P.; Ofial, A. R.; Mayr, H. Cyclobutane Formation by the Reaction of Ethenesulfonyl Fluoride with Dimethyl Diazomalonate. *Eur. J. Org. Chem.* **2022**, e202200865.
- (19) (a) Aggarwal, V. K.; Vicente, J. de; Bonnert, R. V. A Novel One-Pot Method for the Preparation of Pyrazoles by 1,3-Dipolar Cycloadditions of Diazo Compounds Generated in Situ. *J. Org. Chem.* **2003**, *68*, 5381–5383. (b) Gladow, D.; Doniz-Kettenmann, S.; Reissig, H.-U. 1,3-Dipolar Cycloadditions of Ethyl 2-Diazo-3,3,3-trifluoropropanoate to Alkynes and [1,5] Sigmatropic Rearrangements of the Resulting 3H-Pyrazoles: Synthesis of Mono-, Bis- and Tris(trifluoromethyl)-Substituted Pyrazoles. *Helv. Chim. Acta* **2014**, *97*, 808–821.
- (20) Atkins, P.; Paula, J. de; Keeler, J. *Atkins' Physical Chemistry*, 11th ed., Oxford Univ. Press, Oxford (UK), 2018, p 733.
- (21) (a) Reissig, H. U. *Neue Beiträge zu den Additionen der Diazoalkane und zur Chemie der 3H-Pyrazole*. Ludwig-Maximilians-Universität München (Germany), Dissertation, 1978. (b) Huisgen, R.; Reissig, H.-U. Cycloadditions of α -Diazo Carbonyl Compounds to Enamines. *Angew. Chem. Int. Ed. Engl.* **1979**, *18*, 330–331.
- (22) (a) Geittner, J. *Kinetik und Mechanismus der Cycloadditionen von Diazoalkanen*. Ludwig-Maximilians-Universität München (Germany), Dissertation, 1973. (b) Fisera, L.; Geittner, J.; Huisgen, R.; Reissig, H.-U. Cycloaddition Rates of Diazomethane and Diphenyldiazomethane. *Heterocycles* **1978**, *10*, 153–158. (c) Huisgen, R.; Stangl, H.; Sturm, H. J.; Wagenhofer, H. Kinetik und Mechanismus der 1,3-Dipolaren Additionen der Diazoalkane. *Angew. Chem.* **1961**, *73*, 170.
- (23) (a) As illustrated in **Figure 3**, generally $(\lg k_2)/s_N$ is plotted vs N to obtain linear correlations for reaction series including nucleophiles with variable s_N values. (b) The exact position of **3a** in this graph shall not be discussed, since the corresponding rate constant had to be extrapolated from reported measurements at 110 °C, and neither the original investigators (ref **21a**) nor we have been able to identify products of this reaction. (c) The deviation of this number from $N(\mathbf{1b}) = -1.24$ is due to the fact that the slope of the green correlation line in **Figures 7A** and **7C** differs slightly from $s_N(\mathbf{1b})$.
- (24) Because of the missing product studies, the reported experimental rate constants for the reactions of **1a** and **1b** with **3a** and **3b** (Table 3) should be considered with caution.
- (25) Uncatalyzed dimerization of diazoalkanes usually do not take place. Diazoacetates were reported to undergo a base-promoted dimerization: (a) Curtius, T.; Lang, J. Diazo- und Azoverbindungen der Fettreihe. III. Abhandlung. Ueber Tri-Azoverbindungen. *J. Prakt. Chem.* **1888**, *38*, 531–558. (b) Sauer, J.; Mielert, A.; Lang, D.; Peter, D. Eine Studie der Diels-Alder-Reaktion, III: Umsetzungen von 1,2,4,5-Tetrazinen mit Olefinen. Zur Struktur von Dihydropyridazinen. *Chem. Ber.* **1965**, *98*, 1435–1445. (c) Boger, D. L.; Coleman, R. S.; Panek, J. S. A Detailed, Convenient Preparation of Dimethyl 1,2,4,5-Tetrazine-3,6-Dicarboxylate. *J. Org. Chem.* **1985**, *50*, 5377–5379.
- (26) Zhang, J.; Chen, Q.; Mayer, R. J.; Yang, J.-D.; Ofial, A. R.; Cheng, J.-P.; Mayr, H. Predicting Absolute Rate Constants for Huisgen Reactions of Unsaturated Iminium Ions with Diazoalkanes. *Angew. Chem. Int. Ed.* **2020**, *59*, 12527–12533.

(27) Geittner, J.; Huisgen, R.; Reissig, H.-U. Solvent Dependence of Cycloaddition Rates of Phenyl diazomethane and Activation Parameters. *Heterocycles* **1978**, *11*, 109–120.

(28) Huisgen, R.; Koszinowski, J.; Ohta, A.; Schiffer, R. Cycloadditions of Diazoalkanes to 1-Alkenes. *Angew. Chem., Int. Ed. Engl.* **1980**, *19*, 202–203.

(29) Analogously, DFT calculated values for **TS1** are slightly higher than those obtained by eq. (1) for the stepwise reactions of ketene acetal **3a** and vinyl ether **3b**. The reason for the huge differences of **TS1**(DFT) and **TS1**(eq. 1) for the reactions of hex-1-ene (**3h** or model **3h'**) is presently not known.

(30) (a) Bickelhaupt, F. M.; Houk, K. N. Analyzing Reaction Rates with the Distortion/Interaction-Activation Strain Model. *Angew. Chem., Int. Ed.* **2017**, *56*, 10070–10086. (b) Vermeeren, P.; van der Lubbe, S. C. C. C.; Guerra, F.; Bickelhaupt, F. M.; Hamlin, T. A. Understanding Chemical Reactivity Using the Activation Strain Model. *Nat. Protoc.* **2020**, *15*, 649–667.

(31) The potential formation of diradical intermediates is not covered by this approach. (a) Firestone, R. A. On the Mechanism of 1,3-Dipolar Cycloadditions. *J. Org. Chem.* **1968**, *33*, 2285–2290. (b) Huisgen, R. On the Mechanism of 1,3-Dipolar Cycloadditions. A Reply. *J. Org. Chem.* **1968**, *33*, 2291–2297.

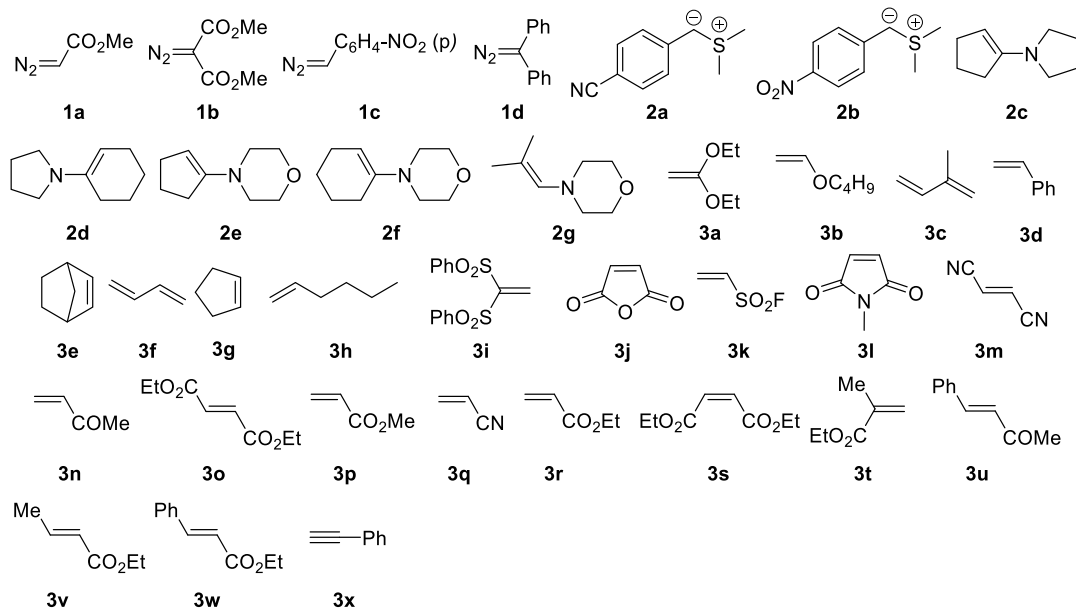
(32) Please note that the degree of concertedness has to be derived from the deviation from the respective correlation line. Thus, the fact that styrene (**3d**) is located far above the green, nucleophile-specific correlation line in [Figure 8B](#) indicates a high degree of concertedness though it is below the blue, electrophile-specific correlation line. Future work has to show how ambiphilic dipolarophiles will integrate in these correlations.

(33) Allgäuer, D. S.; Jangra, H.; Asahara, H.; Li, Z.; Chen, Q.; Zipse, H.; Ofial, A. R.; Mayr, H. Quantification and Theoretical Analysis of the Electrophilicities of Michael Acceptors. *J. Am. Chem. Soc.* **2017**, *139*, 13318–13329.

6.2 Supporting Information

6.2.1 General

Chemicals. Diazo compound **1a** (Scheme S1) was synthesized from glycine methyl ester hydrochloride based on literature procedure,^{S1} **1b** was obtained from *N*-acetylsulfanyl chloride as described,^{S2} **1c** was synthesized from 4-nitrobenzaldehyde as mentioned.^{S3} ESF (**3k**) was synthesized from 2-chloro-ethanesulfonyl chloride as described.^{S4} All other compounds were purchased and purified by distillation or recrystallization when necessary.



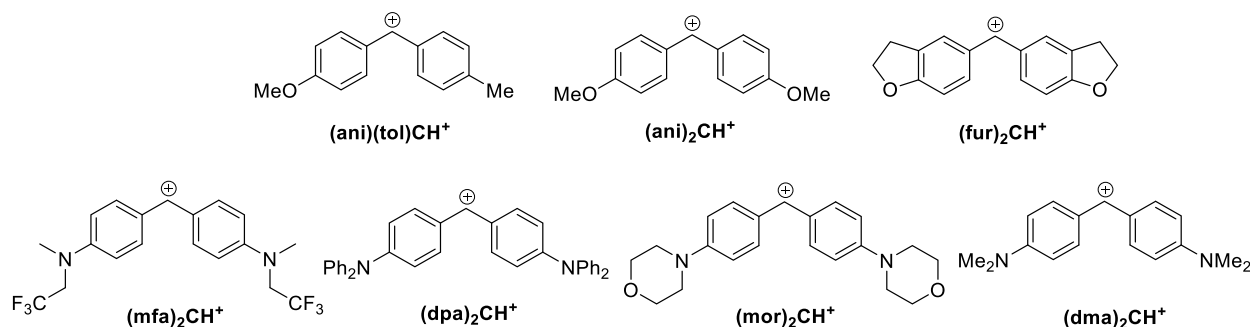
Scheme S1. Nucleophiles **2** and dipolarophiles **3** in this work.

Analytics. ¹H and ¹³C{¹H} NMR spectra were recorded in CDCl₃ (δ_{H} 7.26, δ_{C} 77.16 ppm), CD₂Cl₂ (δ_{H} 5.32, δ_{C} 53.84 ppm) or d₆-DMSO (δ_{H} 2.50, δ_{C} 39.52 ppm) on 400 or 600 MHz NMR spectrometers.^{S5}

The following abbreviations were used for designation of chemical shift multiplicities: br = broad, s = singlet, d = doublet, t = triplet, q = quartet, quint = quintet, m = multiplet. NMR signals were assigned by additional 2D NMR experiments (COSY, HSQC, HMBC and NOESY). HRMS were recorded on a Thermo Finnigan LTQ FT Ultra (ESI) or a Finnigan MAT 95Q (EI) mass spectrometer. Melting points were determined on a Büchi B540 device and are not corrected. IR spectra were recorded on a FTIR Spectrometer SPECTRUM BX II (Perkin Elmer).

The X-ray intensity data were measured on a Bruker D8 Venture TXS system equipped with a multilayer mirror monochromator and a Mo K α rotating anode X-ray tube ($\lambda = 0.71073 \text{ \AA}$). The frames were integrated with the Bruker SAINT software package.^{S6} Data were corrected for absorption effects using the MultiScan method (SADABS).^{S7} The structure was solved and refined using the Bruker SHELXTL Software Package.^{S8} The figures have been drawn at the 25% ellipsoid probability level.^{S9}

Kinetics. The kinetic investigations of the reactions of **1a** or **1b** with the reference electrophiles (ani)(tol)CH⁺, (ani)₂CH⁺, (fur)₂CH⁺, (mfa)₂CH⁺, (dpa)₂CH⁺, (mor)₂CH⁺ and (dma)₂CH⁺ (Scheme S2) were performed in dry dichloromethane at 20 °C by using a diode array spectrometer (J&M TIDAS). The decrease of the absorbance of the colored reference electrophile solutions in dichloromethane was observed by photometric methods.^{S10a} The benzhydrylium triflates (ani)(tol)CH⁺ TfO⁻, (ani)₂CH⁺ TfO⁻, and (fur)₂CH⁺ TfO⁻ were freshly prepared by adding a solution of TMSOTf (4 equivs) in dry dichloromethane into the solution of (ani)(tol)CHCl, (ani)₂CHCl, or (fur)₂CHCl in dry dichloromethane. The benzhydrylium tetrafluoroborates (mfa)₂CH⁺ BF₄⁻, (dpa)₂CH⁺ BF₄⁻, (mor)₂CH⁺ BF₄⁻, and (dma)₂CH⁺ BF₄⁻ were prepared as described before.^{S10b}



Scheme S2. Benzhydrylium ions used in this work to determine N and s_N parameters of **1a** and **1b**.

The kinetic investigations of the reactions of **1c** with the Michael acceptors **3n-o**, **3r** or **3t** were performed in dry dichloromethane at 20 °C by using a diode array spectrometer (J&M TIDAS) and evaluating the decrease of the absorbance of **1c**.^{S11}

The kinetics of the reactions of **1a** and **1b** with the dipolarophiles **3** as well as of **1c** with **3d** were monitored by ¹H NMR spectroscopy in well-sealed NMR tubes under argon atmosphere at constant temperatures.^{S12} All online NMR kinetic measurements were performed with internal standards (dibromomethane, mesitylene or 1,1,2,2-tetrachloroethane) at variable temperatures (over a ΔT range of at least 20 K) by following the integration of a certain hydrogen atom (marked red in the NMR kinetic part of this work) to derive the second-order rate constants k_2 at +20, +80.3 or +110 °C based on the Eyring activation parameters ΔH^\ddagger and ΔS^\ddagger . Generally, equal initial concentrations of the reactants were used in the reactions for NMR kinetic measurements. In the kinetics of the reactions of **1b** with **3r**, 3 equiv. of **1b** were used and the second-order rate constants of the reactions were obtained from the equation^{S13}

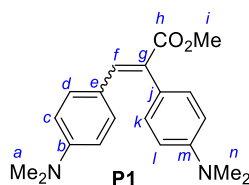
$$k_2 t = \frac{1}{\Delta} \ln \frac{[\mathbf{3r}]_0 ([\mathbf{3r}]_t + \Delta)}{([\mathbf{3r}]_0 + \Delta) [\mathbf{3r}]_t}, \text{ with } \Delta = [\mathbf{1b}]_0 - [\mathbf{3r}]_0.$$

6.2.2 Product Studies

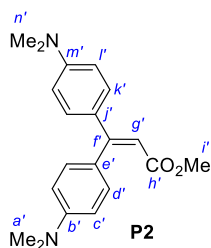
Reaction of methyl diazoacetate (**1a**) with the $(\text{dma})_2\text{CH}^+ \text{BF}_4^-$

Methyl (*E*)-2,3-bis(4-(dimethylamino)phenyl)acrylate (P1**)** and **methyl 3,3-bis(4-(dimethylamino)phenyl)acrylate (**P2**)** were obtained from **1a** (239 mg, 2.39 mmol) and $(\text{dma})_2\text{CH}^+ \text{BF}_4^-$ (396 mg, 1.16 mmol) in CH_2Cl_2 according to a previously reported procedure.^{S10} A pure sample of **P1** (60.0 mg) was isolated by column chromatography as a yellow solid, and a mixture of the isomers **P1** and **P2** (56.0 mg, ratio **P1**:**P2** \approx 5:4 by ^1H NMR integration) was also obtained as yellow solid. The overall yield of **P1** and **P2** was 116 mg (31%).

The ^{13}C NMR spectra of **P1** and **P2** were measured after repeating of the reaction of **1a** and $(\text{dma})_2\text{CH}^+ \text{BF}_4^-$. The mixture of **P1** and **P2** isolated the second time gives a ratio of **P1**:**P2** \approx 3:5 by ^1H NMR spectroscopy.



P1: ^1H NMR (600 MHz, CDCl_3): δ = 2.93 (s, 6 H, H^a), 3.00 (br s, 6 H, H^n), 3.76 (s, 3 H, H^i), 6.48 (d, J = 8.6 Hz, 2 H, H^c), 6.76 (br s, 2 H, H^l), 7.02 (d, J = 8.5 Hz, 2 H, H^d), 7.12 (d, J = 7.4 Hz, 2 H, H^k), 7.73 (s, 1 H, H^f). ^{13}C NMR (101 MHz, CDCl_3): δ = 40.2 (CH_3 , C^a), 40.6 (CH_3 , C^n), 52.2 (CH_3 , C^i), 111.5 (CH, C^c), 112.8 (CH, C^l), 123.0 (C, C^e), 124.7 (C, C^j), 127.4 (C, C^g), 130.8 (CH, C^k), 132.5 (CH, C^d), 140.6 (CH, C^f), 149.8 (C, C^m), 150.6 (C, C^b), 169.7 (C, C^h). **HRMS** (ESI⁺): m/z calcd for $\text{C}_{20}\text{H}_{25}\text{N}_2\text{O}_2^+$ ($\text{M} + \text{H}^+$): 325.1911, found 325.1913. **IR** (neat, ATR): 2884, 2803, 1719, 1691, 1609, 1585, 1519, 1482, 1445, 1427, 1354, 1320, 1257, 1220, 1182, 1168, 1153, 1065, 945, 822, 798, 771, 730 cm^{-1} . mp 194.7 $^\circ\text{C}$.



P2 (based on the NMR spectra of the 3:5-mixture of **P1** and **P2**): ^1H NMR (600 MHz, CDCl_3): δ = 2.99 (s, 6 H, $\text{H}^{n'}$, partially superimposed with H^n of **P1**), 3.01 (s, 6 H, $\text{H}^{a'}$), 3.63 (s, 3 H, $\text{H}^{i'}$), 6.12 (s, 1 H, $\text{H}^{g'}$), 6.62–6.64 (m, 2 H, $\text{H}^{l'}$), 6.69–6.74 (m, 2 H, $\text{H}^{c'}$), 7.11–7.15 (m, 2 H, $\text{H}^{d'}$, superimposed with H^k of **P1**), 7.22–7.25 (m, 2 H, $\text{H}^{k'}$). ^{13}C NMR (101 MHz, CDCl_3): δ = 40.3 (CH_3 , $\text{C}^{n'}$), 40.5 (CH_3 , $\text{C}^{a'}$), 51.0 (CH_3 , $\text{C}^{i'}$), 110.8 (CH, $\text{C}^{g'}$), 111.2 (CH, $\text{C}^{c'}$), 111.5 (CH, $\text{C}^{l'}$), 126.7 (C, $\text{C}^{e'}$), 129.5 (C, $\text{C}^{j'}$), 130.3 (CH, $\text{C}^{k'}$), 131.2 (CH, $\text{C}^{d'}$), 150.6 (C, $\text{C}^{b'}$), 151.3 (C, $\text{C}^{m'}$), 158.8 (C, $\text{C}^{f'}$), 167.4 (C, $\text{C}^{h'}$).

Reactions of diazo compounds **1** with dipolarophiles **3**

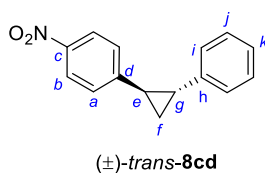
General procedure A (GP A). Diazo compound **1a** or **1b** was added dropwise to dipolarophile solution in CHCl₃, CDCl₃, toluene, d₈-toluene, d₈-toluene:mesitylene = 1:1 or neat in an oven-dried vial (a round-bottom flask or a NMR tube) under argon atmosphere. The mixture was kept at room temperature or heated (50–90 °C) for a certain time (till reactions completed or reached a sufficiently high degree of conversion). The reaction mixture was then concentrated and recrystallized or worked up by column chromatography on silica gel (*n*-pentane/diethyl ether = 2:1 or *n*-pentane/EtOAc = 5:1–1:1) to give the purified products.

General procedure B (GP B). Diazo compound **1c** were added dropwise to dipolarophile solution in dry CH₂Cl₂ or CD₂Cl₂ in a round-bottom flask (or a NMR tube) under argon atmosphere. The mixture was stirred at room temperature till reaction completed. The resulting mixture was then concentrated and worked up by column chromatography on silica gel (*n*-pentane/diethyl ether = 5:1 ~ diethyl ether or *n*-pentane/EtOAc = 5:1–2:1) to give the purified products.

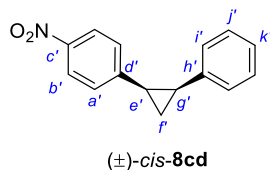
Reaction of *p*-nitrophenyldiazomethane (**1c**) with styrene (**3d**)

1-Nitro-4-((1*S,2*S**)-2-phenylcyclopropyl)benzene (±)-*trans*-(**8cd**)** and **1-nitro-4-((1*S**,2*R**)-2-phenylcyclopropyl)benzene (±)-*cis*-(**8cd**)** were obtained from **1c** (508 mg, 3.11 mmol) and **3d** (388 mg, 3.73 mmol) in CH₂Cl₂ (1.5 mL) as a mixture (*trans*:*cis* = 5:2, NMR integration) according to *GP B* (round-bottom flask, 22 days, *n*-pentane/diethyl ether = 5:1): light-yellow solid (490 mg, yield 66%).

The *trans/cis* mixture of **8cd** was recrystallized from EtOH (2×) to give pure *trans*-**8cd**: white crystals (198 mg, yield 27%); mp 88.5 °C (ref.^{S14a}: mp 88.5-89.5 °C). ¹H NMR spectral data are consistent with those reported in ref.^{S14b}



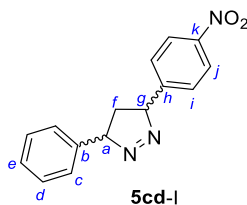
trans-**8cd**: ¹H NMR (400 MHz, CDCl₃): δ = 1.45–1.50 (m, 1 H, H^f), 1.53–1.59 (m, 1 H, H^f), 2.15–2.22 (m, 2 H, H^e and H^g), 7.07 (d, *J* = 7.4 Hz, 2 H, Hⁱ), 7.15–7.17 (m, 3 H, H^a and H^k, superimposed with solvent peak), 7.24 (t, *J* = 7.4 Hz, 2.0 H, H^j), 8.07 (d, *J* = 8.5 Hz, 2 H, H^b). ¹³C NMR (101 MHz, CDCl₃): δ = 19.5 (CH₂, C^f), 28.2 (CH, C^e), 29.9 (CH, C^g), 123.9 (CH, C^b), 125.9 (CH, Cⁱ), 126.2 (CH, C^a), 126.5 (CH, C^k), 128.7 (CH, C^j), 141.3 (C, C^h), 146.1 (C, C^c), 150.9 (C, C^d). **HRMS** (EI): *m/z* calcd for C₁₅H₁₃NO₂⁺(M⁺): 239.0941; found 239.0939. **IR** (neat, ATR): 3028, 1593, 1508, 1494, 1342, 1211, 1111, 1073, 1044, 939, 900, 855, 820, 779, 754, 736, 694 cm⁻¹.



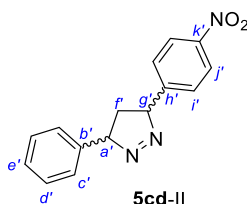
cis-**8cd** (based on the NMR spectra of the 5:2 mixture of *trans*- and *cis*-**8cd**): ¹H NMR (400 MHz, CDCl₃): δ = 1.41–1.53 (m, 2.0 H, H^f, superimposed with H^f of *trans*-**8cd**), 2.46 (td, *J* = 8.8, 6.3 Hz, 0.4 H, H^{e'}), 2.62 (td, *J* = 8.9, 6.3 Hz, 0.4 H, H^{g'}), 6.89–6.95 (m, 1.6 H, H^{a'} and H^{i'}), 6.99–7.06 (m, 1.1 H, H^{j'} and H^{k'}), 7.83–7.87 (m, 0.8 H, H^{b'}). ¹³C NMR (101 MHz, CDCl₃): δ = 12.4 (CH₂, C^f), 24.1 (CH, C^{e'}), 26.2 (CH, C^{g'}), 123.0 (CH, C^{b'}), 126.5 (CH, C^{k'}), 128.2 (CH, C^{j'}), 129.1 (CH, C^{a'}), 129.5 (CH, C^{i'}), 136.9 (C, C^{h'}), 146.0 (C, C^{c'}), 147.4 (C, C^{d'}).

NMR monitoring of the reaction of **1c** (1.01 M) with **3d** (1.07 M) in CD₂Cl₂ at +6 °C to ambient temperature showed the initial formation of diastereomeric pyrazoles **5cd-I** and **5cd-II** (I:II = 5:4, Figure S1B). When the reactions mixture was allowed to warm up from +6 °C to ambient temperature, the concentration of **5cd-I** decreased while the concentrations of **5cd-II** and cyclopropane **8cd** kept increasing (Figure S1C). When stored at ambient temperature over a period of another 12 days, **8cd** kept increasing in concentration until the reaction completed (Figure S1D).

Resonances for **5cd** were assigned based on NMR spectra (**5cd-I**:**5cd-II** = 5:4 by ¹H NMR integration) measured for the reaction of **1c** (96.3 mg, 0.590 mM) with **3d** (65.5 mg, 0.629 mM) in CD₂Cl₂ (400 μL) after 2 days at 6 °C.



5cd-I: ¹H NMR (400 MHz, CD₂Cl₂): δ = 1.46 (dt, *J* = 12.7, 11.0 Hz, 1 H, H^f), 2.91 (dt, *J* = 12.8, 7.9 Hz, 1 H, H^f), 5.38–5.45 m, 2 H, H^a and H^g), 7.64 (d, *J* = 8.8 Hz, 2 H, Hⁱ), 8.28–8.34 (m, 2 H, H^j). ¹³C NMR (101 MHz, CD₂Cl₂): δ = 36.1 (CH₂, C^f), 90.9 (CH, C^g), 92.5 (CH, C^a), 124.2 (CH, C^j), 127.6 (CH, C^c), 128.5 (CH, Cⁱ), 139.0 (C, C^b), 146.6 (C, C^h), 147.80 (C, C^k). The ¹H NMR signals of protons at the phenyl group superimposed with those of the starting material. The resonances of C^d and C^e could not be assigned unambiguously.



5cd-II: ¹H NMR (400 MHz, CD₂Cl₂): δ = 2.15 (ddd, *J* = 13.4, 9.4, 6.9, Hz, 1 H, H^f), 2.28 (ddd, *J* = 13.4, 9.4, 5.8 Hz, 1 H, H^f), 5.98 (m, 2 H, H^{a'} and H^{g'}). ¹³C NMR (101 MHz, CD₂Cl₂): δ = 33.8 (CH₂, C^f), 91.5 (CH, C^{g'}), 93.1 (CH, C^{a'}), 124.3 (CH, C^{j'}), 127.3 (CH, C^{c'}), 128.4 (CH, C^{i'}), 138.3

(C, C^b), 146.2 (C, C^h), 147.76 (C, C^k). The ¹H NMR signals of protons at the phenyl group superimposed with those of the starting material. The resonances of C^d and C^e could not be assigned unambiguously.

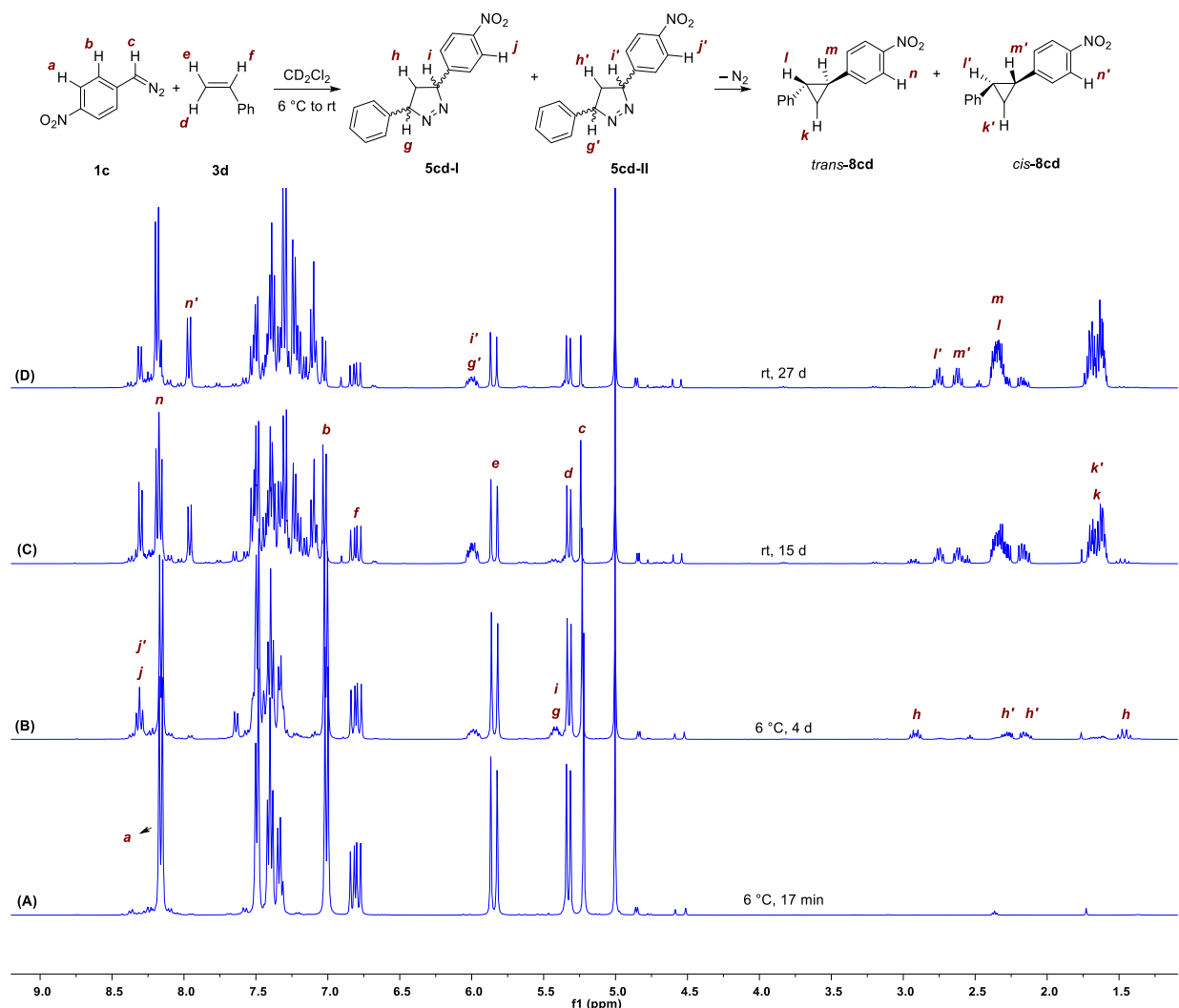
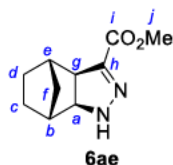


Figure S1. ¹H NMR (400 MHz) monitoring of the reaction of **1c** (1.01 M) with **3d** (1.07 M) in CD₂Cl₂ at 6 °C to ambient temperature over a period of 27 days.

Reaction of methyl diazoacetate (**1a**) with norbornene (**3e**)

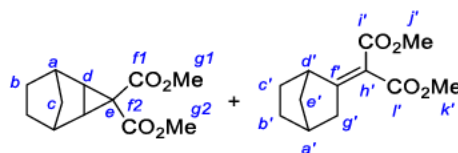
Methyl (3aR*,4S*,7R*,7aS*)-3a,4,5,6,7,7a-hexahydro-1H-4,7-methanoindazole-3-carboxylate (±)-(6ae) was obtained from **1a** (202 mg, 2.02 mmol) and **3e** (190 mg, 2.02 mmol) in CHCl₃ (0.5 mL) according to *GP A* (sealed vial, 50 °C, 4 days, recrystallization: EtOAc/*n*-pentane): colorless crystals (310 mg, yield 79%); mp 140.6 °C. Spectroscopic data consistent with those reported in ref.^{S15}



¹H NMR (400 MHz, CDCl₃): δ = 1.13–1.58 (m, 6 H, H^c, H^d, and H^f), 2.32 (s, 1 H, H^b), 2.56 (s, 1 H, H^e), 3.20 (dd, *J* = 9.9, 4.3 Hz, 1 H, H^g), 3.79–3.81 (m, 3 H, Hⁱ), 3.93 (dd, *J* = 10.2, 2.7 Hz, 1 H, H^a) 6.18 (br s, 1 H, NH). **¹³C NMR** (101 MHz, CDCl₃): δ = 24.6 (CH₂, C^c), 28.1 (CH₂, C^d), 33.2 (CH₂, C^f), 40.5 (CH, C^e), 44.6 (CH, C^b), 52.0 (CH₃, C^j), 53.7 (CH, C^g), 68.4 (CH, C^a), 142.0 (C, C^h), 163.6 (C, Cⁱ). **HRMS** (ESI⁺): *m/z* calcd for C₁₀H₁₅N₂O₂⁺ (M + H⁺): 195.1128; found 195.1127. **IR** (neat, ATR): 3286, 2951, 2872, 1685, 1527, 1434, 1352, 1334, 1319, 1293, 1258, 1208, 1160, 1131, 1106, 977, 839, 796, 768, 746 cm⁻¹.

Reaction of dimethyl diazomalonate (**1b**) with norbornene (**3e**)

Dimethyl tricyclo[3.2.1.0]octane-3,3-dicarboxylate (8be) and **dimethyl 2-(bicyclo[2.2.1]heptan-2-ylidene)malonate (7be)** were obtained from **1b** (203 mg, 1.28 mmol) and **3e** (116 mg, 1.23 mmol) in CDCl₃ (300 μL) as a mixture (**8be**:**7be** = 3:1, NMR integration) according to *GP A* (sealed NMR tube, 55°C, 4 months, column chromatography on silica gel, *n*-pentane/EtOAc = 1:1): **8be** colorless solid and **7be** colorless oil (230 mg, total yield 84%).

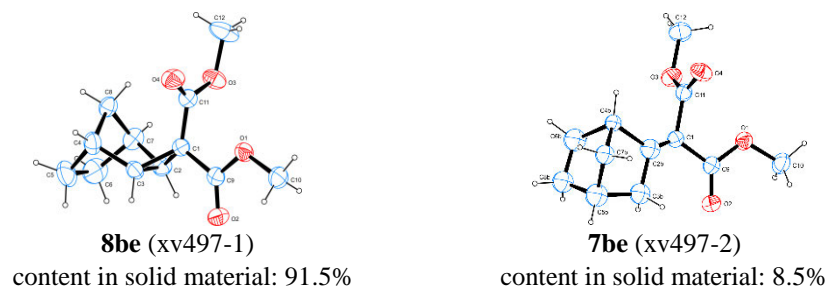


8be (**8be**:**7be** = 3:1) **7be**

8be: **¹H NMR** (400 MHz, CDCl₃): δ = 0.72 (dt, *J* = 12.1, 2.2 Hz, 1 H, H^c), 0.81 (dt, *J* = 12.1, 1.3 Hz, 1 H, H^c), 1.34 (qt, *J* = 5.6, 3.1 Hz, 2 H, H^b), 1.49–1.55 (m, 2 H, H^b), 1.66 (s, 2 H, H^d), 2.58 (s, 2 H, H^a), 3.68 (s, 3 H, H^{g1} or H^{g2}), 3.75 (s, 3 H, H^{g1} or H^{g2}). **¹³C NMR** (101 MHz, CDCl₃): δ = 28.9 (CH₂, C^b), 30.7 (CH₂, C^c), 33.2 (CH, C^d), 33.5 (C, C^e), 36.4 (CH, C^a), 52.8 (CH₃, C^{g1} or C^{g2}), 53.0 (CH₃, C^{g1} or C^{g2}), 169.9 (C, C^{f1} or C^{f2}), 171.2 (C, C^{g1} or C^{g2}).

7be: **¹H NMR** (400 MHz, CDCl₃): δ = 1.25 (ddq, *J* = 13.9, 7.1, 2.0 Hz, 0.5 H, H^b), 1.39–1.47 (m, 0.9 H, H^e and H^c), 1.59–1.64 (m, 0.3 H, H^b), 1.78 (tdd, *J* = 12.0, 6.5, 2.9 Hz, 0.3 H, H^c), 2.36 (dd, *J* = 18.7, 3.8 Hz, 0.3 H, H^g), 2.47 (q, *J* = 4.0 Hz, 0.3 H, H^a), 2.53–2.55 (m, 0.2 H, H^g), 3.25 (d, *J* = 4.5 Hz, 0.3 H, H^d), 3.74 (s, 0.9 H, Hⁱ or H^k), 3.79 (s, 0.9 H, Hⁱ or H^k). **¹³C NMR** (101 MHz, CDCl₃): δ = 27.4 (CH₂, C^b), 28.0 (CH₂, C^c), 36.0 (CH, C^a), 39.4 (CH₂, C^e), 41.1 (CH₂, C^g), 45.3 (CH, C^d), 51.9 (CH₃, C^j or C^k), 52.2 (CH₃, C^j or C^k), 117.5 (C, C^h), 165.5 (C, Cⁱ or C^l), 166.9 (C, Cⁱ or C^l), 172.0 (C, C^f).

The ¹H NMR spectral data for both **7be** and **8be** differ from those reported in refs.^{S16,S17} However, X-ray crystal structures of low quality could be obtained from the solid isolated after column chromatography, which support the structural assignments for **7be** and **8be**.



Furthermore, repeating the reaction of **1b** (505 mg, 3.19 mmol) with **3e** (301 mg, 3.20 mmol) in CDCl_3 (0.2 mL) according to *GP A* (sealed NMR tube, 55 °C, 4 months, column chromatography on silica gel, *n*-pentane/EtOAc = 10:1) furnished a 8:1-mixture of **7be** and **8be** (594 mg, yield 83%). NMR signal assignments for **7be** were confirmed by the spectral data of this **7be**-enriched sample.

The reaction of **1b** (182 mg, 1.15 mM) with **3e** (111 mg, 1.18 mM) in CDCl_3 (350 μL) was repeated by mixing the reactants at room temperature (Figure S2). After heating to +55 °C for 2 days, the initial product formed in the reaction of **1b** with **3e** was detected by NMR monitoring to be pyrazole **5be**, which gave **7be** after elimination of N_2 during the further progress of the reaction (Figure S2). The cyclopropane **8be** was not detected in the reaction mixture. Presumably, **8be** was generated from **5be** only during work up by column chromatography on silica gel.

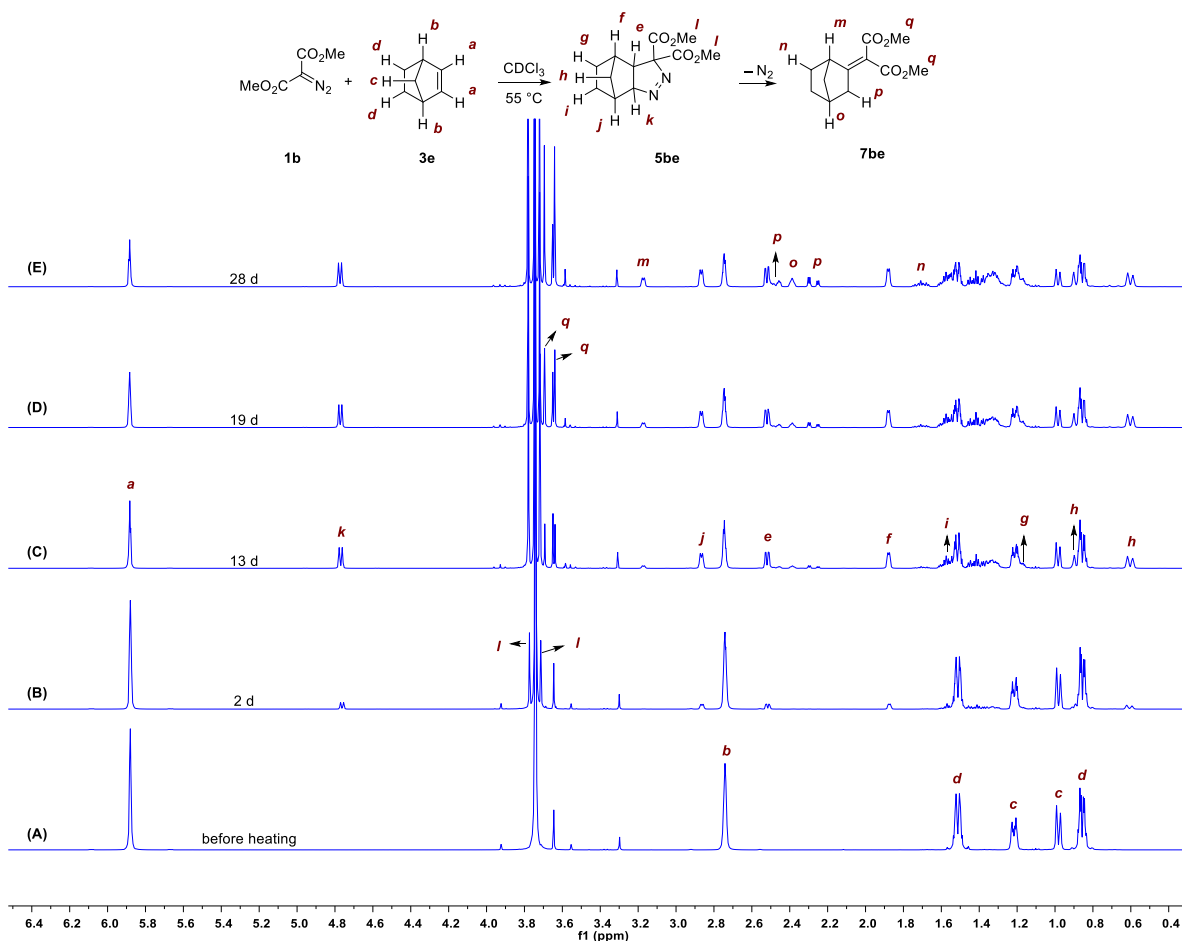
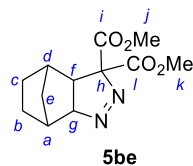


Figure S2. ^1H NMR (400 MHz) monitoring of the reaction of **1b** (1.01 M) with **3e** (1.07 M) in CDCl_3 at 55°C .

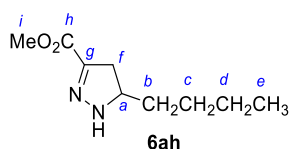
The NMR spectroscopic data for **5be** were assigned based on NMR spectra of the reaction mixture measured after 8 days at 55°C (Figure S2C).



5be: ^1H NMR (400 MHz, CDCl_3): $\delta = 0.51$ (d, $J = 11.0$ Hz, 1 H, H^e), 0.80 (s, 1 H, H^c), 1.08 (dd, $J = 5.7, 2.7$ Hz, 1 H, H^b), 1.20 – 1.27 (m, 1 H, H^c), 1.33 (ddt, $J = 15.6, 11.2, 3.8$ Hz, 1 H, H^c), 1.48 (ddd, $J = 9.6, 6.6, 3.7$ Hz, 1 H, H^b), 1.78 (d, $J = 4.0$ Hz, 1 H, H^d), 2.43 (dd, $J = 6.5, 1.5$ Hz, 1 H, H^a), 2.77 (d, $J = 4.6$ Hz, 1 H, H^f), 3.63 (s, 3 H, H^j or H^k), 3.69 (s, 3 H, H^j or H^k), 4.68 (d, $J = 6.5$ Hz, 1 H, H^g). ^{13}C NMR (101 MHz, CDCl_3): $\delta = 24.9$ (CH_2 , C^c), 28.3 (CH_2 , C^b), 32.2 (CH_2 , C^e), 37.5 (CH , C^a), 38.0 (CH , C^d), 43.7 (CH , C^f), 52.3 (CH_3 , C^j or C^k), 53.3 (CH_3 , C^j or C^k), 100.1 (CH , C^g), 104.5 (C , C^h), 165.0 (C , C^i or C^l), 165.9 (C , C^i or C^l).

Reaction of methyl diazoacetate (**1a**) with 1-hexene (**3h**)

Methyl 5-butyl-4,5-dihydro-1H-pyrazole-3-carboxylate (6ah) was obtained from **1a** (257 mg, 2.57 mmol) and **3h** (216 mg, 2.57 mmol) in CDCl_3 (200 μL) according to *GP A* (sealed NMR tube, 50°C , 44 days, conversion ratio 68%, mesitylene as internal standard, column chromatography on silica gel, *n*-pentane/diethyl ether = 2:1) as colorless oil (310 mg, 65%). **6ah** is unstable upon heating or exposure to air.^{S18}

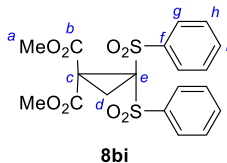


^1H NMR (400 MHz, CDCl_3): $\delta = 0.90$ (t, $J = 6.9$ Hz, 3 H, H^e), 1.32 – 1.37 (m, 4 H, H^c and H^d), 1.47 – 1.62 (m, 2 H, H^b), 2.61 (dd, $J = 17.0, 8.8$ Hz, 1 H, H^f), 3.01 (dd, 1 H, $J = 16.9, 11.0$ Hz, H^f), 3.83 (s, 3 H, H^i) 3.90 – 3.98 (m, 1 H, H^a). The NH signal was not detectable presumably due to fast exchange in CDCl_3 . ^{13}C NMR (101 MHz, CDCl_3): $\delta = 14.1$ (CH_3 , C^e), 22.7 (CH_2 , C^d), 28.2 (CH_2 , C^c), 34.7 (CH_2 , C^b), 36.4 (CH_2 , C^f), 52.2 (CH_3 , C^i), 62.4 (CH , C^a), 142.6 (C , C^g), 163.4 (C , C^h). **HRMS** (ESI): m/z calcd for $\text{C}_9\text{H}_{15}\text{N}_2\text{O}_2^-$ ($\text{M} - \text{H}^+$): 183.1139; found 183.1138.

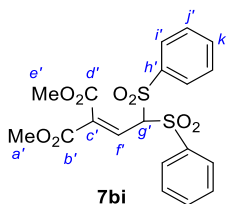
Reaction of dimethyl diazomalonate (**1b**) with 1,1-bis(phenylsulfonyl)ethylene (**3i**)

Dimethyl 2,2-bis(phenylsulfonyl)cyclopropane-1,1-dicarboxylate (8bi) and **dimethyl 2-(2,2-bis(phenylsulfonyl)ethylidene)malonate (7bi)** were obtained from **1b** (182 mg, 1.15 mmol) and **3i** (299 mg, 0.97 mmol) in CDCl_3 (0.5 mL) according to *GP A* (sealed NMR tube, 50°C , 14 days,

column chromatography on silica gel, *n*-pentane/diethyl ether = 2:1): **8bi** white powder (87.2 mg, yield 21%); mp 58.1 °C and **7bi** light yellow oil (300 mg, yield 70%).



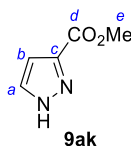
8bi: $^1\text{H NMR}$ (400 MHz, CDCl_3): δ = 2.66 (s, 2 H, H^d), 3.82 (s, 6 H, H^a), 7.55–7.60 (m, 4 H, H^h), 7.69–7.72 (m, 2 H, H^i), 7.97–8.00 (m, 4 H, H^g). $^{13}\text{C NMR}$ (101 MHz, CDCl_3): δ = 21.9 (CH_2 , C^d), 46.4 (C, C^c), 54.4 (CH_3 , C^a), 67.5 (C, C^e), 129.1 (CH, C^h), 129.6 (CH, C^g), 134.8 (CH, C^i), 138.6 (C, C^f), 163.6 (C, C^b). **HRMS** (ESI): m/z calcd for $\text{C}_{19}\text{H}_{17}\text{O}_8\text{S}_2^-$ ($\text{M} - \text{H}^+$): 437.0370; found 437.0372. **IR** (neat, ATR): 3101, 3067, 3010, 2956, 2361, 2339, 1743, 1584, 1448, 1434, 1328, 1263, 1232, 1152, 1129, 1084, 1062, 798, 743, 683 cm^{-1} .



7bi: $^1\text{H NMR}$ (400 MHz, CDCl_3): δ = 3.59 (s, 3 H, $\text{H}^{a'}$ or $\text{H}^{e'}$), 3.78 (s, 3 H, $\text{H}^{a'}$ or $\text{H}^{e'}$), 6.19 (d, J = 11.4 Hz, 1 H, $\text{H}^{g'}$), 6.91 (d, J = 11.4 Hz, 1 H, $\text{H}^{f'}$), 7.55–7.59 (m, 4 H, $\text{H}^{j'}$), 7.68–7.72 (m, 2 H, $\text{H}^{k'}$), 7.89–7.91 (m, 4 H, $\text{H}^{i'}$). $^{13}\text{C NMR}$ (101 MHz, CDCl_3): δ = 52.9 (CH_3 , $\text{C}^{a'}$ or $\text{C}^{e'}$), 53.2 (CH_3 , $\text{C}^{a'}$ or $\text{C}^{e'}$), 81.3 (CH, $\text{C}^{g'}$), 129.4 (CH, $\text{C}^{j'}$), 129.6 (CH, $\text{C}^{i'}$), 132.2 (CH, $\text{C}^{f'}$), 135.2 (CH, $\text{C}^{k'}$), 135.7 (C, $\text{C}^{c'}$), 137.7 (C, $\text{C}^{h'}$), 162.9 (C, $\text{C}^{b'}$ or $\text{C}^{d'}$), 163.1 (C, $\text{C}^{b'}$ or $\text{C}^{d'}$). **HRMS** (ESI): m/z calcd for $\text{C}_{19}\text{H}_{17}\text{O}_8\text{S}_2^-$ ($\text{M} - \text{H}^+$): 437.0370; found 437.0364. **IR** (neat, ATR): 3065, 2957, 1722, 1642, 1583, 1447, 1437, 1364, 1335, 1313, 1278, 1236, 1152, 1100, 1077, 1051, 911, 805, 726, 683 cm^{-1} .

Reaction of methyl diazoacetate (**1a**) with ESF (**3k**)

Methyl 1H-pyrazole-3-carboxylate (9ak) was obtained from **1a** (252 mg, 2.52 mmol) and **3k** (201 mg, 1.83 mmol) in toluene (5 mL) according to *GP A* (round bottom flask, room temperature, overnight, column chromatography on silica gel, *n*-pentane/EtOAc = 5:1 ~ 1:1): white powder (205 mg, yield 89%); mp 142.0 °C (ref. ^{S19a}: mp 140-142 °C). Spectroscopic data are consistent with those reported in literature.^{S19}

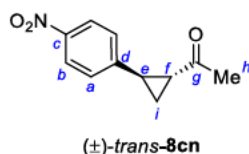


$^1\text{H NMR}$ (400 MHz, CDCl_3): δ = 3.97 (s, 3 H, H^e), 6.86 (d, J = 2.3 Hz, 1 H, H^b), 7.85 (dd, J = 2.2, 1.1 Hz, 1 H, H^a), 14.1 (br s, 1 H, NH). $^{13}\text{C NMR}$ (101 MHz, CDCl_3): δ = 52.1 (CH_3 , C^e), 107.8

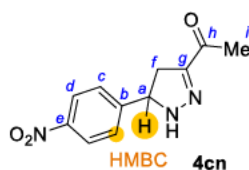
(CH, C^b), 131.7 (CH, C^a), 142.3 (C, C^c), 162.9 (C, C^d). **HRMS** (EI): m/z calcd for C₃H₆N₂O₂⁺ (M⁺): 126.0424; found 126.0424. **IR** (neat, ATR): 3128, 3032, 2959, 2882, 2835, 2758, 1731, 1461, 1422, 1369, 1307, 1220, 1197, 1190, 1157, 1097, 1058, 999, 944, 901, 803, 778, 763 cm⁻¹.

Reaction of *p*-nitrophenyldiazomethane (**1c**) with 1-butene-3-one (**3n**)

1-((1*S,2*S**)-2-(4-Nitrophenyl)cyclopropyl)ethan-1-one** ((±)-*trans*-**8cn**) and **1-(5-(4-nitrophenyl)-4,5-dihydro-1*H*-pyrazol-3-yl)ethan-1-one** (**4cn**) were obtained from **1c** (197 mg, 1.21 mmol) in dry CH₂Cl₂ (2 mL) and **3n** (103 mg, 1.47 mmol) in dry CH₂Cl₂ (0.5 mL) according to *GP B* (3 days, column chromatography on silica gel, *n*-pentane/EtOAc = 4:1 ~ 2:1): (±)-*trans*-**8cn** white solid (120 mg, yield 48%); mp 103.3 °C (ref.^{S20}: mp 98-99 °C) and **4cn** orange-red solid (72.0 mg, yield 26%); mp 136.5 °C.



trans-**8cn**: ¹H NMR (600 MHz, CDCl₃): δ = 1.44 (ddd, $J = 8.3, 6.4, 4.5$ Hz, 1 H, Hⁱ), 1.76 (ddd, $J = 9.1, 5.3, 4.6$ Hz, 1 H, Hⁱ), 2.30 (ddd, $J = 8.6, 5.4, 4.1$ Hz, 1 H, H^f), 2.34 (s, 3 H, H^h), 2.61 (ddd, $J = 9.2, 6.4, 4.0$ Hz, 1 H, H^e), 7.20–7.23 (m, 2 H, H^a), 8.13–8.16 (m, 2 H, H^b). ¹³C NMR (151 MHz, CDCl₃): δ = 20.0 (CH₂, Cⁱ), 28.3 (CH, C^e), 31.2 (CH₃, C^h), 33.5 (CH, C^f), 124.0 (CH, C^b), 126.7 (CH, C^a), 146.7 (C, C^c), 148.5 (C, C^d), 205.9 (C, C^g). **HRMS** (ED): m/z calcd for C₁₁H₁₁NO₃⁺ (M⁺): 205.0733; found 205.0732. **IR** (neat, ATR): 3110, 3081, 3003, 1923, 1691, 1600, 1509, 1397, 1341, 1316, 1193, 1180, 1172, 1109, 1018, 966, 907, 852, 818, 764, 740, 694 cm⁻¹.



4cn: ¹H NMR (600 MHz, CDCl₃): δ = 2.45 (s, 3 H, Hⁱ), 2.81 (dd, $J = 17.3, 10.0$ Hz, 1 H, H^f), 3.41 (dd, $J = 17.3, 12.1$ Hz, 1 H, H^f), 5.11 (ddd, $J = 12.0, 9.9, 2.0$ Hz, 1 H, H^a), 6.58 (br s, 1 H, NH), 7.47–7.49 (m, 2 H, H^c), 8.21–8.23 (m, 2 H, H^d). ¹³C NMR (151 MHz, CDCl₃): δ = 25.7 (CH₃, Cⁱ), 38.8 (CH₂, C^f), 65.1 (CH, C^a), 124.4 (CH, C^d), 127.4 (CH, C^c), 147.9 (C, C^e), 148.7 (C, C^b), 149.9 (C, C^g), 194.4 (C, C^h). The structure of **4cn** in chloroform solution was assigned because of the correlation of H^a with C^c in the HMBC spectrum. **HRMS** (EI): m/z calcd for C₁₁H₁₁N₃O₃⁺ (M⁺): 233.0795; found 233.0798. **IR** (neat, ATR): 3315, 3069, 1646, 1606, 1539, 1518, 1448, 1414, 1339, 1280, 1239, 1171, 1101, 1084, 1014, 982, 949, 938, 869, 858, 837, 750, 721, 698, 658 cm⁻¹.

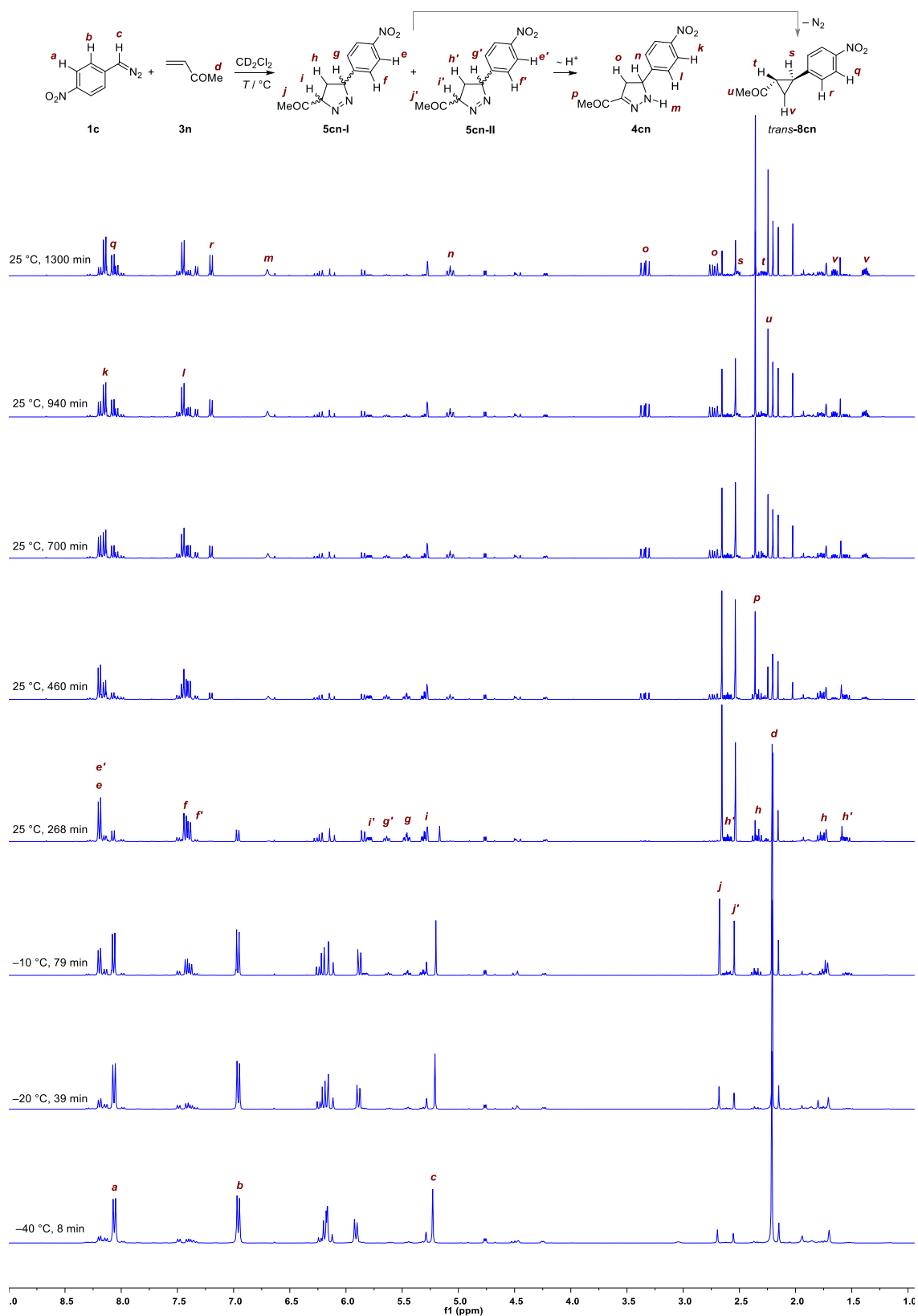
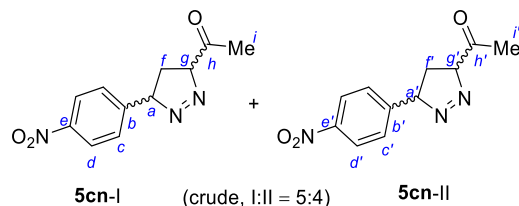


Figure S3. 1H NMR (400 MHz) monitoring of the reaction of **1c** (0.233 M) with **3n** (0.258 M) in CD_2Cl_2 at -40 to 25 °C.

NMR monitoring of the reaction of **1c** (0.233 M) and **3n** (0.258 M) in CD₂Cl₂ at -40 °C to ambient temperature suggested the initial formation of a diastereomeric mixture of the 3*H*-pyrazoles **5cn-I** and **5cn-II** (I:II = 5:4), which underwent proton shift to give the isolated 1*H*-pyrazole **4cn** as well as elimination of N₂ to furnish the cyclopropane **8cn** (Figure S3).

The structures of intermediate **5cn-I** and **5cn-II** were assigned on the basis of additional 2D NMR spectra.



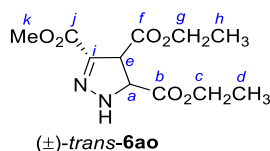
5cn-I: ¹H NMR (400 MHz, CD₂Cl₂): δ = 1.79–1.84 (m, 1 H, H^f), 2.38 (dt, *J* = 13.2, 9.1 Hz, 1 H, H^f), 2.70 (s, 3 H, Hⁱ), 5.31–5.37 (m, 1 H, H^g, superimposed with solvent peak), 5.50 (td, *J* = 9.4, 3.0 Hz, 1 H, H^a), 7.47 (d, *J* = 8.4 Hz, 2 H, H^c), 8.23 (d, *J* = 8.5 Hz, 2 H, H^d, superimposed with H^d). ¹³C NMR (at -40 °C, 101 MHz, CD₂Cl₂): δ = 25.9 (CH₂, C^f), 30.0 (CH₃, Cⁱ), 91.5 (CH, C^a), 99.9 (CH, C^g), 124.0 (CH, C^d), 128.4 (CH, C^c), 145.6 (C, C^b), 147.2 (C, C^e), 201.6 (C, C^h).

5cn-II: ¹H NMR (400 MHz, CD₂Cl₂): δ = 1.60 (ddd, = 13.3, 9.7, 7.7 Hz, 0.7 H, H^f, superimposed with resonance of residue H₂O), 2.58 (s, 2.2 H, Hⁱ), 2.61–2.68 (m, 0.8 H, H^f), 5.65–5.70 (m, 0.7 H, H^g), 5.81–5.85 (m, 0.7 H, H^a), 7.44 (d, *J* = 8.5 Hz, 1.5 H, H^c), 8.23 (d, *J* = 8.5 Hz, 1.4 H, H^d, superimposed with H^d). ¹³C NMR (at -40 °C, 101 MHz, CD₂Cl₂): δ = 26.1 (CH₂, C^f), 29.96 (CH₃, Cⁱ), 91.3 (CH, C^a), 99.7 (CH, C^g), 124.04 (CH, C^d), 128.1 (CH, C^c), 145.7 (C, C^b), 147.1 (C, C^e), 200.1 (C, C^h).

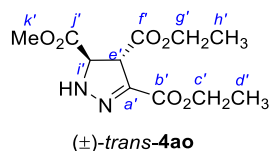
Reaction of methyl diazoacetate (**1a**) with diethyl fumarate (**3o**)

4,5-Diethyl 3-methyl (4*S,5*R**)-4,5-dihydro-1*H*-pyrazole-3,4,5-tricarboxylate (±)-*trans*-(**6ao**)** and **3,4-diethyl 5-methyl (4*R**,5*S**)-4,5-dihydro-1*H*-pyrazole-3,4,5-tricarboxylate (±)-*trans*-(**4ao**)** were obtained from **1a** (202 mg, 2.02 mmol) and **3o** (294 mg, 1.71 mmol) in toluene (0.5 mL) as a mixture (**6ao**:**4ao** = 5:2, NMR integration) according to *GP A* (sealed GC vial, 50 °C, 3 days, column chromatography on silica gel, *n*-pentane/EtOAc = 5:1–2:1): white solid (385 mg, yield 82%).

Pure *trans*-**6ao** (white needles, 135 mg, yield 13%) was obtained by repeated (6×) recrystallization from EtOH of the 937 mg (yield 86%) product isolated from another batch of the reaction of **1a** (410 mg, 4.00 mmol) and **3o** (843 mg, 4.90 mmol) (neat, 50 °C, 44 h, column chromatography on silica gel, *n*-pentane/EtOAc = 2:1). mp 97.9 °C



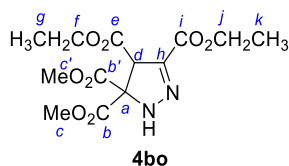
trans-**6ao**: $^1\text{H NMR}$ (400 MHz, CDCl_3): $\delta = 1.26\text{--}1.32$ (m, 6 H, H^{d} and H^{h}), 3.85 (s, 3 H, H^{k}), 4.20–4.27 (m, 4 H, H^{c} and H^{g}), 4.42 (d, $J = 5.3$ Hz, 1 H, H^{e}), 4.75 (d, $J = 5.4$ Hz, 1 H, H^{a}), 6.80 (br s, 1 H, NH). $^{13}\text{C NMR}$ (101 MHz, CDCl_3): $\delta = 14.1$ (CH_3 , C^{h}), 14.2 (CH_3 , C^{d}), 52.5 (CH_3 , C^{e}), 52.6 (CH , C^{k}), 62.4 (CH_2 , C^{c}), 62.8 (CH_2 , C^{g}), 66.3 (CH , C^{a}), 140.0 (C, C^{i}), 161.8 (C, C^{j}), 169.1 (C, C^{b}), 169.9 (C, C^{f}). The structure of **6ao** in chloroform solution was assigned on the fundament of the correlation of H^{k} and C^{i} in HMBC and the low chemical shift of C^{j} (161.8 ppm) due to conjugation with the double bond. **HRMS** (ESI $^+$): m/z calcd for $\text{C}_{11}\text{H}_{17}\text{N}_2\text{O}_6^+$ ($\text{M} + \text{H}^+$): 273.1081; found 273.1082. **IR** (neat, ATR): 3289, 2962, 1732, 1701, 1561, 1447, 1369, 1342, 1313, 1272, 1222, 1183, 1112, 1030, 981, 866, 820, 765 cm^{-1} . **Single crystal X-ray crystallography** (*trans*-**6ao**): $\text{C}_{11}\text{H}_{16}\text{N}_2\text{O}_6$ (av017).



trans-**4ao** (from the NMR spectra of the 5:2 mixture of **6ao/4ao**): $^1\text{H NMR}$ (400 MHz, CDCl_3): $\delta = 1.26\text{--}1.36$ (m, 2.6 H, $\text{H}^{\text{d}'}$ and $\text{H}^{\text{h}'}$, superimposed with H^{d} and H^{h} of *trans*-**6ao**), 3.80 (s, 1.2 H, $\text{H}^{\text{k}'}$), 4.20–4.34 (m, 1.7 H, $\text{H}^{\text{c}'}$ and $\text{H}^{\text{g}'}$, superimposed with H^{c} and H^{g} of *trans*-**6ao**), 4.42 (d, $J = 5.3$ Hz, 0.4 H, $\text{H}^{\text{e}'}$, superimposed with H^{e} of *trans*-**6ao**), 4.77 (d, $J = 6.0$ Hz, 0.4 H, $\text{H}^{\text{a}'}$, superimposed with H^{a} of *trans*-**6ao**), 6.78 (s, 0.4 H, NH). $^{13}\text{C NMR}$ (101 MHz, CDCl_3): $\delta = 14.1$ (CH_3 , $\text{C}^{\text{h}'}$, superimposed with C^{h} of *trans*-**6ao**), 14.3 (CH_3 , $\text{C}^{\text{d}'}$), 52.6 (CH , $\text{C}^{\text{e}'}$), 53.4 (CH_3 , $\text{C}^{\text{k}'}$), 61.7 (CH_2 , $\text{C}^{\text{c}'}$), 62.4 (CH_2 , $\text{C}^{\text{g}'}$, superimposed with C^{c} of *trans*-**6ao**), 66.2 (CH , $\text{C}^{\text{i}'}$), 140.4 (C, $\text{C}^{\text{a}'}$), 161.3 (C, $\text{C}^{\text{b}'}$), 169.1 (C, $\text{C}^{\text{f}'}$), 170.5 (C, $\text{C}^{\text{j}'}$). A pure sample of *trans*-**4ao** was characterized as *trans*-**4as** (from the reaction of **1a** with **3s**, see below).

Reaction of dimethyl diazomalonate (**1b**) with diethyl fumarate (**3o**)

4,5-Diethyl 3,3-dimethyl 2,4-dihydro-3H-pyrazole-3,3,4,5-tetracarboxylate (4bo) was obtained from **1b** (188 mg, 1.19 mmol) and **3o** (244 mg, 1.42 mmol) according to *GP A* (neat, sealed GC vial, 90 °C, 11 days, column chromatography on silica gel, *n*-pentane/EtOAc = 5:1–1:1): colorless crystals (282 mg, yield 71%); mp 85.4 °C.

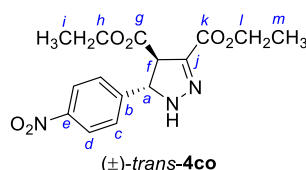


$^1\text{H NMR}$ (400 MHz, CDCl_3): $\delta = 1.27\text{--}1.34$ (m, 6 H, H^{g} and H^{k}), 3.77 (s, 3 H, H^{c} or $\text{H}^{\text{c}'}$), 3.85 (s, 3 H, H^{c} or $\text{H}^{\text{c}'}$), 4.20 (q, $J = 7.1$ Hz, 2 H, H^{f}), 4.27–4.32 (m, 2 H, H^{j}), 4.87 (d, $J = 1.0$ Hz, 1 H, H^{d}), 7.04 (br s, 1 H, NH). $^{13}\text{C NMR}$ (101 MHz, CDCl_3): $\delta = 14.1$ (CH_3 , C^{g} or C^{k}), 14.3 (CH_3 , C^{g} or C^{k}), 53.9 (CH_3 , C^{c} or $\text{C}^{\text{c}'}$), 54.3 (CH_3 , C^{c} or $\text{C}^{\text{c}'}$), 56.3 (CH , C^{d}), 61.9 (CH_2 , C^{j}), 62.4 (CH_2 , C^{f}), 78.9 (C, C^{a}), 140.9 (C, C^{h}), 160.7 (C, C^{i}), 166.80 (C, C^{b} or $\text{C}^{\text{b}'}$), 166.83 (C, C^{b} or $\text{C}^{\text{b}'}$), 167.7 (C, C^{e}). **HRMS** (EI): m/z calcd for $\text{C}_{13}\text{H}_{18}\text{N}_2\text{O}_8^+$ (M^+): 330.1058; found 330.1055. **IR** (neat, ATR):

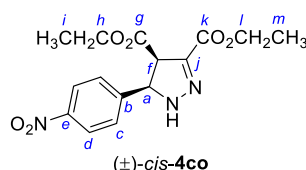
3329, 3310, 2983, 2954, 1733, 1708, 1592, 1476, 1437, 1374, 1341, 1284, 1252, 1218, 1178, 1156, 1133, 1093, 1070, 1039, 1028, 947, 931, 837, 784, 715, 688 cm^{-1} .

Reaction of *p*-nitrophenyldiazomethane (1c) with diethyl fumarate (3o)

Diethyl (4*S**,5*R**)-5-(4-nitrophenyl)-4,5-dihydro-1*H*-pyrazole-3,4-dicarboxylate (\pm)-*trans*-4co) and diethyl (4*S**,5*S**)-5-(4-nitrophenyl)-4,5-dihydro-1*H*-pyrazole-3,4-dicarboxylate (\pm)-*cis*-4co) were obtained from 1c (200 mg, 1.23 mmol) in dry CH_2Cl_2 (2.5 mL) and 3o (221 mg, 1.28 mmol) in dry CH_2Cl_2 (0.5 mL) according to *GP B* (27 hours, column chromatography on silica gel, *n*-pentane/EtOAc = 5:1–2:1): *trans*-4co yellow solid (253 mg, yield 61%); mp 113.8 °C and *cis*-4co light-yellow solid (75 mg, yield 18%); mp 117.0 °C.



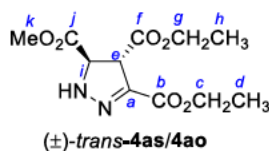
trans-4co: $^1\text{H NMR}$ (400 MHz, CDCl_3): δ = 1.29 (t, J = 7.1 Hz, 3 H, H^i), 1.34 (t, J = 7.1 Hz, 3 H, H^m), 3.95 (d, J = 10.3 Hz, 1 H, H^f), 4.24–4.35 (m, 4 H, H^h and H^l), 5.36 (dd, J = 10.4 Hz, 1.9 Hz, 1 H, H^a), 6.64 (br s, 1 H, NH), 7.50–7.53 (m, 2 H, H^c), 8.22–8.26 (m, 2 H, H^d). $^{13}\text{C NMR}$ (101 MHz, CDCl_3): δ = 14.2 (CH_3 , C^i), 14.3 (CH_3 , C^m), 58.7 (CH, C^f), 61.8 (CH_2 , C^l), 62.4 (CH_2 , C^h), 69.7 (CH, C^a), 124.5 (CH, C^d), 127.5 (CH, C^c), 139.3 (C, C^j), 146.5 (C, C^b), 148.2 (C, C^e), 161.5 (C, C^k), 169.9 (C, C^g). **HRMS** (EI): m/z calcd for $\text{C}_{15}\text{H}_{17}\text{N}_3\text{O}_6^+$ (M^+): 335.1112; found 335.1111. **IR** (neat, ATR): 3518, 3357, 3110, 3083, 2982, 2940, 1725, 1700, 1605, 1572, 1514, 1428, 1341, 1290, 1222, 1189, 1136, 1108, 1053, 1027, 981, 921, 858, 844, 756, 724, 710 cm^{-1} .



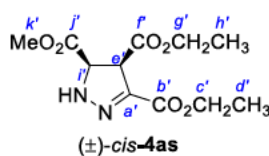
cis-4co: $^1\text{H NMR}$ (400 MHz, CDCl_3): δ = 0.86 (t, J = 7.1 Hz, 3 H, H^i), 1.35 (t, J = 7.1 Hz, 3 H, H^m), 3.65–3.79 (m, 2 H, H^h), 4.30–4.36 (m, 2 H, H^l), 4.39 (d, J = 13.0 Hz, 1 H, H^f), 5.46 (dd, J = 13.0, 2.4 Hz, 1 H, H^a), 6.56 (s, 1 H, NH), 7.56 (d, J = 8.7 Hz, 2 H, H^c), 8.21 (d, J = 8.7 Hz, 2 H, H^d). $^{13}\text{C NMR}$ (101 MHz, CDCl_3): δ = 13.9 (CH_3 , C^i), 14.4 (CH_3 , C^m), 55.2 (CH, C^f), 61.5 (CH_2 , C^h), 61.8 (CH_2 , C^l), 67.5 (CH, C^a), 123.8 (CH, C^d), 128.8 (CH, C^c), 140.3 (C, C^j), 143.3 (C, C^b), 148.2 (C, C^e), 161.7 (C, C^k), 167.2 (C, C^g). **HRMS** (EI): m/z calcd for $\text{C}_{15}\text{H}_{17}\text{N}_3\text{O}_6^+$ (M^+): 335.1112; found 335.1112. **IR** (neat, ATR): 3292, 2981, 2940, 1732, 1702, 1607, 1571, 1520, 1468, 1430, 1343, 1295, 1221, 1200, 1105, 1059, 1020, 914, 871, 852, 822, 775, 753, 734, 693 cm^{-1} .

Reaction of methyl diazoacetate (1a) with diethyl maleate (3s)

3,4-Diethyl 5-methyl (4*R,5*S**)-4,5-dihydro-1*H*-pyrazole-3,4,5-tricarboxylate (±)-*trans*-4as** (= (±)-*trans*-4ao, white solid, 350 mg, 76%) and a mixture of *cis*-4as and *cis*-6as (colorless oil, *cis*-4as: *cis*-6as = 5:4, total yield 8.9%) were obtained from **1a** (203 mg, 2.03 mmol) and **3s** (291 mg, 1.69 mmol) in toluene (0.5 mL) according to *GP A* (sealed GC vial, 50 °C, 5 days, column chromatography on silica gel, *n*-pentane/EtOAc = 1:1); mp (*trans*-4as) 58.6 °C.



trans-4as: $^1\text{H NMR}$ (400 MHz, CDCl_3): δ = 1.27 (t, J = 7.1 Hz, 3 H, H^{h}), 1.34 (t, J = 7.2 Hz, 3 H, H^{d}), 3.80 (s, 3 H, H^{k}), 4.19–4.25 (m, 2 H, H^{g}), 4.31 (q, J = 7.2 Hz, 2 H, H^{c}), 4.42 (d, J = 5.3 Hz, 1 H, H^{e}), 4.77 (d, J = 5.3 Hz, 1 H, H^{f}), 6.79 (br s, 1 H, NH). $^{13}\text{C NMR}$ (101 MHz, CDCl_3): δ = 14.1 (CH_3 , C^{h}), 14.3 (CH_3 , C^{d}), 52.6 (CH, C^{e}), 53.4 (CH, C^{k}), 61.7 (CH_2 , C^{c}), 62.4 (CH_2 , C^{g}), 66.2 (CH, C^{i}), 140.4 (C, C^{a}), 161.3 (C, C^{b}), 169.1 (C, C^{f}), 170.5 (C, C^{j}). **HRMS** (ESI^+): m/z calcd for $\text{C}_{11}\text{H}_{17}\text{N}_2\text{O}_6^+$ ($\text{M} + \text{H}^+$): 273.1080; found 273.1081. **IR** (neat, ATR): 3286, 2987, 2951, 1730, 1695, 1549, 1440, 1374, 1337, 1309, 1214, 1185, 1128, 1023, 968, 797, 770 cm^{-1} . **Single crystal X-ray crystallography** (*trans*-4as): $\text{C}_{11}\text{H}_{16}\text{N}_2\text{O}_6$ (av173).



cis-4as (based on the NMR spectra of the mixture of *cis*-4as and *cis*-6as): $^1\text{H NMR}$ (400 MHz, CDCl_3): δ = 1.23–1.28 (m, 3 H, H^{h} , superimposed with $\text{H}^{\text{d}'}$ and $\text{H}^{\text{h}'}$ of *cis*-6as), 1.30 (t, J = 7.1 Hz, 3 H, H^{d}), 3.72 (s, 3 H, H^{k}), 4.08–4.30 (m, 4 H, H^{c} and H^{g} , superimposed with $\text{H}^{\text{c}'}$ and $\text{H}^{\text{g}'}$ of *cis*-6as), 4.33 (d, J = 13.0 Hz, 1 H, H^{e} , superimposed with $\text{H}^{\text{e}'}$ of *cis*-6as), 4.78 (dd, J = 13.0, 0.8 Hz, 1 H, H^{f}), 6.67 (s, 1 H, NH). $^{13}\text{C NMR}$ (101 MHz, CDCl_3): δ = 14.1 (CH_3 , C^{h}), 14.2 (CH_3 , C^{d}), 52.9 (CH, C^{e}), 53.0 (CH_3 , C^{k}), 61.7 (CH_2 , C^{c}), 62.0 (CH_2 , C^{g}), 65.1 (CH, C^{i}), 140.4 (C, C^{a}), 161.2 (C, C^{b}), 168.1 (C, C^{f}), 169.5 (C, C^{j}).



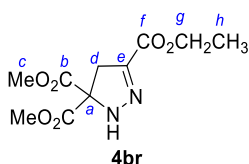
cis-6as (based on the NMR spectra of the mixture of *cis*-4as and *cis*-6as): $^1\text{H NMR}$ (400 MHz, CDCl_3): δ = 1.23–1.28 (m, 5.5 H, $\text{H}^{\text{d}'}$ and $\text{H}^{\text{h}'}$, superimposed with H^{h} of *cis*-4as), 3.80 (s, 2.5 H, H^{k}), 4.08–4.30 (m, 3.9 H, $\text{H}^{\text{c}'}$ and $\text{H}^{\text{g}'}$, superimposed with H^{c} and H^{g} of *cis*-4as), 4.31 (d, J = 13.0 Hz, 0.9 H, $\text{H}^{\text{e}'}$, superimposed with H^{e} of *cis*-4as), 4.76 (dd, J = 13.1, 0.9 Hz, 0.9 H, H^{f}), 6.69 (br s, 0.8 H, NH). $^{13}\text{C NMR}$ (101 MHz, CDCl_3): δ = 14.0 (CH_3 , $\text{C}^{\text{d}'}$ or $\text{C}^{\text{h}'}$), 14.1 (CH_3 , $\text{C}^{\text{d}''}$ or $\text{C}^{\text{h}''}$), 52.5 (CH_3 , $\text{C}^{\text{k}''}$), 52.8 (CH, $\text{C}^{\text{e}''}$), 62.0 (CH_2 , $\text{C}^{\text{g}''}$), 62.4 (CH_2 , $\text{C}^{\text{c}''}$), 65.0 (CH, $\text{C}^{\text{a}''}$), 140.0 (C, $\text{C}^{\text{i}''}$), 161.7 (C, $\text{C}^{\text{j}''}$), 168.0 (C, $\text{C}^{\text{f}''}$), 169.0 (C, $\text{C}^{\text{b}''}$).

Reaction of dimethyl diazomalonate (1b) with diethyl maleate (3s)

4bs (=4bo) (30.3 mg, yield 11%) was also obtained from **1b** (130 mg, 0.82 mmol) and **3s** (137 mg, 0.80 mmol) in d_8 -toluene:mesitylene = 1:1 (350 μ L) according to *GP A* (sealed NMR tube, 85 °C, 137 days, conversion ratio 60%, 1,1,2,2-tetrachloroethane as internal standard, column chromatography on silica gel: *n*-pentane/EtOAc = 5:1–1:1).

Reaction of dimethyl diazomalonate (1b) with ethyl acrylate (3r)

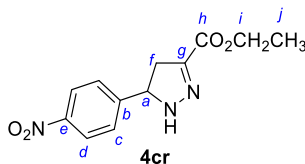
5-Ethyl 3,3-dimethyl 2,4-dihydro-3H-pyrazole-3,3,5-tricarboxylate (4br) was obtained from **1b** (711 mg, 4.50 mmol) and **3r** (300 mg, 3.00 mmol) in d_8 -toluene: mesitylene = 1:1 (200 μ L) according to *GP A* (sealed NMR tube, 30 mg hydroquinone, 50 °C, 45 days, column chromatography on silica gel, *n*-pentane/EtOAc = 5:1–1:1): colorless oil (577 mg, yield 74%). Isolated **4br** decomposed at room temperature upon exposure to air.



¹H NMR (400 MHz, CDCl₃): δ = 1.33 (t, J = 7.1 Hz, 3 H, H^h), 3.58 (s, 2 H, H^d), 3.81 (s, 6 H, H^c), 4.29 (q, J = 7.1 Hz, 2 H, H^e), 7.07 (br s, 1 H, NH). **¹³C NMR** (101 MHz, CDCl₃): δ = 14.3 (CH₃, C^h), 39.1 (CH₂, C^d), 53.9 (CH₃, C^c), 61.7 (CH₂, C^g), 75.2 (C, C^a), 116.2 (residue hydroquinone), 143.0 (C, C^e), 161.5 (C, C^f), 168.6 (C, C^b). **HRMS** (ESI⁺): m/z calcd for C₁₀H₁₅N₂O₆⁺ (M + H⁺): 259.0925; found 259.0926. **IR** (neat, ATR): 3338, 2985, 2959, 1736, 1707, 1435, 1288, 1240, 1153, 1129, 1061, 1046, 828, 778, 751 cm⁻¹.

Reaction of *p*-nitrophenyldiazomethane (1c) with ethyl acrylate (3r)

Ethyl 5-(4-nitrophenyl)-4,5-dihydro-1H-pyrazole-3-carboxylate (4cr) was obtained from **1c** (146 mg, 0.89 mmol) in dry CH₂Cl₂ (1.5 mL) and **3r** (113 mg, 1.13 mmol) in dry CH₂Cl₂ (0.5 mL) according to *GP B* (21 hours, column chromatography on silica gel, *n*-pentane/diethyl ether = 1:2–diethyl ether): yellow solid (156 mg, yield 66%); mp 137.8 °C. **4cr** decomposed at room temperature upon exposure to air.

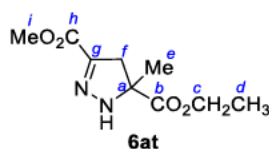


¹H NMR (400 MHz, CDCl₃): δ = 1.36 (t, J = 7.1 Hz, 3 H, H^j), 2.89 (dd, J = 17.3, 10.3 Hz, 1 H, H^f), 3.48 (dd, J = 17.3, 11.9 Hz, 1 H, H^f), 4.32 (q, J = 7.2 Hz, 2 H, Hⁱ), 5.13 (dd, J = 11.9, 10.3 Hz,

1 H, H^a), 7.49–7.53 (m, 2 H, H^c), 8.21–8.24 (m, 2 H, H^d). ¹³C NMR (101 MHz, CDCl₃): δ = 14.3 (CH₃, C^j), 40.3 (CH₂, C^f), 61.4 (CH₂, Cⁱ), 64.8 (CH, C^a), 124.2 (CH, C^d), 127.3 (CH, C^c), 141.8 (C, C^g), 147.7 (C, C^e), 148.7 (C, C^b), 162.3 (C, C^h). HRMS (ESI⁺): *m/z* calcd for C₁₂H₁₄N₃O₄⁺ (M + H⁺): 264.0979; found 264.0983. IR (neat, ATR): 3321, 3113, 2991, 2950, 2901, 1682, 1606, 1559, 1524, 1480, 1443, 1420, 1384, 1341, 1330, 1279, 1224, 1147, 1087, 1027, 1009, 854, 764, 659 cm⁻¹.

Reaction of methyl diazoacetate (1a) with methyl methacrylate (3t)

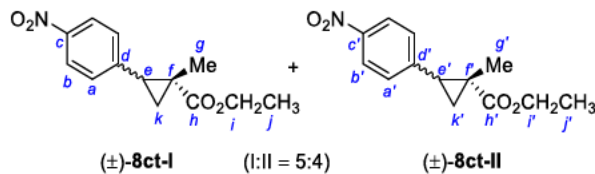
5-Ethyl 3-methyl 5-methyl-4,5-dihydro-1H-pyrazole-3,5-dicarboxylate (6at) was obtained from **1a** (206 mg, 2.06 mmol) and **3t** (232 mg, 2.03 mmol) in toluene (0.5 mL) according to *GP A* (sealed GC vial, 50 °C, 4 days, column chromatography on silica gel, *n*-pentane/EtOAc = 5:1–2:1): colorless oil (348 mg, yield 80%).



¹H NMR (400 MHz, CDCl₃): δ = 1.28 (t, *J* = 7.1 Hz, 3 H, H^d), 1.54 (s, 3 H, H^e), 2.80 (d, *J* = 17.6 Hz, 1 H, H^f), 3.50 (d, *J* = 17.6 Hz, 1 H, H^f), 3.82 (s, 3 H, Hⁱ), 4.20 (q, *J* = 7.1 Hz, 2 H, H^c), 6.70 (br s, 1 H, NH). ¹³C NMR (101 MHz, CDCl₃): δ = 14.2 (CH₃, C^d), 24.3 (CH₃, C^e), 41.2 (CH₂, C^f), 52.4 (CH₃, Cⁱ), 62.2 (CH₂, C^c), 69.9 (C, C^a), 142.4 (C, C^g), 162.7 (C, C^h), 173.9 (C, C^b). HRMS (ESI⁺): *m/z* calcd for C₉H₁₄N₂NaO₄⁺ (M + H⁺): 237.0846; found 237.0846. IR (neat, ATR): 3336, 2983, 2955, 1728, 1701, 1566, 1444, 1408, 1374, 1344, 1248, 1180, 1145, 1115, 1091, 1018, 970, 859, 791, 767, 750 cm⁻¹.

Reaction of *p*-nitrophenyldiazomethane (1c) with methyl methacrylate (3t)

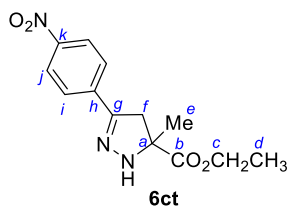
Ethyl-1-methyl-2-(4-nitrophenyl)cyclopropane-1-carboxylate (±)-(8ct) and a mixture of two diastereomers (I:II = 5:4, NMR integration) and **ethyl 5-methyl-3-(4-nitrophenyl)-4,5-dihydro-1H-pyrazole-5-carboxylate (6ct)** were obtained from **1c** (190 mg, 1.16 mmol) and **3t** (172 mg, 1.51 mmol) in dry CH₂Cl₂ (1 mL) according to *GP B* (15 h, column chromatography on silica gel, *n*-pentane/diethyl ether = 10:1–2:1): **8ct** light-yellow oil (142 mg, yield 49%), **6ct** yellow solid (125 mg, yield 39%); mp 83.4 °C.



8ct-I: ¹H NMR (400 MHz, CDCl₃): δ = 0.99 (s, 3 H, H^g), 1.22–1.27 (m, 1 H, H^k, superimposed with H^k of **8ct-II**), 1.29 (t, *J* = 7.1 Hz, 3 H, Hⁱ), 1.78 (dd, *J* = 9.0, 4.8 Hz, 1 H, H^k), 2.87 (dd, *J* =

8.7, 7.3 Hz, 1 H, H^e), 4.19 (q, $J = 7.1$ Hz, 2 H, Hⁱ), 7.34–7.39 (m, 2 H, H^a, superimposed with H^{a'} of **8ct-II**), 8.15–8.18 (m, 2 H, H^b). ¹³C NMR (101 MHz, CDCl₃): $\delta = 14.4$ (CH₃, C^j), 14.6 (CH₃, C^g), 20.4 (CH₂, C^k), 26.1 (C, C^f), 31.1 (CH, C^e), 61.3 (CH₂, Cⁱ), 123.6 (CH, C^b), 130.2 (CH, C^a), 145.2 (C, C^d), 146.9 (C, C^c), 174.8 (C, C^h).

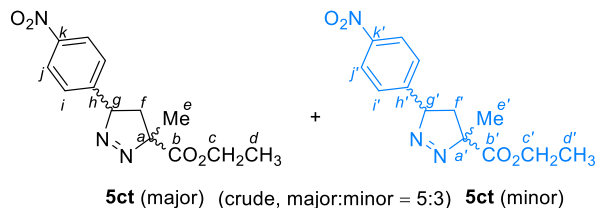
8ct-II: ¹H NMR (400 MHz, CDCl₃): $\delta = 0.90$ (t, $J = 7.1$ Hz, 2.4 H, Hⁱ), 1.22–1.27 (0.9 H, H^k, superimposed with H^k of **8ct-I**), 1.52 (s, 2.4 H, H^g), 2.00 (dd, $J = 7.3, 5.2$ Hz, 0.8 H, H^k), 2.38 (t, $J = 7.9$ Hz, 0.8 H, H^e), 3.75–3.87 (m, 1.6 H, Hⁱ), 7.34–7.39 (m, 1.6 H, H^{a'}, superimposed with H^a of **8ct-I**), 8.10–8.13 (m, 1.6 H, H^b). ¹³C NMR (101 MHz, CDCl₃): $\delta = 14.1$ (CH₃, C^j), 19.6 (CH₂, C^k), 21.4 (CH₃, C^g), 28.9 (CH, C^f), 33.4 (CH, C^e), 60.7 (CH₂, Cⁱ), 123.2 (CH, C^b), 130.1 (CH, C^a), 145.4 (C, C^d), 146.7 (C, C^c), 171.9 (C, C^h).



¹H NMR (400 MHz, CDCl₃): $\delta = 1.30$ (t, $J = 7.1$ Hz, 3 H, H^d), 1.62 (s, 3 H, H^e), 2.93 (d, $J = 16.7$ Hz, 1 H, H^f), 3.67 (d, $J = 16.7$ Hz, 1 H, H^f), 4.22 (q, $J = 7.1$ Hz, 2 H, H^c), 6.57 (br s, 1 H, NH), 7.75 (d, $J = 8.9$ Hz, 2 H, Hⁱ), 8.21 (d, $J = 8.6$ Hz, 2 H, H^j). ¹³C NMR (101 MHz, CDCl₃): $\delta = 14.2$ (CH₃, C^d), 24.4 (CH₃, C^e), 42.0 (CH₂, C^f), 62.3 (CH₂, C^c), 69.3 (C, C^a), 124.0 (CH, C^j), 126.5 (CH, Cⁱ), 138.8 (C, C^h), 147.6 (C, C^k), 149.1 (C, C^g), 174.7 (C, C^b). HRMS (ESI⁺): m/z calcd for C₁₃H₁₆N₃O₄⁺ (M + H⁺): 278.1135; found 278.1136. IR (neat, ATR): 3322, 2974, 2931, 2872, 1720, 1596, 1564, 1508, 1425, 1342, 1305, 1251, 1201, 1133, 1112, 1069, 1019, 857, 844, 836, 770, 752, 688 cm⁻¹.

By NMR monitoring of the reaction of **1c** with **3t**, formation of a diastereomeric mixture of **5ct** (major:minor = 5:3) was observed at the initial stages of the reaction, which furnished **8ct** by elimination of N₂ (Figure S4). The 1H-pyrazole **6ct** resulted probably from tautomerization of **5ct** upon work up by column chromatography. The structures of **5ct**-major and **5ct**-minor were assigned on the basis of 2D NMR spectra.

The NMR spectra for the structural assignment of **5ct** were measured for the reaction of **1c** (30.0 mg, 0.184 mM) with **3t** (25.0 mg, 0.219 mM) in CD₂Cl₂ (500 μ L) after 5 hours at ambient temperature.



NMR data assigned to **5ct**: ¹H NMR (400 MHz, CDCl₃): $\delta = 1.27$ – 1.30 (m, 11.9 H, H^d, H^{d'} and

H^f , superimposed with resonances of OCH_3 of **3v**), 1.54 (s, 3 H, H^e), 1.80 (s, 1.7 H, H^e), 1.97 (dd, $J = 13.1, 9.0$ Hz, 1 H, H^f), 2.21 (dd, $J = 13.1, 8.9$ Hz, 1 H, H^f), 2.81 (dd, $J = 13.2, 8.8$ Hz, 0.6 H, H^f), 4.18–4.28 (m, 3.8 H, H^c and H^c), 5.68–5.74 (m, 1.5 H, H^g and H^g), 7.48–7.51 (m, 3 H, H^i and H^i), 8.22–8.27 (m, 3 H, H^j and H^j). ^{13}C NMR (101 MHz, $CDCl_3$): $\delta = 14.2$ (CH_3 , C^d and $C^{d'}$), 20.9 (CH_3 , C^e), 22.8 (CH_3 , $C^{e'}$), 36.9 (CH_2 , C^f), 38.2 (CH_2 , $C^{f'}$), 62.45 (CH_2 , C^c), 62.48 (CH_2 , $C^{c'}$), 91.6 (CH , C^g), 92.9 (CH , $C^{g'}$), 96.7 (C, C^a), 97.3 (C, $C^{a'}$), 124.3 (CH, C^j), 124.4 (CH, $C^{j'}$), 128.4 (CH, C^i), 128.7 (CH, C^i), 145.9 (C, C^h), 146.4 (C, $C^{h'}$), 147.95 (C, C^k), 147.99 (C, C^k), 169.8 (C, C^b), 171.0 (C, C^b).

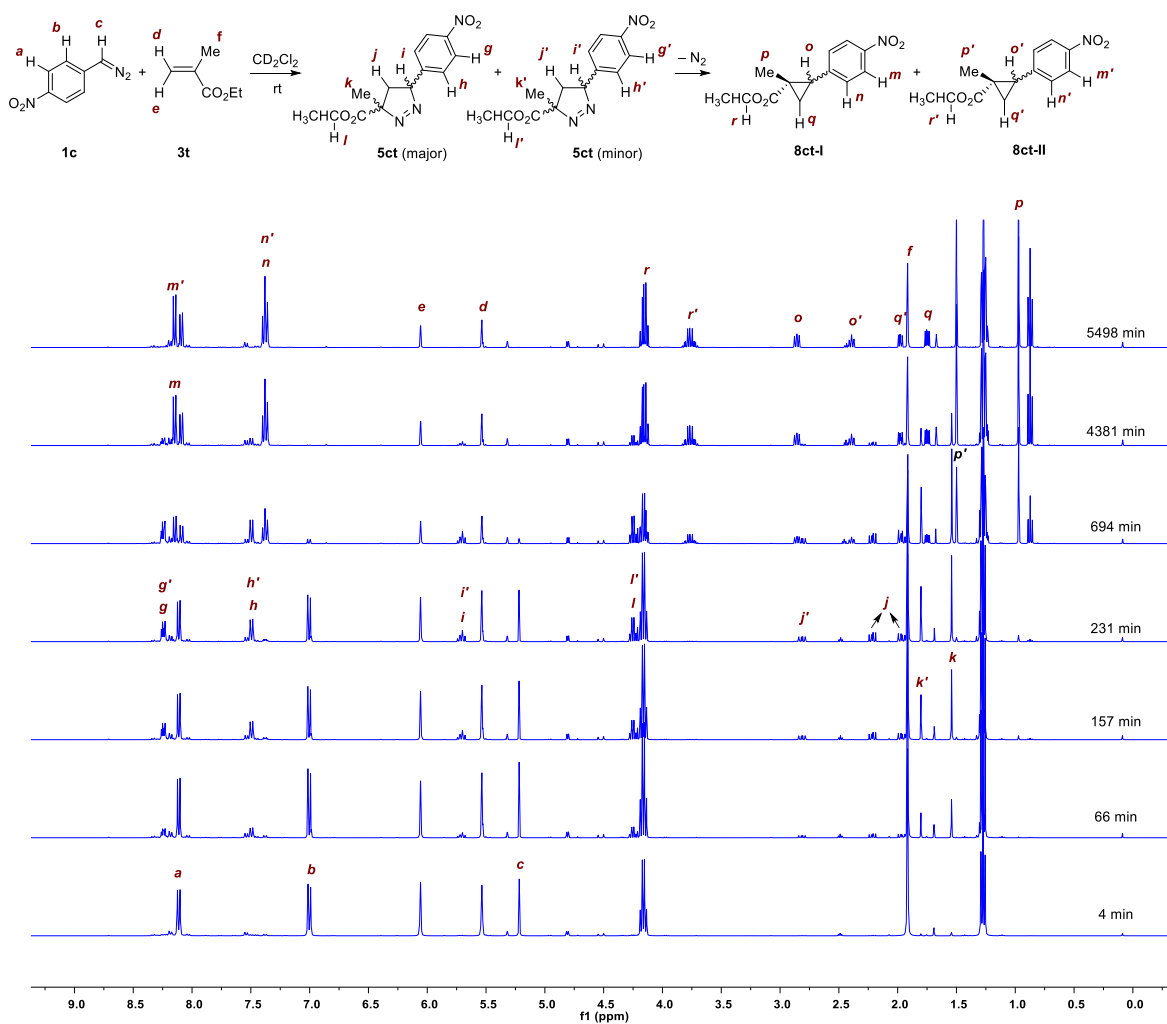
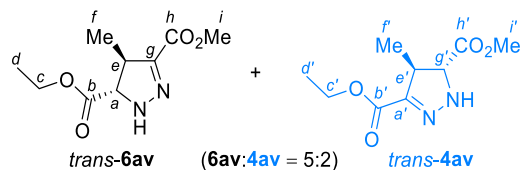


Figure S4. 1H NMR (400 MHz) monitoring of the reaction of **1c** (0.330 M) with **3t** (0.393 M) in CD_2Cl_2 at ambient temperature.

Reaction of methyl diazoacetate (**1a**) with ethyl (*E*)-crotonate (**3v**)

5-Ethyl 3-methyl (4*S,5*R**)-4-methyl-4,5-dihydro-1*H*-pyrazole-3,5-dicarboxylate (±)-*trans*-**

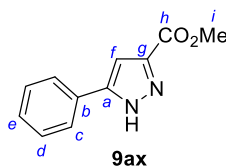
(**6av**) and **3-ethyl 5-methyl (4S*,5R*)-4-methyl-4,5-dihydro-1H-pyrazole-3,5-dicarboxylate** (\pm)-*trans*-(**4av**) were obtained from **1a** (207 mg, 2.07 mmol) and **3v** (233 mg, 2.04 mmol) in *d*₈-toluene (250 μ L) as a mixture (**6av**:**4av** = 5:2, NMR integration) according to *GP A* (sealed NMR tube, 80 °C, 5 days, column chromatography on silica gel, *n*-pentane/EtOAc = 4:1): colorless oil (304 mg, yield 70%).



¹H NMR (400 MHz, CDCl₃): δ = 1.28 (t, *J* = 7.1 Hz, 3 H, H^d), 1.32–1.36 (m, 5.6 H, H^f, H^{d'} and H^{f'}), 3.54–3.60 (m, 1.4 H, H^e, H^{e'}), 3.75 (s, 1.2 H, Hⁱ), 3.83 (s, 3 H, Hⁱ), 4.00 (d, *J* = 4.1 Hz, 1 H, H^a), 4.02 (d, *J* = 4.1 Hz, 0.4 H, H^{g'}), 4.20 (q, *J* = 7.1 Hz, 2 H, H^c), 4.25–4.33 (m, 0.8 H, H^{c'}), 6.66 (br s, 1.2 H, NH). **¹³C NMR** (101 MHz, CDCl₃): δ = 14.2 (CH₃, C^d), 14.3 (CH₃, C^{d'}), 17.29 (CH₃, C^f), 17.34 (CH₃, C^{f'}), 43.1 (CH, C^e), 43.2 (CH, C^{e'}), 52.3 (CH₃, Cⁱ), 52.9 (CH₃, C^{i'}), 61.4 (CH₂, C^c), 62.2 (CH₂, C^{c'}), 68.9 (CH, C^g), 69.0 (CH, C^a), 146.4 (C, C^g), 146.8 (C, C^{a'}), 161.8 (C, C^{b'}), 162.3 (C, C^h), 171.6 (C, C^b), 172.1 (C, C^{h'}).

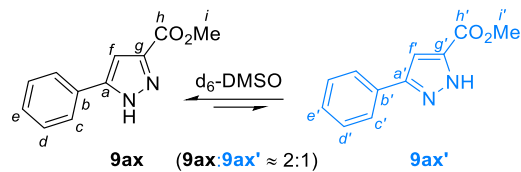
Reaction of methyl diazoacetate (**1a**) with phenylacetylene (**3x**)

Methyl 5-phenyl-1H-pyrazole-3-carboxylate (9ax) was obtained from **1a** (208 mg, 2.08 mmol) and **3x** (218 mg, 2.13 mmol) in *d*₈-toluene (250 μ L) according to *GP A* (sealed NMR tube, 80 °C, 2 days, filtration then recrystallization: CH₂Cl₂/hexane): white crystals (243 mg, yield 58%); mp 184.4 °C (ref. S21a: mp 182–183 °C). Spectroscopic data are consistent with those reported in ref. S21



¹H NMR (400 MHz, CDCl₃): δ = 3.92 (s, 3 H, Hⁱ), 7.11 (s, 1 H, H^f), 7.35–7.39 (m, 1 H, H^e), 7.41–7.46 (m, 2 H, H^d), 7.74 (s, 2 H, H^c), 11.4 (br s, 1 H, NH). **¹³C NMR** (101 MHz, CDCl₃): δ = 52.4, 105.8, 125.8, 128.8, 129.1, resonances of further carbon atoms were broadened because of fast proton transfer in **9ax**. **HRMS** (ESI⁺): *m/z* calcd for C₁₁H₁₁N₂O₂⁺ (M + H⁺): 203.0815; found 203.0815. **IR** (neat, ATR): 3203, 3169, 3137, 3062, 3017, 2982, 2954, 1729, 1491, 1432, 1405, 1274, 1241, 1194, 1132, 1009, 944, 845, 806, 782, 758, 684, 672 cm⁻¹.

¹H and ¹³C NMR spectra of **9ax** in *d*₆-DMSO suggest a mixture of **9ax** with a tautomer, presumably **9ax'** (**9ax**:**9ax'** \approx 2:1).

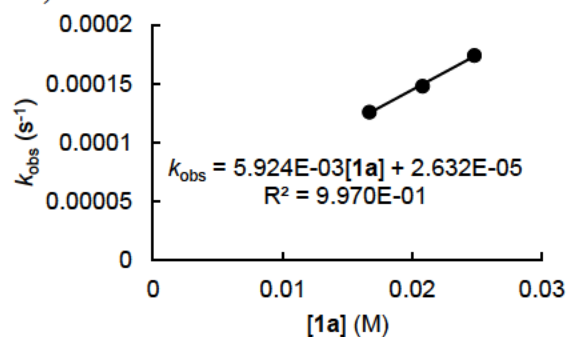


^1H NMR (400 MHz, $\text{d}_6\text{-DMSO}$): $\delta = 3.82$ (s, 3 H, H^i), **3.87** (s, 2.0 H, $\text{H}^{i'}$), 7.21 (d, $J = 1.9$ Hz, 1 H, H^f), 7.31–7.49 (m, 6.0 H, H^d , H^e , **$\text{H}^{d'}$** , **$\text{H}^{e'}$** , H^f), 7.82 (d, $J = 7.4$ Hz, 2 H, H^c), **7.88** (d, $J = 7.4$ Hz, 1.4 H, $\text{H}^{c'}$), 14.0 (br s, 1 H, NH of **9ax**), **14.1** (br s, 0.7 H, NH of **9ax'**). **^{13}C NMR** (101 MHz, CDCl_3): $\delta = 51.6$ (CH_3 , C^i), **52.1** (CH_3 , $\text{C}^{i'}$), 104.9 (CH, C^f), **105.8** (CH, $\text{C}^{f'}$), **125.3** (CH, C^c), 125.4 (CH, C^c), **128.0** (CH, $\text{C}^{c'}$), 128.4 (C, C^b), 128.7 (C, C^e), **128.8** (C, $\text{C}^{d'}$), 129.1 (C, C^d), **132.7** (C, $\text{C}^{b'}$), **134.5** (C, C^g), 143.5 (C, C^a), 143.9 (C, C^g), **151.3** (C, $\text{C}^{a'}$), **159.5** (C, C^h), 162.5 (C, C^h).

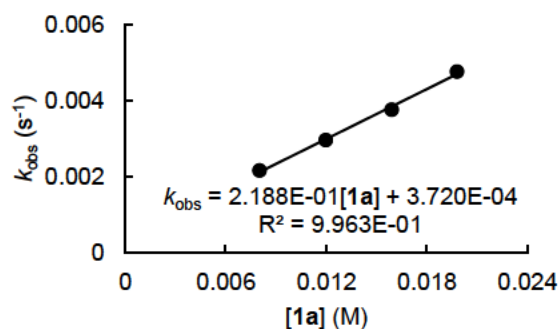
6.2.3 Kinetics

Determination of Nucleophilic Reactivity Parameters N and s_N for **1a** and **1b** in CH_2Cl_2 **Table S1.** Kinetics of the reactions of methyl diazoacetate (**1a**) with $(\text{dma})_2\text{CH}^+\text{BF}_4^-$ in dichloromethane at 20 °C (conventional UV-Vis technique, detection at 612 nm).

$[(\text{dma})_2\text{CH}^+]$ (M)	[1a] (M)	k_{obs} (s^{-1})
1.02×10^{-5}	1.67×10^{-2}	1.26×10^{-4}
1.02×10^{-5}	2.08×10^{-2}	1.48×10^{-4}
1.01×10^{-5}	2.48×10^{-2}	1.74×10^{-4}
$k_2 = 5.92 \times 10^{-3} \text{ M}^{-1} \text{ s}^{-1}$		

**Table S2.** Kinetics of the reactions of methyl diazoacetate (**1a**) with $(\text{mor})_2\text{CH}^+\text{BF}_4^-$ in dichloromethane at 20 °C (conventional UV-Vis technique, detection at 620 nm).

$[(\text{mor})_2\text{CH}^+]$ (M)	[1a] (M)	k_{obs} (s^{-1})
1.65×10^{-5}	8.02×10^{-3}	2.17×10^{-3}
1.64×10^{-5}	1.20×10^{-2}	2.97×10^{-3}
1.64×10^{-5}	1.59×10^{-2}	3.77×10^{-3}
1.63×10^{-5}	1.98×10^{-2}	4.77×10^{-3}
$k_2 = 0.219 \text{ M}^{-1} \text{ s}^{-1}$		

**Table S3.** Kinetics of the reaction of methyl diazoacetate (**1a**) with $(\text{dpa})_2\text{CH}^+\text{BF}_4^-$ in dichloromethane at 20 °C (conventional UV-Vis technique, detection at 677 nm).

$[(\text{dpa})_2\text{CH}^+]$ (M)	[1a] (M)	k_{obs} (s^{-1})
1.68×10^{-5}	4.20×10^{-3}	3.59×10^{-3}
1.67×10^{-5}	6.27×10^{-3}	4.52×10^{-3}
1.66×10^{-5}	8.33×10^{-3}	5.87×10^{-3}
1.66×10^{-5}	1.04×10^{-2}	7.05×10^{-3}
1.65×10^{-5}	1.24×10^{-2}	8.70×10^{-3}
$k_2 = 0.622 \text{ M}^{-1} \text{ s}^{-1}$		

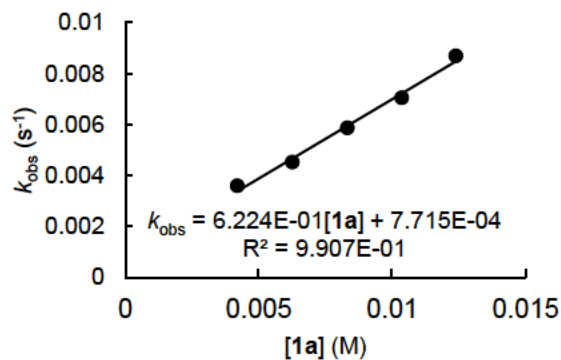
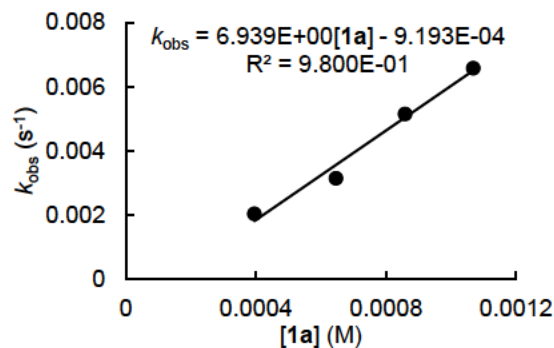
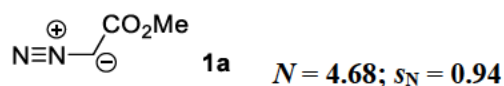
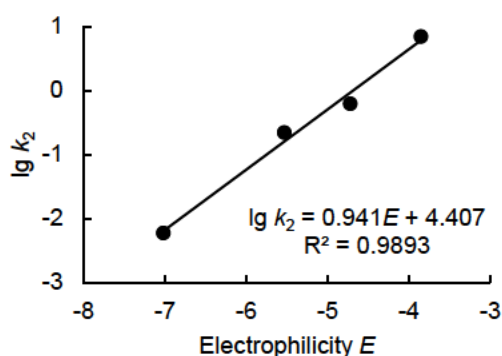


Table S4. Kinetics of the reaction of methyl diazoacetate (**1a**) with (mfa)₂CH⁺BF₄⁻ in dichloromethane at 20 °C (conventional UV-Vis technique, detection at 592 nm).

[(mfa) ₂ CH ⁺] (M)	[1a] (M)	<i>k</i> _{obs} (s ⁻¹)
1.08 × 10 ⁻⁵	3.95 × 10 ⁻⁴	2.05 × 10 ⁻³
1.08 × 10 ⁻⁵	6.47 × 10 ⁻⁴	3.15 × 10 ⁻³
1.07 × 10 ⁻⁵	8.59 × 10 ⁻⁴	5.15 × 10 ⁻³
1.07 × 10 ⁻⁵	1.07 × 10 ⁻³	6.58 × 10 ⁻³
<i>k</i>₂ = 6.94 M⁻¹ s⁻¹		

**Table S5.** Determination of the nucleophilicity parameters *N* and *s_N* for **1a** in dichloromethane.

Electrophile	<i>E</i>	<i>k</i> ₂ (20 °C) (M ⁻¹ s ⁻¹)	lg <i>k</i> ₂
(dma) ₂ CH ⁺	-7.02	5.92 × 10 ⁻³	-2.23
(mor) ₂ CH ⁺	-5.53	2.19 × 10 ⁻¹	-0.66
(dpa) ₂ CH ⁺	-4.72	6.22 × 10 ⁻¹	-0.21
(mfa) ₂ CH ⁺	-3.85	6.94	0.84

**Table S6.** Kinetics of the reactions of dimethyl diazomalonate (**1b**) with (fur)₂CH⁺TfO⁻ in dichloromethane at 20 °C (conventional UV-Vis technique, detection at 535 nm, (fur)₂CH⁺TfO⁻ generated by the reaction of (fur)₂CH-Cl with 4.0 equiv TMSOTf).

[(fur) ₂ CH ⁺] (M)	[1b] (M)	<i>k</i> _{obs} (s ⁻¹)
1.11 × 10 ⁻⁵	2.96 × 10 ⁻²	3.82 × 10 ⁻⁴
1.10 × 10 ⁻⁵	3.94 × 10 ⁻²	4.32 × 10 ⁻⁴
1.10 × 10 ⁻⁵	4.90 × 10 ⁻²	4.76 × 10 ⁻⁴
1.09 × 10 ⁻⁵	5.86 × 10 ⁻²	5.82 × 10 ⁻⁴
<i>k</i>₂ = 6.67 × 10⁻³ M⁻¹ s⁻¹		

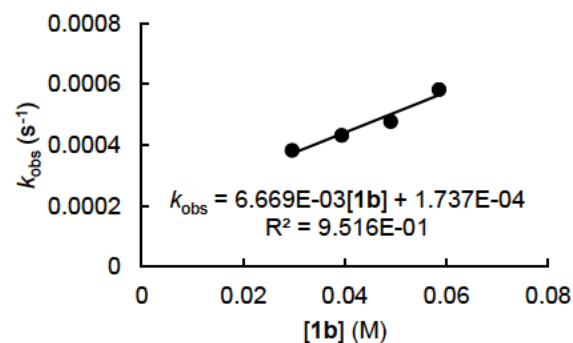
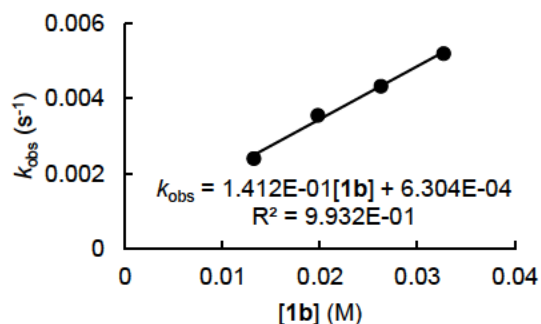
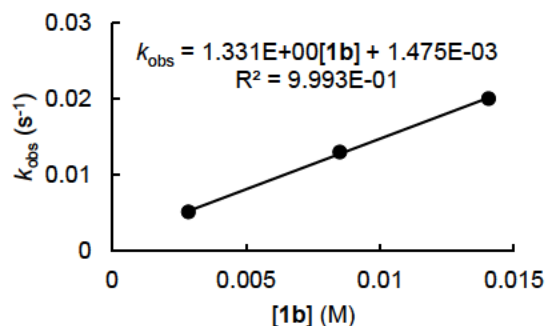


Table S7. Kinetics of the reactions of dimethyl diazomalonate (**1b**) with (ani)₂CH⁺TfO⁻ in dichloromethane at 20 °C (conventional UV-Vis technique, detection at 512 nm, (ani)₂CH⁺TfO⁻ generated by the reaction of (ani)₂CH-Cl with 4.3 equiv TMSOTf).

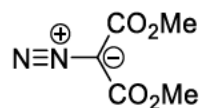
[(ani) ₂ CH ⁺] (M)	[1b] (M)	<i>k</i> _{obs} (s ⁻¹)
1.95 × 10 ⁻⁵	1.32 × 10 ⁻²	2.41 × 10 ⁻³
1.94 × 10 ⁻⁵	1.98 × 10 ⁻²	3.56 × 10 ⁻³
1.93 × 10 ⁻⁵	2.63 × 10 ⁻²	4.34 × 10 ⁻³
1.93 × 10 ⁻⁵	3.27 × 10 ⁻²	5.20 × 10 ⁻³
<i>k</i>₂ = 0.141 M⁻¹ s⁻¹		

**Table S8.** Kinetics of the reactions of dimethyl diazomalonate (**1b**) with (ani)(tol)CH⁺TfO⁻ in dichloromethane at 20 °C (conventional UV-Vis technique, detection at 488 nm, (ani)(tol)CH⁺TfO⁻ generated by the reaction of (ani)(tol)CH-Cl with 4.0 equiv TMSOTf).

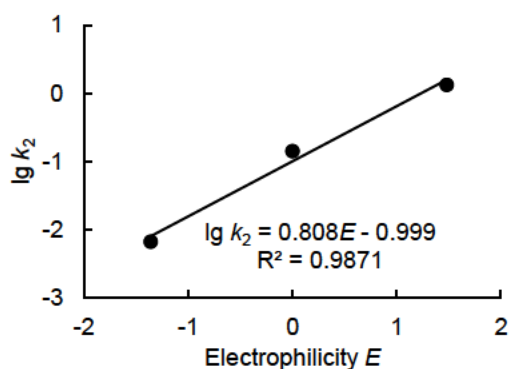
[(ani)(tol)CH ⁺] (M)	[1b] (M)	<i>k</i> _{obs} (s ⁻¹)
4.14 × 10 ⁻⁵	2.86 × 10 ⁻³	5.17 × 10 ⁻³
4.10 × 10 ⁻⁵	8.50 × 10 ⁻³	1.30 × 10 ⁻²
4.07 × 10 ⁻⁵	1.41 × 10 ⁻²	2.01 × 10 ⁻²
<i>k</i>₂ = 1.33 M⁻¹ s⁻¹		

**Table S9.** Determination of the nucleophilicity parameters *N* and *s_N* for **1b** in dichloromethane.

Electrophile	<i>E</i>	<i>k</i> ₂ (20 °C) (M ⁻¹ s ⁻¹)	lg <i>k</i> ₂
(fur) ₂ CH ⁺	-1.36	6.67 × 10 ⁻³	-2.18
(ani) ₂ CH ⁺	0.00	1.41 × 10 ⁻¹	-0.85
(ani)(tol)CH ⁺	1.48	1.33	0.12



1b *N* = -1.24; *s_N* = 0.81



Kinetic investigations of **1c** with Michael acceptors in CH₂Cl₂

The kinetics of the reactions of the diazo compound **1c** (1,3-dipole) with the Michael acceptors **3n**, **3o**, **3r**, and **3t** (dipolarophiles) in dichloromethane at 20 °C were followed by using conventional photometry.

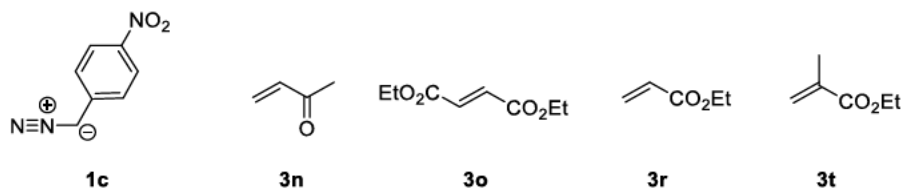


Table S10. Kinetics of the reactions of **1c** with **3n** in CH₂Cl₂ at 20 °C (detection at 380 nm).

[1c] (M)	[3n] (M)	k_{obs} (s ⁻¹)
8.10×10^{-5}	2.29×10^{-2}	1.69×10^{-4}
8.03×10^{-5}	3.18×10^{-2}	2.28×10^{-4}
8.03×10^{-5}	5.90×10^{-2}	4.25×10^{-4}
7.94×10^{-5}	8.33×10^{-2}	5.45×10^{-4}
8.00×10^{-5}	1.44×10^{-1}	1.07×10^{-3}
$k_2 = 7.35 \times 10^{-3} \text{ M}^{-1} \text{ s}^{-1}$		

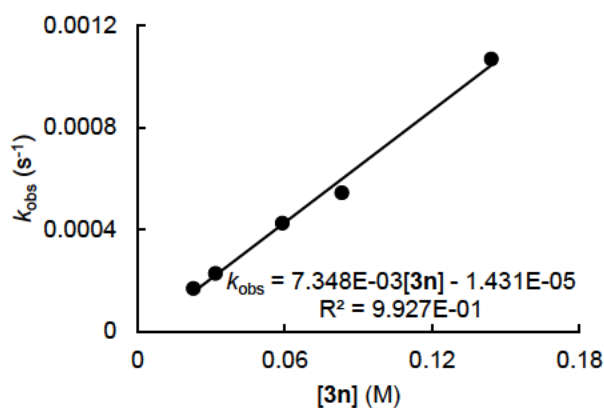


Table S11. Kinetics of the reaction of **1c** with **3o** in CH₂Cl₂ at 20 °C (detection at 380 nm).

[1c] (M)	[3o] (M)	k_{obs} (s ⁻¹)
8.93×10^{-5}	4.29×10^{-2}	3.95×10^{-4}
8.86×10^{-5}	5.68×10^{-2}	5.19×10^{-4}
9.15×10^{-5}	6.78×10^{-2}	6.62×10^{-4}
9.07×10^{-5}	8.65×10^{-2}	8.52×10^{-4}
$k_2 = 1.07 \times 10^{-2} \text{ M}^{-1} \text{ s}^{-1}$		

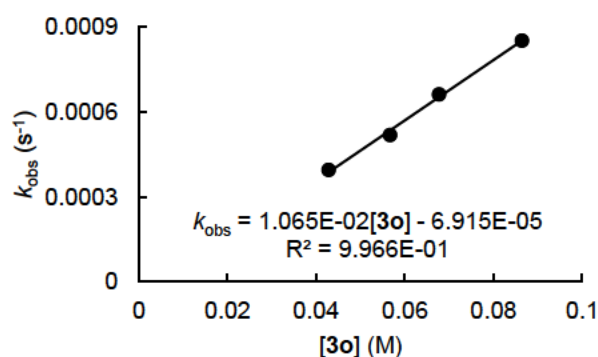
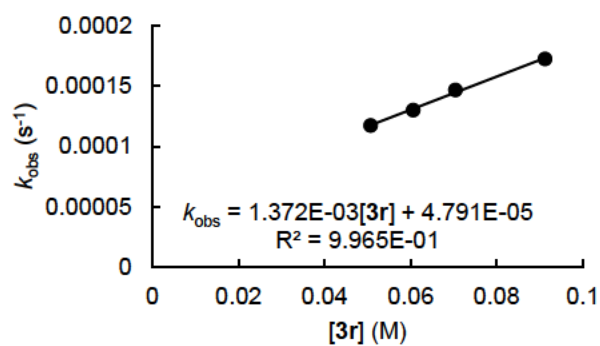
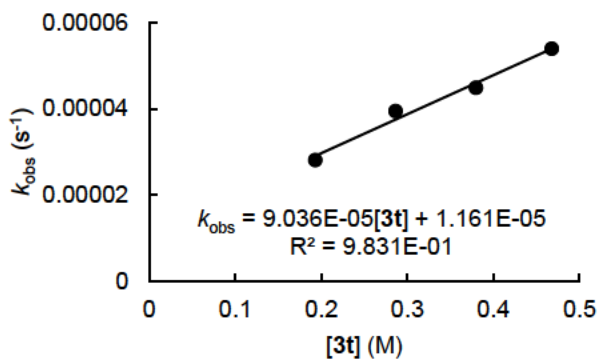


Table S12. Kinetics of the reaction of **1c** with **3r** in CH₂Cl₂ at 20 °C (detection at 380 nm).

[1c] (M)	[3r] (M)	<i>k</i> _{obs} (s ⁻¹)
8.10 × 10 ⁻⁵	5.07 × 10 ⁻²	1.17 × 10 ⁻⁴
8.07 × 10 ⁻⁵	6.06 × 10 ⁻²	1.30 × 10 ⁻⁴
8.03 × 10 ⁻⁵	7.04 × 10 ⁻²	1.47 × 10 ⁻⁴
8.86 × 10 ⁻⁵	9.13 × 10 ⁻²	1.72 × 10 ⁻⁴
<i>k</i>₂ = 1.37 × 10⁻³ M⁻¹ s⁻¹		

**Table S13.** Kinetics of the reaction of **1c** with **3t** in CH₂Cl₂ at 20 °C (detection at 380 nm).

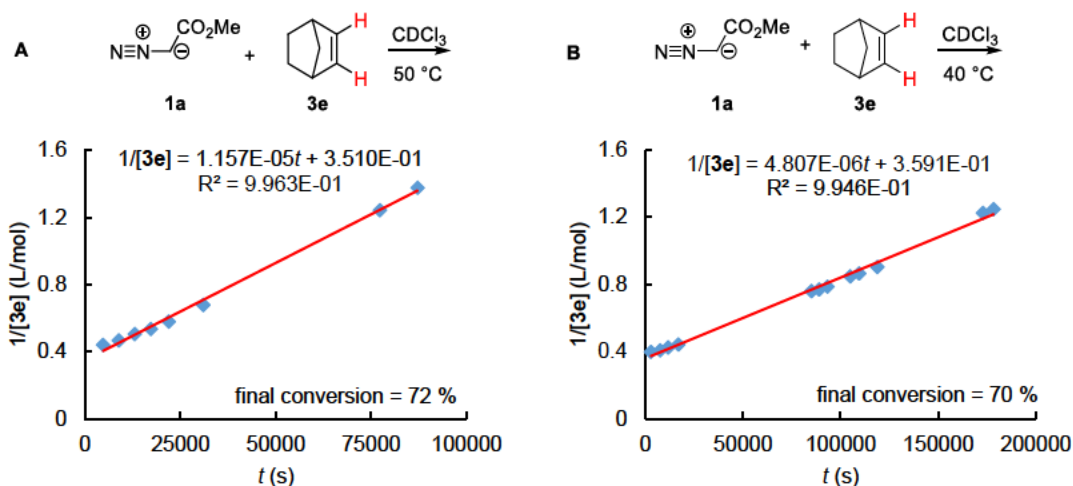
[1c] (M)	[3t] (M)	<i>k</i> _{obs} (s ⁻¹)
8.31 × 10 ⁻⁵	1.93 × 10 ⁻¹	2.81 × 10 ⁻⁵
8.21 × 10 ⁻⁵	2.86 × 10 ⁻¹	3.95 × 10 ⁻⁵
8.12 × 10 ⁻⁵	3.80 × 10 ⁻¹	4.49 × 10 ⁻⁵
8.02 × 10 ⁻⁵	4.68 × 10 ⁻¹	5.39 × 10 ⁻⁵
<i>k</i>₂ = 9.04 × 10⁻⁵ M⁻¹ s⁻¹		



Kinetic investigations of **1a** with dipolarophiles in CDCl₃

Table S14. Second-order rate constants k_2^{exptl} of the reactions of **1a** with **3e** in CDCl₃ at +50 (A), +40 (B), +30 °C (C), and +20 °C (D) (¹H NMR kinetics, 1,1,2,2-tetrachloroethane as the internal standard IS). Activation parameters from the Eyring plot (E) were used to calculate $k_2(20\text{ °C})$ and $k_2(80.3\text{ °C})$. Initial reactant concentrations were determined by using the integration ranges of the IS from +50 to +20 °C at 6.05–5.88, 6.03–5.95, 6.03–5.94, 6.03–5.94 ppm, respectively, of the vinylic hydrogen of **3e** at 5.89–5.73, 5.94–5.78, 5.92–5.76, 5.91–5.77 ppm, respectively, and of the CH hydrogen of **1a** at 4.90–4.45, 4.94–4.54, 4.95–4.55, 4.91–4.59 ppm, respectively. Relaxation delay and acquisition time are always 1.00 and 4.09 s, respectively.

T (°C)	1a ₀ (M)	3e ₀ (M)	[IS] ₀ (M)	k_2^{exptl} (M ⁻¹ s ⁻¹)	k_2 (M ⁻¹ s ⁻¹)	ΔG^\ddagger (kJ mol ⁻¹)
50	2.56	2.60	6.39×10^{-1}	1.16×10^{-5}		
40	2.59	2.64	4.37×10^{-1}	4.81×10^{-6}		
30	2.48	2.58	4.72×10^{-1}	2.22×10^{-6}		
20	2.20	2.34	7.69×10^{-1}	6.50×10^{-7}		
20					$(7.06 \pm 0.58) \times 10^{-7}$	106
25						107
80.3					$(1.29 \pm 0.28) \times 10^{-4}$	



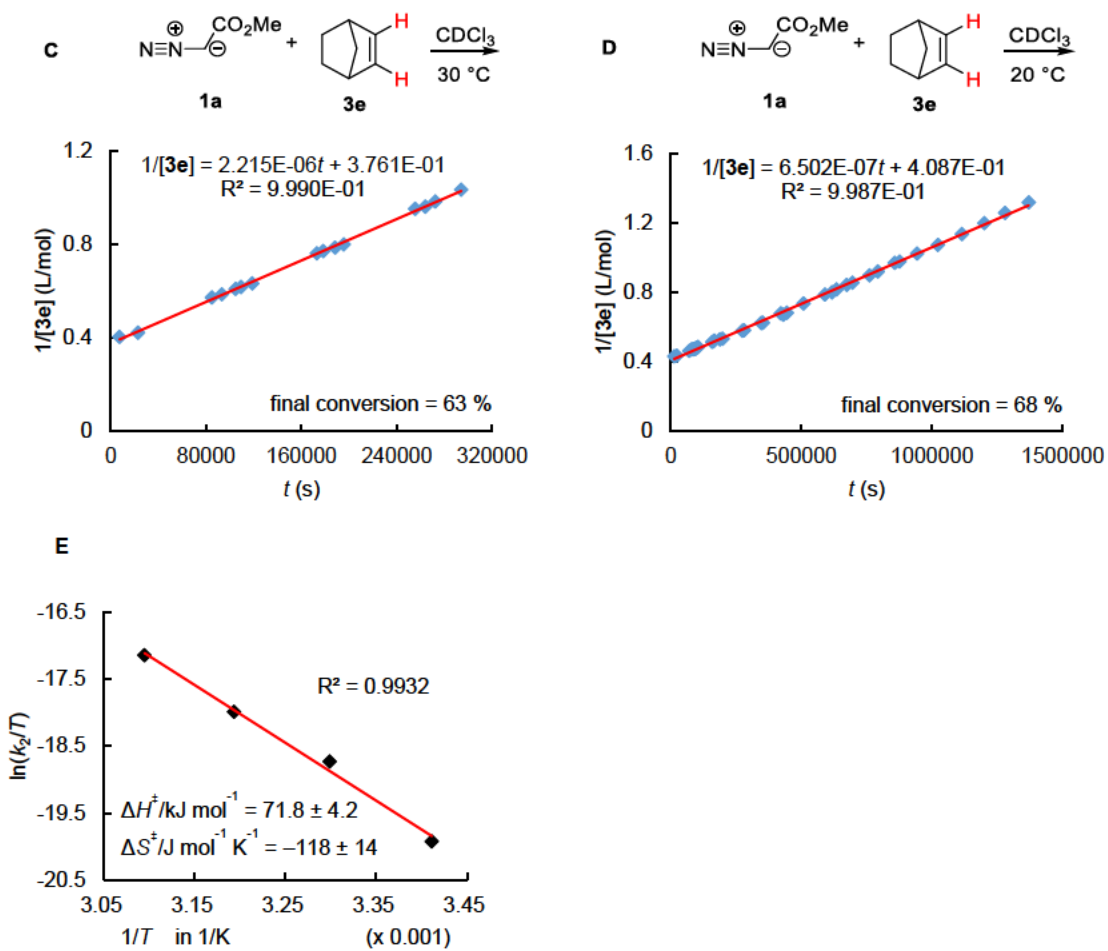
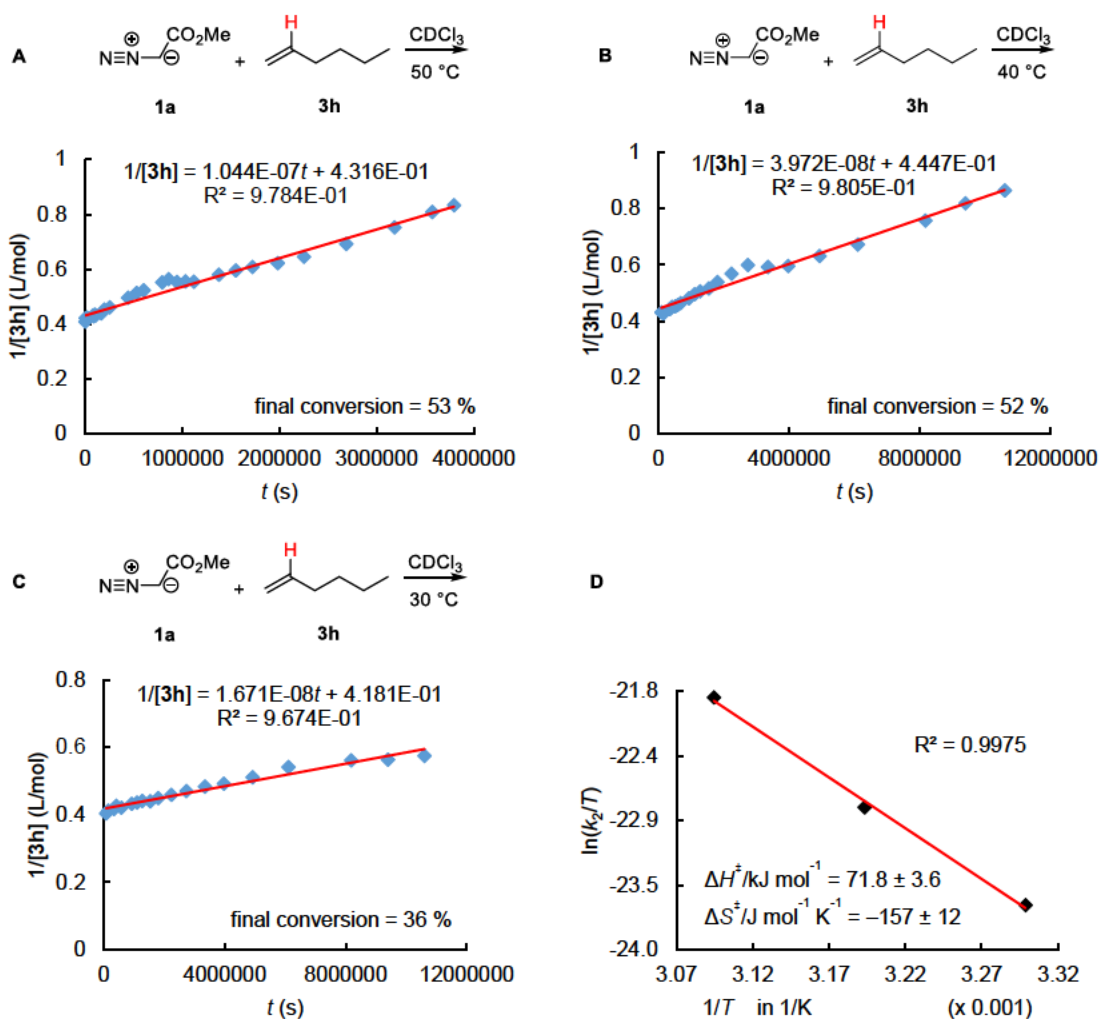


Table S15. Second-order rate constants k_2^{exptl} of the reactions of **1a** with **3h** in CDCl_3 at +50 (A), +40 (B), and +30 °C (C) (^1H NMR kinetics, mesitylene as the internal standard IS). Activation parameters from the Eyring plot (D) were used to calculate $k_2(20^\circ\text{C})$. Initial reactant concentrations were determined by using the integration ranges of the IS from +50 to +30 °C at 6.59–6.69, 6.61–6.72, 6.58–6.71 ppm, respectively, of the hydrogen at C-2 of **3h** at 5.84–5.58, 5.85–5.61, 5.85–5.61 ppm, respectively, and of the CH hydrogen of **1a** at 4.78–4.63, 4.78–4.64, 4.78–4.65 ppm, respectively. Relaxation delay and acquisition time are always 1.00 and 4.09 s, respectively.

T (°C)	$[\mathbf{1a}]_0$ (M)	$[\mathbf{3h}]_0$ (M)	$[\text{IS}]_0$ (M)	k_2^{exptl} ($\text{M}^{-1} \text{s}^{-1}$)	k_2 ($\text{M}^{-1} \text{s}^{-1}$)	ΔG^\ddagger (kJ mol^{-1})
50	2.90	2.57	9.38×10^{-1}	1.04×10^{-7}		
40	2.49	2.41	9.57×10^{-1}	3.97×10^{-8}		
30	2.52	2.72	9.10×10^{-1}	1.67×10^{-8}		
20					$(5.96 \pm 0.56) \times 10^{-9}$	118
25						119



Kinetic investigations of **1a** with dipolarophiles in *d*₈-toluene

Table S16. Second-order rate constants k_2^{exptl} of the reactions of **1a** with ESF (**3k**) in *d*₈-toluene at +50 (A), +40 (B), and +30 °C (C) (¹H NMR kinetics, mesitylene as the internal standard IS). Activation parameters from the Eyring plot (D) were used to calculate $k_2(20\text{ °C})$. Initial reactant concentrations were determined by using the integration ranges of the IS from +50 °C to +30 °C at 6.74–6.44, 6.74–6.50, 6.72–6.46 ppm, respectively, of the hydrogen at C-1 of **3k** at 5.88–5.54, 5.88–5.54, 5.88–5.56 ppm, respectively, and of the CH hydrogen of **1a** at always 4.07–3.87 ppm. Relaxation delay and acquisition time are always 0.10 and 3.65 s, respectively.

<i>T</i> (°C)	[1a] ₀ (M)	[3k] ₀ (M)	[IS] ₀ (M)	k_2^{exptl} (M ⁻¹ s ⁻¹)	k_2 (M ⁻¹ s ⁻¹)	ΔG^\ddagger (kJ mol ⁻¹)
50	2.73×10^{-1}	2.65×10^{-1}	5.54×10^{-1}	3.53×10^{-3}		
40	2.51×10^{-1}	2.71×10^{-1}	2.52×10^{-1}	2.18×10^{-3}		
30	2.30×10^{-1}	2.88×10^{-1}	2.79×10^{-1}	1.35×10^{-3}		
20					$(7.92 \pm 0.16) \times 10^{-4}$	89.3
25						90.1

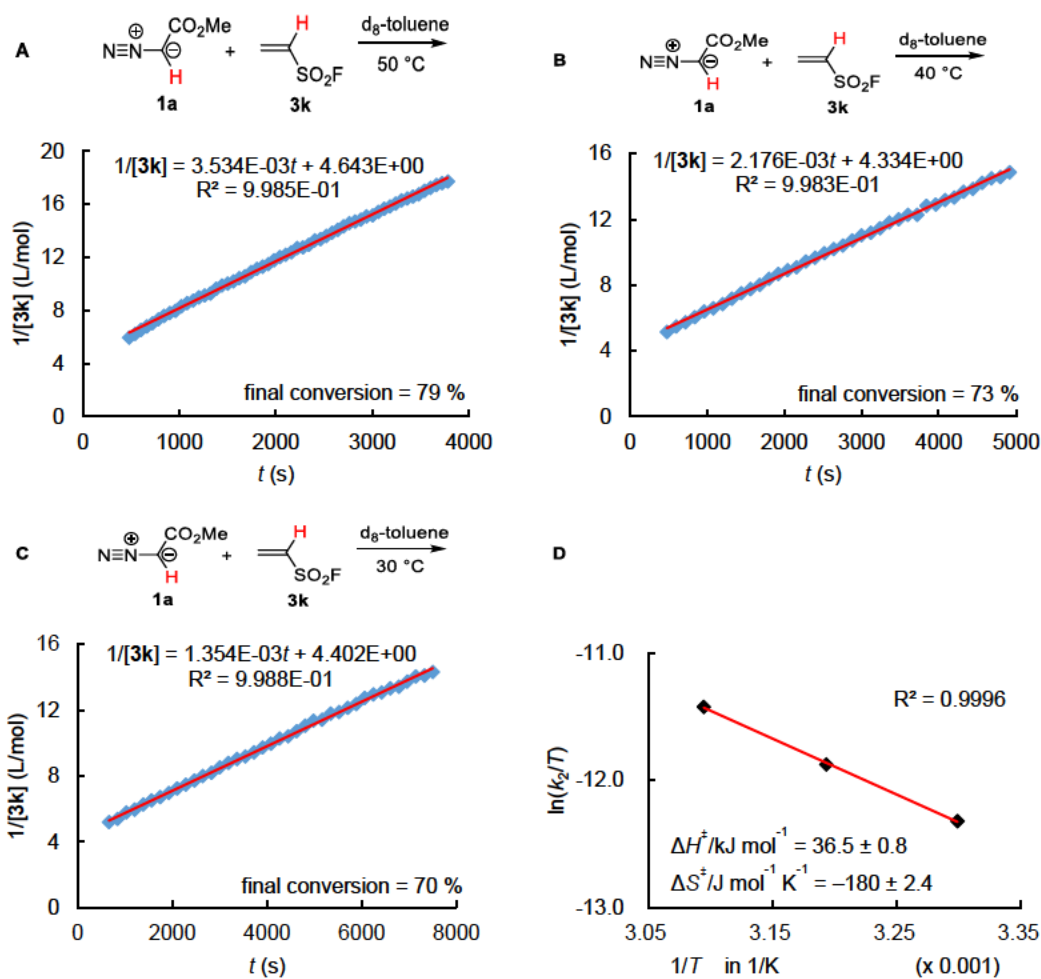
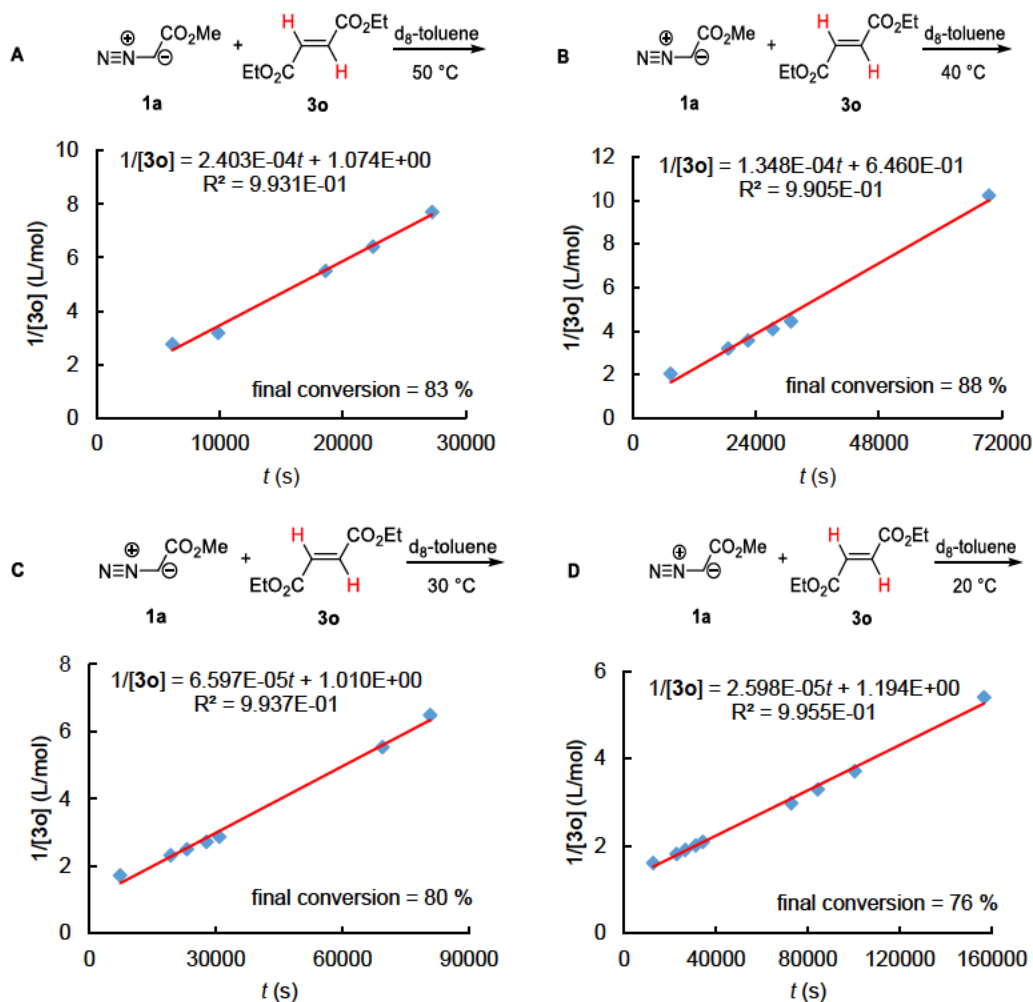


Table S17. Second-order rate constants k_2^{exptl} of the reactions of **1a** with **3o** in d_8 -toluene at +50 (A), +40 (B), +30 (C), and +20 °C (D) (^1H NMR kinetics, 1,1,2,2-tetrachloroethane as the internal standard IS). Activation parameters from the Eyring plot (E) were used to calculate $k_2(20\text{ °C})$ and $k_2(80.3\text{ °C})$. Initial reactant concentrations were determined by using the integration ranges of the IS from +50 to +20 °C at 5.16–5.10, 5.17–5.12, 5.19–5.11, 5.20–5.12 ppm, respectively, of the vinylic hydrogens of **3o** at 6.61–6.55, 6.60–6.56, 6.61–6.55, 6.61–6.55 ppm, respectively, and of the OCH_3 hydrogens of **1a** at 3.21–3.13, 3.21–3.14, 3.23–3.15, 3.22–3.15 ppm, respectively. Relaxation delay and acquisition time are always 1.00 and 4.09 s, respectively.

T (°C)	$[\mathbf{1a}]_0$ (M)	$[\mathbf{3o}]_0$ (M)	$[\text{IS}]_0$ (M)	k_2^{exptl} ($\text{M}^{-1}\text{ s}^{-1}$)	k_2 ($\text{M}^{-1}\text{ s}^{-1}$)	ΔG^\ddagger (kJ mol^{-1})
50	1.04	7.67×10^{-1}	2.27×10^{-1}	2.40×10^{-4}		
40	1.11	8.07×10^{-1}	2.30×10^{-1}	1.35×10^{-4}		
30	1.15	7.68×10^{-1}	2.99×10^{-1}	6.60×10^{-5}		
20	9.79×10^{-1}	7.58×10^{-1}	2.09×10^{-1}	2.60×10^{-5}		
20					$(2.78 \pm 0.18) \times 10^{-5}$	97.3
25						98.0
80.3					$(1.66 \pm 0.28) \times 10^{-3}$	



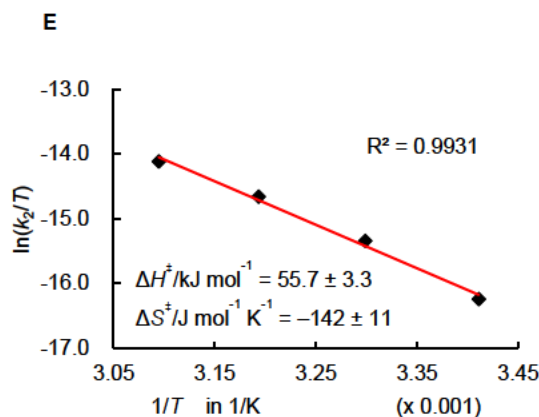


Table S18. Second-order rate constants k_2^{exptl} of the reactions of **1a** with **3s** in d_8 -toluene at +50 (A), +40 (B), +30 (C), and +20 °C (D) (^1H NMR kinetics, 1,1,2,2-tetrachloroethane as the internal standard IS). Activation parameters from the Eyring plot (E) were used to calculate $k_2(20\text{ °C})$ and $k_2(80.3\text{ °C})$. Initial reactant concentrations were determined by using the integration ranges of the IS from +50 to +20 °C at 5.55–5.50, 5.53–5.49, 5.59–5.49, 5.56–5.51 ppm, respectively, of the vinylic hydrogens of **3s** at 5.83–5.76, 5.82–5.76, 5.85–5.75, 5.83–5.77 ppm, respectively, and of the CH hydrogen of **1a** at 4.46–4.25, 4.45–4.22, 4.48–4.22, 4.46–4.20 ppm, respectively. Relaxation delay and acquisition time are always 1.00 and 4.09 s, respectively.

T (°C)	$[\mathbf{1a}]_0$ (M)	$[\mathbf{3s}]_0$ (M)	$[\text{IS}]_0$ (M)	k_2^{exptl} ($\text{M}^{-1} \text{s}^{-1}$)	k_2 ($\text{M}^{-1} \text{s}^{-1}$)	ΔG^\ddagger (kJ mol^{-1})
50	1.22	1.56	5.55×10^{-1}	2.50×10^{-5}		
40	1.18	1.67	4.56×10^{-1}	1.59×10^{-5}		
30	1.26	1.56	4.03×10^{-1}	8.51×10^{-6}		
20	1.27	1.83	4.02×10^{-1}	2.74×10^{-6}		
20					$(3.21 \pm 0.47) \times 10^{-6}$	103
25						103
80.3					$(1.81 \pm 0.71) \times 10^{-4}$	

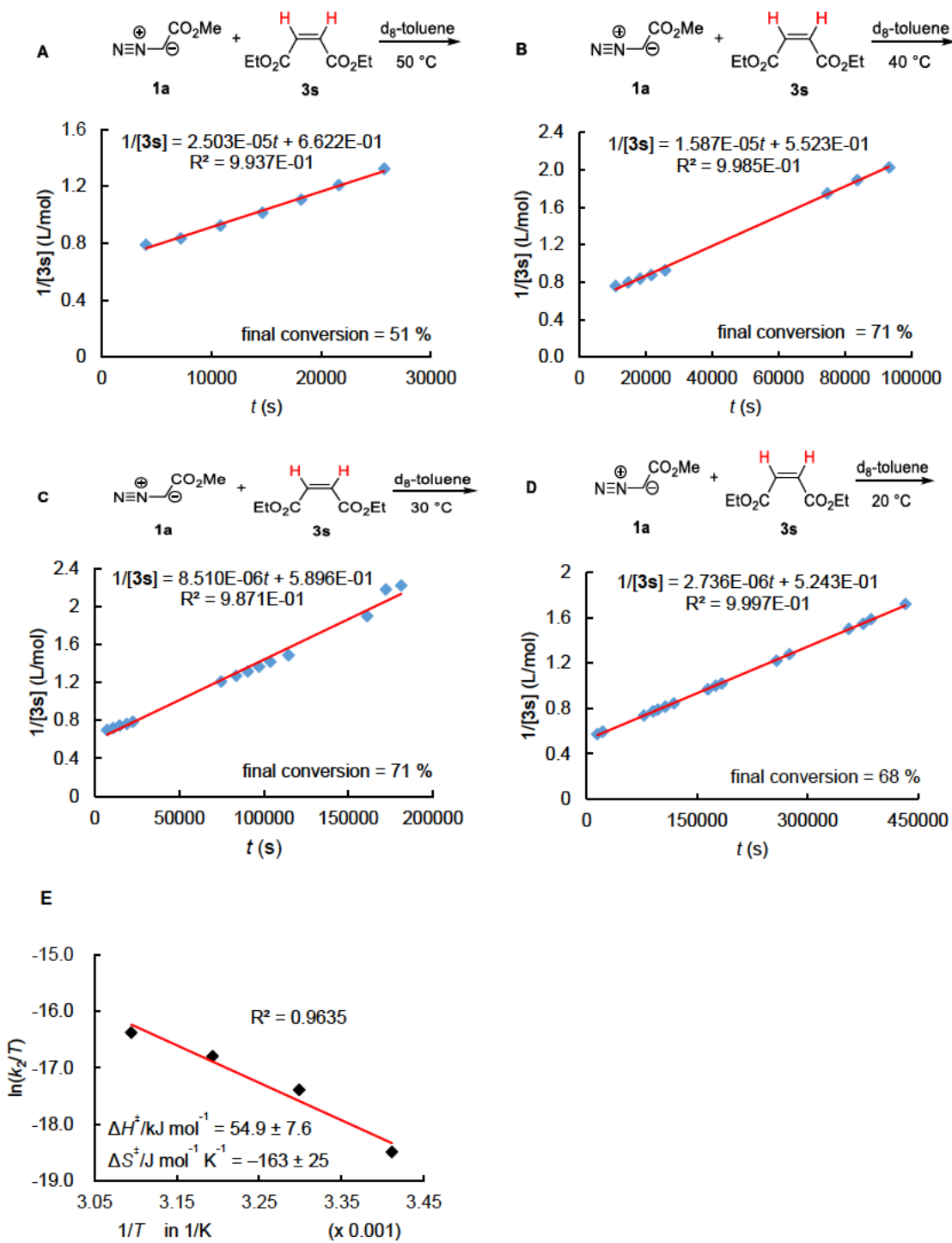


Table S19. Second-order rate constants k_2^{exptl} of the reactions of **1a** with **3t** in d_8 -toluene at +60 (A), +40 (B), and +30 °C (C) (^1H NMR kinetics, 1,1,2,2-tetrachloroethane as the internal standard IS). Activation parameters from the Eyring plot (D) were used to calculate $k_2(20\text{ °C})$. Initial reactant concentrations were determined by using the integration ranges of the IS from +60 to +30 °C at always 5.48–5.44 ppm, of the hydrogen at C-3 of **3t** at always 5.88–5.81 ppm, and of the OCH_3 hydrogens of **1a** at 3.33–3.20, 3.30–3.16, 3.33–3.19 ppm, respectively. Relaxation delay and acquisition time are always 1.00 and 4.09 s, respectively.

T (°C)	$[\mathbf{1a}]_0$ (M)	$[\mathbf{3t}]_0$ (M)	$[\text{IS}]_0$ (M)	k_2^{exptl} ($\text{M}^{-1} \text{s}^{-1}$)	k_2 ($\text{M}^{-1} \text{s}^{-1}$)	ΔG^\ddagger (kJ mol^{-1})
60	2.37	2.00	5.07×10^{-1}	3.95×10^{-5}		
40	2.28	1.86	6.75×10^{-1}	1.26×10^{-5}		
30	2.43	1.96	4.70×10^{-1}	5.63×10^{-6}		
20					$(2.85 \pm 0.31) \times 10^{-6}$	103
25						104

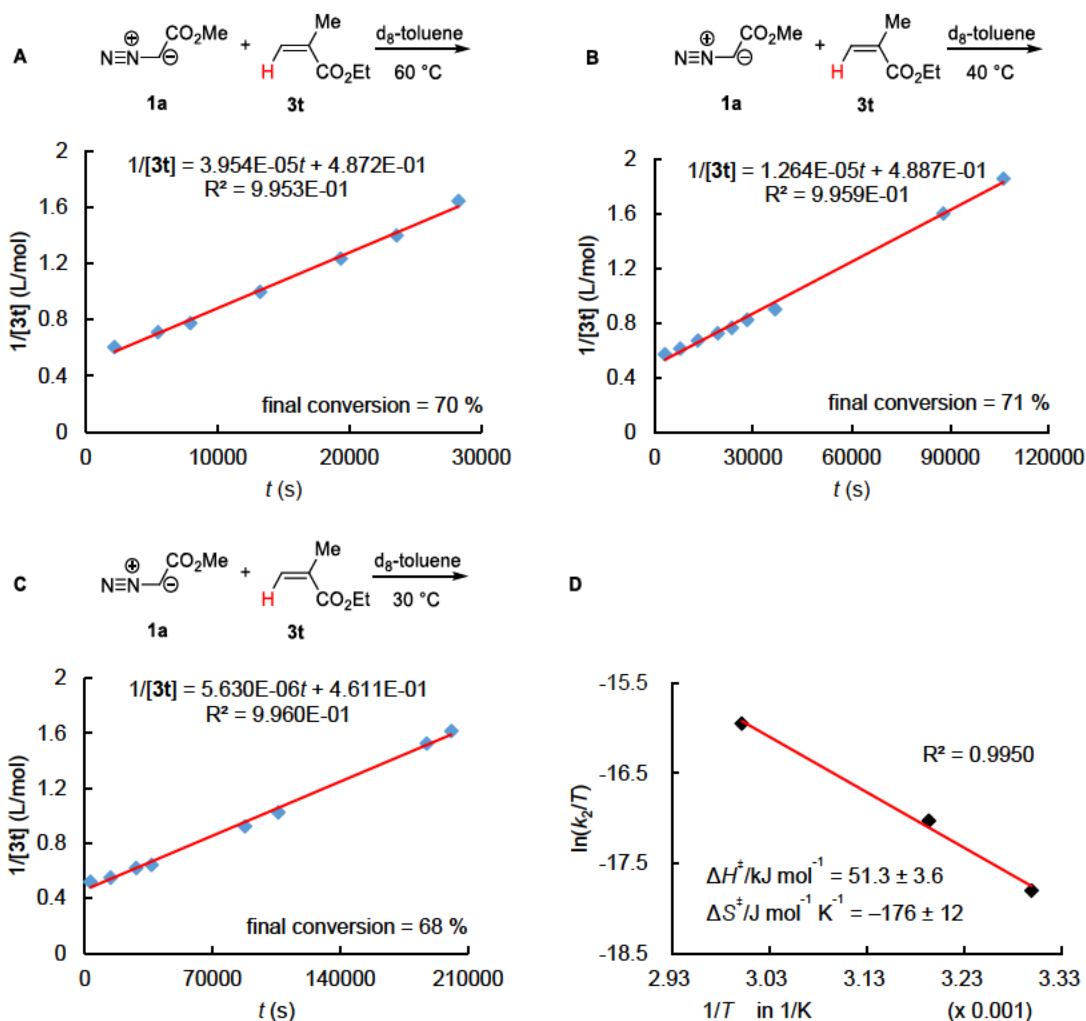


Table S20. Second-order rate constants k_2^{exptl} of the reactions of **1a** with **3v** in d_8 -toluene at +80 (A), +60 (B), and +50 °C (C) (^1H NMR kinetics, 1,1,2,2-tetrachloroethane (60, 80 °C) or mesitylene (50 °C) as the internal standard IS). Activation parameters from Eyring plot (D) were used to calculate $k_2(20\text{ °C})$. Initial reactant concentrations were determined by using the integration ranges of the IS from 80 °C to 50 °C at 5.87–5.77, 5.72–5.66, 6.68–6.54 ppm, respectively, of the hydrogen at C-3 of **3v** at 6.89–6.71, 6.79–6.59, 6.89–6.71 ppm, respectively, and of the CH hydrogen of **1a** at 4.85–4.40, 4.75–4.30, 4.86–4.42 ppm, respectively. Relaxation delay and acquisition time are always 1.00 and 4.09 s, respectively.

T (°C)	$[\mathbf{1a}]_0$ (M)	$[\mathbf{3v}]_0$ (M)	$[\text{IS}]_0$ (M)	k_2^{exptl} ($\text{M}^{-1} \text{s}^{-1}$)	k_2 ($\text{M}^{-1} \text{s}^{-1}$)	ΔG^\ddagger (kJ mol^{-1})
80	2.29	2.30	5.53×10^{-1}	1.47×10^{-5}		
60	1.82	1.84	5.19×10^{-1}	4.99×10^{-6}		
50	1.94	2.19	8.44×10^{-1}	1.99×10^{-6}		
20					$(2.07 \pm 0.85) \times 10^{-7}$	109
25						110
80.3					$(1.57 \pm 0.21) \times 10^{-5}$	

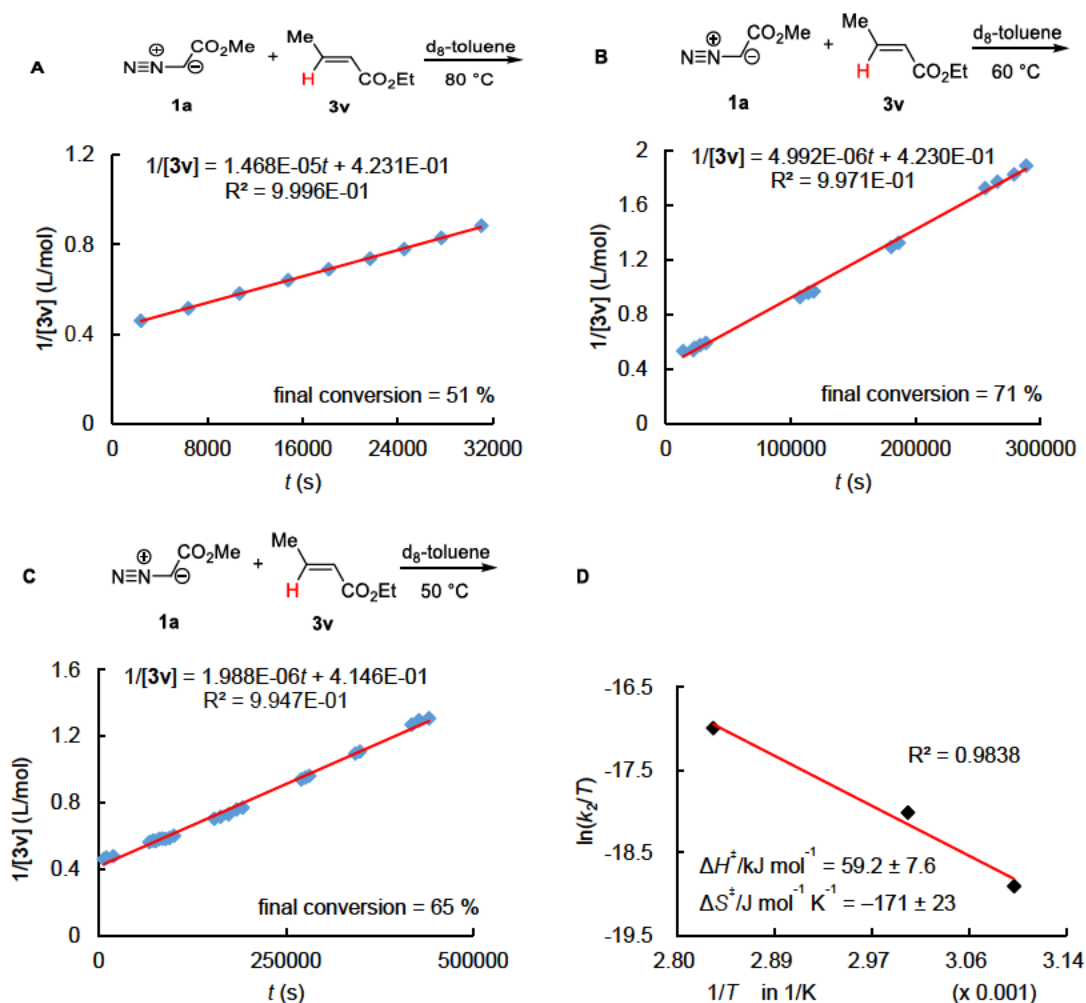
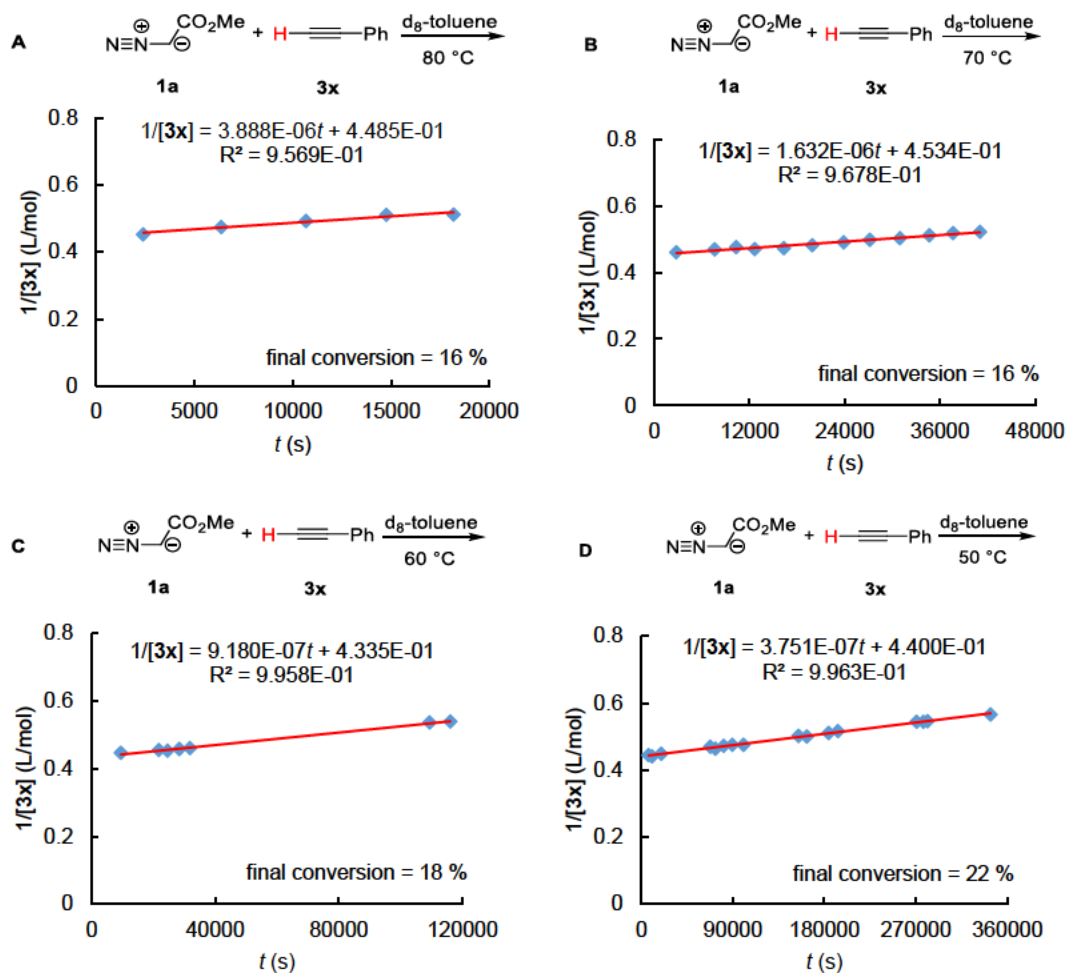
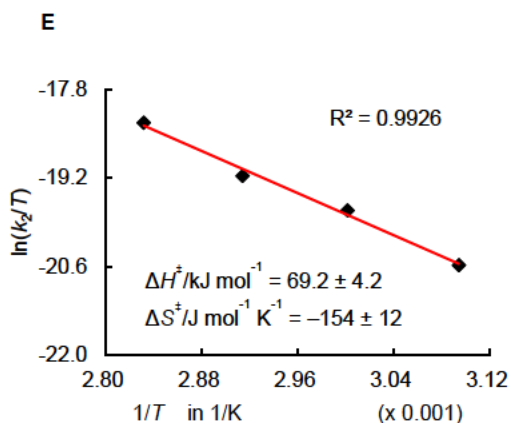


Table S21. Second-order rate constants k_2^{exptl} of the reactions of **1a** with **3x** in d_8 -toluene at +80 (A), +70 (B), +60 (C), and +50 °C (D) (^1H NMR kinetics, 1,1,2,2-tetrachloroethane as the internal standard IS). Activation parameters from the Eyring plot (E) were used to calculate $k_2(20\text{ °C})$ and $k_2(80.3\text{ °C})$. Initial reactant concentrations were determined by using the integration ranges of the IS from +80 to +50 °C at 5.50–5.39, 5.49–5.38, 5.68–5.59, 5.66–5.54 ppm, respectively, of the alkynyl hydrogen of **3x** at 2.92–2.78, 2.93–2.81, 3.09–3.00, 3.09–2.98 ppm, respectively, and of the CH hydrogen of **1a** at 4.50–4.10, 4.50–4.10, 4.70–4.28, 4.68–4.26 ppm, respectively. Relaxation delay and acquisition time are always 1.00 and 4.09 s, respectively.

T (°C)	$[\mathbf{1a}]_0$ (M)	$[\mathbf{3x}]_0$ (M)	$[\text{IS}]_0$ (M)	k_2^{exptl} ($\text{M}^{-1}\text{ s}^{-1}$)	k_2 ($\text{M}^{-1}\text{ s}^{-1}$)	ΔG^\ddagger (kJ mol^{-1})
80	2.45	2.34	6.93×10^{-1}	3.89×10^{-6}		
70	2.53	2.29	7.77×10^{-1}	1.63×10^{-6}		
60	2.63	2.26	6.34×10^{-1}	9.18×10^{-7}		
50	2.52	2.25	7.02×10^{-1}	3.75×10^{-7}		
20					$(2.48 \pm 0.57) \times 10^{-8}$	114
25						115
80.3					$(3.79 \pm 0.25) \times 10^{-6}$	





Kinetic investigations of **1b** with dipolarophiles in CDCl_3

Table S22. Second-order rate constants k_2^{exptl} of the reactions of **1b** with **3e** in CDCl_3 at +55 (**A**), +45 (**B**), and +35 °C (**C**) (^1H NMR kinetics, 1,1,2,2-tetrachloroethane as the internal standard IS). Activation parameters from the Eyring plot (**D**) were used to calculate $k_2(20\text{ °C})$ and $k_2(110\text{ °C})$. Initial reactant concentrations were determined by using the integration ranges of the IS from +55 to +35 °C at 6.03–5.94, 6.03–5.93, 6.03–5.93 ppm, respectively, of the olefinic hydrogens of **3e** at 5.875–5.79, 5.875–5.81, 5.88–5.79 ppm, respectively, and of the OCH_3 hydrogens of **1b** at 3.80–3.62, 3.78–3.63, 3.83–3.63 ppm, respectively. Relaxation delay and acquisition time are always 1.00 and 4.09 s, respectively.

T (°C)	$[\mathbf{1b}]_0$ (M)	$[\mathbf{3e}]_0$ (M)	$[\text{IS}]_0$ (M)	k_2^{exptl} ($\text{M}^{-1} \text{s}^{-1}$)	k_2 ($\text{M}^{-1} \text{s}^{-1}$)	ΔG^\ddagger (kJ mol^{-1})
55	1.66	1.41	9.53×10^{-1}	5.52×10^{-7}		
45	1.61	1.35	1.14	2.32×10^{-7}		
35	1.67	1.43	9.53×10^{-1}	1.02×10^{-7}		
20					$(2.44 \pm 0.18) \times 10^{-8}$	115
25						115
110					$(2.30 \pm 0.35) \times 10^{-5}$	

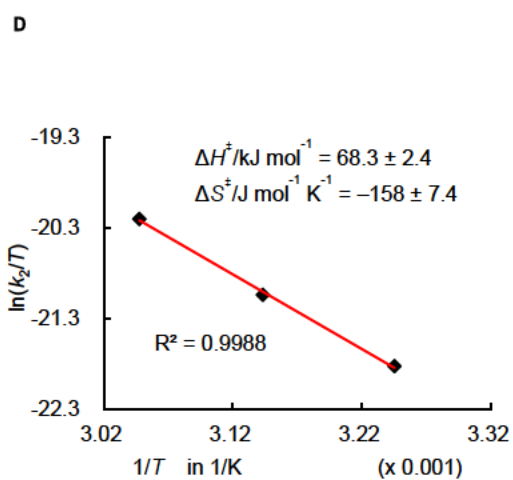
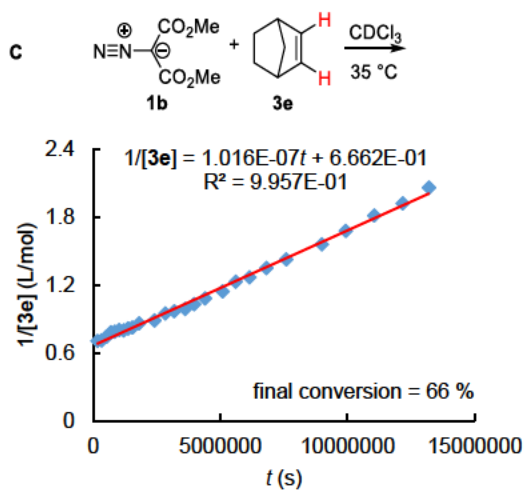
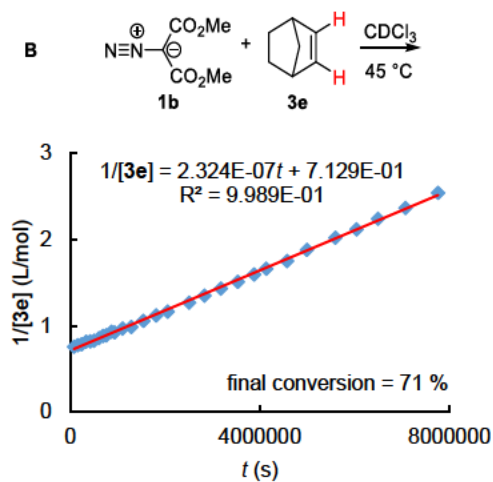
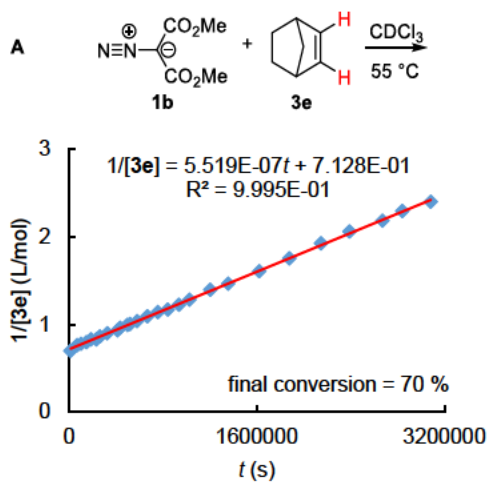
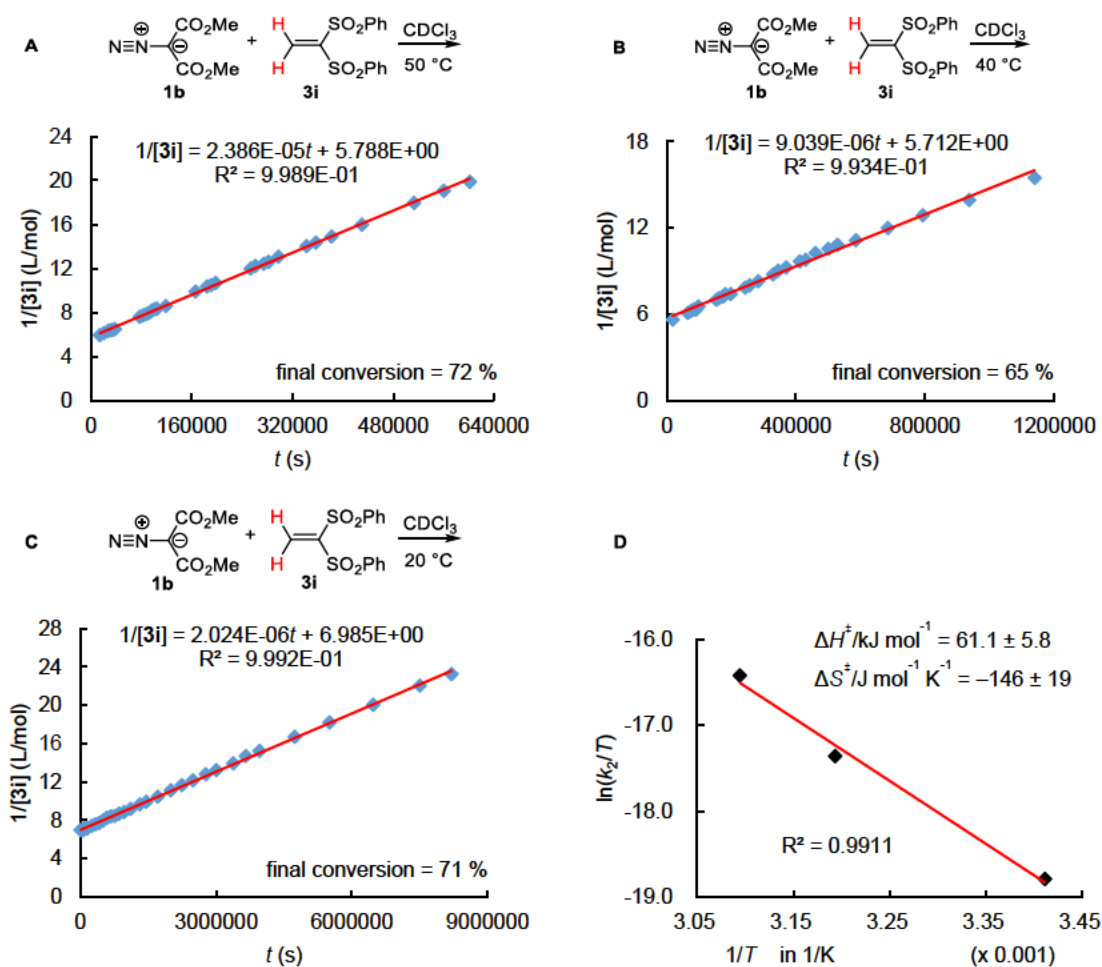


Table S23. Second-order rate constants k_2^{exptl} of the reactions of **1b** with **3i** in CDCl_3 at +50 (A), +40 (B), and +20 °C (C) (^1H NMR kinetics, dibromomethane as the internal standard IS). Activation parameters from the Eyring plot (D) were used to calculate $k_2(20\text{ °C})$. Initial reactant concentrations were determined by using the integration ranges of the IS from +50 to +20 °C at 4.88–4.84, 4.88–4.825, 4.88–4.84 ppm, respectively, of the Me hydrogens of **1b** at 3.80–3.72, 3.80–3.72, 3.85–3.69 ppm, respectively, and of the vinylic hydrogens of **3i** at always 7.175–7.145 ppm. Relaxation delay and acquisition time are always 1.00 and 4.09 s, respectively.

T (°C)	$[\mathbf{1b}]_0$ (M)	$[\mathbf{3i}]_0$ (M)	$[\text{IS}]_0$ (M)	k_2^{exptl} ($\text{M}^{-1}\text{ s}^{-1}$)	k_2 ($\text{M}^{-1}\text{ s}^{-1}$)	ΔG^\ddagger (kJ mol^{-1})
50	1.58×10^{-1}	1.82×10^{-1}	2.39×10^{-1}	2.39×10^{-5}		
40	1.44×10^{-1}	1.83×10^{-1}	3.70×10^{-1}	9.04×10^{-6}		
20	1.31×10^{-1}	1.46×10^{-1}	3.99×10^{-1}	2.02×10^{-6}		
20					$(1.94 \pm 0.24) \times 10^{-6}$	104
25						105



Kinetic investigations of **1b** with dipolarophiles in *d*₈-toluene:mesitylene = 1:1

Table S24. Second-order rate constants k_2^{exptl} of the reactions of **1b** with **3k** in *d*₈-toluene:mesitylene = 1:1 at +90 (A), +80 (B), and +50 °C (C) (¹H NMR kinetics, dibromomethane as the internal standard IS). Activation parameters from the Eyring plot (D) were used to calculate $k_2(20\text{ °C})$. Initial reactant concentrations were determined by using the integration ranges of the IS from +90 to +50 °C at always 3.94–3.85 ppm, and of the α -hydrogen of **3k** at 5.13–5.07, 5.15–5.05, 5.14–5.06 ppm, respectively. Relaxation delay and acquisition time are always 1.00 and 4.09 s, respectively.

<i>T</i> (°C)	[1b] ₀ (M) ^a	[3k] ₀ (M)	[IS] ₀ (M)	k_2^{exptl} (M ⁻¹ s ⁻¹)	k_2 (M ⁻¹ s ⁻¹)	ΔG^\ddagger (kJ mol ⁻¹)
90	5.33×10^{-1}	5.63×10^{-1}	2.28×10^{-1}	1.85×10^{-5}		
80	4.05×10^{-1}	4.95×10^{-1}	4.75×10^{-1}	8.55×10^{-6}		
50	5.22×10^{-1}	5.45×10^{-1}	5.18×10^{-1}	9.52×10^{-7}		
20					$(6.21 \pm 0.91) \times 10^{-8}$	112
25						113

^a Calculated from weighed mass of **1b** because of the superimposition of the NMR resonances for the Me group of **1b** with those of the Me groups in mesitylene (solvent).

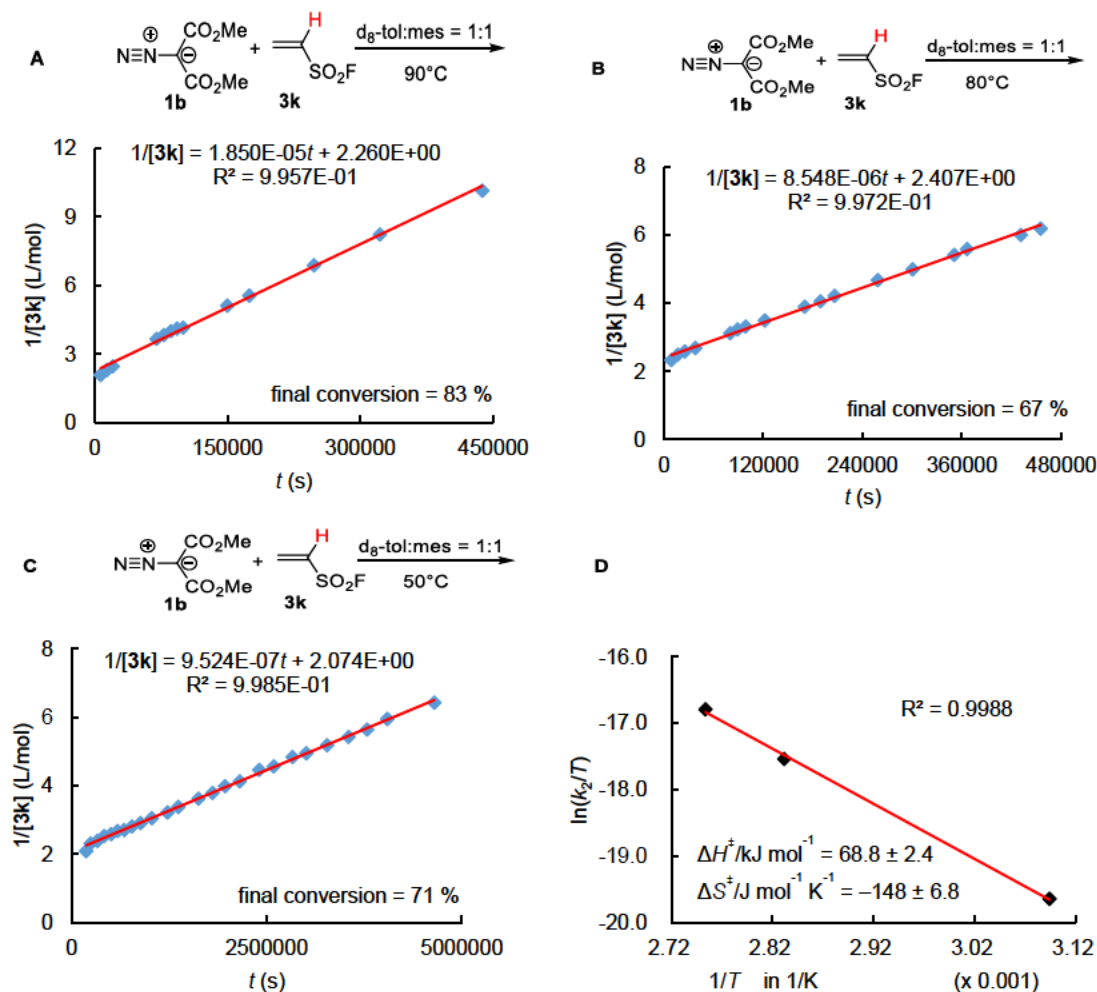
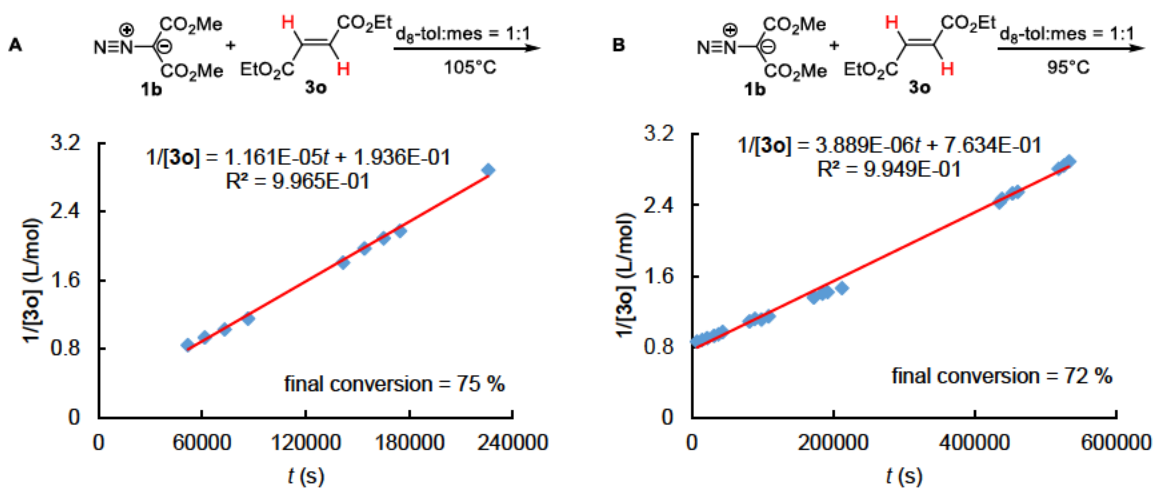


Table S25. Second-order rate constants k_2^{exptl} of the reactions of **1b** with **3o** in d_8 -toluene:mesitylene = 1:1 at +95 (A), +85 (B), +75 (C), and +65 °C (D) (^1H NMR kinetics, 1,1,2,2-tetrachloroethane as the internal standard IS). Activation parameters from the Eyring plot (E) were used to calculate $k_2(20\text{ °C})$ and $k_2(110\text{ °C})$. Initial reactant concentrations were determined by using the integration ranges of the IS from +95 to +65 °C at 5.61–5.54, 5.64–5.52, 5.64–5.56, 5.76–5.42 ppm, respectively, and of the vinylic hydrogens of **3o** at 6.59–6.54, 6.59–6.54, 6.60–6.53, 6.70–6.59 ppm, respectively. Relaxation delay and acquisition time are always 1.00 and 4.09 s, respectively.

T (°C)	$[\mathbf{1b}]_0$ (M) ^a	$[\mathbf{3o}]_0$ (M)	$[\text{IS}]_0$ (M)	k_2^{exptl} ($\text{M}^{-1}\text{ s}^{-1}$)	k_2 ($\text{M}^{-1}\text{ s}^{-1}$)	ΔG^\ddagger (kJ mol^{-1})
105	1.33	1.41	5.90×10^{-1}	1.16×10^{-5}		
95	1.25	1.22	8.98×10^{-1}	3.89×10^{-6}		
85	1.26	1.29	1.00	1.34×10^{-6}		
75	1.25	1.32	9.71×10^{-1}	4.16×10^{-7}		
65	1.29	1.42	8.66×10^{-1}	1.42×10^{-7}		
20					$(2.25 \pm 0.34) \times 10^{-10}$	125
25						125
110					$(1.80 \pm 0.08) \times 10^{-5}$	

^a Calculated from weighed mass of **1b** because of the superimposition of the NMR resonances for the Me group of **1b** with those of the Me groups in mesitylene (solvent).



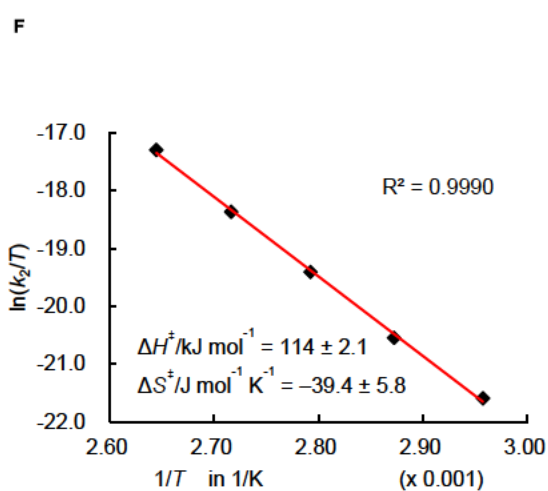
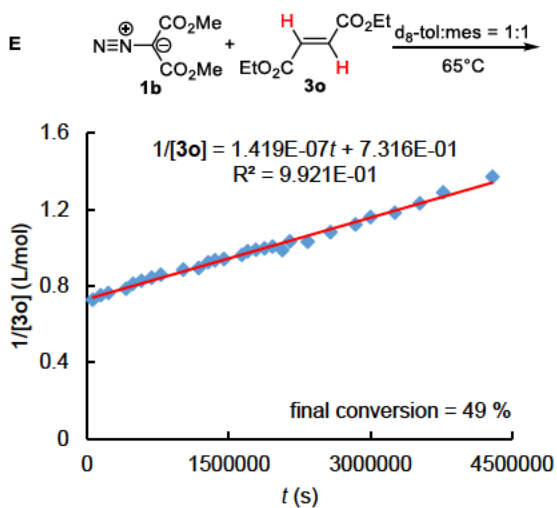
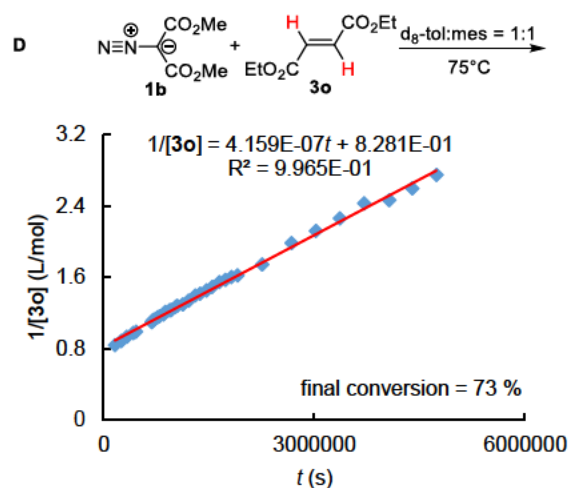
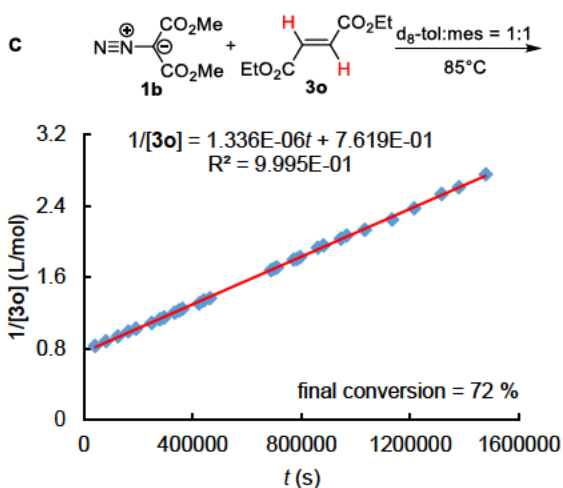


Table S26. Second-order rate constants k_2^{exptl} of the reactions of **1b** with **3r** in d_8 -toluene:mesitylene = 1:1 at +50 (A), +40 (B), and +20 °C (C) (^1H NMR technique, 1,1,2,2-tetrachloroethane as the internal standard IS). Activation parameters from the Eyring plot (D) were used to calculate $k_2(20\text{ °C})$. Initial reactant concentrations were determined by using the integration ranges of the IS from +50 to +20 °C at 6.10–6.00, 6.09–6.01, 5.74–5.66 ppm, respectively, and of the =CH₂ group of **3r** at 5.66–5.44, 5.65–5.44, 5.53–5.27 ppm, respectively. Relaxation delay and acquisition time are always 1.00 and 4.09 s, respectively.

T (°C)	$[\mathbf{1b}]_0$ (M) ^a	$[\mathbf{3r}]_0$ (M)	$[\text{IS}]_0$ (M)	k_2^{exptl} (M ⁻¹ s ⁻¹)	k_2 (M ⁻¹ s ⁻¹)	ΔG^\ddagger (kJ mol ⁻¹)
50	3.90	1.30	6.69×10^{-1}	3.85×10^{-7}		
40	3.96	1.27	6.30×10^{-1}	1.33×10^{-7}		
20	1.81	2.66	8.32×10^{-1}	1.21×10^{-8}	$(1.21 \pm 0.01) \times 10^{-8}$	116
25						117

^a Calculated from weighed mass of **1b** because of the superimposition of the NMR resonances for the Me group of **1b** with those of the Me groups in mesitylene (solvent).

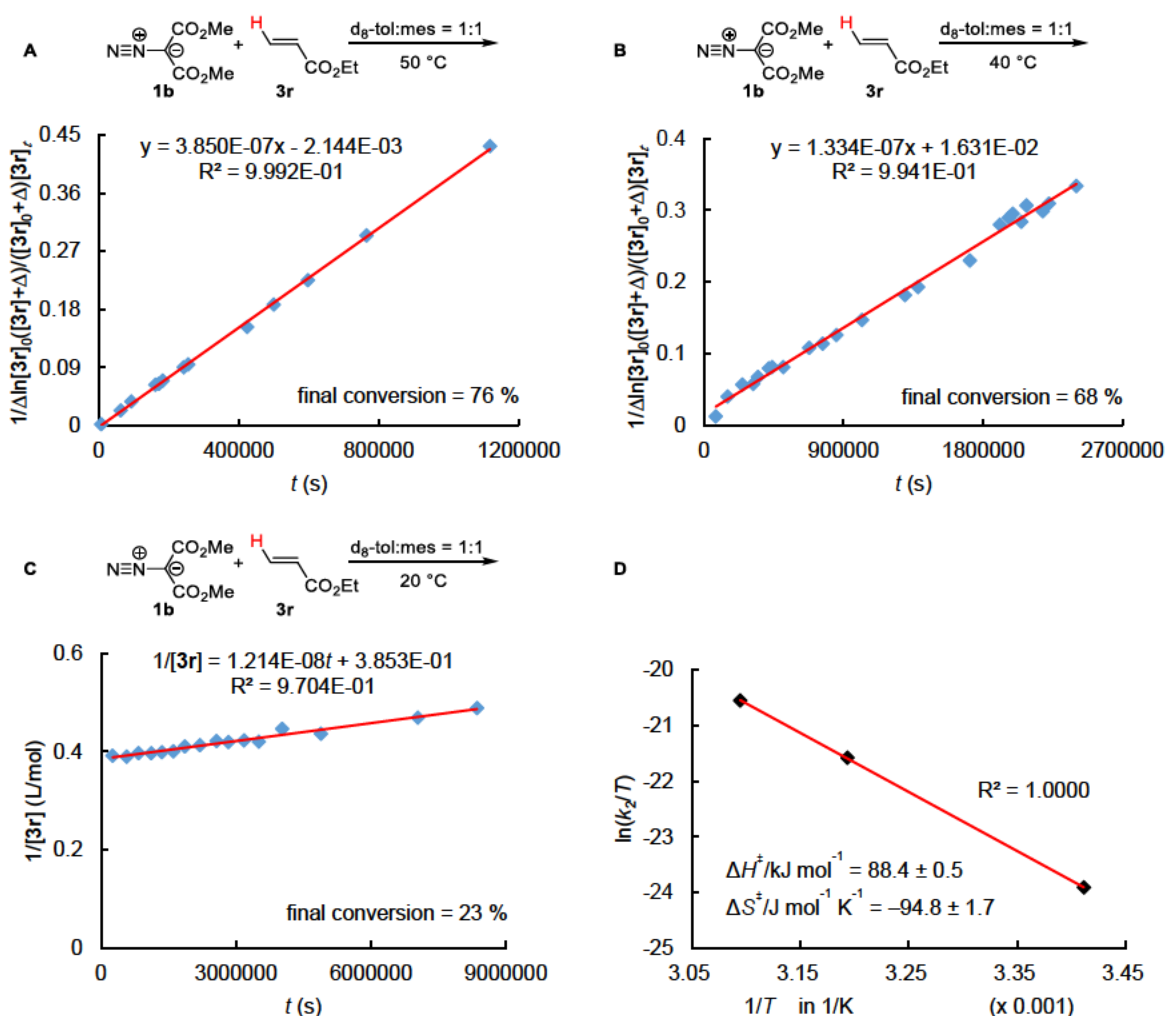
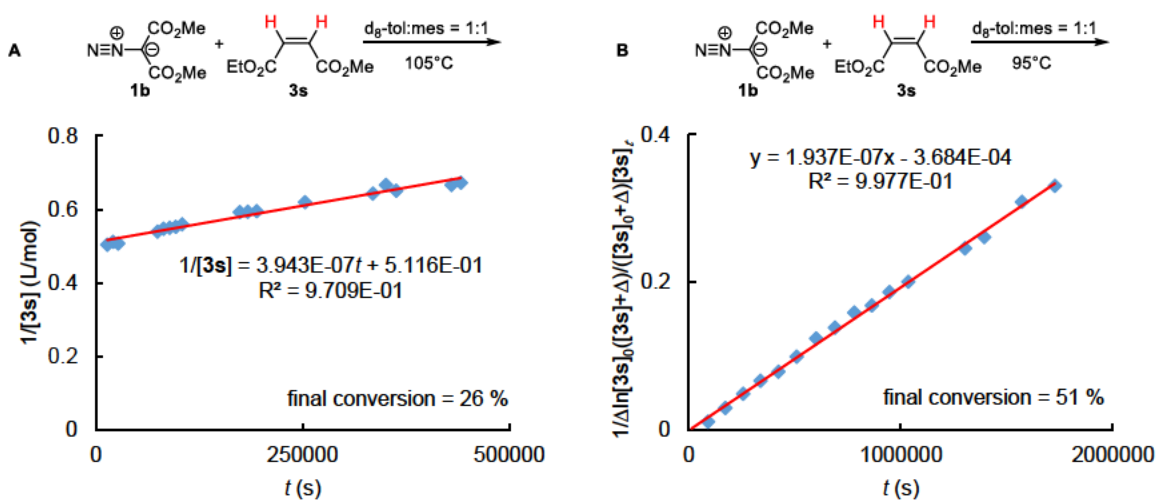
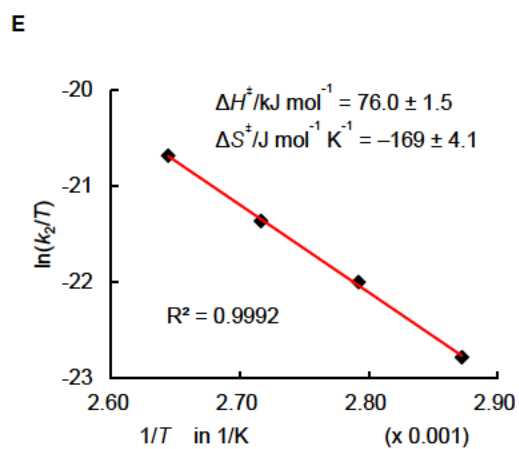
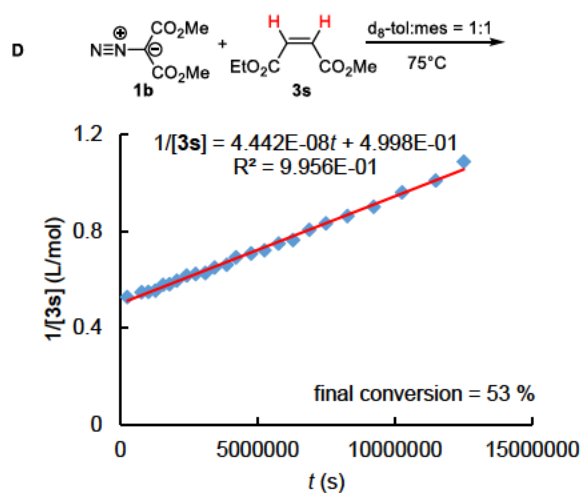
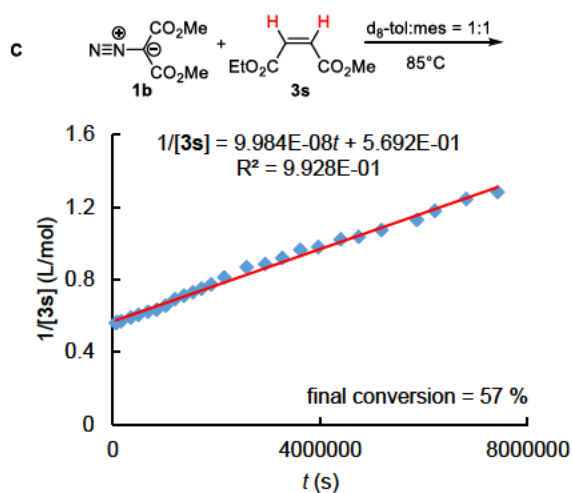


Table S27. Second-order rate constants k_2^{exptl} of the reactions of **1b** with **3s** in d_8 -toluene:mesitylene = 1:1 at +105 (A), +95 (B), +85 (C), and +75 °C (D) (^1H NMR technique, 1,1,2,2-tetrachloroethane as the internal standard IS). Activation parameters from the Eyring plot (E) were used to calculate $k_2(20\text{ °C})$ and $k_2(110\text{ °C})$. Initial reactant concentrations were determined by using the integration ranges of the IS from +105 to +75 °C at 5.71–5.51, 5.66–5.52, 5.69–5.45, 5.69–5.49 ppm, respectively, and of the vinylic hydrogens of **3s** at 5.93–5.70, 5.83–5.75, 5.91–5.67, 5.88–5.68 ppm, respectively. Relaxation delay and acquisition time are always 1.00 and 4.09 s, respectively.

T (°C)	$[\mathbf{1b}]_0$ (M) ^a	$[\mathbf{3s}]_0$ (M)	$[\text{IS}]_0$ (M)	k_2^{exptl} ($\text{M}^{-1}\text{ s}^{-1}$)	k_2 ($\text{M}^{-1}\text{ s}^{-1}$)	ΔG^\ddagger (kJ mol^{-1})
105	1.41	2.00	4.96×10^{-1}	3.94×10^{-7}		
95	1.23	1.92	9.80×10^{-1}	1.94×10^{-7}		
85	1.27	1.79	9.59×10^{-1}	9.98×10^{-8}		
75	1.26	1.94	9.48×10^{-1}	4.44×10^{-8}		
20					$(2.76 \pm 0.33) \times 10^{-10}$	126
25						126
110					$(5.45 \pm 0.14) \times 10^{-7}$	

^a Calculated from weighed mass of **1b** because of the superimposition of the NMR resonances for the Me group of **1b** with those of the Me groups in mesitylene (solvent).

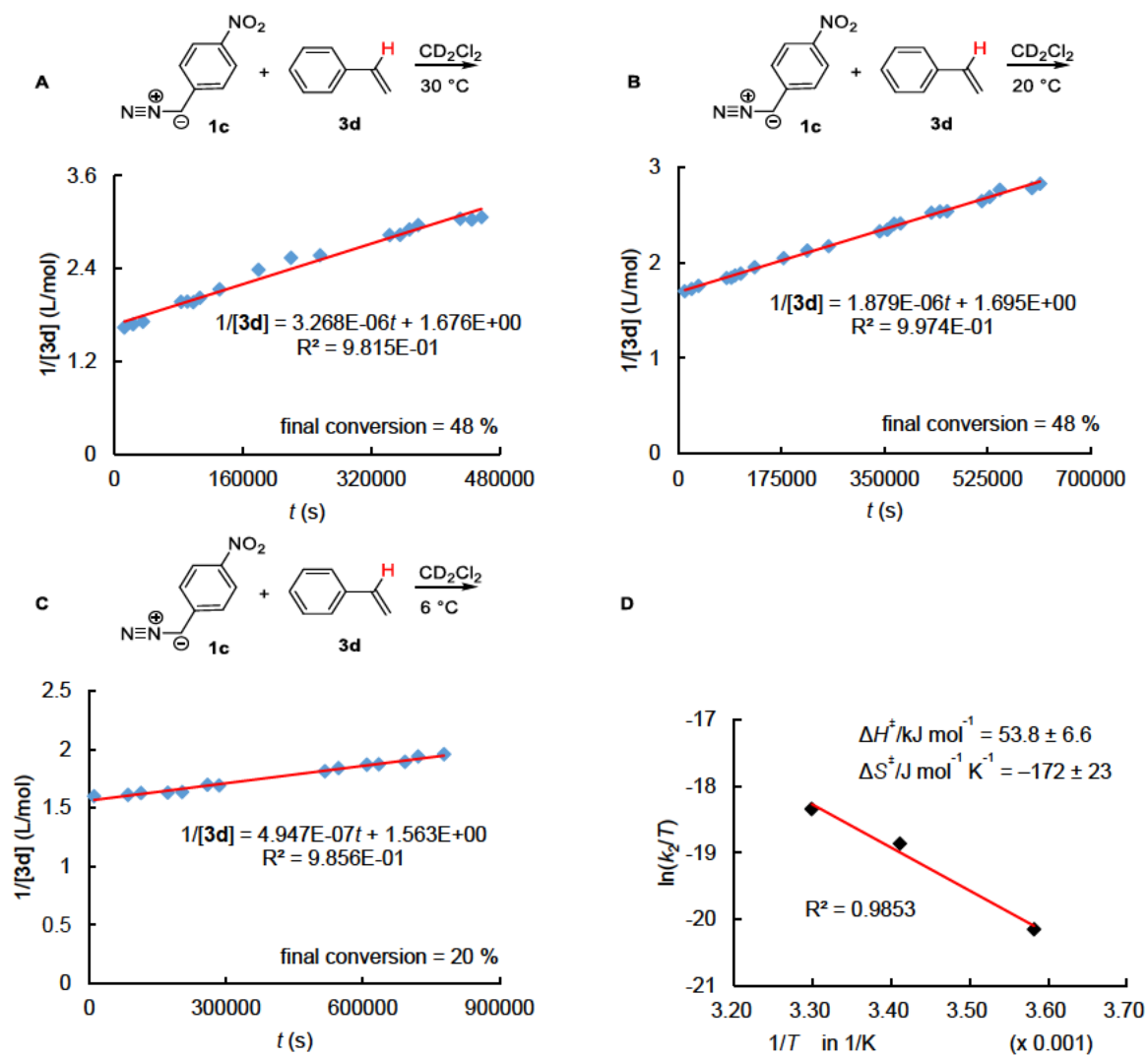




Kinetic investigations of the reactions of **1c** with styrene **3d** in CD_2Cl_2

Table S28. Second-order rate constants k_2^{exptl} of the reactions of **1c** with **3d** in CD_2Cl_2 at +30 (A), +20 (B), and +6 °C (C) (^1H NMR kinetics, dibromomethane as the internal standard IS). Activation parameters from the Eyring plot (D) were used to calculate $k_2(20\text{ °C})$. Initial reactant concentrations were determined by using the integration ranges of the IS from +30 to +6 °C at always 4.96–4.70 ppm, of the $-\text{CH}=\text{C}$ group of **3d** at 6.685–6.50 ppm, and of the aliphatic hydrogen of **1c** at 5.08–4.95 ppm. Relaxation delay and acquisition time are always 1.00 and 4.09 s, respectively.

T (°C)	$[\mathbf{1c}]_0$ (M)	$[\mathbf{3d}]_0$ (M)	$[\text{IS}]_0$ (M)	k_2^{exptl} ($\text{M}^{-1}\text{s}^{-1}$)	k_2 ($\text{M}^{-1}\text{s}^{-1}$)	ΔG^\ddagger (kJ mol^{-1})
30	5.83×10^{-1}	6.31×10^{-1}	2.96×10^{-1}	3.27×10^{-6}		
20	5.54×10^{-1}	5.94×10^{-1}	3.39×10^{-1}	1.88×10^{-6}		
6	5.60×10^{-1}	6.37×10^{-1}	3.61×10^{-1}	4.95×10^{-7}		
20					$(1.65 \pm 0.26) \times 10^{-6}$	104
25						105



List of Eyring activation parameters for the reactions of 1a-c with dipolarophiles

Table S29. Second-order rate constants $k_2(20^\circ\text{C})$ and Eyring activation parameters ΔG^\ddagger , ΔH^\ddagger , and ΔS^\ddagger for the reactions of diazo compounds 1a–c with dipolarophiles.

1	Dipolarophiles	Solvents	$k_2(20^\circ\text{C})$ ($\text{M}^{-1} \text{s}^{-1}$)	$\Delta G^\ddagger(20^\circ\text{C})$ (kJ mol^{-1})	ΔH^\ddagger (kJ mol^{-1})	ΔS^\ddagger ($\text{J mol}^{-1} \text{K}^{-1}$)	T-Range
1a	3e	CDCl_3	$(7.06 \pm 0.58) \times 10^{-7}$	106	71.8 ± 4.2	-118 ± 14	+20 to +50 °C
1a	3h	CDCl_3	$(5.96 \pm 0.56) \times 10^{-9}$	118	71.8 ± 3.6	-157 ± 12	+30 to +50 °C
1a	3k	<i>d</i> ₈ -toluene	$(7.92 \pm 0.16) \times 10^{-4}$	89.3	36.5 ± 0.8	-180 ± 2.4	+30 to +50 °C
1a	3o	<i>d</i> ₈ -toluene	$(2.78 \pm 0.18) \times 10^{-5}$	97.3	55.7 ± 3.3	-142 ± 11	+20 to +50 °C
1a	3s	<i>d</i> ₈ -toluene	$(3.21 \pm 0.47) \times 10^{-6}$	103	54.9 ± 7.6	-163 ± 25	+20 to +50 °C
1a	3t	<i>d</i> ₈ -toluene	$(2.85 \pm 0.31) \times 10^{-6}$	103	51.3 ± 3.6	-176 ± 12	+30 to +60 °C
1a	3v	<i>d</i> ₈ -toluene	$(2.07 \pm 0.85) \times 10^{-7}$	109	59.2 ± 7.6	-171 ± 23	+50 to +80 °C
1a	3x	<i>d</i> ₈ -toluene	$(2.48 \pm 0.57) \times 10^{-8}$	114	69.2 ± 4.2	-154 ± 12	+50 to +80 °C
1b	3e	CDCl_3	$(2.44 \pm 0.18) \times 10^{-8}$	115	68.3 ± 2.4	-158 ± 7.4	+35 to +55 °C
1b	3i	CDCl_3	$(1.94 \pm 0.24) \times 10^{-6}$	104	61.1 ± 5.8	-146 ± 19	+20 to +50 °C
1b	3k	T+M ^a	$(6.21 \pm 0.91) \times 10^{-8}$	112	68.8 ± 2.4	-148 ± 6.8	+50 to +90 °C
1b	3o	T+M ^a	$(2.25 \pm 0.34) \times 10^{-10}$	126	114 ± 2.1	-39.4 ± 5.8	+65 to +105 °C
1b	3r	T+M ^a	$(1.21 \pm 0.01) \times 10^{-8}$	116	88.4 ± 0.5	-94.8 ± 1.7	+20 to +50 °C
1b	3s	T+M ^a	$(2.76 \pm 0.33) \times 10^{-10}$	126	76.0 ± 1.5	-169 ± 4.1	+75 to +105 °C
1c	3d	CD_2Cl_2	$(1.65 \pm 0.26) \times 10^{-6}$	104	53.8 ± 6.6	-172 ± 23	+6 to +30 °C

^a Solvent T+M = *d*₈-toluene/mesitylene (v/v = 1/1).

Comparison of rate constants k_2 with reported k_2 values**Table S30.** Comparison of the second-order rate constants k_2 extrapolated from experimental data (this work) with Reissig's data (ref. S17) for the reactions of **1a** with dipolarophiles at 80.3 °C and of **1b** with dipolarophiles at 110 °C.

Diazo Compounds	Dipolarophiles	T (°C)	$k_2(T)$ ($M^{-1} s^{-1}$) this work	$k_2(T)$ ($M^{-1} s^{-1}$) ref. S17	Ratio
1a	3e	80.3	$1.29 \times 10^{-4},^a$	$7.46 \times 10^{-5},^b$	1.7
1a	3o	80.3	$1.66 \times 10^{-3},^c$	$1.23 \times 10^{-3},^b$	1.4
1a	3s	80.3	$1.81 \times 10^{-4},^c$	$3.05 \times 10^{-4},^b$	1/1.7
1a	3v	80.3	$1.57 \times 10^{-5},^c$	$1.62 \times 10^{-5},^b$	1.0
1a	3x	80.3	$3.79 \times 10^{-6},^c$	$3.75 \times 10^{-6},^d$	1.0
1b	3e	110	$2.30 \times 10^{-5},^a$	$3.18 \times 10^{-5},^e$	1/1.4
1b	3o	110	$1.80 \times 10^{-5},^f$	$9.20 \times 10^{-6},^e$	2.0
1b	3s	110	$6.37 \times 10^{-7},^f$	$1.50 \times 10^{-6},^e$	1/2.4

^a Extrapolated from rate constants in $CDCl_3$ at lower temperatures by using the Eyring equation. ^b In toluene at 80.3 °C measured by IR spectroscopy. ^c Extrapolated from rate constants in d_8 -toluene at lower temperatures by using the Eyring equation. ^d In toluene at 80.3 °C measured by NMR spectroscopy. ^e In mesitylene at 110 °C measured by IR spectroscopy. ^f Extrapolated from rate constants in d_8 -toluene:mesitylene = 1:1 at lower temperatures by using the Eyring equation.

Determination of the energy of concert for the reactions of 1a-c with dipolarophiles

Table S31. Determination of the energy of concert ($\Delta G^{\ddagger}_{\text{concert}}$) from the ratio of experimental (k_2^{exptl}) and calculated (k_2^{Eq1}) second-order rate constants for the reactions of 1a-c with dipolarophiles at 20 °C.

Diazo compounds	Dipolarophiles	k_2^{exptl} ($\text{M}^{-1} \text{s}^{-1}$)	Solvents	k_2^{Eq1} ($\text{M}^{-1} \text{s}^{-1}$)	$k_2^{\text{exptl}}/k_2^{\text{Eq1}}$	$\Delta G^{\ddagger}_{\text{concert}}$ (kJ mol^{-1})
1a ($E = -18.5$)	3e ($N = -0.25, s_N = 1.09$)	7.06×10^{-7}	CDCl_3	3.65×10^{-21}	1.9×10^{14}	80
	3h ($N = -2.77, s_N = 1.41$)	5.96×10^{-9}	CDCl_3	1.02×10^{-30}	5.8×10^{21}	122
	3x ($N = -0.04, s_N = 0.77$)	2.48×10^{-8}	<i>d</i> ₈ -toluene	5.30×10^{-15}	4.7×10^6	37
1a ($N = 4.68, s_N = 0.94$)	3k ($E = -12.09$)	7.92×10^{-4}	<i>d</i> ₈ -toluene	1.08×10^{-7}	7.3×10^3	22
	3o ($E = -17.79$)	2.78×10^{-5}	<i>d</i> ₈ -toluene	4.75×10^{-13}	5.9×10^7	44
	3q ($E = -19.05$)	$1 \times 10^{-5, a}$	toluene	3.11×10^{-14}	3.2×10^8	48
	3s ($E = -19.49$)	3.21×10^{-6}	<i>d</i> ₈ -toluene	1.20×10^{-14}	2.7×10^8	47
	3t ($E = -22.77$)	2.85×10^{-6}	<i>d</i> ₈ -toluene	9.89×10^{-18}	2.9×10^{11}	64
	3v ($E = -23.59$)	2.07×10^{-7}	<i>d</i> ₈ -toluene	1.68×10^{-18}	1.2×10^{11}	62
1b ($E = -18.2$)	3e ($N = -0.25, s_N = 1.09$)	2.44×10^{-8}	CDCl_3	7.75×10^{-21}	3.1×10^{12}	70
1b ($N = -1.24, s_N = 0.81$)	3i ($E = -7.50$)	1.94×10^{-6}	CDCl_3	8.33×10^{-8}	2.3×10^1	8
	3k ($E = -12.09$)	6.21×10^{-8}	T+M ^b	1.59×10^{-11}	3.9×10^3	20
	3o ($E = -17.79$)	2.25×10^{-10}	T+M ^b	3.85×10^{-16}	5.8×10^5	32
	3q ($E = -19.05$)	$4 \times 10^{-9, c}$	mesitylene	3.67×10^{-17}	1.1×10^8	45
	3r ($E = -19.07$)	1.21×10^{-8}	T+M ^b	3.54×10^{-17}	3.4×10^8	48
	3s ($E = -19.49$)	2.76×10^{-10}	T+M ^b	1.62×10^{-17}	1.7×10^7	41
	3t ($E = -22.77$)	$3 \times 10^{-9, c}$	mesitylene	3.56×10^{-20}	8.4×10^{10}	61
3v ($E = -23.59$)	$2 \times 10^{-10, c}$	mesitylene	7.72×10^{-21}	2.6×10^{10}	58	
1c ($E = -18.3$)	3d ($N = 0.78, s_N = 0.95$)	1.65×10^{-6}	CD_2Cl_2	2.27×10^{-17}	7.3×10^{10}	61
1c ($N = 7.17, s_N = 0.83$)	3i ($E = -7.50$)	$2.16 \times 10^{1, d}$	CH_2Cl_2	5.32×10^{-1}	4.1×10^1	9
	3k ($E = -12.09$)	$5.82 \times 10^{-2, d}$	CH_2Cl_2	8.25×10^{-5}	7.1×10^2	16
	3l ($E = -14.07$)	$1.74 \times 10^{-2, d}$	CH_2Cl_2	1.87×10^{-6}	9.3×10^3	22
	3n ($E = -16.76$)	7.35×10^{-3}	CH_2Cl_2	1.10×10^{-8}	6.7×10^5	33
	3o ($E = -17.79$)	1.07×10^{-2}	CH_2Cl_2	1.53×10^{-9}	7.0×10^6	38
	3r ($E = -19.07$)	1.37×10^{-3}	CH_2Cl_2	1.33×10^{-10}	1.0×10^7	39
	3t ($E = -22.77$)	9.04×10^{-5}	CH_2Cl_2	1.13×10^{-13}	8.0×10^8	50

^a Calculated from $k_2(80.3 \text{ °C})$ reported in refs. S17 and S22 by assuming $\Delta S^{\ddagger} = -150 \text{ J mol}^{-1} \text{ K}^{-1}$. ^b Solvent T+M = *d*₈-toluene/mesitylene (1/1). ^c Calculated from $k_2(110 \text{ °C})$ reported in refs. S17 and S22 by assuming $\Delta S^{\ddagger} = -150 \text{ J mol}^{-1} \text{ K}^{-1}$. ^d Second-order rate constants k_2^{exptl} from ref. S11.

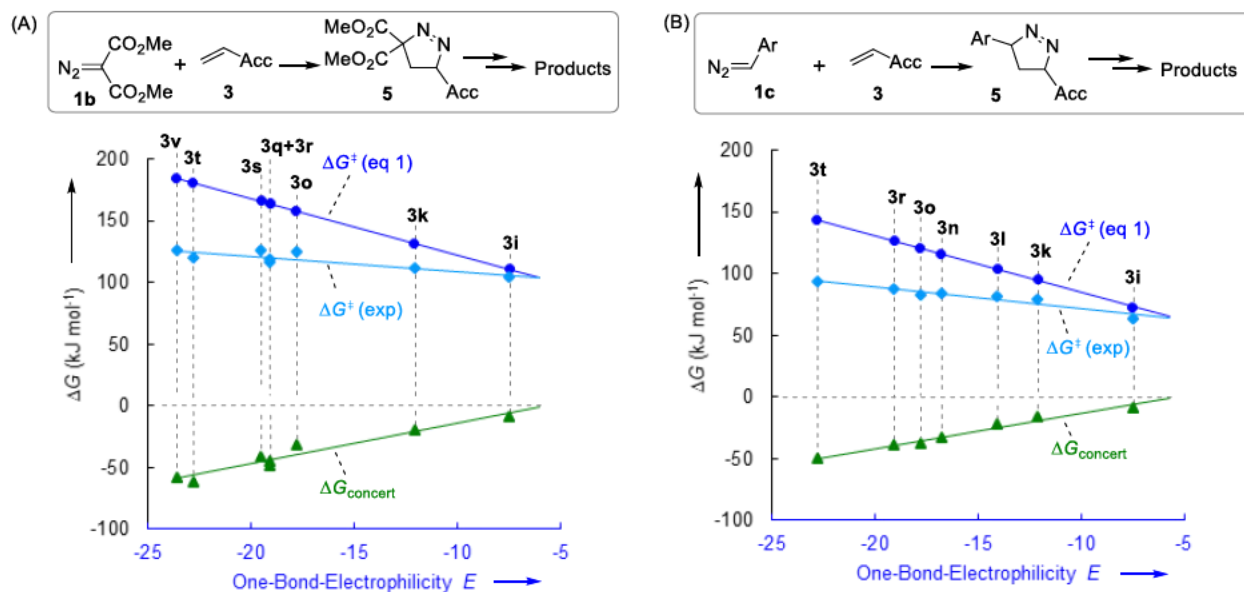
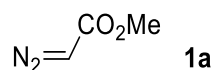


Figure S5. Correlation of Gibbs energies ΔG (at 20 °C) for the 1,3-dipolar cycloadditions of electrophilic 1,3-dipolarophiles **3** with diazo compounds (A) **1b** and (B) **1c**, respectively, vs. the one-bond electrophilicities E of **3**. – ΔG^+ (eq 1): Gibbs activation energy calculated from eq. (1); ΔG^+ (exp): Gibbs activation energy measured experimentally; $\Delta G_{\text{concert}}$: energy of concert, i.e., stabilization of the concerted transition state relative to the transition state yielding a zwitterion.

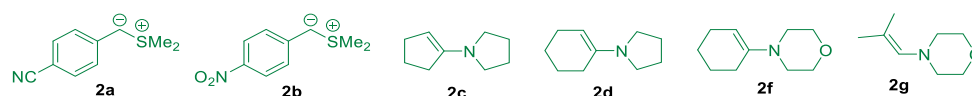
Construction of $\lg k_2$ vs. N and E correlations for the reactions of diazo compounds **1** with electrophiles, nucleophiles, and dipolarophiles

Methyl diazoacetate (**1a**)



The $\lg k_2$ vs. N and E correlations for methyl diazoacetate (**1a**) were constructed by using second-order rate constants $k_2(20\text{ }^\circ\text{C})$ of the reactions of **1a** with reference one-bond nucleophiles **2** (Table S32), reference one-bond electrophiles (Ar_2CH^+ , Table S33), and dipolarophiles **3** (Table S34).

Table S32. Second-order rate constants $k_2(20\text{ }^\circ\text{C})$ for the reactions of **1a** with reference one-bond nucleophiles **2** and resulting electrophilicity parameter $E(\mathbf{1a})$.

		Solvents	$k_2(20\text{ }^\circ\text{C})^a/$ ($\text{M}^{-1}\text{ s}^{-1}$)	$\lg k_2$
Nucleophiles 2				
2a ($N = 21.07$, $s_N = 0.68$)		DMSO	1.18×10^2	2.07
2b ($N = 18.42$, $s_N = 0.65$)		DMSO	2.17	0.34
2c ($N = 15.91$, $s_N = 0.86$)		CDCl_3	1.83×10^{-3}	-2.74
2d ($N = 14.91$, $s_N = 0.86$)		CDCl_3	4.68×10^{-4}	-3.33
2f ($N = 11.40$, $s_N = 0.83$)		CDCl_3	7.03×10^{-7}	-6.15
2g ($N = 10.04$, $s_N = 0.82$)		CDCl_3	2.20×10^{-7}	-6.66
E of 1a			-18.5	

^a From refs S12a and S12b.

Table S33. Second-order rate constants $k_2(20\text{ }^\circ\text{C})$ for the reactions of **1a** with reference one-bond electrophiles Ar_2CH^+ (counterion: BF_4^-) in CH_2Cl_2 and resulting reactivity parameters N and s_N .

$\text{Ar}_2\text{CH}^+{}^a$	E	$k_2(20\text{ }^\circ\text{C})^a/$ ($\text{M}^{-1}\text{ s}^{-1}$)	$\lg k_2$
$(\text{mfa})_2\text{CH}^+$	-3.85	6.94	0.84
$(\text{dpa})_2\text{CH}^+$	-4.72	6.22×10^{-1}	-0.21
$(\text{mor})_2\text{CH}^+$	-5.53	2.19×10^{-1}	-0.66
$(\text{dma})_2\text{CH}^+$	-7.02	5.92×10^{-3}	-2.23
$N(s_N)$ of 1a		4.68 (0.94)	

^a This work.**Table S34.** Second-order rate constants $k_2(20\text{ }^\circ\text{C})$ for the reactions of **1a** with dipolarophiles **3**.

Dipolarophiles 3	Solvents	$k_2(80.3\text{ }^\circ\text{C})^a/$ ($\text{M}^{-1}\text{ s}^{-1}$)	$k_2(20\text{ }^\circ\text{C})^b/$ ($\text{M}^{-1}\text{ s}^{-1}$)	$\lg k_2$
3a ($N = 9.81$)	toluene	7.2×10^{-6}	$5 \times 10^{-8},^c$	-7.3
3b ($N = 3.76$)	toluene	2×10^{-7}	$6 \times 10^{-10},^c$	-9.2
3d ($N = 0.78$)	toluene	1.14×10^{-5}	$8 \times 10^{-8},^c$	-7.1
3e ($N = -0.25$)	CDCl_3		7.06×10^{-7}	-6.2
3h ($N = -2.77$)	CDCl_3		5.96×10^{-9}	-8.2
3x ($N = -0.04$)	d_8 -toluene		2.48×10^{-8}	-7.6
3k ($E = -12.09$)	d_8 -toluene		7.92×10^{-4}	-3.1
3o ($E = -17.79$)	d_8 -toluene		2.78×10^{-5}	-4.6
3q ($E = -19.05$)	toluene	7.22×10^{-4}	$1 \times 10^{-5},^c$	-5.0
3s ($E = -19.49$)	d_8 -toluene		3.21×10^{-6}	-5.5
3t ($E = -22.77$)	d_8 -toluene		2.85×10^{-6}	-5.5
3v ($E = -23.59$)	d_8 -toluene		2.07×10^{-7}	-6.7

^a Second-order rate constants $k_2(80.3\text{ }^\circ\text{C})$ from refs S17 and S22. ^b This work, if not mentioned otherwise.^c Calculated from $k_2(80.3\text{ }^\circ\text{C})$ with an assumed $\Delta S^\ddagger = -150\text{ J mol}^{-1}\text{ K}^{-1}$.

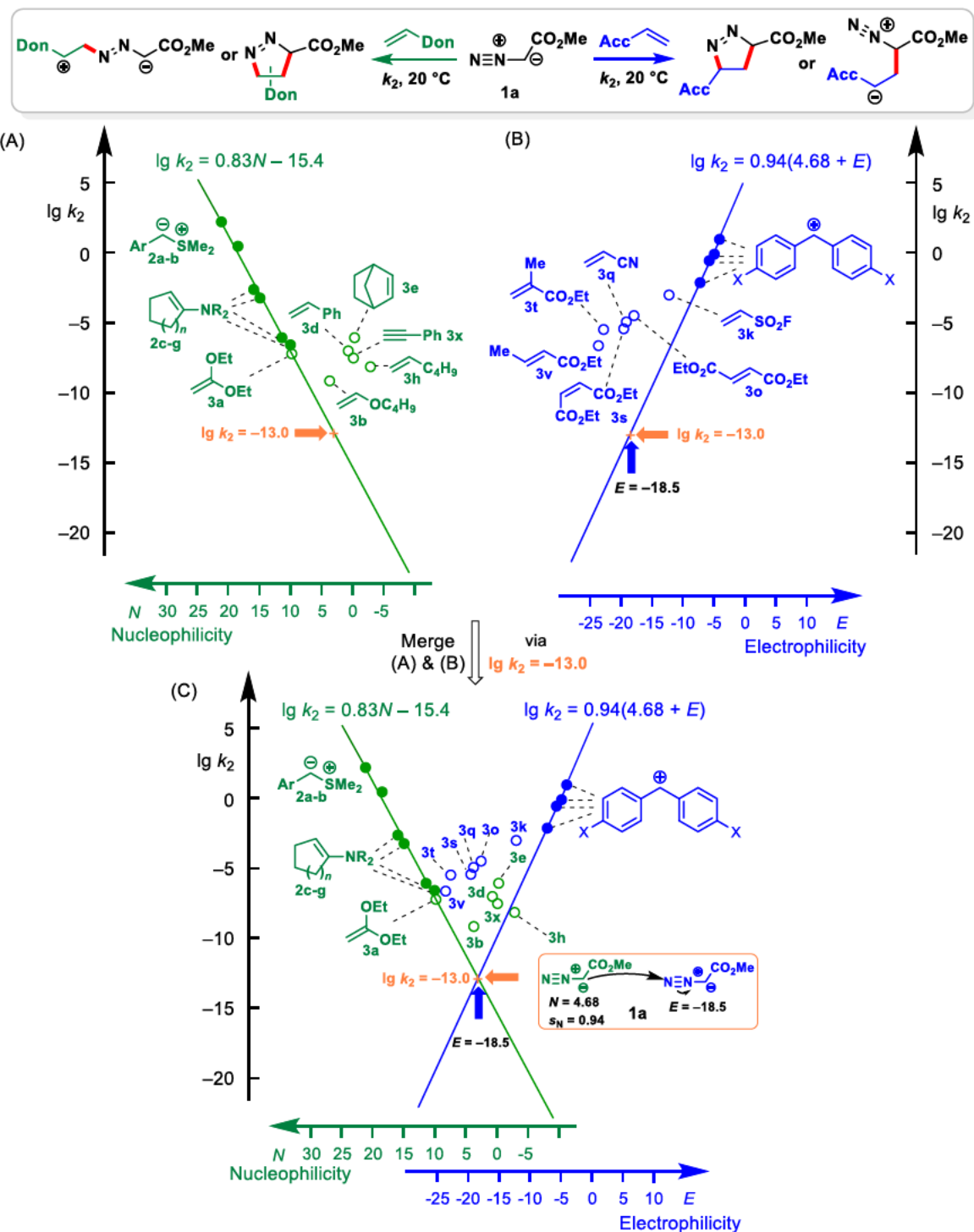
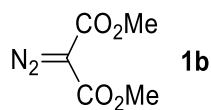
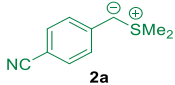
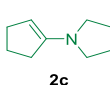
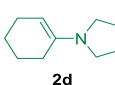
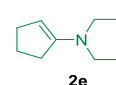
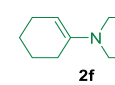


Figure S6. (A) Plot of $\lg k_2$ vs. N parameters for the reactions of **1a** with reference nucleophiles **2** (filled green dots, used to construct the green correlation line) and nucleophilic dipolarophiles **3** (open green dots). (B) Plot of $\lg k_2$ vs. E parameters for the reactions of **1a** with reference electrophiles Ar_2CH^+ (filled blue dots, used to construct the blue correlation line) and electrophilic dipolarophiles **3**. (C) Merging the plots of (A) and (B) by crossing the green and blue correlation lines at $\lg k_2 = -13.0$, which reflects the hypothetical rate constant for the reaction of an electrophilic molecule **1a** with a nucleophilic molecule **1a** as calculated by using Equation (1).

Dimethyl diazomalonate (1b)

The $\lg k_2$ vs. N and E correlations for dimethyl diazomalonate (**1b**) were constructed by using second-order rate constants $k_2(20\text{ }^\circ\text{C})$ of the reactions of **1b** with reference one-bond nucleophiles **2** (Table S35), reference one-bond electrophiles (Ar_2CH^+ , Table S36), and dipolarophiles **3** (Table S37).

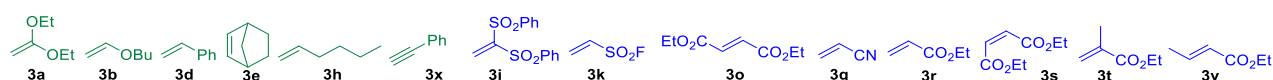
Table S35. Second-order rate constants $k_2(20\text{ }^\circ\text{C})$ for the reactions of **1b** with reference one-bond nucleophiles **2** and resulting electrophilicity parameter $E(\mathbf{1b})$.

Nucleophiles 2	Solvents	$k_2(20\text{ }^\circ\text{C})^a /$ ($\text{M}^{-1}\text{ s}^{-1}$)	$\lg k_2$
 2a ($N = 21.07$, $s_N = 0.68$)	DMSO	4.22×10^1	1.62
 2c ($N = 15.91$, $s_N = 0.86$)	CDCl_3	2.59×10^{-2}	-1.59
 2d ($N = 14.91$, $s_N = 0.86$)	CDCl_3	7.59×10^{-4}	-3.12
 2e ($N = 13.41$, $s_N = 0.82$)	CDCl_3	9.91×10^{-5}	-4.00
 2f ($N = 11.40$, $s_N = 0.83$)	CDCl_3	4.81×10^{-6}	-5.32
E of 1b		-18.2	

^a From ref. S12b.

Table S36. Second-order rate constants $k_2(20\text{ }^\circ\text{C})$ for the reactions of **1b** with reference one-bond electrophiles Ar_2CH^+ (counterion: TfO^-) in CH_2Cl_2 and resulting nucleophilicity parameters $N(s_N)$ for **1b**.

Ar_2CH^+ ^a	E	$k_2(20\text{ }^\circ\text{C})^a/$ ($\text{M}^{-1}\text{ s}^{-1}$)	$\lg k_2$
(ani)(tol) CH^+	1.48	1.33	0.12
(ani) ₂ CH^+	0	1.41×10^{-1}	-0.85
(fur) ₂ CH^+	-1.36	6.67×10^{-3}	-2.18
$N(s_N)$ of 1b		-1.24 (0.81)	

^a This work.**Table S37.** Second-order rate constants $k_2(20\text{ }^\circ\text{C})$ for the reactions of **1b** with dipolarophiles **3**.

Dipolarophiles 3	Solvents	$k_2(110\text{ }^\circ\text{C})^a/$ ($\text{M}^{-1}\text{ s}^{-1}$)	$k_2(20\text{ }^\circ\text{C})^b/$ ($\text{M}^{-1}\text{ s}^{-1}$)	$\lg k_2$
3a ($N = 9.81$)	mesitylene	1.2×10^{-6}	$4 \times 10^{-10}, c$	-9.4
3b ($N = 3.76$)	mesitylene	2×10^{-7}	$4 \times 10^{-11}, c$	-10.4
3d ($N = 0.78$)	mesitylene	1.4×10^{-6}	$5 \times 10^{-10}, c$	-9.3
3e ($N = -0.25$)	CDCl_3		2.44×10^{-8}	-7.6
3h ($N = -2.77$)	mesitylene	1.3×10^{-6}	$4 \times 10^{-10}, c$	-9.4
3x ($N = -0.04$)	mesitylene	1.6×10^{-6}	$6 \times 10^{-10}, c$	-9.2
3i ($E = -7.50$)	CDCl_3		1.94×10^{-6}	-5.7
3k ($E = -12.09$)	T+M ^d		6.21×10^{-8}	-7.2
3o ($E = -17.79$)	T+M ^d		2.25×10^{-10}	-9.6
3q ($E = -19.05$)	mesitylene	6.7×10^{-6}	$4 \times 10^{-9}, c$	-8.4
3r ($E = -19.07$)	T+M ^d		1.21×10^{-8}	-7.9
3s ($E = -19.49$)	T+M ^d		2.76×10^{-10}	-9.6
3t ($E = -22.77$)	mesitylene	$6.1 \times 10^{-6}, e$	$3 \times 10^{-9}, c$	-8.5
3v ($E = -23.59$)	mesitylene	6×10^{-7}	$2 \times 10^{-10}, c$	-9.7

^a Second-order rate constants $k_2(110\text{ }^\circ\text{C})$ from refs [S17](#) and [S22](#). ^b This work, if not mentioned otherwise. ^c Calculated from $k_2(110\text{ }^\circ\text{C})$ with an assumed $\Delta S^\ddagger = -150\text{ J mol}^{-1}\text{ K}^{-1}$. ^d Solvent mixture T+M = *d*₃-toluene/mesitylene (1/1). ^e Rate constant $k_2(110\text{ }^\circ\text{C})$ for the reaction of **1b** with methyl methacrylate.

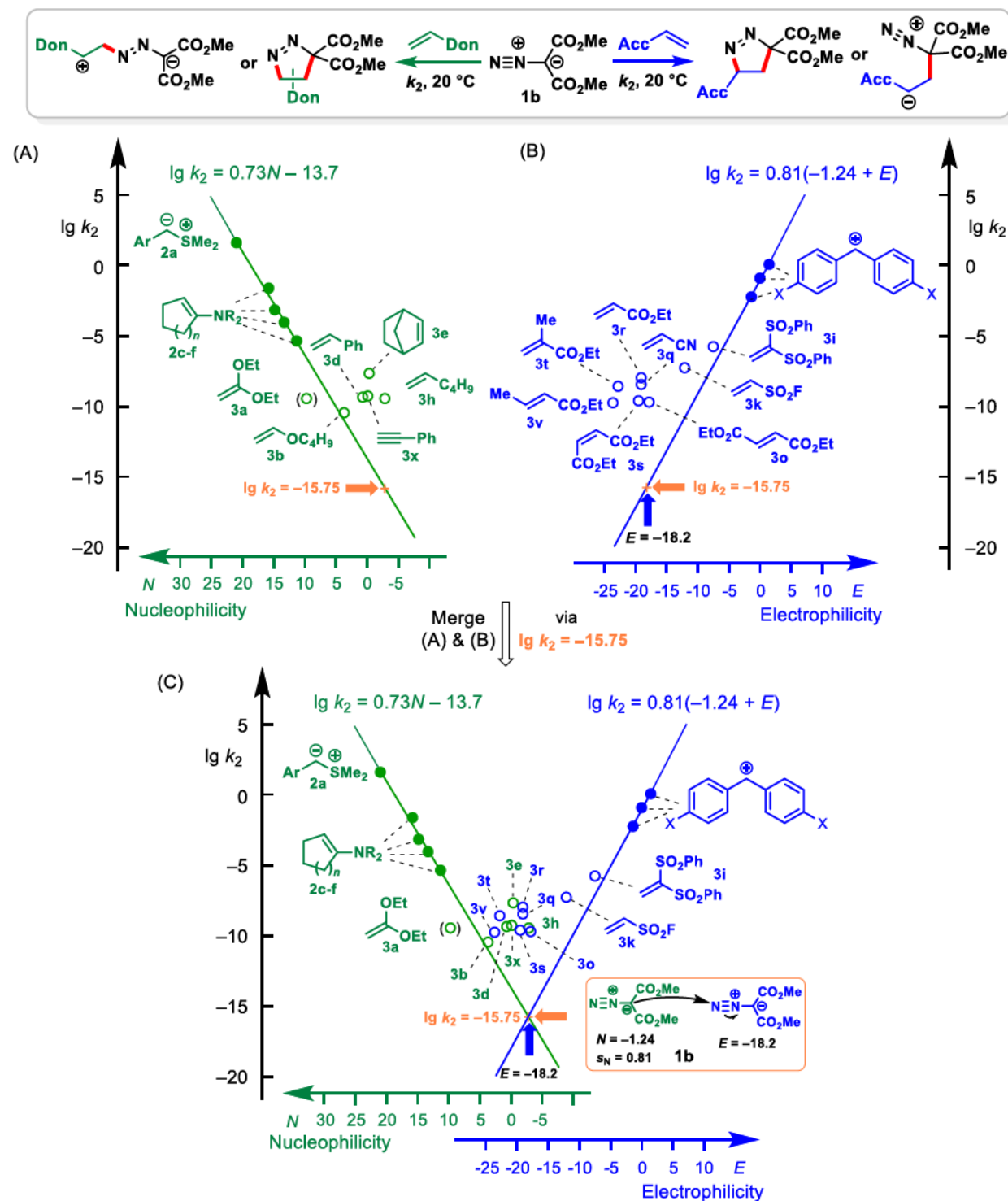
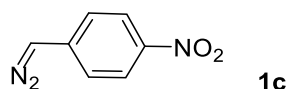
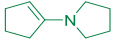
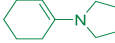
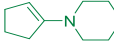


Figure S7. (A) Plot of $\lg k_2$ vs. N parameters for the reactions of **1b** with reference nucleophiles **2** (filled green dots, used to construct the green correlation line) and nucleophilic dipolarophiles **3** (open green dots). (B) Plot of $\lg k_2$ vs. E parameters for the reactions of **1b** with reference electrophiles Ar_2CH^+ (filled blue dots, used to construct the blue correlation line) and electrophilic dipolarophiles **3**. (C) Merging the plots of (A) and (B) by crossing the green and blue correlation lines at $\lg k_2 = -15.75$, which reflects the hypothetical rate constant for the reaction of an electrophilic molecule **1b** with a nucleophilic molecule **1b** as calculated by using Equation (1).

(*p*-Nitrophenyl)diazomethane (1c)

The $\lg k_2$ vs. N and E correlations for (*p*-nitrophenyl)diazomethane (**1c**) were constructed by using second-order rate constants $k_2(20\text{ }^\circ\text{C})$ of the reactions of **1c** with reference one-bond nucleophiles **2** (Table S38), reference one-bond electrophiles (Ar_2CH^+ , Table S39), and dipolarophiles **3** (Table S40).

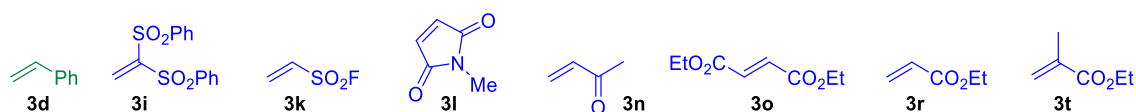
Table S38. Second-order rate constants $k_2(20\text{ }^\circ\text{C})$ for the reactions of **1c** with reference one-bond nucleophiles **2** and resulting electrophilicity parameter $E(\mathbf{1c})$.

 2c	 2d	 2e	 2f
Nucleophiles 2			
Solvents	$k_2(20\text{ }^\circ\text{C})^a/$ ($\text{M}^{-1}\text{ s}^{-1}$)	$\lg k_2$	
2c ($N = 15.91$, $s_N = 0.86$)	7.20×10^{-3}	-2.14	CD_2Cl_2
2d ($N = 14.91$, $s_N = 0.86$)	1.93×10^{-3}	-2.71	CD_2Cl_2
2e ($N = 13.41$, $s_N = 0.82$)	7.59×10^{-5}	-4.12	CD_2Cl_2
2f ($N = 11.40$, $s_N = 0.83$)	1.80×10^{-6}	-5.74	CD_2Cl_2
E of 1b		-18.3	

^a From ref. S12b.

Table S39. Second-order rate constants $k_2(20\text{ }^\circ\text{C})$ for the reactions of **1c** with reference one-bond electrophiles Ar_2CH^+ (counterion: BF_4^-) in CH_2Cl_2 and resulting reactivity parameters N and s_N .

$\text{Ar}_2\text{CH}^+{}^a$	E	$k_2(20\text{ }^\circ\text{C})^a/$ ($\text{M}^{-1}\text{ s}^{-1}$)	$\lg k_2$
(dpa) $_2\text{CH}^+$	-4.72	1.26×10^2	2.10
(mor) $_2\text{CH}^+$	-5.53	2.16×10^1	1.33
(mpa) $_2\text{CH}^+$	-5.89	9.49	0.98
(dma) $_2\text{CH}^+$	-7.02	1.51	0.18
$N(s_N)$ of 1c		7.17 (0.83)	

^a Data from ref. S11.**Table S40.** Second-order rate constants $k_2(20\text{ }^\circ\text{C})$ for the reactions of **1c** with dipolarophiles **3**.

Dipolarophiles 3	Solvents	$k_2(20\text{ }^\circ\text{C})^a/$ ($\text{M}^{-1}\text{ s}^{-1}$)	$\lg k_2$
3d ($N = 0.78$)	CD_2Cl_2	1.65×10^{-6}	-5.78
3i ($E = -7.5$)	CH_2Cl_2	$2.16 \times 10^{1,b}$	1.33
3k ($E = -12.09$)	CH_2Cl_2	$5.82 \times 10^{-2,b}$	-1.24
3l ($E = -14.07$)	CH_2Cl_2	$1.74 \times 10^{-2,b}$	-1.80
3n ($E = -16.76$)	CH_2Cl_2	7.35×10^{-3}	-2.13
3o ($E = -17.79$)	CH_2Cl_2	1.07×10^{-2}	-1.97
3r ($E = -19.07$)	CH_2Cl_2	1.37×10^{-3}	-2.86
3t ($E = -22.77$)	CH_2Cl_2	9.04×10^{-5}	-4.04

^a This work, if not mentioned otherwise. ^b From ref. S11.

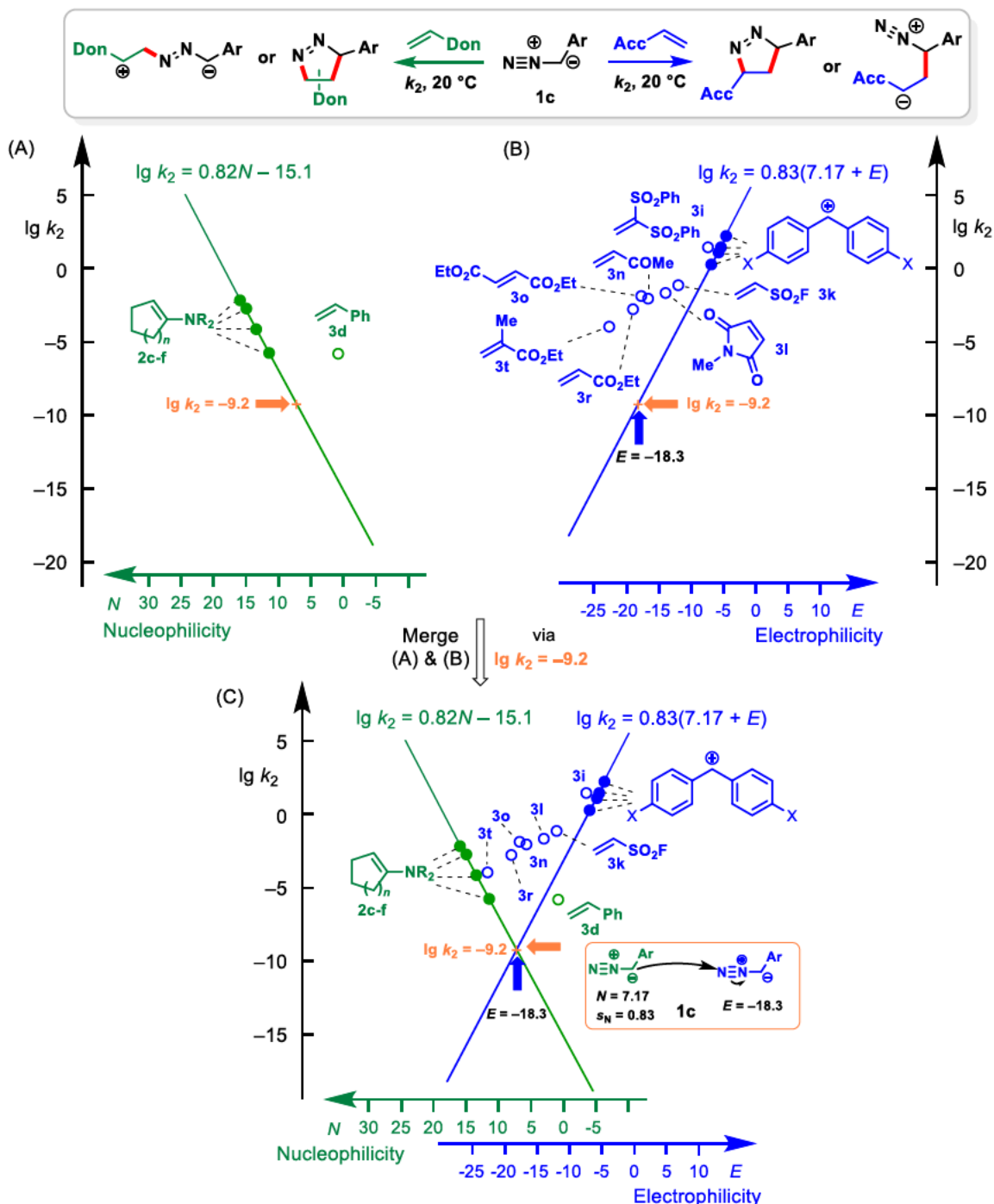
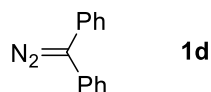


Figure S8. (A) Plot of $\lg k_2$ vs. N parameters for the reactions of 1c with reference nucleophiles 2 (filled green dots, used to construct the green correlation line) and the nucleophilic dipolarophile 3d (open green dots). (B) Plot of $\lg k_2$ vs. E parameters for the reactions of 1c with reference electrophiles Ar_2CH^+ (filled blue dots, used to construct the blue correlation line) and electrophilic dipolarophiles 3. (C) Merging the plots of (A) and (B) by crossing the green and blue correlation lines at $\lg k_2 = -9.2$, which reflects the hypothetical rate constant for the reaction of an electrophilic molecule 1c with a nucleophilic molecule 1c as calculated by using Equation (1).

Diphenyldiazomethane (1d)

The $\lg k_2$ vs. N and E correlations for diphenyldiazomethane (**1d**) were constructed by using second-order rate constants $k_2(20\text{ }^\circ\text{C})$ of the reactions of **1d** with reference one-bond nucleophiles **2** (Table S41), reference one-bond electrophiles (Ar_2CH^+ , Table S42), and dipolarophiles **3** (Table S43).

Table S41. Second-order rate constant $k_2(20\text{ }^\circ\text{C})$ for the reaction of **1d** with the reference one-bond nucleophile **2d** and resulting electrophilicity parameter $E(\mathbf{1d})$.

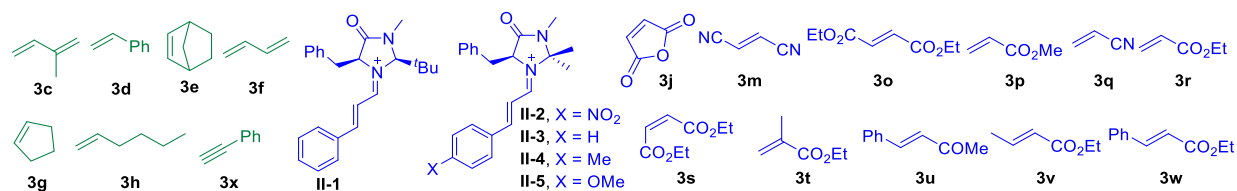
Nucleophiles 2	Solvents	$k_2(20\text{ }^\circ\text{C})^a/$ ($\text{M}^{-1}\text{ s}^{-1}$)	$\lg k_2$
2d ($N = 14.91$, $s_N = 0.86$)	CD_2Cl_2	2.89×10^{-6}	-5.54
E of 1d		-21.4	

^a From ref. S12b.

Table S42. Second-order rate constants $k_2(20\text{ }^\circ\text{C})$ for the reactions of **1d** with reference one-bond electrophiles Ar_2CH^+ (counterion: BF_4^-) in CH_2Cl_2 and resulting reactivity parameters N and s_N .

$\text{Ar}_2\text{CH}^+{}^a$	E	$k_2(20\text{ }^\circ\text{C})^a/$ ($\text{M}^{-1}\text{ s}^{-1}$)	$\lg k_2$
$(\text{mfa})_2\text{CH}^+$	-3.85	2.30×10^1	1.36
$(\text{dpa})_2\text{CH}^+$	-4.72	2.93	0.47
$(\text{mpa})_2\text{CH}^+$	-5.89	2.88×10^{-1}	-0.54
$(\text{dma})_2\text{CH}^+$	-7.02	2.71×10^{-2}	-1.57
N (s_N) of 1d		5.29 (0.92)	

^a Data from ref. S10.

Table S43. Second-order rate constants $k_2(20^\circ\text{C})$ for the reactions of **1d** with dipolarophiles **3** as calculated from the experimentally determined $k_2(40^\circ\text{C})$ in DMF.

Dipolarophiles 3	$k_2(40^\circ\text{C})^a$ ($\text{M}^{-1}\text{s}^{-1}$)	ΔS^\ddagger ($\text{J mol}^{-1}\text{K}^{-1}$)	$k_2(20^\circ\text{C})^b$ ($\text{M}^{-1}\text{s}^{-1}$)	$\lg k_2$
3c ($N = 1.10$)	2.85×10^{-6}	-138 ± 4^c	5×10^{-7}	-6.3
3d ($N = 0.78$)	1.23×10^{-5}		2×10^{-6}	-5.7
3e ($N = -0.25$)	3.83×10^{-5}		$7 \times 10^{-6},^c$	-5.2
3f ($N = -0.87$)	7.85×10^{-6}		1×10^{-6}	-6.0
3g ($N = -1.55$)	4.45×10^{-7}		6×10^{-8}	-7.2
3h ($N = -2.77$)	6×10^{-7}		9×10^{-8}	-7.0
3x ($N = -0.04$)	1.18×10^{-5}		2×10^{-6}	-5.7
II-1 ($E = -5.52$)			$5.54 \times 10^{-1},^d$	-0.3
II-2 ($E = -5.90$)			$4.73 \times 10^{-1},^d$	-0.3
II-3 ($E = -7.20$)			$1.48 \times 10^{-1},^d$	-0.8
II-4 ($E = -7.20$)			$6.48 \times 10^{-2},^d$	-1.2
II-5 ($E = -8.00$)			$1.76 \times 10^{-2},^d$	-1.8
3j ($E = -11.31$)	7.88×10^{-2}	-141 ± 1^c	3×10^{-2}	-1.5
3m ($E = -15.71$)	4.02×10^{-3}		1×10^{-3}	-3.0
3o ($E = -17.79$)	2.47×10^{-2}		8×10^{-3}	-2.1
3p ($E = -18.84$)	8.31×10^{-3}		2×10^{-3}	-2.7
3q ($E = -19.05$)	4.74×10^{-3}		1×10^{-3}	-3.0
3r ($E = -19.07$)	8.12×10^{-3}		2×10^{-3}	-2.7
3s ($E = -19.49$)	$6.85 \times 10^{-4},^e$		2×10^{-4}	-3.7
3t ($E = -22.77$)	5.05×10^{-4}		1×10^{-4}	-4.0
3u ($E = -23.01$)	7.20×10^{-6}		1×10^{-6}	-6.0
3v ($E = -23.59$)	2.46×10^{-5}		4×10^{-6}	-5.4
3w ($E = -24.52$)	1.25×10^{-5}		2×10^{-6}	-5.7

^a Second-order rate constants $k_2(40^\circ\text{C})$ from refs **S23** and **S24**. ^b Calculated from $k_2(40^\circ\text{C})$ with an assumed $\Delta S^\ddagger = -140 \text{ J mol}^{-1} \text{ K}^{-1}$ derived from ref. **S23**. ^c Calculated from rate constants reported in ref. **S23**. ^d Data from ref. **S25**. ^e Rate constant $k_2(40^\circ\text{C})$ for the reaction of **1d** with dimethyl maleate.

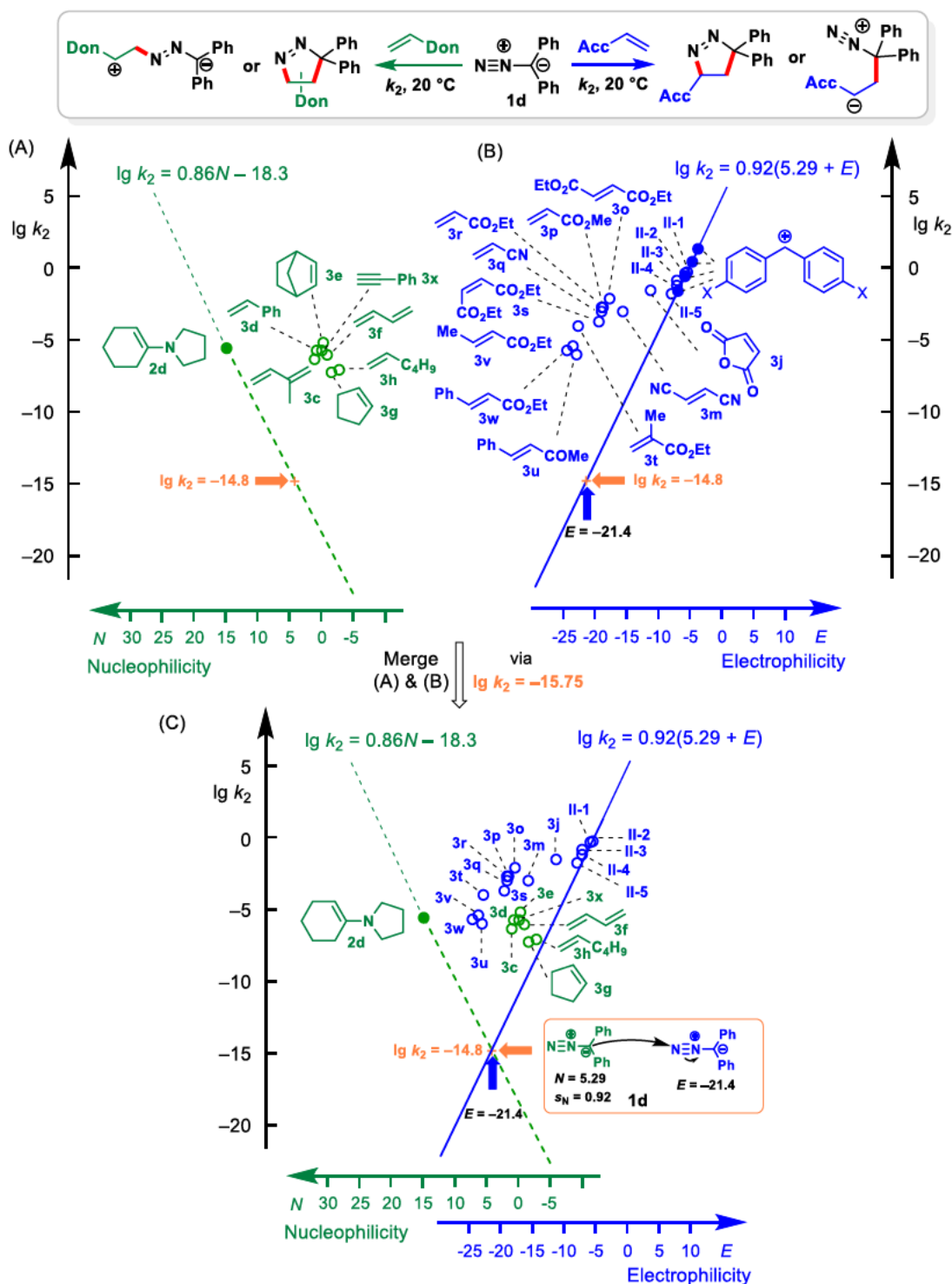
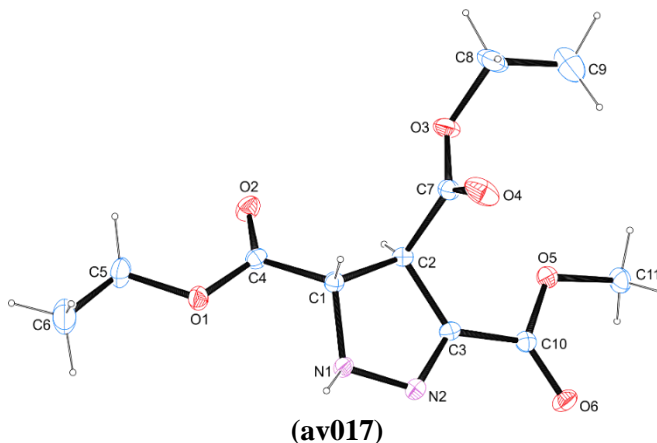


Figure S9. (A) Plot of $\lg k_2$ vs. N parameters for the reactions of **1d** with the reference nucleophile **2d** (filled green dots, $s_N = 0.86$ of **2d** was used to construct the green correlation line) and nucleophilic dipolarophiles **3** (open green dots). (B) Plot of $\lg k_2$ vs. E parameters for the reactions of **1d** with reference electrophiles Ar_2CH^+ (filled blue dots, used to construct the blue correlation line) and electrophilic dipolarophiles **3**. (C) Merging the plots of (A) and (B) by crossing the green and blue correlation lines at $\lg k_2 = -14.8$, which reflects the hypothetical rate constant for the reaction of an electrophilic molecule **1d** with a nucleophilic molecule **1d** as calculated by using Equation (1).

6.2.4 Single Crystal X-ray Crystallography

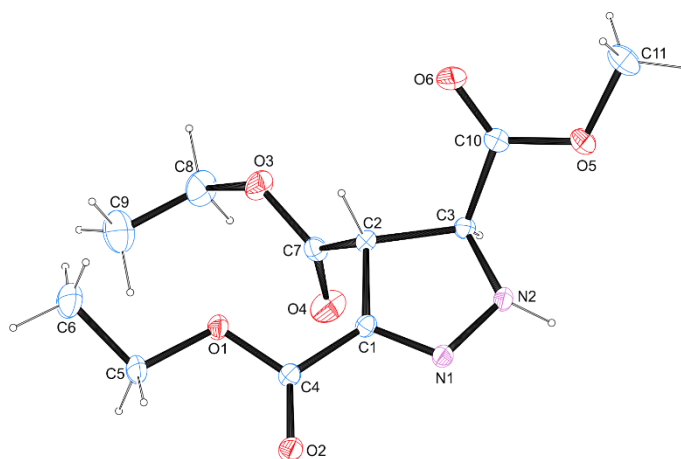
4,5-Diethyl 3-methyl (4*S**,5*R**)-4,5-dihydro-1*H*-pyrazole-3,4,5-tricarboxylate *trans*-(6a*o*)**Crystallographic data.**

net formula	C ₁₁ H ₁₆ N ₂ O ₆
<i>M</i> _r /g mol ⁻¹	272.26
crystal size/mm	0.100 × 0.030 × 0.030
<i>T</i> /K	173.(2)
radiation	MoKα
diffractometer	'Bruker D8 Venture TXS'
crystal system	orthorhombic
space group	'P c a 21'
<i>a</i> /Å	16.0043(10)
<i>b</i> /Å	10.5037(8)
<i>c</i> /Å	7.7419(6)
α/°	90
β/°	90
γ/°	90
<i>V</i> /Å ³	1301.45(16)
<i>Z</i>	4
calc. density/g cm ⁻³	1.390
μ/mm ⁻¹	0.114
absorption correction	Multi-Scan
transmission factor range	0.91–1.00
refls. measured	6930
<i>R</i> _{int}	0.0449
mean σ(<i>I</i>)/ <i>I</i>	0.0514
θ range	3.200–25.348
observed refls.	2008
<i>x</i> , <i>y</i> (weighting scheme)	0.0473, 0.2364
hydrogen refinement	mixed
Flack parameter	0.5
refls in refinement	2328
parameters	179
restraints	1
<i>R</i> (<i>F</i> _{obs})	0.0417
<i>R</i> _w (<i>F</i> ²)	0.0993

S	1.081
shift/error _{max}	0.001
max electron density/e Å ⁻³	0.312
min electron density/e Å ⁻³	-0.167

All C-bound hydrogen atoms have been calculated in ideal geometry riding on their parent atoms while the N-bound one has been refined freely. The structure has been refined as a 2-component perfect inversion twin.

3,4-Diethyl 5-methyl (4*R**,5*S**)-4,5-dihydro-1*H*-pyrazole-3,4,5-tricarboxylate (±)-*trans*-4as



(av173)

Crystallographic data.

net formula	C ₁₁ H ₁₆ N ₂ O ₆
M_r /g mol ⁻¹	272.26
crystal size/mm	0.120 × 0.090 × 0.060
T /K	173.(2)
radiation	MoK α
diffractometer	'Bruker D8 Venture TXS'
crystal system	orthorhombic
space group	'P 21 21 21'
a /Å	7.7451(3)
b /Å	10.1134(4)
c /Å	17.2325(7)
α /°	90
β /°	90
γ /°	90
V /Å ³	1349.81(9)
Z	4
calc. density/g cm ⁻³	1.340
μ /mm ⁻¹	0.110
absorption correction	Multi-Scan
transmission factor range	0.95–0.99

refls. measured	16630
R_{int}	0.0293
mean $\sigma(I)/I$	0.0198
θ range	2.883–26.733
observed refls.	2722
x, y (weighting scheme)	0.0559, 0.3942
hydrogen refinement	mixed
Flack parameter	0.5
refls in refinement	2848
parameters	178
restraints	0
$R(F_{\text{obs}})$	0.0359
$R_w(F^2)$	0.1057
S	1.114
shift/error _{max}	0.001
max electron density/e \AA^{-3}	0.263
min electron density/e \AA^{-3}	-0.175

All C-bound hydrogen atoms have been calculated in ideal geometry riding on their parent atoms, the N-bound hydrogen atom has been refined freely. The structure has been refined as a 2-component perfect inversion twin.

The X-ray structure of triethyl *trans*-4,5-dihydro-1*H*-pyrazole-3,4,5-tricarboxylate has previously been reported.^{S26}

6.2.5 References

- (S1) a) Shi, T. D.; Teng, S. H.; Wei, Y. J.; Guo, X.; Hu, W. H. *Green Chem.* **2019**, *21*, 4936–4940. b) Kornilova, T. A.; Ukolov, A. I.; Kostikov, R. R.; Zenkevich, I. G. *Russ. J. Gen. Chem.* **2012**, *82*, 1675–1685.
- (S2) Baum, J. S.; Shook, D. A.; Davies, H. M. L.; Smith, H. D. *Synthetic Commun.* **1987**, *17*, 1709–1716.
- (S3) Arunprasath, D.; Sekar, G. *Adv. Synth. Catal.* **2017**, *359*, 698–708.
- (S4) Zheng, Q. H.; Dong, J. J.; Sharpless, K. B. *J. Org. Chem.* **2016**, *81*, 11360–11362.
- (S5) Fulmer, G. R.; Miller, A. J. M.; Sherden, N. H.; Gottlieb, H. E.; Nudelman, A.; Stoltz, B. M.; Bercaw, J. E.; Goldberg, K. I. *Organometallics*. **2010**, *29*, 2176–2179.
- (S6) SAINT. Bruker AXS Inc., Madison, Wisconsin, USA, 2012.
- (S7) Sheldrick, G. M. *SADABS, TWINABS*, University of Göttingen, Germany, 1996.
- (S8) Sheldrick, G. M. *Acta Cryst. A* **2015**, *71*, 3–8.
- (S9) Farrugia, L. J. *J. Appl. Cryst.* **2012**, *45*, 849–854.
- (S10) (a) Bug, T.; Hartnagel, M.; Schlierf, C.; Mayr, H. *Chem. Eur. J.* **2003**, *9*, 4068–4076. (b) Mayer, R. J.; Hampel, N.; Mayer, P.; Ofial, A. R.; Mayr, H. *Eur. J. Org. Chem.* **2019**, 412–421.
- (S11) Jangra, H.; Chen, Q.; Fuks, E.; Zenz, I.; Mayer, P.; Ofial, A. R.; Zipse, H.; Mayr, H. *J. Am. Chem. Soc.* **2018**, *140*, 16758–16772.
- (S12) (a) Li, L.; Mayer, P.; Stephenson, D. S.; Ofial, A. R.; Mayer, R. J.; Mayr, H. *Angew. Chem. Int. Ed.* **2022**, *61*, e202117047. (b) Li, L.; Mayer, R. J.; Stephenson, D. S.; Mayer, P.; Ofial, A. R.; Mayr, H. *Chem. Eur. J.* **2022**, *28*, e202201376.
- (S13) Atkins, P.; de Paula, J.; Keeler, J. *Atkins' Physical Chemistry*, 11th ed.; Oxford Univ. Press: Oxford (UK), **2018**; p 733.
- (S14) (a) Applequist, D. E.; Gdanski, R. D. *J. Org. Chem.* 1981, *46*, 2502–2510. (b) Yao, M.-L.; Deng, M. Z. *Synthesis* 2000, 1095–1100.
- (S15) Gorpinchenko, V. A.; Petrov, D. V.; Spirikhin, L. V.; Dokichev, V. A.; Tomilov, Yu. V. *Russ. J. Org. Chem.* **2006**, *42*, 1706–1710.
- (S16) Zhu, C. J.; Yoshimura, A.; Ji, L.; Wei, Y. Y.; Nemykin, V. N.; Zhdankin, V. V. *Org. Lett.* **2012**, *14*, 3170–3173.
- (S17) Reissig, H.-U. *Neue Beiträge zu den Additionen der Diazoalkane und zur Chemie der 3H-Pyrazole*, Dissertation, Ludwig-Maximilians-Universität München, **1978**.
- (S18) Huisgen, R.; Koszinowski, J.; Ohta, A.; Schiffer, R. *Angew. Chem. Int. Ed. Engl.* **1980**, *19*, 202–203.
- (S19) (a) Davies, H. M. L.; Hougland, P. W.; Cantrell Jr., W. R. *Synth. Commun.* **1992**, *22*, 971–978. (b) Bulychov, Yu. N.; Preobrazhenskaya, M. N.; Chernyshev, A. I.; Esipov, S. E. *Chem. Heterocycl. Compd.* **1988**, *24*, 751–755.

- (S20) Johnston, R. L.; Jones, L. A. *J. Chem. Eng. Data* **1971**, *16*, 112–115.
- (S21) (a) Felcht, U.; Regitz, M. *Liebigs Ann.* **1977**, 1309–1320. (b) Driermann, D.; Kerndl, V.; Görls, H.; Vilotijevic, I. *Synlett* **2020**, *31*, 1158–1162. (c) O'Connor, N. R.; Bolgar, P.; Stoltz, B. M. *Tetrahedron Lett.* **2016**, *57*, 849–851.
- (S22) Bihlmaier, W.; Huisgen, R.; Reissig, H.-U.; Voss, S. *Tetrahedron Lett.* **1979**, *20*, 2621–2624.
- (S23) Geittner, J. *Kinetik und Mechanismus der Cycloadditionen von Diazoalkanen*, Dissertation, Ludwig-Maximilians-Universität München, **1973**.
- (S24) Huisgen, R.; Stangl, H.; Sturm, H. J.; Wagenhofer, H. *Angew. Chem.* **1961**, *73*, 170.
- (S25) Zhang, J.; Chen, Q.; Mayer, R. J.; Yang, J.-D.; Ofial, A. R.; Cheng, J.-P.; Mayr, H. *Angew. Chem. Int. Ed.* **2020**, *59*, 12527–12533.
- (S26) (a) Egli, D. H.; Linden, A.; Heimgartner, H. *Helv. Chim. Acta* **2007**, *90*, 86–100. (b) X. Jia, Y. Li, L. Xiao, L. Liu, *Polym. Chem.* **2014**, *5*, 4781–4789.